Pseudo-Sugar Mimics of D-Glucosamine-6-phosphate are Activators of the *glmS* Ribozyme

Dissertation

zur
Erlangung des Doktorgrades (Dr. rer. nat.)
der
Mathematisch-Naturwissenschaftlichen Fakultät
der
Rheinischen Friedrich-Wilhelms-Universität Bonn

vorgelegt von

Daniel Matzner

aus

Troisdorf

Bonn 2018

Angefertigt mit Genehmigung der Mathematisch-Naturwissenschaftlichen Fakultät der
Rheinischen Friedrich-Wilhelms-Universität Bonn

1. Gutachter: Prof. Dr. Günter Mayer
2. Gutachter: Prof. Dr. Andreas Gansäuer

Tag der Promotion: 29. Juni 2018
Erscheinungsjahr: 2018

Parts of this thesis have been published in:

- Matzner, D.; Schüller, A.; Seitz, T.; Wittmann, V.; Mayer, G. Fluoro-carba-sugars are Glycomimetic Activators of the *glmS* Ribozyme, *Chem. Eur. J.* **2017**, *23*, 12604-12612.
- Schüller, A.; Matzner, D.; Lünse, C.; Wittmann, V.; Schumacher, C.; Unsleber, S.; Brötz-Oesterhelt, H.; Mayer, C.; Bierbraum, G.; Mayer, G. Activation of the *glmS* Ribozyme Confers Bacterial Growth Inhibition, *ChemBioChem* **2017**, *18*, 435-440.
- Matzner, D.; Mayer, G. (Dis)similar Analogues of Riboswitch Metabolites as Antibacterial Lead Compounds, *J. Med. Chem.* **2015**, *58*, 3275-3286

Danksagung

An diesem Punkt möchte ich den zahlreichen Personen danken ohne deren Beitrag und Unterstützung diese Arbeit nicht möglich gewesen wäre.

Als erstes gilt mein besonderer Dank *Prof. Dr. Günter Mayer*, der mir mit einer überaus interessanten Themenstellung eine spannende wissenschaftliche Arbeit in den letzten Jahren ermöglicht hat. Seine Motivation, Förderung, Forderung aber auch das Vertrauen in meine eigene Entscheidungsfähigkeit haben mir die Entwicklung zu dem Wissenschaftler ermöglicht der ich heute bin.

Allen Mitgliedern meiner Prüfungskommission möchte ich danken, dass sie sich bereit erklärt haben die vorliegende Arbeit zu begutachten. Insbesondere danke ich *Prof. Dr. Andreas Gansäuer* für die Übernahme des Koreferates.

Ohne die unschätzbaren Beiträge in Form von Kollaborationen wäre die erfolgreiche Umsetzung der Projekte, die zu dieser Arbeit führten, nicht möglich gewesen. Bedanken möchte ich mich bei *Prof. Dr. Valentin Wittmann* und seinen Labormitarbeitern, vor allem *Dr. Torben Seitz*, *Dr. Daniel Wieland* und *Dr. Magnus Schmidt*. Die Arbeiten während meiner zwei Forschungsaufenthalte in den Laboren in der AG Wittmann legten den Grundstein für die Etablierung der Synthese von Carba-Zucker-Derivaten. Die Hilfe bei synthetischen Fragestellungen, der Analytik und die zahlreichen Meetings und Skype-Konferenzen leisteten einen entscheidenden Beitrag. Es ist mir ein besonderes Vergnügen *Dr. Torben Seitz* dafür zu danken, dass nicht nur die Sauerei im Labor unvergessen bleibt. Seine Arbeit sowie die Motivation und Unterstützung auch an frustrierenden Stellen nicht aufzugeben waren entscheidend für den erfolgreichen Abschluss der Synthese. Das Gesamtpaket aus seiner offenen Art, dem täglichen Fitnessprogramm und dem Spass im Labor haben für eine großartige Zeit in Konstanz gesorgt.

Ich möchte allen Mitgliedern der Forschergruppe FOR 854 der DFG und im besonderen *Prof. Dr. Hans-Georg Sahl* danken. Weiterhin danke ich *Prof. Heike Brötz-Oesterhelt*, *Prof. Dr. Christoph Mayer* und ihren Laboren dafür, dass sie erste mikrobiologische Experimente meiner Zielverbindungen durchführten, die zukünftige Kollaborationen sichern.

Stefan Künne danke ich neben der hervorragenden Organisation des Labors auch für die spannenden Kicker-Duelle in der Mittagspause. *Kordula Bellinghausen*, *Dr. Sven*

Freudenthal, *Sarah Hensel* und *Sandra Ullrich* danke ich für die Hilfe in allen organisatorischen Belangen.

Bei den Mitarbeitern der zentralen Analytik des Kekulé-Institutes, der NMR-core-facility der Universität Konstanz sowie der NMR-Abteilung der Universität Hamburg danke ich für die unzähligen gemessenen Massen- und NMR-Spektren. Besonderer Dank gilt *Anke Friemel*; *Dr. Senada Nozinovic* und *Dr. Thomas Hackl* für Sondermessungen in Konstanz, Bonn und Hamburg.

Dr. Andreas Meyer danke ich für seine Hilfe bei der quantenchemischen Berechnung meiner Verbindungen.

Ich danke meinen Praktikanten, Bachelor-, Master- und Diplomstudenten für die tatkräftige Unterstützung bei der Synthese, insbesondere *Waldemar Grunwald*, *Thomas Meyer* und *Rita Zimmermann*.

Für das Korrekturlesen dieser Arbeit danke ich *Ignazio Geraci*, *Dr. Silvana Haßel*, *Mark Kerzhner*, *Dr. Andreas Meyer*, *Franziska Pfeiffer* und *Shannon Smith*.

Weiterhin möchte ich mich bei den gesamten aktuellen und ehemaligen Mitgliedern der Arbeitsgruppen Mayer, Famulok und Kath-Schorr für die gute Arbeitsatmosphäre und die großartige Zeit im Labor bedanken. Mein besonderer Dank gilt *Ignazio Geraci*, *Dr. Silvana Haßel*, *Dr. Stefanie Kath-Schorr*, *Franziska Pfeiffer*, *Dr. Fabian Tolle*. Weiterhin gilt mein Dank meinen Mitstreitern *Anna Schüller* und *Dr. Christina Lünse* für die gute Zusammenarbeit. *Anna Schüller* danke ich insbesondere für ihr Durchhaltevermögen bei unzähligen radioaktiven Gelen und Herausforderungen im Projekt. Mein großer Dank gilt meinem Laborpartner *Mark Kerzhner* für die Unterstützung bei synthetischer Unwegsamkeit, aber vor allem für den guten Zusammenhalt und den Spaß im Laboralltag.

Für die ausgleichenden Abende beim Bouldern/Klettern und die sportlichen Events wie Triathlons oder kurze „Bring Sally Up“-Challenges möchte ich mich bei allen Teilnehmern bedanken, insbesondere *Christof Domnick*, *Iganzio Geraci*, *Dr. Stefanie Kath-Schorr*, *Mark Kerzhner*, *Dr. Björn Niebel*, *Sebastian Pilsl*, *Malte Rosenthal*, *Dr. Fabian Tolle* und *Dr. Benjamin Weiche.*

Von ganzem Herzen möchte ich mich bei meinen Eltern bedanken, die durch ihre Unterstützung und ihr Vertrauen während Doktorarbeit und Studium diese Arbeit erst möglich gemacht haben. Zuletzt danke ich meiner geliebten Frau *Mirjam Wingender* und meinem Sohn *Bjarne Matzner* die durch ihr Lachen und ihre Wärme mein Leben erhellen.

Abstract

The *glmS* ribozyme is a gene-regulating riboswitch in bacteria whose enzymatic activity is dependent on D-glucosamine-6-phosphate (GlcN6P) as a natural cofactor. The GlmS enzyme plays a major role in the bacterial cell wall synthesis as it produces GlcN6P, an early intermediate in the biosynthesis of UDP-GlcNAc, which is an essential precursor of peptidoglycan. It is due to the presence of this ribozyme in human pathogens, including MRSA, *Listeria monocytogenes*, and *Clostridium difficile* that it represents an attractive target for the development of artificial activators. Carbohydrate mimics that possess significant structural dissimilarity to their natural counterparts, but efficiently mimic the activity of GlcN6P, could function as novel therapeutic entities.

The substitution of the ring oxygen of natural sugars by functionalized methylene yields 5a-substituted carba-sugars. These promising synthetic glycomimetics could potentially interfere with their target structures in biological systems due to new functionalities. In the course of the project presented herein, the synthesis of fluoro-carba-sugar analogs of α-D-glucosamine and β-L-idosamine as well as a phenyl-carba-sugar variant of α-D-glucosamine was established. Titanocene(III)-catalyzed radical epoxide opening was used in the synthesis of (5a*R*)-fluoro-carba-α-D-glucosamine-6-phosphate as part of a new route towards base-labile carbocycles. The high diastereoselectivity of the hydrogen transfer step was rationalized by computation of the transition states involved in this step.

In studies of the biological activity of the carba-sugar mimics on *glmS* ribozymes from different bacteria, fluoro-carba-GlcN6P effectively promoted the *glmS* ribozyme self-cleavage reaction, although with a significant loss of activity compared to its non-fluorinated analog. Docking of all synthesized carba-sugars to the rigid *glmS* binding pocket supported the experimental data, thereby allowing an in-depth structure-activity relationship. In contrast, the inhibiting effect of fluoro-carba-GlcN on *B. subtilis* growth, which is dependent on the GlcN-specific phosphoenolpyruvate:sugar phosphotransferase system, was comparable with that of carba-GlcN. The specific induction of cell envelope stress, thus, paves the way for a comprehensive analysis of the mode of action of fluoro-carba-GlcN.

Zusammenfassung

Das *glmS*-Ribozym ist ein genregulierender Riboswitch in Bakterien, dessen enzymatische Aktivität von D-Glucosamin-6-phosphat (GlcN6P) als natürlicher Cofaktor abhängt. Das GlmS-Enzym spielt bei der bakteriellen Zellwand-Synthese eine wichtige Rolle, da es GlcN6P, eine frühe Zwischenstufe in der Biosynthese von UDP-GlcNAc, produziert, das wiederum ein wesentlicher Vorläufer des Peptidoglycans ist. Die Anwesenheit dieses Ribozyms in menschlichen Pathogenen, wie MRSA, *Listeria monocytogenes* und *Clostridium difficile*, macht es zu einem attraktiven Ziel für die Entwicklung von künstlichen Aktivatoren. Kohlenhydrat-Mimetika, die eine wesentliche strukturelle Veränderung gegenüber ihren natürlichen Gegenstücken besitzen dabei aber die Aktivität von GlcN6P effizient nachahmen, könnten als neuartige Wirkstoffe fungieren.

Die Substitution des Ring-Sauerstoffs von natürlichen Zuckern durch funktionalisierte Methylengruppen ergibt 5a-substituierte Carba-Zucker. Diese vielversprechenden synthetischen Glycomimetika können durch neue Funktionalitäten eine potente Interaktion mit ihren Zielstrukturen in biologischen Systemen eingehen. Im Rahmen des hier vorgestellten Projektes wurde die Synthese von Fluoro-Carba-Zucker-Analoga von α-D-Glucosamin und β-L-Idosamin sowie einer Phenyl-Carba-Zucker-Variante von α-D-Glucosamin etabliert. Die Titanocen(III)-katalysierte radikalische Epoxidöffnung wurde bei der Synthese von (5a*R*)-fluoro-carba-α-D-glucosamin-6-phosphat als Teil einer neuen Route zur Darstellung von basisch-labilen Carbocyclen eingesetzt. Die hohe Diastereoselektivität des Wasserstoffübertragungsschrittes wurde durch Berechnungen der in diesem Schritt beteiligten Übergangszustände rationalisiert.

In Studien über die biologische Aktivität der Carba-Zucker-Mimetika auf *glmS*-Ribozyme aus verschiedenen Bakterien, induzierte Fluoro-carba-GlcN6P effektiv die Selbstspaltungsreaktion des Ribozyms, jedoch mit signifikant niedriger Aktivität als das nicht-fluorierte Analogon. Docking-Studien von allen synthetisierten Carba-Zuckern mit der starren *glmS*-Bindungstasche unterstützten die experimentellen Daten, so dass eine tiefgehende Struktur-Aktivitäts-Beziehung aufgestellt werden konnte. Im Gegensatz dazu war die hemmende Wirkung von Fluoro-carba-GlcN auf das *B. subtilis*-Wachstum in Abhängigkeit vom GlcN-spezifischen Phosphoenolpyruvat: Zucker-Phosphotransferase-System vergleichbar mit der von Carba-GlcN. Eine spezifische Stressinduktion in der

bakteriellen Zellhülle ebnet den Weg für eine umfassende Analyse der genauen Wirkungsweise von Fluoro-carba-GlcN.

Contents

1 Introduction

1.1 Carbohydrate mimics

The diet of most people relies on carbohydrates as a primary source of energy.[1] The perception of the sweet taste of low molecular weight dietary carbohydrates is thereby associated with advantageous food.[2] Besides their role as an energy source, carbohydrates are one of the essential building blocks of living systems, along with proteins, lipids, and nucleic acids.[3] The sugar components of carbohydrate macromolecules are referred to as glycans and comprise linked monomeric sugar molecules.[4] In contrast to biopolymers composed of nucleotides (RNA/DNA) or amino acids (proteins), glycans far exceed their potential structural diversity.[5] The complex structure of glycans, due to strong branching and sequence diversity, enables them to encode information for a correspondingly large number of roles in molecular recognition.[6] Glycans play central roles in various cellular processes, including signaling, cell-cell communication[7], and mediation of immune responses.[8] Thereby, recognition of carbohydrates is involved in diseases and infections. Viruses and bacteria adhere, species- and tissue-specific, to the cell-surface of their host through carbohydrate-mediated cell recognition.[7,9] Because of their pivotal role, the elucidation of their functions and the decryption of the sugar-code are major challenges in glycobiology.[10] However, the structural diversity of these glycoconjugates is accompanied by the complex analytic that lags behind the achievements in the field of RNA and protein analysis. The synthesis of oligosaccharides thereby helps to understand their biological function and opens the way for carbohydrate-based vaccines or the synthesis of specific inhibitors of glycoconjugate function.[6]

Of particular importance in this context are compounds that mimic interactions of carbohydrates with their target structure and are therefore termed “carbohydrate mimics.”[11] These allow the intervention with protein- or nucleic acid-carbohydrate interactions as potential therapeutic agents.[12] Mimics that are dissimilar to their natural carbohydrate counterparts can thereby overcome some disadvantages of therapeutics based on natural products. Oligosaccharides are rapidly degraded by glycosidases, while low molecular weight carbohydrates often lack specificity and low biostability due to, among others, off-target effects and metabolization.[13] Nature already provides carbohydrate mimics such as *C*-glycosides, in the case of which the substitution of the

O-glycosidic bond by C-C prevents hydrolysis by glycosidases. **Figure 1** shows the chemical structure of two natural product C-glycosides, carminic acid and altromycin B. Carminic acid is the free acid of carmine, which is a red pigment produced from cochineal scale already used in ancient times.[14,15]

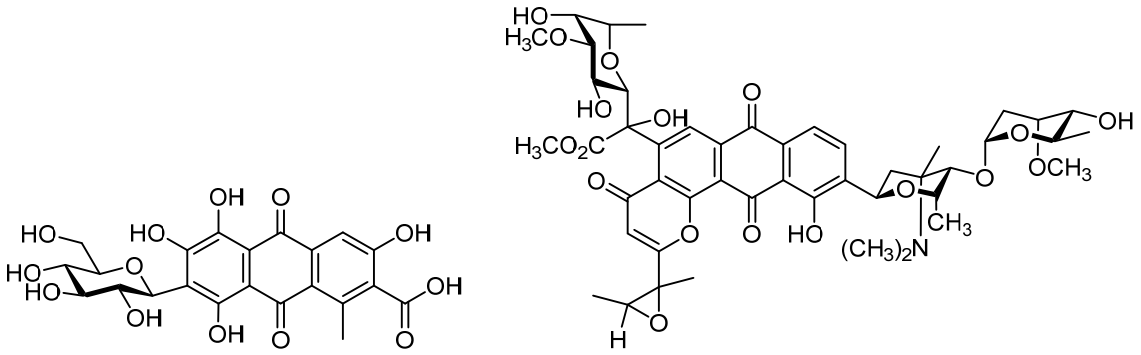

Figure 1 **Two examples of natural product C-glycosides**
The aluminum salt of carminic acid, which is isolated from cochineal scale, is used as the pigment carmine. Altromycin B is an antitumor antibiotic from the pluramycin family, which is produced by an actinomycete from a South African bushveld soil.[16,17]

Altromycin B, on the other hand, shows antibacterial activity against Streptococci and Staphylococci with a low minimal inhibitory concentration (MIC).[16] The mechanism of action of altromycin B, as for other compounds from the pluramycin family, is the alkylation of DNA, whereby altromycin B also exhibits activity against several kinds of cancer.[17,18] Synthetic C-glycosides are prepared as potent inhibitors of glycosidases and glycosyltransferases. Intensively studied synthetic representatives of carbohydrate mimics are carbocyclic analogs of natural sugar pyranoses and furanoses termed pseudo- or more accurate carba-sugars.[19-21]

1.1.1 Carba-sugars

Carba-sugars result from the formal substitution of the ring oxygen by methylene (**Figure 2**). The prefix “carba” thereby has been established by Ogawa *et al.* instead of “pseudo,” and the locant “5a” is used for indexing and distinguishing of 5a-carba-pyranoses from 4a-carba-furanose.[20] Thus, the carbocyclic analogs of the cyclic form of carbohydrates lack the intramolecular hemiacetal which is the most reactive functional group of sugars. Removal of the acetal moiety by a C-C bond thereby increases the chemical and biochemical stability of carba-sugar compared to their natural counterparts since natural carbohydrates are susceptible to hydrolytic cleavage.[13,22]

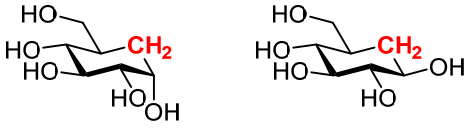

5a-carba-α-D-glucose 5a-carba-β-D-glucose

Figure 2 Chemical structure of the two isomers of the carba-sugar analog of D-glucose.

Moreover, the interconversion of the α- and β-isomers, which is depicted in **Figure 3** for the example of D-glucose, is no longer possible.[23,24] Consequently, the respective carba-sugar isomers do not exist in a steady-state but could be produced in their pure isomeric form.[25] Besides the synthetic accessibility of pure isomers, the carba-sugars differ in their properties in many ways. These include the absence of the anomeric effect, a different hydrogen-bond pattern due the missing hydrogen-acceptor and changed flexibility due to altered conformational behavior.[26,27]

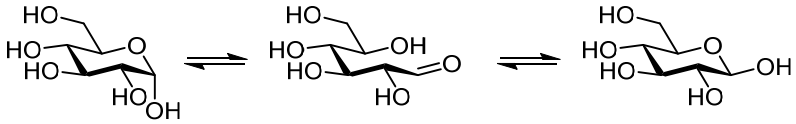

36% <<1% 64%

Figure 3 Interconversion of the α- and β-pyranose forms of D-glucose via the open chain form. The percentages given for each form refers to the aqueous solution of glucose.

The anomeric effect in the case of the α-isomers of natural sugar greatly stabilizes the C-O bond at C1 and thereby shifts the equilibrium between α- and β-isomer towards α-glucopyranose.[23] The absence of the anomeric effect in carba-sugars especially increases the flexibility in the interglycosidic linkage of disaccharides.[20,28] The existence of more conformations induces an entropic penalty to the interaction of carbonated sugar mimics with their target structures, e.g., proteins. The binding free energy increases with ligand flexibility because the binding pocket needs to freeze out the desirable binding conformation which is not necessary in the case of pre-organized ligands.[29] In the case of carba-sugar analogs of monosaccharides, there is the interplay between altered

conformational flexibility and the absence of the interconversion between α- and β-isomers. Whereas the presence of only one isomer increases the ligand pre-organization, the conformational population distributions need to be investigated individually. Unione *et al.*, for instance, observed that the carba-sugar analog of 5-hydroxymethyl-carba-β-L-idopyranoside loses its conformational flexibility compared to the natural analog.[27] In the same study, they could show that substitution of the ring-oxygen by difluoromethylene restores the conformational plasticity. In the case of the iduronic acid moieties in heparin, the ability to adopt different ring conformations is essential for the interaction with protein receptors, as distinct conformations are recognized depending on the respective receptor.[30]

A property of carbohydrate ligands, which is inseparably connected to the ring flexibility described above, is their hydrogen-bond pattern. In the case of carba-sugars, the number and configuration of the hydroxyl groups resemble that of their natural counterparts. However, due to the substitution of the ring-oxygen one potential hydrogen bond acceptor is lost.

The first reported carba-sugar 5a-carba-α-DL-talopyranose[31] was synthesized by McCasland *et al.* in 1966, followed by 5a-carba-β-DL-gulopyranose[32] and 5a-carba-α-DL-galactopyranose[33]. Not before 1973, 5a-carba-α-D-galactopyranose was detected in the fermentation broth of *Streptomyces* sp. MA-4145, which shows inhibitory activity against *Klebsiella pneumonia*.[22,34] There are several examples of naturally occurring carba-sugars or carba-sugar elements in larger structures that exhibit antibacterial activity. Prominent representatives are the carba-trisaccharides of the validamycin compound class[34], which have antibacterial and antifungal activity and are used as potent antibiotics in agriculture. Due to their close similarity to natural sugars, carba-sugars can also function as glycosidase inhibitors (**Figure 4**). Acarbose, which shares the unsaturated amino carba-sugar substructure valienamine with validamycins, is a carba-oligosaccharide that is used for the treatment of diabetes mellitus type 2 (**Figure 4**).[35,36]

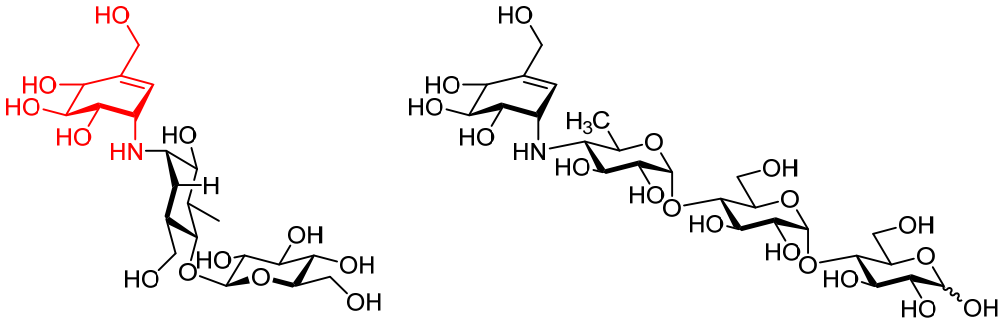

Validamycin A Acarbose

Figure 4 Chemical structure of two examples of natural carba-sugars with biological activity
Validamycin A is a representative of antibacterial validamycins. Acarbose functions as a potent inhibitor of alpha-glycosidase and is thereby used as a drug for the treatment of diabetes. The unsaturated amino carba-sugar substructure valienamine is indicated in red.

The promising mimicking abilities of carba-sugars, which are supported by the biological activity of the examples given above, inspired the synthesis of carba-sugars with different synthetic approaches. Especially noteworthy is the pioneering work of Ogawa *et al.* who contributed, among others, studies on validamine and the synthesis of many carba-sugars utilizing the Diels-Alder reaction on nonsugar substrates.[20,37,38] Synthesis of carba-sugars from natural sugar templates, however, enables the preservation of their chiral centers. Also, nature utilizes this source of chiral natural products for the synthesis of carbocycles (e.g., shikimic acid, cyclitols).[39] A comprehensive view on the synthesis carba-sugar analogs of pyranoses as well as furanoses can be found in the review article of Arjona *et al.*, which gives an overview of the substrate, the number of steps and the overall yield.[22] The carbocyclisation described by Ferrier *et al.* in 1979, represents a versatile synthetic tool for the transformation of 5,6-unsaturated hexopyranose compounds into functionalized cyclohexanones (**Scheme 1**).[40,41] These cyclohexanones can then be easily converted into the respective carba-sugar analogs.[42-44] **Scheme 1** shows the unexpected rearrangement of the hex-5-enopyranoside of glucose **1** observed by Ferrier *et al.* in the presence of equimolar quantities of mercury(II) chloride.[40] In this example, compared to the sugar substrate glucose that was used as the chiral template, all stereocenters except for C5 were retained in the main product **4**. In a more detailed investigation, both α- and β-isomers of the cyclohexanones could be isolated. However, a significant stereoselectivity depending on the 5-ene substrates was observed.[45-47]

Scheme 1 Ferrier rearrangement of hex-5-enopyranoside 1 via the methoxymercuration intermediate 2 and the hemiacetal 3 to the cyclohexanone 4.

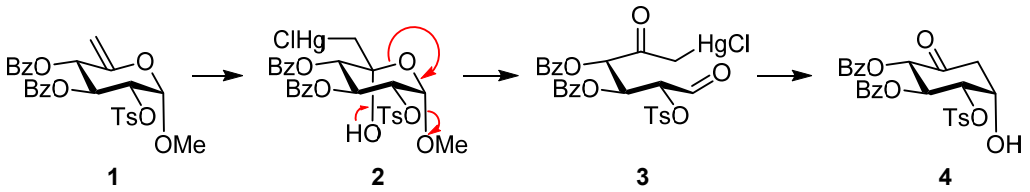

1 **2** **3** **4**

The comparative analysis of the stereochemistry at C1 of the cyclohexanone for a variety of substrates indicated a preference for a *trans*-orientation to the substituent at C3.[41,48-52] This leads to a yield of 89% of the α-ketone **4** for the example shown in **Scheme 1**.[48] The observed stereochemistry of the reaction can be rationalized with the help of **Scheme 2**.[41] The two possible transition states **3'a** and **3'b** differ by the conformation of the ring and the intramolecular coordination of the mercury atom. In the case shown, the chair-like transition state 3'a most probably would be favored leading to **4** as the main product. With a large axial substituent at C3, however, axial repulsion between the substituent at C3 and the coordinated substituents at C1 and C5 would increase the energy of **3'a** and thus the relative amount of the β-isomer **5**.

Scheme 2 Proposed mechanism for the Ferrier rearrangement of 6-deoxyhex-5-enoside 1.

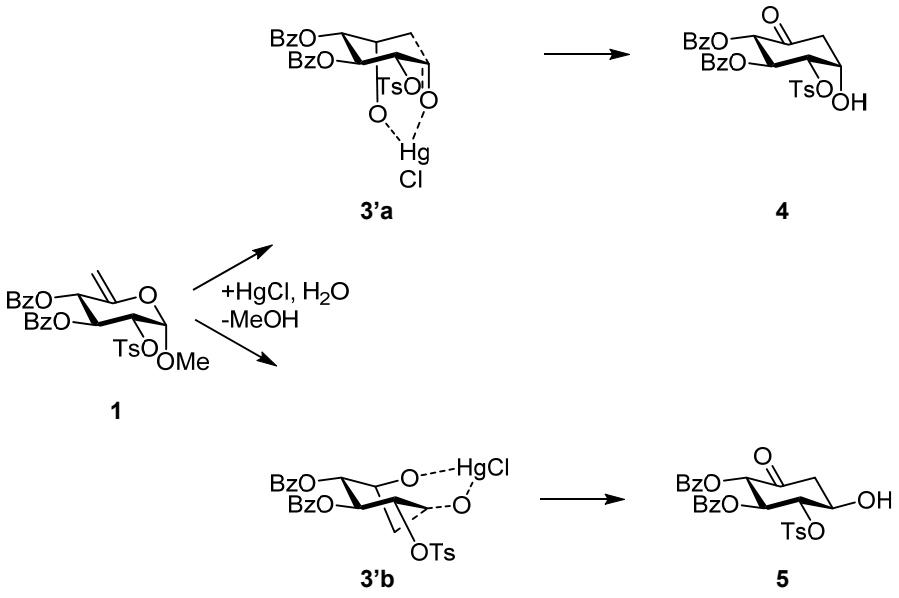

3'a **4**

1

3'b **5**

The Ferrier-rearrangement was successfully applied in the synthesis of the carba-sugar analogs D-glucosamine[42], β-L-idose[53], a carbatrisaccharide component of amilostatins[54] and valienamine[55,56]. Another feature of the Ferrier carbocyclisation that is of utmost interest is the possibility to introduce modifications at C5a in one step with the rearrangement. 6-substituted hex-5-enose derivatives are tolerated and readily transformed into the 5a-substituted carba-sugar derivatives. **Scheme 3** shows this

feature in the case of enol acetate **7** derived from aldehyde **6**, which enables the preparation of *myo*-inositol derivative **8**.[57]

Scheme 3 Synthesis of *myo*-inositol derivative 8.

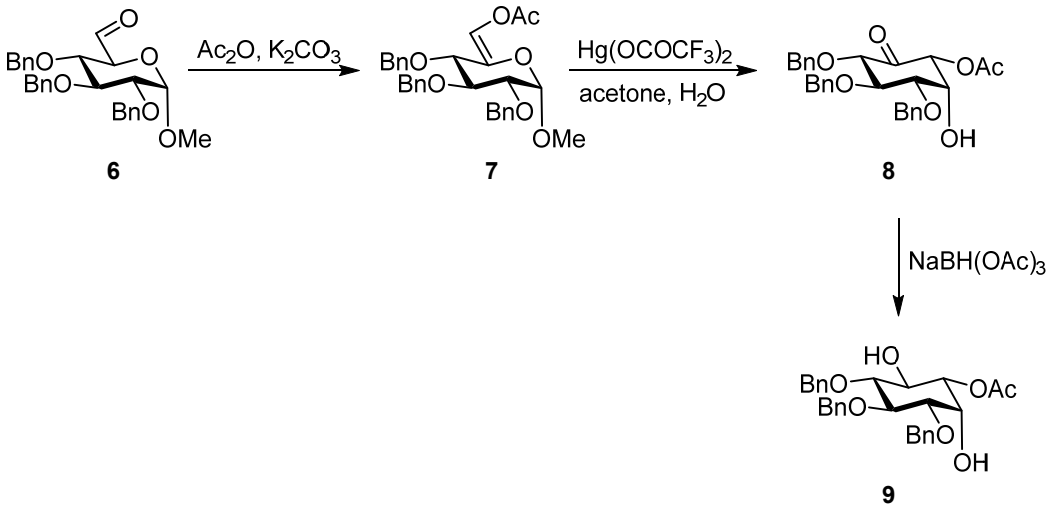

6 **7** **8** **9**

Even bulky substituents at C6 are tolerated, as a demonstrated by Park and Danishefsky during the synthesis of pancratistatin derivative **11** starting from hex-5-enose **10** (**Scheme 4**).[58]

Scheme 4 Synthesis of pancratistatin 11

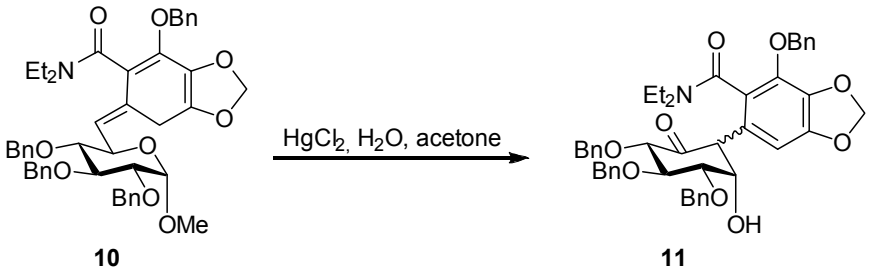

10 **11**

Consequently, the Ferrier rearrangement enables the synthesis of 5a-substituted carbocycles while maintaining the stereo information of the starting material, which is typically derived from sugar templates. The possibility of introducing modifications at C5a thereby allows the synthesis of more complex carba-sugar[a] conjugates. Furthermore, with the possibility of a modular approach towards 5a-modified carba-sugars, new interactions of bioactive carbohydrate mimics with their respective target structures can be addressed.

[a] According to the originally definition of carba-sugars, 5a-modified carbacyclic derivatives would not be considered as carba-sugars but rather as pseudo carba-sugar. However, to simplify the nomenclature used in the present work, carbocyclic mimics of sugars bearing substituents other than hydrogen are herein also referred to as carba-sugars.

1.2 Riboswitches

The control of gene expression is essential for the flow of genetic information and therefore fundamental in all living organisms.[59,60] In every living cell, even of the simplest cellular organism, the whole gene-control system needs to react to an immense number of chemical signals and cellular needs.[61] Until two decades ago, it was assumed that gene expression is mostly regulated by protein factors, however, already the catalytically active RNA subunit of ribonuclease P and the self-splicing group I introns challenged this view.[62,63] In the last decades it became apparent that functional non-coding RNAs are not only molecular fossils of a primordial "RNA world," but play crucial roles in the control of bacterial gene expression as among others antisense or attenuator RNAs.[64,65] In the context of attenuators, which are part of the same mRNA that they regulate, metabolite-sensing RNAs mostly found in the 5' untranslated region (5'UTR) of bacterial mRNA comprise a major class among *cis*-regulatory RNAs. The direct recognition of metabolites by mRNA without the need for proteins was thereby demonstrated by Nahvi *et al.*[66] and Winkler *et al.*[67]. These so-called riboswitches serve as genetic switches in many fundamental metabolic pathways.[68,69]

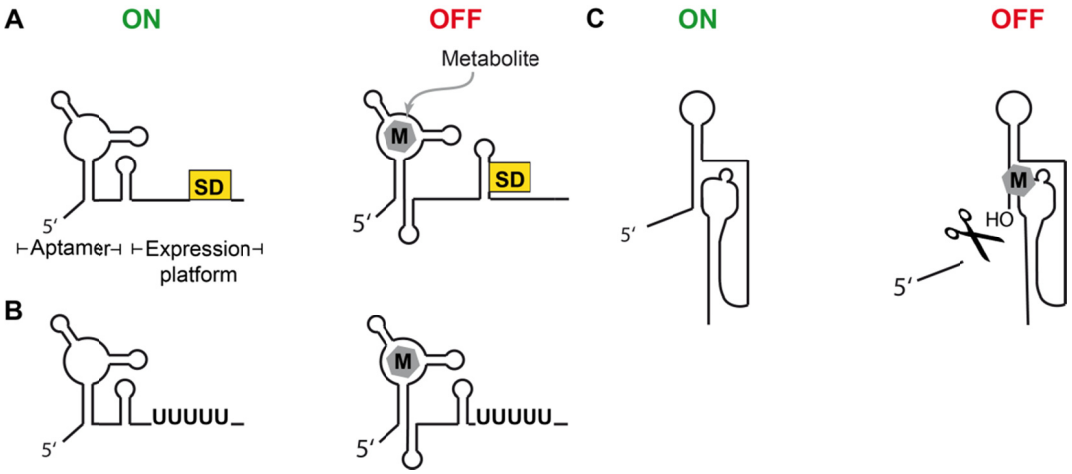

Figure 5 Schematic explanation of the most common mechanism of gene expression by riboswitches and the unique self-cleavage mechanism of the *glmS* riboswitch
In this figure, only OFF-switches are considered. (A) Shown is the inhibition of translation that is initiation by sequestering the Shine-Dalgarno sequence (SD) upon binding of the metabolite (M). (B) In the case of transcription termination, metabolite binding induces the formation of a terminator stem in front of a stretch of five to nine uridines. (C) The natural metabolite of the *glmS* ribozyme is α-D-glucosamine-6-phosphate (GlcN6P) that acts as the cofactor of the self-cleavage mechanism. The resulting 5'-hydroxy group is detected by RNase J1 and leads to hydrolysis of the *glmS* gene. Modified from Matzner *et al.*[70]

Riboswitches consist of an aptamer region with an adjoined expression platform. The aptamer (from aptus = fit and meros = part) senses the respective metabolite by specific and high-affinity binding. The binding of the metabolite induces a conformational change

in the expression platform, which leads to the control of gene expression by mostly transcription termination (**Figure 5B**) or inhibition of translation initiation (**Figure 5A**).[71,72] In the case of transcription termination, the ongoing transcription is terminated by a terminator stem followed by five to nine uridines (OFF). This structure leads to the stop of the RNA polymerase, ending the transcription of the template prematurely. An anti-terminator is formed in the absence of the metabolite, which allows regular mRNA synthesis (ON).[69] Genetic control by riboswitches on the level of translation initiation takes place through conformational switching. The RNA conformation in "ON" position enables the excess of the ribosome to the Shine-Dalgarno sequence (SD). In the case of an OFF-switch, an anti-SD sequence sequesters the ribosome binding site in the presence of the metabolite and thereby prevents the start of translation.[69] A unique mechanism for regulation of translation is utilized by the *glmS* riboswitch, which functions as a cofactor depending self-cleaving ribozyme (**Figure 5C**).[73] Upon binding of α-D-glucosamine-6-phosphate (GlcN6P), self-cleavage of the riboswitch leads to the formation of a 5'OH group at the cleavage site, which is prone to hydrolysis by RNase J1.[73,74] This results in down-regulation of the levels of *glmS* mRNA. Apart from these mechanisms, gene expression by riboswitches takes place through a combination of both, regulation of translation and mRNA decay, as for the *lysC* riboswitch.[75] Other mechanisms include the Rho-dependent transcription termination of the *mgtA* and the *ribB* riboswitches[76], as well as the *trans*-acting riboswitches SreA and SreB[77]. Currently known are almost 40 distinct classes of riboswitches accompanied by several orphan riboswitches that are distinguished by their respective aptamer region and consequently by the recognized metabolite.[78] Riboswitches are not restricted to bacteria; there are mainly two riboswitch classes, fluoride riboswitches[79], which are found in archaea and thiamin pyrophosphate (TPP) riboswitches[67,80], which are present in archaea and very common among fungi[81,82], plants[83] and algae[84].

1.3 The *glmS* ribozyme

The unique role of *glmS* riboswitches among all classes of regulatory-active mRNA is defined by their function as metabolite-cofactor-dependent ribozymes (catalytically active RNA) (depicted in **Figure 5C**)[73], whereas other riboswitch-triggered ribozymes are described.[78,85] The irreversible cleavage of the *glmS* mRNA is triggered by α-D-glucosamine-6-phosphate, which is also the natural cofactor of the cleavage reaction (**Figure 6**).[86,87] The mechanism of the *glmS* ribozyme cleavage reaction was comprehensively studied by different means. Besides its structural investigation by high-resolution crystal structures[88], the determination of the ligand requirements[89] and

computational simulations/calculations[90,91] helped to understand the cleavage mechanism. As a result, several mechanisms were proposed[90,92,93] that are, however, similar to those of other self-cleaving ribozymes.[94] Consequently, cleavage of the *glmS* ribozyme yields the 5' cleavage product with a 2',3'-cyclic phosphate and the 3' part with a 5'-OH terminus.[92] The cleavage requires the presence of a base for deprotonation of the 2'-OH and an acid that protonates the 5'-oxygen.The proposed mechanisms of the *glmS* ribozyme differ in the definition of the precise role of GlcN6P. However, they agree on the function of the protonated GlcN6P as the general acid transferring a proton from its amino group to the 5'-oxygen of G1. The role of G40, whose G40A mutation leads to complete inactivation of the ribozyme[92], is not that clear-cut. However, quantum mechanical/molecular mechanical (QM/MM) simulations predicted the lowest energy barrier for the mechanism that involved deprotonation of G40 by an external base, which then fills the role of the general base (**Figure 6**).[90] Metal-bound hydroxide ions, buffer-molecules or basic residues of the ribozyme could deprotonate G40. However, additional studies are needed to clarify the identity of the external base.[90]

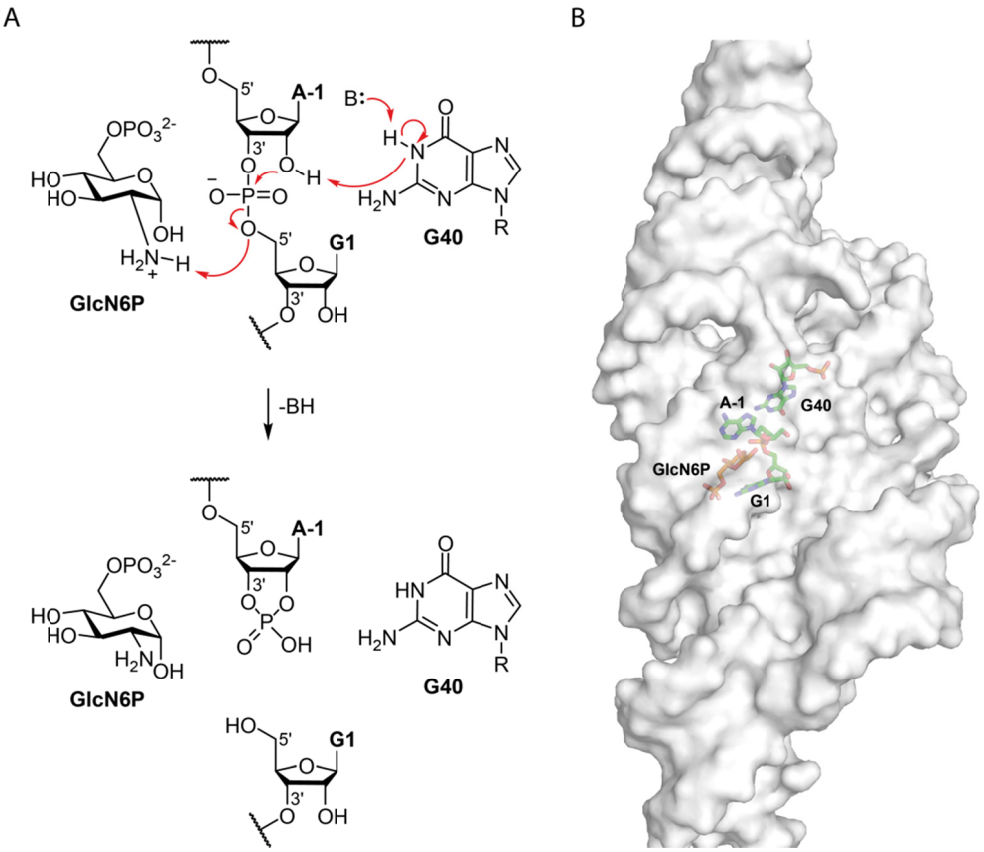

Figure 6 The self-cleavage mechanism of the *glmS* ribozyme from *Thermoanaerobacter tengcongensis*
(A) In the shown acid-base mechanism, the natural cofactor GlcN6P functions as the general acid and the deprotonated N1 of G40 acts as the base. The self-cleavage yields two RNA-strands, one with a 2',3'-cyclic phosphate and the 3' part of the RNA containing the *glmS* coding region with a 5'-OH terminus.[91-93] The external base that deprotonates G40 is denoted 'B:'. (B) Crystal structure of the *glmS* ribozyme from *Thermoanaerobacter tengcongensis* bound to the cleavage-inhibitor Glc6P (PDB 2Z74)[95]. The surface of the ribozyme RNA is shown in transparent grey, while Glc6P, the scissile phosphate and the crucial nucleosides (A-1, G1' and G40) are shown in a colored stick-model. The crystal is shown from the opposite side of the binding pocket.

In the absence of the natural cofactor, the *B. subtilis glmS* ribozyme exhibits a half-life of 4 h, which is reduced to 15 s in the presence of saturating concentrations of GlcN6P. This corresponds to an acceleration of the *glmS* ribozyme self-cleavage reaction by a factor of 1,000-fold[73]. In the case of the *B. cereus glmS* ribozyme, the rate enhancement by GlcN6P is even more pronounced, demonstrated by a 100,000-fold increase in cleavage rates. Thus, the half-life of the *glmS* RNA is reduced from approximately 48 days to below 1 min upon saturation with ligand.[89]

Regulation of gene expression by the *glmS* ribozyme is accomplished by the degradation of the 5'OH cleavage product by RNase J1, an enzyme, which is conserved among bacteria.[74,96] The *glmS* ribozyme is part of a negative-feedback loop, as it senses the concentration of GlcN6P and down-regulates gene expression accordingly. This is

possible since the *glmS* gene encodes for the fructose-6-phosphate amidotransferase (GlmS), which produces GlcN6P from fructose-6-phosphate and D-glutamine.[97] The regulation of *glmS* expression by ribozymes discovered until now is mostly limited to Gram-positive bacteria, and only a few *glmS* ribozymes in Gram-negative bacteria were identified mainly belonging to phylum of synergestetes.[98]

1.3.1 Ligand recognition by the *glmS* ribozyme

The recognition of the natural *glmS* ribozyme ligand GlcN6P is mediated by several hydrogen bonds between all functional group of the sugar and the nucleotides forming the binding pocket (**Figure 7**).

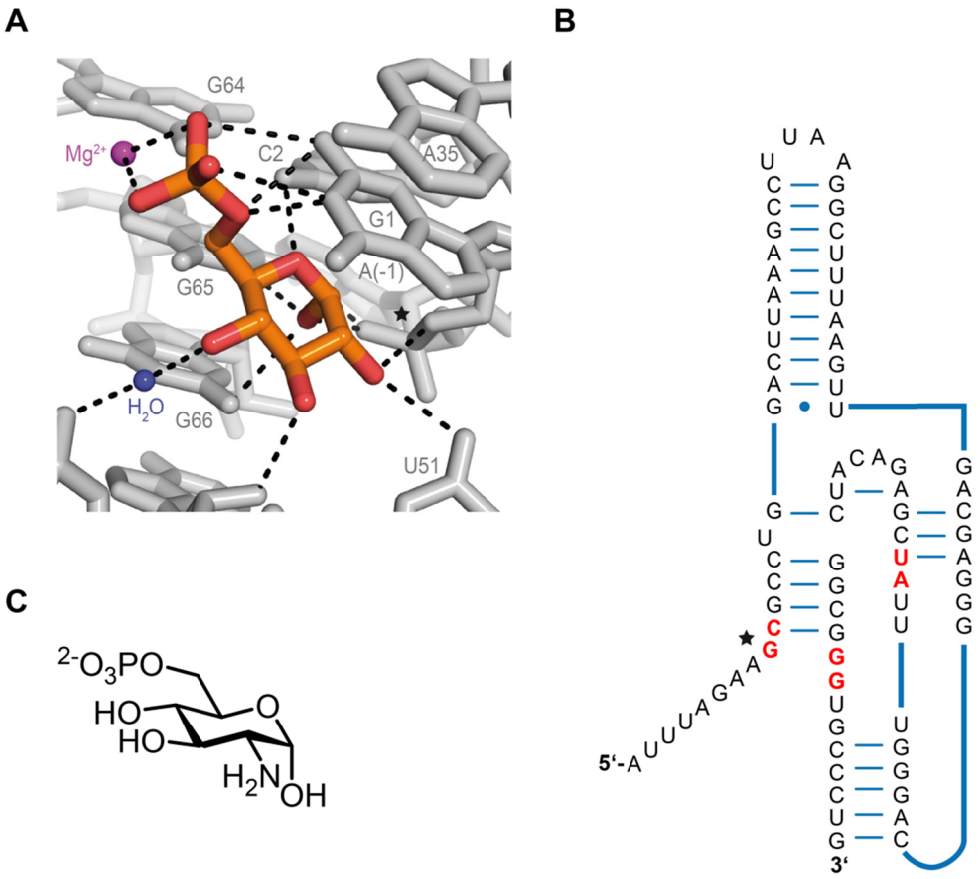

Figure 7 The ligand-recognition of α-D-glucose-6-phosphate by the catalytic core of the *glmS* ribozyme
(A) Glc6P bound to the ligand binding site of the *glmS* ribozyme from *Thermoanaerobacter tengcongensis*. Shown is a detail of the crystal structure (PDB 2Z74) modified from Klein *et al.*.[88] Hydrogen bonds involving Glc6P are depicted as black, dotted lines. The scissile phosphate between G1 and A-1 is marked with a star (★). (B) The schematic secondary structure of the catalytic core of the *glmS* ribozyme from *T. tengcongensis*. The six nucleotides that form hydrogen bonds with the ligand are colored red. (C) Chemical structure of α-D-glucosamine-6-phosphate **12**, the natural metabolite of the *glmS* ribozyme.

Currently, there are crystal structures available of *glmS* ribozymes from *Thermoanaerobacter tengcongensis* and *Bacillus antracis*.[88,92,95,99] From crystals in the absence of D-glucose-6-phosphate it is known that, unlike other riboswitches, the ligand binding site is preformed and does not considerably rearrange upon binding of the ligand.[88] This finding indicates low flexibility of the ribozyme binding pocket and contradicts an induced fit mechanism. Highly altered or modified analogs of GlcN6P are therefore less likely to fit into the rigid binding site, which leads to reduced affinity or, respectively, cleavage activity.[100] However, the preformed *glmS* binding pocket is of advantage for computational methods as molecular docking, to predict the affinity of artificial activators[101,102] or perform *in silico* screenings[103]. The high discrimination of the *glmS* ribozyme is also reflected by the high failure rate of attempts to find alternative natural or artificial high-affinity activators.[89,100,104,105] As a result, even high-throughput screening approaches of the library of more than 5000 drug-like compounds[105,106] or 960 bioactive compounds[104] failed to identify activators of the *glmS* self-cleavage other than GlcN. However, the rational screening of GlcN6P analogs provided detailed insights into the ligand requirements of *glmS* ribozymes.[89,100]

The decisive factor that affects affinity and correct positioning of the ligand in the binding pocket of the *glmS* RNA is the number of hydrogen bonds. In the case of GlcN6P and Glc6P every ring-substituent, the phosphate group, and the ring oxygen make hydrogen-bonds with the RNA (**Figure 7A**). Glc6P, which acts as an inhibitor of the *glmS* ribozyme cleavage due to the missing amine, shows a similar hydrogen-bond pattern as GlcN6P and competes for the binding to the ribozyme.[89] The sugar functional groups interact with the ribozyme by multiple hydrogen bonds and, additionally, by the mediation of well-ordered water molecules and Mg^{2+}-ions (**Figure 7B**). However, only six nucleotides, which are highly conserved among *glmS* ribozymes, are forming the binding pocket and are involved in the ligand recognition.[98]

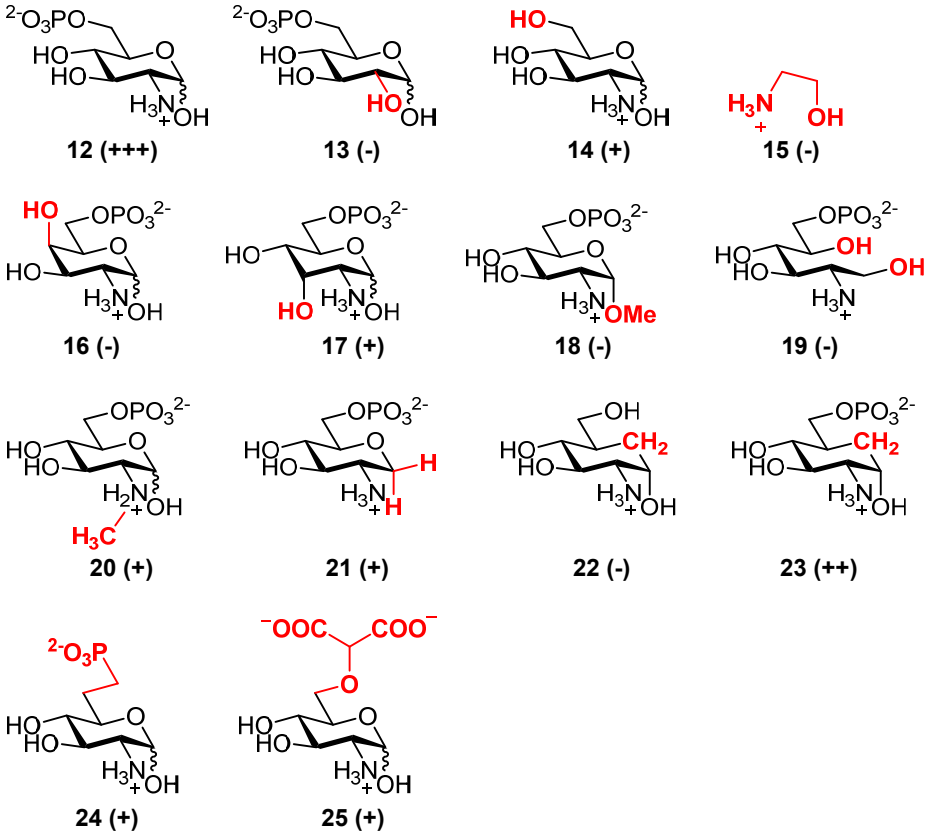

Figure 8 Overview on previously described analogs of GlcN6P that were tested in different screening formats and methods.[100,101,104,105,107]
A rating of their effectiveness as ribozyme activators *in vitro* are given in: (+++) strong, (++) moderate, (+) weak, and (-) inactive.

From the results of several screening experiments of close analogs of GlcN6P, summarized in **Figure 8**, structure-activity relationships (SAR) can be concluded. On the one hand, the phosphate is crucial for high-affinity binding especially through complexation of the highly conserved Mg^{2+}-ion, demonstrated by a 30-fold decrease in cleavage rates in the case of GlcN **14** compared to GlcN6P **12**.[89] The amino function, on the other hand, is essential for the role of the ligand as a general acid in the cleavage mechanism explained above. Removal (**13**) leads to complete inactivity, while methylation (**20**) is partly tolerated. Particular importance is assigned to the anomeric hydroxy group, as GlcN6P and Glc6P exclusively bind in the α-conformation. Removal of the OH group (**21**) leads to a significant 70-fold decrease in activity, while modification (**18**) results in complete inactivity.[100] The amine functionality together with and an adjacent hydroxyl group, as in ethanolamine (**15**), forms the minimal motive of a potential cofactor of the *glmS* ribozyme self-cleavage. This minimum requirement is demonstrated by the low activity of ethanolamine, tris(hydroxy methylene)aminomethane (TRIS) and serinol at very high ligand concentrations.[89] Alterations to the hydroxyl group at C3 and C4 differently affect activity. Inversion of the configuration of C4-OH (**17**) does not yield

an active compound, whereas inversion at C3 (**16**) leads to a 4-fold reduction in cleavage rates.[108] This can be rationalized with the solvent accessible opening of the binding pocket close to the hydroxyl group at C3, which apparently tolerates modification at this position. Also crucial for activation is the intact ring structure as the acyclic form of GlcN6P **19** did not show considerable cleavage.[100] Taking this requirement into account, the carba-sugar analog (**23**) of GlcN6P bears an intact cyclohexane ring and shows very similar *in vitro* activity as GlcN6P. Furthermore, the influence of the phosphate demonstrated by low activity of carba-α-D-GlcN (**22**) is also consistent with its natural counterpart.[105] As a conclusion, considering the modifications of GlcN6P investigated until now, the substitution of the ring-oxygen by methylene leads to the most potent artificial activator of the *glmS* ribozymes tested.

A different approach leading to potential phosphatase-inert mimics of GlcN6P is the substitution of the phosphate group by phosphate surrogates, e.g., phosphonate (**24**) or malonate (**25**).[101] Both showed 7-fold reduced activity compared to GlcN6P. However, similar binding to the ligand binding site could be predicted with the help of molecular docking studies.

1.4 Threat of multi-resistant bacteria

The persistent threat of multi-resistant, human-pathogenic bacteria is leading to mounting health care costs, challenges in adequate treatment and deaths.[109] Multi-resistant bacteria or so-called “superbugs” developed through overuse and misuse of antibiotics in human medicine and preventative use on healthy animals on livestock breeding and agriculture.[110] The resulting global health challenge can be attributed to a gap of innovation in the antimicrobial field after the golden era of antibiotic discovery from 1940 to 1960 and the misbelief that the problem of bacterial infections was solved.[111,112] The lack of new chemical entities in the pipeline of antimicrobial research have led to a post-antibiotic era in, which sophisticated interventions, e.g., organ transplantations, care of pre-term infants or joint replacements, once again could represent challenges and causes of death.[113,114] Bacteria that are a particular threat to humans due to the development of antibiotic resistance, hard-to-treat infections, and death are listed in the recent reports of the Center for Disease Control and Prevention (CDC) and the European Centre for Disease Prevention and Control (ecdc) (**Table 1**).[115,116]

Table 1 Bacteria that are immediate threats to public health and require urgent action according to CDC
Numbers are given for infections and death in the United States each year. Data from the year 2011[115]

	C. difficile	*S. aureus*	*Enterobacteriaceae*	*N. gonorrhoeae*
Resistance	Clindamycin	Methicillin	Carbapenem	Tetracycline
Infections (p.a.)	500,000	80,500	9,000	246,000
Deaths (p.a.)	15,000	11,300	600	-

Among these microorganisms that require urgent, global actions are *Clostridium difficile*, methicillin-resistant *Staphylococcus aureus*, carbapenem-resistant *Enterobacteriaceae,* and *Neisseria gonorrhoeae*. A high number of gonorrhea infections of 246,000 in the US (2011)[115] and 39,179 in Europe (2011)[117] are caused by *N. gonorrhoeae* resistant to multiple antibiotic classes. The resistance to tetracycline, which is most prevalent among isolates and high levels of decreased susceptibility to cefixime as well as the appearance of resistance to drugs of last resort, require surveillance. The trend of resistance development and the ease of sexual transmission thereby are main factors that make drug-resistant *N. gonorrhoeae* infection a global problem.[109] Even though infections with methicillin-resistant *S. aureus* (MRSA) are decreasing according to the annual report of the ecdc from 2012[117], MRSA are among the most common healthcare-associated infections (HAI) and a high number of 11285 related deaths in the US in 2011.[115] Infections from *Enterobacteriaceae* (9000 in the US in 2011) caused by multidrug-resistant *E. coli* or *Klebsiella* spp., however, are increasing in Europe.[109] *Enterobacteriaceae* possess a dangerous threat to public health in the case of resistance to nearly all antibiotics, including last-line antimicrobials as carbapenems. Thus, the death-rate of bloodstream infections from carbapenem-resistant *Enterobacteriaceae* is high at almost 50%.[115] *C. difficile* tops the chart of bacterial threats that require urgent countermeasures published by the CDC. However, this is not due to resistance to the antibiotics used to treat *C. difficile* infections (CDI). The Gram-positive bacterium forms spores that can be found in the human colon.[118] Life-threatening diarrhea, inflammatory lesions, sepsis, shock, and death are the severe clinical outcomes of CDI.[119] The natural resistance of the spores to many antimicrobial drugs and the large numbers of infections in the US each year of 500000, resulting in 15000 deaths, thereby reflect the immediate impact of CDI on public health. Furthermore, CDI mostly develop after hospitalization

and antibiotic treatment since the absence of the regular microbiota in the gut enables pathological *C. difficile* colonization in the first place.[119]

National efforts in infection prevention and healthcare control show promising results in a stable number of infections with MRSA in Europe. Nevertheless, the pharmaceutical industry, as well as academic research facilities, are required to invest in the research and development of antimicrobials, although the return of investment is low. Also, in 2015, most of the developed countries agreed on a “global action plan on antimicrobial resistance” whereby the political support and awareness is set to take actions against antimicrobial resistance.[120] To keep these developments at pace, there is a static need for the identification of new targets in bacteria to counteract the development of drug-resistance to the previously known limited number of addressed cellular processes.[121]

1.4.1 Drug development in the post-antibiotic era

By listing the discovery of crucial antibiotics on a timeline (**Figure 9**), it becomes apparent that the development of new antibacterial drugs slowed down after the golden era of antibiotic discovery between 1940 and 1960.[122]

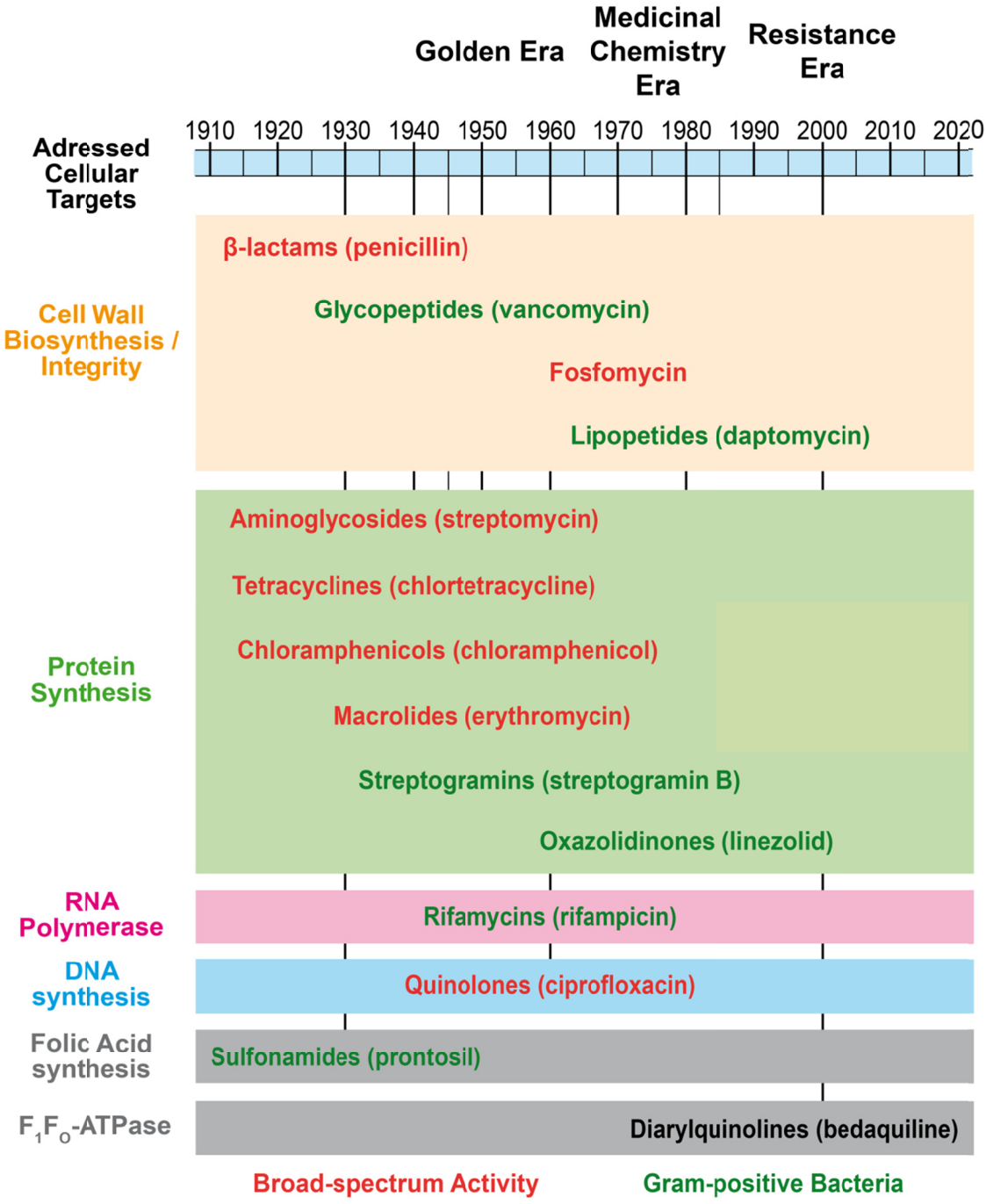

Figure 9 Timeline of the discovery of antibiotics. Listed are important classes of antibiotics with their respective important representative

Indicated is the common model of antibiotic drug discovery of each era.[114] The antibiotics are sorted into their different classes of cellular targets in bacteria: the cell wall biosynthesis or integrity (orange), the 30S or 50S ribosomal subunit and thereby protein synthesis (green), the RNA polymerase β-subunit (pink), DNA synthesis (blue), folic acid synthesis (grey) and F_1F_O-ATPase of *Mycobacterium tuberculosis* (grey). Furthermore, the antibiotics are differentiated by either broad-spectrum activity (red text) or targeting of Gram-positive bacteria (green text). Diarylquinolines are colored black since they only show activity against *Mycobacterium tuberculosis*.[122,123]

With the isolation of Streptomycin A from a soil actinomycete, *Streptomyces griseus*, a first screening platform for antibiotics was introduced by Selman Waksman in 1943, for which he was later honored with the Nobel Prize in Physiology or Medicine in 1952.[124] Based on the detection of growth-inhibition zones of a susceptible microorganism caused by soil-derived streptomycetes, his approach was similar to the method used by Alexander Fleming that led to the discovery of penicillin.[122,124] In the next 20 years, the whole-cell screening of bacterial extracts and its adoption by pharmaceutical companies resulted in the discovery of a majority of the drug classes that serve as an antibiotic arsenal today (streptomycin, tetracyclines, chloramphenicol, and erythromycin).[122] The golden era of drug discovery and the success of the Waksman platform ended because of overmining of cultivable soil microorganisms as a limited resource and the resulting rediscovery of known compounds.[125] Afterwards, in the medicinal chemistry era, the development of new drugs was restricted to the improvement and modification of existing chemical scaffolds, while the discovery of new chemical classes ground to a halt.[114] Although the FDA has approved potent antibiotics with the oxazolidinones (linezolid) and the lipopeptides (daptomycin), they are still based on well-known classes.[126] Badequiline, which inhibits the F_1F_O-ATPase of *M. tuberculosis*, was discovered in 2005 after no tuberculosis-specific drugs were discovered in 40 years.[127] Without counteraction to the emergence of multidrug-resistant bacteria, this could be the starting point of a post-antibiotic era as the introduction of new antibiotics did not keep up with the resistance mechanisms in bacteria. The trial of strength between drug development and bacterial evolution of resistance, however, is highly discouraging because resistance has evolved against every antibiotic that has been introduced to the market.

Currently, known antibiotics are derived from natural compounds and address a limited number of processes in bacterial cells. The mainly addressed targets are the cell wall biosynthesis or its integrity, the protein synthesis through binding to the 30S or 50S ribosomal subunit, the DNA synthesis through inhibition of gyrase, and the synthesis of folic acid (**Figure 9**). However, the activity of antibiotics is often far more complex than this simple picture would suggest. For example, β-lactams not only target penicillin-binding proteins (PBPs) but induce malfunction of cell wall synthesis in a way that is more complex than simple enzyme inhibition.[128] One reason for the success of drugs against the above mentioned few targets could be that they are in fact addressing multiple targets, thereby lowering the potential of endogenous resistance development.[129] Modern target-based screenings for antibiotic leads, conducted by the pharmaceutical industry, focused on single targets or macromolecular biosynthetic pathways derived from essential genes after complete genome sequencing.[130,131] This

approach allows both the addressing of an incredible number of new targets as well as the avoidance of susceptibility to existing resistance mechanism.[130] The results of target-based high-throughput screening (HTS) of large libraries of synthetic compounds, however, are disappointing as not a single antibacterial drug was found. One reason for the failure of this approach is the limited area of chemical space that synthetic libraries of pharmaceutical companies cover. The optimization of these libraries for the human biology and their oral availability following Lipinski's rule of five[132] does not cover the unique property-space of antibiotics.[133] This is evident from antibacterial drugs currently used in the clinic that are natural products or their derivatives and show higher molecular weight and polarity. One of the special challenges in the development of new antibiotics is their ability to penetrate the cell envelope of bacteria, which also requires a differentiation between Gram-positive and Gram-negative cell architecture.[133] In the case of Gram-negative bacteria the outer membrane keeps out drugs that are amphipathic while membrane-associated pumps mediate active efflux, particularly multidrug resistance (MDR) pumps.[134]

In the resistance era, there are several conceivable solutions to counter the threat of multidrug-resistant bacteria and increase the output of antibacterial drug development. The application of rules of permeability to compound libraries would increase the success rate of large HTS approaches. Alternatively, mimics of natural products could trick the bacteria similar to a "Trojan horse." This is possible when they are actively transported into the bacterial cell and yield the active compound through, e.g., specific enzymatic activity.[135] Furthermore, innovative strategies to cultivate previously unculturable bacteria[136] could revive the Waksman platform. Indeed this approach led to the discovery of teixobactin, an inhibitor of cell wall biosynthesis from *Eleftheria terrae*, which challenges the assumption of inevitable resistance as no resistance development was observed.[137] Focus on the development of species-specific antibiotics is another popular suggestion for improvement of future antibacterial drug development. This approach requires an in-depth understanding of the disease-causing microorganism. However, fewer off-target effects and the protection of the gut microbiome are significant benefits.[122] The later thereby diminishes the risk of infections associated with *C. difficile*.

1.4.2 The *glmS* ribozyme as antibacterial drug targets

Due to the very narrow spectrum of bacterial targets that are addressed by currently known antibiotics, there is a static need for unconventional innovation to affect multidrug-resistant bacteria. The identification of drugs with novel mode of actions or combination therapies are approaches that are recently followed.[138] Combination therapy, in

particular, is desirable as it prevents the emergence of reduced susceptibility or resistance due to a narrow mutant-selection window.[139] Synergistic effects would allow for overcoming deficiencies of the respective drugs, such as limited tissue penetration and poor activity of vancomycin against organisms growing in a biofilm.[138,140]

Riboswitches are such a promising novel target for antibacterial drug development. Among the 40 distinct classes known today, several regulate metabolic genes that are essential for the survival or growth of their host microorganism.[141,142] This assumption is widely supported by the discoveries that the activity of well-known antimicrobial compounds (pyrithiamine (PT), DL-4-oxalysine and roseflavin) is directly related to the regulation of riboswitches.[143-145] Given the high specificity with which the aptamer region of riboswitches recognizes their cognate ligand, riboswitch-targeting compounds can be designed that show low binding to other cellular targets.[142] As riboswitch are usually located next to genes that are involved in the synthesis or the transport of their metabolite ligand they can be part of negative feedback loops.[146] Structural dissimilar small molecules that mimic the interaction of the natural metabolite to the aptamer of riboswitches could downregulate essential biosynthetic genes, thereby inhibiting growth.[70,141,142,147] That riboswitches are indeed druggable targets was already demonstrated in the case of the synthetic mimic Ribocil, which modulates the riboflavin riboswitch and shows antibacterial efficacy in mice infected with *E. coli*.[148]

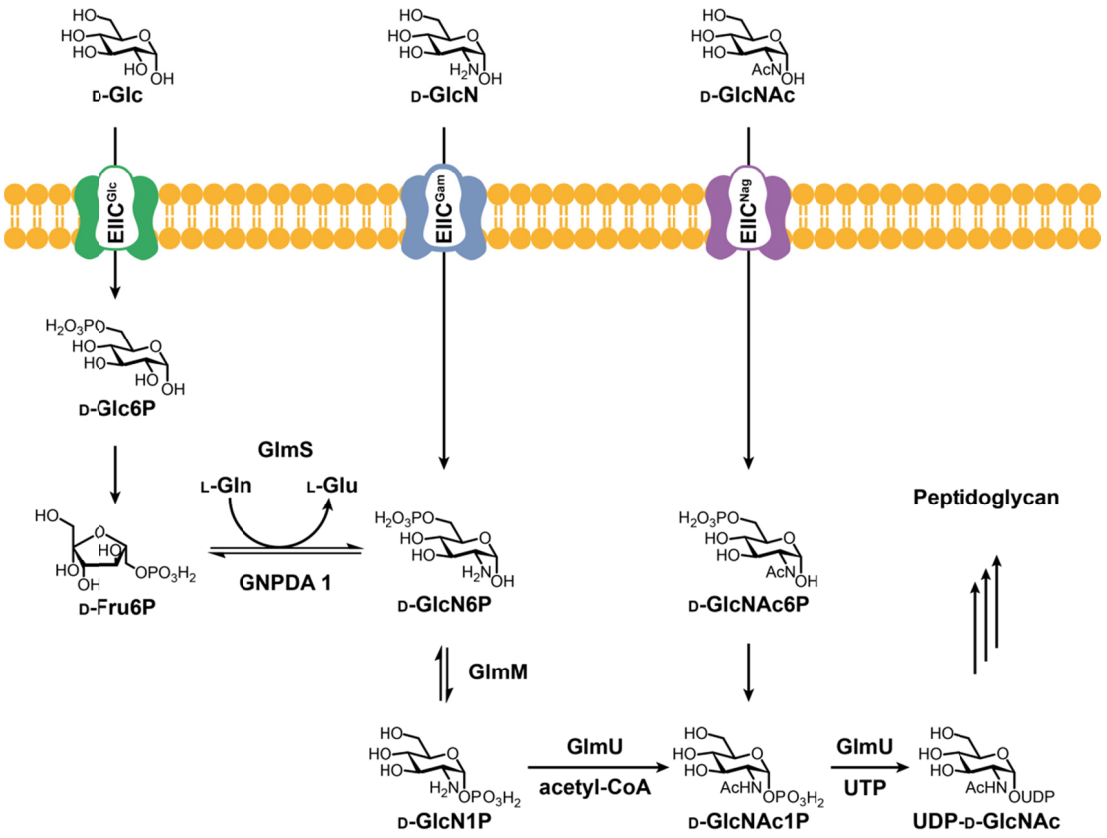

Figure 10 Schematic part of the amino sugar metabolism in *B. subtilis* yielding UDP-*N*-acetyl-D-glucosamine, which is an essential precursor of the peptidoglycan
D-glucose, D-glucosamine, and *N*-acetyl-D-glucosamine are phosphorylated and actively transported into the cell by the sugar-specific phosphoenolpyruvate: sugar phosphotransferase system (PTS). The crucial role of the glutamine-fructose-6-phosphate transaminase (GlmS) in the production of the important precursor GlcN6P from extracellular D-Glc becomes clear.[97,149-151]

The biosynthesis of GlcN6P by the glutamine-fructose-6-phosphate transaminase (GlmS) represents one attractive target for this approach (**Figure 10**).[141,152-154] GlmS is part of the general amino sugar and nucleotide sugar metabolism. Its synthesis product GlcN6P is an early intermediate in the cytoplasmic steps of UDP-*N*-acetyl-D-glucosamine synthesis.[154] The GlmS catalyzes the transfer of an amino group from L-glutamine (L-Gln) to D-fructose-6-phosphate (D-Fru6P) and subsequent isomerization to GlcN6P. The reverse step is catalyzed by the GlcN6P deaminase NagB.[155] The biosynthetic pathway of UDP-GlcNAc is fueled by extracellular D-glucose, which is transported and subsequently phosphorylated by the sugar-specific phosphoenolpyruvate sugar phosphotransferase system (PTS) glcP. In the next step, Fru6P is formed from Glc6P as a part of glycolysis. In prokaryotes, GlmS is an essential enzyme for cell survival, if exogenous GlcN or GlcNAc are not available in adequate amounts.[152,156,157] However, the concentration of GlcN in the human body fluids is not sufficient to allow growth of bacteria with *glmS* mutations.[157,158] That the supply of amino sugars bypasses GlmS is comprehensible since GlcN and GlcNAc are also actively transported and

phosphorylated by the PTS, concretely by gamP and nagP (**Figure 10**). Both, GlcN6P that is either synthesized by GlmS or the result of PTS-transport and GlcNAc6P are converted into UDP-*N*-acetyl-D-glucosamine. GlcN6P is first converted to D-glucosamine-1-phosphate (GlcN1P) by the phosphoglucosamine mutase (GlmM) followed by acetyl transfer by GlmU yielding GlcNAc1P.[154] The bifunctional enzyme GlmU also catalyzes the last step the uridyltransfer from UTP to GlcNAc1P. The product of this pathway, UDP-GlcNAc, is an essential precursor of peptidoglycan and therefore needed for the synthesis of the bacterial cell wall.[154]

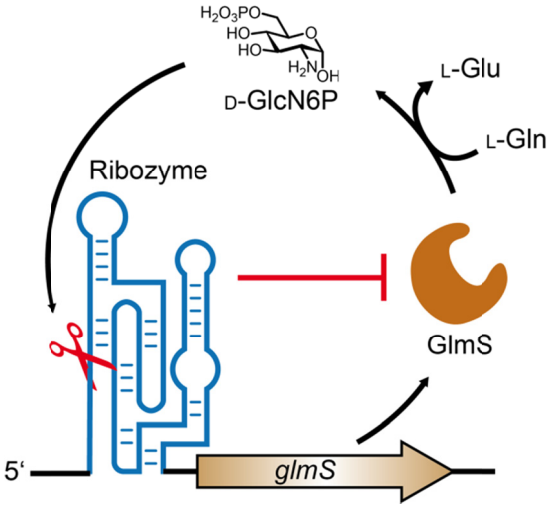

Figure 11 Negative feedback circuit involving the *glmS* ribozyme
The *glmS* ribozyme senses the concentration of GlcN6P, which is the natural cofactor of its self-cleavage, leading to the down-regulation of *glmS*. Thus, the production of GlmS is regulated, which, in turn, catalyzes the synthesis of GlcN6P, thereby closing the negative feedback circuit.

In Gram-positive bacteria, GlmS is regulated via the *glmS* riboswitch in the 5'-untranslated region, which is correctly called ribozyme due to the promotion of self-cleavage.[73] The g*lmS* ribozyme is part of a negative feedback circuit (**Figure 11**) through which *glmS* expression is regulated. This regulatory RNA senses the GlcN6P in micromolar concentrations and is conserved among several human pathogens, including *C. difficile*, *S. aureus* and *Listeria monocytogenes*.[141,142,159] In contrast, most Gram-negative bacteria employ two small RNAs (sRNAs), GlmY and GlmZ in the interplay with the adapter protein RapZ, for *glmS* gene-regulation.[157,160,161]

Activation of the *glmS* ribozyme by synthetic GlcN6P mimics allows the targeting of the early supply of the cell wall biosynthesis. Considering the rigid ligand binding pocket of the RNA (**Figure 7**), the design of suitable mimics requires thorough consideration of the ligand-RNA interactions, in other words, a sufficient similarity to GlcN6P.[100] In view of the complexity of the biosynthetic pathway of peptidoglycan, however, a high degree of dissimilarity of artificial actuators is crucial to minimize undesired off-target effects.[70] In

the case of GlcN6P-mimics, off-target effects on GlmM (**Figure 10**) are very likely.[162] Carba-GlcN represents a promising example for antibacterial compounds targeting the *glmS* ribozyme, as antibacterial activity was demonstrated for VISA strain Mu50[163] and *B. subtilis*.[153]

2 Aim of this study

The persisting threat of multidrug-resistant bacteria can be attributed to the fact that the golden era of antibiotic development led to the misbelief that the problem of antibacterial infections was solved. Over- and misuse of antibiotics in healthcare, agriculture and livestock breeding together with stagnation of innovations in antibacterial drug development are major consequences.

there is an urgent need for the discovery of new drug targets in bacteria to stay ahead of emerging antibiotic resistance in highly pathogenic microorganisms. A class of non-coding RNAs found in bacteria referred to as riboswitches regulate gene expression in response to cognate small molecules. Synthetic small molecules that mimic the activity of the natural ligand thereby showing antibacterial properties have been developed. Among these is carba-α-D-glucosamine, whose phosphorylated variant carba-α-D-glucosamine-6-phosphate efficiently activates the *glmS* riboswitch, a self-cleaving ribozyme.

The aim of this study was the development of carba-sugar mimics of GlcN6P with modifications at the 5a-carba position. It was hypothesized that these variants, similar to carba-GlcN, are taken up via the sugar-specific PTS, releasing their phosphorylated variants into the cytoplasm (**Figure 12**). Induction of the negative feedback mechanism of the *glmS* ribozyme by high-affinity ligands would lead to a down-regulation of the translation of the GlmS protein and immediate reduction of the intracellular GlcN6P concentration. This interference with an early step of peptidoglycan biosynthesis through a limited supply of UDP-GlcNAc would ultimately lead to inhibition of the cell wall biosynthesis and consequently of bacterial growth.

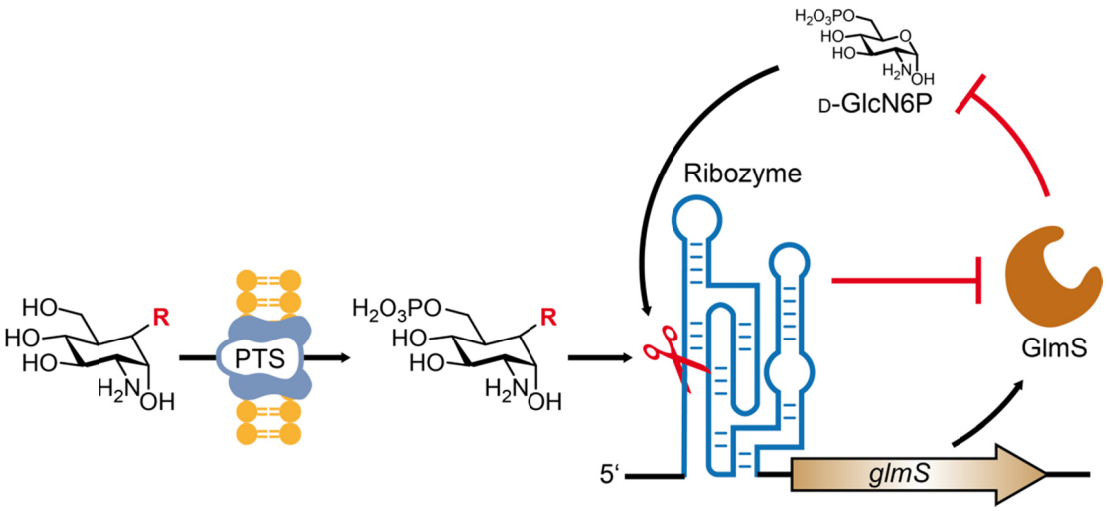

Figure 12 Proposed mechanism of 5a-modified carba-sugar analogs of GlcN6P targeting the *glmS* ribozyme

Similar to carba-GlcN, carba-sugars with 5a-modifications would function as prodrugs of their phosphorylated variants that activate the *glmS* ribozyme, thereby reducing the translation of the GlmS protein and the intracellular concentration of GlcN6P. The mechanism of GlcN-transport and metabolism is illustrated by black arrows, while inhibition arrows and pictograms depicted in red indicate the effect of (modified) carba-sugars.

3 Results and Discussion

3.1 Synthesis of amino-carba-sugars bearing modifications at the 5a-position

D-Glucosamine-6-phosphate is the natural metabolite of the *glmS* ribozyme acting as a cofactor in the self-cleavage reaction in the low micromolar range (EC_{50} = 3.6 µM for *S. aureus*).[105] Huge efforts have been made to identify natural and artificial ligands that would activate the riboswitch to a similar extent (**Figure 8**). Different screening setups have been utilized to find small molecules from collections of bioactive compounds[104,106] or small libraries of analogs of GlcN6P[100,105]. In the wake of this, carba-D-α-glucosamine-6-phosphate **30** (**Scheme 5**) has been identified and represents the most active artificial cofactor so far (EC_{50} = 6.2 µM for *S. aureus*).[105]

There are currently two procedures described for the synthesis of carba-GlcN6P **30** sharing the same carbocyclic precursor **27** (**Scheme 5**). The synthesis of **27** in eight steps from methyl glucopyranoside **26** in a total yield of 9% was first described by Barton *et al.*[164] For the synthesis of **30**, Lünse *et al.* employed basic conditions to open the oxazolidone ring of **27** followed by phosphorylation analog to Sowa *et al*[165] and final deprotection.[105] Wang *et al.*, on the other hand, directly transformed **27** to the phosphorylated variant **31** followed by opening of the oxazolidone ring and final deprotection yielding **30**.[166] The main difference between the two procedures and different yield lies in the different phosphorylation strategies. Phosphorylation of **28** resulted in poor yield (23%) while Wang *et al.* succeeded in the synthesis of the fully protect phosphate **31** in very good yield (86%) after treatment with dibenzyl *N*,*N*-diisopropylphosphoramidite and subsequent oxidation.[166]

Scheme 5 Synthesis of carba-GlcN6P 30 by two alternative procedures described by (A) Lünse *et al.*[105] and (B) Wang *et al.*[166]

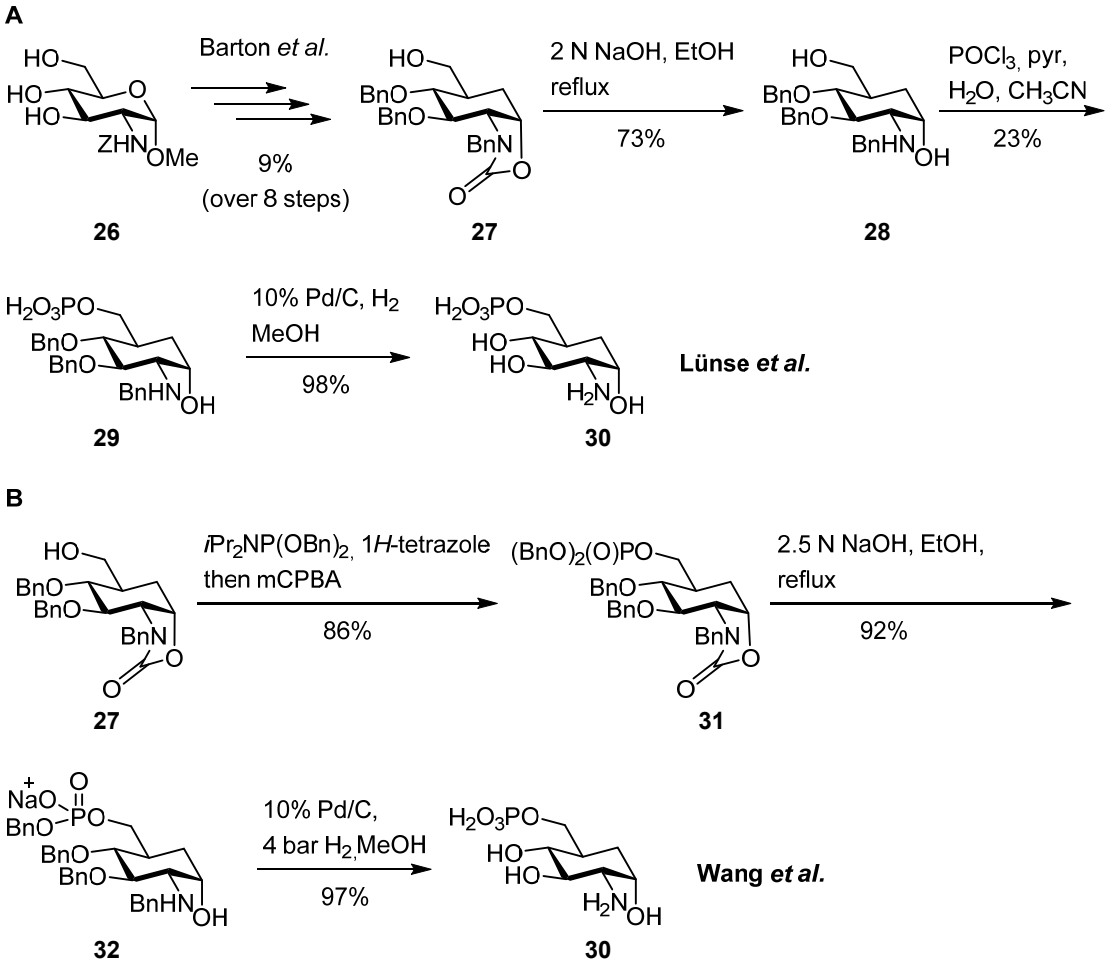

The substitution of the ring-oxygen in GlcN6P yielding carba-GlcN6P is a relatively small modification considering the high discrimination of the *glmS* riboswitch binding pocket and the resulting ligand requirements. The hydrogen bonds between functional groups of the ligand and the RNA can be extracted from high-resolution crystal structures.[95] Certainly, all of these hydrogen bonds contribute to high-affinity binding, whereby their individual strength differs among all of them. It is well known that GlcN6P and GlcN both are activators of the *glmS* ribozyme. However, they have largely different EC_{50}-values of EC_{50}(GlcN) = 189 µM and EC_{50}(GlcN6P) = 3.6 µM for *S. aureus.*[105] This reflects the major role of the phosphate in affinity to the RNA. The ring-oxygen of the sugar ligand is capable of acting as a hydrogen bond donor with adjacent nucleobases. However, a lower influence to *in vitro* ribozyme activation can be assumed. This is evident from almost identical EC_{50} of carba-GlcN6P and GlcN6P. Besides a strong similarity to the natural ligand, the newly introduced methylene group has vastly different chemical properties compared to the ring-oxygen. Of these, the possibility to introduce

modifications and functionalities at this position is the main synthetic task of the present study.

3.1.1 Synthesis of 5a-fluoro modified carba-sugars

Fluorinated compounds play a remarkable role as lead compounds in drug development, which is reflected by the fact that 30% of the drugs leading the pharmaceutical sales of the US in 2013 bear at least one fluorine atom.[167,168] This widespread use of fluorinated compounds in drug design can be attributed to the versatile ability to alter compound properties by introducing fluorine in the drug design.[29] Because of fluorine modifications, among others, pharmacokinetics, pk_A-values, conformational flexibility[27] and membrane permeability[169] can be altered.[170] In recent years the availability of synthetic methodologies to introduce fluorine in numerous building blocks continuously improved.[171-173] This includes stereoselective as well as mild fluorination reactions that permit late-stage introduction of fluorine.[174,175] Recently, the synthesis of carba-sugar was combined with fluorination strategies.[28,176,177] Only a few examples for the synthesis of fluoro-carba-sugars have been described until now, which is most probably due to the challenges related to their synthesis.[178] As far as biological applications are concerned, studies that describe their biological activity are even more limited, and hence the use of fluorinated carbohydrate-based drugs is still in its infancy.[179]

In the case of artificial activators of the *glmS* ribozyme, the synthesis of fluorinated carba-sugars was considered as a promising approach towards potent mimics of D-glucosamine-6-phosphate. In view of the rigid ligand binding pocket of the *glmS* RNA, the introduction of fluorine as a chemically small modification should cause only a minimal steric strain between ligand and RNA. In contrast, the high electronegativity may influence properties of the carba-sugar such as the pk_A of the amine or the H-bond of the hydroxyl groups more diversely and more unpredictably.[174,178,180]

Scheme 6 Retrosynthetic analysis of 5a-fluorinated carba-sugar analogs of β-L-idosamine-6-phosphate 33 and α-D-glucosamine-6-phosphate 35

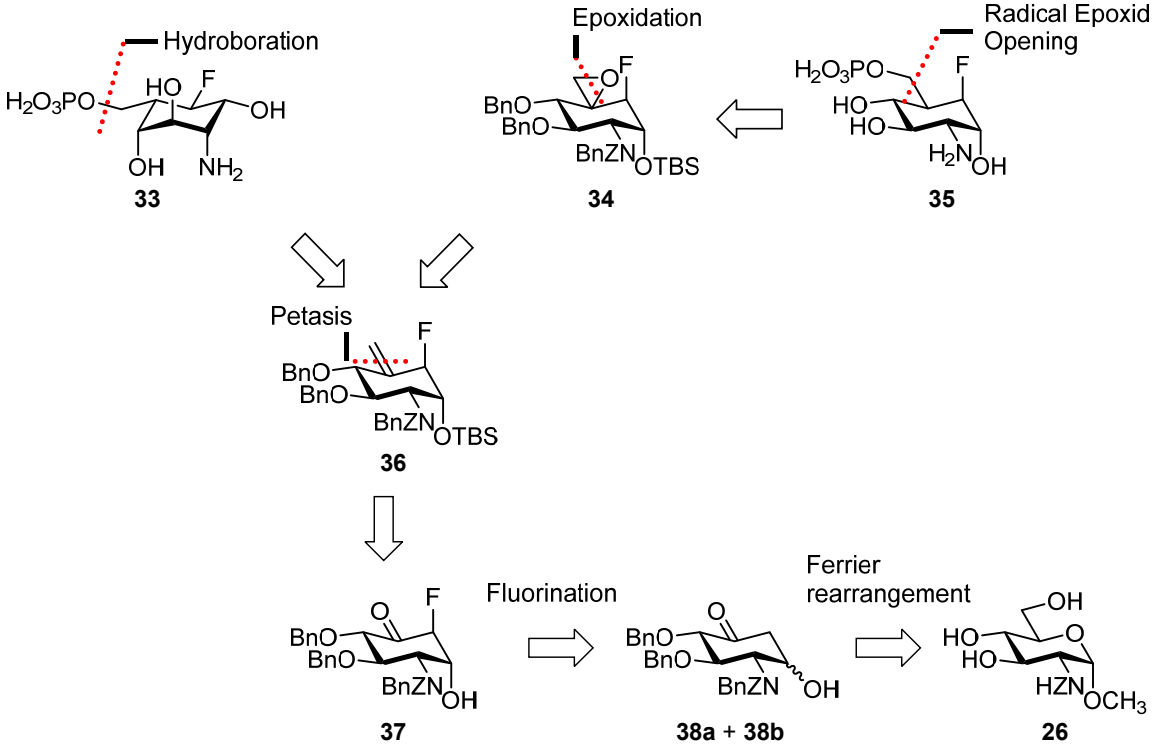

Scheme 6 depicts the retrosynthetic analysis of 5a-*mono*-fluorinated carba-sugar analogs of β-L-idosamine-6-phosphate **33** and α-D-glucosamine-6-phosphate **35**. For both target compounds, the same deprotection and phosphorylation strategy was used. The crucial installation of the hydroxy methylene group was accomplished starting from the same fluorinated precursor, the alkene **36**. Two highly stereoselective approaches gave the hydroxy methylene group in different configurations, leading to the two C5 epimers. Hydroboration (**36**→**33**) gave the fluoro-carba-β-L-idosamine precursor, whereas epoxidation (**36**→**34**) followed by regioselective radical epoxide opening (**34**→**35**) furnished the fluoro-carba-α-D-glucosamine precursor. The alkene **36** was formed by olefination of the cyclohexanone **37** under Petasis-Tebbe conditions following α-fluorination of the α-anomeric cyclohexanone **38a**. A mixture of **38a** and **38b** is the result of the Ferrier rearrangement after elimination of the alcohol **26**.

The starting point of this synthesis, the methyl-*N*-benzyloxycarbonyl-glucopyranoside **26**, was prepared according to literature.[181] Benzylation of the hydroxy groups at position C3 and C4 by an orthogonal protection strategy afforded **39** in moderate yield of 51% over three steps. (**Scheme 7**) The alcohol **39** was transformed to the iodo-compound **40** by an Appel-analog reaction followed by elimination affording the terminal olefin **41**.[42]

Scheme 7 Synthesis of the hex-6-enopyranoside 41.

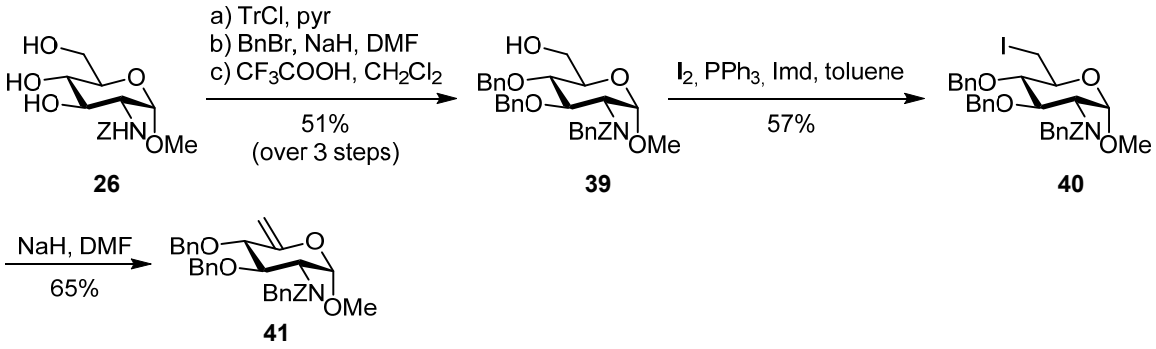

An alternative procedure for the synthesis of the hex-6-enopyranoside **41** by Amano *et al.*[182] yielded varying amounts of the side-product **43** with the endo-cyclic double bond (**Scheme 8A**). This side-reaction can be explained by the formation of the desired exo-methylene derivative **41** at first followed by base-induced isomerization to the thermodynamically favored endocyclic double bond in **43**. Observations by Weyershausen *et al.* support this. In their study, they treated a 6-iodo-galacto-pyranose **44** with an excess of *t*BuOK (5 eq) and prolonged reaction time (20h), yielding the enol ether **45**.[183]

Scheme 8 (A) Side-product formation for alternative elimination procedure and (B) analog reaction of a similar 6-iodo-galacto-pyranose derivative 44.[183]

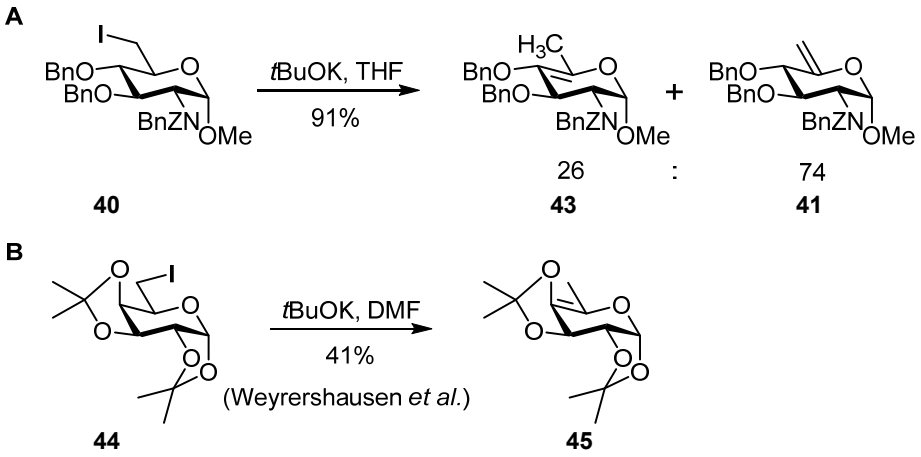

The first key-intermediate of the synthesis of mono-fluorinated carba-sugar analogs of GlcN6P is the carbocyclic intermediate **42** (**Scheme 9**). The cyclohexanone was readily available as an isomeric mixture of 77:23 (alpha/beta) via Ferrier rearrangement[40] of **41** in the presence of catalytic amounts of $HgSO_4$.[50,164,184] The yield of this reaction (86%) could be improved compared to that reported by Barton *et al.* (70%) (**Scheme 9**).[164] Next, the 1-OH of the isomeric mixture was protected with TBS in good yield (89%).[185] The TBS protection was necessary to prevent base-mediated β-elimination in the next step. Furthermore, the introduction of the TBS-groups was found to simplify the separation of the two isomers **38a** and **38b** by column chromatography.

Scheme 9 Synthesis of protected cyclohexanone 38a and 38b.

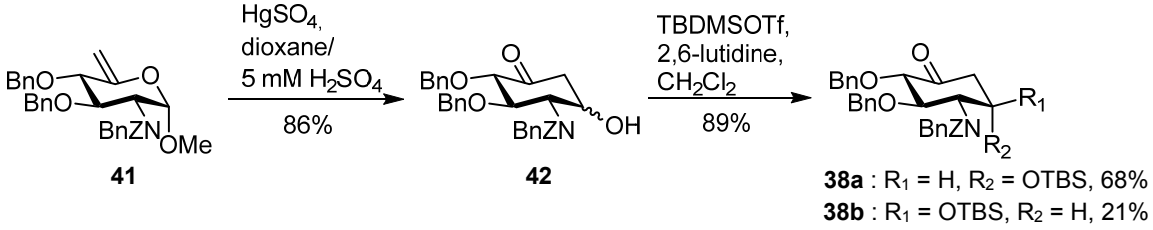

41 **42**

38a : R_1 = H, R_2 = OTBS, 68%
38b : R_1 = OTBS, R_2 = H, 21%

For the regioselective introduction of a single fluorine atom at the 5a-methylene position (**Scheme 10**), the electrophilic fluorination reagents N-fluorobenzene sulfonimide (NFSI) (**Table 2**, **Entry 2**)[186] and Selectfluor® (**Table 2**, **Entry 1**)[187] were tested. To achieve regioselective fluorination at the carba-position, isolation of the kinetic silyl enol ether (**Table 2**, **Entry 1**)[188] or intermediated formation of the kinetic enolate through metalation (**Table 2**, **Entry 2**)[185] were investigated. The yield of **37** was higher when NFSI was used even though Selectfluor® is known to be more reactive. As salt, Selectfluor® could not be used for direct fluorination in THF. Instead, isolation of the silyl enol ether was required adding another step to the synthesis procedure, thus lowering the yield. Only one diastereomer could be isolated following either of the two procedures. Unfortunately, the orientation of the fluorine substituent could not be determined at this point due to unfavorable signal-overlapping in NMR and a high flexibility of the ring due to the carbonyl at C5.[189,190] The axial configuration, however, could be determined for compound **68** after introduction of the equatorial hydroxy methylene group and removal of the TBS-group (**Scheme 21**).

Scheme 10 Synthesis of 5a-fluoro-cyclohexanone 37[b].

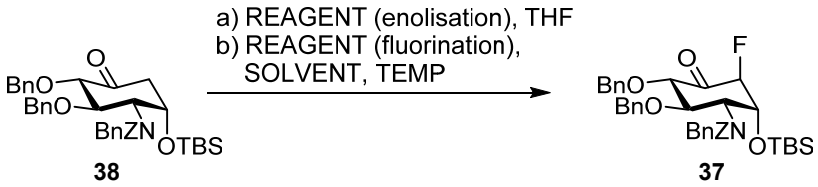

38 **37**

Table 2 Representative results for 5a-fluorination of cyclohexanone 38.

Entry	Reagent (enolisation)	Reagent (fluorination)	Temp.	Solvent (fluorination)	Yield
1	LDA, TMSCl	Selectfluor®	rt	DMF	36%
2	LDA	NFSI	-78 °C	THF	46%

[b] The axial orientation of the 5a-fluorine of compound **37** is depicted, as verified at a later step of the synthesis of the 5a-fluoro-carba-sugar.

A high diastereomeric excess (de) ≥98 of the fluorination process can be explained by the influence of the bulky substituents, especially of the OTBS-group at C-1, at the α-face of the enolate (**Figure 13**). These bulky substituents direct the approach of the electrophilic fluorination reagent towards the β-face, resulting in the observed axial orientation of the fluorine in compound **37**.

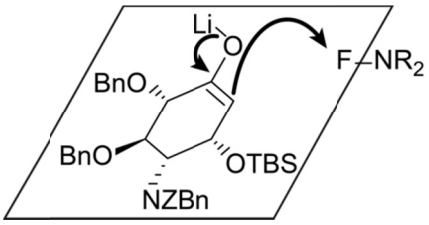

Figure 13 Approach of the electrophilic fluorine to the enolate intermediate from the less hindered β-face of the ring.

Both the better yield for the direct fluorination of the lithium enolate and the high de are in good agreement with the findings of Enders *et al.* in the region- and enantioselective synthesis of α-fluoroketones.[188] They employed TBS at the α-position of ketones as a directing group and achieved high de, especially in the case of α-silyl-cyclohexanone, for the electrophilic fluorination of the corresponding lithium enolate with NFSI.

Next, the ketone **37** needed to be homologated to build up the sugar structure of the fluorinated pseudo sugar. For the synthesis of the unmodified carba-analog of GlcN, Barton *et al.* carried out a Wittig reaction with methoxy methylene.[164] The strong basic conditions had the side-effect that an oxazolidine ring between position C1 and C2 was formed. In the case of the 5a-fluoro-ketone **37**, however, the treatment with the Wittig reagent led to a complex mixture and no product could be isolated (**Scheme 11**). To avoid the strongly basic conditions under Wittig-reaction conditions, the alternative Tebbe-Petasis olefination was used.[191] With this, only one-carbon homologation is possible, but base-labile substrates are tolerated.[192,193] For example, Howell *et al.* used the Petasis-reagent to obtain 2-methyleneazetidines from *Z*-protected β-lactams successfully.[194] This also provided evidence that *Z*-protected amines in substrates are tolerated.

Scheme 11 Attempted Wittig reaction with cyclohexanone 37.

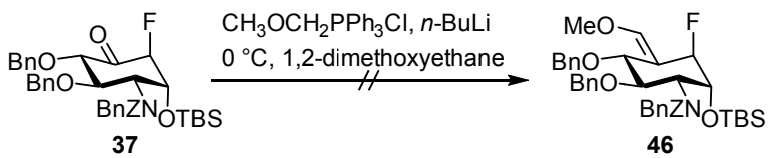

37 **46**

The Petasis-Tebbe olefination was used to generate both olefins **36** and **47** (**Scheme 12**). In the case of fluorine-substituted cyclohexanone **37**, two equivalents of Petasis-

reagent only led to slow conversion and the onset of side-reactions. After 20h reaction time, no product was present, but side-products with the mass of the hydrogen fluoride elimination products of both the ketone and olefin could be identified via LC-MS analysis. An increase of Petasis-reagent to four equivalents led to a reduction of the reaction time to 3h and a yield of **36** of 61%. The 5a-unsubstituted β-1OH cyclohexanone **38b** was converted to the corresponding olefin **47** under similar conditions in a moderate yield of 41%.

Scheme 12 Petasis-Tebbe olefination of fluorinated cyclohexanone 37 and cyclohexanone 38b.

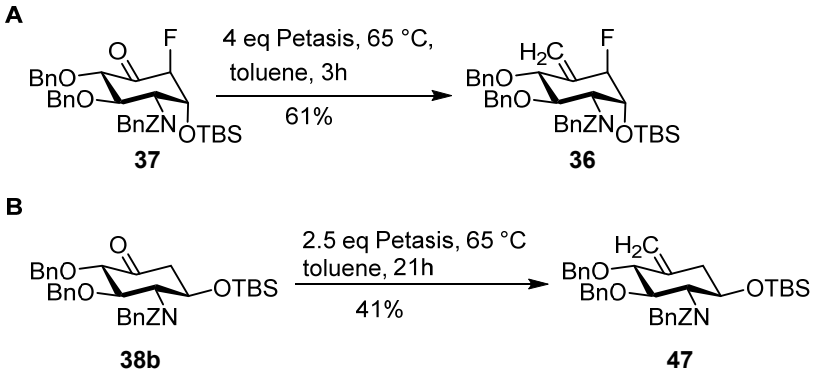

With the terminal olefin **36** in place, the following task was the stereoselective conversion of **36** to **48** (**Scheme 13**). Hydroboration with 9-BBN at 66 °C followed by oxidative workup yielded **48** in 50% yield. 2D-HH-NOESY and analysis of the HH-coupling constants at -40 °C confirmed the stereoselective formation of the L-isomer. An NOE-correlation between H5 and H3 was absent while a $^{3}J_{H4\text{-}H5}$ coupling constant of 5.4 Hz could be determined. This stereoselectivity has already been observed by Sun *et al.* for the hydroboration of the 5a-unmodified carba-sugar precursor of mannose .[43]

Scheme 13 Hydroboration of olefin 36 yielding exclusively the axial hydroxy methylene derivative 48.

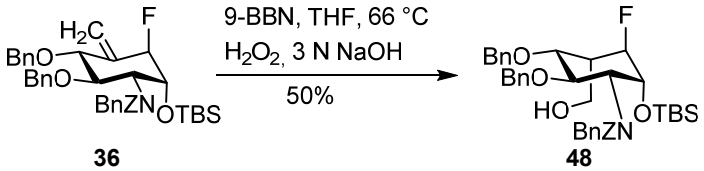

A well-described approach to obtain the equatorial hydroxy methylene group includes the oxidation of the carbocyclic alcohol to the aldehyde followed by epimerization under mildly basic conditions and subsequent reduction.[24,41,189] The epimerization of the L-carba-sugar precursor **48** and similar conditions failed (**Scheme 14**). The oxidation of **48** to the L-aldehyde **49** with IBX was completed after 14h. At this point, however, already 21% HF-elimination product was formed (determined by LC-MS). LC-MS monitoring of

the subsequent isomerization of the L-aldehyde **49** to the D-aldehyde **50** in a mixture of methanol and 10% pyridine at 60 °C showed complete elimination after 10h.

Scheme 14 Attempt to isomerize aldehyde 49 to the D-conformer of the 5a-fluoro-carba-sugar precursor 50.

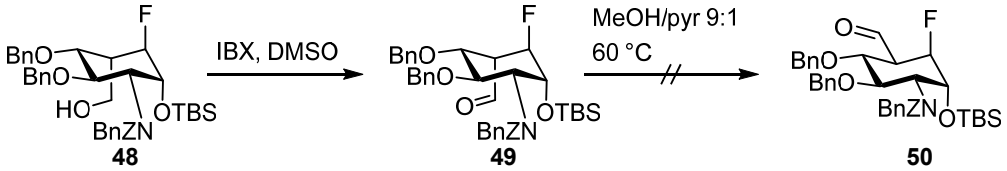

The search for an alternative synthesis route towards the D-conformer of **48** led to the synthetic sequence of epoxidation and subsequent regioselective epoxid-opening. Epoxidation of **36** was carried out with *meta*-chloroperoxybenzoic acid (*m*CPBA) under standard conditions (**Scheme 15**).[195] Similar to already described epoxidations of terminal olefins with allylic fluorine, prolonged reaction times were necessary.[196] Almost complete consumption of starting material **36** was reached after 14 days, and the epoxide **34** could be isolated in 59% yield. The long reaction time of the epoxidation is likely due to the strong electron-withdrawing effect of the adjacent fluorine.[196] For comparison, the epoxidation of the unmodified β-cyclohexanone **47** was finished after a reaction time of 4 days in a yield of 67%. However, the epoxide was isolated as a mixture of two isomers **51** and **52** in the ratio of 25:75, respectively.

Scheme 15 Synthesis of the fluorinated epoxide 34 compared to the unmodified epoxides 51 and 52.

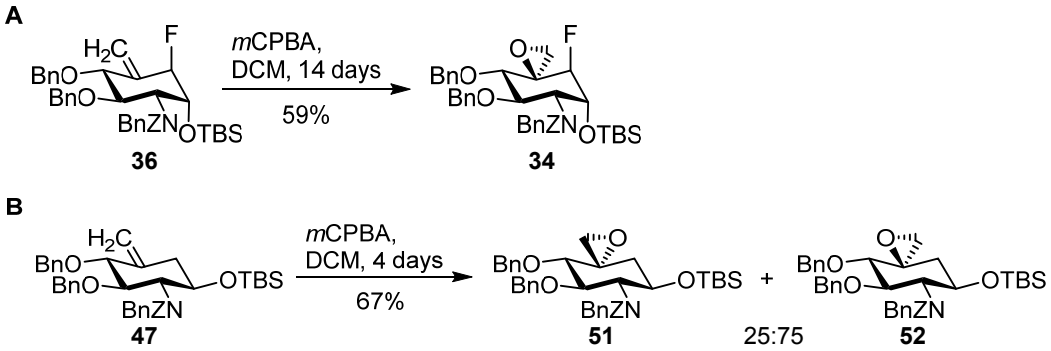

To determine the configuration of C5 in **34**, NOE-correlations were extracted from ROESY experiments. **Figure 14** shows the fully optimized structures (BP/def2-TZVP) of the two possible isomers of the epoxide **34**, whereas benzyl was replaced by methyl to reduce calculation times. Indicated are the expected NOE-correlations crucial for the determination of the orientation of the oxirane ring. In the 2D-ROESY experiment of **34**, NOE-correlation between H6a and H5a as well as H6b and H3 was observed, while a correlation between H4 and H6b was absent. In accordance with **Figure 14**, these NOE-correlations are indicative of an equatorial position of the oxygen and a 5*R* configuration

of **34**. Similar considerations led to the assignment of the configurations at C5 in the unmodified carba-sugar precursors **51** and **52**. In this respect again, the equatorial position of the oxygen **52** (5*R*) is favored with a ratio of 75:25 compared to **51** (5*S*). However, there is a higher selectivity for an epoxidation occurring from the equatorial position of the olefin in **36** compared to **47**. It can be assumed that the different stereoselectivity depends on the different orientation of the bulky OTBS group. Its axial orientation in **36** is blocking the β face of the ring, leading to the observed high preference for an equatorial epoxidation. In the case of the β-cyclohexane **47**, the steric effect of the TBS group is negligible leading to the low stereoselectivity for **52**. The observed predominant equatorial transfer of oxygen for **36** is in good agreement with other hindered olefins.[197] However, the high ratio of equatorial attack in the epoxidation of **47** cannot be explained simply by steric factors. For comparison, in the case of unmodified and unhindered methylene cyclohexanes, the axial attack would be preferred.[198,199]

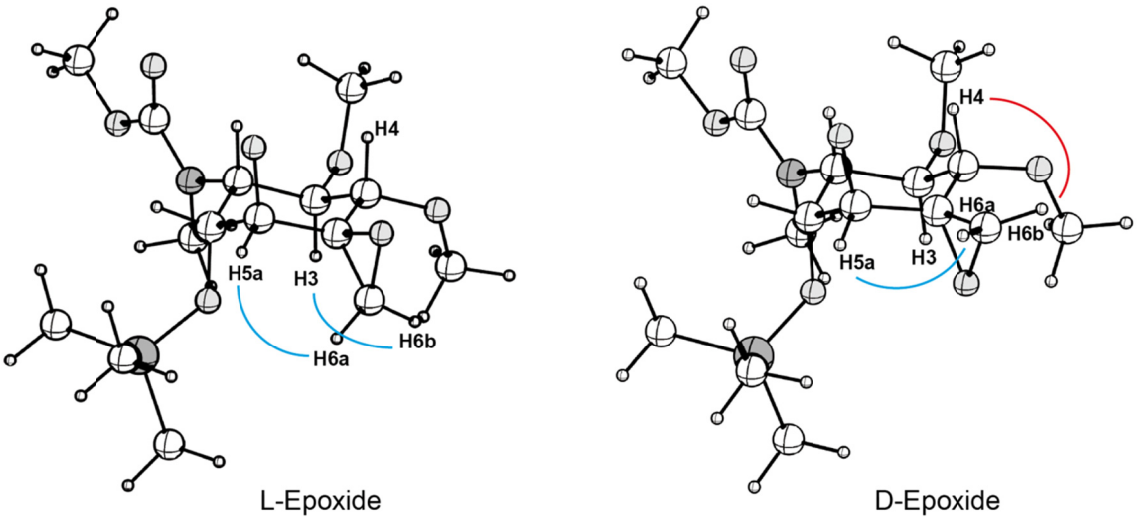

Figure 14 Optimized structures (BP/def2-TZVP) of the two possible isomers of 34
The protection groups were simplified to reduce calculation times. Therefore, all benzyl-groups were replaced by methyl prior to calculations. Indicated with colored lines are NOE-correlations of interest that should be observed for each isomer. Blue: NOE correlations that were found in 2D-ROESY experiments at -40 °C. Red: NOE correlations that were absent in 2D-ROESY experiments at -40 °C. The structures were visualized with the ChemCraft program.[200]

For the next step towards fluoro-carba-GlcN, radical reaction conditions were used for the regioselective epoxide opening of **34** and the epimeric mixture of **51**/**52** (**Scheme 16**). In this reaction, first, a titanium oxide radical is formed by the opening of the epoxide with paramagnetic Cp_2TiCl. Next, hydrogen atom transfer from 1,4-cyclohexadiene (CHD) yields the corresponding alcohol as a mixture of C5-isomers (pseudo L- or D-configuration) (**Scheme 16A**).[201] The regioselectivity, thereby, is opposite to classical

S_N2-type reductive epoxide openings. As a first try, a procedure utilizing stoichiometric amounts of Cp_2TiCl were employed (**Scheme 16B**, **Table 3**, **Entry 1**, **3**, and **4**).[201,202] In the case of fluoro-carba epoxide **34**, due to the slow conversion at room temperature, the temperature was increased incrementally to 60 °C, and additional portions of Cp_2TiCl were added over time up to 170 mol% relative to the substrate. Nevertheless, full conversion was not reached after four hours, and the formation of side-products could be observed via TLC-monitoring. The product was isolated as a mixture of the D- isomer **53** and L-isomer **48** in a poor yield (11%) (**Table 3**, **Entry 1**). Despite a high diastereomer ratio (dr 86:14) for the **53**, both isomers were separable via HPLC. As side-products of the opening of **34**, the HF-elimination product **58** (**Figure 15**) and a complex mixture of compounds with a high retention time (RP-HPLC), where observed.

Scheme 16 Regioselective titanocene-mediated radical epoxide opening of the unmodified epoxide 51 or 52 and the fluorinated epoxide 34

(A) Crucial steps of the titanocene-mediated radical epoxide opening are shown. (B) The Stoichiometric approach for **34**, **51** and **52**. (C) The catalytic radical epoxide opening of **34**.

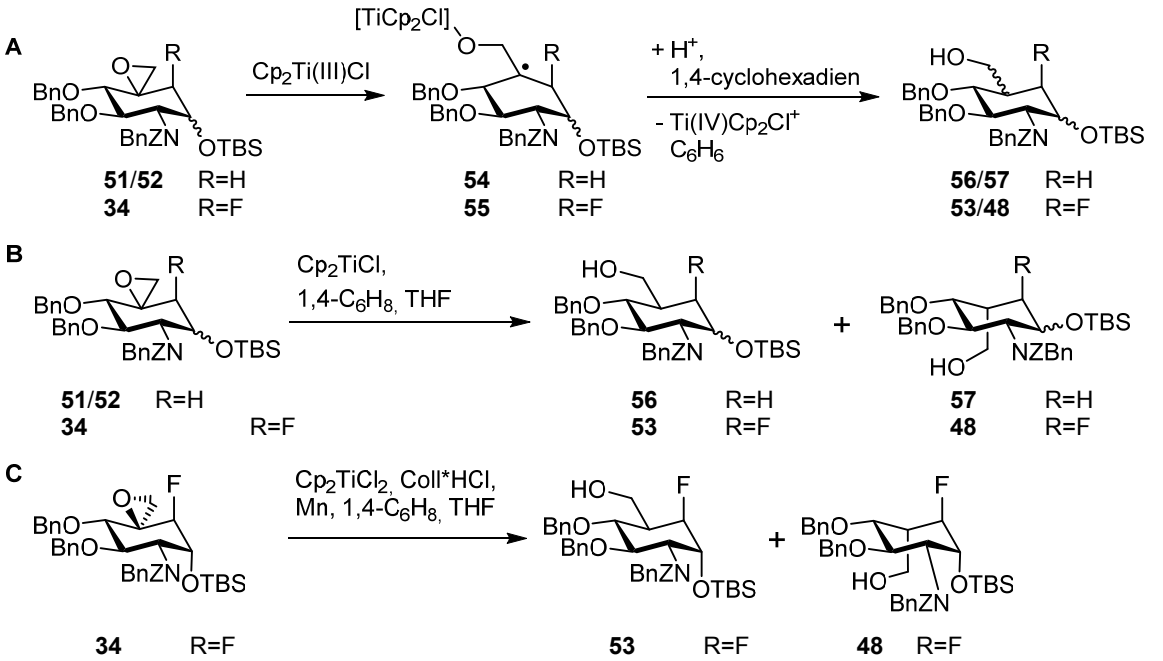

The epoxide opening of the individual C5-isomers of the unmodified carba-sugar epoxides **51** and **52** was performed at room temperature as sufficient conversion could be observed. Complete consumption of the starting material was determined via TLC-monitoring after two hours. For both substrates, the epoxide opening proceeded in high yields, and the D-isomer **56** was predominantly formed for both substrates. The **56**/**57**-ratio was determined by LC-MS as 64:36 for substrate **51**, compared to 72:28 for **52**.

Table 3 Product ratios and reaction conditions of the radical epoxid opening of 5a-fluoro carba-sugar epoxide 34 and the unmodified epoxides 51 and 52.

Entry	Substrate	Cp_2TiCl_2 [mol%]	Additives	T [°C]	Product ratio D/L*	Yield [%]
1	**34**	170	CHD	25 to 60	86:14	11
2	**34**	30	CHD, coll, Mn	50 to 58	93:7	33
3	**51**	210	CHD	25	64:36	72
4	**52**	210	CHD	25	72:28	62*

*determined by LC-MS

Due to the low yield of the stoichiometric reaction for **34**, a catalytic variant of the radical epoxide opening was tested. (**Scheme 16C**) This approach was assumed to reduce side-reactions that are related to Ti(III)-species. Under these conditions introduced by Gansäuer *et al.*, catalytic quantities of titanocene dichloride are reduced by stoichiometric manganese. The 2,4,6-collidine hydrochloride (col) is added to protonate the titanium oxide and regenerate titanocene dichloride.[203] As a consequence, the amount of titanocene dichloride was reduced to 30 mol% (**Table 3**, **Entry 2**). In this case, a short temperature-gradient from 50 to 58 °C was used. Compared to the stoichiometric approach, the isolated yield of the D-isomer **53** was improved to 33%, while 12% of the starting material could be recovered. Considering the stereoselectivity, a high dr of 93:7 in favor of **53** could be retained.

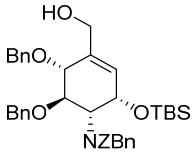

58

Figure 15 Side-product 58 of epoxide opening of 5a-fluoro-epoxide 34

The increased yield of the catalytic (**Scheme 16B**, **Table 3**, **Entry 2**) compared to the stoichiometric epoxide opening of **34** (**Scheme 16C**, **Table 3**, **Entry 1**) is likely due to the reduction of the relative amount of titanocene radical. The trapping of the intermediate carbon-centered radical by a second Cp_2TiCl leads to elimination, which is thereby depending on the concentration of the active species Cp_2TiCl.[201] The use of the additive Coll*HCl that mediates turnover, further reduces Cp_2TiCl concentration in the catalytic approach through reversible $[Cp_2TiCl_2]^-$ formation (resting state of the catalyst).[204]

3.1.1.1 Mechanistic study of the titanocene(III) catalyzed epoxid-opening of the fluoro-carba-sugar precursor

The significant formation of side-product **58** through HF-elimination seems to contradict the generally expected thermodynamic inertness of carbon-fluorine bonds. Therefore the different possible reaction paths starting from the titanium oxide radical intermediate **55** need to be considered (**Scheme 17**). Immediate hydrogen transfer from 1,4-cyclohexadiene to **55** leads to the desired protected carba-sugar **53** or **48** (**Scheme 17**, **path A**). An excess of the catalyst titanocene(III) chloride, however, leads to the competitive electron transfer reduction of the carbon-centered radical intermediate **55** yielding **59** (**Scheme 17**, **path B**). Subsequent β-elimination of the good leaving group $OTiCp_2Cl$ would give the terminal olefin **36** in the course of the well-described process of deoxygenation of epoxides.[201,202] Elimination of fluoride from **59** would yield side-product **60** instead. However, the elimination of fluoride as a poor leaving group is expected to be less likely than the elimination of $OTiCp_2Cl$, yet the terminal olefin **36** was not observed. Thus path B, which describes the competition of these two reactions does not satisfactorily explain the reaction outcome.

Scheme 17 Mechanistic hypothesis for Cp_2TiCl opening of epoxide 34
(A) Hydrogen-transfer leading to the desired product **53** or **48**. (B) Deoxygenation leading to not-observed side-product **36**. (C) A mixed radical disproportionation process is yielding the elimination product **58** that is formed in significant amounts.

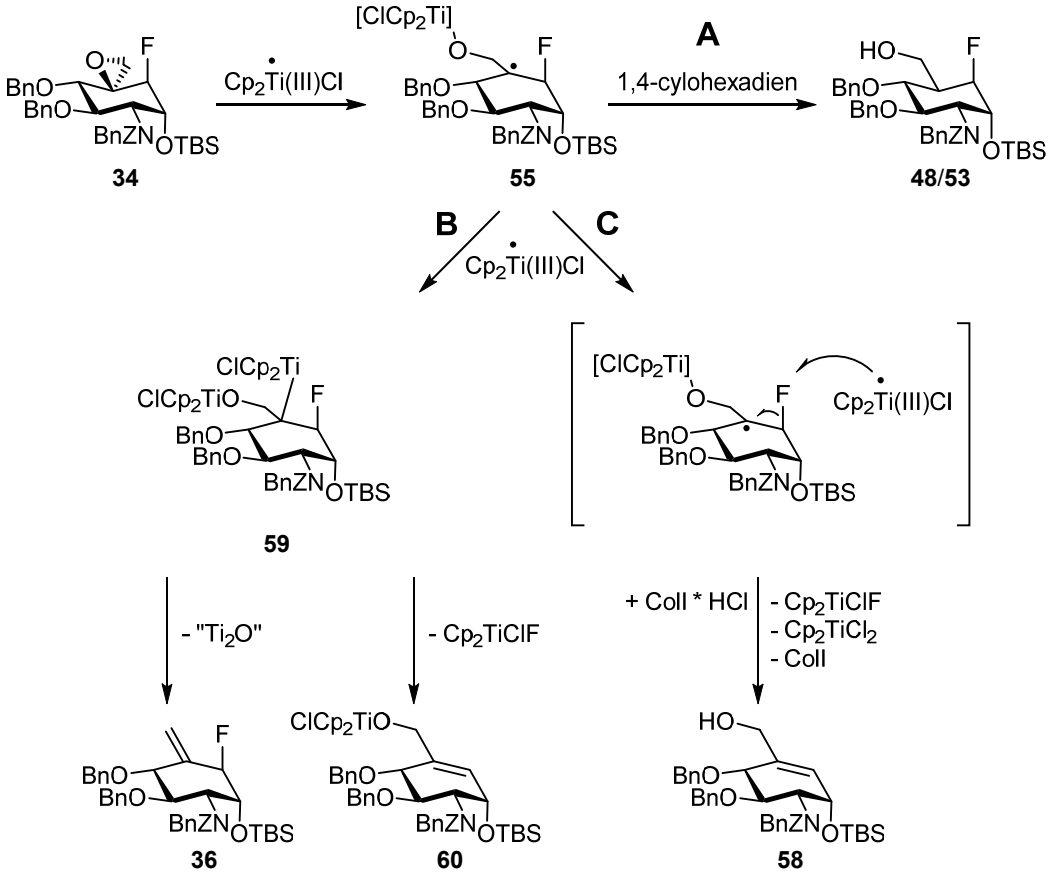

An alternative process, which fits the experimental results better is shown as path C (**Scheme 17**, **path C**). In this side-reaction, a second Cp_2TiCl reacts with intermediate **55** in a radical disproportionation. Instead of recombination of the carbon-centered radical and Cp_2TiCl, the titanocene radical abstracts the fluorine and a double bond is formed between C5 and C5a. A similar radical disproportionation after titanocene-mediated epoxide opening was observed by Justicia *et al*. [205] Unlike the loss of fluorine in the example presented herein, their epoxide opening was followed by abstraction of hydrogen yielding the allylic alcohol. This side-reaction was substrate-dependent. They stated that the trapping of the radical intermediate (equals **55**) by bulky Cp_2TiCl (**Scheme 17**, **path B**) occurred very slowly making the disproportionation reaction more likely.[205] In the case of the fluorinated radical intermediate **55**, the high affinity of titanium to form a Ti-F bond could be the driving force of this reaction. The bond dissociation energy of Ti-F is 569 ± 33 kJ/mol[206] compared to 491.2 ± 8.4 kJ/mol[207] for the C-F bond (in fluoro cyclohexane). Titanium-catalyzed C-F activation with Cp_2TiH as the active species has already been used for the hydrodefluorination of fluoroalkenes.[208] Furthermore, oxidative

addition of the C-F bond to low-valent titanocene generated from titanocene dichloride was assumed as the key step in the defluorination of saturated perfluorocyclohexane.[209]

As a result, reaction path C can be assumed to be most probable, if abstraction of fluorine by the titanocene radical proceeds faster than the hydrogen transfer from 1,4-cyclohexadiene. Because of the bulky titanocene substituent at the oxygen in **55**, the tertiary radical center is hard to access by 1,4-cyclohexadiene, which increases the likelihood of the radical disproportionation.

To explain the high diastereoselectivity of the epoxide opening of the fluorinated α-substrate, the different intermediate steps of the titanocene catalyzed epoxide opening have to be considered (**Scheme 16A**). The carbon-centered radical intermediate **55** with the titanocene bound to the oxygen is formed through regio divergent epoxide opening. Epoxide opening by single-electron-transfer (SET) is the rate-limiting step in the sequence,[210] followed by reduction of the radical with 1,4-cyclohexadiene (CHD). In most cases, the carbon-centered radical occupies an orbital with mainly p-character, so attack from two sides is possible. A high p-character of the radical center is also the case for **55**, which is confirmed by calculations of the Mulliken spin populations (C-5 p: 0.83) of the simplified molecule (**Figure 22**). The significant stability of this intermediate is the requirement for the loss of the stereo information at C-5 and the observed selectivity. Decisive for the stereoselectivity of the following H-abstraction from either axial or equatorial position is the transition state of this step. In general, steric strain by the torsional effect disfavors equatorial attacks while 1,3-diaxial repulsion disfavors axial attacks.

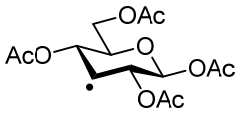

61

Figure 16 Chemical structure of the C-3 radical of β-D-glucose pentaacetate

Six-membered cyclic radicals and their selectivity in abstraction reactions have thoroughly been investigated.[211] Giese *et al.* investigated the D-abstraction from Bu_3SnD by the C-3 radical of β-D-glucose pentaacetate (**Figure 16**).[211] No selectivity was observed (ratio of equatorial:axial 53:47), most likely because the torsional effect and the 1,3-diaxial repulsion canceled each outer out. Unlike the sterically small acetyl groups, the C-5 radical intermediate of the unmodified β-DL-carba-GlcN **54** bears the bulky $CH_2O[TiCp_2Cl]$ group at the radical center (**Figure 17**). This influences the relative energy of the two transition states resulting from either axial or equatorial attack of CHD. It can be assumed that the substituents of the radical center already adopt a near-

tetrahedral conformation in the transition state. As a consequence, the $CH_2O[TiCp_2Cl]$ group is oriented either near-axial (**Figure 17B**), leading to repulsive interactions with axial protons at C-1 and C-3 or near- equatorial, which is the sterically preferred position of the titanocene (**Figure 17A**). The steric effect of the bound titanocene is counteracted by steric repulsion between the hydrogen transfer reagent CHD that approaches the radical from the respectively other site. Due to the absence of bulky axial substituents, the influence of 1,3-diaxial strain is small leading to the observed low selectivity for the axial hydrogen abstraction of 64:36 or 72:28. These results are in good agreement with experiments by Giese *et al.* that large substituents at the methylene group guide the H-abstraction *trans* to substituents at the stereogenic center.[212]

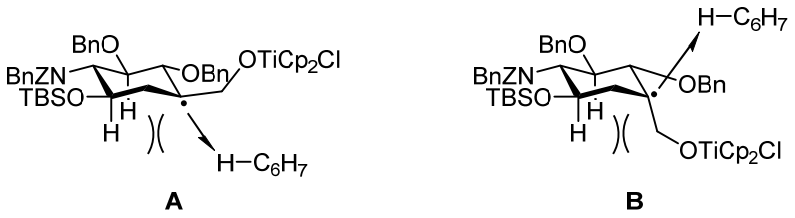

Figure 17 Proposed transition states (TS) of the axial (A) or equatorial (B) hydrogen transfer from 1,4-CHD to the carbon-based radical intermediate 54
The molecule is turned at 120° compared to the representation before.

In the case of the mono-fluorinated α-carba-sugar precursor **34**, the major difference is the axial configuration of the OTBS group at C-1. The bulky group in the α-plane of the ring greatly changes the interactions with other axial groups in the α-plane. In the proposed transition states **TS2A** and **TS2B**, the substituents at C-3 and C-5 are thereby crucial (**Figure 18**). Therefore, the steric strain between OTBS and $CH_2O[TiCp_2Cl]$ increases the energy of **TS2B**. However, a significant steric strain between OTBS and the incoming CHD can be expected in the case of **TS2A**. The evaluation of these two contributions to determine the favored transition state and therefore explain the diastereoselectivity of the reaction is hardly possible solely on the basis of **Figure 18**. A way to experimentally address this issue is varying the ligands of the titanocene. Bulky substituents of the cyclopentadienyl ligands would increase the steric strain in transition state **TS2B** while the steric effect of titanocene in equatorial position in **TS2A** should be negligible. This effect, an increase in diastereoselectivity in the opening-reaction of *meso* epoxides was observed when bis(*tert*-butylcyclopentadienyl) titanium dichloride was used as a catalyst instead of titanocene dichloride.[213] Variation of the hydrogen donor (alkyl mercury hydride, tributyltin hydride, cyclohexane) on the other hand was shown to have little effect on the stereoselectivity of substituted maleic anhydride radicals.[211]

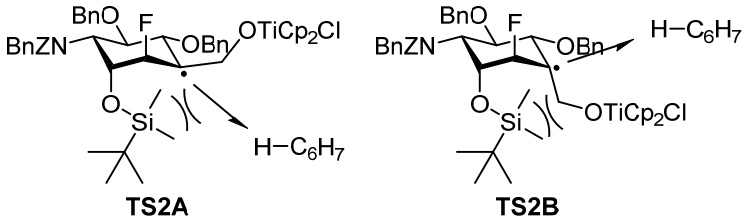

Figure 18 Proposed structures of the transition states TS2A and TS2B of hydrogen abstraction of the radical intermediate from 1,4-cyclohexadiene during epoxide opening of 34

The molecule is turned at 120° compared to the representation before.

Besides the steric effect of the bulky TBSO-group also the influence of fluorine at C-5a on the stereoselectivity needs to be considered. Its steric effect, on the one hand, can most probably be neglected due to its small size. The electronic nature of fluorine, on the contrary, influences the reactivity of the radical.[214] Fluorination most probably increases the reactivity of the radical, thus decreases selectivity. In the case of hydrogen atom abstraction from *n*-Bu_3SnH, β,β-difluorinated radicals showed five times higher reactivity compared to the hydrogenated analog.[214] Due to only one fluorine atom in the case of **34**, the influence on reactivity would be accordingly smaller.[215] Furthermore, the directing effect of β-substituents in six-membered rings to the *anti*-side is well described.[211]

3.1.1.2 Computational study of the hydrogen atom abstraction step in the epoxide opening reaction

The preference for the axial hydrogen atom abstraction (**TS2A**, **Figure 18**) could not be conclusively clarified due to a variety of effects. Besides steric strain between OTBS and either CHD or $CH_2O[TiCp_2Cl]$, the electronic effects of fluorine are difficult to predict. For this purpose, DFT calculations were carried out to evaluate TS2 (**Figure 19**) computationally. All calculations were done with the ORCA program package.[216] For initial optimizations of structures and scans of the potential energy surfaces (PES), the BP86 functional[217,218] with the Ahlrichs' def2-SVP basis set and the def2-TZVP basis set for the titanium were used. To lower the computational time the benzyl protection groups were substituted by methyl.

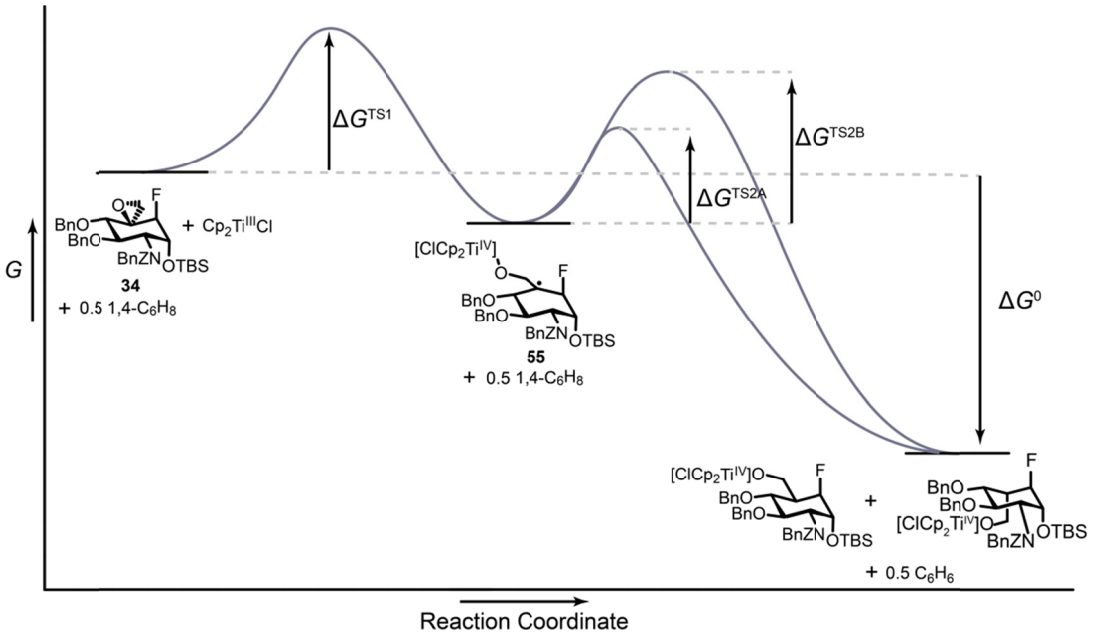

Figure 19 Proposed energy diagram of the epoxide opening of 34
Indicated are the Gibbs free energies of activation of both reaction steps, the opening of the epoxide ring (ΔG^{TS1}) and both reaction paths of the hydrogen abstraction leading to pseudo-D-isomer **53** and L-isomer **48**.

First, the structure of the carbon-centered radical intermediate **55** was calculated. A scan of one coordinate of the PES was performed to find the most favored orientation of the CH_2OTiCp_2Cl group. Therefore the energy was calculated depending on the dihedral angle between C5a-C5-C6-O (**Figure 20**). A definite ground state of **55** was hoped to already allow conclusions about the favored transition state on the assumption of an "early", thus reactant-like transition state (**Figure 19**). Giese *et al.* used this approach for the determination of the transition state and stereoselectivity of an H-abstraction by carbohydrate-radicals.[212]

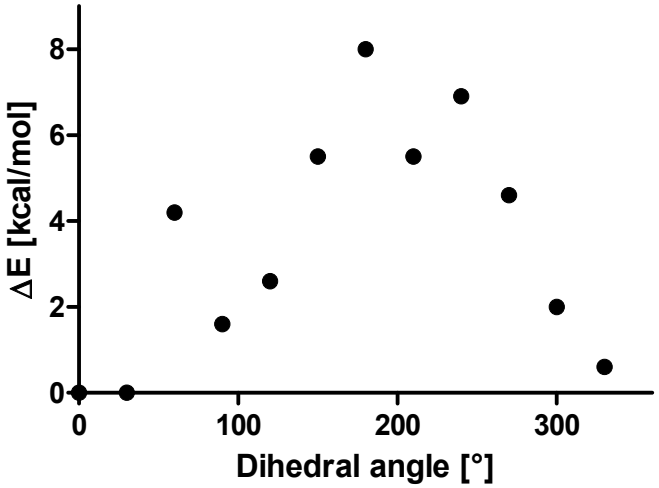

Figure 20 Relative energy of 55 as a function of the dihedral angle between C5a-C5-C6-O
The energy difference is given relative to the single point energy at an angle of 0°.

All optimized conformers of intermediate **55** adopt the chair-like conformation. From the PES, two minima with an energy difference of less than 2 kcal/mol emerged (**Figure 21**). Optimization of the structure of intermediate **55** without constrained angles resulted in a structure with a dihedral angle of 22° which fits the PSE scan and the conformations with the lowest energy (dihedral angle 0° and 30°) (**Figure 22**).

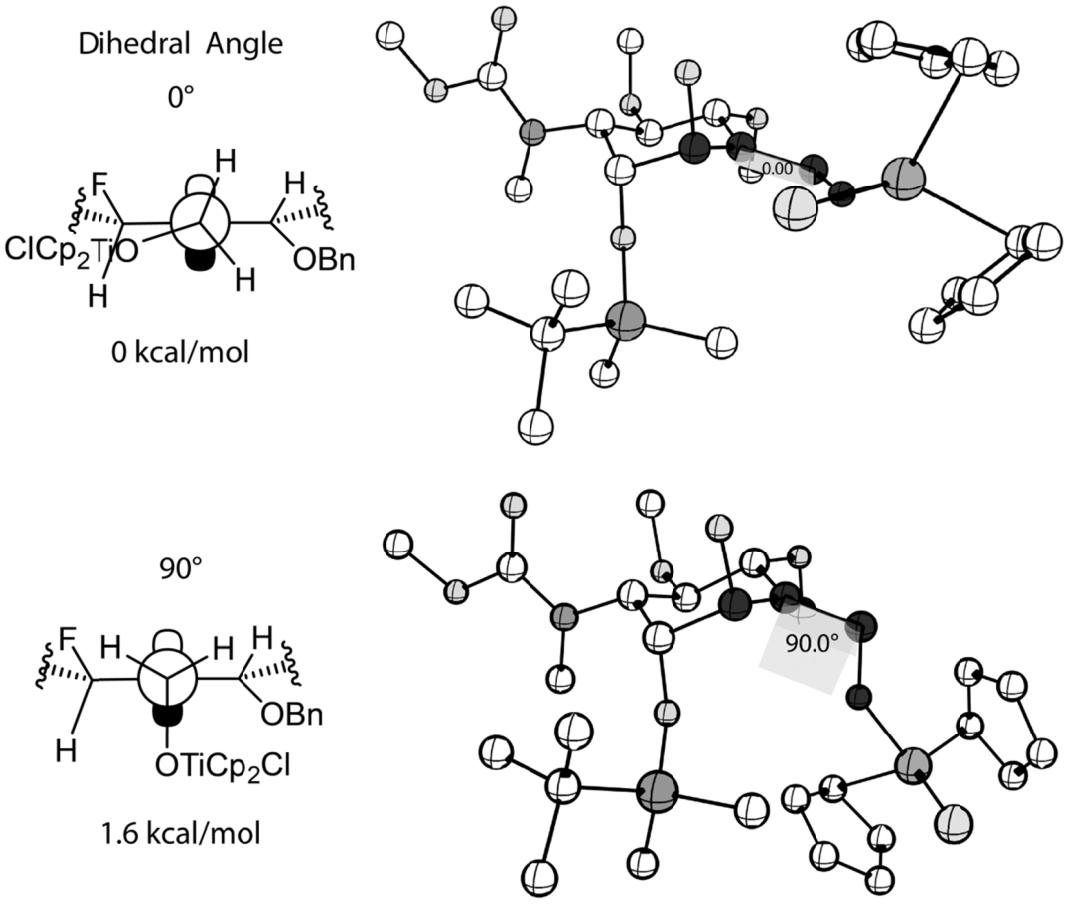

Figure 21 Comparison of the structures of the carbon-centered radical intermediate 55 that correspond to the minima of the PSE scan with constrained dihedral angles C5a-C5-C6-O
Both the schematic Newman-projection of each conformer and the respective optimized structures employing the BP86/def2-SVP level of theory are shown. The given energy for each conformer is the single point energy relative to the lowest energy conformer with a dihedral angle of 0°. For better visibility hydrogens are hidden in the optimized structures.

Hence, the optimized structure with a dihedral angle of 0° closely resembles **TS2A**, while an angle close to 90° would be expected for **TS2B**. However, due to the small energy difference between these two, a clear statement about the preference of one of the two proposed transition state cannot be made. This is the case even though the transition state can be predicted to be "early", thus reactant-like according to the Hammond postulate (**Figure 19**).[219] The similar energy of both conformers in contrast to the study of Giese *et al.*[212] can be attributed to non-existent steric strain through bulky substituents in β-position concerning the radical center. As fluorine is too small to guide the titanocene into the *anti*-orientation, the present study is not as clear-cut as a comparable model by Giese *et al.*, which showed an *anti*-orientation of the bulky substituent at the prochiral center (analog to $OTiCp_2Cl$) to a *t*-butyl β-substituent, favored by 5 kcal/mol.[212]

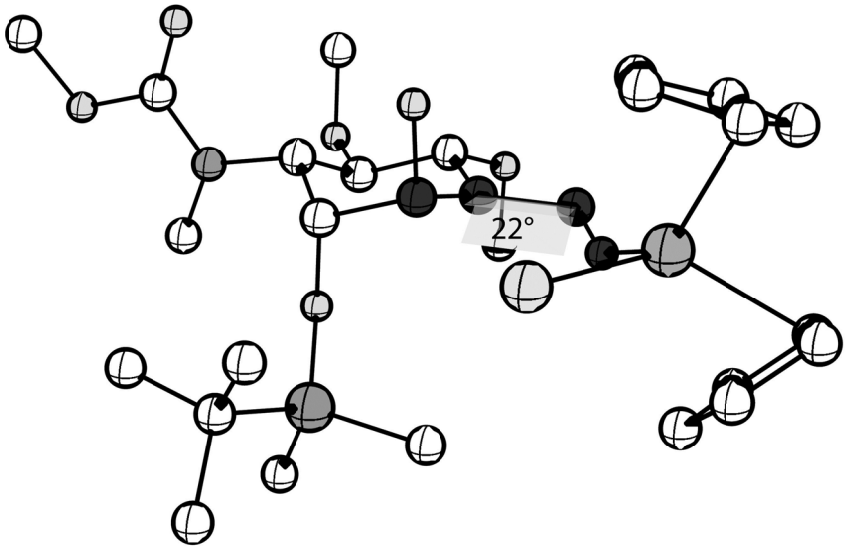

Figure 22 Structure of the β-titanoxy radical 55 optimized with the TPSS-D3/def2-TZVP level of theory.

Therefore, the transition structures of **TS2A** and **TS2B**, as well as their corresponding activation energies, were calculated. For this, a PES scan was carried out to find a structure that is close to the TS. In the PES scan, constrained optimizations for different values of the distance between CHD and radical center were performed. The distance between the hydrogen of CHD and the radical center was varied between 2.0 to 1.0 Å in five steps with the BP86/def2-SVP level of theory. The structure with the highest energy was then used for further constrained optimizations with smaller steps at a higher level of theory (TPSS-D3/def2-TZVP). Finally, TS-optimization was performed with the respective initial guessed structure for both **TS2A** and **TS2B**. Thereby, distances between hydrogen and radical center of 1.52 Å (**TS2A**) or 1.49 Å (**TS2B**) were used. The vibrational frequencies of the fully optimized molecules show a single imaginary frequency, which confirms that the structures are indeed TS structures.

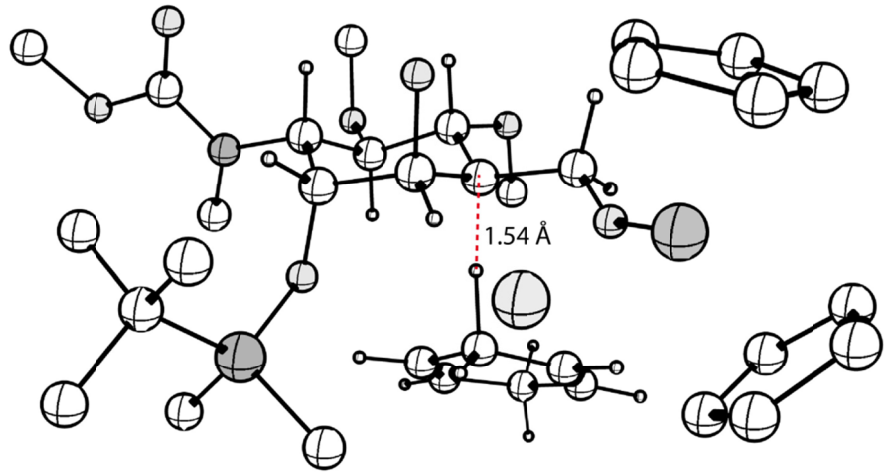

ΔG^{TS2A} = 11.6 kcal/mol

Figure 23 Optimized structure of transition state TS2A of the axial hydrogen abstraction and its Gibbs free energy of activation ΔG^{TS2A} (TPSS-D3/def2-TZVP)
The activation energy is given relatively to **55**.

As already predicted by the Hammond-postulate, the early transition state **TS2A** (**Figure 23**) closely resembles the structure of the β-titanoxy radical **55**. Transition state **TS2B** (**Figure 24**), which is 2.5 kcal/mol higher in energy than **TS2A**, on the other hand, looks similar to the conformer with a dihedral angle of 90° (**Figure 21**).

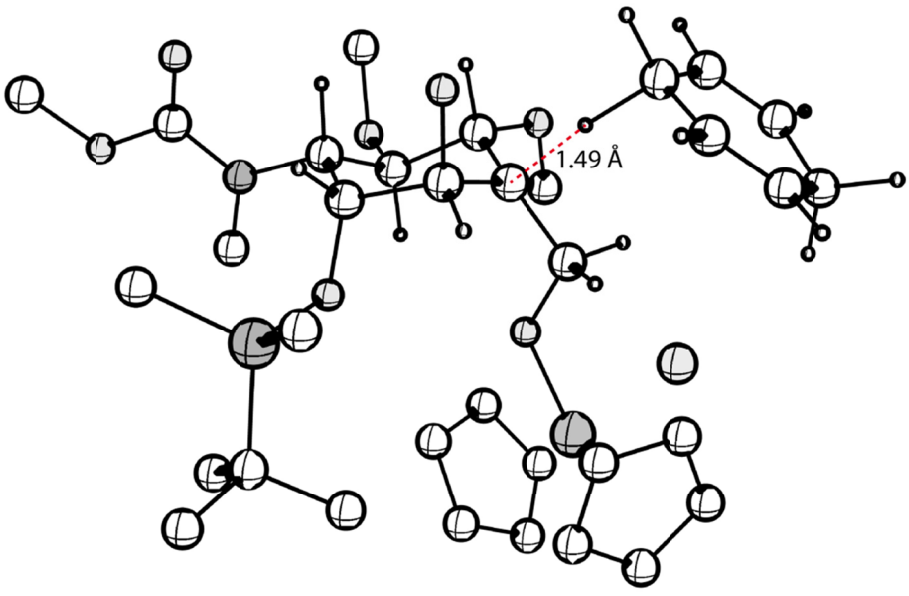

ΔG^{TS2B} = 14.3 kcal/mol

Figure 24 Optimized structure of transition state TS2B of the equatorial hydrogen abstraction and its Gibbs free energy of activation ΔG^{TS2B} (TPSS-D3/def2-TZVP)
The activation energy is given relatively to **55**.

The range of the free energy of activation of 12-14 kcal/mol indicates that hydrogen transfer should be facile at room temperature. However, from related studies on radical epoxide opening with subsequent hydrogen transfer, it is known that the epoxide opening is rate determining and thus should have the highest activation energy.[210] In **TS2B**, the titanocene is pointing down, near the bulky TBS-group leading to steric strain as already predicted from a comparison of the schematic TS (**Figure 18**). The observed difference in energy of **TS2A** and **TS2B** ($\Delta\Delta G^{TS}$ = 2.6 kcal/mol) at 60 °C, corresponds to a predicted ratio of equatorial to axial hydrogen transfer of 98:2. This correlates well with the experimentally observed high preference for the formation of the D-isomer **53**.

The Gibbs free energies of activation ΔG^{TS2A} = 11.6 kcal/mol and ΔG^{TS2B} = 14.3 kcal/mol were calculated relative to **55**. Consideration of different conformations of the β-titanoxy radical intermediate for **TS2A** and **TS2B** results in the energy diagram shown in **Figure 25**. However, it can be assumed that the rates of the H-abstraction step are much slower than the rates of conformational interconversion. The small rotational barrier around the C5-C6 bond in the PSE scan of the dihedral angle (**Figure 20**) reflects this assumption. In this case, the Curtin-Hammett principle applies and "the product composition does not depend on the relative proportions of the conformational isomers in the substrate but only on the standard Gibbs energies of the respective transition states".[220]

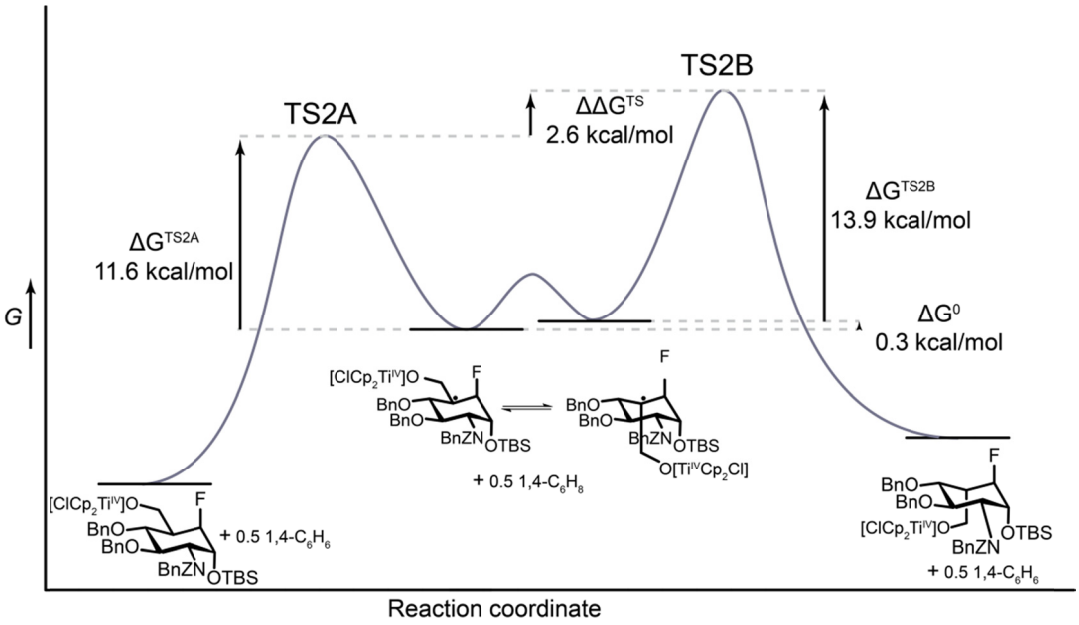

Figure 25 Energy diagram of the hydrogen atom transfer to the quickly interchanging conformers of intermediate 55
Hydrogen atom transfer is possible via two competing transition states **TS2A** and **TS2B** leading to the hydroxy methylene group at C5 in either axial or equatorial orientation.

An optimization of **TS2B,** starting from the same conformation of **55** as **TS2A** led to **TS2B*** (**Figure 26**). Here the cyclohexane ring adopts a boat-like conformation, which very likely reduces the steric strain between the titanoxy- and the OTBS-group. However, the Gibbs free energy of activation is very high (ΔG^{TS2B*} = 17.0 kcal/mol) most likely due to the disfavored ring conformation.

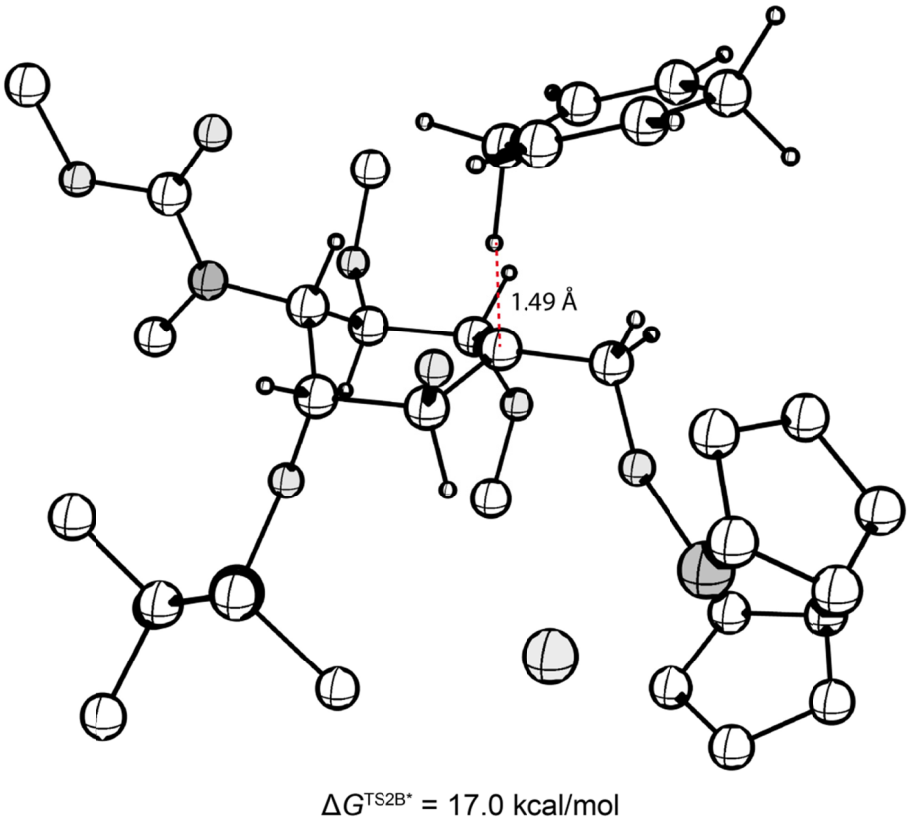

Figure 26 Optimized structure of transition state TS2B*
The free energy of activation $\Delta G^{\ddagger}$ (TPSS-D3/def2-TZVP) is given relatively to **55**.

Both **TS2B** and **TS2B*** that would lead to the hydroxy methylene group to adopt a pseudo L-configuration show a shorter distance between the hydrogen of CHD and the carbon-radical center (**Figure 24**, **Figure 26**). This is in agreement with the Hammond-postulate since the L-isomer **48** is thermodynamically less stable and the respective TS is predicted to be later, or rather, product-like.

As a conclusion, the conducted DFT calculations greatly helped to explain the stereoselectivity of the H-abstraction step in the epoxide-opening of **34**. The PSE scan of the dihedral angle between C5a-C5-C6-O of the β-titanoxy radical **55** showed two conformations that correspond to minima of the PSE (**Figure 20**). Two transition structures were found, of which TS2A (**Figure 23**) is similar to the stable conformation with a dihedral angle of 0°. Transition structure TS2B (**Figure 24**), in contrast, resembles the conformation with an angle of 90°. According to the Curtin-Hammett principle, the

Boltzmann distribution of the two conformations of radical intermediate **55** does not influence the composition of the product, the pseudo-D-isomer **53** and L-isomer **48**. The reason for this is the rapid interconversion of the conformers compared to the significantly slower H-abstraction from CHD. As a consequence, the energy diagram shown in **Figure 25** results, which shows a preference for a transition state that leads to the hydrogen-abstraction proceeding from an equatorial line of attack. The theoretical dr of 98:2, thereby closely resembles that of the experiment (dr 93:7).

3.1.1.3 Final steps of the synthesis of (5a*R*)-fluoro-carba-β-L-idosamine, (5a*R*)-fluoro-carba-α-D-glucosamine, and their phosphorylated variants

For the synthesis of the final pseudo-β-L-idosamine **63**, complete removal of the protection groups from **48** was carried out (**Scheme 18**). Removal of the silyl-group from the hydroxyl-group at C1 to yield **62** was tested under different conditions and monitored via HPLC (**Table 4**). With an excess of TBAF (*tetra-n*-butylammonium fluoride) (**Table 4**, **Entry 1**) no starting material could be detected after 45 min, but the formation of a side-product with a mass-difference of 107 m/z was detected via LC-MS. This difference correlates with the elimination of the OH-group at C1 and removal of one of the benzyl protection group on the hydroxy-groups at C3 **64** or C4 **65** (**Table 4**). This observation can most probably be associated with the excess of highly basic TBAF. Therefore, alternative deprotection strategies were tested, including alternative reagents (**Entry 2** and **5**), smaller amounts of TBAF and shortened reaction time (**Entry 3**), or buffered, catalytic deprotection with TBAF (**Entry 4**).

Scheme 18 Synthesis of 1OH fluoro-carba-IdoN precursor 62.

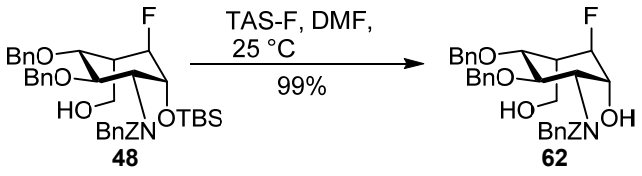

In summary, high reactivity of substrate **48** with all fluoride sources (TAS-F and TBAF) could be observed leading to the completeness of the reaction yielding **62** in short reaction times (15 to 90 min) (**Table 4**). However, a molar excess of TBAF led to the significant formation of elimination products **64** or **65** based on LC-MS (**Table 4**, **Entry 1**). With regard to side-reactions, reducing the amount of TBAF to 1.5 equivalents already prevented the formation of either **64** or **65** for more than 15 min (**Table 4**, **Entry 3**). Further reduction of TBAF under buffered conditions showed similar results and complete deprotection after 15 min (**Table 4**, **Entry 4**). For the use of acetic acid (**Table**

4, **Entry 2**) no side-product was detected, but the reaction proved to be very slow with less than 10% conversion after 18 hours of reaction time. The procedure used for removal of TBS in a larger scale (**Table 4**, **Entry 5**) was successful under mild conditions with tris(dimethylamino)sulfonium difluorotrimehtylsilicate (TAS-F) and an excellent yield of 99% of the isolated product (**Scheme 18**).

Table 4 Overview of the tested conditions for the removal of TBS from 48.

Entry	Reagent	Reagent Amount	T/°C	Time	Ratio **62**/**64**+**65***
1	TBAF	400 mol%	25	45 min	77/23
2[a]	Acetic acid – water - THF	3:1:1	23	18 h	<10% product, no side product
3[b]	TBAF	150 mol%	23	15 min	99/1
4[c]	TBAF, THF/K_2HPO_4 (100:1)	50 mol%	23	15 min	99/1
5	TAS-F	150 mol%	25	90 min	99/1

[a] Corey *et al.*[221] [b] Meyer *et al.*[222] [c] DiLauro *et al.*[223] [d] Scheidt *et al.*

*Formation of side-product **64** and **65** was assumed based on LC-MS without further analysis.

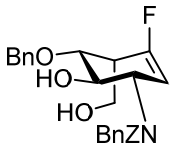

64

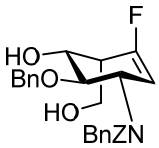

65

Simultaneous removal of the benzyl protection groups and the carboxy benzyl group was accomplished in one step via heterogeneous hydrogenation in 34% yield (**Scheme 19**). 100% (w/w) of 10% Pd/C relative to the substrate **62** was necessary, in the presence of 10% trifluoroacetic acid (TFA) and a hydrogen pressure of 10 bar, to cleave all benzyl ethers and remove the protection groups from the amine. If lower amounts of Pd/C were used, a complex mixture of compounds with varying degrees of benzylation was observed by LC-MS monitoring. The occurrence of side-products is most probably due to the poisoning of the Pd/C catalyst by the *in situ* formed, partly deprotected, amine at C2.[224] To ensure a high purity of the final product **63**, suitable for tests in bacterial cell culture, the raw product was purified via hydrophilic interaction chromatography (HILIC). However, it was not possible to collect the product through threshold detection of its

signal in the chromatogram because of missing UV-absorption. Therefore, chromatography-fractions were collected in time-slices and each fraction was analyzed via LC-MS. Since 20 mM NH_4OAc-buffer (pH 5.4) was used during HILIC-purification, **63** was isolated as the acetate salt.

Scheme 19 Synthesis of (5a*R*)-fluoro-carba-β-L-idosamine 63.

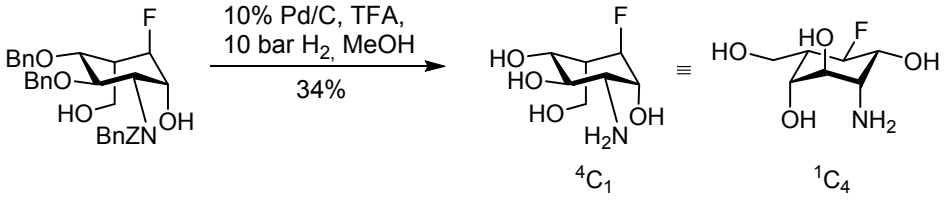

62 **63**

Phosphorylation of **48** was conducted with dibenzyl *N*,*N*-diisopropyl phosphoramidite and subsequent oxidation with *m*CPBA affording **66** in excellent yield (99%, **Scheme 20**).[166] For subsequent cleavage of the TBS ether, under-stoichiometric quantities of TBAF and buffered conditions were used. In contrast to **Entry 4** in **Table 4**, only 92% conversion to **67** could be observed after three hours. The significantly lower yield (41%) of isolated product, however, can be attributed to losses during HPLC-purification. Final cleavage of benzyl ethers and removal of the carboxy benzyl group was achieved in good yield (68%) of **33** after 24 hours. In conclusion, the (5a)-fluorinated carbocylic variant of IdoN **63** could be obtained in twelve steps starting from **26** and an overall yield of 0.7%. The synthesis of (5a*R*)-fluoro-carba-β-L-IdoN6P **33** could be complete in a total of thirteen steps and an overall yield of 0.6%.

During NMR-analysis of **63** and **33**, coupling constants $^3J_{H3\text{-}H4}=^3J_{H2\text{-}H3}$= 6.1 Hz were determined. These coupling constants lie between the expected value of *gauche*- or *anti*-orientation of the respective protons in the two most stable ring-conformations $^1C_4$ and $^4C_1$ (**Scheme 19**). Besides strong NOE correlations between H2 and H4 which are indicative of the $^4C_1$ conformation, also NOE correlations between H1 and H5 characteristic for the $^1C_4$ conformation were observed. However, NOE correlation between H5a and H2 were absent which would have indicated a $^2S_{5a}$ skew-boat conformation.[225] In the case of both conformations $^1C_4$ and $^4C_1$, three substituents occupy the axial orientation, thereby similar thermodynamical stability can be expected. This explains the averaged coupling constants as well as the presence of both characteristic NOE correlations due to rapid $^1C_4 \leftrightarrow ^4C_1$ interconversion that is not distinguishable on an NMR timescale at room temperature. Similar flexibility of the ring in fluoro-carba-sugars was already demonstrated for the *gem*-difluorocarba-sugar analog of methyl β-L-idopyranoside.[27] On this basis, the fluorine in **33** was determined to be *R*-configurated due to large coupling constants of H5a ($^3J_{H5a\text{-}H5}$ $^3J_{H5a\text{-}H1}$= 7.3 Hz) which is

indicative for a proportion of *anti*-orientation of H5a and H4/H1 in the case of the $^1C_4$ ring conformation.

Scheme 20 Synthesis of (5a*R*)-fluoro-carba-β-L-idosamine-6-phosphate 33.

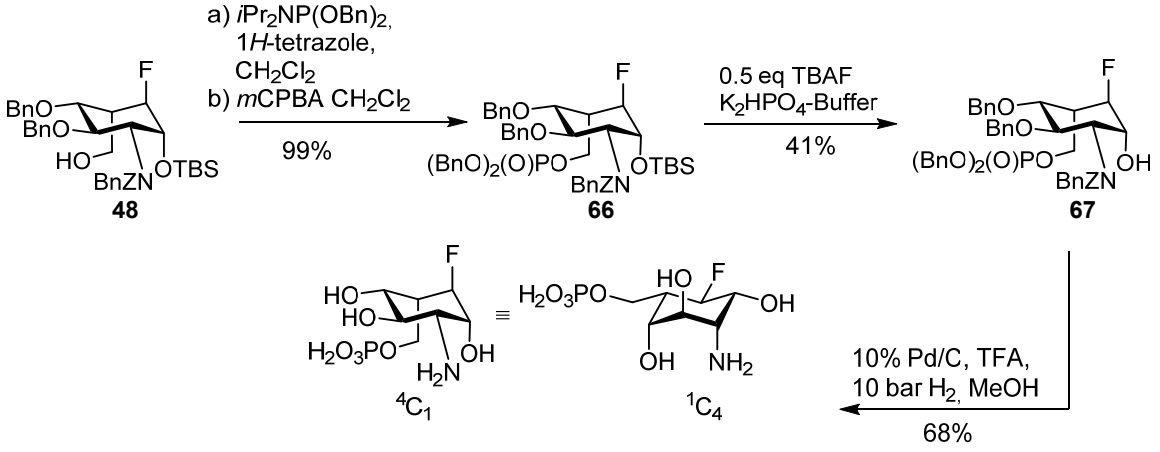

The last steps in the synthesis of the 5a-fluorinated carbocyclic variants of GlcN and GlcN6P starting from **53** were performed analog to that of the respective idosamine derivatives (**Scheme 21**). Significantly higher stability of **53** and **70** towards basic conditions compared to **48** and **66** was observed during TBS ether cleavage. A molar excess of TBAF in a mixture of THF and phosphate-buffer according to Dilauro *et al.*[223] was used for the deprotection of the carba-GlcN precursors **53** and **70**. However, no formation of side-product was observed after four hours. Consequently, **68** and **71** could be obtained at high yields of 90% and 87%, respectively. Also in the case of **68**, small coupling constants for H5a ($^3J_{H5a-H1}$ = 2.1 Hz, $^3J_{H5a-H5}$ = 4.0 Hz) were clear indicators for the axial orientation of fluorine. In this case, the verification is even more apparent since equatorial fluorine would lead to large coupling constants between H5 and H5a. At this point, the equatorial orientation of the methylene hydroxy group at C5 could be determined because of large coupling constants of H4 ($^3J_{H4-H3}$ = $^3J_{H4-H5}$ = 10.0 Hz). Phosphorylation of **53** was achieved utilizing the same phosphoramidite strategies as for **48**, leading to **70** in excellent yield (94%). Deprotection of **68** and **71** following the same protocol already described for the fluoro-carba-idosamine derivatives, provided (5a*R*)-fluoro-carba-α-D-glucosamine **69** and (5a*R*)-fluoro-carba-α-D-glucosamine-6-phosphate **35** in good yields of 53% and 70%, respectively. Due to the use of 20 mM NH_4OAc-buffer (pH 5.4) during HILIC-purification, **69** was isolated as the acetate salt. The synthesis of fluoro-carba-GlcN **69** could be completed in a total of thirteen steps starting from **26** and an overall yield 0.4%. The synthesis of fluoro-carba-GlcN6P **35** required a total of 14 steps while the overall yield was 0.5%. Due to lower yields during epoxidation and

radical-catalyzed epoxide-opening, the overall yield of the presented synthesis of **69** and **35** is slightly lower than that for **63** and **33**.

Scheme 21 Synthesis of (5a*R*)-fluoro-carba-α-D-glucosamine 69 and of (5a*R*)-fluoro-carba-α-D-glucosamine-6-phosphate 35.

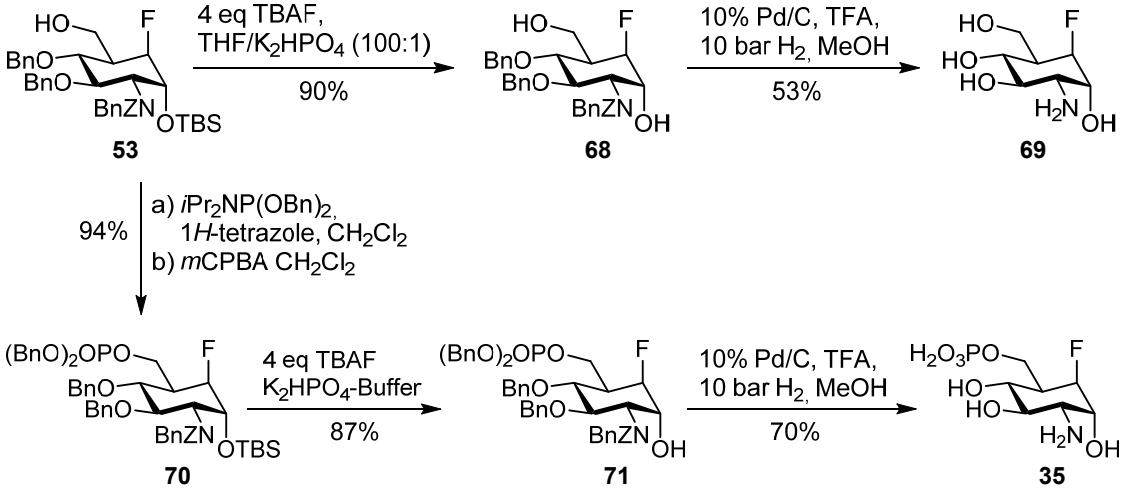

3.1.2 Synthesis of 5a-phenyl modified carba-D-glucosamine

In contrast to fluorine, as a chemically small modification, also sterically more demanding substituents were introduced at the 5a-carba-position of D-glucosamine mimics. Phenyl bound to the 5a-carbon via a C-C bond was chosen to further investigate the ligand requirements of the *glmS* ribozyme ligand binding site in relation to 5a-modified carba-aminosugars. Along with repulsive steric strain, attracting interactions are possible, since phenyl is capable of forming π-π-stacking interaction with nucleobases, which would increase the affinity to the ribozyme.[226,227] Furthermore, independent of the use as artificial *glmS* ribozyme activators, the present synthesis of phenyl-modified carbohydrate mimics represents a proof of concept of the versatile introduction of C-linked modifications at the 5a-position of carba-sugars.

Scheme 22 depicts the retrosynthetic analysis of the 5a-phenyl-carba-sugar variants of α-D-glucosamine **72** and β-D-glucosamine **75**. Besides opposing configuration at C-1, both compounds differ in the configuration of the phenyl. **72** is 5a*R*-configurated, while the phenyl in **75** is 5a*S*-configurated. In contrast to the completely deprotected **72**, the retrosynthesis of protected **75** is shown, because the final heterogeneous hydrogenolysis only provided a side-product. Up to this point, the same phosphorylation and deprotection strategy was used. Furthermore, for both compounds, the olefin-precursor **76** or **77** was used. The installation of the D-configured hydroxy methylene group, however, required different approaches. In the case of **72**, a sequence of hydroboration and subsequent isomerization of the corresponding aldehyde was used (**76**→**73**). The hydroxy methylene group of **75** was introduced via epoxidation (**77**→**74**) followed by the regioselective radical epoxide opening. Synthesis of the olefins **76** and **77** was achieved through Tebbe olefination of the corresponding cyclohexanones **103** and **104**. A mixture of the cyclohexanones, in turn, resulted from the Ferrier rearrangement of the 6-phenyl enolic ortho ester **80**. **80** is the product of an elimination reaction after the introduction of the phenyl at C-6 after oxidation of the alcohol **26**, which was the starting material of both synthetic routes.

Scheme 22 Retrosynthetic analysis of 5a-phenyl modified carba-sugar derivatives 75 and 72

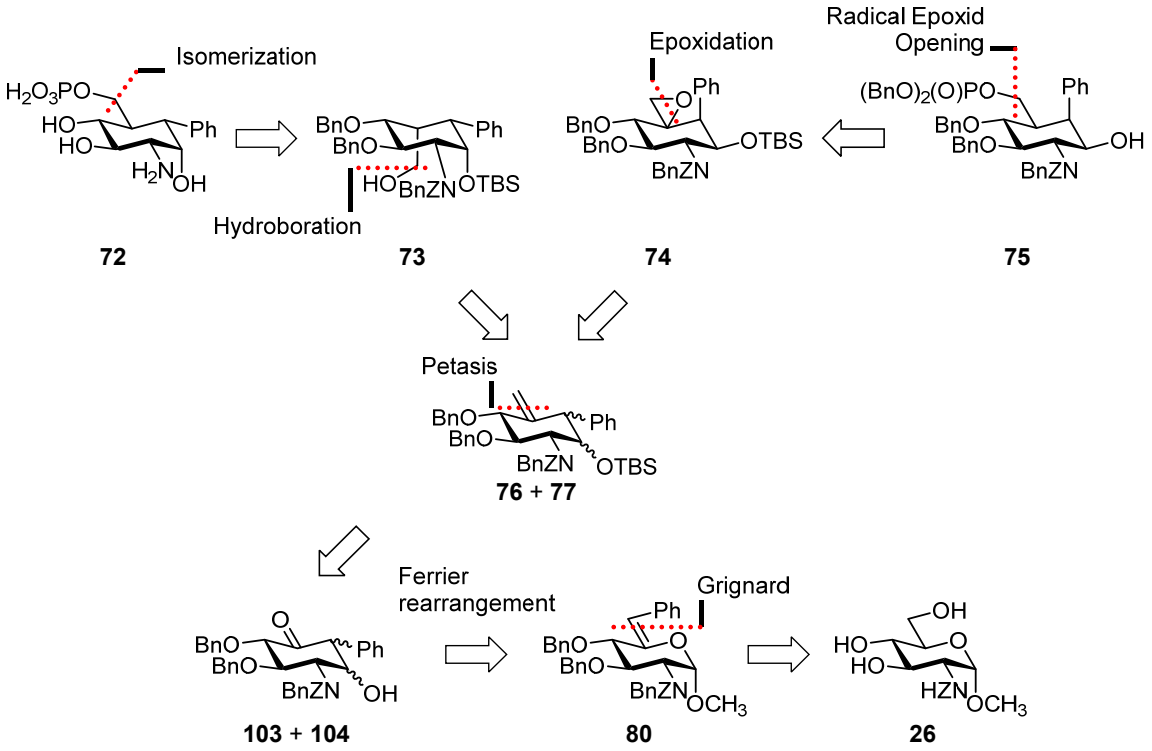

The synthesis of phenyl-carba-sugars was performed using an approach similar to that for the fluoro-carba-sugars. The core difference between both synthesis routes lies in the time point of the introduction of the modification. Phenyl is introduced in an early step, already before the carbocyclisation under Ferrier conditions (**Scheme 23**). Therefore, selectively protected glucosamine **39**, which bears a free 6-OH group, was used as a starting material. **39** was synthesized as already described (**Scheme 7**, **Section 3.1.1**) and indicates the branching point of the synthesis routes of fluoro- and phenyl-carba-sugars.

Scheme 23 Synthesis of 6-phenyl enolic ortho ester 80.

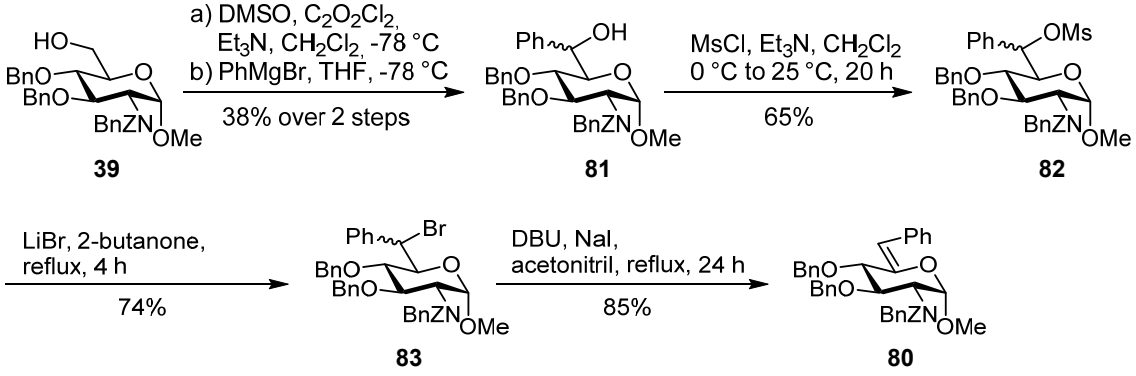

Synthesis of 6-phenyl enolic ortho ester **80** was performed analog to a procedure by Collins *et al.*[228] for the synthesis of glucose derivatives. The alcohol **39** was converted to

the aldehyde under Swern conditions followed by the introduction of phenyl via a Grignard-reaction with phenylmagnesium bromide. **81** was isolated as an *R*/*S*-isomeric mixture in a moderate 38% yield over two steps. Since benzyl carbamates are readily cleaved by nucleophiles[229], the Grignard-reaction was conducted at a low temperature of -78 °C resulting in a selective reaction of the aldehyde. Elimination was performed in a sequence of three steps. The reaction sequence consisting of mesylation to **82**, conversion into the corresponding bromides **83** and subsequent elimination was completed in moderate yield. The yield of **83** could be improved by using the raw product after mesylation, whereby a high yield of 80% over two steps was achieved. Elimination was performed under the same conditions as previously described by Collins *et al.* yielding **80** as a single isomer. Therefore, the (*Z*)-hexenpyranose **84** could be used as a reference to explain the *Z*-selectivity of the elimination reaction (**Figure 27**). The olefinic proton H6 in **80** showed a chemical shift of 6.18 ppm, which is in good accordance with enolic ortho ester **84** (6.26 ppm). The (*Z*)-configuration of the double bond in **84** could be verified with the help of X-ray crystallography.[228,230]

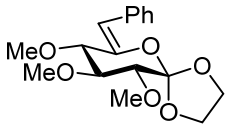

84

Figure 27 (*Z*)-Hexenopyranose 84[228]

The following carbocyclizaton (**Scheme 24**) is a key step of the presented synthesis since it yields the cyclohexanone ring structure with the phenyl group bound to the 5a-carba-position. This is accomplished under modified Ferrier-conditions[40], with mercury(II) sulfate as a promoter. For comparison, the rearrangement of the unmodified olefin **41** was accomplished in high yields (86%) using catalytically amounts of mercury(II) sulfate (**Scheme 9**). In the case of **80**, however, higher equivalents of the promotor $PdCl_2$ or $HgSO_4$ were necessary (**Table 5**). The product was obtained as a mixture of the isomers **78** and **79**. Through an increase of $HgSO_4$ from 20 mol% (**Table 5**, **Entry 2**) to 50 mol% (**Table 5**, **Entry 3**) the yield could be increased from 30% to 57%. The initially published reaction temperature of 80 °C led to the significant formation of a water-elimination side-product indicated by LC-MS. This elimination reaction is a well-described side-reaction as highly oxygenated cyclohexanones are prone to β-elimination and aromatization.[42,58] Therefore, the reaction temperature was decreased to 55 °C (**Table 5**, **Entry 4**), which led to a slight increase in product yield whereby the elimination product was not observed.

Scheme 24 Synthesis of cyclohexanones 78 and 79
Carbocyclisation of **80** through Ferrier rearrangement of **80**.

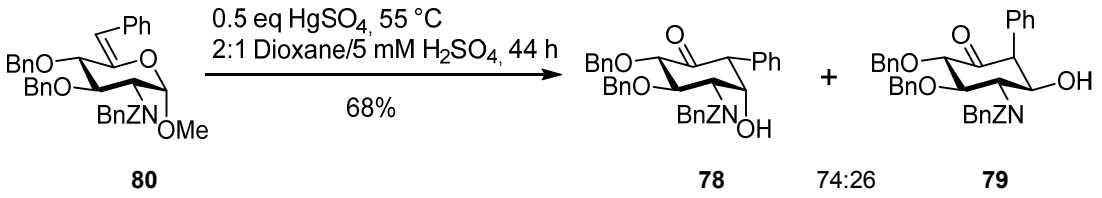

80 **78** 74:26 **79**

Table 5 Overview of the tested conditions for the Ferrier-rearrangement of 80.

Entry	Reagent	Amount reagent	T [°C]	Time	Amount elimination	Yield (**78**+**79**)	Ratio **78**:**79**
1	$PdCl_2$	60 mol%	80	113 h	20%	37%	n.d.
2	$HgSO_4$	20 mol%	80	20 h	9%	30%	n.d.
3	$HgSO_4$	50 mol%	80	18 h	23%	57%	73:27
4	$HgSO_4$	50 mol%	55	44 h	0%	68%	74:26

A moderate stereoselectivity of the rearrangement, with a product ratio of 74:26 in favor of the (5a*R*)-α-isomer was observed. The ratio of axial (**78**) to equatorial (**79**) orientation of the hydroxyl-group at C1 is almost identical to that of the unmodified cyclohexanones **42** (77:23, **Scheme 7**). This is in accordance with studies that showed a preference of the OH at C1 *trans* to the substituent at C3 (the mechanism and stereoselectivity of the Ferrier-rearrangement is described in **Section 1.1.1**, **Scheme 2**).[41] Influence by the configuration of the double bond of the substrate **80** could be excluded from studies utilizing a 6-deuterated hex-5-enose derivatives of glucose have shown that the stereoinformation of the olefin is lost during the Ferrier-reaction.[231]

Scheme 25 Ferrier Reaction of 6-*O*-acetyl-5-enopyranosides 85 and 86

The reaction mediated by $PdCl_2$ or $Hg(OCOCF_3)_2$ is shown with the respective ratio of 5a-OAc-cyclohexanones **87**, **88**, **89**, **90** (glucose) and **91**, **92**, **93**, **94** (galactose).

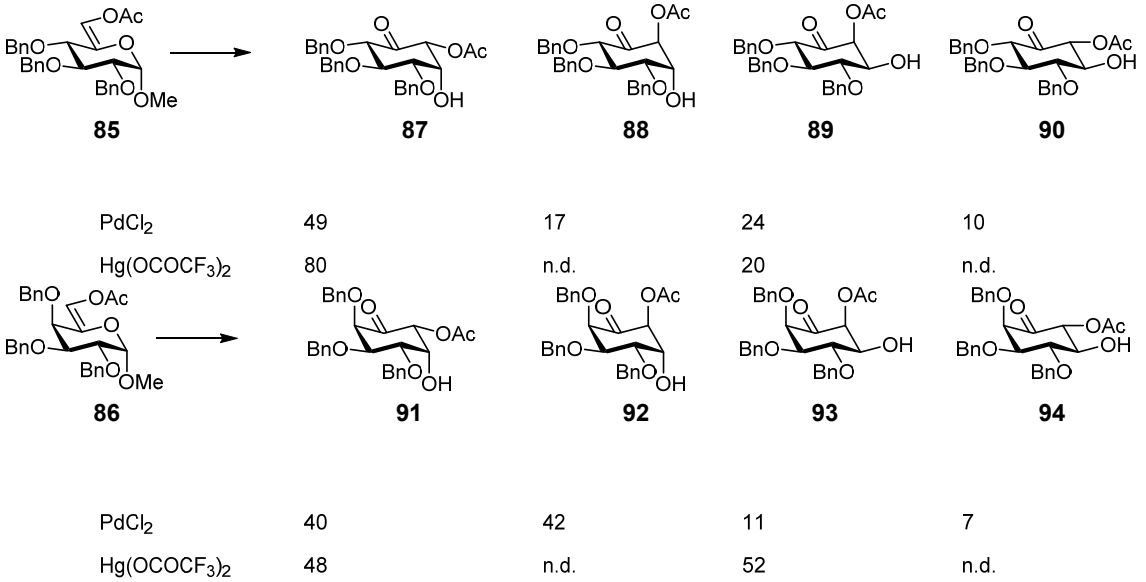

Upon synthesis of 5a-substituted carba-sugar through rearrangement of the respective hex-5-enose, both the stereochemistry at C1 as well as the possible orientations of the substituent at C5a needs to be considered. Takahashi *et al.*[44] have investigated the stereoselectivity of the Ferrier reaction using 6-*O*-acetyl-5-enopyranosides derived from glucose, galactose and mannose, mediated by either $PdCl_2$ or $Hg(OCOCF_3)_2$ (**Scheme 25**).[44] Even though the reasons for the stereochemistry at C5a are not entirely clear, the mechanism most probably differs depending on the promoter. The $Hg(OCOCF_3)_2$-catalyzed process yields only two diastereomers in the case of enol acetates of glucose **85** or galactose **86**. The $Pd(Cl)_2$ variant, however, provides four isomers. Considering the orientation of the substituent at C1 for **85**, $Hg(OCOCF_3)_2$ showed higher selectivity for the axially orientated hydroxyl group compared to $PdCl_2$ (80% vs. 66% axial). Surprisingly, **86** showed the opposite promotor-dependency (48% vs. 82 %), even though studies on 6-deoxyhex-5-enose derived from galactose stated an exclusive formation of the axial product in a Hg(II)-mediated Ferrier reaction.[41]

Scheme 26 Proposed mechanism for the Ferrier rearrangement of 80

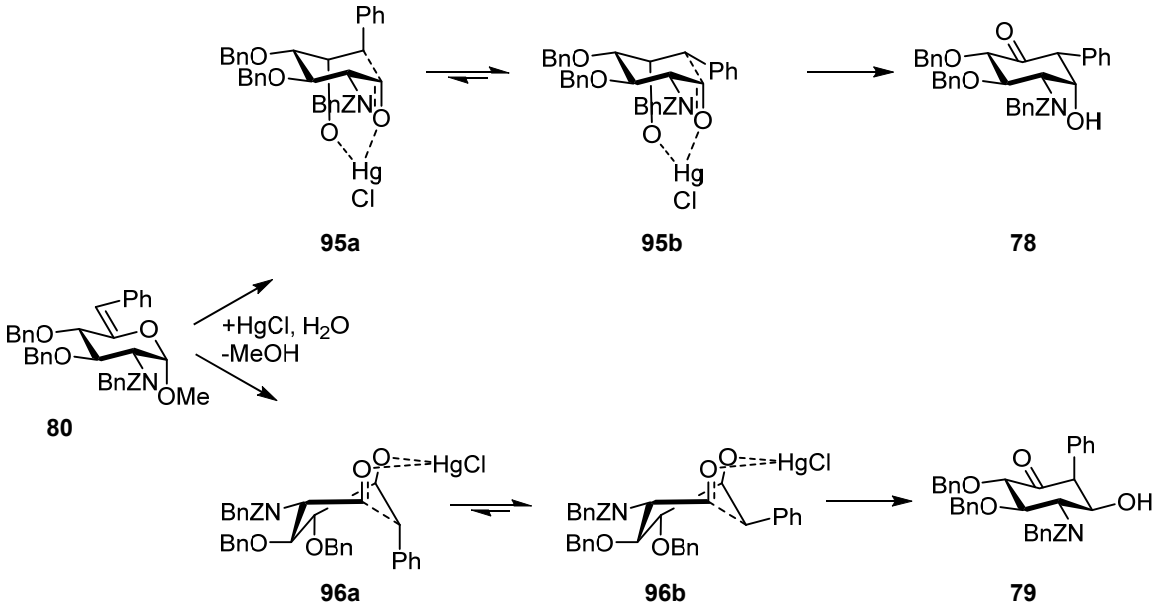

In the case of 6-phenyl-5-enopyranoide **80**, almost no difference could be observed in the ratio of axial to equatorial OH at C1 compared to the respective 6-deoxy-5-enopyranoside **41**. This finding implies that the phenyl-modification does not influence the relative stability of the transition states of the rearrangement leading to the axial or equatorial orientation of the hydroxyl group at C1 (**Scheme 26**). The proposed transition structures **95a**, **95b**, **96a**, and **96b** can be used to explain this observation. In general, the chair-like ring conformations of **95a** and **95b** can be expected to be favored compared to the twist boat-like conformations of transition states **96a** and **96b**. This is because of angle strain and eclipsing strain that are typical for boat conformation that both increase the energy relative to the chair-conformation.[232] The phenyl occupies a neutral position in either of the favored transition states **95b** and **96b**. Therefore, the effect of phenyl on the stereochemistry at C1 could be neglected. Furthermore, the equatorial phenyl in **95b** and **96b** correlates to the observed stereoselectivity in **78** and **79**. Although the proposed mechanism and transition states explain the experimental results, DFT calculation of the transition states involved in the Ferrier-reaction of both substrates **41** and **80** would allow a more comprehensive validation of the mechanism involved.

3.1.2.1 Alternatives for the Wittig reaction in the homologation reactions of 5a-phenyl-cyclohexanones

The objective of the following steps was the transformation of the C5 carbonyl of **78** and **79** into the hydroxy methylene group. The original synthesis of carba-sugars proposed by Barton *et al.* utilized a Wittig-reaction with methoxy methylenetriphenylphosphorane to

yield the olefin **97** (**Scheme 27A**). Due to the basic reaction conditions, an oxazolidine ring is formed from the *Z*-protection group and the 1OH group in the α-isomer of **42**. As β-isomers are not able to form the ring, this reaction increases the separability of the α-product. However, analog reaction conditions to synthesize **98** were not successful (**Scheme 27B**). Also, alternative olefination reactions such as HWE and Peterson olefination failed to yield the homologation product, even though the more stable unmodified cyclohexanones **42** were used as substrates. Drawbacks related to methoxy methylenetriphenylphosphorane are known. Besides the formation of butylidene ylides[233], low yields[43] and loss of substituents at C1 (methoxy or hydroxy)[234] are described for the use in carba-sugar preparation. Improvements concerning the yield of the Wittig reaction through utilization of methylenetriphenylphosphorane were described.[43] Indeed, the olefination of cyclohexanones **42** with methylenetriphenylphosphorane afforded the expected olefin in moderate 44% yield (yield regarding both isomers) (**Scheme 27C**). However, when the mixture of **78** and **79** was used as the substrate, only the elimination product **100** could be isolated (**Scheme 27D**).

Scheme 27 Comparison of Wittig homologation reactions of cyclohexanone 78, 79 and 42 for different reaction conditions.

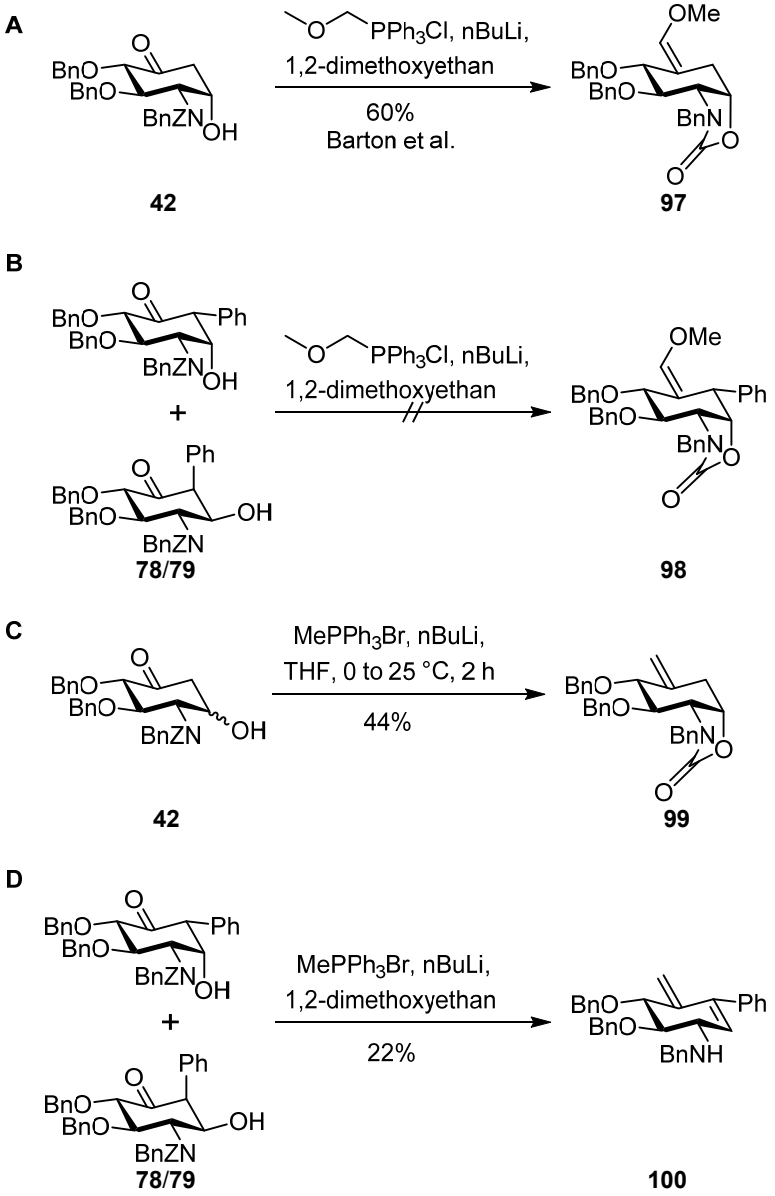

To decrease the risk of elimination due to the high basicity of the Wittig reaction conditions, Tebbe's olefination[235,236] was used. The direct olefination of the isomeric mixture of **78** and **79** only gave the olefination product **101** in a low yield of 16% (**Scheme 28**). The low yield and the isolation of only the equatorial 1OH product were associated with multiple reasons: First, TLC-analysis showed very similar retention of the olefin compared to the starting material, thereby impeding column purification. Second, the titanocene reagent and side-products thereof complicated the purification via flash chromatography, so that an additional purification step via RP-HPLC was required.

Scheme 28 Tebbe olefination of 78 and 79.

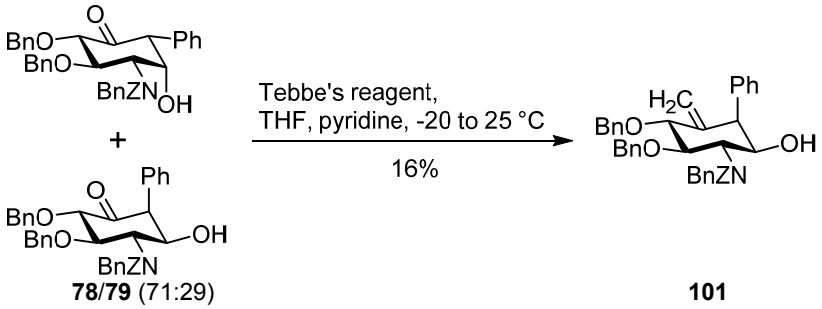

Tebbe olefination of the isolated axial isomer **78** (**Scheme 29**) afforded the olefin **102** in very low yield accompanied by separation problems during product isolation. Reaction monitoring after 3 h showed 84% consumption of the starting material and formation of several new peaks in the chromatogram. Via Flash chromatography of the reaction solution only insufficient separation of starting material and olefin was achieved.

Scheme 29 Tebbe olefination of the isolated isomer 78 with the 1OH-group in the axial orientation.

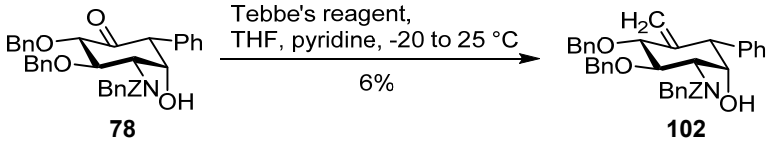

Due to the reasons that are given above (bad separation, low yield) and since the highly reactive Tebbe's reagent is known to also react with carbamates, Petasis reagent[191] was used as an alternative. It was shown that Z-protection groups remain stable if Petasis reagent was used for olefination at 70 °C.[194] Since thermolysis of dimethyltitanocene to the titanium carbene requires temperatures of 60 to 70 °C, the stability of the substrates **78** and **79** at 70°°C in varying solvents were tested (**Table 6**). Toluene and THF were tested as these are commonly used solvents in Petasis and Tebbe reactions. Cyclohexanones **78** and **79** both were stable in toluene for 16 h at 70 °C (**Table 6**, **Entry 1** and **3**). In THF, however, the formation of new peaks could be detected via HPLC. The remaining amount of both cyclohexanones was similar, with 82% in the case of **78** (**Table 6**, **Entry 2**) compared to 73% for **79** (**Table 6**, **Entry 3**).

Table 6 Overview of the stability of 78 and 79 at 70 °C depending on the solvent and the time.

Entry	Substrate	Solvent	T/°C	Time	Amount **78** or **79**
1	**78**	Toluene	70	16 h	100%
2	**78**	THF	70	16 h	82%
3	**79**	Toluene	70	16 h	100%
4	**79**	THF	70	16 h	73%

By this stability study, methylenation of **78** was performed with Petasis reagent in toluene at 65 °C. However, the reaction gave similar results as the Tebbe variant (**Scheme 30**). Although conversion of the starting material could be brought to almost completeness, mainly water-elimination side-product was detected via HPLC/LC-MS. Furthermore, the olefin **100** was formed, as previously observed in the Wittig-reaction (**Scheme 27**). Also in the case of the olefination of the β-1OH cyclohexanone **79**, a high ratio of water-elimination product was observed, while **100** was absent.

Scheme 30 Olefination of the isolated isomer 78 with Petasis reagent.

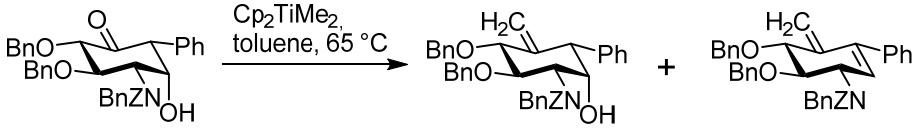

78 **102** **100**

Concerning the conducted stability tests in toluene at 70 °C (**Table 6**, **Entry 1** and **3**), the observed side-reactions can most probably be associated with the titanocene reagent. The protection of the 1OH group to decrease the probability of elimination was accomplished in the form of a silyl ether (**Scheme 31**).

Silylation of the hydroxyl group at C1 was conducted with the mixture of cyclohexanones **78** and **79** (**Scheme 31A**) analog to that of the 5a-unmodified cyclohexanones **42** (**Section 3.1.1**, **Scheme 9**). The difference in R_f (TLC) of **103** and **104** on normal phase silica was $\Delta R_f \approx 0.05$, thus represents a challenging separation problem. Nevertheless, 75% of the total amount of the axial-OH isomer **104** could be isolated in a single fraction, while the rest of **103** and **104** formed a mixed fraction (**103**/**104**-ratio of 69:31). The latter was transformed into the corresponding olefins **76** and **77** in a low yield of 33%. The isomeric mixture of **76** and **77** was separable via normal phase flash chromatography. For comparison, the olefination of pure **103** (**Scheme 31B**), gave **76** in a yield of 33%,

while 13% of starting material could be recovered. In conclusion, protection of the 1OH group in cyclohexanones **78** and **79** as *tert*-butyldimethylsilyl ethers significantly increased the yield of olefination with Petasis-reagent.

Scheme 31 Synthesis of both isomers 76 and 77 of the 5a-phenyl modified olefin.

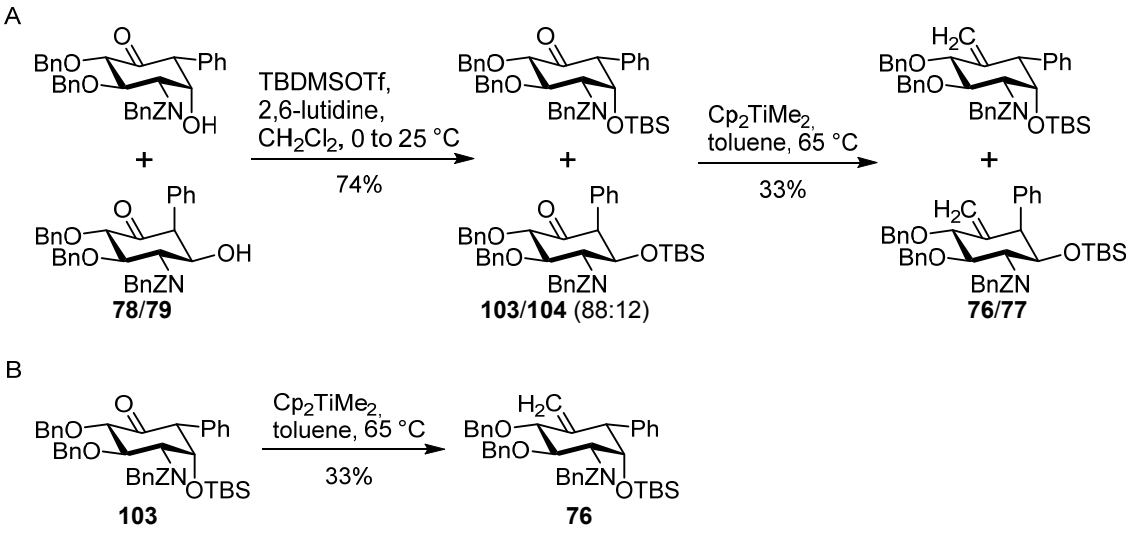

For the transformation of olefins **76** and **77** to the respectively protected carba-sugars with the hydroxy methylene group at C5, two different synthetic approaches were necessary. In the case of **76**, the olefin was transformed to the hydroxy methylene group by hydroboration and subsequent oxidation (**Scheme 32**). **73** was afforded as a single product in a good yield of 86%. The axial configuration at C5 could be determined by a small coupling constant ($^3J_{H4\text{-}H5}$ = 5.09 Hz)[c] between H4 and H5, while an NOE correlation between H3 and H5 was absent. The thermodynamically favored isomer **107** was accessible through oxidation to the corresponding aldehyde **105** followed by isomerization, analog to procedures described for unmodified carba-sugars.[43,237] The alcohol was transformed to the aldehyde by treatment with 2-iodoxybenzoic acid (IBX) in good yield (72%) with a $^3J_{H4\text{-}H5}$ = 5.2 Hz coupling as a clear indicator of the axial configuration at C5.

[c] Determined via H,H-COSY

Scheme 32 Synthesis of protected (5a*R*)-phenyl-carba-sugar analog of α-D-glucosamine 107.

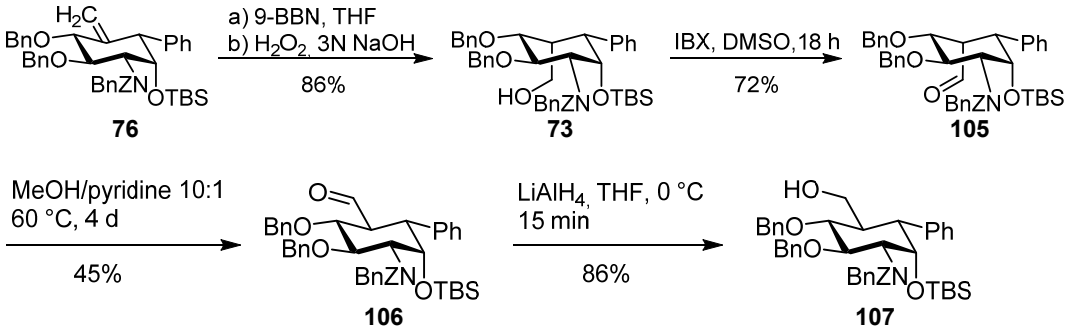

Monitoring of the isomerization of **105** in a mixture of MeOH and pyridine (60:30) at 60 °C[43] to give **106**, led to a large ratio of side-product due to the loss of OBn, as determined by LC-MS. Therefore, different conditions were screened via HPLC monitoring of each reaction over time (**Table 7**). The temperature was fixed at 60 °C, whereas both the concentration of the substrate **105** and the ratio of MeOH and pyridine was varied. A clear change of retention time from **105** to **106** could be observed indicating the progress of isomerization. The conducted study indicated that significant elimination arose for all reaction conditions and could only be decreased to 33% (**Table 7**, **Entry 7**). A major factor that influenced the amount of isomerization product **106** was the concentration of the starting material. The decrease of **105** concentration showed a dramatic effect that led to the almost complete loss of the aldehyde at a substrate concentration of 5 mM (**Table 7**, **Entry 6**). The increase of the MeOH/pyridine ratio showed a slightly positive effect (**Table 7**, **Entry 2**), as it increased the yield of **106** while the amount of elimination remained stable. In the case of very high proportions of MeOH (89:1, **Table 7**, **Entry 3**) or pure methanol (**Table 7**, **Entry 4**), however, the isomerization was slowed down. This led to low conversions of starting material within 78 hours while elimination in a range of 40 to 50% occurred. Nonetheless, a yield of the isolated **106** of 45% was achieved when the conditions from **Entry 7** were used on a larger scale (**Scheme 32**). Besides a difference in retention time (3.1 min **105** vs. 3.5 min **106**, 80-87% MeCN in 5 min, Kinetex EVO C18, 2.6 µm, 0.8 mL/min) the different isomers could also be distinguished by the chemical shifts of the aldehyde protons (10.29 ppm **105** vs. 9.65 ppm **106**). Furthermore, large $^3J_{HH}$ coupling constant of 12.6 Hz between H5a and H5 indicated the equatorial orientation of the aldehyde at C5. Transformation to the corresponding alcohol **107** succeeded in a rapid reduction with lithium aluminum hydride in high yield (86%).

Table 7 Overview of different conditions tested for the isomerization of the aldehyde 105. Only the end-point of each reaction after 78 hours is shown

Entry	Ratio MeOH/pyr	Conc. **105**/mM	T/°C	Time/ h	Amount **106**	Amount elimination	Amount **105**
1	60:30	25	60	78 h	41%	52%	6%
2	80:10	25	60	78 h	48%	49%	3%
3	89:1	25	60	78 h	18%	52%.	30%
4	90:0	25	60	78 h	12%	41%.	47%
5	60:30	10	60	78 h	13%	86%	1%.
6	60:30	5	60	78 h	5%	95%	n.d.
7	80:10	100	60	64 h	63%	33%	3%

For the conversion of the terminal olefin of **77** into the hydroxy methylene group, a different approach was followed (**Scheme 33**). It comprised the epoxidation and the subsequent radical epoxide opening analog to the synthesis of the protected (5a*R*)-fluoro-carba-α-D-GlcN **53** (**Scheme 16**). Epoxidation to **74** was accomplished after eight hours in a yield of 82%. NMR-analysis of **74** was challenging because conformational flexibility led to signal broadening. Through NMR measurements at -40 °C, however, three conformers could be distinguished. Nevertheless, particular assignment of ring-conformations to the different sets of signals was not possible. The configuration of C5 was determined through ROESY experiments that showed strong NOE correlation between the two methylene protons and both H3 and H1. This indicates an axial orientation of the methylene in the most stable $^4C_1$ chair conformation, while the oxygen of the epoxide occupies the equatorial position (**Scheme 33**). The epoxidation reaction of **77** with 8 hours was considerably faster compared to the epoxidation of the fluorinated olefin **36** with 14 days (**Scheme 15**). Thus, this change in kinetics reflects the electronic effect of the fluorine, which most probably lowered the reactivity of **36**. Transformation of **74** to the terminal alcohol **108** was accomplished regioselectively by titanocene promoted radical epoxide opening.[201,202] **108** was isolated as the 5a*S*-isomer in a good yield of 65%. The equatorial configuration of the hydroxy methylene group was confirmed by large coupling constants for H4 of $^3J_{HH}$ = 11.6 and 9.1 Hz

Scheme 33 Synthesis of protected (5a*S*)-phenyl-carba-sugar analog of β-D-glucosamine 108.

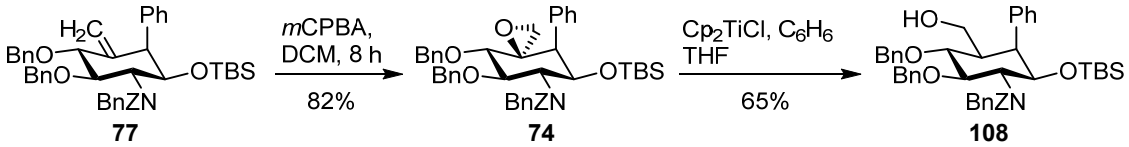

The observed stereoselectivity resembles that of the analog epoxide opening of the fluorinated α-carba-sugar precursor **34** (**Section 3.1.1**, **Table 3**). The effects that influence the stability of the proposed transition states, however, differ from the fluoro-carba-precursor.The high stereoselectivity of the epoxide opening can be explained with the help of the proposed transition structures of the hydrogen abstraction by the carbon-centered radical intermediate of **74** (**Figure 28**). On the one hand, the steric impact of the OTBS group with the incoming CHD in **TSA** (transition structure A) as well as the CH_2OTiCp_2Cl group in **TSB** is absent. On the other hand, the steric effect of the β-substituent becomes a key factor due to the size of phenyl compared to fluorine. Steric repulsion between the phenyl group and the incoming CHD in the case of **TSB** makes a reaction via this transition state unlikely. The preference for **TSA** is in good agreement with the observed D-configuration of **108**. It is well described in the literature that the attack of six-membered cyclic radicals occurs anti to axial substituents in β-position to the radical center.[211]

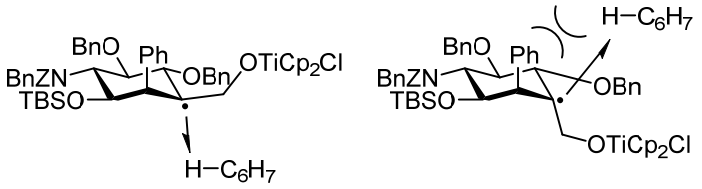

Figure 28 Schematic structures of the proposed transition states of the hydrogen abstraction of the radical intermediate during the epoxide opening of 74.

A test reaction to synthesize the 5a*R*-phenyl-carba-α-D-sugar **107** from **76** with the sequence of epoxidation and regioselective epoxid-opening resulted in two isomers of the epoxide. However, none of these gave the desired product upon treatment with Cp_2TiCl.

Since phosphorylation of sugar-derivatives greatly increases the rate of self-cleavage of the *glmS* ribozyme[89], both isomers of the 5a-phenyl-carba-sugar were phosphorylated. **107** was transformed into the protected phosphate **109** in good yield (78%) by treatment with dibenzyl *N*,*N*-diisopropylphosphoramidite and subsequent oxidation with *m*CPBA.

(**Scheme 34A**).[166] The analog reaction with **108** gave **110** in a slightly lower yield of 61% (**Scheme 34B**).

Scheme 34 Phosphorylation of 107 and 108.

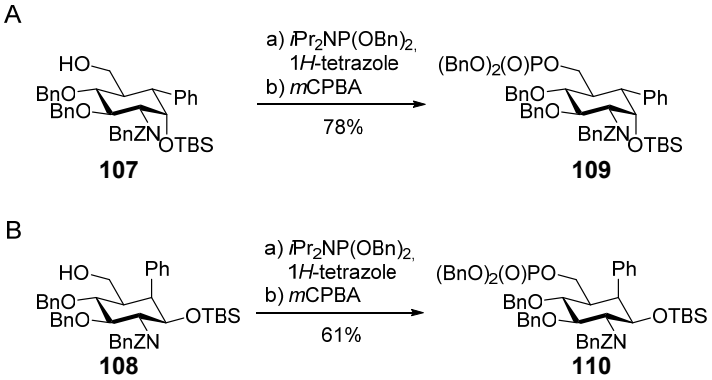

In the next step, the TBS-group was removed from the phosphorylated carba-sugars **109** and **110**. Desilylation of **109** was conducted under buffered conditions with an excess of TBAF (12 equivalents) (**Scheme 35A**). After a reaction time of 20 h, HPLC-analysis showed a conversion of 99%. The product **111** was isolated in 43% yield. However, large amounts of side-product (51%) were formed. Mass analysis of the side-product equals **112**, which could be explained by the formation of an oxazolidine ring due to the high basicity of TBAF. Deprotection of **109** under less basic conditions with TAS-F (12 equivalents) and water (10 equivalents) provided **111** in high yield (63%) (**Scheme 35B**). Although the reaction was carried out for 66 h, the conversion of the substrate only reached 73% (HPLC). Nevertheless, only 6% of side-product was observed via HPLC. The analog desilylation of the phenyl-β-carba-GlcN6P precursor **110 (Scheme 35C**) with TBAF was completed after 56 hours, and the alcohol **75** was isolated in 58% yield.

Scheme 35 Comparison of the removal of the TBS protection group from 109 and 110.

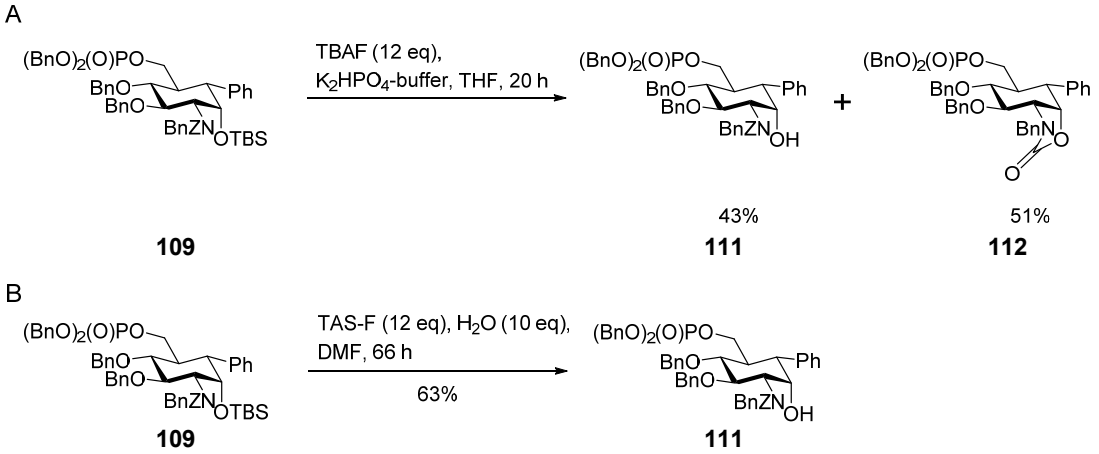

C

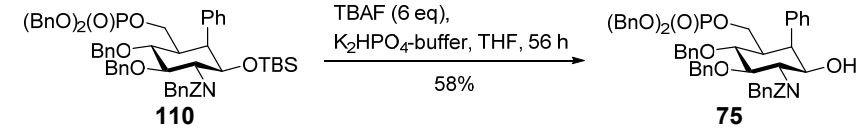

The final removal of the benzyl protection groups from **109** was accomplished via heterogeneous hydrogenolysis (**Scheme 36**). The conditions that were already successfully applied for final deprotection of the fluoro-carba variants **67** (**Scheme 20**) and **71** (**Scheme 21**) gave **72** in an isolated yield of 76% after RP-HPLC purification. In conclusion, the synthesis of 5aS-phenyl-carba-α-D-GLCN6P **72** starting from methyl-glucopyranoside **26** required 18 steps with an overall yield of 0.1%. Upon comparison of the synthesis **72** to the fluoro-derivative, an additional four steps were required, mainly due to the three-step elimination sequence (**Scheme 23**).

Scheme 36 Synthesis of (5aS)-phenyl-carba-α-D-glucosamine-6-phosphate 72.

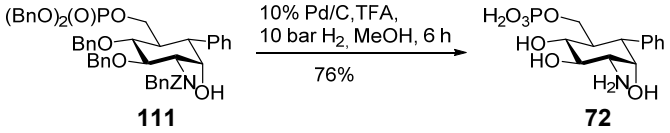

The analog debenzylation of **75** proceeded slower, and completeness of the reaction was observed only after 23 h compared to 6 h for **111** (**Scheme 37**). Surprisingly, the phenyl-carba-sugar **113** was not detected via LC-MS analysis. Instead a peak with significantly higher retention time (t_r = 4.8 min) to **72** (t_r = 0.4 min) was found (gradient 0-40% acetonitrile in 20 min, C18-HPLC). The detected mass (236.127 m/z) corresponded to the molecular formula $C_{13}H_{17}NO_3H^+$ that indicated the loss of the phosphate and one double bond equivalent (DBE=6 for **113**, DBE=5 for **112**) more than expected. As double bonds could be excluded with the help of NMR, the formation of the bicyclic ether **114** explains both the observation in LC-MS and NMR. The ring formation between C6 and 1OH requires a $^1C_4$ chair conformation to bring 1OH near C6. Two opposing influences determine the energy of the $^1C_4$ conformation. On the one hand, five substituents in an axial configuration increase the energy, on the other hand, the equatorial configuration of the bulky phenyl group decreases steric strain. Two conformers of **75**, which were distinguishable via NMR, indicated conformational flexibility. A strong downfield shift of C1 (78.8 ppm) and small coupling constants $^3J_{H2\text{-}H3}$ = 5.8 Hz and $^3J_{H2\text{-}H3}$ = 2.1 Hz confirm the assumed bicyclic structure of **114**.

Scheme 37 Final deprotection of phenyl-carba-β-D-glucosamine-6-phosphate precursor 75 leading to solely formation of bicyclic ether 114.

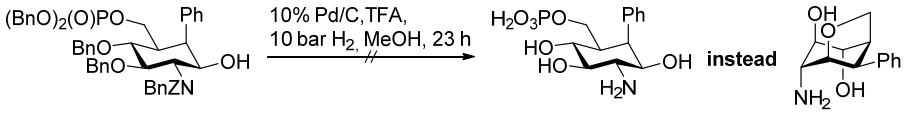

75 **113** **114**

Sun *et al.* observed a similar bicyclic derivative of carba-β-L-gulose **116**.[43] They used the reaction shown in **Scheme 38** to support the axial configuration of the hydroxy methylene group at C5 in **115**. In their case, the resulting bicyclic lactone occupied the $^4C_1$ conformation, bringing C6 and 1OH nearby because of the inverted configuration at C5 and C1 compared to **75**. To explain the unexpected side-reaction of **75**, the ability of the phosphate to act as a leaving group needed to be analyzed. From a chemical view, phosphate represents a poor leaving group. In nature, however, phosphate is the leaving group of choice that requires tunable stability towards hydrolysis in the absence or presence of enzymes.[238] Because of this contrast, intensive research has been carried out to understand the reactivity and mechanism of the cleavage of phosphate esters.[239,240] Cleavage of either the C-O or P-O bond can occur, whereas a preference for C-O cleavage could be demonstrated at low pH.[241,242] This effect could also be crucial for the formation of **114** as TFA in methanol was used in the heterogeneous hydrogenolysis of **75**. The low pH may have led to selective C-O over P-O cleavage.[242]

Scheme 38 Transformation of the carba-β-L-gulose derivative 115 into the lactone 116 performed by Sun *et al.* to prove the axial conformation at C5.[43]

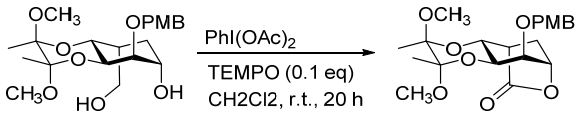

115 **116**

3.2 Induction of *glmS* ribozyme self-cleavage by 5a-modified carba-sugar analogs of GlcN6P

In a screening of a small library of synthetic analogs of GlcN6P Lünse *et al.* identified carba-α-D-glucosamine-6-phosphate as the most potent artificial cofactor of *glmS* ribozyme cleavage known.[105] The 5a-carba position represents a versatile entity for the study of structure-activity relationship (SAR). This is the case since the methylene group is readily modified during synthesis, in contrast to the ring oxygen of natural carbohydrates. Thus, the 5a-modified carba-sugars shown in **Figure 29A** were investigated for their influence on *glmS* ribozyme self-cleavage in a metabolite-induced

self-cleavage assay (**Figure 29B**). For this experiment, the well-characterized *glmS* ribozymes of the two bacterial species *B. subtilis* and *S. aureus* were used.[73,105]

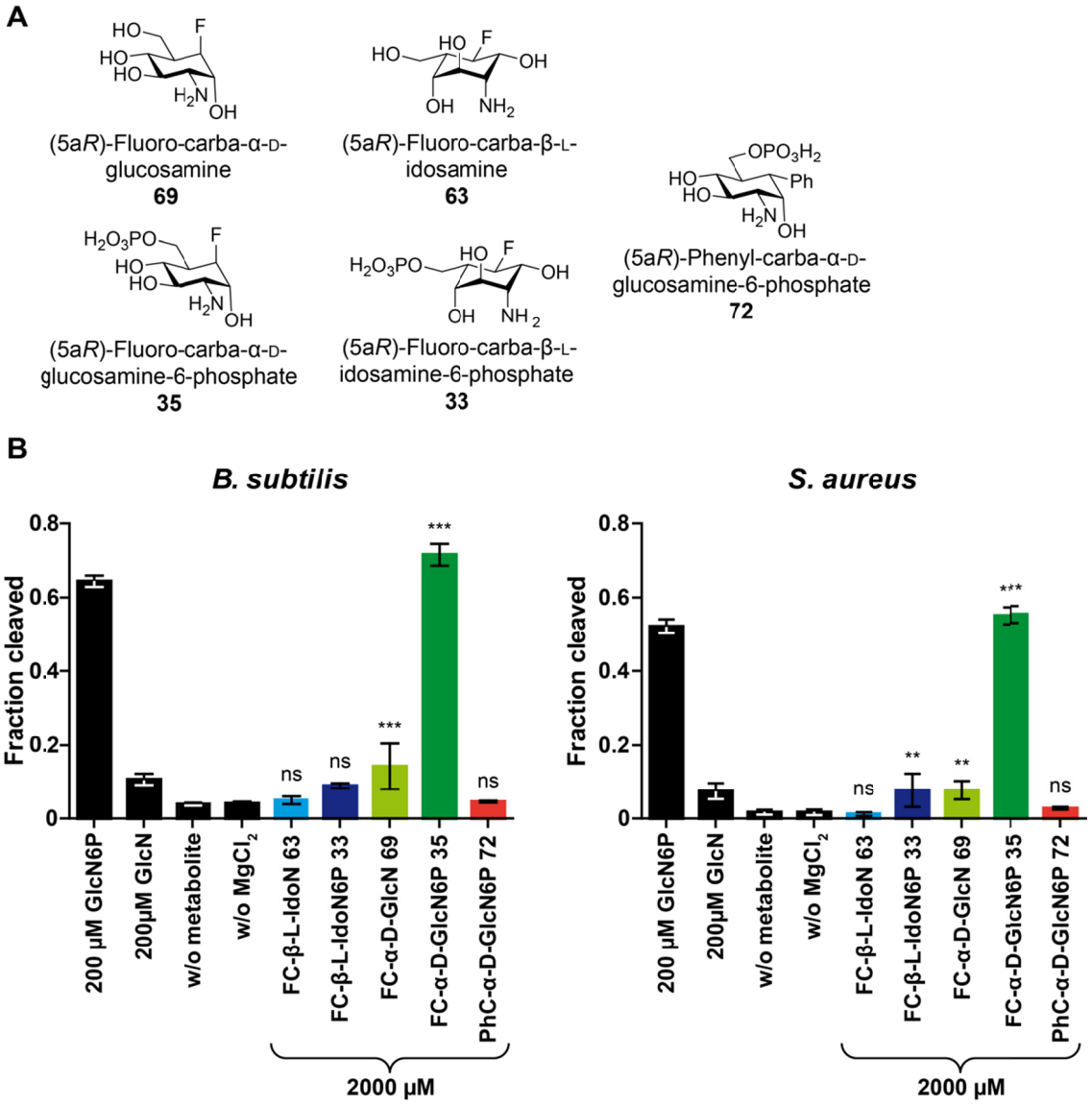

Figure 29 *In vitro* activity of the 5a-modified carba-sugar analogs of GlcN and GlcN6P for *S. aureus* and *B. subtilis glmS* ribozyme cleavage
(A) Carba-sugars synthesized in this work and used in this screening. (B) Screening results depicted as fraction cleaved of 5'-^{32}P-labeled *glmS* ribozyme RNA mediated by 2000 µM of the respective carba-sugar analogs of unphosphorylated carbohydrates **63** (blue), **69** (green), or phosphorylated variants **33** (dark blue), **35** (dark green), and **72** (red). For comparison, the cleavage in the presence of 200 µM GlcN6P and GlcN and the absence of metabolite or Mg^{2+} is shown (black). Error bars are s.d. of experiments carried out at least in triplicate. One-way ANOVA with Tukey's multiple comparison test demonstrates statistically significant (*** $P < 0.001$, ** $P < 0.01$) or not significant (ns $P > 0.05$) fraction of cleaved RNA compared to both negative controls w/o $MgCl_2$ and w/o metabolite. All experiments were carried out by Anna Schüller.

Among all screened compounds, (5a*R*)-fluoro-carba-α-D-glucosamine-6-phosphate **35** shows the highest cleavage ratio at a concentration of 2000 µM, which is comparable to

that of the GlcN6P (control) at 200 µM. **69**, the unphosphorylated variant of **35**, showed significant cleavage with a ratio of 0.14 or 0.08 cleaved RNA (*B. subtilis* or *S. aureus*, respectively). The cleavage is much lower compared to **35**, but similar to the respective unphosphorylated control GlcN at 200 µM. The fraction of cleaved RNA in the presence of **69** and **35** relative to GlcN6P was independent of the bacterial species. However, the absolute values vary between *S. aureus* and *B. subtilis* as higher cleavage was observed in the case of *B. subtilis*. Fluoro-carba-β-L-idosamine derivatives **63** and **33**, on the other hand, did not show consistent activity between the ribozymes of both species. The unphosphorylated variant **63** did not induce any cleavage, while **33** showed significant ($P < 0.01$) self-cleavage only of the ribozyme from *S. aureus*. The 5a-phenyl variant of α-D-glucosamine-6-phosphate **72** was completely inactive in the induction of *glmS* ribozyme self-cleavage.

For GlcN6P as well as carba-α-D-GlcN6P it was shown that the phosphate group is critical for the binding to the RNA in the binding pocket.[100,105] Indeed, this is also the case for fluoro-carba-GlcN **69**, which induced far less self-cleavage of the *glmS* ribozymes compared to its phosphorylated variant **35**. Besides the well-characterized *glmS* ribozymes of *S. aureus*[105] and *B. subtilis* also the counterparts from *C. difficile* and *L. monocytogenes* were used to investigate metabolite-induced self-cleavage in the presence of the 5a-fluorinated carba-sugars **63**, **33**, **69** and **35** (**Figure 30**).[243] These two *glmS* ribozymes present in human pathogenic strains were synthesized after the prediction in the 5'-UTR of the *glmS* RNA by McCown *et al.*.[98] A complete characterization of both ribozymes performed by Anna Schüller validated their functionality as cofactor-dependent self-cleaving ribozymes.[244] The cleavage of *C. difficile* and *L. monocytogenes glmS* ribozymes in the presence of **35** resembles that of GlcN6P, thus showing consistent behavior among bacterial species if compared to *S. aureus* and *B. subtilis*. However, in the case of the ribozyme from *C. difficile,* only weak cleavage by fluoro-carba sugar derivatives **63**, **33** and **69** as compared to controls was observed. This resulted in a low significance ($P < 0.05$) activity only in the case of fluoro-carba-GlcN **69**. The high background cleavage and the large error bars of the controls, however, explain this discrepancy to the other *glmS* ribozymes. The tendencies in the cleavage of *L. monocytogenes*, in turn, reflected those of *S. aureus*, with significant cleavage for both fluoro-carba-IdoN6P **33** and fluoro-carba-GlcN **69**. The phosphorylation of fluoro-carba-GlcN **69** strongly affected the *L. monocytogenes glmS* ribozyme self-cleavage. This is consistent with concentration-dependent analyses of GlcN- and GlcN6P-induced cleavage, which revealed a factor of ~5000 between their EC_{50} values (unpublished results). The *glmS* ribozymes generally show high

discrimination between phosphorylated and unphosphorylated sugars. However, this is especially pronounced in the case of *L. monocytogenes*.

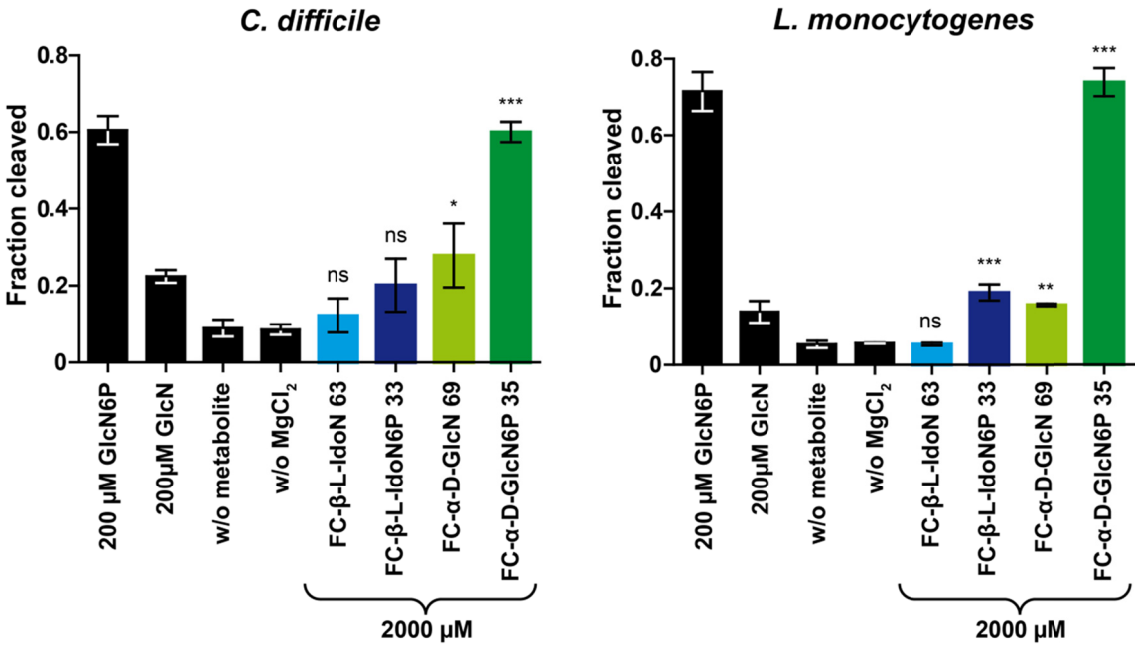

Figure 30 *In vitro* activity of the 5a-fluorinated carba-sugar analogs of GlcN and GlcN6P for *C. difficile* and *L. monocytogenes glmS* ribozyme cleavage
The fraction of cleaved *glmS* ribozyme induced by GlcN6P and GlcN (black, 200 µM) is compared to carba-sugar derivatives **63** (blue), **69** (green), **33** (dark blue), **35** (dark green) at a concentration of 2000 µM. All experiments were carried out by Anna Schüller.

On the basis of the screening of the 5a-modified carba-sugars for *glmS* ribozyme cleavage at a high concentration, the most active (5a*R*)-fluoro-carba-α-D-GlcN6P **35** was used to investigate the induction of *glmS* ribozyme self-cleavage in a concentration-dependent analysis (**Figure 31**). For these experiments, only the well-established *glmS* ribozymes of *B. subtilis* and *S. aureus* were used.

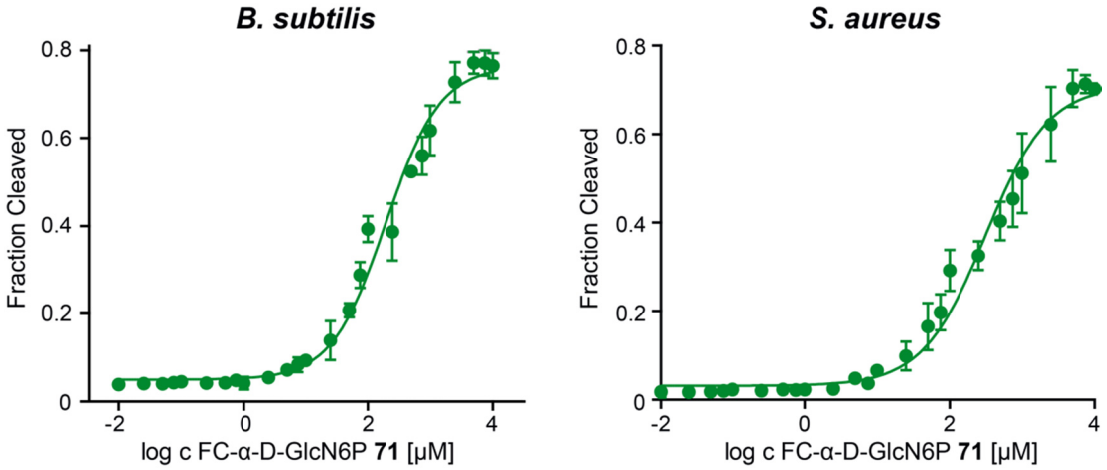

Figure 31 Self-cleavage reaction of the *glmS* ribozymes from *B. subtilis* and *S. aureus* in the presence of increasing concentrations of (5a*R*)-fluoro-carba-α-D-GlcN6P 35.
Error bars are s.d. of experiments carried out at least in triplicate. All experiments were performed by Anna Schüller.

The plotted data of the fraction of cleaved *glmS* RNA against the logarithmic concentrations of **35** were fitted by non-linear regression to a sigmoidal dose-response curve. Half-maximal effective concentrations (EC_{50}) were determined, which allow a valid comparison between the effectivity of **35** and the natural co-factor GlcN6P as well as the established artificial activator carba-GlcN (**Table 8**).The EC_{50}-values of **35** are much higher with 312 ± 32 µM and 196 ± 17 µM for *S. aureus* and *B. subtilis*, respectively. **35** is a factor of ~50 less active on the *S. aureus glmS* ribozyme compared to carba-GlcN6P and even ~100-times less active compared to GlcN6P. In the case of the *B. subtilis glmS* ribozyme, only the EC_{50} of carba-GlcN6P is known to literature, which is also ~100-times more effective compared to **35**. This difference is discussed on the basis of molecular docking studies later in this work (**Section 3.3**).

Table 8 EC_{50}-values of metabolite-induced self-cleavage of *glmS* ribozymes from *S.aureus* and *B. subtilis* by 35, carba-GlcN6P and GlcN6P.

	35	carba-GlcN6P	GlcN6P
		EC_{50} [µM]	
S. aureus	312 ± 32	6.2 ± 0.7[105]	3.6 ± 0.4[105]
B. subtilis	196 ± 17	2.2 ± 0.4[245]	n.d.

The determination of pseudo-first-order rate constants (k_{obs}) for the promotion of *glmS* ribozyme self-cleavage of *B. subtilis* and *S. aureus* (**Figure 32**, **Table 9**) confirmed the results of the concentration-dependent cleavage (**Figure 31**, **Table 8**).

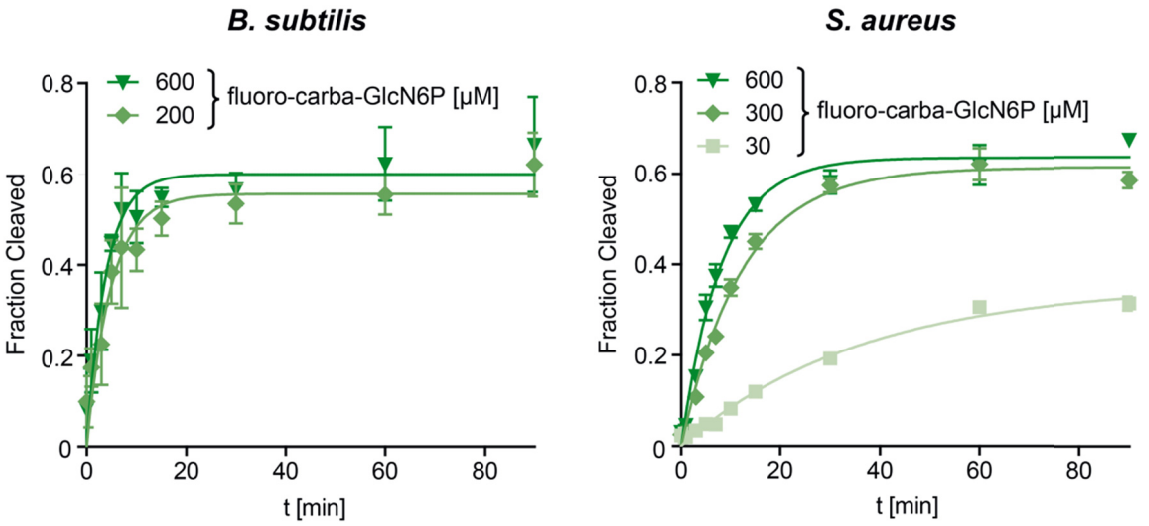

Figure 32 Cleavage rates of *B. subtilis* and *S. aureus glmS* ribozymes at different concentrations of 35 (shades of green)
The fraction of cleaved RNA as a function of time is shown. Error bars are s.d. of experiments carried out at least in triplicates. Experiments were performed by Anna Schüller.

In general, much higher self-cleavage rates were determined for the *glmS* ribozyme of *B. subtilis* when the same concentration of **35** was used (k_{obs}(*B. subtilis*, 600 µM) = 0.258 ± 0.036 and k_{obs}(*S. aureus*, 600 µM) = 0.122 ± 0.007 min^{-1}). About the self-cleavage of *B. subtilis glmS* ribozyme in the presence of 200 µM GlcN, fluoro-carba-GlcN6P **35** showed a significantly higher self-cleavage rate. The direct comparison to carba-GlcN6P and GlcN6P, however, reflects the drop in activity of **35** already observed by a higher EC_{50}. Very similar k_{obs}-values were determined at concentrations that resemble the EC_{50}-values of **35** and GlcN6P, respectively (k_{obs}(*B. subtilis*, **35**, 200 µM) = 0.204 ± 0.030 min^{-1} and k_{obs}(*B. subtilis*, GlcN6P, 2 µM) = 0.187 ± 0.048 min^{-1}). Similar trends among the listed *glmS* ribozyme activators were observed in the case of *S. aureus glmS* ribozyme. For instance, 300 µM and 2 µM of **35** and GlcN6P show similar rate-constants of 0.081 ± 0.003 min^{-1} and 0.068 ± 0.014 min^{-1}, respectively.

Table 9 k_{obs}-values of 35, carba-GlcN6P and GlcN6P, determined for the cleavage of the *glmS* ribozymes of *B. subtilis* and *S. aureus*.

B. subtilis

Conc.	**35**	carba-GlcN6P^{245}	GlcN6P^{245}	GlcN^{245}
[µM]	k_{obs} [min^{-1}]			
600	0.258 ± 0.036	n.d.	n.d.	n.d
200	0.204 ± 0.030	1.190 ± 0.302	1.749 ± 0.588	0.128 ± 0.019
20	n.d.	0.222 ± 0.027	0.397 ± 0.054	n.d
2	n.d.	0.083 ± 0.016	0.187 ± 0.048	n.d.

S.aureus

Conc.	**35**	carba-GlcN6P^{105}	GlcN6P^{105}	GlcN^{245}
[µM]	k_{obs} [min^{-1}]			
600	0.122 ± 0.007	n.d.	n.d.	n.d.
300	0.081 ± 0.003	n.d.	n.d	n.d.
200	n.d.	0.153 ± 0.012	0.177 ± 0.015	0.065 ± 0.005
30	0.027 ± 0.002	n.d.	n.d.	n.d.
20	n.d.	0.095 ± 0.008	0.107 ± 0.010	n.d.
2	n.d.	0.060 ± 0.012	0.068 ± 0.014	n.d.

3.3 Molecular docking studies

The noticeable difference between the EC_{50} of carba-GlcN6P and its 5a-fluorinated counterpart **35** are surprising considering the small alteration given by the substitution of the axial hydrogen at C5a by fluorine. Therefore the influence of the 5a-fluorine on *glmS* ribozyme cleavage was evaluated and the binding to RNA in the catalytic core and the ability to act as an acid-base catalyst[93] were taken into account.

As already described in **Section 1.3.1**, the ligand binding pocket of the *glmS* ribozyme is rigid and the binding of the natural metabolite GlcN6P does not induce a considerable rearrangement.[88] Furthermore, the sequences of the *glmS* ribozymes identified so far exhibit a high uniformity leading to a consensus model.[98] As a highly-conserved part of this model, the nucleotides G1, C2, and G65 are at least 97% conserved while A50 and

U51 are 90% conserved (The numbering of the nucleotides corresponds to *T. tengcongensis*, **Figure 33**). Position 66 is occupied by a nucleotide with a pyrimidine base which is also 97% conserved.[98] The latter alters the hydrogen-bond pattern and thus the recognition of the natural metabolite GlcN6P. The N2 of G66 in *T. tengcongensis*, as well as *L. monocytogenes,* can form a hydrogen bond to the anomeric OH of the sugar ligand, whereas this contact is lost in the case of *S. aureus*, *B. subtilis,* and *C. difficile* (**Figure 33**). Nevertheless, more than ten other potential hydrogen-bonds are preserved among the *glmS* ribozymes discussed in this work.[86] Therefore, the high-resolution crystal structures of the *T. tengcongensis glmS* ribozyme is a good starting point for reliable predictions about the suitability of potential activators.

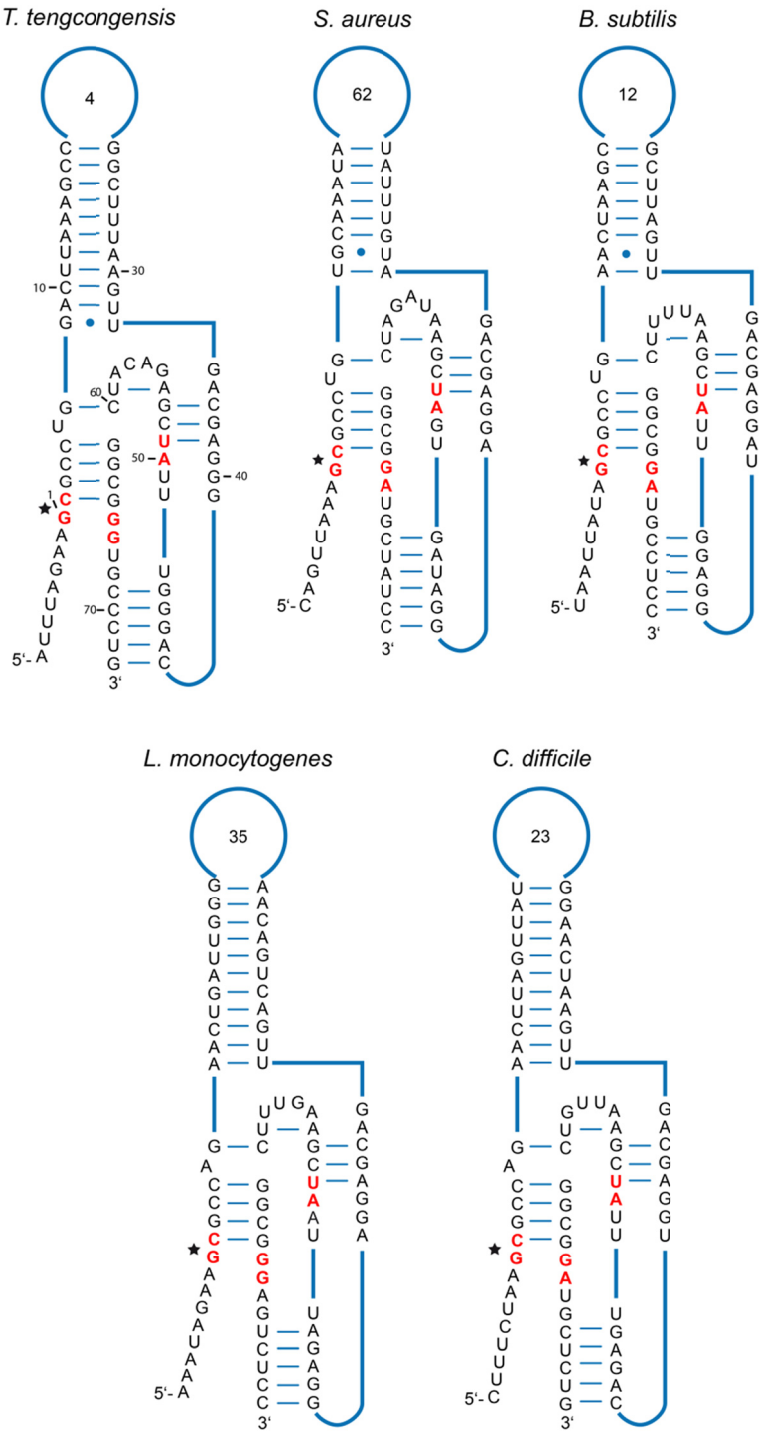

Figure 33 Predicted secondary structure of the minimal functional core of the *glmS* ribozymes from *T. tengcongensis*, *S. aureus*, *B. subtilis*, *L. monocytogenes* and *C. difficile*
The numbering of the nucleotides that is shown for *T. tengcongensis* is used for the nucleotides that correspond to these positions in the other species, even though the different loop size would change the counting. The nucleotides that form hydrogen bonds with the natural metabolite GlcN6P according to crystal structures[88,95] are colored red.

In the case of the artificial *glmS* ribozyme activator carba-GlcN6P, the substitution of the ring oxygen with methylene leads to the loss of one hydrogen-bond acceptor. It is hard to estimate if the replacement of either of the methylene-hydrogen atoms by fluorine would

be able to restore this interaction. The potential of fluorine to act as a hydrogen-bond acceptor is still widely debated.[246,247] Although sufficient proof is given to accept that organic fluorine is capable of forming hydrogen bonds, it is considered a weak interaction.[248]

In addition to the above-mentioned attracting interaction with the *glmS* ribozyme, the repulsive interaction of the modifications at C5a and the ligand binding pocket must be considered. These steric factors have a significant influence on the ligand affinity because of the rigid *glmS* ligand binding site. The substitution of the axial hydrogen of carba-GlcN6P by fluorine could be considered a small modification. However, the van-der-Waals (VdW) radius of fluorine is closer to oxygen than hydrogen (r(F) = 1.47 Å, r(H) = 1.20 Å, r(O) = 1.52 Å)[249]. Furthermore, the C-F bond is approximately 0.3 Å longer compared to C-H (d(C-F) = 1.40 Å, d(C-H) = 1.10 Å)[250d]. Both values are well confirmed by DFT calculations on **35** and carba-GlcN6P (d(C-F) = 1.43 Å, d(C-H) = 1.10 Å, **Table 10**). The structures of **35** and carba-GlcN6P were optimized at the TPSS-D3/def2-TZVP level of theory and solvent effects were considered using the COSMO model[251] with the dielectric constant and refractive index of water. In the case of the phenyl-group at the C5a of **72** much larger steric strain with adjacent nucleobases in the rigid binding site can be expected.

Table 10 Selected bond lengths for the optimized structures of 35 and carba-GlcN6P. Bond lengths are given in Å.

	35	carba-GlcN6P
	d [Å]	
C5a-H_{ax}	-	1.10
C5a-H_{eq}	1.10	1.10
C5a-F_{ax}	1.43	-

The influence of these modifications, firstly assessed with the cleavage assay (**Section 3.2**), were further evaluated by molecular docking studies. Molecular docking is a powerful tool to rate the artificial activators discussed in this work against carba-GlcN6P and the natural metabolite GlcN6P. With regard to the highly conserved catalytic core of the *glmS* ribozymes and similar ligand-recognition, the crystal structure of the *glmS* ribozyme from *T. tengcongensis* without the ligand was used as the receptor for molecular docking. The structures of the dianionic, phosphorylated carba-sugars and GlcN6P were optimized using the BP86 functional and the def2-TZVPP/J basis set[252] including the COSMO model[251]. In the case of fluoro-carba-β-L-IdoN6P two chair-

[d] C-F refers to C_2CH-F; C-H refers to C_2-C-H_2

conformations, $^{1}C_4$ and $^{4}C_1$ were optimized and used for docking (**Figure 34**). The docking was performed with the AutoDock Vina program while the results of GlcN6P served as reference (**Section 5.2**). From the docking results of each compound, the ligand pose that best resembles the binding of Glc6P in the crystal was chosen for discussion.

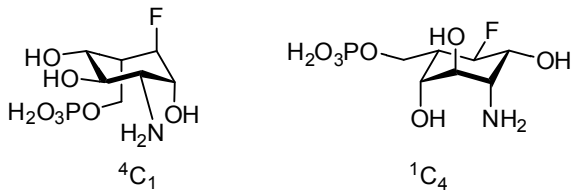

Figure 34 The two chair conformations $^{4}C_1$ and $^{1}C_4$ of (5a*R*)-fluoro-carba-β-L-IdoN6P

The predicted structure of GlcN6P closely overlaps with Glc6P from the crystal structure (**Figure 35A**). This result illustrates the fitness of the molecular docking studies and reproduces the perfect superimposition of both ligands bound to the *glmS* RNA in the crystal structure (**Figure 35B**).

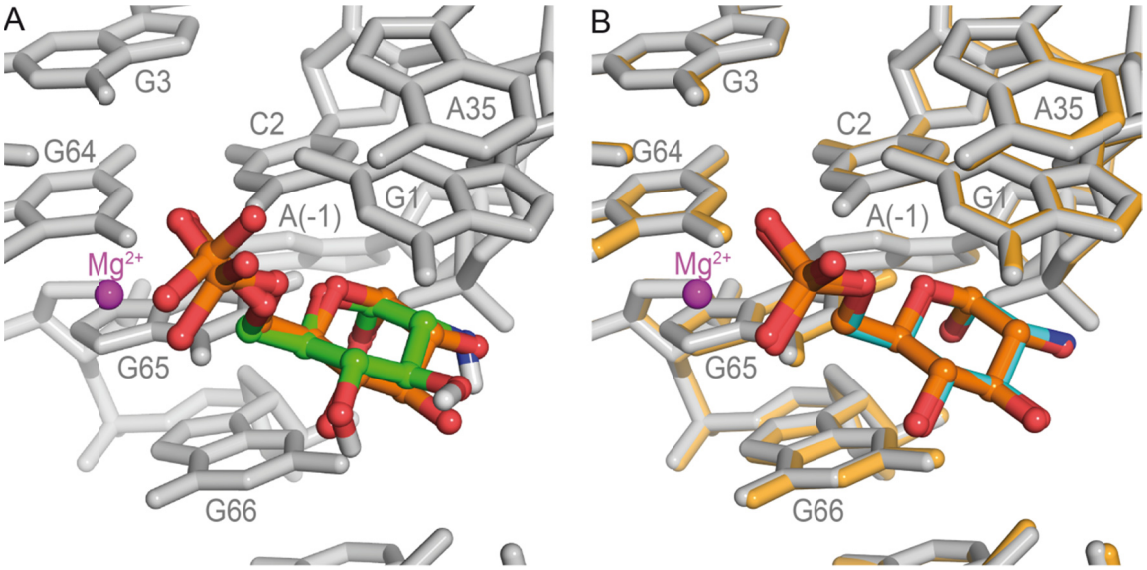

Figure 35 Docking results of GlcN6P and superposition of PDB 2Z74 and 2Z75
(A) Overlay of the docked structure of GlcN6P (green) with the crystal structure of the *glmS* ribozyme from *T. tengcongensis* (gray) and bound Glc6P (orange). The predicted structure closely matches Glc6P and thereby confirms the fitness of the molecular docking results. The distance between the nitrogen of the amine of GlcN6P and the oxygen of the scissile-phosphate is d(N-O) = 3.1 Å (B) Superposition of the Glc6P-bound *glmS* ribozyme from *T. tengcongensis* (grey RNA, orange ligand) and GlcN6P-bound *glmS* ribozyme (orange RNA, cyan ligand) from PDB 2Z74 and 2Z75, respectively.[88,95]

The molecular docking results of the carba-sugar analogs of GlcN6P, carba-GlcN6P and **35**, both closely resemble Glc6P in the crystal (**Figure 36**). In particular, the distance

between the ligand amine group and the scissile phosphate (carba-GlcN6P: *d*(N-O) = 3.1 Å; **35**: *d*(N-O) = 2.9 Å) compared to GlcN6P (Glc6P: d(N-O) = 3.1 Å) supports ribozyme self-cleavage promotion. The correct prediction of the position of the phosphate for both docked molecules would allow Mg^{2+}-coordination, which is crucial for high-affinity binding to the RNA.[73,89,101] Distances between the nitrogen of the amine and the phosphate-oxygen at the cleavage position of *d*(N-O, carba-GlcN6P) = 3.1 Å and *d*(**35**, N-O) = 2.9 Å could be determined. These distances closely match the respective value of the natural ligand *d*(N-O, GlcN6P) = 3.1 Å and are consistent with the activity seen in the cleavage assay. A notable factor that distinguishes the carba-sugars from the natural ligand is the distortion of the ring around the C2-C5 axis, which is even more pronounced in the case of **35**. This distortion brings the fluorine in close contact with the amine of C^2 (d(N-H···F) = 1.86 Å; ∠(N-H···F) = 141°). Thus, there is the possibility of a hydrogen bond, whereas the distance between amine and fluorine is shorter than normally described for X-H···F-interactions.[253] The twisting of **35** at the binding site can be attributed to the fact that the axial hydrogen and the fluorine at C5a would otherwise cause steric repulsion with G^1. Consequently, the substitution of the ring oxygen with methylene or fluoromethylene leads to the loss of a strong hydrogen bond to C^2 and a distortion of the hydroxy groups on C3 and C4. The different degree of the displacement of **35** and carba-GlcN6P at the binding site is also reflected by their predicted affinities. AutoDock Vina predicted a 0.6 kcal/mol higher affinity for carba-GlcN6P compared to **35** (**Table 11**).

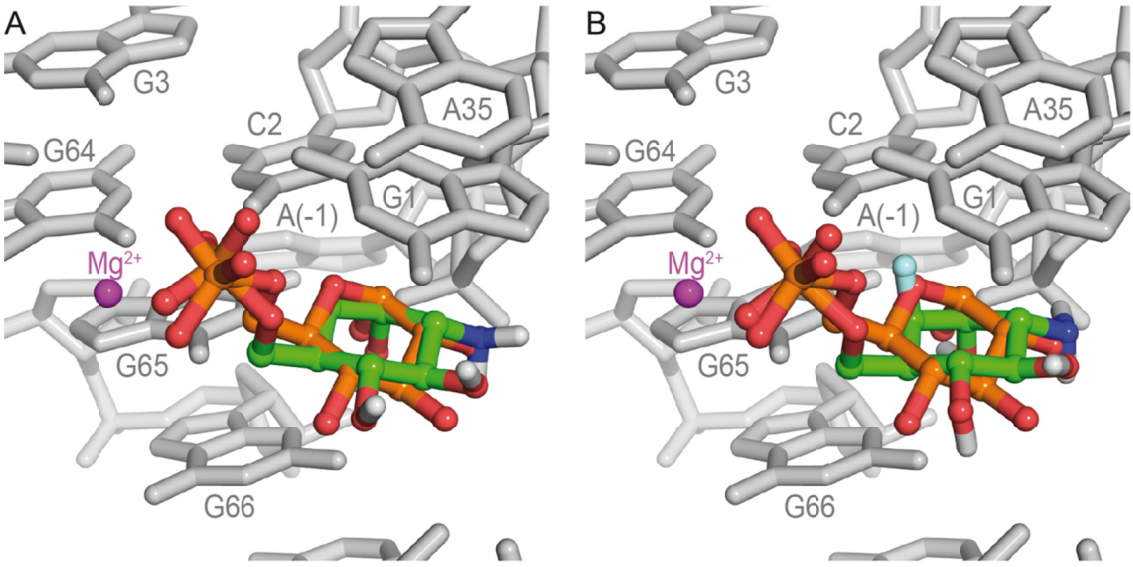

Figure 36 Docking results of carba-GlcN6P and (5a*R*)-fluoro-carba-GlcN6P 35
Docked structures of (A) carba-GlcN6P and (B) (5a*R*)-fluoro-carba-GlcN6P **35** (both green) overlayed with the crystal structure of the catalytic core of *T. tengcongensis glmS* ribozyme and bound Glc6P (gray RNA, orange ligand). Both artificial ligands bind similarly to Glc6P with the correct positioning of the amine group to promote the catalytic self-cleavage of the ribozyme. The distance between the nitrogen of the carba-sugar and the oxygen of the scissile phosphate is (A) carba-GlcN6P: *d*(N-O) = 3.1 Å; (B) **35**: *d*(N-O) = 2.9 Å.

In conclusion, the reduced activity of **71** in the cleavage assay can be attributed, to some extent, to steric encumbrance (**Section 3.2**). However, the small difference in distortion of fluoro-carba-GlcN6P and carba-GlcN6P does not explain the large differences in EC_{50} values. Therefore, co-crystallization of both compounds bound to the *glmS* ribozyme would allow more detailed SAR.

Table 11 Predicted binding affinity of the carba-sugars to the binding site of the *T. tengcongensis glmS* ribozyme relative to GlcN6P

Compound	Affinity [kcal/mol]
GlcN6P	0
carba-GlcN6P	0.2
(5a*R*)-fluoro-carba-α-D-GlcN6P **35**	0.8
(5a*R*)-fluoro-carba-β-L-IdoN6P $^{1}C_4$ **33**	1.3
(5a*R*)-fluoro-carba-β-L-IdoN6P $^{4}C_1$ **33**	n.d.
phenyl-carba-α-D-GlcN6P **72**	1.3

Besides the structurally very similar carba-sugar analogs of GlcN6P, the affinity of fluoro-carba-IdoN6P **33** to the *glmS* ribozyme was also investigated via molecular docking. Two chair-conformations $^{1}C_4$ and $^{4}C_1$ of **33** were considered (**Table 11**) and docked to the

binding site of the *glmS* ribozyme (**Figure 37A**). Docking of the $^{4}C_{1}$-chair did not result in a structure that binds at the ligand-binding site. Since the phosphate is the primary factor that influences affinity, a loss of recognition of the $^{4}C_{1}$-fluoro-carba-IdoN6P by the RNA can be explained with the inversion at C5. Either the ring or the phosphate could bind similarly to Glc6P, while the other part of the molecule would cause steric repulsion with the rigid binding site. The predicted structure for the flipped chair $^{1}C_{4}$, in contrast, places the phosphate in the correct distance to the Mg^{2+} that allows coordination (**Figure 37A**). The ring of the molecule, however, is largely misplaced compared to Glc6P, leading to a distance between the amine and scissile phosphate of *d*(N-O) = 5.2 Å. It must be taken into account that compared to GlcN6P, all functional groups except for the methylene-phosphate are inverted due to the ring-flip. Accordingly, this leads to the observed prediction of a widely altered placement of the ligand in the binding pocket of the ribozyme. The docking results of **33**, therefore, do not explain the promotion of *glmS* ribozyme self-cleavage, which although weak, is significantly higher than background in the case of *L. monocytogenes* and *S. aureus*. However, only two conformations of **33** were considered so the possibility persists that the *glmS* binding pocket is capable of freezing out a little-occupied ring conformation, which would lead to the observed activity *in vitro*.

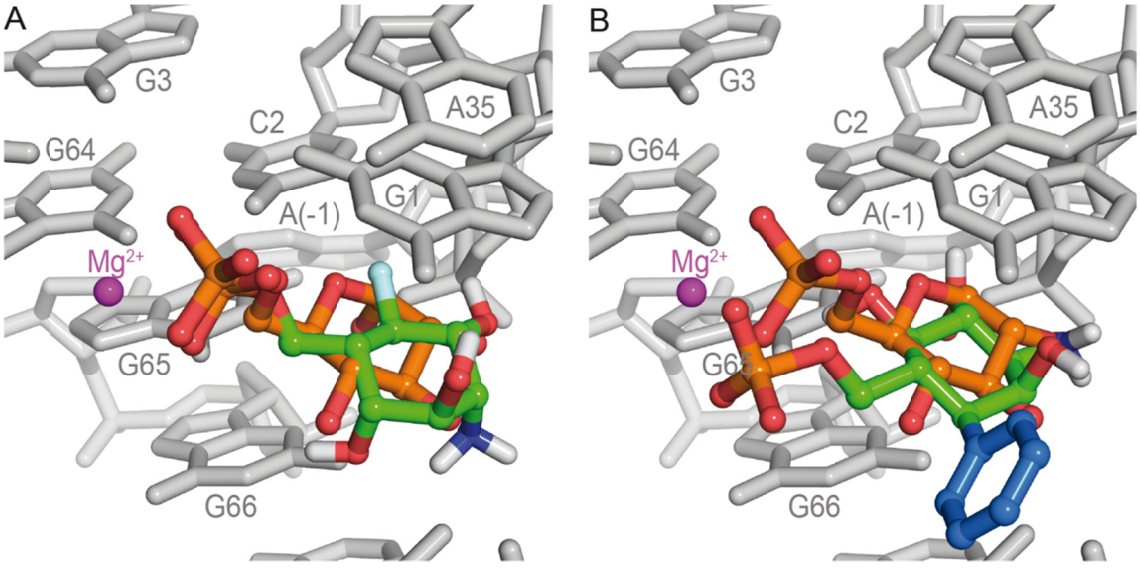

Figure 37 Docking results of fluoro-carba-IdoN6P 33 and phenyl-carba-GlcN6P 72
Docked structures of (A) fluoro-carba-IdoN6P **33** in its $^{1}C_{4}$ conformation and (B) phenyl-carba-GlcN6P **72** (both green) overlayed with the structure of the catalytic core of *T. tengcongensis glmS* ribozyme and bound Glc6P (gray RNA, orange ligand). Both predicted structures are heavily misplaced at the binding site of the RNA. The distance between the nitrogen of the carba-sugar and the oxygen of the scissile-phosphate is: (A) **33**: *d*(N-O) = 5.2 Å; (B) **72**: *d*(N-O) = 3.2 Å. The 5a-phenyl modification is highlighted (blue).

Docking of **72** predicts a binding mode at the ribozyme core, which is rotated by 180° around the C2-C5 axis (**Figure 37B**). This arrangement places the phosphate near the shown Mg^{2+}-ion, by which coordination would still be possible. Also, the amine is positioned in the distance to the scissile-phosphate that would still allow proton transfer (*d*(N-O) = 3.2 Å). However, through rotation of the entire molecule, the orientation of the adjacent OH relative to the amine is distorted. As a result, the minimally required motive for activity is lost, which is in agreement with complete inactivity observed in the cleavage-assay. Nevertheless, the orientation of the phenyl-ring towards the opening of the binding pocket[88] demonstrates that bulky modifications on this site of the molecule are possibly tolerated. The affinity of **72** to the *glmS* binding pocket predicted by AutoDock Vina is equal to that of fluoro-carba-IdoN6P **33** in its $^1C_4$ conformation, which is only 1.3 kcal/mol lower than that of GlcN6P. With regard to the total inactivity in the *in vitro* experiments, **72**, therefore, could act as an inhibitor of *glmS* ribozyme cleavage.

A huge advantage of molecular docking is that it allows docking of molecules that are not yet described in the literature. Thus, the optimized structures of two promising GlcN6P-mimics, (5a*S*)-fluoro-carba-GlcN6P **117** and (5a*S*)-hydroxy-carba-GlcN6P **118**, were docked to the *glmS* ribozyme binding pocket (**Figure 38**, **Figure 39**). These molecules bear fluorine or hydroxyl in an equatorial configuration at C5a, which can be expected to alter the binding to the RNA compared to **35** significantly. Both predicted structures are equally distorted compared to Glc6P, which can be explained by similar predicted bond lengths of C5a-F and C5a-OH (*d*(C5a-X) = 1.44 and 1.43 Å respectively) and VdW-radii (*r*(O) = *r*(F) = 1.5)[254]. The distortion is caused by a steric clash between the substituents and the nucleobases C2 as well as G65. The phosphate and the amine of nucleobase C2, however, are positioned similarly to the natural ligand and would most probably allow cofactor activity. The equatorial fluorine is less likely to form a hydrogen bond to the nucleobase C2 (*d*(N4-H···F) = 2.22 Å, ∠(N4-H···F) = 101°), comparing the position of the equatorial fluorine to the axial fluorine of **35**. The hydroxy-group of the (5a*S*)-hydroxy-carba variant, on the other hand, is in close contact with the O6 of G65 (*d*(O-H···O6) = 2.72 Å). Therefore, a hydrogen bond with the 5aOH group as hydrogen donor would be possible. Under the circumstances predicted by molecular docking both 5a*S*-modified carba-sugar mimics of GlcN6P **117** and **118** are most probably activators of the *glmS* ribozyme. However, the 5a-hydroxy group has more potential to increase affinity to the RNA than fluorine due to strong hydrogen bonds to adjacent nucleobases, e.g., G65.

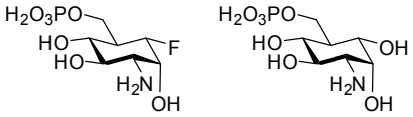

117 **118**

Figure 38 Chemical structure of (5a*S*)-fluoro-carba-α-D-GlcN6P 117 and (5a*S*)-hydroxy-carba-α-D-GlcN6P 118

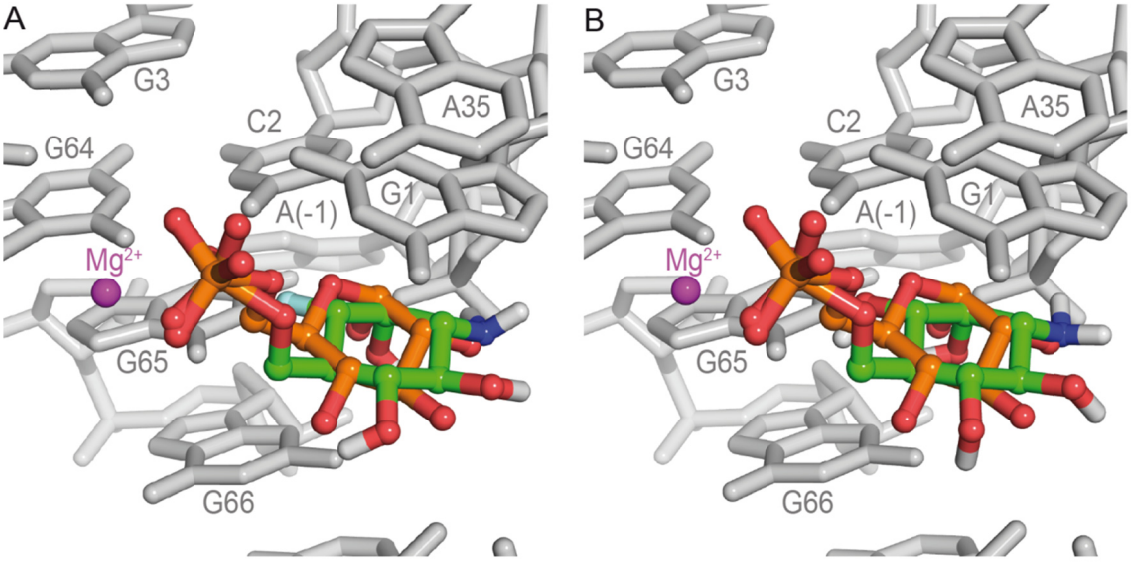

Figure 39 Docking results of (5a*S*)-fluoro-carba-α-D-GlcN6P and (5a*S*)-hydroxy-carba-α-D-GlcN6P

Docked structures of (A) (5a*S*)-fluoro-carba-α-D-GlcN6P **117** (B) (5a*S*)-hydroxy-carba-α-D-GlcN6P **118** overlaid with the crystal structure of the catalytic core of *T. tengcongensis glmS* ribozyme and bound Glc6P (gray RNA, orange ligand). Both compounds that are not yet described in literature bear an equatorial-modification (F or OH) at C5a. The distance between the nitrogen of the carba-sugar and the oxygen of the scissile-phosphate is: (A) (5a*S*)-fluoro-carba-GlcN6P: *d*(N-O) = 2.9 Å; (B) (5a*S*)-hydroxy-carba-GlcN6P: *d*(N-O) = 2.9 Å.

As a conclusion, molecular docking is a powerful tool to extract SAR from libraries of artificial activators of the *glmS* ribozyme. SAR from molecular docking to the *glmS* ribozyme are only possible as long as the assumption of a rigid binding pocket of the ribozyme is valid. As far as carba-analogs of α-D-GlcN6P are concerned, molecular docking correctly predicts the steric clash that modifications at the 5a-carba-position cause with the back of the binding pocket. Therefore, the substitution of the ring-oxygen with methylene already leads to a distortion of the ligand. This effect is more pronounced in the case of fluorine by its larger bond length and VdW-radius. With a bulky substituent like phenyl, no binding with the same orientation as Glc6P is possible. Interestingly, the molecular docking studies show the accurate positioning of the phosphate-group for all compounds but phenyl-carba-GlcN6P. It can, therefore, be concluded that the essential contribution of the phosphate to the ligand affinity is correctly predicted. The rotation around the C5-C6 and C6-O bonds, thereby, contribute to the flexibility necessary for

arranging the phosphate. This is also the case for fluoro-carba-IdoN6P **33** that otherwise show strong steric clash with the binding pocket. Furthermore, the C2-NH_2 group is predicted to occupy a position close to the scissile-phosphate that would allow proton transfer. However, in the case of the fluoro-carba-analog of β-L-idosamine, the docking results do not reflect the, albeit weak, activity in the cleavage assay. From NMR-experiments and calculations shown in this work as well as studies on *gem*-difluoro-β-L-carba-idose[27], the high conformational flexibility of this compound class is known. Thus, it is hard to conclude reliable SAR from the docking studies alone. Possibly, the *glmS* ribozyme can freeze out thermodynamically *meta*-stable conformations, which are not considered by the docking algorithm but act as cofactors of the self-cleavage reaction.

Concerning the 50- to 100-fold reduced activity of (5a*R*)-fluoro-carba-α-D-GlcN6P **35** *in vitro* compared to carba-GlcN6P **22**, besides [252,255-257]repulsive interaction, the electronic effect of fluorine on the other functional groups also needs to be considered.[246,249-251] The basicity of the amine is very likely decreased in **35** due to fluorine[258], which means that its ability to function as an acid-base catalyst during the ribozyme self-cleavage reaction would also be altered. Similar effects of the fluorine on the pK_A of the hydroxy groups, thereby altering their H-bond acidity is likely.[180] Graton *et al.* analyzed the influence of *mono*-fluorination (axial and equatorial) and *gem*-difluorination on axial and equatorial hydroxy groups in conformationally restricted fluorohydrins.[180] Studies of the H-bond acidities showed a strong dependency on the relative configuration of the fluorine and the hydroxy group. Concerning the configuration in (5a*R*)-fluoro-carba-GlcN6P **35**, in 1,2-fluorohydrins an axial configuration of fluorine and equatorial orientation of the adjacent hydroxy group led to a decrease of H-bond acidity. The transfer of these finding to the activity of **35** on *glmS* ribozyme cleavage would explain its decrease in affinity. The strongest increase of H-bond acidity for 1,3-fluorohydrins was observed in the case of axial fluorine configuration. A similar effect on the amine in **35** would explain reduced activity in ribozyme cleavage due to reduced basicity.

3.4 Antibacterial effect of fluoro-carba-GlcN

Since (5a*R*)-fluoro-carba-α-D-GlcN6P **35** showed *in vitro* activity in the micromolar range, its potential effect on bacterial growth was investigated. For the transmembrane transportation of sugars in Gram-positive and Gram-negative bacteria the phosphoenolpyruvate: sugar phosphotransferase system (PTS) is used.[259] The PTS consists of several catalytic compounds that detect, transport and phosphorylate sugar substrates. Natural sugar substrates also include the essential, early cell-wall precursor

GlcN, which, unlike its intracellular phosphorylated variant GlcN6P, is uncharged under physiological conditions. The negative charge of the phosphate prevents GlcN6P and other hydrophilic compounds from crossing the lipid bilayer membrane that surrounds bacterial cells.[260] Although fluorine-substitution is used to increase the lipophilicity of drugs[29,168], it is highly unlikely that **35** can enter bacterial cells by passive diffusion. Therefore, the non-phosphorylated variant **69** was employed in bacterial assays, assuming that carba-sugar mimics of GlcN are also transported into the cell and phosphorylated by the PTS.

3.4.1 Growth inhibition of *B. subtilis* in the presence of (5a*R*)-fluoro-carba-α-D-GlcN

The analysis of the growth of *B. subtilis* was performed in chemically defined medium (CDM) without glucose (**Section 5.1.3**) to exclude the competition between glucose and sugar-mimics for PTS. Cells of *B. subtilis* strain 168 were incubated in the presence (4.7 to 300 µM) and absence of **69** (**Figure 40A**) to investigate the antibacterial effect of fluoro-carba-GlcN **69**. The resulting growth-curves over ten hours show concentration-dependent inhibition of bacterial growth. Close investigation of the fractional growth after seven hours showed significantly more than 50% growth inhibition at a concentration of 18.8 µM (**Figure 40B**). Concentrations of 150 µM or more caused complete growth inhibition in accordance with a minimum inhibitory concentration (MIC) of 150 µM (**Figure 40C**). Assuming that **35** is formed upon uptake and that this is the active species, the observed performance is surprising considering the *in vitro* activity of **35** on the *glmS* ribozyme with an EC_{50} (**35**, *B. subtilis*) of 196 ± 17 µM. The non-fluorinated carba-GlcN analog showed the same MIC of 150 µM. However, compared to the 18.8 µM of **69**, 75 µM of carba-GlcN **22** were necessary to induce significant growth inhibition after seven hours (**Figure 40D**).[153]

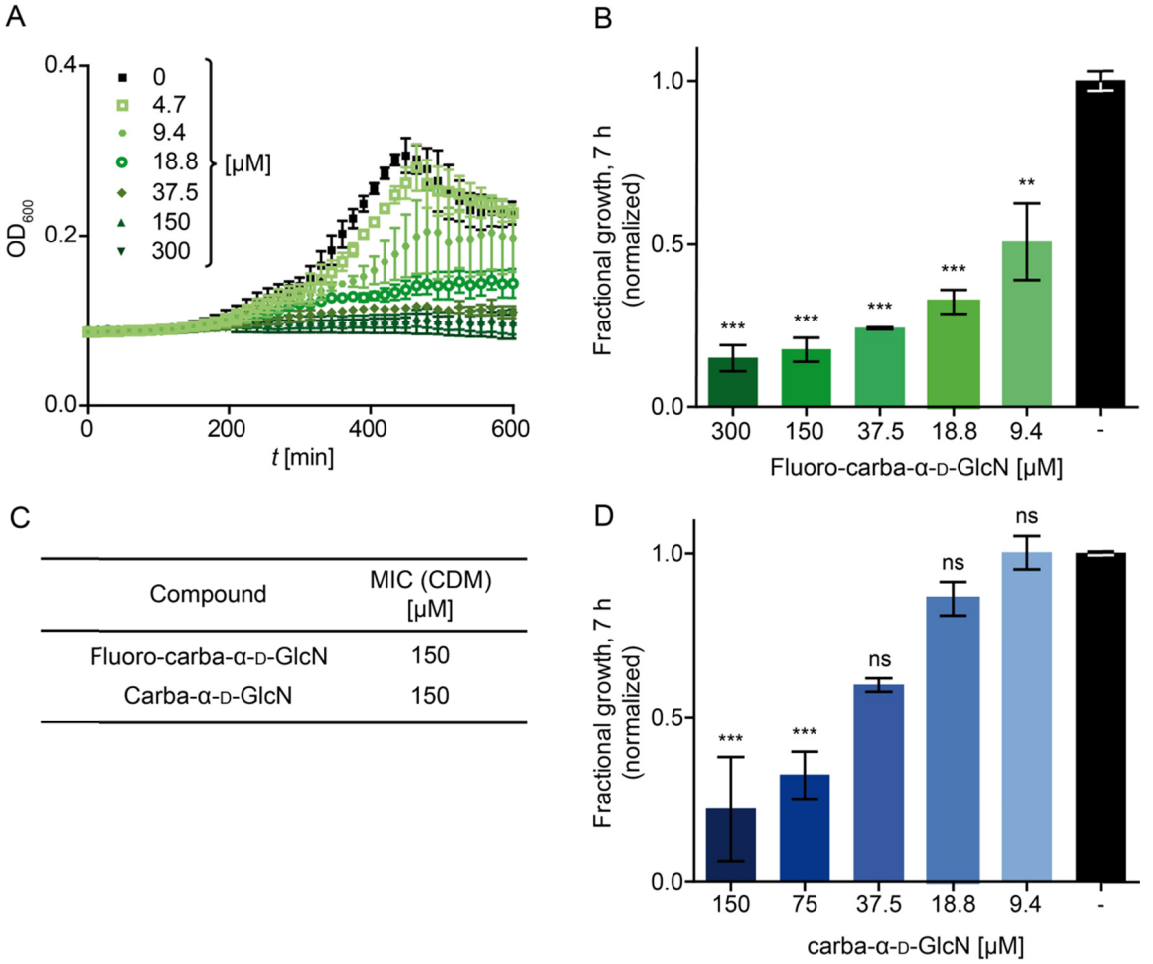

C

Compound	MIC (CDM) [µM]
Fluoro-carba-α-D-GlcN	150
Carba-α-D-GlcN	150

Figure 40 Cell growth inhibition of *B. subtilis* 168 in the presence of (5a*R*)-fluoro-carba-α-D-GlcN 69 or carba-GlcN 22

(A) Inhibition of *B. subtilis* cell growth depending on the concentration of **69** (0 to 300 µM, shades of green). The shown error bars are the s.d. of two independent experiments. (B) The growth of *B. subtilis* cells in the presence of **69** (shades of green) after 7 h, normalized to the growth in the absence of **69** (black). (C) Determined minimum inhibitory concentrations (MIC) for **69** and carba-GlcN[153]. (D) The growth of *B. subtilis* cells in the presence of carba-GlcN **22** (shades of blue) after 7 h, normalized to the growth in the absence of carba-GlcN, respectively (black). (B, D) The data is baseline corrected by subtracting the absorption of the chemical defined medium. The shown error bars are the s.d. of two independent experiments. One-way ANOVA with Tukey's multiple comparison test demonstrates statistically significant (*** $P < 0.001$, ** $P < 0.01$) or no significance (ns $P > 0.05$) growth inhibition compared to growth without compound. Error bars are s.d. of experiments carried out at least in duplicate. Experiments were carried out by Anna Schüller

3.4.2 (5a*R*)-fluoro-carba-α-D-GlcN hijacks the GlcN-specific PTS

To investigate whether the antibacterial effect of **69** depends on the PTS and, in particular, if a specific transporter is necessary for transport of the carbohydrate-mimic, PTS-specific deletion mutants of *B subtilis* were used. **Figure 41A** shows the schematic structure of the gam- and nag-PTS. Furthermore, the role of the histidine-rich protein

(HPr) as the general component in the PTS-facilitated transport and phosphorylation is shown. The membrane domain enzyme II (EIIC) and the cytosolic components of the fused EII complex are substrate-specific, while the HPr component is part of the phosphorylation cascade. In general, the transport of carbohydrates by PTS is accompanied by their direct phosphorylation.[261] However, phosphorylation and transport of PTS-substrates are two mechanistically separated steps that are performed by two distinct components of the substrate-specific EII complex. Although their interplay is not entirely understood, the membrane-spanning EIIC binds its substrate, while phosphorylation by EIIB takes places at the cytoplasmic-facing site of EII.[262] Therefore, in principle, the transport of the unphosphorylated substrate through facilitated diffusion is possible if the cytoplasmic release is not gated. Transport that was not coupled to phosphorylation was shown in the case of mannitol and the EII^{Man} as well as EII^{Glc} mutants of *E. coli*.[263,264] However, translocation of substrates by unphosphorylated EII that was not coupled to phosphorylation was 2 to 3 orders of magnitude slower compared to phosphorylated EII.[263,265]

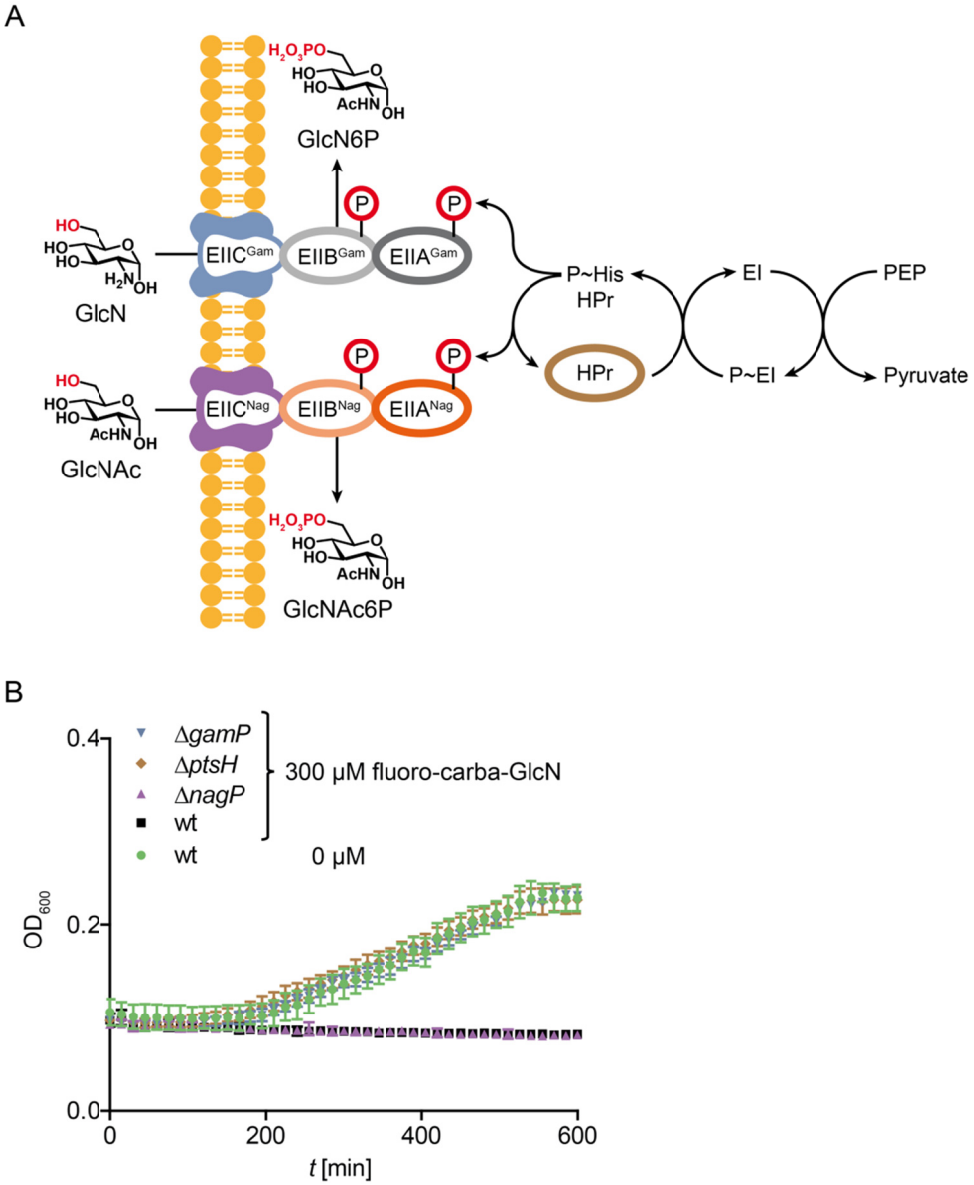

Figure 41 Analysis of the antibacterial effect of (5a*R*)-fluoro-carba-α-D-GlcN 69 depending on the uptake by specific PTS

(A) Shown is the schematic presentation of the structure and mechanism of the *B. subtilis* PTS nagP and gamP. The EII complexes of both gamP and nagP are fused to one substrate-specific protein.[266] Each comprises the membrane-spanning EIIC and the cytoplasmic EIIBA pair. EIIAB, which transfers the phosphate to the respective PTS-substrate, is part of the phosphorylation cascade. This cascade includes the general PTS component HPr and begins with EI, which uses PEP as an energy source and phosphoryl donor.[267] (B) Bacterial growth of Δ*gamP* (GlcN-specific, blue downward triangles), Δ*ptsH* (phosphorylation subunit, brown diamonds), Δ*nagP* (GlcNAc-specific, purple triangles) *B. subtilis* strains over time was compared to wild-type (black squares) and the untreated control (green circles). The wild-type and Δ*nagP* strain both show complete growth inhibition in the presence of 300 µM **69** (2x MIC) over the investigated time. The Δ*gamP*, Δ*ptsH* strain both show the same growth over time as the untreated control. Experiments were carried out by Anna Schüller in triplicate.

Growth curves for deletion mutants for the N-acetylglucosamine specific transporter (NagP), the glucosamine specific PTS (GamP) and the global phosphorylation unit

(PtsH) were analyzed in in the presence of **69** and compared to the wildtype (wt) (**Figure 41B**).[268] As shown in **Figure 41B**, the *B. subtilis* growth curves in the presence of **69** for the Δ*nagP* strain and wild-type (wt) overlap. Conversely, Δ*ptsH* and Δ*gamP* deletion strains show growth equal to the untreated wild-type control. These results indicate that **69** specifically addresses the GlcN-specific permease of the PTS and therefore possesses GlcN-mimicking capabilities in the interaction with this substrate-specific protein. This specificity for *gamP* is in contradiction to the growth of *B. subtilis* PTS mutants in minimal medium with GlcN by Gaugue *et al.*[269] In their case, deletion of *gamP* or even double deletion of *gamP* and *nagP* still led to normal growth on GlcN as a carbon source. However, Reizer *et al.* observed growth inhibition of gamP mutant strains and even stronger inhibition in the case of *ptsH* mutation with GlcN as a single carbon source.[270] The uptake of **69**, however, is solely dependent on *gamP*, demonstrated by the same growth of *gamP* and *ptsH* mutants as well as the untreated wild-type strain. The *gamP*-specific growth inhibition of **69** is in good agreement with analog experiments on the antibacterial effect of CGlcN.[153] In the case of the strain defective in the function of HPr, the substrate-specific EII are normally expressed, however, no growth inhibition due to facilitated diffusion of **69** could be detected. This supports the initial assumption that simultaneous transportation and phosphorylation of **69** is necessary to yield the preferred *glmS* ribozyme activator fluoro-carba-GlcN6P **35**. As stated previously, facilitated diffusion is expected to be slowed down in the case of the unphosphorylated EII. Therefore, it is hard to predict to which extent growth inhibition in the present assay setup would be detectable. Thus, only direct measurement of intracellular quantities of **69** or **35**, e.g., by LC-MS, would allow a final statement about the active species that is responsible for the observed growth inhibition of *B. subtilis*.

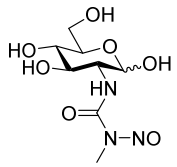

Figure 42 Chemical structure of streptozotocin.

Streptozotocin is a nitrosourea derivative of D-glucosamine, whereby it has natural mimicking abilities of GlcN and GlcNAc with regard to the PTS of bacteria. This aspect has been extensively studied due to the use of streptozotocin as a broad spectrum antibiotic with activity against Gram-positive and -negative bacteria.[271,272] It could be shown that *E. coli* strains resistant to streptozotocin possess mutations in the *nagE* transport system, which is responsible for GlcN- and GlcNAc-transport.[273] The *nagE* gene is therefore homologous to *gamP* and *nagP* in *B. subtilis*.[269] The PTS-dependent

uptake and activity was further investigated for PTS mutants of *E. coli*, *S. aureus* and *B. subtilis* defective in the function of the general PTS components EI and HPr.[274] In the same study, Ammer *et al.* showed that transport of streptozotocin is inevitably accompanied by its phosphorylation.[250] Considering the utilization of the bacterial PTS for uptake and their structural similarity to GlcN, the parallels between streptozotocin and CGlcN are striking. The direct linkage of transport and phosphorylation in the case of streptozotocin supports the assumption of a similar mechanism for CGlcN and fluoro-carba-GlcN **69**. However, the example of mannose uptake which is independent of phosphorylation is contrary to this. Future experiments must, therefore, prove the presence of CGlcN6P or fluoro-carba-GlcN6P in the cytoplasm.

3.4.3 (5a*R*)-Fluoro-carba-α-D-GlcN specifically acts on the bacterial cell envelope

Artificial activation of the *glmS* ribozyme in bacterial cells would inevitably lead to reduced levels of GlcN6P and impairment of cell-wall synthesis. To test if treatment of *B. subtilis* cells with (5a*R*)-fluoro-carba-α-D-GlcN **69** impairs the cell wall structure, *B. subtilis* strains to carry plasmids encoding the promoter of stress-inducible genes fused to the firefly luciferase gene were used. Hence, increasing levels of luciferase luminescence directly correlate with the induction of the respective stress-responsive promoter. The promoters analyzed in this study indicate cell envelope damage (*ypuA*), DNA damage (*yorB*), RNA damage (*helD*) and translational arrest (*bmrC*).[275] P*ypuA,* indicates cell wall synthesis inhibition or cell envelope stress and is responsive to, among others, vancomycin, polymyxin B, and β-lactams. The incubation of all four strains with **69** revealed concentration-dependent induction of P*ypuA* and no effect on the other stress-responsive promoters. Thus, **69** specifically inhibits the cell wall synthesis of *B. substilis*, while interference with other major biosynthetic pathways (DNA, RNA, and protein biosynthesis) could be excluded. This specificity for cell envelope stress is in accordance with the already demonstrated effect of CGlcN.[153]

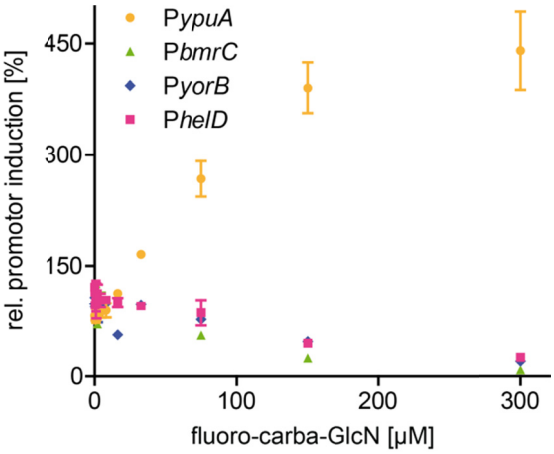

Figure 43 Relative induction of stress-responsive promoters measured as bioluminescence of the firefly-luciferase cloned behind the indicated stress-inducible promoter in *B. subtilis*
Treatment with increasing concentrations of (5a*R*)-fluoro-carba-α-D-GlcN **69** specifically induced the P*ypuA* (yellow circles), which is indicative of cell envelope stress or cell wall biosynthesis inhibition. The stress-responsive promoters associated with protein synthesis inhibition (P*bmrC*, green triangles), DNA synthesis inhibition/damage (P*yorB*, blue diamonds), and RNA biosynthesis inhibition (P*helD*, pink squares) were not induced by fluoro-carba-GlcN. Experiments were carried out by Anna Schüller in duplicate.

These experiments show that the antibacterial effect of **69** is indeed related to the cell wall synthesis of *B. subtilis*. On the one hand, this supports the assumption that *glmS* ribozyme activation in the cell would reduce the level of the essential cell-wall precursor GlcN6P and thereby peptidoglycan biosynthesis. On the other hand, induction of cell-envelope stress exclusively by action on the *glmS* ribozyme cannot be proven by P*ypuA* induction. Effects of **69** or phosphorylated **35** on other targets in bacterial cell wall synthesis is highly probable because of the high chemical similarity of **69** to the other carbohydrate-substrates involved. It appears very likely that intracellular (5a*R*)-fluoro-carba-α-D-GlcN6P **35** would mimic GlcN6P as a substrate of phosphoglucosamine mutase GlmM. GlmM catalysis the synthesis of glucosamine-1-phosphate (GlcN1P) from GlcN6P as the second step of the peptidoglycan synthesis starting from fructose-6-phosphate (**Section 1.4.2**, **Figure 10**).[162] The uridyltransfer reaction, which is the fourth step in cell wall biosynthesis, is catalyzed by GlcN1P acetyltransferase and N-acetylglucosamine-1-phosphate uridyltransferase GlmU and yields UDP-GlcNAc.[276] Seo *et al.* could show that carba-α-GlcNAc-1-phosphate can indeed function as a carba-sugar substrate of GlmU yielding UDP-carba-GlcNAc.[277] Apart from this step, no reference on the utilization of carba-sugar mimics by enzymes involved in the cell wall synthesis is available. Therefore, it is of utmost importance for future studies to investigate the inhibiting effects of carba-sugar analogs of GlcN and GlcN6P on the enzymes involved in the biosynthesis of peptidoglycan. In this context, the possibility of

insertion of carba-sugar into the bacterial cell wall is especially relevant for the elucidation of the mode of action of carba-sugars.

3.4.4 Comparison of *glmS* ribozyme activation and antibacterial growth inhibition by fluoro-carba-GlcN and carba-GlcN

(5a*R*)-fluoro-carba-α-D-GlcN **69** showed activity as a promoter of the *glmS* ribozyme self-cleavage mechanism in the micromolar range (**Figure 31**). However, compared to carba-GlcN that only differs by the substitution of fluorine by hydrogen at C5a, concentrations of **69** which are 50 to 100 times higher are required to achieve half-maximal ribozyme activation (**Table 8**). This drop in activity is partly explained through the increased steric clash with the back of the ligand binding pocket of the *glmS* ribozyme, while electronic effects of the fluorine lead to the reduced basicity of the amine (**Section 3.3**). In contrast, (5a*R*)-fluoro-carba-α-D-GlcN **69** shows very similar growth inhibition of *B. subtilis* cells, which is reflected by an equally high MIC of 150 µM (**Figure 40C**). Looking at the growth of *B. subtilis* after 7h, which is the stationary phase of bacterial growth, 19 µM of **69** are sufficient to reduce growth below 50% of the control (**Figure 40B**). In contrast, 75 µM of carba-GlcN are required to induce comparable inhibition (**Figure 40D**). Thus, the significantly lower in vitro activity of (5a*R*)-fluoro-carba-α-D-GlcN6P **35** compared to carba-GlcN6P is not reflected by the similar inhibiting capabilities of *B. subtilis* cell growth of the respective non-phosphorylated variants **69** and carba-GlcN. However, this difference could be attributed to a deviation between the intra- and extracellular concentration of the fluoro-carba sugar caused by active transportation via PTS. A significant concentration difference was already observed in the case of streptozotocin, whose active transport led to 70 times higher intracellular concentrations of phosphorylated streptozotocin compared to its precursor in the external medium.[274] The intracellular accumulation of phosphorylated sugars or sugar-mimics is counteracted by their possible dephosphorylation by intracellular phosphatases and efflux by the substrate-specific EII.[278,279] This results in a complex interplay of active PTS uptake and phosphorylation, dephosphorylation by cytosolic phosphatases and potential metabolisation. Vastly improved uptake of fluoro-carba-GlcN **69** and higher resistance to active efflux compared to carba-GlcN could thereby explain the discrepancy between *in vitro* and antibacterial activity of both mimics. Tracking of the fluorinated carba-sugar with the help of, e.g. LC-MS[280,281] or ^{32}P-labeled phosphoenolpyruvate[274], especially considering the path of cell-wall biosynthesis, could allow future studies a precise impression of its mode of action.

4 Outlook

The synthesis of new 5a-phenylated and 5a-fluorinated glycomimetics of α-D-glucosamine and α-D-glucosamine-6-phosphate, as well as 5a-fluorinated mimics of β-L-idosamine and β-L-idosamine-6-phosphate, was established. In the course of the synthesis of 5a-fluorinated analogs of carba-GlcN and carba-GlcN6P, the synthesis sequence of epoxidation and titanocene(III)-catalyzed radical epoxide opening was established as a versatile approach towards base-labile carbocyclic analogs of carbohydrates in general.

Fluorinated bioactive compounds are of utmost value in drug development, which is reflected by versatile improvement of pharmacokinetics through fluorination[282] on the one hand and by the impressively high portion of fluorinated drugs or agrochemicals that are introduced to the market each year on the contrary.[29,173] The fluorination of glycomimetics as highly functionalized molecules is difficult[174], thus synthetic strategies of the kind described here that introduce fluorine early while tolerating a number of different functional groups in the following steps are of particular value. In the present study, fluorinated glycomimetics that possess antibacterial activity were developed and investigated. In the course of this, the mode of action of fluorinated carba-GlcN analogs needs to be explained in detail. This point is of highest priority for upcoming studies, as the discrepancy between *in vitro* and *in vivo* activity of (5a*R*)-fluoro-carba-α-D-GlcN compared to carba-α-D-GlcN cannot be explained on the basis of the currently available data (**Section 3.4.4**.). It is very likely that fluoro-carba-GlcN acts as a prodrug of fluoro-carba-GlcN6P due to the proven dependency of bacterial growth inhibition on the sugar-specific transport via PTS (**Section 3.4.2**, **Figure 41)**. Nevertheless, as a PTS-facilitated transport without simultaneous phosphorylation cannot be excluded on the basis of current data, LC-MS analysis should be used to prove the intracellular presence of fluoro-carba-GlcN6P. Metabolomics[281], as already demonstrated by Meyer *et al.* for the intracellular metabolome of *S. aureus* or cryo-electron microscopy that allows insight into the cell envelope of *B. subtilis*[283] would give a better understanding of the impact of carba-sugars and whereabouts of fluoro-carba-GlcN after potential metabolisation. The investigation of the fate of fluoro-carba-sugars could benefit from the fluorine atom that could be used as a spin-active ^{19}F-nucleus label.[284] Since fluorine-containing metabolites are very rare in bacteria, detection of fluorine in different compartments of the cell can easily be traced back to the applied fluoro-carba-sugars.[285,286]

One major finding presented herein is the immense impact of chemically small modifications, as the substitution of hydrogen by fluorine, on the activity as a cofactor of the *glmS* ribozyme self-cleavage reaction. Therefore, future approaches towards artificial activators that are focused on minimal modifications compared to GlcN6P are beneficial. This leads to the following two GlcN6P mimetics as promising synthetic targets.

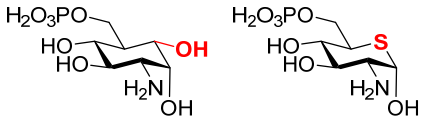

118 **119**

Figure 44 Chemical structures of 5a-hydroxy-carba-GlcN6P 118 and 2-amino-2-deoxy-5-thio-d-glucopyranose (thio-GlcN6P) 119
Both compounds are promising artificial activators of the *glmS* ribozyme bearing minimal modifications compared to their natural counterpart GlcN6P.

The synthesis of thio-GlcN6P **119** could easily be derived from the already described synthesis of thio-GlcNAc,[287] Gloster and Vocadlo *et al.* successfully used thio-GlcNAc as a prodrug of UDP-thio-GlcNAc by hijacking the mammalian hexamine biosynthetic pathway.[288] UDP-thio-GlcNAc acted as a potent inhibitor of uridine diphospho-*N*-acetylglucosamine:polypeptide β-*N*-acetylglucosaminyltransferase leading to decreased cellular *O*-GlcNAc levels. These findings could be the starting point for the design of other glycosyltransferase inhibitors with an effect on diabetes, inflammation, and cancer. On the one hand, the natural analogies between the mammalian and the bacterial hexamine biosynthetic pathway make thio-GlcN6P a promising artificial activator of the *glmS* ribozyme. On the contrary, the substitution of the ring-oxygen with sulfur represents a minimal modification that is very likely to be tolerated by the *glmS* ribozyme ligand binding pocket. Furthermore, the demonstrated high tolerance of the mammalian hexamine biosynthetic pathway could be an excellent target for fluoro-carba-sugars or unmodified carba-sugar variants of GlcNAc as potent glycosyltransferase inhibitors.

Torben Seitz was able to develop major parts of the synthesis of 5a-hydroxy-carba-GlcN6P **118**, which involves a Ferrier rearrangement of 6-O-acetyl-5-enoglycopyranosides as a crucial step.[44,289] Currently, the synthesis of **118** following an alternative synthesis approach including olefin metathesis is conducted by David Stängle also under the supervision of Valentin Wittmann. Molecular docking of (5a*S*)-fluoro-carba-α-D-GlcN6P and (5a*S*)-hydroxy-carba-α-D-GlcN6P predicts similar steric strain between both 5a-modifications and the back of the *glmS* ribozyme ligand binding pocket (**Figure 39**). However, the hydroxyl group might function as a hydrogen bond donor whereby the affinity to the RNA would potentially be increased compared to carba-GlcN6P.

Alternative approaches for the synthesis of artificial activators of the *glmS* ribozyme focus on surrogating the phosphate with malonates or phosphonates.[101] This alteration renders the phosphate-mimicking group inert to phosphatases, thereby preventing phosphate hydrolysis in the bacterial cell and the resulting decrease of *glmS* ribozyme ligand concentration. However, besides their low activity, the currently developed phosphatase-inert *glmS* ribozyme activators are charged under physiological conditions. Therefore, it is a major obstacle for these molecules to cross the lipid bilayer class. Nevertheless, variants of fluoro-carba-GlcN6P or carba-GlcN6P, which are able to enter the bacterial cell by passive diffusion, would be a promising approach to increase their cytoplasmic concentration. This, moreover, would counteract the development of resistance through mutation of gamP and thereby prevention of the uptake of carba-sugar analogs of GlcN6P. Alternative bacterial targets of carba-sugars beside the *glmS* ribozyme are protein targets within the peptidoglycan biosynthetic pathway. The substrate of GlmM, which catalyzes the next biosynthetic step after GlmS, is GlcN6P (**Figure 10**). Therefore, carba-sugar mimics of GlcN6P are very likely to interact or even become a substrate of GlmM. As GlmM catalyzes the phosphate transfer from C6 to C1, phosphatase-inert GlcN6P mimics would not be metabolized. However, inhibition of GlmM is rather likely. Similar to other off-targets that are connected to the cell wall biosynthesis this could potentially still lead to an inhibition of cell wall synthesis. Thus, a comprehensive investigation of the obvious off-targets and their interaction with carba-sugar mimics of GlcN6P is a major requirement for a complete mode of action analysis in the case of fluoro-carba-GlcN.

5 Experimental Section

5.1 Molecular Biological Methods

5.1.1 Preparation of RNA

The *glmS* RNA including the ribozyme from *S. aureus*, *B. subtilis*, *C. difficile* and *L. monocytogenes* were prepared as previously described.[105] Templates for transcription of *glmS* RNA were prepared from genomic DNA by Pfu DNA-polymerase and 5'-primers containing the T7 promoter sequence. The *glmS* ribozymes were prepared by in vitro transcription using T7 RNA polymerase (37 °C, 17 h). The transcription products were treated with DNase and separated by denaturing polyacrylamide gel electrophoresis (PAGE). The RNAs were dephosphorylated using calf intestine alkaline phosphatase (CIAP, Promega). Radioactive labeling was accomplished by phosphorylation of the 5'-end using the T4 polynucleotide kinase (PNK, NEB) and γ-^{32}P-ATP (10 mCi/mL BEBm Zaventem, Belgium). The ribozymes were desalted on G25 columns (GE Healthcare), which had been equilibrated with DEPC-treated water before.[105]

5.1.2 Radioactive *glmS* ribozyme self-cleavage assay

The ribozyme self-cleavage assay was performed as previously described.[105] The ^{32}P-labeled *glmS*-RNA from either *S. aureus*, *B. subtilis*, *C. difficile* or *L. monocytogenes* was incubated at 37 °C with GlcN, GlcN6P, carba-sugars synthesized in this work **33**, **35**, **63**, **69**, **72**, or without metabolite in the presence of 10 mM $MgCl_2$, 50 mM HEPES (pH 7.5) and 200 mM KCl. The reaction was stopped after 30 min at 37 °C by adding EDTA containing sucrose buffer. After addition of PAGE loading buffer (95% formamide, 10 mM EDTA, 0.1% (v/v) xylene cyanol and 0.1% (v/v) bromophenol blue), the reaction products were separated by 17% denaturing PAGE. The radiolabeled cleavage products were detected via autoradiography on a phosphorimager FLA-3000 (Fujifilm) and AIDA software. Kinetik parameters (k_{obs}-values) for ribozyme cleavage were determined using trace amounts of ^{32}P-labeled RNA incubated at 37 °C as described above with indicated concentration of fluoro-carba-α-D-GlcN6P **35**. Aliquots were withdrawn at various time points and the reaction quenched by addition of PAGE loading buffer. The cleavage products were separated by denaturing PAGE and k_{obs} were determined by plotting the

fraction cleaved as a function of time. Curves were then fitted according to pseudo-first order association kinetics.

5.1.3 Growth curve analysis

Growth curve analysis was performed as previously described.[153] Growth of *B. subtilis* 168 in the presence of fluoro-carba-α-D-glucosamine **69** was monitored. Bacterial cells were pre-cultured in 5 mL lysogeny-broth (LB) medium overnight at 37 °C and mixing at 130 rpm. 5 mL chemically defined medium (CDM, modified after van de Rijn & Kessler[290] without glucose) were inoculated 1:100 with the pre-culture and incubated to an OD_{600} of ~1. The culture was transferred to a prepared 96-well plate containing a dilution series of **69**. A Tecan plate reader Sunrise was used to monitor absorbance at 600 nm every 180 s over ten hours under vigorous shaking for 3 s before each measurement. The tested concentration of **69** ranged from 4.7 to 1200 µM (Data is only shown for 4.7 to 300 µM).

5.1.4 ΔPTS-dependent growth curves

The impact of fluoro-carba-α-D-glucosamine **69** on the growth of *B. subtilis* 168 PTS deletion strains was analyzed as previously described.[141] *B. subtilis* 168 Δ*ptsH*::ermR, *B. subtilis* 168 Δ*gamP*::ermR and *B. subtilis* 168 Δ*nagP*::ermR were ordered at the *B. subtilis* genetic stock center (BGSC.org). 3 ml CD medium were inoculated with the different strains and incubated overnight at 37 °C. 20 µl of the preculture was diluted with 100 µl CD medium and 80 µl of either **69** or CD medium, leading to a final OD_{600} of 0.1. The final concentration of fluoro-carba-α-D-glucosamine **69** was 300 µM which equals twice the minimal concentration that needed to inhibit B. subtilis growth in growth curve analysis completely. The OD_{600} was monitored every 45 s over 24 h and vigorous shaking for 3 s before each measurement.

5.1.5 *B. subtilis* stress promotor induction

The effect of fluoro-carba-α-D-glucosamine **69** on *B. subtilis* reporter strains (listed in Table 12) was analyzed as previously described.[153,275] Pre-cultures of each *B. subtilis* strain were prepared in 10 ml LB medium with 5 µg/mL erythromycin at 37 °C overnight. The precultures were diluted to an OD_{600} of 0.05 in 5 ml CD medium and allowed to grow to an OD_{600} of ~0.2. The cultures were transferred to well plates containing a serial dilution of fluoro-carba-α-D-glucosamine **69**, yielding a final OD_{600} of 0.01. After incubation at 37 °C for 3.5 h, a 2 mM luciferin solution in 0.1 M citrate buffer (pH 5) was injected, and luminescence was subsequently measured.

Table 12 List of stress-inducible *B. subtilis* strains investigated.

Bacterial strain	Stress-inducible promotor
B. subtilis 1S34	None
B. subtilis 1S34 pS 63	*helD, synonym yvgS* (inhibition of RNA synthesis)
B. subtilis 1S34 pS 72	*bmrC,* synonym *yheI* (inhibition of protein synthesis)
B. subtilis 1S34 pS 77	*yorB* (inhibition of DNA synthesis or DNA damage)
B. subtilis 1S34 pS 107	*ypuA* (cell envelope stress)

5.2 Molecular Docking

As a target structure for molecular docking studies, the crystal structure of the *glmS* ribozyme from *T. tengcongensis* (PDB 2Z74) was used. Before docking of artificial ligands to the RNA, the native ligand Glc6P was removed, and polar hydrogen atoms were added to the crystal structure using the WHAT IF program.[291] The chemical structures of GlcN6P and carba-sugars discussed in this work were optimized using DFT calculation in the ORCA[216] program package at the BP86/def2-TZVPP/J level of theory including the COSMO model with the dielectric constant and refractive index of water. For docking, the AutoDock Vina 1.1.2 program[292] was used. The grid map for docking was set to a dimension of 30x30x20 Å (XYZ-dimensions) centered at x = 42.845 y = 12.244 z = 13.958, which corresponds to the oxygen at C2 of Glc6P. The number of runs (exhaustiveness) was set to 100 and a maximal number of 50 modes were printed in the output. The docking poses of each artificial ligand were analyzed with the Pymol program, and the poses selected that show a close resemblance to Glc6P in the crystal structure. From these, the pose with the lowest binding energy was used for discussion.

5.3 General Methods

All reactions involving moisture or air sensitive compounds were carried out under an argon atmosphere with dry solvents and heat-dried glassware. Anhydrous

tetrahydrofuran (THF) and dimethylformamide (DMF) were purchased from Acros Organics and stored under argon. Toluene and Dichloromethane (ACS grade) purchased from Fisher Scientific were dried by allowing them to stand over 3 Å molecular sieves for at least two days under argon.[293]

Yields refer to chromatographically (LC-MS) homogeneous material unless otherwise stated. All reagents were purchased from commercial suppliers and used without further purification. Reactions were monitored by LC-MS, or analytical thin-layer chromatography (TLC) carried out on silica gel 60 F254 coated aluminum sheets (Merck) using UV light for visualization. A solution of ammonium molybdate tetrahydrate (2.5 g), $Ce(SO_4)_2 \cdot 4H_2O$ (1.0 g), H_2SO_4 (6 mL) in H_2O (94 mL) and heat was used as the developing agent. Macherey-Nagel silica gel (60, particle size 0.040 – 0.063 mm) was used for manual flash column chromatography. Automated flash column chromatography was conducted on a puriFlash®430 system (Interchim) with puriFlash high-performance silica columns.

High-resolution mass spectra (HRMS) were recorded on an Orbitrap XL mass spectrometer (Bruker) using ESI (electrospray ionization).

General Procedure 1 (GP1): Heterogenous hydrogenolysis of benzyl ethers and removal of Z-protection group

The benzylated pseudo-sugar was dissolved in 2 mL of Methanol (LC-MS grade), and 10% Pd/C (25% *w/w*) is added. After addition of trifluoroacetic acid (10 equiv.), the reaction was placed in a laboratory autoclave and is stirred at room temperature under 10 bar hydrogen pressure for 1 hour. Then another 10% Pd/C (25% *w/w*) was added, and the reaction stirred until HPLC-monitoring shows complete consumption of the starting material. The reaction was filtered through RC (regenerated cellulose) syringe filters (0.2 µm pore size), methanol was removed under reduced pressure and the resulting pseudo-sugar lyophilized.

5.4 Analytics

5.4.1 High-performance liquid chromatography (HPLC) and high-performance liquid chromatography coupled mass spectrometry (LC-MS)

High-performance liquid chromatography was performed on either an analytical Agilent Infinity 1260 or on a preparative Agilent Infinity 1100 system. As eluent a gradient of A:

H_2O + 0.1% formic acid and B: acetonitrile was used, unless otherwise noted. High-performance liquid chromatography coupled mass spectra (LC-MS) were recorded on an Agilent Infinity 1100 HPLC system coupled to a Bruker HCT esquire ESI mass spectrometer. The stationary phase, gradient, and flow used to analyze the compounds synthesized in this work are mentioned in the respective experimental description.

5.4.2 Mass spectrometry

High-resolution mass spectra (HRMS) were recorded on an Orbitrap XL mass spectrometer (Bruker) using ESI (electrospray ionization). The calculated and experimental determined mass is given as m/z with an accuracy of four significant decimal places.

5.4.3 NMR spectroscopy

NMR spectra were recorded in $CDCl_3$ or D_2O on Bruker Avance III HD Cryo 700 MHz, Avance III 600 MHz, Avance I 500 MHz or Avance III 400 MHz instruments. Chemical shifts are given as given as δ in ppm. Residual undeuterated solvents ($CDCl_3$: δH = 7.26 ppm; δC = 77.1 ppm and D_2O: δH = 4.79 ppm) were used as internal references. Assignments were based on 2D correlation spectroscopy (HH-COSY, HSQC, HMBC, NOESY, ROESY). In the case of signal-broadening due to high conformational flexibility, NMR spectra were acquired at -40 °C and the different conformations assigned individually.

5.5 Synthesis and physical data of fluoro-carba-sugars

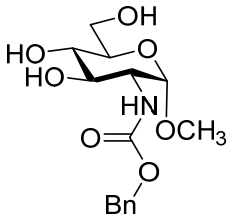

2-Amino-*N*-benzyloxycarbonyl-2-deoxy-1-*O*-methyl-α-D-glycopyranoside (26)
The methyl-*N*-benzyloxycarbonyl-glucopyranoside **26** was prepared according to a literature procedure from Sofia *et al.*[181]

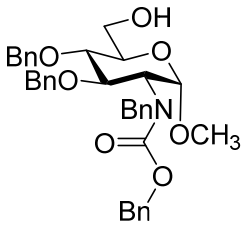

2-Amino-*N*-benzyl-*N*-benzyloxycarbonyl-3,4-*O*-benzyl-2-deoxy-1-*O*-methyl-α-D-Glycopyranoside (39) Trityl chloride (53.7 g, 0.193 mol) was presented in a 500 mL flask, and methyl glycoside **26**[181] (30.0 g, 0.0917 mol) in pyridine (300 mL) was added and stirred at room temperature for 40 h. The solution was diluted with CH_2Cl_2 (500 mL), washed with brine (3x200 mL) and dried ($MgSO_4$). The solvents were removed under reduced pressure and the orange oil used in the next step without further purification.

NaH (22.1 g, 0.552 mol, 60% in mineral oil) was added to anhydrous DMF (200 mL) and cooled to 0 °C in an ice bath. Benzyl bromide (65.6 mL, 0.552 mol) was added dropwise to the suspension. The crude product of tritylation was solved in anhydrous DMF (300 mL) and added dropwise to the suspension at 0 °C. The ice bath was removed, the suspension allowed to reach room temperature and stirred at room temperature for 17 h. Methanol (50 mL) and water (200 mL) were added successively to quench the reaction, and then the pH was adjusted to pH 7 with acidic acid. The suspension was diluted with ethyl acetate (250 mL), the organic layer separated and the aqueous layer extracted with ethyl acetate (2x250 mL). The organic layers were combined and dried ($MgSO_4$). The solvents were removed under reduced pressure and the brown oil used in the next step without further purification.

The benzylated crude product was solved in CH_2Cl_2 (500 mL) and cooled to 0 °C in an ice bath. Trifluoroacetic acid (60 mL) and triisopropylsilane (30 mL) were added successively at 0 °C. The ice bath was removed, and the solution stirred at room temperature for 1.5 h. The solvents were reduced at reduced pressure and the brown crude product purified by manual flash chromatography (5:1 to 1:1 petroleum ether/ethyl acetate) yielding the alcohol **39** (27.8 g, 51% over three steps) as a yellow oil.

R_f = 0.45 (silica, petroleum ether/ethyl acetate 1:1), Seebach-reagent; **^{1}H-NMR (400 MHz, $CDCl_3$, 25 °C)**: δ [ppm] = 7.35-7.01 (m, 20H, Ar-H), 5.21-5.05 (m, 2H, -N-C(O)-O-CH_2-Ph), 4.89-4.27 (m, 8H, 2xO-CH_2-Ph, N-CH_2-Ph, H-1, H-2), 4.09 (br, 1H, H-3), 3.82-3.69 (m, 4H, H-4, H-5, H-6), 2.82 (s, 3H, CH3); **^{13}C-NMR (100 MHz, $CDCl_3$, 25 °C)**: δ [ppm] = 138.1-125.7 (C^{Ar}), 99.9 (C-1), 79.7 (C-4), 77.4 (C-3), 75.0, 74.0 (2xO-CH_2-Ph), 71.3 (C-5), 67.7 (-N-C(O)-O-CH_2-Ph), 62.0 (C-6), 58.8 (br, C-2), 54.7 (CH_3); **RP-HPLC**: t_r = 15.1 min (ZORBAX SB-C18, 5 µm, 0.4 mL/min, 20-100% MeCN in 20 min); **MS (ESI)**: calcd for $C_{36}H_{39}NO_7Na$ $[M+Na]^+$, 620.2622, found, 620.2622.

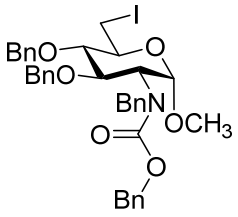

2-Amino-N-benzyl-N-benzyloxycarbonyl-3,4-di-*O*-benzyl-2-deoxy-6-iodo-1-*O*-methyl-α-D-glucopyranoside (40). The methyl glycoside **39** (2.64 g, 4.42 mmol) was solved in anhydrous toluene (20 mL), triphenylphosphine (0.83 g, 7.52 mmol) and imidazole (0.72 g, 10.61 mmol) were added. The mixture was heated to 60 °C and iodine (1.35 g, 5.30 mmol) was added. After heating to 80 °C the reaction was stirred at 80 °C for 6 h. The solvent was removed under reduced pressure and the residue purified via flash chromatography (petroleum ether/ethyl acetate 1:1) yielding the iodo-sugar **40** (1.96 g, 63%) as colorless foam.

R_f = 0.59 (petroleum ether/ethyl acetate 5:1), Seebach-reagent; **^{1}H-NMR (400 MHz, $CDCl_3$)**: δ [ppm] = 7.28-6.93 (m, 20H, Ar-H), 5.15-4.97 (m, 2H, -N-C(O)-O-CH_2-Ph), 4.87-4.64 (m, 7H, O-CH_2-Ph, H-1, H-2, N-CH_2-Ph), 4.25-4.14 (m, 1H, N-CH_2-Ph), 4.00 (br, 1H, H-3), 3.52-3.20 (m, 4H, H-4, H-5, H-6ab), 2.77 (s, 3H, CH_3); **^{13}C-NMR (125.7 MHz, $CDCl_3$)**: δ [ppm] = 157.8 (C=O), 140.1-125.6 (C^{Ar}), 99.7 (C-1), 83.6 (C-4), 81.9 (C-4), 76.8 (C-3), 75.3 (O-CH_2-Ph), 74.1 (O-CH_2-Ph), 70.0 (C-5), 67.7 (-N-C(O)-O-CH_2-Ph), 58.6 (br, C-2), 55.0 (CH_3), 47.3 (br, N-CH_2-Ph) 7.4 (C-6); **RP-HPLC**: t_r = 11.3 min (EC 125/4 Nucleodur C-18 Gravity, 3 µm, 0.4 mL/min, 80-100% MeCN in 10 min); **HRMS**: calcd for $C_{36}H_{38}INO_6Na$ $[M+Na]^+$, 730.1636, found, 730.1631.

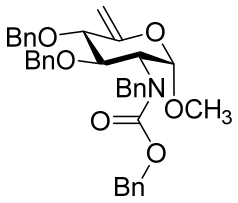

2-Amino-N-benzyl-N-benzyloxycarbonyl-3,4-di-*O*-benzyl-2-deoxy-1-*O*-methyl-α-D-gluco-hex-5-enopyranoside (41). The iodo sugar **40** (1.00 g, 1.41 mmol) was solved in anhydrous DMF (10 mL) and added dropwise to a suspension of NaH (60% in mineral oil, 0.23 g, 5.64 mmol) in anhydrous DMF (10 mL) at 0 °C. The suspension was stirred at room temperature for 2 h. The reaction was cooled to 0 °C and methanol was added dropwise to quench residual NaH. The solution was concentrated under reduced pressure and the residue diluted with ethyl acetate (50 mL). Aqueous 1M HCl was carefully added until the aqueous reached a slightly acidic pH. The organic layer was separated and the pH of the aqueous phase adjusted to pH > 8. The aqueous phase was extracted with ethyl acetate (3x100 mL). The combined organic layers were washed with

aqueous sat. $NaHCO_3$ (100 mL), aqueous sat. NaCl (100 mL) and dried ($MgSO_4$). The solvent was removed under reduced pressure and the residue purified by automated flash chromatography (100% petroleum ether to 80:20 petroleum ether/ethyl acetate in 30 min) yielding the alkene **41** (0.51 g, 62%) as a colorless oil.

R_f = 0.50 (petroleum ether/ethyl acetate 5:1), Seebach-reagent; **^{1}H-NMR (400 MHz, $CDCl_3$)**: δ [ppm] = 7.41-6.99 (m, 20H, Ar-H), 5.22-5.07 (m, 2H, -N-C(O)-O-CH_2-Ph), 4.89-4.45 (m, 8H, O-CH_2-Ph, H-1, H-2, H-6ab), 4.26-4.01 (m, 4H, N-CH_2-Ph, H-3, H-4), 2.90 (s, CH_3); **^{13}C-NMR (125.7 MHz, $CDCl_3$)**: δ [ppm] = 157.9 (C=O), 153.9 (C=CH_2), 140.0-125.7 (C^{Ar}), 100.5 (C-1), 97.1 (C-6), 81.9 (C-4), 76.0 (C-3), 74.4 (O-CH_2-Ph), 74.1 (O-CH_2-Ph), 67.7 (-N-C(O)-O-CH_2-Ph), 58.5 (br, C-2), 55.0 (CH_3), 47.0 (N-CH_2-Ph); **RP-HPLC**: t_r = 19.1 min (ZORBAX SB-C18, 5 µm, 0.4 mL/min, 80-100% MeCN in 20 min); **HRMS**: calcd for $C_{36}H_{37}NO_6Na$ $[M+Na]^+$, 602.2513; found, 602.2515.

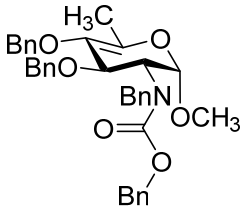

2-Amino-N-benzyl-N-benzyloxycarbonyl-3,4-di-*O*-benzyl-2-deoxy-1-*O*-methyl-5-methyl-α-D-gluco-hex-4-enopyranoside (43) To the iodo sugar **40** (0.99 g, 1.43 mmol) solved in THF (200 mL) was added potassium *tert*-butoxide (0.48 g, 4.24 mmol) as a solid at room temperature. The solution was stirred at room temperature for 5 h. The reaction was diluted with ethyl acetate (400 mL) and washed with aqueous 1M HCl, aqueous sat. $NaHCO_3$ (100 mL), aqueous sat. NaCl (100 mL) and dried ($MgSO_4$). The solvent was removed under reduced pressure and the residue purified by automated flash chromatography (85:15 petroleum ether/ethyl acetate to 100% ethyl acetate in 8 min) yielding a mixture of enolether **43** and exo-methylene **41** (0.75 g, 91 %) as colorless oil. A product ratio between endo- and exo-product of 26:74 could be determined by NMR.

R_f = 0.50 (petroleum ether/ethyl acetate 5:1), Seebach-reagent; Assignment of NMR for endocyclic product: **^{1}H-NMR (400 MHz, $CDCl_3$)**: δ [ppm] = 7.41-6.99 (m, 20H, Ar-H), 5.23-5.07 (m, 2H, -N-C(O)-O-CH_2-Ph), 4.90-4.45 (m, 6H, 2xO-CH_2-Ph, H-1, H-2), 4.26-4.01 (m, 4H, N-CH_2-Ph, H-3, H-4), 3.17 (s, CH_3), 1.72 (s, CH_3); **^{13}C-NMR (125.7 MHz, $CDCl_3$)**: δ [ppm] = 157.9 (C=O), 153.9 (C=CH_2), 140.0-125.7 (C^{Ar}), 100.4 (C-1), 81.8 (C-4), 76.0 (C-3), 74.4 (O-CH_2-Ph), 74.1 (O-CH_2-Ph), 67.7 (-N-C(O)-O-CH_2-Ph), 58.5 (br, C-2), 55.0 (CH_3), 47.0 (N-CH_2-Ph) 14.1 (CH_3);

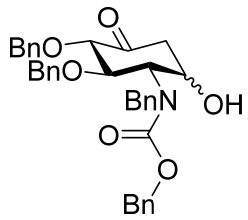

Benzyl benzyl((1R,2R,3S)-2,3-bis(benzyloxy)-6-hydroxy-4-oxocyclohexyl)-carbamate. (42) The alkene **41** (14.7 g, 19.5 mmol) was solved in 2:1 dioxane/aqueous 5 mM H_2SO_4 (225 mL), $HgSO_4$ (0.174 g, 0.585 mmol) was added, and the resulting mixture was stirred at 80 °C for 3 h. Aqueous sat. NaCl (100 mL) and CH_2Cl_2, (400 mL) were added. The organic layer was separated, and the aqueous phase was extracted with CH_2Cl_2 (3x200 mL). The organic phases were combined, dried ($MgSO_4$) and the solvent was removed under reduced pressure. The residue was purified via flash chromatography (2x40 g silica, 100% petroleum ether to 100% ethyl acetate in 60 min) yielding the cyclohexanone **42** as a mixture of isomers (9.55 g, 86%, 77:23 axial/equatorial ratio) as a colorless foam. The isomers were not separated before the next step.

R_f(axial) = 0.60, **R_f(equatorial)** = 0.50 (petroleum ether/ethyl acetate 1:1), Seebach-reagent; Assignment for most abundant isomer with 1-OH in axial configuration: **^{1}H-NMR (500 MHz, $CDCl_3$)**: δ [ppm] = 7.45-7.21 (m, 20H, Ar-H), 5.18-5.14 (m, 2H, -N-C(O)-O-CH_2-Ph), 5.01-4.48 (m, 5H, O-CH_2-Ph, H-2), 5.37-4.01 (m, 2H, N-CH_2-Ph), 4.11 (br, 1H, H-1), 4.73 (m, 1H, H-3),), 4.07 (s, 1H, H-4), 2.53 (dd, *J* = 14.3, 3.9 Hz, 1H, H-5aa), 2.29, (d, *J* = 11.7 Hz, 1H, H-5ab); **^{13}C-NMR (125.7 MHz, $CDCl_3$)**: δ [ppm] = 203.7 (C=O), 158.4 (N-C=O), 138.3-127.5 (C^{Ar}), 88.2 (C-4), 77.2 (C-3), 75.6 (O-CH_2-Ph), 73.7 (O-CH2-Ph), 69.5 (C-1), 68.3 (-N-C(O)-O-CH_2-Ph), 55.2 (br, C-2), 53.6, 53.2 (N-CH_2-Ph), 46.4 (C-5a); **RP-HPLC**: t_r(axial) = 16.7 min, t_r(equatorial) = 16.0 min (ZORBAX SB-C18, 5 µm, 0.4 mL/min, 80-100% MeCN in 20 min); **HRMS**: calcd for $C_{35}H_{35}NO_6Na$ $[M+Na]^+$, 588.2357; found, 588.2348.

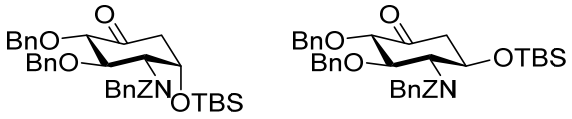

Benzyl benzyl((1R,2R,3S,6R)-2,3-bis(benzyloxy)-6-((tert-butyldimethylsilyl)-oxy)-4-oxocyclohexyl)carbamate (38/38b) The isomeric mixture of cyclohexanone **42** (2.00 g, 3.54 mmol) was presented in a heat-dried schlenk tube and solved in anhydrous CH_2Cl_2 (20 mL). The solution was cooled to 0 °C and 2,6-lutidine (0.9 mL, 8.13 mmol) and *tert*-butyldimethylsilyl trifluoromethanesulfonate (1.9 mL, 8.13 mmol) were added successively at 0 °C. The cooling was removed and the reaction was stirred at room

temperature for 1.5 h. The reaction mixture was diluted with CH_2Cl_2 (20 mL) and washed with 1N aqueous HCl (20 mL) and sat. aqueous NaCl (20 mL). The organic layer was dried ($MgSO_4$) and the solvent removed under reduced pressure. The residue was purified via automated flash chromatography (100% petroleum ether to 73:27 petroleum ether/ethyl acetate in 54 min) yielding the protected α-cyclohexanone **38** (1.64 g, 68%) and the β-cyclohexanone **38b** (0.49 g, 21%) as colorless oils.

R_f38 = 0.45, **R_f38b** = 0.40 (petroleum ether/ethyl acetate 3:1), Seebach-reagent; assignment of **38**: **^{1}H-NMR (400 MHz, $CDCl_3$, 25 °C)**: δ [ppm] = 7.40-6.98 (m, 20H, Ar-H), 5.11 and 5.05 (d, *J* = 12.5 Hz, 2H, -N-C(O)-O-CH_2-Ph), 4.93-3.68 (m, 12H, 3xO-CH_2-Ph, N-CH_2-Ph, H-2, H-1, H-3, H-4), 2.70 (d, *J* = 13.5 Hz, 1H, H-5a, eq), 2.59 (dd, *J* = 14.0, 4.0 Hz, 1H, H-5a,ax), 0.88 (s, 9H, Si-*t*-Bu), 0.11 (s, 3H, Si-CH_3), (-0.11) (s, 3H, Si-CH_3); **^{13}C-NMR (100 MHz, $CDCl_3$, 25 °C)**: δ [ppm] = 203.5 (C-5), 157.4 (C=O), 138.9-126.1 (C^{Ar}), 88.1 (C-4), 77.0 (C-3), 73.6 (O-CH_2-Ph), 73.2 (O-CH_2-Ph), 70.4 (H-1), 67.4 (O-CH_2-Ph), 61.6 (C-2), 48.5 (N-CH_2-Ph), 46.4 (C-5a), 25.8 (Si-*t*-Bu), -4.0, -5.1 (Si-CH_3); assignment of **38b**: **^{1}H-NMR (400 MHz, $CDCl_3$, 25 °C)**: δ [ppm] = 7.40-7.04 (m, 20H, Ar-H), 5.20 and 5.07 (d, *J* = 12.3 Hz, 2H, -N-C(O)-O-CH_2-Ph), 4.94-4.36 (m, 11H, 3xO-CH_2-Ph, N-CH_2-Ph, H-2, H-1, H-3), 4.10 (d, *J* = 9.5 Hz, 1H, H-4), 2.75 (dd, *J* = 13.7, 5.0 Hz, 1H, H-5a,eq), 2.51 (dd, *J* = 13.8, 10.8 Hz, 1H, H-5a,ax), 0.89 (s, 9H, Si-*t*-Bu), 0.9 (s, 3H, Si-CH_3), (-0.03) (s, 3H, Si-CH_3); **^{13}C-NMR (100 MHz, $CDCl_3$, 25 °C)**: δ [ppm] = 203.5 (C-5), 155.5 (C=O), 138.4-127.2 (C^{Ar}), 87.0 (C-4), 76.4 (C-3), 75.1 (O-CH_2-Ph), 73.4 (O-CH_2-Ph), 70.0 (H-2), 67.1 (O-CH_2-Ph), 66.2 (C-1), 56.0 (N-CH_2-Ph), 48.2 (C-5a), 25.8 (Si-*t*-Bu), -4.8, -4.9 (Si-CH_3); **RP-HPLC**: t_r**38** = 4.8 min, t_r**38b** = 5.9 min (ZORBAX SB-C18, 5 µm, 0.4 mL/min, 80-100% MeCN in 20 min); **HRMS**: calcd for $C_{41}H_{49}FNO_6SiNa$ $[M+Na]^+$, 702.3221; found, 702.3225.

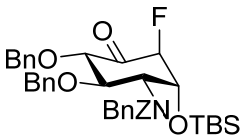

Benzyl benzyl((1R,2R,3S,5S,6R)-2,3-bis(benzyloxy)-6-((tert-butyldimethylsilyl)oxy)-5-fluoro-4-oxocyclohexyl)carbamate (37) LDA-solution in anhydrous THF (0.2 M) was freshly prepared by addition of *n*-BuLi (1.01 mL, 1.62 mmol, 1.6 M in hexane) to an ice-cold solution of (*i*-Pr)$_2$NH (0.25 mL, 1.78 mmol) in anhydrous THF (6.8 mL), stirred for 30 min at 0 °C. The cyclohexanone **38** (1.00 g, 1.477 mmol) was solved in anhydrous THF (7 mL) under argon atmosphere, cooled to -74 °C and the LDA-solution added dropwise over 15 min. After stirring at -74 °C for 3.5 h, NFSI (0.51 g, 1.62 mmol) solved in THF (6.5 mL) was added slowly. After 1.5 h water (3 mL) and CH_2Cl_2 were added to the cold solution and the aqueous acidified with sat. aqueous

NH_4Cl. The organic layer was separated and the aqueous layer extracted with CH_2Cl_2 (4x20 mL) and the combined organic phases dried ($MgSO_4$) and the solvent removed under reduced pressure. The residue was purified via flash chromatography (98:2 to 85:15 petroleum ether/ethyl acetate in 60 min) yielding the fluorocyclohexanone **37** (476.52 mg, 46%) as colorless oil.

R_f = 0.50 (petroleum ether/ethyl acetate 5:1), Seebach-reagent; ^{19}F-NMR at -40°°C shows three distinct signals, indicating three conformers A, B, C in a ratio 1.00:3.49:1.52. Assignment for conformer A: **^{19}F-NMR (470 MHz, $CDCl_3$, -40 °C)**: δ [ppm] = -187.1. Most probably the least abundant conformer A is not observed/distinguishable in HMQC, thus no assignment could be made for ^{1}H- or ^{13}C-NMR. Assignment for conformer B: **^{1}H-NMR (500 MHz, $CDCl_3$, -40 °C)**: δ [ppm] = 7.43-6.95 (m, 20H, Ar-H), 5.40-5.04 (m, 2H, -N-C(O)-O-CH_2-Ph), 4.99 (d, *J* = 11.7 Hz, 1H, H-2), 4.87-4.31 (m, 4H, N-CH_2-Ph), 4.73-4.70 (m, 1H, H-4), 4.53 (dd, *J* = 50.9, 6.0 Hz, 1H, H-5a), 4.31-4.26 (m, 1H, H-1b), 4.05-3.98 (m, 1H, H-3), 0.84 (s, 9H, Si-*t*-Bu), 0.09, -0.21 (s, 6H, Si-CH_3), **^{13}C-NMR (126 MHz, $CDCl_3$, -40 °C)**: δ [ppm] = 200.6 or 200.3 (d, *J* = 19.7 or 19.3 Hz, C=O), 157.5 (C=O (CBz)), 128.8-125.9 (C^{Ar}), 90.8 (d, *J* = 186 Hz, C-5a), 85.6 or 85.4 (C-4), 76.9 (C-3), 73.7 (O-CH_2-Ph), 73.1 (O-CH2-Ph), 71.7 (d, *J* = 23.9 Hz, C-1), 67.7 or 67.6 (-N-C(O)-O-CH_2-Ph), 56.8 or 56.6 (C-2), 48.9 (N-CH_2-Ph), 25.7 (-Si-C-CH_3), 18.0 (-Si-C-CH_3), (-4.0)-(-5.6) (-Si-CH_3-); **^{19}F-NMR (470 MHz, $CDCl_3$, -40 °C)**: δ [ppm] = -187.9; Assignment for conformer C: **^{1}H-NMR (500 MHz, $CDCl_3$, -40 °C)**: δ [ppm] = 7.43-6.95 (m, 20H, Ar-H), 5.40-5.04 (m, 2H, -N-C(O)-O-CH_2-Ph), 5.14-5.10 (m, 1H, H-2), 4.87-4.31 (m, 4H, N-CH_2-Ph), 4.78-4.76 (m, 1H, H-4), 4.57 (dd, J = 49.4, 7.4 Hz, 1H, H-5a), 4.53-4.48 (m, 1H, H-1), 4.05-3.98 (m, 1H, H-3), 0.87, (s, 9H, Si-*t*-Bu), 0.03, 0.17 (s, 3H, CH_3); **^{13}C-NMR (126 MHz, $CDCl_3$, -40 °C)**: δ [ppm] = 200.6 or 200.3 (d, *J* = 19.7 or 19.4 Hz, C=O), 156.6 (C=O (CBz)), 128.8-125.9 (C^{Ar}), 91.0 (d, *J* = 185 Hz, C-5a), 85.4 (C-4), 76.4 (C-3), 73.7 (O-CH_2-Ph), 73.1 (O-CH2-Ph), 70.8 (d, *J* = 38.4 Hz, C-1), 67.8 (-N-C(O)-O-CH_2-Ph), 56.8 or 56.6 (C-2), 48.0 (N-CH_2-Ph), 25.7 (-Si-C-CH_3), 17.9 (-Si-C-CH_3), (-4.0)-(-5.6) (-Si-CH_3-); **^{19}F-NMR (470 MHz, $CDCl_3$, -40°C)**: δ [ppm] = -188.4; **RP-HPLC**: t_r = 5.9 min (ZORBAX SB-C18, 5 µm, 0.4 mL/min, 80-100% MeCN in 20 min); **HRMS**: calcd for $C_{41}H_{48}FNO_6SiNa$ $[M+Na]^+$, 720.3127; found, 720.3121.

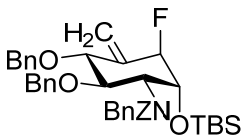

Benzyl benzyl((1R,2R,3R,5S)-2,3-bis(benzyloxy)-6-((tert-butyldimethylsilyl)oxy)-5-fluoro-4-methylenecyclohexyl)carbamate (36)

Cyclohexanone **37** (290.60 mg, 0.416 mmol) was presented in a heat-dried schlenk-

tube, coevaporated two times with toluene and dried under vacuum for 19 h. The starting material was solved in anhydrous toluene (2 mL) and freshly prepared Cp_2TiMe_2[294] (0.25 M, 6.7 mL, 1.66 mmol) was added under argon atmosphere. The reaction was heated in an oil-bath to 70 °C and stirred for 3 h, after which the solution was allowed to reach room temperature. Water (5 mL) and petroleum ether/ethyl acetate (5:1, 10 mL) were added and the mixture stirred at room temperature for 24 h, resulting in an orange suspension. After filtration through Celite® 545, the filter cake was washed with ethyl acetate and the filtrate was washed with sat. aqueous NaCl and dried ($MgSO_4$). The solvents were removed under reduced pressure and the residue purified by automated flash chromatography (100% cyclohexane to 9:1 cyclohexane/ethyl acetate in 45 min) yielding olefin **36** (175.72 mg, 61%) as slightly yellow oil.

R_f = 0.75 (petroleum ether/ethyl acetate 5:1), Seebach-reagent; The ^{19}F-NMR at -40 °C shows four distinct signals, indicating four conformers A, B, C, D in a ratio of 1.00:3.48:15.91:8.36. Only two sets of signals are observed in HMQC, most probably belonging to most abundant conformers C and D. Assignment for conformer A: **^{19}F-NMR (471 MHz, $CDCl_3$, -40 °C)**: δ [ppm] = -176.1; Assignment for conformer B: **^{19}F-NMR (471 MHz, $CDCl_3$, -40 °C)**: δ [ppm] = -176.6; Assignment for conformer C: **^{1}H-NMR (500 MHz, $CDCl_3$, -40 °C)**: δ [ppm] = 7.45-6.92 (m, 20H, Ar-H), 5.56 (s, 1H, H-6a), 5.40-5.04 (m, 2H, N-C(O)-O-C$\underline{H}_2$-Ph), 5.28 (s, 1H, H-6b), 4.91-3.39 (m, 2H, (C-3)-O-C$\underline{H}_2$-Ph), 4.87-4.85 (m, 1H, H-2), 4.83 (dd, *J* = 48.6, 5.4 Hz, 1H, H-5a), 4.82-4.37 (m, 2H, N-C$\underline{H}_2$-Ph), 4.64-4.55 (m, 2H, (C-4)-O-C$\underline{H}_2$-Ph), 4.45-4.38 (m, 1H, H-4), 3.80 (q, J = 8.8 Hz, 1H, H-3), 0.86 or 0.84 (s, 9H, *t*-Bu), 0.09-(-0.22) (s, 3H, CH_3); **^{13}C-NMR (160 MHz, $CDCl_3$, -40 °C)**: δ [ppm] = 157.3 or 156.6 (C=O), 139.3-125.9 (C^{Ar}), 116.9 (C-6), 92.5 (d, *J* = 171 Hz, C-5a), 82.3 (C-4), 77.2 (C-3), 73.6 or 73.5 (O-$\underline{C}H_2$-Ph), 72.7 (O-$\underline{C}H_2$-Ph), 71.1 (d, *J* = 29 Hz, C-1), 67.3 or 67.2 (N-C(O)-O-$\underline{C}H_2$-Ph), 57.5 (C-2), 49.1 or 48.3 (N-$\underline{C}H_2$-Ph), 25.7 (-Si-$\underline{C}$-CH_3), 17.8-17.4 (-Si-C-$\underline{C}H_3$), (-3.8)-(-5.6) (-Si-CH_3-); **^{19}F-NMR (471 MHz, $CDCl_3$, -40 °C)**: δ [ppm] = -177.9; Assignment for conformer D: **^{1}H-NMR (500 MHz, $CDCl_3$, -40 °C)**: δ [ppm] = 7.45-6.92 (m, 20H, Ar-H), 5.56 (s, 1H, H-6a), 5.40-5.04 (m, 2H, N-C(O)-O-C$\underline{H}_2$-Ph), 5.28 (s, 1H, H-6b), 4.91-3.39 (m, 2H, (C-3)-O-C$\underline{H}_2$-Ph), 4.82-4.37 (m, 2H, N-C$\underline{H}_2$-Ph), 4.80 (dd, *J* = 46.9, 6.2 Hz, 1H, H-5a), 4.78-4.74 (s, 1H, H-2b), 4.64-4.55 (m, 2H, (C-4)-O-C$\underline{H}_2$-Ph), 4.45-4.38 (m, 1H, H-4), 4.15 (q, *J* = 3.1 Hz, 1H, H-1), 3.80 (q, J = 8.8 Hz, 1H, H-3), 0.86 or 0.84 (s, 9H, *t*-Bu), 0.09-(-0.22) (s, 3H, CH_3); **^{13}C-NMR (160 MHz, $CDCl_3$, -40 °C)**: δ [ppm] = 157.3 or 156.6 (C=O), 139.3-125.9 (C^{Ar}), 116.9 (C-6), 93.8 (d, *J* = 168 Hz, C-5a), 82.6 (C-4), 77.2 (C-3), 73.6 or 73.5 (O-$\underline{C}H_2$-Ph), 72.7 (O-$\underline{C}H_2$-Ph), 72.0 (d, *J* = 29 Hz, C-1), 67.3 or 67.2 (N-C(O)-O-$\underline{C}H_2$-Ph), 57.6 (C-2), 49.1 or 48.3 (N-$\underline{C}H_2$-Ph), 25.7 (-Si-$\underline{C}$-CH_3), 17.8-17.4 (-Si-C-$\underline{C}H_3$), (-3.8)-(-5.6) (-Si-CH_3-);

^{19}F-NMR (471 MHz, $CDCl_3$, -40 °C): δ [ppm] = -178.7; **RP-HPLC**: t_r = 8.9 min (ZORBAX SB-C18, 5 µm, 0.4 mL/min, 80-100% MeCN in 20 min); **HRMS**: calcd for $C_{42}H_{50}FNO_5SiNa$ $[M+Na]^+$, 718.3334; found, 718.3328.

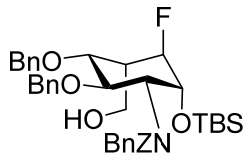

(5a*R*)-2-Amino-*N*-benzyl-N-benzyloxycarbonyl-3,4-di-*O*-benzyl-2-deoxy-5a-fluoro-carba-idose (48) To the olefin **36** (481.36 mg, 0.692 mmol) solved in anhydrous THF (5 mL) was added a solution of 9-BBN in THF (8.3 mL, 4.150 mmol, 0.5 M) at room temperature. After stirring at room temperature for 2 h the temperature was increased to 66 °C. No starting material could be detected via TLC after additional 3.5 h and the solution was cooled to 0 °C. 3N NaOH aqueous solution (2.8 mL, 8.400 mmol) and 35%wt H_2O_2 solution (2.8 mL) were successively added at 0 °C. The solution was stirred for 2 h at room temperature before stopping the reaction with 0.5 N $Na_2S_2O_3$ aqueous solution (10 mL) and diluting with CH_2Cl_2 (60 mL). The organic phase was separated and the aqueous phase extracted with CH_2Cl_2 (3x20 mL). The combined organic layers were washed with sat. aqueous NaCl, followed by drying with $MgSO_4$. The solvent was removed under reduced pressure and the residue purified by automated flash chromatography (40 g silica, 95:5 to 75:25 petroleum ether/ethyl acetate in 90 min) yielding the protected fluoro-carba-β-L-idosamine **48** (249.05 mg, 50%) as a colorless foam.

The ^{19}F-NMR at -40 °C shows three distinct signals, indicating three conformers A, B, C in a ratio of 1.00:10.90:21.98. Assignment for conformer A: **^{1}H-NMR (500 MHz, $CDCl_3$, -40 °C)**: δ [ppm] = 7.48-6.95 (m, 20H, Ar-H), 5.43-3.41 (m, N-C(O)-O-C$\underline{H_2}$-Ph), 5.07-4.49 (m, 4H, O-C$\underline{H_2}$-Ph), 4.89-4.07 (m, 2H, N-C$\underline{H_2}$-Ph), 4.68-4.84 (m, 1H, H-2), 4.65-4.56 (m, 1H, H-5a), 4.30- 3.67 (m, 2H, H6a and b), 4.18 (br, 1H, H-1); 4.17-4.15 (m, 2H, H-3 and H-4), 2.79 (br, 1H, H-5), 0.98-0.95 (m, 9H, *t*-Bu-Si), 0.13-(-0.20) (m, 6H, Me_2-Si); **^{13}C-NMR (126 MHz, $CDCl_3$, -40 °C)**: δ [ppm] 157.0 or 156.4 or 155.2 (C=O), 139.1-125.9 (C^{Ar}), 91.6 or 91.5 or 91.3 (d, *J* = 174 or 175 Hz, C-5a), 82.4 or 82.0 (C-4), 74.1 or 73.7 or 73.2 or 73.1 or 72.4 or 72.1 (O-$\underline{C}H_2$-Ph), 73.6 (C-3), 72.4 (d, *J* = 29 Hz, C-1), 67.4 or 67.2 or 66.5 (N-C(O)-O-$\underline{C}H_2$-Ph), 61.1 or 60.8 or 60.7 (d, *J* = 11 Hz, C-6a and b), 57.8 (C-2), 52.9 or 49.6 or 49.0 (N-$\underline{C}H_2$-Ph), 44.6 or 43.8 or 43.6 (d, *J* = 18 Hz, C-5), 26.0, 25.8 (*t*-Bu-Si), -4.4, -4.7, -5.0, -5.4, -5.9, -6.0 (Me_2-Si); **^{19}F-NMR (470 MHz, $CDCl_3$, -40 °C)**: δ [ppm] = -179.98 (s, 1F); Assignment for conformer B: **^{1}H-NMR (500 MHz, $CDCl_3$, -40 °C)**: δ [ppm] = 7.48-6.95 (m, 20H, Ar-H), 5.49 (t, J = 10.3 Hz, 1H, H-3), 5.43-

3.41 (m, N-C(O)-O-C$\underline{H_2}$-Ph), 5.07-4.49 (m, 4H, O-C$\underline{H_2}$-Ph), 4.89-4.07 (m, 2H, N-C$\underline{H_2}$-Ph), 4.65-4.56 (m, 1H, H-5a), 4.30- 3.67 (m, 2H, H6a and b), 4.13 (m, 1H, H-1), 3.92 (dd, 1H, *J* = 9.6, 5.4 Hz, H-4), 3.22 (br, 1H, H-2), 2.79 (br, 1H, H-5), 0.98-0.95 (m, 9H, *t*-Bu-Si), 0.13-(-0.20) (m, 6H, Me_2-Si); **^{13}C-NMR (126 MHz, $CDCl_3$, -40 °C)**: δ [ppm] = 157.0 or 156.4 or 155.2 (C=O), 139.1-125.9 (C^{Ar}), 91.6 or 91.5 or 91.3 (d, *J* = 174 or 175 Hz, C-5a), 83.1 (C-4), 74.9 (C-3), 74.1 or 73.7 or 73.2 or 73.1 or 72.4 or 72.1 (O-$\underline{C}H_2$-Ph), 70.4 (d, *J* = 28 Hz, C-1), 67.4 or 67.2 or 66.5 (N-C(O)-O-$\underline{C}H_2$-Ph), 63.6 (C-2), 61.1 or 60.8 or 60.7 (d, *J* = 11 Hz, C-6), 52.9 or 49.6 or 49.0 (N-$\underline{C}H_2$-Ph), 44.6 or 43.8 or 43.6 (d, *J* = 18 Hz, C-5), 26.0, 25.8 (*t*-Bu-Si), -4.4, -4.7, -5.0, -5.4, -5.9, -6.0 (Me_2-Si); **^{19}F-NMR (470 MHz, $CDCl_3$, -40 °C)**: δ [ppm] = -180.93 (s, 1F); Assignment for conformer C: **^{1}H-NMR (500 MHz, $CDCl_3$, -40 °C)**: δ [ppm] = 7.48-6.95 (m, 20H, Ar-H), 5.43-3.41 (m, N-C(O)-O-C$\underline{H_2}$-Ph), 5.07-4.49 (m, 4H, O-C$\underline{H_2}$-Ph), 4.89-4.07 (m, 2H, N-C$\underline{H_2}$-Ph), 4.80-4.76 (m, 1H, H-2), 4.70-4.62 (m, 1H, H-5a), 4.40 (br, 1H, H-1), 4.30-3.67 (m, 2H, H6a and b), 4.17-4.15 (m, 2H, H-3 and H-4), 2.79 (br, 1H, H-5), 0.98 or 0.97 or 0.95 (m, 9H, *t*-Bu-Si), 0.13-(-0.20) (m, 6H, Me_2-Si); **^{13}C-NMR (126 MHz, $CDCl_3$, -40 °C)**: δ [ppm] = 157.0 or 156.4 or 155.2 (C=O), 139.1-125.9 (C^{Ar}), 91.6 or 91.5 or 91.3 (d, *J* = 174 or 175 Hz, C-5a), 82.4 or 82.0 (C-4), 74.1 or 73.7 or 73.2 or 73.1 or 72.4 or 72.1 (O-$\underline{C}H_2$-Ph), 73.6 (C-3), 71.0 (d, *J* = 28 Hz, C-1), 67.4 or 67.2 or 66.5 (N-C(O)-O-$\underline{C}H_2$-Ph), 61.1 or 60.8 or 60.7 (d, *J* = 11 Hz, C-6a and b), 58.1 (C-2), 52.9 or 49.6 or 49.0 (N-$\underline{C}H_2$-Ph), 44.6 or 43.8 or 43.6 (d, *J* = 18 Hz, C-5), 26.0, 25.8 (*t*-Bu-Si), -4.4, -4.7, -5.0, -5.4, -5.9, -6.0 (Me_2-Si); **^{19}F-NMR (470 MHz, $CDCl_3$, -40 °C)**: δ [ppm] = -182.03 (s, 1F); **RP-HPLC**: t_r = 14.2 min (ZORBAX SB-C18, 5 µm, 0.4 mL/min, 60-80 % MeCN in 20 min); **HRMS**: calcd for $C_{42}H_{53}FNO_6Si$ $[M+H]^+$, 714.3621 found, 714.3617.

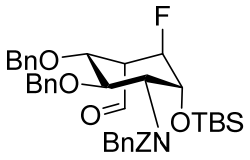

Benzyl benzyl((1R,2R,3R,4R,5R,6R)-2,3-bis(benzyloxy)-6-((tert-butyldimethylsilyl)oxy)-5-fluoro-4-formylcyclohexyl)carbamate (49) To 2-iodoxybenzoic acid (297 mg, 0.466 mmol) solved in anhydrous DMSO (1 mL) was added a solution of the protected fluoro-carba-β-L-idosamine **48** (95.0 mg, 0.133 mmol) in anhydrous DMSO (0.5 mL) at room temperature. The solution was stirred at room temperature for 14 h, as reaction monitoring via LC-MS showed complete consumption of starting material. Water (5 mL) was added and the pH adjusted to pH 7 to 9 with sat aqueous NaHCO3. Then 0.5M solution of Na2SO3 was added (5 mL) and the solution extracted wit CH2Cl2 (4y20 mL). The combined organic layers where dried (MgSO4) and

the solvents removed under reduced pressure. The residue was used in the next step without further purification.

RP-HPLC: t_r = 7.0 min (ZORBAX SB-C18, 5 µm, 0.4 mL/min, 80-100 % MeCN in 20 min); **ESI-MS**: calcd for $C_{42}H_{50}FNO_6Si$ $[M+H]^+$, 712.35 found, 712.34.

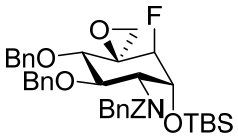

Benzyl benzyl((3S,4S,5R,6R,7R,8S)-4,5-bis(benzyloxy)-7-((tert-butyldimethylsilyl)oxy)-8-fluoro-1-oxaspiro[2.5]octan-6-yl)carbamate (34) The olefin **36** (281.68 mg, 0.4047 mmol) was solved in CH_2Cl_2 (10 mL). The solution was cooled to 0 °C and *m*CPBA (1.2 g, 5.26 mmol, 77%) solved in CH_2Cl_2 (6 mL) was added. The cloudy suspension was stirred at room temperature for 6 days. HPLC shows ~50% conversion, another portion of *m*CPBA (90 mg, 0.40 mmol, 77%) was added. After 10 days again *m*CPBA (90 mg, 0.40 mmol) is added and the reaction stirred at room temperature for additional 4 days after which HPLC-monitoring shows almost complete conversion. Sat. aqueous Na_2SO_3 (10 mL) was added and the suspension through an RC-syringe filter (0.2 µm) and the filtrate diluted with CH_2Cl_2 (60 mL). The organic layer is washed with sat. aqueous Na_2SO_3 (3x30 mL), sat. aqueous $NHCO_3$ and sat. aqueous NaCl, followed by drying with $MgSO_4$. The solvent was removed under reduced pressure and the residue purified by automated flash chromatography (40 g silica, 100% petroleum ether to 90:10 petroleum ether/ethyl acetate in 30 min). Fractions containing product were combined and freeze-dried, yielding the epoxide **34** (170.93 mg, 59%) as colorless solid.

The ^{19}F-NMR at -40 °C shows three distinct signals, indicating three conformers A, B, C in a ratio of 1.00:2.37:1.26. Conformers A and C could not be distinguished in HSQC due to similar intensity. Assignment for conformer A or C: **^{1}H-NMR (500 MHz, $CDCl_3$, -40 °C)**: δ [ppm] = 7.44-6.89 (m, 20H, Ar-H), 5.39-4.94 (m, 2H, N-C(O)-O-C$\underline{H}_2$-Ph), 4.97-4.42 (m, 2H, O-C$\underline{H}_2$-Ph), 4.82-3.39 (m, 2H, O-C$\underline{H}_2$-Ph), 4.79-4.38 (m, 2H, N-C$\underline{H}_2$-Ph), 4.75 (s, 1H, H-2), 4.24 (d, *J* = 8.5 Hz, 1H, H-4), 4.16 (br, 1H, H-1), 4.16 (d, *J* = 46.9 Hz, 1H, H-5a), 3.90 (q, *J* = 10.9 Hz, 1H, H-3), 3.38 (br, 1H, H-6a), 2.69 (br, 1H, H-6b), 0.87 (s, 9H, *t*-Bu), 0.06-(-0.28) (s, 3H, CH_3); **^{13}C-NMR (176 MHz, $CDCl_3$, -20 °C)**: δ [ppm] = 157.2 or 156.5 (C=O), 138.6-125.9 (C^{Ar}), 94.2 (d, *J* = 178 Hz, C-5a), 78.3 (C-4), 75.8 (O-$\underline{C}H_2$-Ph), 75.3 (C-3), 72.7 or 72.5 (O-$\underline{C}H_2$-Ph), 71.5 (d, *J* = 26.4 Hz, H-1), 67.3 (N-C(O)-O-$\underline{C}H_2$-Ph), 57.1 (C-2), 49.1 (N-$\underline{C}H_2$-Ph), 48.4 or 48.2 (C-6), 25.9 (-Si-*t*-Bu), 17.7 (Si-C-), 1.3-(-6.3) (-Si-CH_3-); **^{19}F-NMR (470 MHz, $CDCl_3$, -40 °C, ^{1}H-coupled)**: δ [ppm] = -190.47 (d, *J* = 49.9

Hz) or -191.92 (d, J = 48.6 Hz); Assignment for conformer B: **^{1}H-NMR (500 MHz, $CDCl_3$, -40 °C)**: δ [ppm] = 7.44-6.89 (m, 20H, Ar-H), 5.39-4.94 (m, 2H, N-C(O)-O-C$\underline{H_2}$-Ph), 4.97-4.42 (m, 2H, O-C$\underline{H_2}$-Ph), 4.82-3.39 (m, 2H, O-C$\underline{H_2}$-Ph), 4.70-4.38 (m, 2H, N-C$\underline{H_2}$-Ph), 4.85 (br, 1H, H-2), 4.40 (br, 1H, H-1), 4.28 (d, *J* = 8.8 Hz, 1H, H-4), 4.16 (d, *J* = 46.9 Hz, 1H, H-5a), 3.90 (q, *J* = 10.9 Hz, 1H, H-3), 3.38 (br, 1H, H-6a), 2.69 (br, 1H, H-6b), 0.87 (s, 9H, *t*-Bu), 0.06-(-0.28) (s, 3H, CH_3); **^{13}C-NMR (176 MHz, $CDCl_3$, -20 °C)**: δ [ppm] = 157.2 or 156.5 (C=O), 138.6-125.9 (C^{Ar}), 94.2 (d, *J* = 178 Hz, C-5a), 78.1 (C-4), 75.3 (C-3), 72.7 or 72.5 (O-$\underline{C}H_2$-Ph), 70.4 (d, *J* = 26.1 Hz, H-1), 67.4 (N-C(O)-O-$\underline{C}H_2$-Ph), 57.1 (C-2), 48.4 or 48.2 (C-6), 48.4 or 48.2 (N-$\underline{C}H_2$-Ph), 25.9 (-Si-*t*-Bu), 17.7 (Si-C-), 1.3-(-6.3) (-Si-CH_3-); **^{19}F-NMR (470 MHz, $CDCl_3$, -40 °C, ^{1}H-coupled)**: δ [ppm] = -191.47 (d, J = 48.2 Hz); Assignment for conformer A or C: **^{1}H-NMR (500 MHz, $CDCl_3$, -40 °C)**: δ [ppm] = 7.44-6.89 (m, 20H, Ar-H), 5.39-4.94 (m, 2H, N-C(O)-O-C$\underline{H_2}$-Ph), 5.26 (br, 1H, H-3), 4.97-4.42 (m, 2H, O-C$\underline{H_2}$-Ph), 4.82-3.39 (m, 2H, O-C$\underline{H_2}$-Ph), 4.85-4.08 (m, 2H, N-C$\underline{H_2}$-Ph), 4.16 (d, *J* = 46.9 Hz, 1H, H-5a), 4.12 (br, 1H, H-1), 4.03 (*J* = 9.5 Hz, 1H, H-4), 3.34 (br, 1H, H-2), 3.38 (br, 1H, H-6a), 2.69 (br, 1H, H-6b), 0.87 (s, 9H, *t*-Bu), 0.06-(-0.28) (s, 3H, CH_3); **^{13}C-NMR (176 MHz, $CDCl_3$, -20 °C)**: δ [ppm] = 157.2 or 156.5 (C=O), 138.6-125.9 (C^{Ar}), 94.2 (d, *J* = 178 Hz, C-5a), 78.6 (C-4), 75.8 (O-$\underline{C}H_2$-Ph), 72.7 or 72.5 (O-$\underline{C}H_2$-Ph), 69.4 (d, *J* = 25.2 Hz), 66.5 (N-C(O)-O-$\underline{C}H_2$-Ph), 63.0 (C-2), 52.9 (N-$\underline{C}H_2$-Ph), 48.4 or 48.2 (C-6), 25.9 (-Si-*t*-Bu), 17.7 (Si-C-), 1.3-(-6.3) (-Si-CH_3-); **^{19}F-NMR (470 MHz, $CDCl_3$, -40 °C, ^{1}H-coupled)**: δ [ppm] = -190.47 (d, *J* = 49.9 Hz) or -191.92 (d, J = 48.6 Hz); **RP-HPLC**: t_r = 8.2 min (ZORBAX SB-C18, 5 µm, 0.4 mL/min, 80-100% MeCN in 20 min); **HRMS**: calcd for $C_{42}H_{50}FNO_6SiH$ $[M+H]^+$, 712.3464; found, 712.3450.

*assignment through HSQC

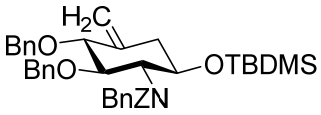

Benzyl benzyl((1R,2R,3R,6R)-2,3-bis(benzyloxy)-6-((tert-butyldimethylsilyl)oxy)-4-methylenecyclohexyl)carbamate (47) Cyclohexanone **38bFehler! Verweisquelle konnte nicht gefunden werden.** (1.05 g, 1.54 mmol) was presented in a heat-dried schlenk-tube and was coevaporated two times with toluene. The starting material was solved in anhydrous toluene (16 mL) and freshly prepared Cp_2TiMe_2 (0.3 M, 10 mL, 3.09 mmol) was added under argon atmosphere. The reaction was heated in an oil-bath to 65 °C and stirred for 6 h, after which again Cp_2TiMe_2 (0.3 M, 2.6 mL, 0.77 mmol) was added under argon atmosphere. The solution was stirred for another 15 h at 65 °C after which the solution was allowed to reach room temperature. Water (20 mL) and petroleum ether/ethyl acetate (5:1, 20 mL) were added and the

mixture stirred at room temperature for 1 h, resulting in an orange suspension. After filtration through celite® 545, the filter cake was washed with ethyl acetate and the filtrate was washed with sat. aqueous NaCl and dried ($MgSO_4$). The solvents were removed under reduced pressure and the residue purified by automated flash chromatography (100% petroleum ether to 9:1 petroleum ether/ethyl acetate in 45 min) yielding olefin **47** (428 mg, 41%) as slightly yellow oil.

R_f = 0.64 (petroleum ether/ethyl acetate 5:1), Seebach-reagent; **major conformer A**: **^{1}H-NMR (600 MHz, $CDCl_3$)**: δ [ppm] = 7.43-7.01 (m, 20H, Ar-H), 5.27-4.99 (m, 2H, N-C(O)-O-C$\underline{H_2}$-Ph), 5.20 (s, 1H, H-6), 4.84-4.27 (m, 2H, N-C$\underline{H_2}$-Ph), 4.80-4.32 (m, 4H, 2x-O-C$\underline{H_2}$-Ph), 4.33 (s, 1H, H-3), 4.04 (s, 1H, H-1), 3.81 (m, 1H, H-4), 3.19 (t, *J* = 9.9 Hz, 1H, H-2), 2.64-1.97 (m, 2H, H-5a), 0.89 (s, 9H, *t*-Bu-O-Si), 0.10 (s, 3H, CH_3-O-Si); **minor conformer B**: **^{1}H-NMR (600 MHz, $CDCl_3$)**: δ [ppm] = 7.43-7.01 (m, 20H, Ar-H), 5.27-4.99 (m, 2H, N-C(O)-O-C$\underline{H_2}$-Ph), 4.96 (s, 1H, H-6), 4.84-4.27 (m, 2H, N-C$\underline{H_2}$-Ph), 4.80-4.32 (m, 4H, 2x-O-C$\underline{H_2}$-Ph), 4.33 (s, 1H, H-1), 4.33 (s, 1H, H-3), 3.81 (m, 1H, H-4), 3.09 (t, *J* = 8.2 Hz, 1H, H-2), 2.64-1.97 (m, 2H, H-5a), 0.89 (s, 9H, *t*-Bu-O-Si), 0.10 (s, 3H, CH_3-O-Si); **RP-HPLC**: t_r = 3.78 min (Kinetex-C18, 2.6 µm, 0.8 mL/min, 80-100 % MeCN in 20 min); **HRMS**: calcd for $C_{42}H_{51}NO_5SiNa$ $[M+Na]^+$, 700.3429; found, 700.3414.

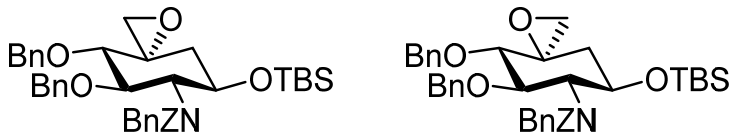

Benzyl benzyl((4S,5R,6R,7R)-4,5-bis(benzyloxy)-7-((tert-butyldimethylsilyl)oxy)-1-oxaspiro[2.5]octan-6-yl)carbamate (51/52) The olefin **47** (300.0 mg, 0.444 mmol) was solved in CH_2Cl_2 (3 mL). The solution was cooled to 0 °C and *m*CPBA (230 mg, 1.021 mmol, 77%) solved in CH_2Cl_2 (2 mL) was added. The cloudy suspension was stirred at room temperature for 4 days, and another portion of *m*CPBA (100 mg, 0.44 mmol, 77%) was added. After another 1.5h again mCPBA (100 mg, 0.40 mmol) is added and the reaction stirred at room temperature for additional 1h. A 10% aqueous solution of Na_2SO_3 (5 mL) was added and the organic layer separated. The organic layer is washed with 10% aqueous solution of Na_2SO_3 (2x100 mL), sat. aqueous $NHCO_3$ and sat. aqueous NaCl, followed by drying with $MgSO_4$. The solvent was removed under reduced pressure and the residue purified by automated flash chromatography (12 g silica, 98% petroleum ether to 88:12 petroleum ether/ethyl acetate in 45 min). Fractions containing product were combined and the

solvent removed under reduced pressure, yielding the 5*S*-epoxide **51** (53.2 mg, 17%) and 5*R*-epoxide **52** (153.3 mg, 50%) as colorless solids.

R_f = 0.33 (5R-epoxide) and 0.50 (5S-epoxide) (petroleum ether/ethyl acetate 5:1), Seebach-reagent; **5S-epoxide: ^{1}H-NMR (600 MHz, $CDCl_3$, 25 °C)**: δ [ppm] = 7.43-6.96 (m, 15H, Ar-H), 5.18 and 5.00 (d, *J* = 12.3 Hz, 2H, O-CH_2-Ph), 4.74-4.30 (8H, N-CH_2-Ph, 2xO-CH_2-Ph, H-1, H-3), 3.64 (d, *J* = 9.2 Hz, 1H, H-4), 3.20 (d, *J* = 5.0 Hz, 1H, H-6a), 3.07 (t, *J* = 10.0 Hz, 1H, H-2), 2.54 (d, *J* = 5.4 Hz, 1H, H-6b), 2.00 (t, *J* = 11.9 Hz, 1H, H5aa), 1.62 – 1.56 (m, 1H, H-5ab), 0.86 (s, 9H, *t*-Bu), 0.08, 0.03. -0.07, -0.13 (s, 3H, CH_3); **^{13}C-NMR (151 MHz, $CDCl_3$, 25 °C)**: δ [ppm] = 155.5 (C=O), 138.9-127.1 (C^{Ar}), 81.4 (C-4), 78.0 (C-3), 75.2 (O-CH_2-Ph), 71.1 (C-2), 66.9 (C-1, O-CH_2-Ph), 57.1 (N-CH_2-Ph), 49.7 (C-6), 40.5, 40.3 (C-5a), 25.9 (-Si-C-(CH_3)$_3$), 18.0 (-Si-C-(CH_3)$_3$), -4.6 (-Si-CH_3-); **5R-epoxide: ^{1}H-NMR (600 MHz, $CDCl_3$, 25 °C)**: δ [ppm] = 7.53-6.97 (m, 15H, Ar-H), 5.31-5.03 (m, 2H, O-CH_2-Ph), 4.93-4.28 (8H, N-CH_2-Ph, 2xO-CH_2-Ph, H-1, H-3), 3.69-3.52 (m, 1H, H-4), 3.15 (t, *J* = 10.4 Hz, 1H), 2.92 (m, 1H, H-6a), 2.52 (br, 1H, H-6b), 1.86-1.48 (m, 2H, H5a), 0.86 (s, 9H, *t*-Bu), 0.06, 0.02. -0.15, -0.21 (s, 3H, CH_3); **^{13}C-NMR (151 MHz, $CDCl_3$, 25 °C)**: δ [ppm] = 156.6 (C=O), 138.9-127.0 (C^{Ar}), 79.9, 79.8, 79.6 (C-4 and C-3), 75.1, 75.0 (O-CH_2-Ph), 69.8 (C-2), 68.4 (C-1), 67.4 (O-CH_2-Ph), 57.6, 56.5 (N-CH_2-Ph), 48.7, 48.5 (C-6), 40.1 (C-5a), 25.9 (-Si-C-(CH_3)$_3$), 17.9 (-Si-C-(CH_3)$_3$), -4.6 (-Si-CH_3-); **RP-HPLC**: t_r = 8.1 min (5S-epoxide) and 6.9 min (5R-epoxide) (ZORBAX SB-C18, 5 µm, 0.4 mL/min, 80-100 % MeCN in 30 min); **HRMS**: calcd for $C_{42}H_{51}NO_6SiNa$ $[M+Na]^+$, 716.3378, found, 716.3366 (5S-epoxide) and 716.3369 (5R-epoxide).

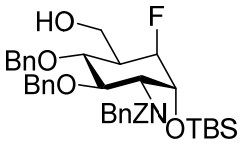

(5a*R*)-2-Amino-*N*-benzyl-*N*-benzyloxycarbonyl-3,4-di-*O*-benzyl-2-deoxy-5a-fluoro-1-O-*tert*-butyldimethylsilyl-carba-glucose (53) The epoxide **34** (47.17 mg, 0.0663 mmol) was transferred to a heat-dried schlenk-tube with toluene. The toluene was removed under reduced pressure and the starting material dried under vacuum (~10^{-2} mbar) for 17 h. Manganese powder (5.46 mg, 0.0994 mmol) together with 2,4,6-collidine hydrochloride (15.67 mg, 0.0994 mmol) were presented in a heat-dried schlenk-tube and heated under oil-pump vacuum until slight sublimation of collidine was observed. The reagents were cooled to room temperature and Cp_2TiCl_2 (4.95 mg, 0.0199 mmol) was added under argon atmosphere. Anhydrous and degassed THF (0.4 mL) was added and the suspension stirred 30 min until color change to green was completed after which 1,4-cyclohexadiene (28 µL) was added. The epoxide was solved

in degassed, anhydrous THF (0.3 mL) and slowly added to the green suspension, upon that a slight color change to light green-yellow could be observed. The reaction was heated to 50 °C in an oil bath and stirred under argon atmosphere for 1 h. The reaction temperature was increased to 55 °C and the reaction stirred for another 30 min. The reaction temperature was increased to 60 °C and the reaction stirred for 1.5 h, when HPLC-monitoring showed 90% consumption of the epoxide. The reaction was cooled to room temperature and 1M HCl (1 mL) was added slowly. The reaction was diluted with 5 mL ethyl acetate, the organic layer was separated and the aqueous phase extracted with ethyl acetate (3x10 mL) and CH_2Cl_2 (2x10 mL). The aqueous phase was basified with sat. aqueous $NaHCO_3$ and extracted with CH_2Cl_2 (2x10 mL). The combined organic phases were washed with sat. aqueous $NaHCO_3$ and, sat. aqueous NaCl and subsequently dried with $MgSO_4$. The solvent was removed under reduced pressure and the residue purified via RP-HPLC (Gemini® C18, 110 Å, 5 µm, 50x30 mm, 80-100% MeCN in 10 min). Fractions containing product were combined and freeze-dried yielding the alcohole **53** (15.41 mg, 33%) as a white solid.

The ^{19}F-NMR shows two broad signals, indicating conformers that interchange quickly at room temperature, thus the conformers were not distinguishable for ^{1}H and ^{13}C-NMR assignment. **^{1}H-NMR (700 MHz, $CDCl_3$)**: δ [ppm] = 7.42–7.00 (m, 20H, Ar-H), 5.36-4.99 (m, 2H, N-C(O)-O-C$\underline{H_2}$-Ph), 4.91-4.51 (m, 8H, 2xO-C$\underline{H_2}$-Ph, N-C$\underline{H_2}$-Ph, H2, H5a), 4.21 (br, 1H, H-1,conformer A), 3.99-3.83 (m, 5H, H-1, conformer B, H-6, H-3, H-4), 2.31-2.23 (m, 1H, H-5), 0.88 (s, 9H, *t*-Bu), 0.04 (s, 3H, CH_3); **^{13}C-NMR (176 MHz, $CDCl_3$)**: δ [ppm] = 156.9 (C=O), 138.7-126.7 (C^{Ar}), 91.8 (d, *J* = 171 Hz, C-5a), 81.1 (C-4), 77.5 (C-3), 75.5 (O-$\underline{C}H_2$-Ph), 72.7 and 72.2 (br, C-1), 67.2 (N-C(O)-O-$\underline{C}H_2$-Ph), 61.6 (C-6), 57.0 (C-2), 49.2 (N-$\underline{C}H_2$-Ph), 43.3 (d, *J* = 18 Hz, C-5), 26.0 (-Si-*t*-Bu), -5.0 (-Si-CH3-); **^{19}F-NMR (470 MHz, $CDCl_3$)**: δ [ppm] = -196.3 (br), -197.0; **RP-HPLC**: t_r =4.1 min (ZORBAX SB-C18, 5 µm, 0.4 mL/min, 80-100% MeCN in 20 min); **HRMS**: calcd for $C_{42}H_{52}FNO_6SiNa$ $[M+Na]^+$, 736.3440; found, 736.3421.

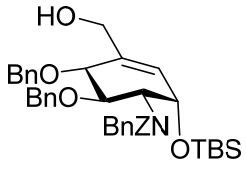

Benzyl benzyl((1R,2S,5R,6R)-5,6-bis(benzyloxy)-2-((tert-butyldimethylsilyl)oxy)-4-(hydroxy methylene)cyclohex-3-en-1-yl)carbamate (58)
Assignment for the most dominant conformer: **^{1}H-NMR (600 MHz, $CDCl_3$)**: δ [ppm] = 7.42–7.08 (m, 20H, Ar-H), 5.83 (d, *J* = 4.7 Hz, 1H, H-5a) 5.15-4.41 (m, 11H, N-C(O)-O-C$\underline{H_2}$-Ph, 2xO-C$\underline{H_2}$-Ph, N-C$\underline{H_2}$-Ph, H-1, H-2, H-3), 4.30 (br, 1H, H-4), 4.15-4.07 (m, 2H, H-

6), 0.98 (s, 9H, *t*-Bu), -0.07 (s, 3H, CH_3); **^{13}C-NMR (151 MHz, $CDCl_3$)**: δ [ppm] = 159.0 (C=O), 140.1 (C-5), 138.6-127.4 (C^{Ar}), 83.0 (C-4), 76.3 (C-3), 74.2, 73.7 (O-$\underline{C}H_2$-Ph), 68.8 (C-1), 68.1 (N-C(O)-O-$\underline{C}H_2$-Ph), 63.7 (C-6), 25.5 (-Si-*t*-Bu), 18.1 (-Si-$\underline{C}$-$(CH_3)_3$) 1.17 (-Si-CH_3-); **RP-HPLC**: t_r =4.6 min (ZORBAX SB-C18, 5 µm, 0.4 mL/min, 80-100 % MeCN in 20 min); **HRMS**: calcd for $C_{42}H_{51}NO_6SiNa$ $[M+Na]^+$, 716.3378; found, 716.3367.

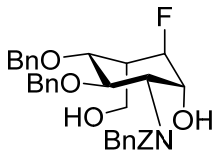

Dibenzyl (5a*R*)-2-Amino-N-benzyl-N-benzyloxycarbonyl-3,4-di-O-benzyl-2-deoxy-5a-fluoro-carba-idose-6-phosphate (62) To the silylated fluoro-carba-sugar precursor **48** (18.01 mg, 0.0252 mmol) solved in DMF (150 µL) was added a solution of TAS-F (30 µL, 0.0303 mmol, 1N in DMF). The reaction was stirred for 1.5 h at 23 °C. The reaction was diluted with 1 mL acetonitrile/water (50:50) and the solution loaded directly onto a C18-HPLC column (Gemini® C18, 110 Å, 5 µm, 50x30 mm), utilizing a gradient of 40-80% MeCN (A: 0.1% formic acid in H_2O) in 10 min. Fractions containing the product were combined and freeze-dried yielding the benzylated pseudo-sugar precursor **62** (15.07 mg, 99%) as colorless foam.

^{1}H-NMR (500 MHz, $CDCl_3$): δ [ppm] = 7.33-7.18 (m, 20H, Ar-H), 5.17 (q, *J* = 12.1 Hz, 2H, N-C(O)-O-C$\underline{H_2}$-Ph), 5.06 and 4.09 (d, *J* = 15.3 Hz, 2H, , N-C$\underline{H_2}$-Ph), 4.86 and 4.44 (d, *J* = 10.8 Hz, 2H, O-C$\underline{H_2}$-Ph), 4.77-4.66 (m, 3H, H-3, O-C$\underline{H_2}$-Ph), 4.57 (dd, *J* = 2.5, 2.8 Hz, 1H, H-5a), 3.99 (dd, *J* = 12.1, 6.7 Hz, 1H, H-6a), 3.92 (br, 1H, H-1), 3.89 (dd, *J* = 9.4, 6.3 Hz, 1H, H-4), 3.84 (dd, *J* = 12.2, 5.4 Hz, 1H, H-6b), 3.37 (d, *J* = 10.9 Hz, 1H, H-2), 2.71 (ddd, *J* = 12.1, 5.9 Hz, 1H, H-5); **^{13}C-NMR (176 MHz, $CDCl_3$)**: δ [ppm] = 159.4 (C=O), 138.6-127.8 (C^{Ar}), 91.3 (d, *J* = 171.7 Hz, C-5a), 82.5 (C-4), 75.6 (O-$\underline{C}H_2$-Ph), 75.3 (C-3), 73.8 (O-$\underline{C}H_2$-Ph), 72.8 (d, *J* = 28.4 Hz, C-1), 68.5 (N-C(O)-O-$\underline{C}H_2$-Ph), 63.7 (C-2), 60.8 (d, *J* = 12.1 Hz, C-6), 56.2 (N-$\underline{C}H_2$-Ph), 44.7 (d, *J* = 17.8 Hz, C-5); **^{19}F-NMR (282 MHz, $CDCl_3$)**: δ [ppm] = -185.40; **RP-HPLC**: t_r = 14.3 min (ZORBAX SB-C18, 5 µm, 0.4 mL/min, 20-100% MeCN in 20 min); **HRMS**: calcd for $C_{36}H_{38}FNO_6Na$ $[M+Na]^+$, 622.2575; found, 622.2579.

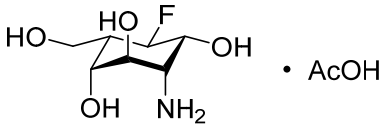

(5a*R*)-2-Amino-2-deoxy-5a-fluoro-carba-idose acetate (63) Perbenzylated fluoro-carba compound **62** (22.65 mg, 0.0378 mmol) was deprotected according to **GP1**, with the difference that only one portion of 10% Pd/C (100% *w/w*) was added. The

reaction was finished after 7 h. The lyophilized pseudo-sugar was purified via HILIC (NUCLEODUR® HILIC 5 µm, 150x4.6 mm, 98-90% MeCN in 20 min, A: 20 mM NH_4OAc in water pH 5.4). Due to missing UV-absorption of the product the fractions collected in time slices were analyzed via LC-MS (0-100% MeCN in 2 min). Fractions containing the target-mass were combined and freeze-dried yielding the pseudo-sugar **63** (3.26 mg, 34%) as the acetate salt.

^{1}H-NMR (700 MHz, $CDCl_3$): δ [ppm] = 4.90 (dt, *J* = 47.4, 7.2 Hz, 1H, H-5a), 4.33 (ddd, *J* = 11.1, 6.9, 4.5 Hz, 1H, H-1), 4.13 (dt, *J* = 6.2, 2.8 Hz, 1H, H-4), 4.09 (t, *J* = 5.9 Hz, 1H, H-3), 3.95 (ddd, *J* = 11.4, 6.0 Hz, 2H, H-6), 3.58 (brt, *J* = 6.0 Hz, 1H, H-2), 2.48 (dp, *J* = 11.8, 6.4 Hz, 1H, H-5); **^{13}C-NMR (176 MHz, $CDCl_3$)**: δ [ppm] = 91.0 (d, *J* = 171.9 Hz, C-5a), 70.7 (d, *J* = 5.8 Hz, C-4), 68.1 (C-3), 67.4 (d, *J* = 23.9 Hz, C-1), 58.28 (d, *J* = 6.6 Hz, C-6), 54.86 (d, *J* = 5.3 Hz, C-2), 43.41 (d, *J* = 17.2 Hz, C-5); **^{19}F-NMR (282 MHz, $CDCl_3$)**: δ [ppm] = -125.18; **HRMS**: calcd for $C_7H_{15}FNO_4Na$ $[M+H]^+$, 196.0980; found,196.0977.

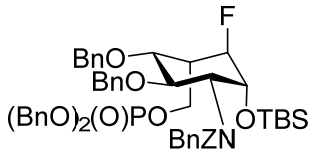

Dibenzyl (5a*R*)-2-Amino-*N*-benzyl-*N*-benzyloxycarbonyl-3,4-di-*O*-benzyl-2-deoxy-5a-fluoro-1-O-*tert*-butyldimethylsilyl-carba-idose-6-phosphate (66) The unphosphorylated fluoro-carba-sugar precursor **48** (24.63 mg, 0.0345 mmol) was transferred to a heat-dried schlenk-tube with anhydrous CH_2Cl_2. The CH_2Cl_2 was removed under reduced pressure and 1H-Tetrazole (12.08 mg, 0.173 mmol), anhydrous CH_2Cl_2 (4 mL) and dibenzyl *N,N*-diisopropylphosphoramidite (29 µL, 0.0862 mmol) were added successively. The mixture was stirred for 3 h at room temperature and HPLC-monitoring showed complete consumption of starting material. The reaction was cooled to 0 °C and *m*-CPBA (70%, 25.5 mg, 0.104 mmol) was added. After another hour HPLC shows completion of the reaction, the mixture was diluted with CH_2Cl_2 (30 mL) and 10 mL of aqueous 10% Na_2SO_3 was added. The mixture was stirred for 15 min, then the organic layer was separated and washed with aqueous 10% Na_2SO_3 (1x10 mL), 1M HCl (2x10 mL), saturated $NaHCO_3$ (2x10 mL) and brine (1x10 mL). The organic layer was dried ($MgSO_4$) and the solvent removed under reduced pressure. The reaction was purified via RP-HPLC (Gemini® C18, 110 Å, 5 µm, 50x30 mm, 80-100% MeCN in 10 min, A: 0.1% formic acid in H_2O). Fractions containing product were combined and freeze-dried yielding the phosphorylated pseudo-sugar precursor **66** (43.42 mg, 99%) as colorless foam.

^{1}H-NMR (500 MHz, $CDCl_3$): δ [ppm] = 7.41-6.89 (m, 30H, Ar-H), 5.32 and 5.15 (d, *J* = 12.4 Hz, 2H, N-C(O)-O-C$\underline{H_2}$-Ph), 5.03-4.98 (m, 4H, P-O-C$\underline{H_2}$-Ph), 4.85-4.32 (m, 10H, 2xO-C$\underline{H_2}$-Ph, N-C$\underline{H_2}$-Ph, H-5a, H-2, H-6), 4.21 (d, *J* = 12.0 Hz, 1H, H-1), 3.93 (br, 1H, H-4), 3.77 (br, 1H, H-3), 2.82-2.75 (m, 1H, H-5), 0.89 (s, 9H, *t*-Bu), 0.07 and 0.01 (s, 6H, 2xCH_3); **^{13}C-NMR (176 MHz, $CDCl_3$)**: δ [ppm] = 156.6 (C=O), 138.8-125.7 (C^{Ar}), 90.67 (d, *J* = 173.1 Hz, C-5a) and 90.00 (d, *J* = 170.5 Hz), 78.7 (C-4), 73.8 (C-3), 73.57 (d, *J* = 27.4 Hz, C-1), 72.3, 72.2. 71.6 (O-$\underline{C}H_2$-Ph), 69.4 (P(O)-(O-C$\underline{H_2}$-Ph)$_2$), 67.5 (N-C(O)-O-$\underline{C}H_2$-Ph), 64.28 (dd, *J* = 10.0, 5.6 Hz, C-6), 58.3 (C-2), 50.0 (N-$\underline{C}H_2$-Ph), 42.12 (d, *J* = 19.0 Hz, H-5), 34.4 (Si-$\underline{C}$-$(CH_3)_3$), 26.1 (Si-C-($\underline{C}H_3$))$_3$, -4.5, -5.3, -5.5 (Si-CH_3); **^{31}P-NMR (121 MHz, $CDCl_3$)**: δ [ppm] = -0.02; **^{19}F-NMR (282 MHz, $CDCl_3$)**: δ [ppm] = -185.12, -185.92 (br); **RP-HPLC**: t_r =9.6 min (ZORBAX SB-C18, 5 µm, 0.4 mL/min, 80-100% MeCN in 20 min); **HRMS**: calcd for $C_{56}H_{66}FNO_9PSi$ $[M+H]^+$, 974.4223; found, 996.4230.

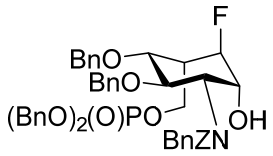

Dibenzyl (5a*R*)-2-Amino-*N*-benzyl-*N*-benzyloxycarbonyl-3,4-di-*O*-benzyl-2-deoxy-5a-fluoro-carba-idose-6-phosphate (67) To the silylated fluoro-carba precursor **66** (15.0 mg, 0.0154 mmol) solved in anhydrous THF (192.5 µL), were added K_2HPO_4-Buffer (1.8 µL, pH 7) and a solution of TBAF (7.7 µL, 0.0077 mmol, 1M in anhydrous THF stored over 2 Å molecular sieve). The reaction was stirred at 23 °C and after 4 h HPLC showed completion of the reaction. After dilution with 500 µL of Acetonitril/H_2O (1:1) the reaction was directly loaded onto a C18-HPLC column (Gemini® C18, 110 Å, 5 µm, 50x30 mm), utilizing a gradient of 40-100% MeCN (A: 0.1% formic acid in H_2O) in 15 min. Fractions containing the target-mass were combined and freeze-dried yielding the benzylated pseudo-sugar precursor **67** (5.44 mg, 41%) as colorless foam.

^{1}H-NMR (700 MHz, $CDCl_3$): δ [ppm] = 7.45-6.99 (m, 30H, Ar-H), 5.18 and 5.12 (d, *J* = 12.3 Hz, 2H, N-C(O)-O-C$\underline{H_2}$-Ph), 5.03-5.02 (m, 4H, P-O-C$\underline{H_2}$-Ph), 4.98 and 4.10 (d, *J* = 15.5 Hz, 2H, N-C$\underline{H_2}$-Ph); 4.74-4.34 (m, 8H, 2xO-C$\underline{H_2}$-Ph, H-5a, H-3, H-6), 4.01 (br, 1H, H-1), 3.83 (t, J = 7.6 Hz, 1H, H-4), 3.28 (br, 1H, H-2), 2.82 (br, 1H, H-5); **^{13}C-NMR (176 MHz, $CDCl_3$)**: δ [ppm] = 159.3 (C=O), 138.7-127.8 (C^{Ar}), 89.08 (d, *J* = 173.3 Hz, C-5a), 80.8 (C-4), 75.6 (O-$\underline{C}H_2$-Ph), 74.6 (C-3), 73.5 (br, C-1), 72.9 (O-$\underline{C}H_2$-Ph), 69.6 (P(O)-(O-$\underline{C}H_2$-Ph)$_2$), 68.5 (N-C(O)-O-$\underline{C}H_2$-Ph), 64.9 (C-6), 61.3 (C-2)*, 55.5 (N-$\underline{C}H_2$-Ph)*, 43.2 (br, C-5); **^{31}P-NMR (121 MHz, $CDCl_3$)**: δ [ppm] = -1.16; **^{19}F-NMR (282 MHz, $CDCl_3$)**: δ [ppm] = -187.92; **RP-HPLC**: t_r = 17.9 min (ZORBAX SB-C18, 5 µm, 0.4 mL/min, 20-100%

MeCN in 20 min); **HRMS**: calcd for $C_{50}H_{51}FNO_9PNa$ $[M+Na]^+$, 882.3178; found, 882.3179.

*assignment through HSQC

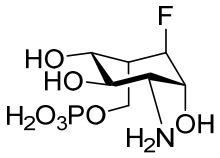

(5a*R*)-2-Amino-2-deoxy-5a-fluoro-carba-idose-6-phosphate (33) Perbenzylated fluoro-carba compound **67** (5.44 mg, 0.00633 mmol) was deprotected according to **GP1**. The reaction was finished after 24 h. The lyophilized pseudo-sugar was purified via HILIC (NUCLEODUR® HILIC 5 µm, 150x4.6 mm, 98-90% MeCN in 20 min, A: 20 mM NH_4OAc in water pH 5.4), due to missing UV-absorption of the product, the fractions collected in time slices were analyzed via LC-MS (0-100% MeCN in 2 min). Fractions containing the target-mass were combined and freeze-dried, yielding the pseudo-sugar **33** (1.18 mg, 68%) as colorless foam.

^{1}H-NMR (500 MHz, D_2O): δ [ppm] = 4.98 (dt, *J* = 46.9, 7.0 Hz, 1H, H-5a), 4.35 (ddd, *J* = 11.2, 6.8, 4.7 Hz, 1H, H-1), 4.22 (t, *J* = 6.1 Hz, 1H, H-3), 4.19 – 4.16 (m, 2H, H-4, H-6a), 4.08 (dt, *J* = 11.2, 6.3 Hz, 1H, H-6b), 3.63 (t, *J* = 6.1 Hz, 1H, H-2), 2.66 – 2.47 (m, 1H, H-5); **^{13}C-NMR (126 MHz, D_2O)**: δ [ppm] = 90.1 (d, *J* = 171.7 Hz, C-5a), 70.4 (d, *J* = 5.3 Hz, C-4), 67.6 (C-3), 67.0 (d, *J* = 24.4 Hz, C-1), 60.6 (C-2), 54.9 (C-5); **^{31}P-NMR (202 MHz, D_2O)**: δ [ppm] = 2.84; **^{19}F-NMR (282 MHz, D_2O)**: δ [ppm] = no signal; **HRMS**: calcd for $C_7H_{14}FNO_7P$ $[M+H]^+$, 274.0486; found, 274.0483.

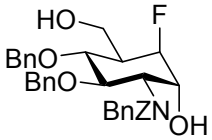

(5a*R*)-2-Amino-*N*-benzyl-*N*-benzyloxycarbonyl-3,4-di-*O*-benzyl-2-deoxy-5a-fluoro-carba-glucose (68) To the silylated fluoro-carba precursor **53** (15.123 mg, 0.0212 mmol) solved in 500 µL anhydrous THF, were added 3.9 µL K_2HPO_4-Buffer (pH 7) and 84.7 µL 1 M TBAF (0.0847 mmol) in anhydrous THF, stored over 2 Å molecular sieve. After 4 h HPLC shows completion of the reaction. After dilution with 500 µL of Acetonitril/H_2O (1:1) the reaction was directly loaded onto C18-HPLC column (Gemini® C18, 110 Å, 5 µm, 50x30 mm), utilizing a gradient of 40-100% MeCN (A: 0.1% formic acid in H_2O) in 15 min. Fractions containing the target-mass were combined and freeze-dried yielding the benzylated pseudo-sugar precursor **68** (11.46 mg, 90%) as colorless foam.

^{1}H-NMR (700 MHz, $CDCl_3$): δ [ppm] = 7.35-7.18 (m, 20H, Ar-H), 5.22 and 5.17 (d, J = 12.2 Hz, N-C(O)-O-C$\underline{H_2}$-Ph), 5.09 and 4.11 (br, 2H, N-C$\underline{H_2}$-Ph), 4.93 and 4.68 (d, *J* = 10.9 Hz, 2H, O-C$\underline{H_2}$-Ph), 4.81 and 4.47 (d, *J* = 10.9 Hz, 2H, O-C$\underline{H_2}$-Ph), 4.69 (ddd, *J* = 47.3, 4.0, 2.1 Hz, 1H, H-5a), 4.63 (br, 1H, H-3), 3.93 (br, 1H, H6a), 3.92 (br, 1H, H-1), 3.84 (br, 1H, H6b), 3.73 (t, *J* = 10.0 Hz, 1H, H-4), 3.32 (br, 1H, H-2), 2.37 (ddt, *J* = 39.5, 10.1, 4.7 Hz, 1H, H-5);**^{13}C-NMR (176 MHz, $CDCl_3$)**: δ [ppm] = 159.3 (C=O), 138.4, 138.2, 135.8, 128.9-127.8 (C^{Ar}), 92.5 (d, *J* = 172 Hz, C-5a) 81.2 (C-4), 78.7 (C-3), 75.5, 75.4 (O-$\underline{C}H_2$-Ph), 72.1 (d, *J* = 26 Hz, C-1), 68.5 (N-C(O)-O-$\underline{C}H_2$-Ph), 63.5 (br, C-2), 62.1 (d, *J* = 2 Hz, C-6), 56.4 (N-$\underline{C}H_2$-Ph), 43.0 (d, *J* = 17 Hz, C-5); **^{19}F-NMR (470 MHz, $CDCl_3$)**: δ [ppm] = -199.03 (s, 1F); **RP-HPLC**: t_r = 14.2 min (ZORBAX SB-C18, 5 µm, 0.4 mL/min, 20-100% MeCN in 20 min); **HRMS**: calcd for $C_{36}H_{39}FNO_6$ $[M+H]^+$, 600.2756; found, 600.2754.

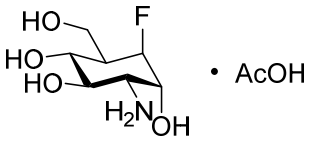

(5a*R*)-2-Amino-2-deoxy-5a-fluoro-carba-glucose (69) The perbenzylated fluoro-carba-idosamine **68** (14.93 mg, 0.0174 mmol) was deprotected according to **GP1**. After a reaction time of 7 h LC-MS monitoring showed completion of the reaction. The lyophilized raw product was purified via HILIC (NUCLEODUR® HILIC 5 µm, 150x4.6 mm, 98-90% MeCN in 20 min, A: 20 mM NH_4OAc in water pH 5.4). Due to missing UV-absorption of the product the fractions collected in time slices were analyzed via LC-MS (0-100% MeCN in 2 min). Fractions containing the target-mass were combined and freeze-dried yielding the pseudo-sugar **69** (2.42 mg, 53%) as the acetate salt.

^{1}H-NMR (500 MHz, $CDCl_3$): δ [ppm] = 4.97 (ddd, *J* = 45.5, 4.0, 2.0 Hz, 1H, H-5a), 4.35 (dd, *J* = 7.2, 3.7 Hz, 1H, H-1), 3.99 (dd, *J* = 11.3, 4.3 Hz, 1H, H-6a), 3.80 (dd, *J* = 11.3, 9.3 Hz, 1H, H-6b), 3.74 (dd, *J* = 10.8, 9.1 Hz, 1H, H-3), 3.54 (dd, *J* = 11.2, 9.2 Hz, 1H, H-4), 3.37 (dt, *J* = 10.8, 3.0 Hz, 1H, H-2), 2.12 (dtdd, *J* = 36.2, 9.3, 4.4, 2.2 Hz, 1H, H-5), **^{13}C-NMR (126 MHz, $CDCl_3$)**: δ [ppm] = 89.8 (d, *J* = 173.7 Hz, C-5a), 71.1 (C-3), 69.7 (d, *J* = 2.0 Hz, C-4); 66.0 (d, *J* = 27.3 Hz, C-1), 58.3 (d, *J* = 3.7 Hz, C-6), 52.9 (C-2), 42.5 (d, *J* = 18.2 Hz, H-5); **^{19}F-NMR (470 MHz, $CDCl_3$)**: δ [ppm] = -201.74 (s, 1F); **RP-HPLC**: t_r = 14.2 min (ZORBAX SB-C18, 5 µm, 0.4 mL/min, 20-100% MeCN in 20 min); **HRMS**: calcd for $C_{36}H_{39}FNO_6$ $[M+H]^+$, 600.2756; found, 600.2754.

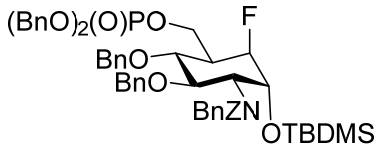

Dibenzyl (5a*R*)-2-amino-*N*-benzyl-*N*-benzyloxycarbonyl-3,4-di-O-benzyl-2-deoxy-5a-fluoro-1-O-*tert*-butyldimethylsilyl-carba-glucose-6-phosphate (70) The unphosphorylated fluoro-carba precursor **53** (17.75 mg, 0.0249 mmol) solved in toluene was transferred to a heat-dried schlenk-tube. The toluene was removed under reduced pressure and the starting material dried under vacuum (~10^{-2} mbar) for 2 h. 1H-Tetrazole (8.71 mg, 0.124 mmol), anhydrous CH_2Cl_2 (2.1 mL) and dibenzyl *N,N*-diisopropylphosphoramidite (21 µL, 0.0622 mmol) were added under argon atmosphere. The mixture was stirred for 2 h at room temperature after which HPLC-monitoring showed completion of the reaction. The reaction was cooled to 0 °C and *m*-CPBA (70%, 18.39 mg, 0.0746 mmol) was added. After another 1 h HPLC shows completion of the reaction, the mixture was diluted with CH_2Cl_2 (20 mL) and 5 mL of aqueous 10% Na_2SO_3 was added and the mixture stirred for 30 min. The organic layer was separated and washed with aqueous 10% Na_2SO_3 (1x10 mL), 1M HCl (2x10 mL), saturated $NaHCO_3$ (2x10 mL) and brine (1x10 mL). The organic layer was dried with $MgSO_4$ and concentrated. The reaction was purified via RP-HPLC (Gemini® C18, 110 Å, 5 µm, 50x30 mm, 80-100% MeCN in 10 min). Fractions containing product were combined and freeze-dried yielding the phosphorylated pseudo-sugar precursor **70** (22.76 mg, 94%) as colorless foam.

^{1}H-NMR (500 MHz, $CDCl_3$): δ [ppm] = 7.50-6.94 (m, 30H, Ar-H), 5.18-5.00 (m, 6H, N-C(O)-O-C$\underline{H}_2$-Ph and P(O)-(O-C$\underline{H}_2$-Ph)$_2$), 4.90-4.42 (m, 6H, O-C$\underline{H}_2$-Ph and N-C$\underline{H}_2$-Ph), 4.73 (d, *J* = 46.4 Hz, 1H, H-5a), 4.67 (br, 1H, H-2), 4.33 (dt, *J* = 9.6, 4.7 Hz, 1H, H-6a), 4.23 (br, 0.5H, H-1), 4.12 (td, *J* = 9.9, 5.5 Hz, 1H, H-6b), 3.97 (br, 1H, H-3), 3.89 (br, 0.5H, H-1), 3.66 (s, 1H, H-4), 2.45 (dt, *J* = 34.5, 9.4 Hz, 1H, H-5), 0.83 (s, 9H, *t*-Bu), 0.03 (s, 3H, CH_3); **^{13}C-NMR (176 MHz, $CDCl_3$)**: δ [ppm] = 156.8 (C=O), 138.6-126.3 (C^{Ar}), 88.8 (d, *J* = 171 Hz, C-5a), 79.5 (C-4), 77.3 (C-3), 75.2 (O-$\underline{C}H_2$-Ph), 72.4 (br, C-1), 69.4 (P(O)-(O-C$\underline{H}_2$-Ph)$_2$), 67.2 (N-C(O)-O-$\underline{C}H_2$-Ph), 64.3 (C-6), 56.8 (C-2), 50.0 (dd, 17.9, 8.0 Hz, C-5), 49.1 (N-$\underline{C}H_2$-Ph), 25.8 (*t*-Bu), -5.2 (CH_3); **^{31}P-NMR (202 MHz, $CDCl_3$)**: δ [ppm] = -0.78, -0.95, -1.02; **^{19}F-NMR (470 MHz, $CDCl_3$)**: δ [ppm] = -198.46 (br), -198.9; **RP-HPLC**: t_r =9.7 min (ZORBAX SB-C18, 5 µm, 0.4 mL/min, 80-100% MeCN in 20 min); **HRMS**: calcd for $C_{56}H_{65}FNO_9PSiNa$ $[M+Na]^+$, 996.4042; found, 996.4054.

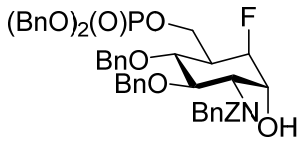

Dibenzyl (5a*R*)-2-amino-*N*-benzyl-*N*-benzyloxycarbonyl-3,4-di-*O*-benzyl-2-deoxy-5a-fluoro-carba-glucose-6-phosphate (71) To the silylated fluoro-carba precursor **70** (14.93 mg, 0.0174 mmol) solved in 500 µL anhydrous THF, were added 3.7 µL K_2HPO_4-Buffer (pH 7) and 56.5 µL 1 M TBAF (4 eq) in anhydrous THF, stored over 2 Å molecular sieve. The reaction was stirred at 23 °C and after 1 h HPLC showed completion of the reaction. After dilution with 500 µL of Acetonitril/H_2O (1:1) the reaction was directly loaded onto a C18-HPLC column (Gemini® C18, 110 Å, 5 µm, 50x30 mm), utilizing a gradient of 40-100% MeCN (A: 0.1% formic acid in H_2O) in 15 min. Fractions containing the target-mass were combined and freeze-dried yielding the benzylated pseudo-sugar precursor **71** (10.62 mg, 87%) as colorless foam.

^{1}H-NMR (500 MHz, $CDCl_3$): δ [ppm] = 7.32-7.16 (m, 30H, Ar-H), 5.24 and 5.18 (d, J = 12.0 Hz, N-C(O)-O-C$\underline{H}_2$-Ph), 5.11 and 4.10 (br, 2H, N-C$\underline{H}_2$-Ph), 5.03 (br, 4H, P(O)-(O-C$\underline{H}_2$-Ph)$_2$), 4.84 and 4.51 (d, *J* = 11.0 Hz, 2H, O-C$\underline{H}_2$-Ph), 4.78 and 4.45 (d, *J* = 11.0 Hz, 2H, O-C$\underline{H}_2$-Ph), 4.65 (d, *J* = 47.8 Hz, 1H, H-5a), 4.62 (br, 1H, H-3), 4.29 (br, 1H, H6a), 4.08 (br, 1H, H6b), 3.92 (br, 1H, H-1), 3.46 (t, *J* = 47.8 Hz, 1H, H-4), 3.30 (br, 1H, H-2), 2.55 (d, *J* = 36.9 Hz, 1H, H-5);**^{13}C-NMR (176 MHz, $CDCl_3$)**: δ [ppm] = 159.0 (C=O), 138.2, 137.9, 128.5-127.7 (C^{Ar}), 89.0 (d, C-5a) 79.7 (C-4), 78.5 (C-3), 75.2 (O-$\underline{C}H_2$-Ph), 75.0 (O-$\underline{C}H_2$-Ph), 71.8 (d, C-1), 69.4 (P(O)-(O-$\underline{C}H_2$-Ph)$_2$), 68.4 (N-C(O)-O-$\underline{C}H_2$-Ph), 64.6 (C-6), 63.3 (br, C-2), 56.2 (N-$\underline{C}H_2$-Ph), 41.5 (C-5); **^{31}P-NMR (202 MHz, $CDCl_3$)**: δ [ppm] = -1.28 (s, 1P); **^{19}F-NMR (470 MHz, $CDCl_3$)**: δ [ppm] = -201.56 (s, 1F); **RP-HPLC**: t_r = 17.8 min (ZORBAX SB-C18, 5 µm, 0.4 mL/min, 20-100% MeCN in 20 min); **HRMS**: calcd for $C_{50}H_{52}FNO_9P$ $[M+H]^+$, 860.3358; found, 860.3357.

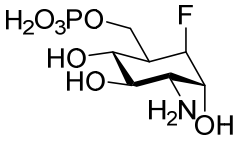

(5a*R*)-2-Amino-2-deoxy-5a-fluoro-carba-glucose-6-phosphate (35) Perbenzylated fluoro-carba compound **71** (10.62 mg, 0.0124 mmol) was deprotected according to **GP1**. The reaction was finished after 3 h. The lyophilized pseudo-sugar was purified via C18-HPLC (NUCLEODUR® C18, 110 Å, 5 µm, 150x4.6 mm, 100% H_2O for 5 min, then 0-100% acetonitrile in 5 min). Due to missing UV-absorption of the product the fractions collected in time slices were analyzed via LC-MS (0-100% MeCN in 2 min).

Fractions containing the target-mass were combined and freeze-dried yielding the pseudo-sugar **35** (2.39 mg, 70%) as colorless foam.

^{1}H-NMR (500 MHz, D_2O): δ [ppm] = 5.03 (d, *J* = 45.3 Hz, 1H, H-5a), 4.38 (d, *J* = 3.6, 1H, H-1), 4.19 (dt, *J* = 10.4, 5.1 Hz, 1H, H-6a), 3.98 (td, *J* = 10.6, 10.1, 7.5 Hz, 1H, H-6b), 3.80 (t, *J* = 9.9 Hz, 1H, H-3), 3.59 (t, *J* = 10.1 Hz, 1H, H-4), 3.44 (dt, *J* = 11.3, 3.2 Hz, 1H, H-2), 2.27 (dt, *J* = 38.3, 11.0 Hz, 1H, H-5); **^{13}C-NMR (126 MHz, D_2O)**: δ [ppm] = 89.5 (d, *J* = 174.1 Hz, C-5a), 70.6 (C-4), 69.5 (C-3); 65.7 (d, *J* = 26.7 Hz, C-1), 61.2 (C-6), 53.1 (C-2); 41.7 (dd, *J* = 18.0, 6.6 Hz, C-5) **^{31}P-NMR (202 MHz, D_2O)**: δ [ppm] = 2.49 (s, 1P); **^{19}F-NMR (471 MHz, D_2O)**: δ [ppm] = -201.77 (br, 1F); **HRMS**: calcd for $C_7H_{14}NO_7PF$ $[M+H]^+$, 274.0486; found, 274.0484.

5.6 Synthesis and physical data of phenyl-carba-sugars

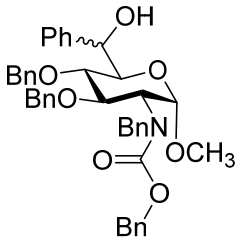

Methyl 3,4-Di-O-benzyl-2-deoxy-6-phenyl-2-((phenylmethoxy)carbonyl)amino-α-D-glucopyranoside (81) Oxalyl chloride (9.1 mL, 0.106 mol) in anhydrous CH_2Cl_2 (250 mL) was presented in a heat-dried flask. At -78 °C a solution of anhydrous DMSO (15.75 mL, 0.222 mol) in CH_2Cl_2 (50 mL) was added dropwise and the reaction was stirred for 30 min at -78 °C. The methyl glycoside **39** (80.74 g, 0.089 mol) was solved in CH_2Cl_2 (100 mL) and slowly added to the reaction. The reaction mixture was stirred for 2h at -78 °C and trimethylamine (30.9 mL, 0.222 mol) was added at -78 °C. The cooling was removed and the reaction allowed to reach room temperature. Water (200 mL) was added, and the organic layer was separated and dried ($MgSO_4$). The crude aldehyde was solved in anhydrous diethyl ether (300 mL), cooled to -74 °C and a freshly prepared solution of phenmagnesium bromide (104.6 mL, 0.133 mol, 1.27 M in diethyl ether) was added dropwise at -74 °C. The reaction solution was stirred at -74 °C for 2h. Ice-cold water (400 mL) was added to the reaction, the organic layer was separated and the aqueous phase extracted with CH_2Cl_2 (3x200 mL). The combined organic layers were washed with sat. aqueous NaCl and dried ($MgSO_4$). The solvents were removed under reduced pressure and the residue purified by manual flash chromatography (3:1 petroleum ether/ethyl acetate) yielding a 6-epimeric mixture of alcohol **81** (22.90 g, 38% over two steps) as slightly yellow oil.

R_f = 0.57, 0.66 (silica, petroleum ether/ethyl acetate 1:1), Seebach-reagent; **^{1}H-NMR (400 MHz, $CDCl_3$, 25 °C)**: δ [ppm] = 7.28-6.86 (m, 25H, Ar-H), 5.10-4.12 (m, 11H, 3xO-C$\underline{H_2}$-Ph, N-C$\underline{H_2}$-Ph, H-6, H-2, H-1), 4.00-3.70 (m, 3H, H-3, H-4, H-5), 2.23 (s, 3H, CH_3). **^{13}C-NMR (100 MHz, $CDCl_3$, 25 °C)**: δ [ppm] = 157.8, 157.3 (C=O), 142.0-124.5 (C^{Ar}), 99.6, 99.4 (H-1), 80.1 (H-4), 77.4 (H-3), 75.2 (O-$\underline{C}H_2$-Ph), 74.0 (O-$\underline{C}H_2$-Ph, H-5), 70.8 (H-6), 67.6 (O-$\underline{C}H_2$-Ph), 58.9 (C-2), 54.2 (CH_3), 47.5 (N-$\underline{C}H_2$-Ph). **RP-HPLC**: t_r = 9.2 and 9.8 min (EC 125/4 Nucleodur C-18 Gravity, 3 µm, 0.4 mL/min, 80–100 % MeCN in 10 min); **MS**: calcd for $C_{42}H_{43}NO_7Na$ $[M+Na]^+$, 696.2932, found, 696.3941.

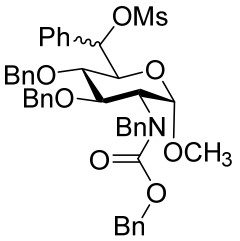

Methyl 3,4-Di-O-benzyl-2-deoxy-6-O-methanesulfonyl-6-phenyl-2-((phenylmethoxy)carbonyl)amino-α-D-glucopyranoside (82) To a solution of the alcohol **81** (0.413 g, 0.613 mmol) in anhydrous CH_2Cl_2 (4 mL) cooled to 0 °C was added triethylamine (0.2 mL) and methanesulfonyl chloride (0.057 mL, 0.736 mmol) successively. The cooling was removed, and the reaction was allowed to reach room temperature. The solution was stirred for 3h at room temperature, then triethylamine (0.2 mL) and methanesulfonyl chloride (0.083 mL, 1.226 mmol) was added at 0 °C. The reaction was stirred for 17h at room temperature, then sat. aqueous $NaHCO_3$ (10 mL) was added, and the organic layer was separated. The organic layer was washed with sat. aqueous $NaHCO_3$ (10 mL), sat. aqueous NaCl and dried ($MgSO_4$). The solvents were removed under reduced pressure and the residue purified by automated flash chromatography (100% petroleum ether to 75:25 petroleum ether/ethyl acetate in 4 min, then 75:25 petroleum ether/ethyl acetate for 6 min) yielding an isomeric mixture of the mesylate **82** (0.30 g, 65%) as colorless oil.

R_f = 0.57 (silica, petroleum ether/ethyl acetate 1:1), Seebach-reagent; **^{1}H-NMR (300 MHz, $CDCl_3$, 25 °C)**: δ [ppm] = 7.49-6.97 (m, 25H, Ar-H), 6.02 (s, 1H, H-6), 5.23-5.09 (m, 2H, O-C$\underline{H_2}$-Ph), 5.04-4.23 (m, 8H, H-6, 2xO-C$\underline{H_2}$-Ph, N-C$\underline{H_2}$-Ph, H-2, H-1), 4.17-3.98 (m, 2H,H-4, H-3), 3.76 (dd, *J* = 9.8, 1.5 Hz, 1H, H-5), 2.70 (s, 3H, CH_3), 2.27 (s, 3H, CH_3); **^{13}C-NMR (75 MHz, $CDCl_3$, 25 °C)**: δ [ppm] = 157.7, 157.2 (C=O), 140.0-125.5 (C^{Ar}), 99.4 (C-1), 80.0 (C-6), 79.1 (C-4), 77.7 (C-3),), 75.0 (O-$\underline{C}H_2$-Ph), 73.8 (O-$\underline{C}H_2$-Ph), 73.4 (C-5), 67.6 (O-$\underline{C}H_2$-Ph), 58.4 (C-2), 54.1 (CH_3), 47.4 (N-$\underline{C}H_2$-Ph), 39.6 (CH_3). **MS**: calcd for $C_{43}H_{45}NO_9SNa$ $[M+Na]^+$, 774.2707, found, 774.2712.

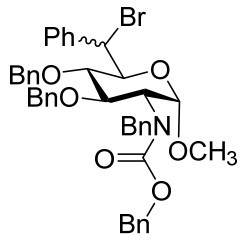

Methyl 6-Bromo-3,4-di-O-benzyl-2-deoxy-6-phenyl-2-((phenylmethoxy)-carbonyl)amino-α-D-glucopyranoside (83) The mesylate **82** (0.025 mol) was solved in butan-2-one (170 mL) and lithium bromide (45.3 g, 0.534 mol) was added. The reaction was heated under reflux for 4h, then water (100 mL) was added and the organic layer separated. The aqueous layer was extracted with CH_2Cl_2 (2x200 mL) and the combined organic layers washed with sat. aqueous NaCl and dried ($MgSO_4$). The solvents were removed under reduced pressure and the residue purified by manual flash chromatography (83:17 petroleum ether/ethyl acetate) yielding a mixture of the two isomers (ratio 53:28) **83** with 16% of the next step elimination product (total 12.27 g, 74% over two steps) as colorless oil.

R_f = 0.67 (silica, petroleum ether/ethyl acetate 3:1), Seebach-reagent; **^{1}H-NMR (300 MHz, $CDCl_3$, 25 °C)**: δ [ppm] = 7.43-6.96 (m, 25H, Ar-H), 5.35 (d, *J* = 2.9 Hz, 1H, H-6), 4.98-3.98 (m, 14H, 3xO-C$\underline{H_2}$-Ph, H-6, N-C$\underline{H_2}$-Ph, H-2, H-1, H-4, H-3, H-5), 2.88 (s, 3H, CH_3); **^{13}C-NMR (75 MHz, $CDCl_3$, 25 °C)**: δ [ppm] = 157.9, 140.0-125.6, 99.4, 82.7, 81.1, 77.8, 75.5, 74.8, 74.4, 67.7 58.6, 55.0, 51.9, 47.2; **RP-HPLC**: t_r = 19.9 min (EC 125/4 Nucleodur C-18 Gravity, 3 µm, 0.4 mL/min, 20–100 % MeCN in 20 min); **MS**: calcd for $C_{42}H_{42}BrNO_6Na$ $[M+Na]^+$, 758.2088, found, 758.2101.

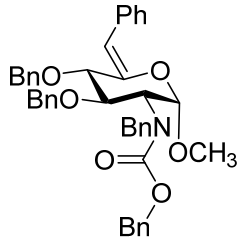

Methyl (*Z*)-3,4-Di-O-benzyl-2,6-dideoxy-6-(phenyl-1-en)-2-((phenylmethoxy)-carbonyl)amino-α-D-glucopyranoside (80) To a solution of the bromide **83** (12.27 g, 16.65 mmol) in acetonitrile (300 mL) sodium iodide (32 g, 216.5 mmol) and 1,8-diazabicyclo[5.4.0]undec-7-ene (7.6 mL, 49.95 mmol) were added. The reaction solution was heated to reflux for 24h. Water (100 mL) was added to the reaction and the aqueous layer extracted with CH_2Cl_2 (3x200 mL). The combined organic layers were washed with sat. aqueous NaCl and dried ($MgSO_4$). The solvents were removed under reduced pressure and the residue purified by automatic flash chromatography (100% petroleum

ether to 56:44 petroleum ether/ethyl acetate in 50min) yielding the enyne **80** (9.30 g, 85%) as colorless oil.

R_f = 0.60 (silica, petroleum ether/ethyl acetate 5:1), Seebach-reagent; **^{1}H-NMR (300 MHz, $CDCl_3$, 25 °C)**: δ [ppm] = 7.58-6.96 (m, 25H, Ar-H), 6.18 (s, 1H, H-6), 5.14 (dd, *J* = 12.3 Hz, 2H, N-C(O)-C$\underline{H_2}$-Ph), 4.91-4.54 (m, 6H, 2xO-C$\underline{H_2}$-Ph, H-2, H-1), 4.34-4.04 (m, 4H, H-3, H-4, N-C$\underline{H_2}$-Ph), 2.57 (s, 3H, CH_3); **^{13}C-NMR (75 MHz, $CDCl_3$, 25 °C)**: δ [ppm] = 157.9 (C=O), 147.5 (C-5), 140.0-125.6 (C^{Ar}), 111.3 (C-6), 101.3 (C-1), 82.4 (C-4), 76.0 (C-3), 74.6 (O-$\underline{C}H_2$-Ph), 74.1 (O-$\underline{C}H_2$-Ph), 67.7 (O-$\underline{C}H_2$-Ph), 58.5 (C-2), 56.5 (CH_3), 47.0 (N-$\underline{C}H_2$-Ph); **RP-HPLC**: t_r = 19.3 min (EC 125/4 Nucleodur C-18 Gravity, 3 µm, 0.4 mL/min, 20–100 % MeCN in 20 min); **MS**: calcd for $C_{42}H_{41}NO_6Na$ $[M+Na]^+$, 678.2836, found, 678.2836.

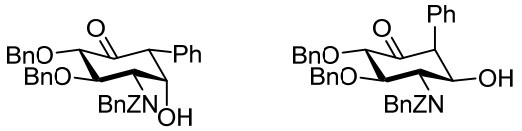

2-Amino-*N*-benzyl-*N*-benzyloxycarbonyl-3,4-*O*-dibenzyl-1-hydroxy-6-phenyl-5-oxo-cyclohexanone (78/79) The Alkene **80** (1.14 g, 1.74 mmol) was solved in a 2:1 mixture of 1,4-dioxane and 5 mM aqueous H_2SO_4 (30 mL). Mecury(II) sulfate (0.26 g, 0.87 mmol) was added and the solution was heated to 50 °C and stirred at this temperature for 17h. Saturated aqueous NaCl (50 mL) was added and the aqueous phase extracted with CH_2Cl_2 (3x70 mL). The combined organic layers were dried ($MgSO_4$), the solvents were removed under reduced pressure. The residue was purified by automatic flash chromatography (100% petroleum ether to 60:40 petroleum ether/ethyl acetate in 20min) yielding a 74:26 mixture of cyclohexanone **78** and **79** (0.76 g, 68%) as colorless powder.

α-isomer: R_f = 0.50 (silica, petroleum ether/ethyl acetate 1:1), Seebach-reagent; **^{1}H-NMR (400 MHz, $CDCl_3$, -40 °C)**: δ [ppm] = 7.44-6.90 (m, 25H, Ar-H), 5.23-4.07 (m, 11H, 3xO-C$\underline{H_2}$-Ph, N-C$\underline{H_2}$-Ph, H-3, H-4, H-1), 3.91 and 3.40 (s, 1H, H-5a), 3.49 (d, *J* = 11.1 Hz, 1H, H-2); **^{13}C-NMR (100 MHz, $CDCl_3$, -40 °C)**: δ [ppm] = 202.6 (C-5), 158.4 (C=O), 137.8-125.3 (C^{Ar}), 87.7 (C-4), 77.1 (C-3), 75.9, 73.7 (2xO-$\underline{C}H_2$-Ph), 74.2 (C-1), 68.3 (O-$\underline{C}H_2$-Ph), 67.1 (C-2), 59.1, 58.7 (C-5a), 56.0 (N-$\underline{C}H_2$-Ph); **RP-HPLC**: t_r = 8.8 min (EC 125/4 Nucleodur C-18 Gravity, 3 µm, 0.4 mL/min, 80–100 % MeCN in 20 min); **MS**: calcd for $C_{41}H_{39}NO_6H$ $[M+H]^+$, 642.2850, found, 642.2843.

β-isomer: R_f = 0.56 (silica, petroleum ether/ethyl acetate 1:1), Seebach-reagent; **^{1}H-NMR (400 MHz, $CDCl_3$, -40 °C)**: δ [ppm] = 7.49-7.10 (m, 25H, Ar-H), 5.48-4.46 (m, 8H, 3xO-C$\underline{H_2}$-Ph, N-C$\underline{H_2}$-Ph), 4.27 (t, *J* = 10.2 Hz, 1H), 4.18-3.72 (m, 4H, H-4, H-1), 3.73 (d,

J = 4.1 Hz, 1H, H-5a), 3.61 (dd, *J* = 10.6, 4.6 Hz, 1H, H-2); **^{13}C-NMR (100 MHz, $CDCl_3$, -40 °C)**: δ [ppm] = 207.1, 206.3 (C-5), 155.8, 155.2 (C=O), 137.7-127.2 (C^{Ar}), 84.7, 84.3 (C-4), 75.5, 72.6 (C-3), 74.9, 74.0 (2xO-$\underline{C}H_2$-Ph), 72.1 (C-1), 68.1, 67.2 (O-$\underline{C}H_2$-Ph), 66.8, 65.3 (C-2), 57.7, 57.3 (C-5a), 55.5, 55.3 (N-$\underline{C}H_2$-Ph); **RP-HPLC**: t_r = 7.8 min (EC 125/4 Nucleodur C-18 Gravity, 3 µm, 0.4 mL/min, 80–100 % MeCN in 20 min).

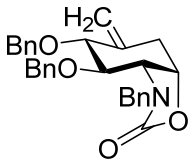

(3aS,4R,5R,7aS)-3-benzyl-4,5-bis(benzyloxy)-6-methylenehexahydrobenzo-[d]oxazol-2(3H)-one (99) Methyltriphenylphosphonium bromide (0.378 g, 1.061 mmol) was presented in a heat-dried schlenk-tube in anhydrous THF (3 mL). A solution of *n*-BuLi (0.66 mL, 1.06 mmol, 1.6 M in hexane) was added to the stirred suspension at 0 °C. After 1h a solution of cyclohexanone **42** (0.100 g, 0.177 mmol) in THF (1 mL) was added dropwise at 0 °C. The solution was stirred two hours at room temperature, after which ethyl acetate (8 mL) and sat. aqueous NH4Cl (4 mL) were added. The organic layer was separated and the aqueous layer extracted with ethyl acetate (3x10 mL). The combined organic phases were washed with sat. aqueous NaCl and dried ($MgSO_4$). The solvents were removed under reduced pressure and the residue purified by automated flash chromatography (100% petroleum ether to 5:95 petroleum ether/ethyl acetate in 30 min) yielding olefin **99** (33.14 mg, 44%) as colorless oil.

R_f = 0.40 (petroleum ether/ethyl acetate 3:1), Seebach-reagent; **^{1}H-NMR (400 MHz, $CDCl_3$, 25 °C)**: δ [ppm] = 7.29-7.03 (m, 15H, Ar-H), 5.16 (d, *J* = 17.2 Hz, 2H, H-6), 4.78 (dd, *J* = 15.0 Hz 1H, N-C$\underline{H}_2$-Ph), 4.69 (d, *J* = 11.7 Hz, 1H, O-C$\underline{H}_2$-Ph), 4.58 (d, *J* = 11.7 Hz, 1H, O-C$\underline{H}_2$-Ph), 4.48 (ddd, *J* = 7.6, 5.6, 4.7 Hz, 1H, H-1), 4.37 (d, *J* = 11.7, 1H, O-C$\underline{H}_2$-Ph), 4.34 (d, *J* = 11.8 Hz, 1H, O-C$\underline{H}_2$-Ph), 3.97 (d, *J* = 15.0 Hz, 1H, N-C$\underline{H}_2$-Ph), 3.87 (d, *J* = 5.9 Hz, 1H, H-4), 3.72 (t, *J* = 5.8 Hz, 1H, H-3), 3.51 (dd, *J* = 7.6, 5.7 Hz, 1H, H-2), 2.63 (dd, *J* = 14.6, 4.7 Hz, 1H, H-5aa), 2.45 (ddt, *J* = 14.5, 5.5, 1.3 Hz, 1H, H-5ab). **^{13}C-NMR (101 MHz, $CDCl_3$, 25 °C)**: δ [ppm] = 158.0 (C=O), 138.0-127.8 (C^{Ar}), 115.6 (C-6), 80.7 (C-4), 80.5 (C-3), 73.6 (C-1), 73.4 (O-$\underline{C}H_2$-Ph), 71.2 (O-$\underline{C}H_2$-Ph), 56.9 (C-2), 46.6 (N-$\underline{C}H_2$-Ph), 33.3 (C-5a). **RP-HPLC**: t_r = 26.5 min (ZORBAX SB-C18, 5 µm, 0.4 mL/min, 20-100 % MeCN in 30 min); **HRMS**: calcd for $C_{29}H_{29}NO_4Na$ $[M+Na]^+$, 478.1989, found, 478.1981.

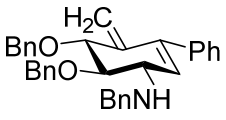

(3S,4R,5R)-N-benzyl-4,5-bis(benzyloxy)-6-methylene-3,4,5,6-tetrahydro-[1,1'-biphenyl]-3-amine (100) Methyltriphenylphosphonium bromide (0.668 g, 1.870 mmol) was presented in a heat-dried schlenk-tube in anhydrous THF (5 mL). A solution of *n*-BuLi (1.17 mL, 1.870 mmol, 1.6 M in hexane) was added to the stirred suspension at 0 °C. The cooling was removed and the suspension was stirred at room temperature. After 2h the yellow solution was cooled to 0 °C and a solution of a mixture of cyclohexanones **78** and **79** (0.200 g, 0.312 mmol) in THF (2 mL) was added dropwise at 0 °C. The solution was stirred two hours at room temperature, after which ethyl acetate (8 mL) and sat. aqueous NH4Cl (4 mL) were added. The organic layer was separated and the aqueous layer extracted with ethyl acetate (3x10 mL). The combined organic phases were washed with sat. aqueous NaCl and dried ($MgSO_4$). The solvents were removed under reduced pressure and the residue purified by automated flash chromatography (silica, 100% petroleum ether to 50:55 petroleum ether/ethyl acetate in 40 min) yielding a complex mixture. A second automated flash chromatography (basic aluminium oxide, 100% petroleum ether to 65:35 petroleum ether/ethyl acetate in 25 min) yielded the eliminated olefin **100** (33.84 mg, 22%) as colorless oil.

R_f = 0.79 (aluminium oxide, petroleum ether/ethyl acetate 3:1), Seebach-reagent; **^{1}H-NMR (300 MHz, $CDCl_3$, 25 °C)**: δ [ppm] = 7.38-7.27 (m, 20H, Ar-H), 5.86 (d, *J* = 2.3 Hz, 1H, H-1), 5.44 (s, 1H, H-6a), 5.16 (s, 1H, H-6b), 4.92-4.68 (m, 4H, O-C$\underline{H_2}$-Ph), 4.32 (dt, *J* = 7.0, 1.1 Hz, 1H, H4), 3.99 (t, *J* = 6.0 Hz, 1H, H-3), 3.83 (s, 2H, N-C$\underline{H_2}$-Ph), 3.63 (t, *J* = 4.4 Hz, 1H, H-2).**^{13}C-NMR (75 MHz, $CDCl_3$, 25 °C)**: δ [ppm] = 141.7 (C-5a), 140.2, 138.6, 138.2 (C^{Ar}), 139. 4 (C-5), 129.0-127.3 (C^{Ar}), 127.0 (C-1), 116.8 (C-6), 81.3 (C-4), 78.9 (C-3), 73.5, 72.6 (O-$\underline{C}H_2$-Ph), 58.0 (C-2), 50.5 (N-$\underline{C}H_2$-Ph). **RP-HPLC**: t_r = 19.6 min (ZORBAX SB-C18, 5 µm, 0.4 mL/min, 0-100 % MeCN in 30 min); **MS**: calcd for $C_{34}H_{34}NO_2$ $[M+H]^+$, 488.3, found, 487.7.

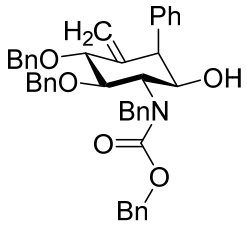

Benzyl benzyl((1R,2R,3R,5S)-2,3-bis(benzyloxy)-5-fluoro-4-methylene-6-oxy-cyclohexyl)carbamate (101) The mixture of cyclohexanones **78** and **79** (200.0 mg, 0.312 mmol) was presented in a heat-dried schlenk-tube and solved in anhydrous THF (5 mL). The solution was cooled to -20 °C after which pyridine (50 µL) and $Cp_2TiCH_2AlCl(CH_3)_2$ (0.5 M in toluene, 1.25 mL, 0.623 mmol) were added under argon atmosphere successively. The reaction was allowed to reach room temperature and was

stirred 17h at room temperature. Sat. aqueous $NaHCO_3$ (5 mL) was added at 0 °C and the reaction was stirred for 15 min. The reaction solution was filtered through celite, the filter cake was washed with CH_2Cl_2.The filtrate was washed with sat. aqueous NaCl and dried ($MgSO_4$). The solvents were removed under reduced pressure and the residue purified by automated flash chromatography (100% petroleum ether to 70:30 petroleum ether/ethyl acetate in 12 min) yielding a mixture of starting material and product. The fraction containing the desired product was purified via RP-HPLC (Gemini® C18, 110 Å, 5 µm, 50x30 mm, 80-100 % MeCN in 10 min). Fractions containing product were combined and freeze-dried yielding the olefin **101** (31.6 mg, 16%) as a colorless foam.

R_f = 0.36 (silica, petroleum ether/ethyl acetate 3:1), Seebach-reagent; **^{1}H-NMR (300 MHz, $CDCl_3$, 25 °C)**: δ [ppm] = 7.35-7.21 (m, 25H, Ar-H), 5.44 (s, 1H, H6a), 5.21-5.18 (m, 2H, H-6b, O-C$\underline{H_2}$-Ph), 4.81-4.44 (m, 8H, N-C$\underline{H_2}$-Ph, O-C$\underline{H_2}$-Ph, H-1, H-3), 4.18-3.77 (m, 3H H-5a, H-4, H-2). **^{13}C-NMR (75 MHz, $CDCl_3$, 25 °C)**: δ [ppm] = 143.8 (C-5), 138.2-126.6 (C^{Ar}), 113.6 (C-6), 82.2 (C-4), 80.4 (C-3 or C-1), 74.4 (O-$\underline{C}H_2$-Ph), 72.9 (O-$\underline{C}H_2$-Ph), 70.3 (C-3 or C-1), 67.5 (O-$\underline{C}H_2$-Ph), 63.6 (C-2 or N-$\underline{C}H_2$-Ph), 62.0 (C-2 or N-$\underline{C}H_2$-Ph), 51.6 (C-5a). **RP-HPLC**: t_r = 21.5 min (ZORBAX SB-C18, 5 µm, 0.4 mL/min, 0-100 % MeCN in 30 min); **MS**: calcd for $C_{42}H_{42}NO_5^+$ $[M+H]^+$, 640.3, found, 639.7.

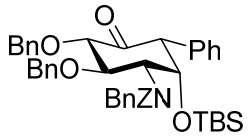

Benzyl benzyl((1R,2R,3S,6R)-2,3-bis(benzyloxy)-6-((tert-butyldimethylsilyl)oxy)-4-oxocyclohexyl)carbamate (103/104) The isomeric mixture cyclohexanone **78** and **79** (0.59 g, 0.927 mmol) was presented in a heat-dried schlenk tube and solved in anhydrous CH_2Cl_2 (5 mL). The solution was cooled to 0 °C and 2,6-lutidine (0.25 mL, 2.13 mmol) and *tert*-butyldimethylsilyl trifluoromethanesulfonate (0.49 mL, 2.13 mmol) were added successively at 0 °C. The cooling was removed and the reaction was stirred at room temperature for 16 h. Reaction monitoring via TLC shows residual starting material. 2,6-lutidine (0.11 mL, 0.948 mmol) and TBDMSOTf (0.21 mL, 0.914 mmol) were added at 0 °C and the reaction was stirred for 7h at room temperature. The reaction mixture was diluted with CH_2Cl_2 (20 mL) and washed with 1N aqueous HCl (15 mL) and sat. aqueous NaCl (15 mL). The organic layer was dried ($MgSO_4$) and the solvent removed under reduced pressure. The residue was purified via flash chromatography (100% petroleum ether to 77:23 petroleum ether/ethyl acetate in 45 min) yielding the protected axial cyclohexanone **78** (0.327 g, 47%) and a mixture of axial **78** and equatorial **79** cyclohexanone (0.186 g, 27%, 66:33 axial/equatorial) as colorless oils. Overall ratio axial/equatorial was 88:12.

$R_f\alpha$ = 0.31, **$R_f\beta$** = 0.36 (petroleum ether/ethyl acetate 7:1), Seebach-reagent; assignment of the α-isomer: **^{1}H-NMR (500 MHz, $CDCl_3$, 25 °C)**: δ [ppm] = 7.66-7.10 (m, 25H, Ar-H), 5.63-5.14 (m, 2H, O-CH_2-Ph), 5.04-4.24 (m, 10H, N-CH_2-Ph 2xO-CH_2-Ph, C-2, C-1, C-4, C-3), 3.89 (s, 1H, H-5a), 3.45 (d, 1H, *J* = 11.3 Hz, O-CH_2-Ph), 0.98 (CH_3-C-Si), (-0.10) (CH_3-Si); **^{13}C-NMR (126 MHz, $CDCl_3$, 25 °C)**: δ [ppm] = 202.1 (C-5), 156.3 (C=O), 137.9-125.4 (C^{Ar}), 88.6 (C-4), 78.2 (C-1), 77.3 (C-3), 73.5, 72.2 (2xO-CH_2-Ph), 67.8 (O-CH_2-Ph), 62.7 (C-2), 56.7 (C-5a), 49.5 (N-CH_2-Ph), 26.4 (Si-C-CH_3), 18.2 (Si-C-CH_3), (-3.7) (Si-CH_3); **RP-HPLC**: $t_r\alpha$ = 7.9 min, $t_r\beta$ = 8.3 min (ZORBAX SB-C18, 5 µm, 0.4 mL/min, 80-100 % MeCN in 20 min); **ESI-MS**: calcd for $C_{47}H_{53}NO_6SiH$ $[M+H]^+$, 756.4; found, 756.5.

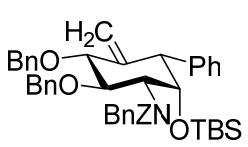

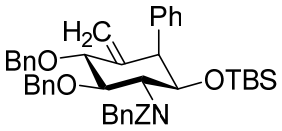

Benzyl benzyl((1R,2R,3R,5S,6S)-2,3-bis(benzyloxy)-6-((tert-butyldimethylsilyl)oxy)-4-methylene-5-phenylcyclohexyl)carbamate (76/77) A mixture of both isomers of the protected cyclohexanone **78** and **79** (1.11 g, 1.47 mmol, 69:31 axial:equatorial) was solved in anhydrous toluene (8 mL). Freshly prepared Cp_2TiMe_2 (6.3 mL, 3.23 mmol, 0.51 M in toluene) was added under an argon atmosphere. The reaction was heated in an oil-bath to 65 °C and stirred for 17 h, after which the solution was allowed to reach room temperature. Water and ethyl acetate were added and the emulsion stirred until no formation of orange precipitate could be detected anymore. After filtration through celite® 545, the filter cake was washed with ethyl acetate. The filtrate was washed with sat. aqueous NaCl and dried ($MgSO_4$). The solvents were removed under reduced pressure and the residue purified by automated flash chromatography (100% petroleum ether to 80:20 petroleum ether/ethyl acetate in 45 min) yielding equatorial-OH olefin **77** (187 mg) and the axial-OH olefin **76** (173 mg) as a yellow oil. The yield calculated with respect to the amount of equatorial protected cyclohexane in the starting material mixture is 41% (**77**), with respect to axial-OH starting material 17% (**76**).

R_f = 0.60 (petroleum ether/ethyl acetate 5:1), Seebach-reagent;

NMR-assignment of the equatorial-OH olefin **77**:

Conformer A: **^{1}H-NMR (600 MHz, $CDCl_3$, -40 °C)**: δ [ppm] = 7.58-7.01 (m, 25H, Ar-H), 5.52-5.22 (m, 2H, H-6a and b), 5.50-5.03 (m, 2H, O-CH_2-Ph), 4.77 and 4.38 (d, 2H, N-CH_2-Ph), 4.81-2.91 (m, 4H, 2xO-CH_2-Ph), 4.80 (br, 1H, H-1), 4.39 (br, 1H, H-3), 4.09-3.83 (m, 1H, H-5a), 3.80 (br, 1H, H-4), 3.75 (t, *J* = 10.5 Hz, 1H, H-2), 0.83 or 0.75 or 0.64 (s, 9H, CH_3-C-Si), 0.19 and 0.03 or 0.11 and 0.00 or -0.11 and -0.21 (s, 3H, 2xCH_3-Si);

^{13}C-NMR (151 MHz, $CDCl_3$, -40 °C): δ [ppm] = 154.8 (C=O), 143-127.8 (C^{Ar}), 112.4 or 112.3 or 112.2 (C-6), 81.8 (C-4), 80.3 (C-3), 75.6 and 72.9 or 72.8 72.6 or 72.3 (O-$\underline{C}H_2$-Ph), 71.4 (C-1), 66.6 (O-$\underline{C}H_2$-Ph), 64.5 (C-2), 56.3 (N-$\underline{C}H_2$-Ph), 52.0 (C-5a), 25.7 (Si-C-$\underline{C}H_3$), 18.0 (Si-$\underline{C}$-CH_3), -4.6 and -5.7 (Si-CH_3);

Conformer B: **^{1}H-NMR (600 MHz, $CDCl_3$, -40 °C)**: δ [ppm] = 7.58-7.01 (m, 25H, Ar-H), 5.52-5.22 (m, 2H, H-6a and b), 5.50-5.03 (m, 2H, O-C$\underline{H_2}$-Ph), 5.22 (br, 1H, H-2), 5.22 and 3.88 (d, 2H, N-C$\underline{H_2}$-Ph), 4.81-2.91 (m, 4H, 2xO-C$\underline{H_2}$-Ph), 4.22 (br, 1H, H-1), 4.09-3.83 (m, 1H, H-5a), 3.80 (br, 1H, H-4), 3.16 (t, *J* = 9.4 Hz, 1H, H-3), 0.83 or 0.75 or 0.64 (s, 9H, CH_3-C-Si), 0.19 and 0.03 or 0.11 and 0.00 or -0.11 and -0.21 (s, 3H, 2xCH_3-Si); **^{13}C-NMR (151 MHz, $CDCl_3$, -40 °C)**: δ [ppm] = 158. 5 (C=O), 143-127.8 (C^{Ar}), 112.4 or 112.3 or 112.2 (C-6), 81.8 or 81.6 (C-4), 79.6 (C-3), 75.6 and 72.9 or 72.8 72.6 or 72.3 (O-$\underline{C}H_2$-Ph), 71.0 (C-1), 67.7 or 67.5 (O-$\underline{C}H_2$-Ph), 59.4 (C-2), 52.2 (C-5a), 45.7 (N-$\underline{C}H_2$-Ph), 25.6 (Si-C-$\underline{C}H_3$), 17.9 (Si-$\underline{C}$-CH_3), 4.2 and -6.1 (Si-CH_3);

Conformer C: **^{1}H-NMR (600 MHz, $CDCl_3$, -40 °C)**: δ [ppm] = 7.58-7.01 (m, 25H, Ar-H), 5.52-5.22 (m, 2H, H-6a and b), 5.50-5.03 (m, 2H, O-C$\underline{H_2}$-Ph), 5.09 and 4.29 (d, 2H, N-C$\underline{H_2}$-Ph), 4.81-2.91 (m, 4H, 2xO-C$\underline{H_2}$-Ph), 4.49 (br, 1H, H-1), 4.39 (br, 1H, H-3), 4.09-3.83 (m, 1H, H-5a), 4.01 (t, 1H, *J* = 9.4 Hz, H-4), 3.88 (br, 1H, H-2), 0.83 or 0.75 or 0.64 (s, 9H, CH_3-C-Si), 0.19 and 0.03 or 0.11 and 0.00 or -0.11 and -0.21 (s, 3H, 2xCH_3-Si); **^{13}C-NMR (151 MHz, $CDCl_3$, -40 °C)**: δ [ppm] = 156.6 (C=O), 143-127.8 (C^{Ar}), 112.4 or 112.3 or 112.2 (C-6), 82.0 (C-4), 75.6 and 72.9 or 72.8 72.6 or 72.3 (O-$\underline{C}H_2$-Ph), 72.9 or 72.8 72.6 or 72.3 (C-1), 67.7 or 67.5 (O-$\underline{C}H_2$-Ph), 63.1 (C-2), 56.6 (N-$\underline{C}H_2$-Ph), 51.7 (C-5a), 25.5 (Si-C-$\underline{C}H_3$), 17.8 (Si-$\underline{C}$-CH_3), 4.1 and -5.0 (Si-CH_3); **RP-HPLC**: t_r = 32.4 min, (NUCLEODUR C18, 150x4.6mm, 5 µm, 0.4 mL/min, 80-100 % MeCN in 40 min); **ESI-MS**: calcd for $C_{48}H_{55}NO_5SiNa$ $[M+Na]^+$, 776.3742; found, 776.3733.

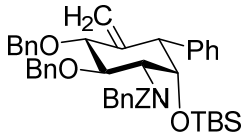

Benzyl benzyl((1R,2R,3R,5S,6S)-2,3-bis(benzyloxy)-6-((tert-butyldimethylsilyl)oxy)-4-methylene-5-phenylcyclohexyl)carbamate (76) The protected cyclohexanone **103** (913 mg, 1.21 mmol) was solved in anhydrous toluene (20 mL) and freshly prepared Cp_2TiMe_2[294] (5.2 mL, 2.66 mmol, 0.51 M in toluene) was added under argon atmosphere. The reaction was heated in an oil-bath to 65 °C and stirred for 17 h, after which the solution was allowed to reach room temperature. Water (20 mL) and ethyl acetate (20 mL) were added and the mixture stirred at room temperature for 1 h, resulting in an orange suspension. After filtration through celite®

545, the filter cake was washed with ethyl acetate. The filtrate was washed with sat. aqueous NaCl and dried ($MgSO_4$). The solvents were removed under reduced pressure and the residue purified by automated flash chromatography (100% petroleum ether to 80:20 petroleum ether/ethyl acetate in 45 min) yielding olefin **76** with residual impurities of the catalyst (304 mg, 33%) as yellow oil.

R_f = 0.57 (petroleum ether/ethyl acetate 5:1), Seebach-reagent; **^{1}H-NMR (500 MHz, $CDCl_3$, 25 °C)**: δ [ppm] = 7.50-6.99 (m, 25H, Ar-H), 5.46-5.04 (m, 2H, O-C$\underline{H_2}$-Ph), 5.40, 5.18 (s, 2H, H-6), 5.00-3.36 (m, 7H, N-C$\underline{H_2}$-Ph, 2xO-C$\underline{H_2}$-Ph, H-2), 4.25 (br, 1H, H-1), 4.03 (br, 2H, H-3, H-4), 3.53 (br, 1H, H-5a), 0.96 (s, 9H, CH_3-C-Si), (-0.12), (-0.80) (s, 3H, CH_3-Si); **^{13}C-NMR (126 MHz, $CDCl_3$, 25 °C)**: δ [ppm] = 152.6 (C=O), 142.2 (C-5), 138.2-126.8 (C^{Ar}), 116.0 (C-6), 85.3 (C-4), 77.9 (C-3), 75.4 (C-1), 73.5, 70.9 (O-$\underline{C}H_2$-Ph), 67.0 (O-$\underline{C}H_2$-Ph), 62.8 (C-2), 52.7 (C-5a), 49.8 (N-$\underline{C}H_2$-Ph), 26.7 (Si-C-$\underline{C}H_3$), (-3.2), (-4.4) (Si-CH_3); **RP-HPLC**: t_r = 32.7 min, (NUCLEODUR C18, 150x4.6mm, 5 µm, 0.4 mL/min, 80-100 % MeCN in 40 min); **ESI-MS**: calcd for $C_{48}H_{55}NO_5SiNa$ $[M+Na]^+$, 776.3742; found, 776.3746.

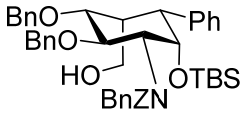

(5aR)-2-Amino-N-benzyl-N-benzyloxycarbonyl-3,4-di-O-benzyl-2-deoxy-5a-phenyl-idose (73) To the olefin **76** (20.0 mg, 0.0265 mmol) solved in anhydrous THF (0.2 mL) was added a solution of 9-BBN (0.16 mL, 0.0796 mmol, 0.5 M in THF) at room temperature. The reaction was heated in an oil bath to 60 °C and was stirred at that temperature for 5h. Again 9-BBN (0.2 mL, 0.0995 mmol) was added to the reaction at room temperature and the reaction was stirred at 60 °C for 17h. The reaction monitoring (TLC) still showed the presence of starting material, another portion of 9-BBN (0.2 mL, 0.0995 mmol) was added do the reaction solution. The stirring was continued for 6h, then the reaction was cooled to 0 °C. 3N NaOH aqueous solution (0.15 mL, 0.477 mmol) and 35%wt H_2O_2 solution (0.15 mL) were successively added at 0 °C. The solution was stirred for 2h at room temperature before the addition of 0.5 N $Na_2S_2O_3$ aqueous solution (10 mL) and diluting with CH_2Cl_2 (30 mL). The organic phase was separated and the aqueous phase extracted with CH_2Cl_2 (3x10 mL). The combined organic layers were washed with sat. aqueous NaCl and dried ($MgSO_4$). The solvents were removed under reduced pressure and the residue purified by automated flash chromatography (12 g silica, 95:5 to 75:25 petroleum ether/ethyl acetate in 90 min) yielding the protected phenyl-carba-β-L-idosamine **73** (17.6 mg, 86%) as a colorless foam.

R_f = 0.44 (petroleum ether/ethyl acetate 5:1), Seebach-reagent; **^{1}H-NMR (500 MHz, $CDCl_3$, 25 °C)**: δ [ppm] = 7.52-6.93 (m, 25H, Ar-H), 5.55, 5.06 (d, *J* = 12.0 Hz, 2H, O-C$\underline{H_2}$-Ph), 4.96, 4.45 (d, *J* = 16.7 Hz, 2H, N-C$\underline{H_2}$-Ph), 4.82, 3.47 (d, *J* = 11.3 Hz, 2H, O-C$\underline{H_2}$-Ph), 4.70, 4.54 (d, *J* = 11.5 Hz, 2H, 2H, O-C$\underline{H_2}$-Ph), 4.52 (br, 1H, H-1), 4.39 (dd, *J* = 11.0, 2.8 Hz, 1H, H-2), 4.25-4.14 (m, 3H, H-3, H-6), 3.91-3.87 (m, 1H, H-4), 2.92-2.90 (m, 2H, H-5, H-5a), 0.90 (s, 9H, CH_3-C-Si), (-0.11), (-0.19) (s, H3, CH_3-Si); **^{13}C-NMR (126 MHz, $CDCl_3$, 25 °C)**: δ [ppm] = 156.6 (C=O), 140.0-126.5 (C^{Ar}), 88.0 (C-4), 77.2 (C-1), 75.0 (C-3), 73.1, 72.9, 72.3 (O-$\underline{C}H_2$-Ph), 67.7 (O-$\underline{C}H_2$-Ph), 63.4 (C-2), 62-1 (C-6), 50.0 (N-$\underline{C}H_2$-Ph), 45.7 (C-5a), 72.9 (C-5), 26.6 (Si-C-$\underline{CH_3}$), (-4.9) (Si-CH_3); **RP-HPLC**: t_r = 7.3 min, (ZORBAX SB-C18, 5 µm, 0.4 mL/min, 80-100 % MeCN in 20 min); **ESI-MS**: calcd for $C_{48}H_{57}NO6SiNa$ $[M+Na]^+$, 794.3847; found, 794.3837.

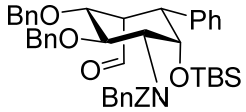

Benzyl benzyl((1R,2R,3R,4R,5R,6S)-2,3-bis(benzyloxy)-6-((tert-butyldimethylsilyl)oxy)-4-formyl-5-phenylcyclohexyl)carbamate (105) To 2-iodoxybenzoic acid (70.0 mg, 0.112 mmol) solved in anhydrous DMSO (0.8 mL) was added a solution of the protected phenyl-carba-β-L-idosamine **73** (24.8 mg, 0.032 mmol) in anhydrous DMSO (0.4 mL) was added at room temperature. The solution was stirred at room temperature for 18h, then water (5 mL) was added and the solution extracted with CH_2Cl_2 (3x10 mL). The combined organic layers were washed with sat. aqueous NaCl and dried ($MgSO_4$). The solvents were removed under reduced pressure and the residue purified by automated flash chromatography (4 g silica, 95:5 to 75:25 petroleum ether/ethyl acetate in 90 min) yielding the aldehyde **105** (17.9 mg, 72%) as a colorless foam.

R_f = 0.54 (petroleum ether/ethyl acetate 5:1), Seebach-reagent; **^{1}H-NMR (500 MHz, $CDCl_3$, 25 °C)**: δ [ppm] = 10.29 (d, *J* = 5.8 Hz, 1H, H-6), 7.51-6.86 (m, 25H, Ar-H), 5.54, 5.08 (d, *J* = 11.9 Hz, 2H, O-C$\underline{H_2}$-Ph), 5.04, 4.45 (d, *J* = 16.7 Hz, 2H, N-C$\underline{H_2}$-Ph), 4.66, 3.23 (d, *J* = 11.4 Hz, 2H, O-C$\underline{H_2}$-Ph), 4.62 (d, *J* = 10.8 Hz, 2H, O-C$\underline{H_2}$-Ph), 4.53 (dd, *J* = 10.9, 3.0 Hz, 1H, H-2), 4.47 (br, 1H, H-1), 4.37 (dd, *J* = 11.0, 8.1 Hz, 1H, H-3), 3.91 (dd, *J* = 8.3, 5.2 Hz, 1H, H-4), 3.53 (td, *J* = 5.4, 2.9 Hz, 1H, H-5), 3.08 (br, 1H, H-5a), 0.85 (s, 9H, CH_3-C-Si), (-0.14), (-0.19) (s, H3, CH_3-Si); **^{13}C-NMR (126 MHz, $CDCl_3$, 25 °C)**: δ [ppm] = 203.9 (C=O), 156.6 (C=O), 140.1-126.7 (C^{Ar}), 84.9, 84.7 (C-4), 77.8, 77.4 (C-1), 75.2 (C-3), 72.3 (O-$\underline{C}H_2$-Ph), 71.1, 71.0 (O-$\underline{C}H_2$-Ph), 67.8 (O-$\underline{C}H_2$-Ph), 63.2 (C-2), 52.6 (C-5), 49.8 (N-$\underline{C}H_2$-Ph), 48.8 (C-5a), 24.0 (Si-C-$\underline{CH_3}$), 18.2 (Si-$\underline{C}$-CH_3), (-4.2), (-5.5) (Si-

CH_3); **RP-HPLC**: t_r = 3.1 min, (Kinetex EVO C18, 2.6 µm, 0.8 mL/min, 80-87 % MeCN in 5 min); **ESI-MS**: calcd for $C_{48}H_{55}NO_6SiNa$ $[M+Na]^+$, 792.3691; found, 792.3680.

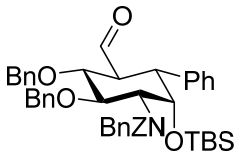

Benzyl benzyl((1R,2R,3R,4S,5R,6S)-2,3-bis(benzyloxy)-6-((tert-butyldimethylsilyl)oxy)-4-formyl-5-phenylcyclohexyl)carbamate (106) A solution of the axial-hydroxy methylene aldehyde **105** (27.1 mg, 0.0317 mmol) in methanol (317 µL) and pyridine (35 µL) was stirred at 60 °C for 4 days. HPLC showed 98% conversion and the solvents were removed under reduced pressure and the residue coevaporated with toluene. The residue was purified by preparative HPLC (Gemini® C18, 110 Å, 5 µm, 50x30 mm, 40-100% acetonitrile in 15 min, A: 0.1% formic acid in H_2O) followed by lyophilisation of product fractions, yielding the aldehyde **106** (11.1 mg, 45%) as colorless foam.

^{1}H-NMR (500 MHz, $CDCl_3$, 25 °C): δ [ppm] = 9.65 (d, *J* = 2.9 Hz, 1H, H-6), 7.50-6.81 (m, 25H, Ar-H), 5.55, 5.02 (d, *J* = 11.9 Hz, 2H, O-C$\underline{H_2}$-Ph), 4.90, 4.31 (d, *J* = 16.7 Hz, 2H, N-C$\underline{H_2}$-Ph), 4.77-3.76 (m, 9H, 2xO-C$\underline{H_2}$-Ph, H-2, H-1, H-3, H-4, H-5), 3.06 (dd, *J* = 12.6, 2.0 Hz, 1H, H-5a), 0.92 (s, 9H, CH_3-C-Si), (-0.18), (-1.17) (s, H3, CH_3-Si); **^{13}C-NMR (126 MHz, $CDCl_3$, 25 °C)**: δ [ppm] = 202.7 (C=O), 156.2 (C=O), 138.0-126.1 (C^{Ar}), 83.5 (C-4), 77.4 (C-1), 76.5 (C-3), 74.9 (O-C$\underline{H_2}$-Ph), 71.3, (O-$\underline{C}$H$_2$-Ph)0, 67.7 (O-$\underline{C}$H$_2$-Ph), 62.5 (C-2), 52.2, 52.0 (C-5), 49.5 (N-$\underline{C}$H$_2$-Ph), 47.2 (C-5a), 26.6 (Si-C-$\underline{CH_3}$), 18.3 (Si-$\underline{C}$-CH_3), (-3.7), (-6.1) (Si-CH_3); **RP-HPLC**: t_r = 3.5 min, (Kinetex EVO C18, 2.6 µm, 0.8 mL/min, 80-87 % MeCN in 5 min); **ESI-MS**: calcd for $C_{48}H_{55}NO_6SiH$ $[M+H]^+$, 770.3871; found, 792.3868.

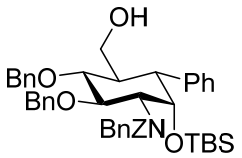

(5aS)-2-Amino-N-benzyl-N-benzyloxycarbonyl-3,4-di-O-benzyl-2-deoxy-5a-phenyl-glucose (107) To the aldehyde **106** (11.1 mg, 0.0144 mmol) solved in anhydrous THF (300 µL) was added a solution of $LiAlH_4$ (18 µL, 0.0180 mmol, 1 M in THF) at 0 °C. The cooling bath was removed and the reaction stirred at room temperature for 15 min. The reaction was cooled and wet $MgSO_4$ was added to quench the reaction. The $MgSO_4$ was removed by filtration through a 0.2 µm syringe filter and washed with CH_2Cl_2 (2x 1 mL). The solvents were removed under reduced pressure and

the residue purified by automated flash chromatography (4 g silica, 98:2 to 78:22 petroleum ether/ethyl acetate in 30 min) yielding the protected phenyl-carba-α-D-glucosamine **107** (9.58 mg, 86%) as a colorless foam.

R_f = 0.26 (petroleum ether/ethyl acetate 5:1), Seebach-reagent; **^{1}H-NMR (600 MHz, $CDCl_3$, -30 °C)**: δ [ppm] = 7.46-6.74 (m, 25H, Ar-H), 5.29 (t, *J* = 9.9 Hz, 1H, H-3c), 5.15-4.61 (m, 6H, 3xO-C$\underline{H_2}$-Ph), 4.92-4.11 (m, 2H, N-C$\underline{H_2}$-Ph), 4.52 (d, *J* = 11.3 Hz, 1H, H-2a), 4.38-4.35 (m, 2H, H-1a, H-2b), 4.11-4.07 (m, 1H, H-3a), 4.01 (H-1c), 3.97 (t, *J* = 9.6 Hz, 1H, H-4a), 3.87 (d, *J* = 12.0 Hz, 1H, H-6aa), 3.82 (d, *J* = 11.2 Hz, 1H, H-6ac), 3.64 (t, *J* = 9.8 Hz, 1H, H-4c), 3.51 (dd, *J* = 11.2, 3.1 Hz, 1H, H-6ba), 3.42 (dd, *J* = 11.2, 3.4 Hz, 1H, H-6bc), 3.08 (d, *J* = 10.8 Hz, 1H, H-2c), 3.04 (d, *J* = 12.5 Hz, 1H, H-5aa), 2.67 (d, *J* = 13.1 Hz, 1H, H-5ab), 2.57-2.45 (m,1H, H-5), 0.88 (s, 9H, CH_3-C-Si), (-0.27), (-1.23) (s, H3, CH_3-Si); **^{13}C-NMR (150 MHz, $CDCl_3$, -30 °C)**: δ [ppm] = 156.9, 154.9 (C=O), 139.8-125.5 (C^{Ar}), 84.1 (C-4c), 77.2 (C-3c), 75.3 (C-1), 73.8, 73.1 (C-3a, H-1a, H-1c, 2xO-$\underline{C}H_2$-Ph), 67.0, 66.4 (C-2c, (O-$\underline{C}H_2$-Ph), 59.6 (C-6), 52.3 (N-$\underline{C}H_2$-Ph), 46.7 (C-5a), 40.6, 40.2 (C-5), 26.3 (Si-C-$\underline{C}H_3$), 8.1 (Si-$\underline{C}$-CH_3), (-3.7), (-7.1) (Si-CH_3); **RP-HPLC**: t_r = 9.2 min, (ZORBAX SB-C18, 5 µm, 0.4 mL/min, 80-100 % MeCN in 20 min); **ESI-MS**: calcd for $C_{48}H_{57}NO6SiNa$ $[M+Na]^+$, 794.3847; found, 794.3837.

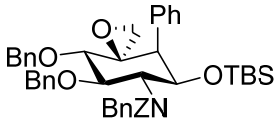

Benzyl benzyl((3S,4S,5R,6R,7R,8S)-4,5-bis(benzyloxy)-7-((tert-butyldimethylsilyl)oxy)-8-fluoro-1-oxaspiro[2.5]octan-6-yl)carbamate (74) The olefin **77** (177.4 mg, 0.235 mmol) was presented in a 10 mL flat bottom flask and solved in CH_2Cl_2 (1.5 mL). The solution was cooled to 0 °C and *m*CPBA (116 mg, 0.52 mmol) solved in CH_2Cl_2 (1 mL) added and the cloudy suspension stirred at room temperature for 1h. TLC shows presence of starting material, so another three additional portions of *m*CPBA (116 mg, 0.52 mmol) were added in an interval of two times 1 h and then 2 h. After stirring for 4 h at room temperature sat. aqueous Na_2SO_3 (10 mL) is added and the suspension stirred for 10 min. The organic layer is separated washed with sat. aqueous $NHCO_3$ (3x10 mL) and sat. aqueous NaCl, followed by drying with $MgSO_4$. The solvent was removed under reduced pressure and the residue purified by flash chromatography (100% petroleum ether to 80:20 petroleum ether/ethyl acetate in 45 min), yielding the epoxide **74** (147.8 mg, 82 %) as colorless solid.

R_f = 0.46 (petroleum ether/ethyl acetate 5:1), Seebach-reagent;

NMR-assignment of conformer A:

^{1}H-NMR (500 MHz, $CDCl_3$, -40 °C): δ [ppm] = 7.64-7.06 (m, 25H, Ar-H), 5.53-5.06 (m, 2H, N-C(O)-O-C$\underline{H_2}$-Ph), 5.26 and 4.03 (d, *J* = 15.6 Hz, 2H, N-C$\underline{H_2}$-Ph), 5.05-4.29 (m, 2H, O-C$\underline{H_2}$-Ph), 4.82 (dd, *J* = 11.2, 5.0 Hz, 1H, H-1), 4.80-4.20 (m, 4H, O-C$\underline{H_2}$-Ph), 4.37–4.29 (m, 1H, H-3), 3.82 (t, *J* = 10.7 Hz, 1H, H-2), 3.68 (d, *J* = 9.4 Hz, 1H, H-4), 3.07 (d, *J* = 5.3 Hz, 1H, H6a), 3.01 (d, *J* = 5.6 Hz, 1H, H-5a), 2.84 (d, *J* = 4.8 Hz, 1H, H6b), 0.74 or 0.69 or 0.58 (s, 9H, CH_3-C-Si), 0.15 and 0.07 or 0.08 and 0.02 or -0.16 and -0.25 (s, 3H, 2xCH_3-Si); **^{13}C-NMR (176 MHz, $CDCl_3$, -40 °C)**: δ [ppm] = 156.6 (C=O), 139.1-126.5 (C^{Ar}), 81.3 (C-3), 75.7 (C-4), 75.6 or 75.1 or 74.9 or 74.7 (O-$\underline{C}H_2$-Ph), 70.7 (C-1), 67.7 or 67.6 or 66.7 (O-$\underline{C}H_2$-Ph), 63.4 (C-2), 56.7 or 56.3 (N-$\underline{C}H_2$-Ph), 50.3 (C-6), 49.9 (C-5a), 25.7 or25.5 (Si-C-$\underline{C}H_3$), 17.8 or 17.7 or 17.6 (Si-$\underline{C}$-CH_3), -4.3 and -4.9 or -4.4 and -6.1 or -4.6 and -5.6 (Si-CH_3);

Conformer B:

^{1}H-NMR (500 MHz, $CDCl_3$, -40 °C): δ [ppm] = 7.64-7.06 (m, 25H, Ar-H), 5.53-5.06 (m, 2H, N-C(O)-O-C$\underline{H_2}$-Ph), 5.26 and 4.03 (d, *J* = 15.6 Hz, 2H, N-C$\underline{H_2}$-Ph), 5.22 (t, *J* = 10.9 Hz, 1H, H-2), 5.05-4.29 (m, 2H, O-C$\underline{H_2}$-Ph), 4.80-4.20 (m, 4H, O-C$\underline{H_2}$-Ph), 4.60 (dd, *J* = 11.0, 5.9 Hz, 1H, H-1), 3.66 (d, *J* = 9.22 Hz, 1H, H-4), 3.54 (t, *J* = 10.1 Hz, 1H, H-3), 3.01 (d, *J* = 5.6 Hz, 1H, H-5a), 2.98 (d, *J* = 5.0 Hz, 1H, H6a), 2.84 (2.93 (d, *J* = 5.1 Hz, 1H, H6b), 0.74 or 0.69 or 0.58 (s, 9H, CH_3-C-Si); **^{13}C-NMR (176 MHz, $CDCl_3$, -40 °C)**: δ [ppm] = 158.4 (C=O), 139.1-126.5 (C^{Ar}), 78.2 (C-3), 77.1 (C-4), 75.6 or 75.1 or 74.9 or 74.7 (O-$\underline{C}H_2$-Ph), 68.2 (C-1), 67.7 or 67.6 or 66.7 (O-$\underline{C}H_2$-Ph), 59.8 (C-2), 56.7 or 56.3 (N-$\underline{C}H_2$-Ph), 50.3 (C-6), 49.7 (C-5a), 25.7 or25.5 (Si-C-$\underline{C}H_3$), 17.8 or 17.7 or 17.6 (Si-$\underline{C}$-CH_3), -4.3 and -4.9 or -4.4 and -6.1 or -4.6 and -5.6 (Si-CH_3);

Conformer C:

^{1}H-NMR (500 MHz, $CDCl_3$, -40 °C): δ [ppm] = 7.64-7.06 (m, 25H, Ar-H), 5.53-5.06 (m, 2H, N-C(O)-O-C$\underline{H_2}$-Ph), 5.26 and 4.03 (d, *J* = 15.6 Hz, 2H, N-C$\underline{H_2}$-Ph), 5.11 (br, 1H, H-1), 5.05-4.29 (m, 2H, O-C$\underline{H_2}$-Ph), 4.80-4.20 (m, 4H, O-C$\underline{H_2}$-Ph), 4.70 (t, *J* = 9.7 Hz, 1H, H-3), 3.72 (d, *J* = 9.6 Hz, 1H, H-4), 3.66 (t, *J* = 9.3 Hz, 1H, H-2), 3.07 (d, *J* = 5.3 Hz, 1H, H6a), 2.84 (d, *J* = 4.8 Hz, 1H, H6b), 2.80 (d, *J* = 4.8 Hz, 1H, H-5a), 0.74 or 0.69 or 0.58 (s, 9H, CH_3-C-Si); **^{13}C-NMR (176 MHz, $CDCl_3$, -40 °C)**: δ [ppm] = 154.8 (C=O), 139.1-126.5 (C^{Ar}), 79.8 (C-3), 76.1 (C-4), 75.6 or 75.1 or 74.9 or 74.7 (O-$\underline{C}H_2$-Ph), 69.8 (C-1), 67.7 or 67.6 or 66.7 (O-$\underline{C}H_2$-Ph), 64 6 (C-2), 56.7 or 56.3 (N-$\underline{C}H_2$-Ph), 50.3 (C-6), 50.0 (C-5a), 25.7 or25.5 (Si-C-$\underline{C}H_3$), 17.8 or 17.7 or 17.6 (Si-$\underline{C}$-CH_3), -4.3 and -4.9 or -4.4 and -6.1 or -4.6 and -5.6 (Si-CH_3);

RP-HPLC: t_r = 9.6 min, (NUCLEODUR C18, 150x4.6mm, 5 µm, 0.4 mL/min, 80-100 % MeCN in 40 min); **HRMS**: calcd for $C_{48}H_{55}NO_6SiNa$ $[M+Na]^+$, 792.3691; found, 792.3696.

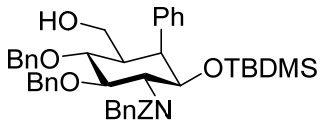

(5aS, 1R)-2-Amino-N-benzyl-N-benzyloxycarbonyl-3,4-di-O-benzyl-2-deoxy-5a-phenyl-1-O-*tert*-butyldimethylsilyl-glucose (108) A fresh solution of Cp_2TiCl in THF was prepared according to Rajanbabu *et al.*[201] To titanocene dichloride (635 mg) solved in anhydrous THF (5.1 mL) was added zinc dust (500 mg). The mixture was stirred at room temperature for 60 min under argon. Unreacted zinc was removed by filtration through a steel cannula with a glass-wool plug at the bottom. The epoxide **74** (82.32 mg, 0.107 mmol) was solved in anhydrous THF (0.25 mL) and 1,4-cyclohexadien (0.1 mL, 1.069 mmol) was added at room temperature. The solution of Cp_2TiCl in THF (0.43 mL, 0.214 mmol, 0.5 M) was added dropwise over 30 min. After 1.5h Cp_2TiCl in THF (0.24 mL, 0.118 mmol) was added at room temperature. The reaction was stirred for another 1h and ice-cold 1 N HCl in water (500 µL) was added to the solution. The organic layer was separated and the aqueous phase extracted with CH_2Cl_2 (3x10 mL). Sat. aqueous $NaHCO_3$ (10 mL) is added to the aqueous phase and again extracted with CH_2Cl_2 (3x 10 mL). The combined organic layers were washed with Sat. aqueous $NaHCO_3$ (10 mL), sat. aqueous NaCl and dried ($MgSO_4$). The solvents were removed under reduced pressure and the residue purified via automated flash chromatography (90% petroleum ether to 75:25 petroleum ether/ethyl acetate in 40 min) yielding the alcohol **108** (53.91 mg, 65%) as slightly yellow oil.

R_f = 0.14 (petroleum ether/ethyl acetate 5:1), Seebach-reagent; **^{1}H-NMR (700 MHz, $CDCl_3$)**: δ [ppm] = 7.32–7.01 (m, 25H, Ar-H), 5.29 and 5.04 (d, *J* = 12.3 Hz, 2H, N-C(O)-O-C$\underline{H_2}$-Ph), 4.88-4.11 (m, 2H, N-C$\underline{H_2}$-Ph), 4.83-4.37 (m, 4H, 2xO-C$\underline{H_2}$-Ph), 4.78-4.69 (m, 2H, H-1 and H-3), 3.84 (dd, *J* = 11.6, 9.1 Hz, 1H, H-4), 3.78-3.76 (m, 1H, H-2), 3.43 (dd, *J* = 7.1, 5.6 Hz, 1H, H-6), 3.39 (dd, *J* = 6.0, 5.3 Hz, 1H, H-5a), 2.18 (dq, *J* = 11.1, 5.7 Hz, 1H, H-5), 0.60 and 0.57 (s, 9H, *t*-Bu), 0.09 and -0.02 (s, 3H, CH_3); **^{13}C-NMR (176 MHz, $CDCl_3$)**: δ [ppm] = 156.5 (C=O), 131.2-128.1 (C^{Ar}), 82.4 (C-4), 81.3 (C-3), 75.2 and 74.8 (O-$\underline{C}H_2$-Ph), 71.0 (C-1), 67.2 (br, C-2) 66.9 (N-C(O)-O-$\underline{C}H_2$-Ph), 64.2 (C-6), 56.8 (br, N-$\underline{C}H_2$-Ph), 50.2 (C-5a), 44.4 (C-5), 25.8 (-Si-*t*-Bu), 17.7 (Si-$\underline{C}$-CH_3), -4.2 and -4.9 (-Si-CH3-); **RP-HPLC**: t_r = 7.5 min (ZORBAX SB-C18, 5 µm, 0.4 mL/min, 80-100 % MeCN in 20 min); **HRMS**: calcd for $C_{48}H_{57}NO_6SiNa$ $[M+Na]^+$, 794.3847; found, 794.3834.

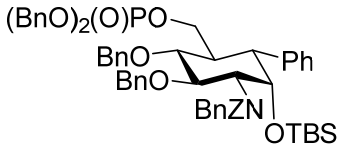

Dibenzyl (5aS)-2-Amino-N-benzyl-N-benzyloxycarbonyl-3,4-di-O-benzyl-2-deoxy-5a-phenyl-1-O-*tert*-butyldimethylsilyl-glucose-6-phosphate (109) The unphosphorylated phenyl-carba precursor **107** (9.58 mg, 0.0124 mmol) was transferred to a heat-dried schlenk-tube with toluene. The toluene was removed under reduced pressure and the starting material dried under vacuum (~10^{-2} mbar) for 17 h. 1H-Tetrazole (4.35 mg, 0.0621 mmol), anhydrous CH_2Cl_2 (1 mL) and dibenzyl *N,N*-diisopropylphosphoramidite (10.4 µL, 0.0310 mmol) were added under argon atmosphere. The mixture was stirred for 2 h at room temperature after which HPLC-monitoring showed completion of the reaction. The reaction was cooled to 0 °C and *m*-CPBA (70%, 9.30 mg, 0.0377 mmol) was added. After 1h HPLC shows completion of the reaction, the mixture was diluted with ethyl acetate (10 mL) and 2 mL of aqueous 10% Na_2SO_3 was added and the mixture stirred for 15 min. The organic layer was separated and washed with aqueous 10% Na_2SO_3 (2x10 mL), 1M HCl (2x10 mL), saturated $NaHCO_3$ (3x10 mL) and brine (2x10 mL). The organic layer was dried with $MgSO_4$ and concentrated. The reaction was purified via RP-HPLC (Gemini® C18, 110 Å, 5 µm, 50x30 mm, 80-100 % MeCN in 10 min). Fractions containing product were combined and freeze-dried yielding the phosphorylated pseudo-sugar precursor **109** (9.94 mg, 78%) as colorless foam.

^{1}H-NMR (700 MHz, $CDCl_3$, 25 °C): δ [ppm] = 7.50-6.85 (m, 35H, Ar-H), 5.24 (br, 1H, H-3b), 5.08-3.76 (m, 18H, 5xO-C$\underline{H_2}$-Ph, N-C$\underline{H_2}$-Ph, H-2, H-6, H-3a, H-1, H-4a), 3.50 (br, 1H, H-4c), 3.02 (m, 1H, H-2), 2.69 (br, 1H, H-5a), 2.63 (br, H-5), 0.90 (s, 9H, CH_3-C-Si), (-0.20), (-1.15) (s, H3, CH_3-Si); **^{13}C-NMR (150 MHz, $CDCl_3$, 25 °C)**: δ [ppm] = 155.0 (C=O), 140.2-125.7 (C^{Ar}), 83.1 (C-4b), 81.9 (C-4a), 78.2 (C-3b), 75.4 (O-$\underline{C}H_2$-Ph), 74.2 (C-1), 73.4 (O-$\underline{C}H_2$-Ph), 69.0 (2xP-O-$\underline{C}H_2$-Ph), 67.4 (C-2b), 66.6 (O-$\underline{C}H_2$-Ph), 67.7 (C-6), 62.4 (C-2a), 52.9 (N-$\underline{C}H_2$-Ph), 46.9 (C-5a), 39.8 (C-5), 26.7 (Si-C-$\underline{CH_3}$), 18.4 (Si-$\underline{C}$-CH_3), (-3.5) (Si-CH_3); **RP-HPLC**: t_r = 22.2 min, (ZORBAX SB-C18, 5 µm, 0.4 mL/min, 20-100 % MeCN in 20 min); **ESI-MS**: calcd for $C_{62}H_{70}NO_9PSiNa$ $[M+Na]^+$, 1054.4450; found, 1054.4481.

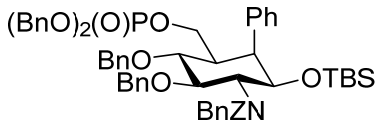

Dibenzyl (5aS)-2-amino-N-benzyl-N-benzyloxycarbonyl-3,4-di-O-benzyl-2-deoxy-5a-phenyl-1-O-*tert*-butyldimethylsilyl-β-D-carba-glucose-6-phosphate (110) The unphosphorylated phenyl-carba precursor **108** (36.76 mg, 0.0476 mmol) in toluene was transferred to a heat-dried schlenk-tub. The toluene was removed under reduced pressure and the starting material dried under vacuum (~10^{-2} mbar) for 17 h.

1H-Tetrazole (16.68 mg, 0.238 mmol), anhydrous CH_2Cl_2 (4 mL) and dibenzyl *N,N*-diisopropylphosphoramidite (40 µL, 0.119 mmol) were added under argon atmosphere. The mixture was stirred at room temperature for 3 h after which TLC-monitoring showed completion of the reaction. The reaction was cooled to 0 °C and *m*CPBA (77%, 32.0 mg, 0.143 mmol) was added. After 1h, 2 mL of aqueous 10% Na_2SO_3 was added at 0 °C and the mixture stirred for 15 min. The organic layer was separated and the aqueous layer extracted with CH_2Cl_2 (3x10 mL). Sat. aqueous NH_4Cl (10 mL) is added to the aqueous layer and extracted with CH_2Cl_2 (3x20 mL). Sat. aqueous $NaHCO_3$ (20 mL) is added to the aqueous layer and extracted with CH_2Cl_2 (3x30 mL). The combined organic layers are washed with brine (10 mL) dried with $MgSO_4$ and the solvents removed under reduced pressure. The residue was purified via prep. RP-HPLC (Gemini® C18, 110 Å, 5 µm, 50x30 mm, 80-100 % MeCN in 10 min). Fractions containing product were combined and freeze-dried yielding the phosphorylated pseudo-sugar precursor **110** (30.03 mg, 61%) as colorless foam.

^{1}H-NMR (700 MHz, $CDCl_3$, 25 °C): δ [ppm] = 7.32-6.98 (m, 35H, Ar-H), 5.28 and 5.04 (d, *J* = 12.3 Hz, 2H, N-C(O)-O-C$\underline{H_2}$-Ph), 4.92 and 4.83 (d, *J* = 7.8 Hz, 2H, P-O-C$\underline{H_2}$-Ph), 4.71 (br, 2H, H-1 and H-3), 4.68 and 4.29 (d, *J* = 11.4 Hz, 2H, O-C$\underline{H_2}$-Ph), 4.23 (dt, *J* = 9.2, 4.3 Hz, 1H, H-6a), 3.61 (dd, *J* = 11.8, 8.9 Hz, 1H, H-4), 3.49 (t, *J* = 5.9 Hz, 1H, H-5a), 3.43 (td, *J* = 9.9, 5.8 Hz, 1H, H-6b), 3.76 (br, 1H, H-2), 2.33 (dt, *J* = 11.0, 5.9 Hz, 1H, H-5), 0.61 and 0.57 (s, 9H, *t*-Bu), 0.07 and -0.04 (s, 3H, CH_3); **^{13}C-NMR (176 MHz, $CDCl_3$)**: δ [ppm] = 155.5 (C=O), 138.2-127.1 (C^{Ar}), 81.2 (C-3), 79.3 (C-4), 74.6 (O-$\underline{C}H_2$-Ph), 70.9 (C-1), 69.2 and 69.2 (d, *J* = 5.4 Hz, P-O-$\underline{C}H_2$-Ph), 66.9 (N-C(O)-O-$\underline{C}H_2$-Ph), 66.3 (d, *J* = 5.8 Hz, C-6), 56.8 (br, N-$\underline{C}H_2$-Ph), 48.5 (C-5a), 43.1 (d, *J* = 8.2 Hz, C-5), 25.9 (-Si-*t*-Bu), 17.7 (Si-$\underline{C}$-CH_3), -4.1 and -4.9 (-Si-CH3-); **RP-HPLC**: t_r = 13.3 min (ZORBAX SB-C18, 5 µm, 0.4 mL/min, 80-100 % MeCN in 20 min); **HRMS**: calcd for $C_{62}H_{70}NO_9PSiNa$ $[M+Na]^+$, 1054.4450 found, 1054.4458.

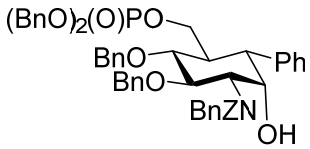

Dibenzyl (5aS)-2-amino-N-benzyl-N-benzyloxycarbonyl-3,4-di-O-benzyl-2-deoxy-5a-phenyl-carba-glucose-6-phosphate (111) To the silylated phenyl-carba-GlcN6P precursor **109** (8.14 mg, 0.00789 mmol) solved in DMF (110 µL) were added water (1.42 µL, 0.0789 mmol) and a solution of TAS-F (39.4 µL, 0.0394 mmol, 1N in DMF). The reaction was stirred for 18h at 23 °C. Another 20 µL of a 1N solution of TAS-F in DMF were added and the reaction stirred at 23 °C. HPLC-monitoring after 27h showed

44% conversion of the reaction and 20 µL of a 1N solution of TAS-F in DMF were added. After 43h water (1.42 µL) and a last portion of 20 µL of a 1N solution of TAS-F in DMF were added. After 66h the reaction was diluted with 1 mL acetonitrile/water (66:34) and the solution was loaded directly onto a C18-HPLC column (Gemini® C18, 110 Å, 5 µm, 50x30 mm), utilizing a gradient of 60-80 % MeCN (A: 0.1% formic acid in H_2O) in 10 min. Fractions containing the product were combined and freeze-dried yielding the benzylated pseudo-sugar precursor **111** (4.59 mg, 63%) as colorless foam.

^{1}H-NMR (700 MHz, $CDCl_3$, 25 °C): δ [ppm] = 7.31-7.13 (m, 35H, Ar-H), 5.12-4.43 (m, 13H, 5xO-C$\underline{H_2}$-Ph, N-C$\underline{H_2}$-Ph, H-3), 4.44 (d, *J* = 9.9 Hz, 1H, H-6a), , 3.85 (br, 1H, H-1), 3.74-3.66 (m, 2H, H-6b, H-4), 3.07 (br, 1H, H-2), 2.68 (br, 1H, H-5), 2.55 (br, 1H, H-5a), 0.90 (s, 9H, CH_3-C-Si), (-0.20), (-1.15) (s, H3, CH_3-Si); **^{13}C-NMR (150 MHz, $CDCl_3$, 25 °C)**: δ [ppm] = 158.8 (C=O), 138.8.2-127.2 (C^{Ar}), 81.8 (C-4), 78.8 (C-3), 75.4 (2xO-$\underline{C}H_2$-Ph), 74.7 (C-1), 69.2, 69.1 (2xP-O-$\underline{C}H_2$-Ph), 68.1 (O-$\underline{C}H_2$-Ph), 65.2 (C-6), 47.2 (N-$\underline{C}$H2-Ph) and 47.2 (C-5a), 41.1 (C-5); **^{31}P-NMR (162 MHz, $CDCl_3$)**: δ [ppm] = -1.08 (s, 1P); **RP-HPLC**: t_r = 17.9 min, (ZORBAX SB-C18, 5 µm, 0.4 mL/min, 20-100 % MeCN in 20 min); **ESI-MS**: calcd for $C_{56}H_{56}NO_9PNa$ $[M+Na]^+$, 940.3585; found, 940.3568.

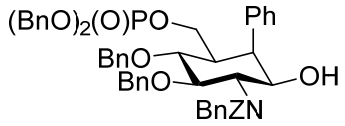

Dibenzyl (5a*S*)-2-amino-*N*-benzyl-*N*-benzyloxycarbonyl-3,4-di-*O*-benzyl-2-deoxy-5a-phenyl-β-D-glucose-6-phosphate (75) To the silylated phenyl-carba precursor **110** (27.6 mg, 0.0267 mmol) solved in THF (395.5 µL) K_2HPO_4-buffer (2.54 µL) was added. A solution of TBAF (107.0 µL, 0.1070 mmol, 1N in THF) was added at room temperature and the reaction was stirred for 24 h at 23 °C. Another 50 µL of a 1N solution of TBAF in THF (0.050 mmol) were added and the reaction stirred at 23 °C for another 29 h. HPLC-monitoring after a total of 56 h showed 90% conversion of the reaction and the reaction was diluted with 1 mL acetonitrile/water (66:34). The solution was loaded directly onto a C18-HPLC column (Gemini® C18, 110 Å, 5 µm, 50x30 mm), utilizing a gradient of 60-80 % MeCN (A: 0.1% formic acid in H_2O) in 10 min. Fractions containing the product were combined and freeze-dried yielding the benzylated phenyl-carba-sugar **75** (14.15 mg, 58%) as colorless foam.

NMR-assignment for conformer A:

^{1}H-NMR (700 MHz, $CDCl_3$, 25 °C): δ [ppm] = 7.36-7.19 (m, 35H, Ar-H), 5.08-5.07 (m, 2H, O-C$\underline{H_2}$-Ph), 4.86 and 4.30 (d, *J* = 14.8 Hz, 2H, N-C$\underline{H_2}$-Ph), 4.76-4.52 (m, 8H, O-C$\underline{H_2}$-Ph), 4.39 (br, 1H, H-4), 4.24 (br, 1H, H-1), 4.01 (br, 1H, H-5a), 3.86 (br, 1H, H-6a), 3.65-

3.61 (m, 2H, H-3, H-6b), 3.50 (br, 1H, H-2), 2.57 (br, 1H, H-5); **^{13}C-NMR (176 MHz, $CDCl_3$, 25 °C)**: δ [ppm] = 156.3 or 155.7 (C=O), 141.1-126.5 (C^{Ar}), 87.4 (C-3), 83.0 (C-4), 77.7 (C-1), 73.9 (2xO-$\underline{C}H_2$-Ph), 71.1 (2xO-$\underline{C}H_2$-Ph), 69.3 (C-6), 67.7 (C-2), 67.2 (O-$\underline{C}H_2$-Ph), 53.9 (N-$\underline{C}$H2-Ph), 44.7 (C-5), 44.2 (C-5a); **^{31}P-NMR (162 MHz, $CDCl_3$)**: δ [ppm] = -1.34 (s, 1P);

NMR-assignment for conformer B:

^{1}H-NMR (700 MHz, $CDCl_3$, 25 °C): δ [ppm] = 7.36-7.19 (m, 35H, Ar-H), 5.08-5.07 (m, 2H, O-C$\underline{H_2}$-Ph), 4.86 and 4.30 (d, *J* = 14.8 Hz, 2H, N-C$\underline{H_2}$-Ph), 4.76-4.52 (m, 8H, O-C$\underline{H_2}$-Ph), 4.24 (br, 1H, H-4), 3.97 (br, 1H, H-1), 3.74 (br, 1H; H-6a), 3.65-3.61 (m, 3H, H-3, H-6b, H-2), 3.41 (br, 1H, H-5a), 2.42 (br, 1H, H-5); **^{13}C-NMR (176 MHz, $CDCl_3$, 25 °C)**: δ [ppm] = 156.3 or 155.7 (C=O), 141.1-126.5 (C^{Ar}), 87.0 (C-3), 82.7 (C-4), 78.1 (C-1), 73.5 (2xO-$\underline{C}H_2$-Ph), 71.1 (2xO-$\underline{C}H_2$-Ph), 68.8 (C-6 and C-2), 68.0 (O-$\underline{C}H_2$-Ph), 45.1 (C-5), 44.0 (C-5a); **^{31}P-NMR (162 MHz, $CDCl_3$)**: δ [ppm] = -1.34 (s, 1P);

RP-HPLC: t_r = 18.0 min, (ZORBAX SB-C18, 5 µm, 0.4 mL/min, 20-100 % MeCN in 20 min); **ESI-MS**: calcd for $C_{56}H_{56}NO_9PNa$ $[M+Na]^+$, 940.3585; found, 940.3577.

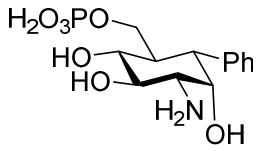

(5aS)-2-Amino-2-deoxy-5a-phenyl-glucose-6-phosphate (72) Perbenzylated phenyl-carba compound **111** (4.59 mg, 0.00500 mmol) was deprotected according to **GP1**. The reaction was finished after 6h. The lyophilized pseudo-sugar was purified via C18-HPLC (Gemini® C18, 110 Å, 5 µm, 50x30 mm, 100% H_2O for 5 min, then 0-40% acetonitrile in 5 min). Fractions containing the product were combined and freeze-dried yielding (5aS)-phenyl-carba-α-D-GlcN6P **72** (1.89 mg, 76%) as colorless foam.

^{1}H-NMR (400 MHz, $CDCl_3$, 25 °C): δ [ppm] = 7.48-7.30 (m, 5H, Ph), 4.13 (ddd, *J* = 10.5, 5.1, 2.0 Hz, 1H, H-6a), 4.10 (t, *J* = 2.4 Hz, 1H, H-1), 3.87 (dd, *J* = 10.7, 9.3 Hz, 1H, H-3), 3.77 (t, *J* = 9.8 Hz, 1H, H-4), 3.50-3.46 (m, 1H, H-6b), 3.46 (dd, *J* = 10.5, 2.9 Hz, 1H, H-2), 3.11 (dd, *J* = 12.7, 2.2 Hz, 1H, H-5a), 2.31 (ddd, *J* = 12.2, 10.2, 2.1 Hz, 1H, H-5); **^{13}C-NMR (176 MHz, $CDCl_3$, 25 °C)**: δ [ppm] = 138.7-127.3 (C^{Ar}), 71.2 (C-4), 70.7 (C-3), 70.3 (C-1), 61.2 (C-6), 56.3 (C-2), 44.8 (C-5a), 40.4 (C-5); **^{31}P-NMR (283 MHz, $CDCl_3$)**: δ [ppm] = 1.32, 0.25; **RP-HPLC**: t_r = 0.4 min, (ZORBAX SB-C18, 5 µm, 0.4 mL/min, 0-40 % MeCN in 20 min); **ESI-MS**: calcd for $C_{13}H_{20}NO_7PNa$ $[M+Na]^+$, 356.0870; found, 356.0877.

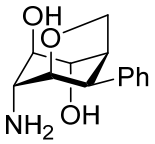

(1*R*,2*R*,3*R*,4*R*,5*R*,8*S*)-4-amino-8-phenyl-6-oxabicyclo[3.2.1]octane-2,3-diol

(114) Perbenzylated phenyl-carba compound **75** (8.86 mg, 0.00965 mmol) was deprotected according to **GP1**. The reaction was finished after 23 h. The lyophilized pseudo-sugar was purified via C18-HPLC (Gemini® C18, 110 Å, 5 µm, 50x30 mm, 100% H_2O for 5 min, then 0-40% acetonitrile in 5 min). Fractions containing the product were combined and freeze-dried yielding the bicyclic ether **114** (1.28 mg, 65%) as colorless foam.

^{1}H-NMR (700 MHz, $CDCl_3$, 25 °C): δ [ppm] = 7.47-7.35 (m, 5H, Ph), 4.68 (br, 1H, H-1), 3.94-3.92 (m, 2H, H-6a, H-4), 3.78 (dd, *J* = 8.9, 4.9 Hz, 1H, H-6b), 3.74-3.72 (m, 2H, H-5a, H-3), 3.26 (dd, *J* = 5.8, 2.1 Hz, 1H, H-2), 2.67 (d, *J* = 4.3 Hz, 1H, H-5); **^{13}C-NMR (176 MHz, $CDCl_3$, 25 °C)**: δ [ppm] = 139.3, 128.9, 127.1, 127.0 (C^{Ar}), 78.8 (C-1), 76.3 (C-4), 72.9 (C-3), 68.7 (C-6), 57.3 (C-2), 47.6 (C-5a), 40.6 (C-5); **RP-HPLC**: t_r = 4.8 min, (ZORBAX SB-C18, 5 µm, 0.4 mL/min, 0-40 % MeCN in 20 min); **ESI-MS**: calcd for $C_{13}H_{17}NO_3H$ $[M+H]^+$, 236.128; found, 236.127.

5.7 Theoretical Section

Cartesian Coordinates of optimized structures:

L-configurated epoxide 34 (BP/def2-TZVP)

C	0.502129	1.183639	-0.333672
C	1.461300	0.033221	0.055388
C	0.738923	-1.336339	-0.000793
C	-0.497418	-1.360713	0.922084
C	-1.462426	-0.237810	0.509682
C	-0.799149	1.123337	0.478787
O	-1.735788	2.196783	0.245387
H	-2.342886	-0.214848	1.169316
O	1.106337	2.475986	-0.308691
C	2.087835	2.735815	0.697279
O	2.670356	0.043789	-0.704790
C	2.539947	-0.024627	-2.127949

N	1.654134	-2.454528	0.239629
C	1.731182	-3.417711	-0.737046
O	2.718855	-4.325803	-0.459469
O	1.014097	-3.485111	-1.729703
C	2.834142	-5.383788	-1.430546
C	2.642471	-2.387579	1.318654
O	-0.142982	-1.176949	2.294719
Si	-0.797480	-2.068547	3.569615
C	-0.349462	-3.887544	3.396873
C	-0.011729	-1.315914	5.096643
C	-2.672557	-1.895303	3.615942
H	0.200970	1.045327	-1.386012
H	1.802331	0.202297	1.088034
H	0.347476	-1.500743	-1.015834
H	-1.009553	-2.327744	0.765365
F	-1.931533	-0.537234	-0.791069
H	-0.366813	-1.822919	6.006293
H	-0.260049	-0.248613	5.188684
H	1.084140	-1.407070	5.068141
H	-3.084483	-2.459212	4.467547
H	-3.149435	-2.294159	2.707782
H	-2.987098	-0.847731	3.732645
C	-1.118440	2.101791	1.536562
H	3.063514	-4.977172	-2.424092
H	1.903254	-5.963600	-1.489558
H	3.657193	-6.013091	-1.074310
H	2.823424	-3.389758	1.720962
H	2.243406	-1.756023	2.118120
H	3.597634	-1.968421	0.966807
H	0.738178	-4.042280	3.437313
H	-0.714375	-4.315459	2.451405
H	-0.802470	-4.470208	4.213766

H	2.309643	3.807721	0.618792
H	3.010547	2.160308	0.522498
H	1.722911	2.529175	1.719262
H	3.563435	-0.111438	-2.512608
H	2.086105	0.890007	-2.543221
H	1.964905	-0.906040	-2.457779
H	-0.401484	2.894928	1.760402
H	-1.781647	1.809063	2.357658

D-configurated epoxide 34 (BP/def2-TZVP)

C	0.435911	1.120390	-0.414906
C	1.439330	0.042059	0.056678
C	0.763158	-1.353617	-0.023038
C	-0.493596	-1.424448	0.871738
C	-1.490692	-0.318109	0.479955
C	-0.856474	1.059444	0.407912
C	-1.716608	2.244893	0.541962
H	-2.329604	-0.298087	1.191901
O	0.975866	2.431458	-0.519379
C	1.822111	2.881651	0.551070
O	2.681051	0.090639	-0.643009
C	2.615738	-0.001667	-2.069089
N	1.703260	-2.446167	0.234857
C	1.832196	-3.401588	-0.742685
O	2.835019	-4.284896	-0.439123
O	1.148311	-3.482414	-1.758216
C	3.011119	-5.331642	-1.412786
C	2.655409	-2.367968	1.346343
O	-0.147469	-1.266906	2.244437
Si	-0.871764	-2.054633	3.546454
C	-0.723255	-3.919646	3.334200
C	0.101754	-1.452685	5.030382
C	-2.689517	-1.586560	3.704654

H	0.132419	0.870703	-1.447305
H	1.715483	0.246041	1.102083
H	0.406380	-1.523606	-1.050528
H	-0.980436	-2.400328	0.687239
F	-2.016690	-0.633727	-0.796480
H	-0.292512	-1.889785	5.959796
H	0.043777	-0.357923	5.119502
H	1.162851	-1.730697	4.953397
H	-3.112547	-2.020284	4.624412
H	-3.293664	-1.963997	2.865777
H	-2.818252	-0.495579	3.759466
O	-0.900989	1.798106	1.649871
H	-1.387010	3.177254	0.077731
H	-2.795628	2.117242	0.678920
H	3.258748	-4.911522	-2.396273
H	2.100179	-5.938406	-1.504167
H	3.841241	-5.939039	-1.035378
H	2.798388	-3.360324	1.788464
H	2.243507	-1.701825	2.109726
H	3.631398	-1.982515	1.014849
H	0.325982	-4.230231	3.224016
H	-1.275788	-4.285120	2.455608
H	-1.134900	-4.440453	4.212795
H	2.052155	3.928435	0.315959
H	2.761780	2.308370	0.580691
H	1.313820	2.832042	1.524933
H	3.656443	-0.065619	-2.409267
H	2.154394	0.895115	-2.514311
H	2.078975	-0.903429	-2.408687

β-titanoxy radical 55 (TPSS-D3/def2-TZVP)

C	0.936583	1.409220	0.707777
C	1.132332	-0.024111	0.166214

C	-0.119134	-0.860405	0.505574
C	-0.262882	-0.955605	2.030877
C	-0.467352	0.440045	2.619875
C	0.545035	1.413601	2.159648
H	-0.555010	0.417360	3.707550
O	2.050457	2.273010	0.441664
C	3.313080	1.744129	0.856691
O	1.480514	-0.053834	-1.213351
C	0.542297	0.558220	-2.106056
N	-0.106475	-2.168811	-0.148132
C	-1.136039	-2.446184	-1.002798
O	-0.936652	-3.646255	-1.629022
O	-2.120109	-1.741912	-1.197105
C	-2.003601	-4.015327	-2.529217
C	1.091096	-3.018447	-0.111010
O	0.926819	-1.522356	2.575150
Si	1.246962	-2.227039	4.058625
C	2.879044	-3.099317	3.741413
C	1.479255	-0.912548	5.376010
C	-0.110921	-3.465228	4.551881
H	0.116383	1.872346	0.133968
H	1.991267	-0.474785	0.668570
H	-1.021115	-0.364511	0.136902
H	-1.135541	-1.574407	2.265320
F	-1.777574	0.878595	2.149125
H	1.841254	-1.359633	6.310565
H	0.549687	-0.376970	5.596311
H	2.220272	-0.174333	5.047051
C	0.806359	2.665561	2.944442
H	-2.111829	-3.266180	-3.317182
H	-2.946496	-4.105345	-1.984466
H	-1.700414	-4.976615	-2.944758

H	0.803883	-4.056406	0.065624
H	1.714993	-2.680700	0.713548
H	1.648240	-2.951253	-1.050777
H	3.607364	-2.392062	3.326904
H	2.770411	-3.922522	3.026518
H	3.303258	-3.508555	4.665183
H	4.011987	2.583177	0.840301
H	3.660228	0.966270	0.165970
H	3.261324	1.330844	1.874868
H	0.886391	0.304437	-3.110631
H	0.543292	1.650291	-1.994090
H	-0.473297	0.168639	-1.963585
H	1.876034	2.921681	2.900276
H	0.279480	3.506772	2.452572
H	-2.008701	3.128151	2.826501
H	-3.653268	2.568884	4.837257
C	-2.107228	3.710008	3.731653
C	-2.978111	3.409046	4.796239
Cl	-1.745394	1.014570	6.041270
O	0.419377	2.555628	4.285233
C	-1.341054	4.849424	4.101910
H	-0.566243	5.320094	3.511057
Ti	-0.717774	3.116575	5.624839
C	-2.751805	4.346154	5.837251
H	1.108728	1.256780	7.261983
H	2.332537	3.271608	5.994849
C	-1.758141	5.256194	5.390119
H	-3.254723	4.364464	6.794284
C	0.834974	2.300035	7.311820
C	1.481548	3.360989	6.654240
C	-0.291540	2.834663	8.008149
H	-1.373854	6.101284	5.942201

H	-1.003145	2.262397	8.584887
C	0.734887	4.542829	6.880151
H	0.969967	5.525784	6.495260
C	-0.341773	4.215578	7.761813
H	-1.084302	4.903033	8.141211
C	-0.429054	-4.399726	3.366654
H	0.459774	-4.947670	3.032802
H	-1.183700	-5.141154	3.664445
H	-0.824536	-3.849043	2.506491
C	-1.400360	-2.748924	5.004360
H	-1.843348	-2.141015	4.208828
H	-2.151490	-3.493139	5.305026
H	-1.222243	-2.089334	5.859186
C	0.410361	-4.315769	5.731819
H	-0.364588	-5.027978	6.048107
H	1.300216	-4.893162	5.457169
H	0.660686	-3.695361	6.600493

TS2A (TPSS-D3/def2-TZVP)

C	0.909878	1.780789	0.966563
C	1.449807	0.410650	0.503122
C	0.355743	-0.635872	0.780648
C	0.001473	-0.722819	2.274742
C	-0.310160	0.660167	2.854110
C	0.639926	1.747764	2.462958
H	-0.456307	0.609966	3.935612
O	1.692012	2.892941	0.532980
C	3.084887	2.820850	0.851655
O	1.882454	0.405689	-0.856350
C	0.892156	0.777670	-1.821206
N	0.687292	-1.948354	0.221873
C	-0.294844	-2.586274	-0.476095
O	0.157908	-3.759472	-1.016788

O	-1.447540	-2.188035	-0.605683
C	-0.864571	-4.509889	-1.707283
C	2.060355	-2.458284	0.280011
O	1.062239	-1.333881	3.003814
Si	0.965688	-2.524874	4.183772
C	2.411289	-3.668271	3.815170
C	1.229117	-1.739520	5.868773
C	-0.673629	-3.499263	4.166245
H	-0.055516	1.952591	0.465072
H	2.353737	0.171404	1.071280
H	-0.565497	-0.325948	0.278432
H	-0.911059	-1.319211	2.360339
F	-1.620574	0.990484	2.306656
H	1.092078	-2.476809	6.669041
H	0.534105	-0.913202	6.054865
H	2.251661	-1.353773	5.958198
C	0.377438	3.109745	3.077347
H	-1.277742	-3.921944	-2.530049
H	-1.667494	-4.780403	-1.017066
H	-0.356185	-5.399328	-2.080338
H	2.039609	-3.544847	0.355884
H	2.536128	-2.051290	1.170784
H	2.628381	-2.161860	-0.607879
H	3.331633	-3.088377	3.677673
H	2.250936	-4.259676	2.907506
H	2.585256	-4.362641	4.645143
H	3.516170	3.760526	0.499479
H	3.566041	1.982549	0.335731
H	3.244902	2.734002	1.932575
H	1.370270	0.649010	-2.794128
H	0.596604	1.826964	-1.700418
H	0.006346	0.131593	-1.768882

H	1.259945	3.749593	2.937192
H	-0.458053	3.594027	2.541570
H	-2.450158	2.880610	3.092010
H	-3.757962	1.860543	5.167616
C	-2.679591	3.409671	4.004871
C	-3.371688	2.865550	5.102734
Cl	-1.435865	0.977860	6.333163
O	0.096246	3.020598	4.451318
C	-2.276135	4.728413	4.349860
H	-1.702220	5.403569	3.728690
Ti	-1.092271	3.281772	5.831874
C	-3.399946	3.835605	6.138163
H	1.400414	2.198470	7.260123
H	1.697291	4.568270	6.015965
C	-2.750184	5.000421	5.655160
H	-3.846363	3.708168	7.114662
C	0.770699	3.068845	7.376026
C	0.927642	4.308990	6.728080
C	-0.411241	3.138274	8.171621
H	-2.624365	5.926661	6.195905
H	-0.815111	2.333328	8.767044
C	-0.175390	5.127572	7.065427
H	-0.339727	6.138305	6.719081
C	-0.986713	4.407174	7.994132
H	-1.898925	4.762841	8.451718
C	-0.993147	-4.088648	2.776968
H	-0.157836	-4.678839	2.382856
H	-1.864066	-4.755339	2.850819
H	-1.235946	-3.317387	2.040880
C	-1.861819	-2.646026	4.658620
H	-2.087905	-1.811736	3.987326
H	-2.764056	-3.270969	4.720730

H	-1.676526	-2.226339	5.652597
C	-0.493860	-4.679114	5.152697
H	-1.426857	-5.257412	5.202101
H	0.302613	-5.360527	4.834037
H	-0.264996	-4.335860	6.167876
C	5.586862	2.032691	3.352778
H	6.567030	1.948348	3.850859
H	5.753442	0.010748	2.449411
H	5.802697	2.609046	2.434865
C	5.075491	0.667124	2.991351
C	3.847936	0.233670	3.321343
H	3.531116	-0.767198	3.044529
H	2.252031	0.533682	4.752603
C	2.868720	1.073733	4.031945
H	1.919546	1.348956	3.219439
C	3.407714	2.344540	4.540520
H	2.761040	2.931103	5.184103
C	4.633305	2.797821	4.225345
H	4.976651	3.751942	4.620664

TS2B (TPSS-D3/def2-TZVP)

C	-1.659075	1.659277	-0.138968
C	-0.433160	0.718673	-0.255814
C	-0.977022	-0.719837	-0.334146
C	-1.811655	-1.128230	0.892325
C	-2.849536	-0.052186	1.272844
C	-2.398693	1.373838	1.158866
H	-3.242084	-0.268999	2.271360
O	-1.379659	3.035559	-0.370860
C	-0.189190	3.576960	0.223524
O	0.413363	1.022144	-1.366976
C	-0.222492	1.032260	-2.649869
N	0.078082	-1.696979	-0.613568

C	-0.223767	-2.688992	-1.497186
O	0.855502	-3.496470	-1.736735
O	-1.321946	-2.864037	-2.014757
C	0.563607	-4.606281	-2.613887
C	1.409090	-1.538657	-0.023446
O	-0.975030	-1.426524	2.019181
Si	-1.177771	-2.941490	2.722238
C	-0.842805	-4.303875	1.473617
C	0.051239	-3.010240	4.164600
C	-2.948815	-3.099060	3.340054
H	-2.341322	1.396186	-0.959208
H	0.205570	0.850923	0.621471
H	-1.665493	-0.777825	-1.182992
H	-2.383636	-2.020150	0.600694
F	-3.941086	-0.263407	0.358082
H	-3.126334	-4.086247	3.782693
H	-3.665632	-2.980676	2.518614
H	-3.185198	-2.344791	4.099278
C	-2.069059	2.109603	2.427859
H	0.214802	-4.243147	-3.583147
H	-0.201789	-5.248416	-2.170929
H	1.508626	-5.140552	-2.714312
H	1.871016	-2.517963	0.093373
H	1.292082	-1.083966	0.959661
H	2.044512	-0.902274	-0.647518
H	0.179387	-4.259264	1.084219
H	-1.525735	-4.244590	0.618506
H	-0.985457	-5.287630	1.937585
H	-0.244484	4.652703	0.048294
H	0.702831	3.166833	-0.264717
H	-0.148671	3.397716	1.300770
H	0.574515	1.235697	-3.367445

H	-0.975696	1.826718	-2.711012
H	-0.679246	0.063076	-2.889058
H	-2.116806	3.192210	2.242489
H	-2.846116	1.868688	3.165019
H	1.884740	2.678345	2.056427
H	2.508027	4.347455	4.060059
C	1.994911	2.405515	3.095218
C	2.316514	3.289389	4.156025
Cl	-0.287231	4.776135	3.700259
O	-0.775885	1.820751	2.965666
C	1.763028	1.125674	3.647233
H	1.427811	0.254675	3.104010
Ti	0.022261	2.563988	4.482162
C	2.273155	2.560077	5.364635
H	-1.155989	4.667684	6.423302
H	-2.915727	3.364604	4.876815
C	1.924364	1.216197	5.050110
H	2.471743	2.955379	6.350272
C	-1.217356	3.596179	6.306381
C	-2.149865	2.905681	5.484432
C	-0.351122	2.647832	6.880656
H	1.823862	0.402922	5.752948
H	0.465045	2.857668	7.556597
C	-1.861562	1.526395	5.565108
H	-2.362700	0.735219	5.025259
C	-0.735415	1.360209	6.406453
H	-0.281336	0.419074	6.674960
C	-0.225240	-1.833915	5.117736
H	-1.218087	-1.911703	5.575607
H	0.514334	-1.828412	5.932420
H	-0.169633	-0.876016	4.592390
C	1.501391	-2.918561	3.651215

H	2.202759	-2.946084	4.497066
H	1.748532	-3.754353	2.987641
H	1.678646	-1.989837	3.101272
C	-0.122824	-4.337207	4.932517
H	-1.135346	-4.443416	5.337864
H	0.082060	-5.205457	4.296048
H	0.578183	-4.374577	5.778055
C	-5.315932	3.750379	3.106944
C	-5.384537	2.762113	2.196986
C	-4.735911	2.858241	0.880572
C	-4.264921	4.201838	0.515654
C	-4.191693	5.203941	1.408033
C	-4.616596	5.053138	2.839922
H	-5.793264	3.628076	4.077432
H	-5.910250	1.839867	2.436383
H	-5.231626	2.301908	0.081248
H	-3.671524	2.117739	0.960479
H	-3.921208	4.357705	-0.502651
H	-3.802314	6.173196	1.105414
H	-5.263593	5.894561	3.136756
H	-3.729993	5.152404	3.493599

TS2B* (TPSS-D3/def2-TZVP)

C	1.326314	1.431996	1.103868
C	1.557620	0.014093	0.523867
C	0.286152	-0.838213	0.671809
C	-0.056119	-0.967808	2.159885
C	-0.444213	0.407375	2.730206
C	0.115398	1.561179	1.979597
H	-0.208582	0.457575	3.801535
O	2.513973	1.963937	1.747153
C	2.795267	1.401407	3.035707
O	2.060745	0.048008	-0.815323

C	1.146181	0.510933	-1.809717
N	0.379106	-2.130759	-0.005363
C	-0.646427	-2.468817	-0.838846
O	-0.410562	-3.674628	-1.438247
O	-1.654984	-1.799961	-1.042882
C	-1.469975	-4.101430	-2.322664
C	1.578557	-2.967096	0.106983
O	1.061561	-1.509580	2.854499
Si	1.142603	-2.571178	4.149207
C	2.577870	-3.721887	3.745391
C	1.557584	-1.577274	5.689343
C	-0.459014	-3.571729	4.389833
H	1.205045	2.119022	0.257892
H	2.366514	-0.454109	1.087975
H	-0.565396	-0.333712	0.205665
H	-0.933470	-1.611143	2.265047
F	-1.880128	0.489583	2.670968
H	1.140580	-2.030078	6.596379
H	1.169580	-0.555732	5.627106
H	2.644409	-1.520158	5.826399
C	-0.349951	2.936949	2.353587
H	-1.604189	-3.378342	-3.130648
H	-2.406937	-4.204545	-1.770186
H	-1.139204	-5.064186	-2.712570
H	1.298433	-3.993762	0.351304
H	2.189701	-2.569296	0.913799
H	2.151334	-2.959546	-0.825033
H	3.291335	-3.217803	3.082993
H	2.259099	-4.644450	3.248089
H	3.118254	-4.001958	4.657012
H	3.743878	1.844043	3.346760
H	2.896460	0.310121	2.991112

H	2.013139	1.659672	3.760932
H	1.681409	0.438571	-2.758260
H	0.860406	1.559758	-1.647539
H	0.237482	-0.102153	-1.855009
H	0.194343	3.684290	1.762032
H	-1.425027	3.044934	2.147109
H	-2.963842	2.429100	3.530617
H	-3.377187	2.051891	6.141305
C	-2.906804	3.191067	4.294404
C	-3.124015	2.991220	5.674861
Cl	-0.722222	1.316735	6.226101
O	-0.087408	3.171902	3.726098
C	-2.534855	4.547998	4.105418
H	-2.272083	5.010434	3.163939
Ti	-0.781455	3.546196	5.385463
C	-2.866406	4.207761	6.349469
H	2.033002	2.660605	6.265963
H	1.944022	4.658098	4.482916
C	-2.516910	5.179397	5.369869
H	-2.934655	4.368224	7.416271
C	1.452215	3.567378	6.350191
C	1.414918	4.622904	5.423991
C	0.533569	3.869067	7.403475
H	-2.275255	6.215190	5.559339
H	0.319270	3.233958	8.250664
C	0.437844	5.553235	5.855397
H	0.165156	6.468123	5.347337
C	-0.071398	5.102222	7.111783
H	-0.816318	5.604613	7.712047
C	-0.880879	-4.307548	3.101709
H	-0.085364	-4.966100	2.734012
H	-1.761020	-4.934350	3.302929

H	-1.145065	-3.621627	2.290897
C	-1.614287	-2.681179	4.894142
H	-1.926624	-1.941788	4.150024
H	-2.490118	-3.302916	5.128535
H	-1.338844	-2.136212	5.803251
C	-0.158230	-4.637231	5.470775
H	-1.051230	-5.256085	5.635474
H	0.658272	-5.304601	5.172452
H	0.108360	-4.180789	6.430732
C	-3.528438	4.680237	0.058239
H	-4.343545	5.184230	-0.486587
H	-4.915419	3.485968	1.313074
H	-3.249606	5.397828	0.848923
C	-4.038868	3.406027	0.672391
C	-3.482395	2.210560	0.459488
H	-3.900897	1.324760	0.931037
H	-2.415225	1.186731	-1.104097
C	-2.260686	2.004966	-0.386265
H	-1.444815	1.640160	0.273316
C	-1.811087	3.258935	-1.076056
H	-0.981518	3.170178	-1.775762
C	-2.364526	4.456056	-0.866613
H	-1.980245	5.327127	-1.395005

α-D-Glucosamine-6-phosphate (BP/def2-TZVPP)

C	0.902343	1.222809	-0.173631
C	1.481217	-0.066088	0.394984
C	0.705494	-1.286143	-0.098944
C	-0.821797	-1.089277	0.096549
O	-1.281725	0.166440	-0.366258
C	-0.589164	1.307624	0.184222
C	-1.267807	2.545609	-0.400211
O	1.641385	2.322970	0.373648

O	2.858238	-0.249562	0.017333
N	1.109423	-2.466138	0.686089
O	-1.151517	-1.271267	1.468097
O	-0.629749	3.699490	0.152297
P	-1.080939	5.236735	-0.492184
O	-0.174126	6.154647	0.331015
O	-0.747096	5.159570	-1.985549
O	-2.578650	5.355011	-0.185878
H	0.997876	1.207387	-1.278203
H	1.410490	-0.010719	1.497883
H	0.893818	-1.397562	-1.181037
H	-1.376576	-1.813977	-0.523467
H	-0.694814	1.317149	1.283400
H	-1.168737	2.540720	-1.501018
H	-2.342319	2.537579	-0.148251
H	1.016449	3.094110	0.318155
H	3.346448	0.521799	0.355693
H	2.123861	-2.462589	0.810209
H	0.881969	-3.327444	0.184794
H	-0.409085	-1.834442	1.802234

Carba-α-D-glucosamine-6-phosphate 23 (BP/def2-TZVPP)

C	0.822410	1.207243	-0.188953
C	1.415534	-0.064880	0.411134
C	0.701941	-1.318086	-0.093463
C	-0.823559	-1.224591	0.143126
C	-1.415754	0.089876	-0.358810
C	-0.669161	1.328975	0.160580
C	-1.282139	2.611054	-0.408279
O	1.598290	2.314921	0.304204
O	2.813018	-0.191562	0.078541
N	1.199414	-2.493684	0.648614
O	-1.089837	-1.377552	1.549069

H	-2.476831	0.136621	-0.070592
O	-0.628542	3.750410	0.172939
P	-0.992783	5.296824	-0.490874
O	-0.095275	6.188775	0.371899
O	-0.592580	5.210161	-1.968124
O	-2.498852	5.473402	-0.257261
H	0.923901	1.154561	-1.293941
H	1.310203	-0.004084	1.510900
H	0.878850	-1.395317	-1.182159
H	-1.300317	-2.059860	-0.405662
H	-1.388769	0.078291	-1.461742
H	-0.756677	1.367111	1.260168
H	-1.159518	2.635089	-1.507682
H	-2.363776	2.649762	-0.187070
H	0.968470	3.085453	0.289194
H	3.231917	0.644181	0.352837
H	2.214946	-2.432257	0.746197
H	1.011221	-3.349976	0.122656
H	-0.366427	-1.981481	1.842174

(5a*R*)-Fluoro-carba-α-D-glucosamine-6-phosphate 35 (BP/def2-TZVPP)

C	0.834963	1.197334	-0.234840
C	1.424064	-0.060262	0.400332
C	0.708531	-1.323249	-0.076881
C	-0.818056	-1.229396	0.159877
C	-1.427046	0.089242	-0.324089
C	-0.657001	1.327912	0.119890
C	-1.284456	2.616732	-0.424778
O	1.600822	2.318974	0.237512
O	2.819179	-0.201093	0.073407
N	1.193045	-2.481088	0.699988
O	-1.094828	-1.367062	1.556997
H	-2.476523	0.149739	0.001056

O	-0.636297	3.736506	0.195525
P	-0.995386	5.300868	-0.438148
O	-0.100569	6.171548	0.447758
O	-0.587761	5.241263	-1.914215
O	-2.502023	5.470474	-0.207222
H	0.941652	1.121634	-1.335028
H	1.315988	0.028933	1.498038
H	0.889318	-1.429678	-1.160904
H	-1.308379	-2.044701	-0.405216
F	-1.459407	0.027438	-1.751977
H	-0.742435	1.353439	1.221093
H	-1.159144	2.676474	-1.519688
H	-2.366319	2.638161	-0.202307
H	0.957999	3.079716	0.254699
H	3.247982	0.629345	0.348253
H	2.205625	-2.411842	0.819221
H	1.020449	-3.349857	0.189562
H	-0.354639	-1.948115	1.861714

(5a*R*)-Fluoro-carba-β-L-idosamine-6-phosphate 33 $^{1}C_{4}$-configuration (BP/def2-TZVPP)

C	0.680988	0.957754	-0.400531
C	1.258523	-0.313453	0.252528
C	0.287268	-1.502274	0.164480
C	-1.118950	-1.172703	0.705655
C	-1.689777	0.109081	0.051732
C	-0.705878	1.271475	0.155022
F	-1.257692	2.374780	-0.573399
O	-2.939883	0.427946	0.674580
N	-1.213705	-1.017631	2.170946
O	1.576105	-0.120981	1.651698
C	1.622843	2.165791	-0.220383
H	2.173276	-0.583265	-0.296367
O	0.172453	-1.878292	-1.225479

H	-1.785480	-2.000575	0.423321
H	-1.887241	-0.080970	-1.013738
H	-0.644603	1.619505	1.199240
H	-2.799027	0.122832	1.603703
H	-0.376822	-0.551254	2.530438
H	-1.258340	-1.932154	2.620754
H	2.331635	0.490790	1.689994
H	0.472022	-2.796651	-1.309921
H	0.705457	-2.335916	0.749558
H	1.274879	3.005302	-0.842522
O	2.984857	1.860445	-0.511921
H	1.580700	2.499131	0.832501
P	3.531628	2.131950	-2.105901
O	5.007195	1.732022	-1.974809
O	3.298562	3.630684	-2.361662
H	0.601195	0.740526	-1.477601
O	2.694761	1.215706	-3.009025

(5a*R*)-Fluoro-carba-β-L-idosamine-6-phosphate 33 $^4C_1$-configuration (BP/def2-TZVPP)

C	0.979516	1.172371	0.152493
C	1.615795	-0.180500	0.469462
C	0.929366	-1.300749	-0.329231
C	-0.574776	-1.340746	-0.038990
C	-1.239667	0.037603	-0.192412
C	-0.526530	1.211491	0.477855
O	1.744230	2.162292	0.876631
O	3.007619	-0.170454	0.098848
N	1.507818	-2.636715	-0.136419
O	-0.753686	-1.834964	1.300298
H	1.111709	1.349589	-0.929407
H	1.530807	-0.388940	1.552171
H	1.038981	-1.044644	-1.396553
H	-1.046888	-2.030981	-0.758584

H	1.583554	3.028006	0.465682
H	3.356879	0.680800	0.423114
H	1.354365	-2.923358	0.833926
H	2.521249	-2.576591	-0.257614
H	-1.697386	-2.030595	1.425798
H	-2.278890	-0.011973	0.161419
F	-1.312184	0.296938	-1.604138
C	-0.836653	1.292012	1.989590
H	-0.965957	2.126472	0.047192
H	-0.474061	0.394587	2.511312
O	-2.239781	1.388321	2.237191
H	-0.315015	2.166101	2.408135
P	-2.927865	2.943401	2.313235
O	-2.711009	3.582123	0.931849
O	-2.188718	3.667708	3.450369
O	-4.389131	2.594078	2.629478

(5a*S*)-fluoro-carba-α-D-GlcN6P 117 (BP/def2-TZVPP)

C	0.811707	1.210529	-0.183406
C	1.413371	-0.066754	0.398386
C	0.693593	-1.319315	-0.103803
C	-0.828143	-1.218978	0.163966
C	-1.388939	0.088206	-0.380368
C	-0.688740	1.331770	0.161515
C	-1.292673	2.617051	-0.417842
O	1.572829	2.313476	0.329766
O	2.801950	-0.191190	0.041078
N	1.184809	-2.491519	0.643214
O	-1.068191	-1.324393	1.569684
F	-2.780596	0.140814	-0.076654
O	-0.636290	3.744833	0.178641
P	-0.985377	5.300436	-0.482245
O	-0.087674	6.179300	0.392422

O	-0.573245	5.212920	-1.955648
O	-2.491523	5.483248	-0.258770
H	0.917891	1.174992	-1.288242
H	1.323268	-0.013778	1.499329
H	0.859591	-1.402098	-1.192954
H	-1.332261	-2.051170	-0.363407
H	-1.323403	0.063792	-1.481079
H	-0.794139	1.347885	1.258932
H	-1.149251	2.639149	-1.514794
H	-2.374361	2.665312	-0.212869
H	0.943656	3.086440	0.306747
H	3.234272	0.630969	0.334718
H	2.200282	-2.432113	0.742000
H	0.992556	-3.350913	0.124122
H	-0.342777	-1.927060	1.863370

(5a*S*)-hydroxy-carba-α-D-GlcN6P 118 (BP/def2-TZVPP)

C	0.851247	1.199583	-0.214923
C	1.459050	-0.058452	0.398102
C	0.734005	-1.318462	-0.070022
C	-0.784691	-1.214178	0.185075
C	-1.400233	0.094696	-0.320411
C	-0.633019	1.339640	0.169137
C	-1.240297	2.624134	-0.404543
O	1.640643	2.316154	0.230759
O	2.846508	-0.192750	0.036227
N	1.226661	-2.478645	0.698974
O	-1.039752	-1.328254	1.594385
O	-0.567089	3.755620	0.170868
P	-0.978459	5.314000	-0.436970
O	-0.051897	6.194760	0.405861
O	-0.645620	5.267130	-1.932559
O	-2.473790	5.465901	-0.130109

H	0.926774	1.121733	-1.320340
H	1.376514	0.023433	1.498280
H	0.900437	-1.424603	-1.157345
H	-1.285311	-2.048797	-0.341998
H	-0.701762	1.382729	1.270335
H	-1.120363	2.640112	-1.504623
H	-2.316672	2.676291	-0.177005
H	1.009680	3.087859	0.232167
H	3.273001	0.647079	0.285690
H	2.242943	-2.420587	0.790759
H	1.030634	-3.346922	0.196119
H	-0.311223	-1.921150	1.899382
H	-1.377757	0.073780	-1.422290
O	-2.795382	0.139227	0.027287
H	-2.849300	-0.057990	0.980380

A. Appendix

1.1 Selected Spectra

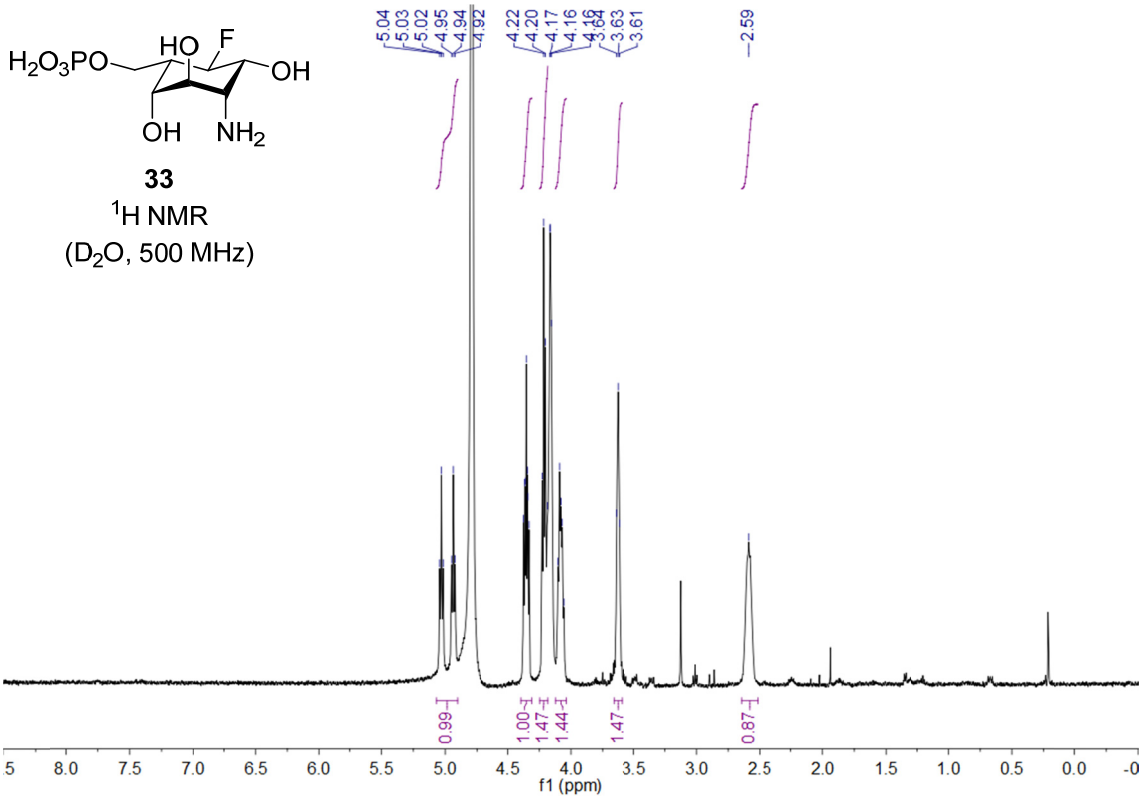

33

^{13}C NMR

(D_2O, 126 MHz)

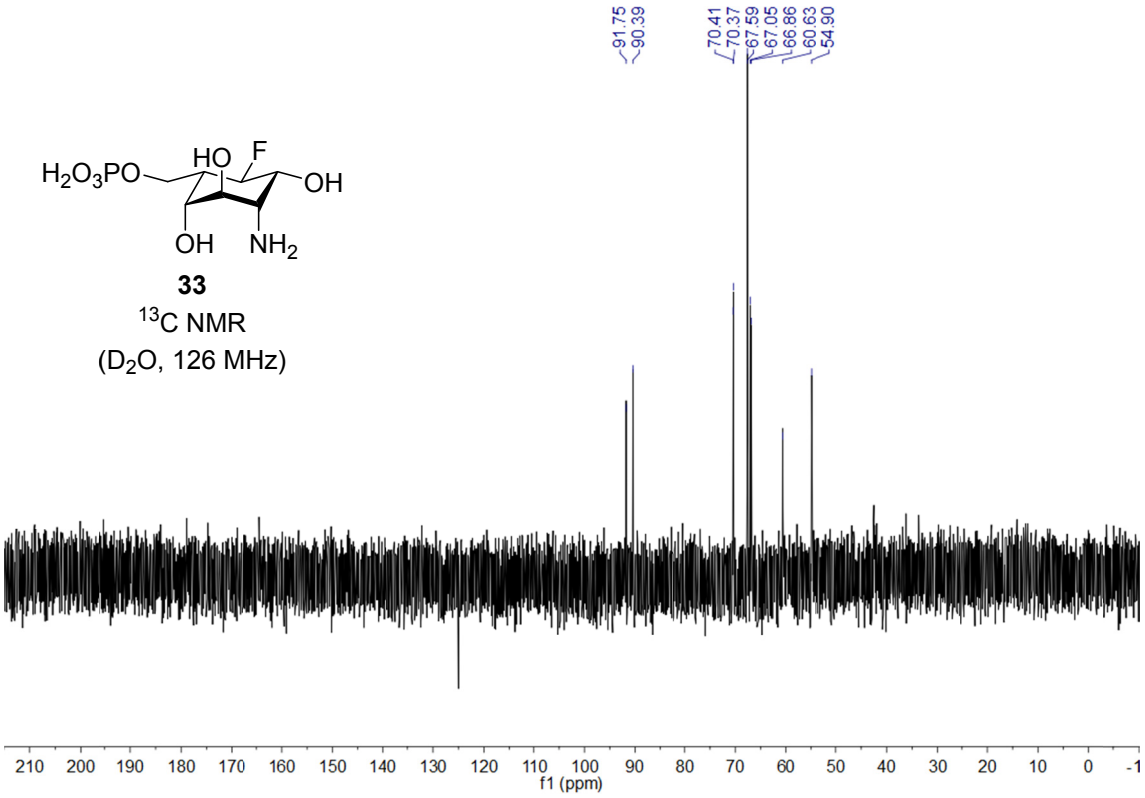

33

^{31}P NMR

(D_2O, 202 MHz)

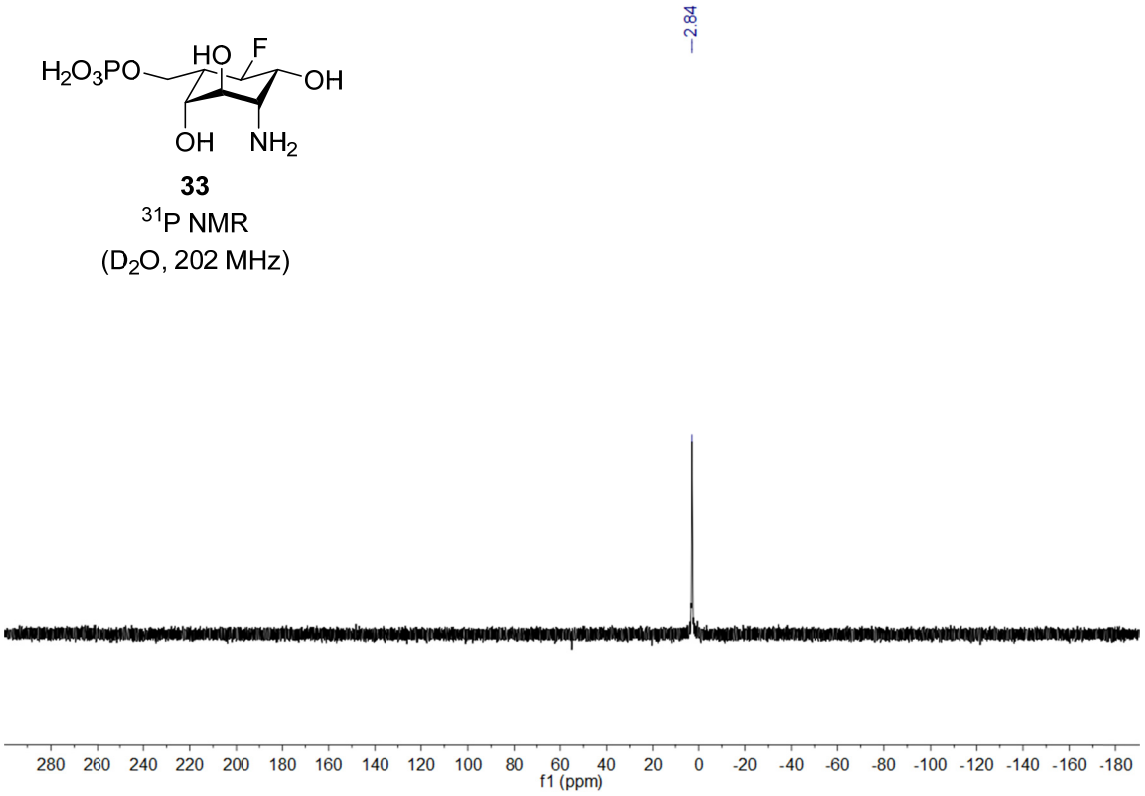

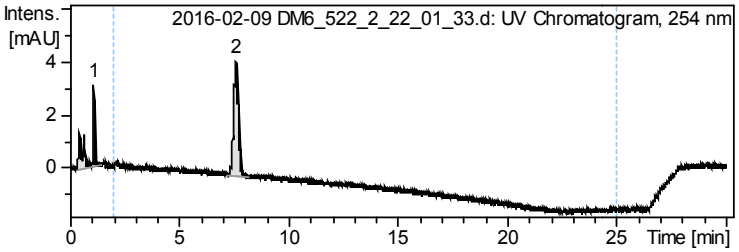

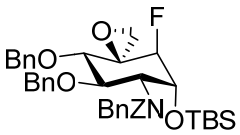

34

HPLC

ZORBAX SB-C18, 5 µm,
0.4 mL/min,
80-100% MeCN in 20 min

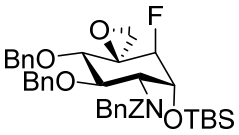

34

^{1}H NMR

($CDCl_3$, 600 MHz, -40 °C)

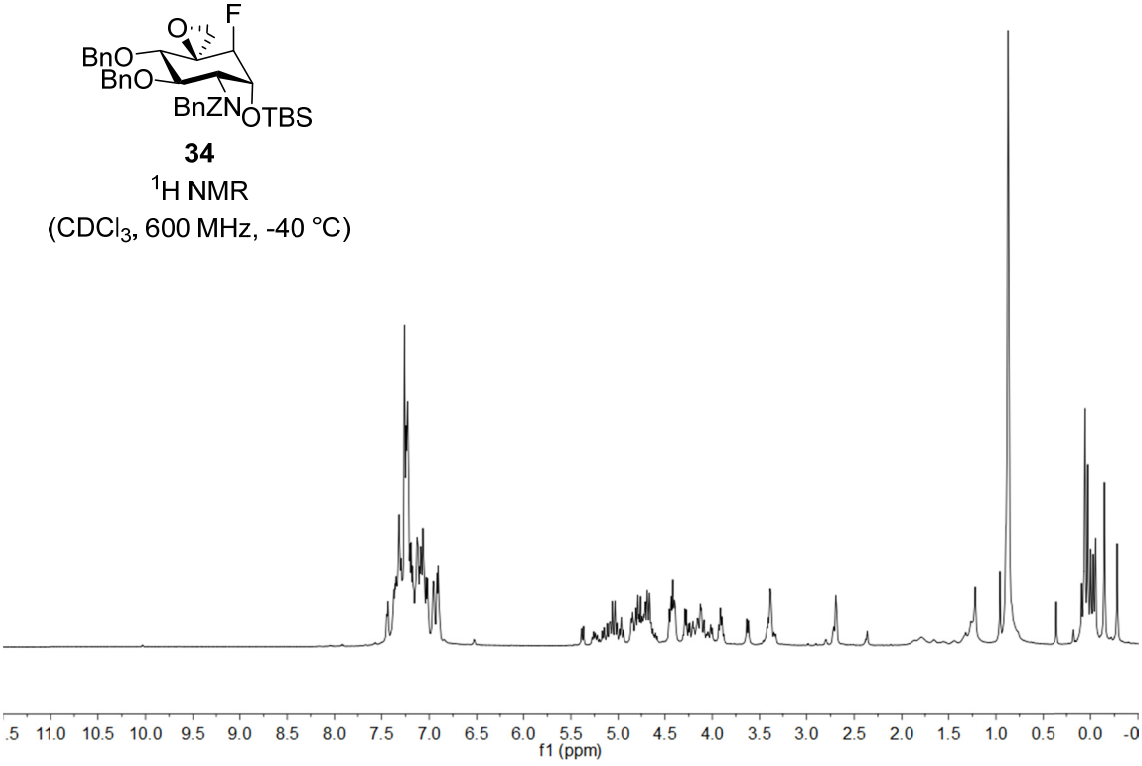

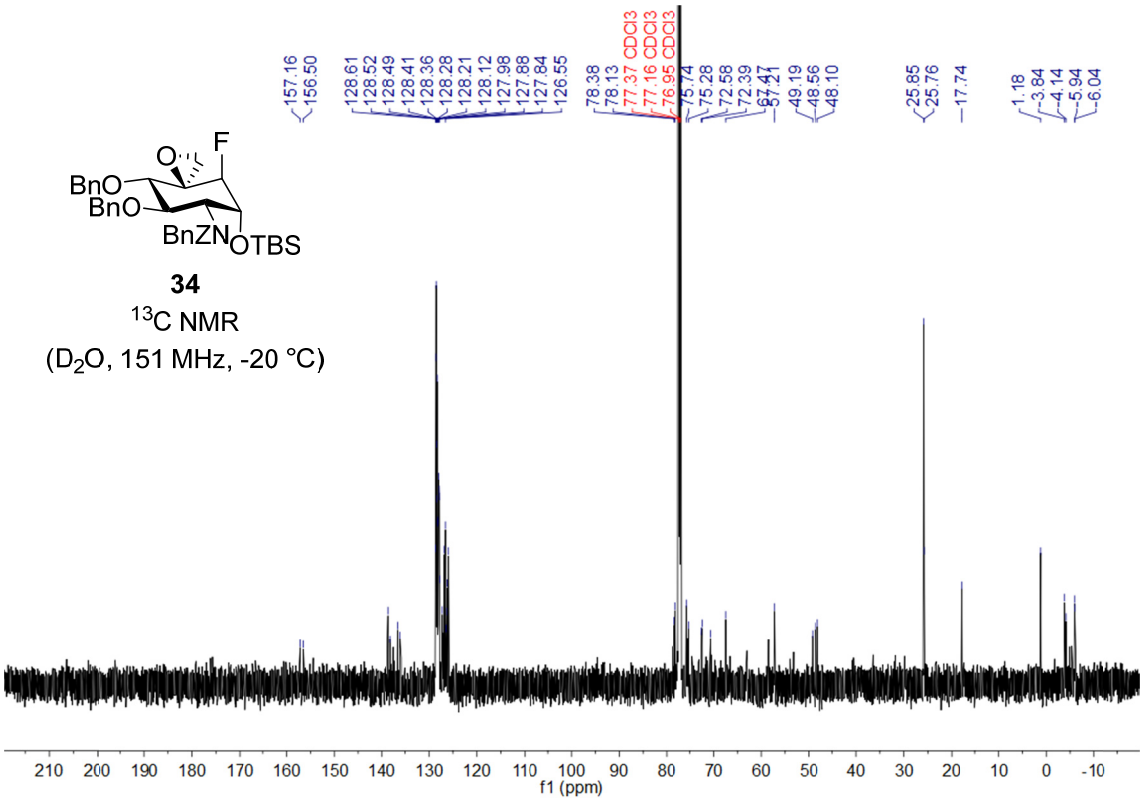
157.16
156.50
128.61
128.52
128.49
128.41
128.36
128.28
128.21
128.12
127.98
127.88
127.84
126.55
78.38
78.13
77.37 CDCl3
77.16 CDCl3
76.95 CDCl3
75.74
75.28
72.58
72.39
67.47
67.21
49.19
48.56
48.10
25.85
25.76
17.74
1.18
-3.84
-4.14
-5.94
-6.04
O
F
BnO
BnO
BnZN
OTBS
34
13C NMR
(D2O, 151 MHz, -20 °C)
f1 (ppm)

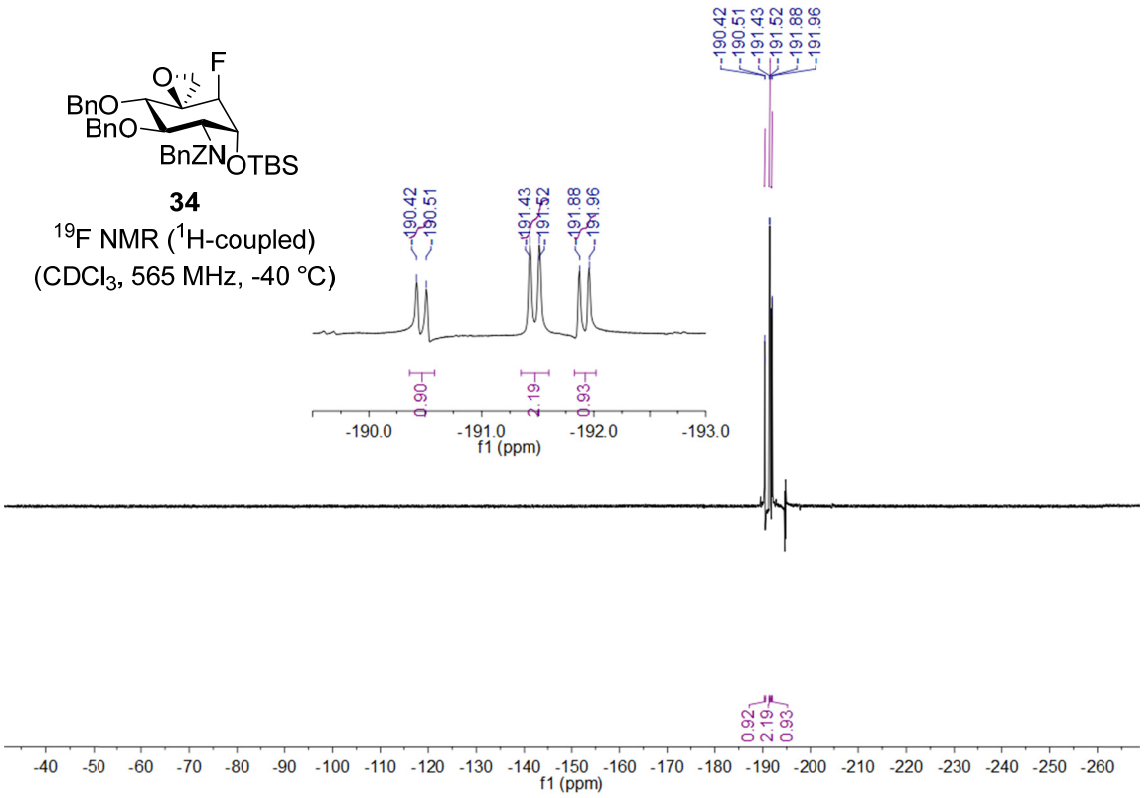
190.42
190.51
191.43
191.52
191.88
191.96
O
F
BnO
BnO
BnZN
OTBS
34
19F NMR (1H-coupled)
(CDCl3, 565 MHz, -40 °C)
0.90
2.19
0.93
f1 (ppm)
0.92
2.19
0.93
f1 (ppm)

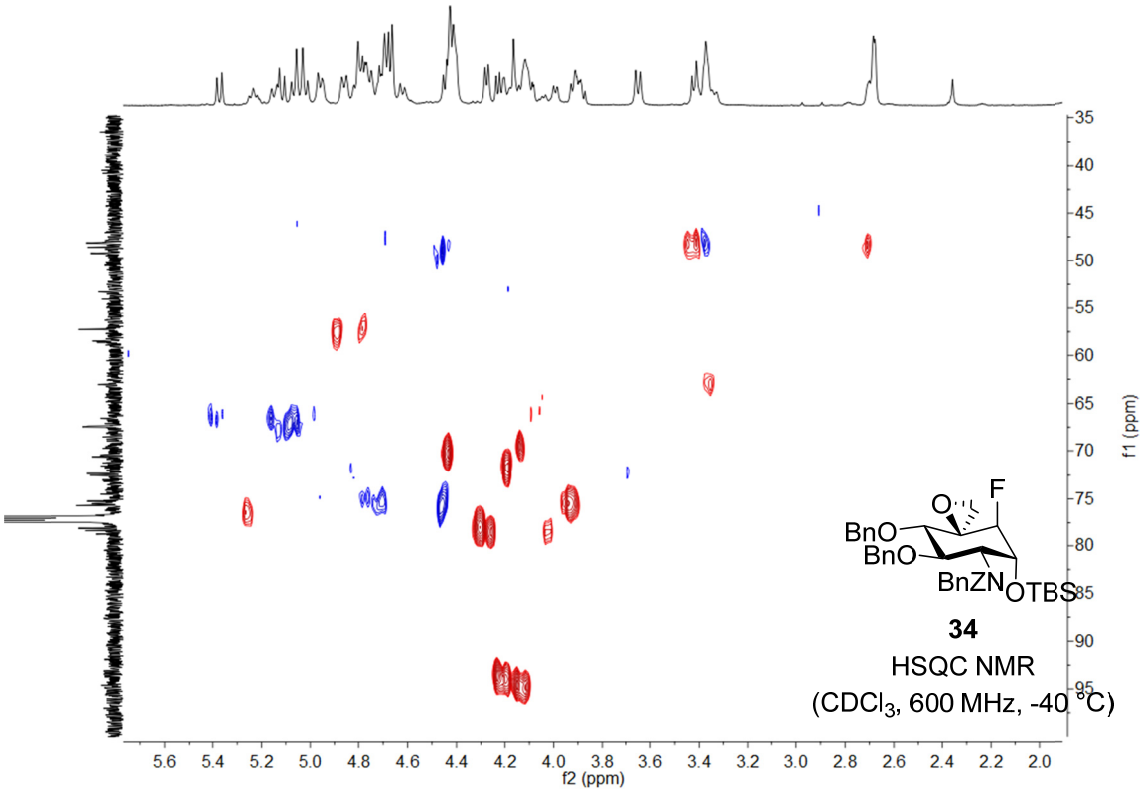

34

HSQC NMR

($CDCl_3$, 600 MHz, -40 °C)

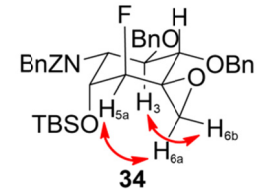

34

NOE Spectrum

($CDCl_3$, 600 MHz, -20 °C)

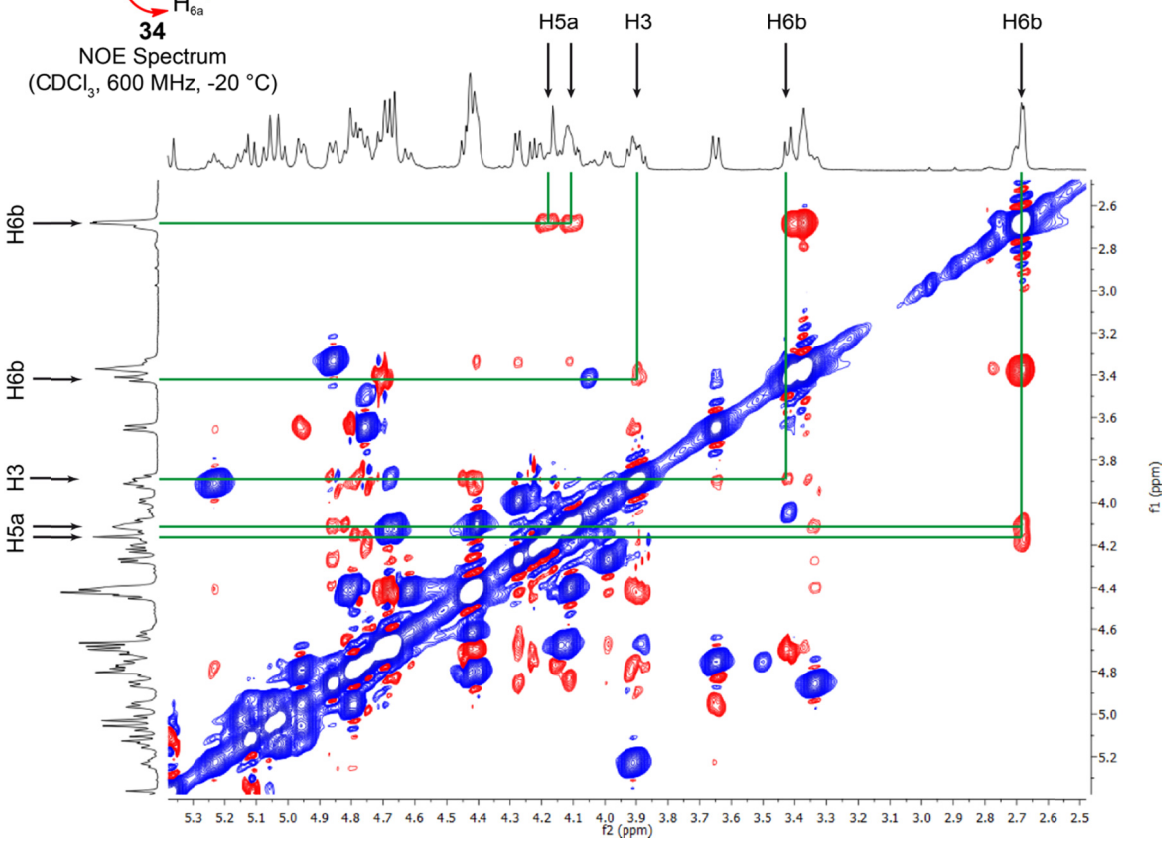

35

^{1}H NMR

(D_2O, 500 MHz)

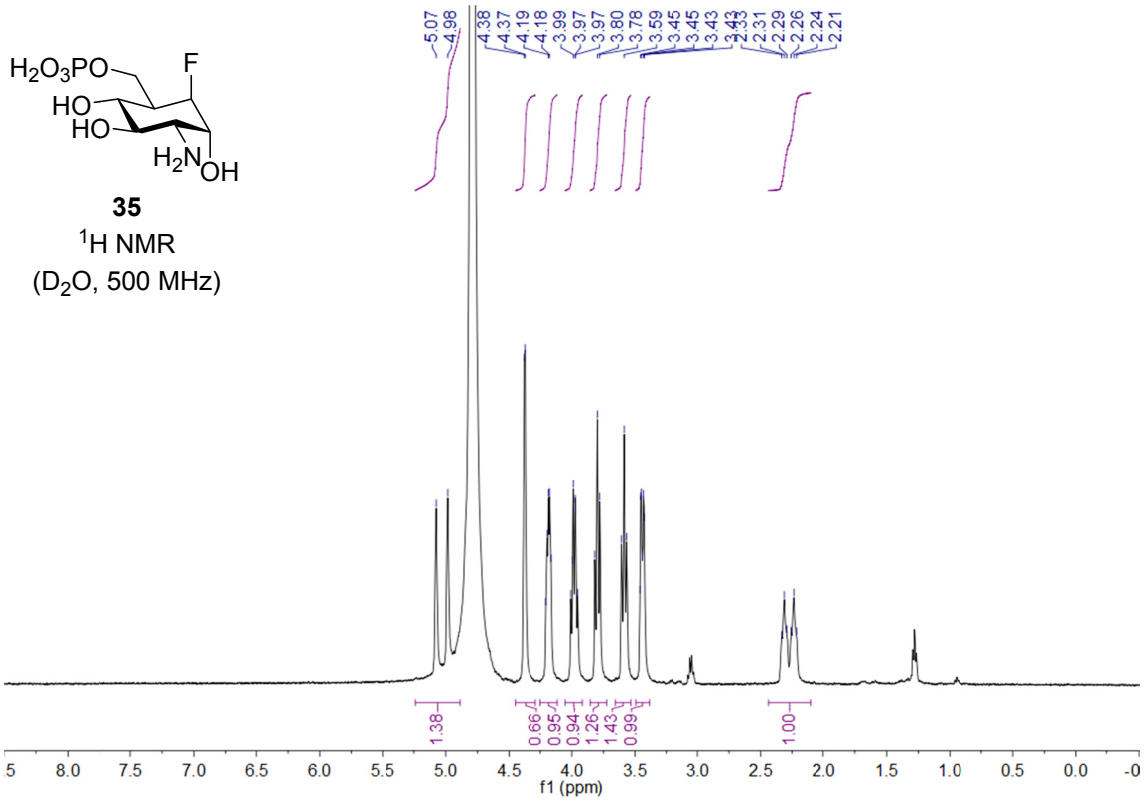

35

^{13}C NMR

(D_2O, 126 MHz)

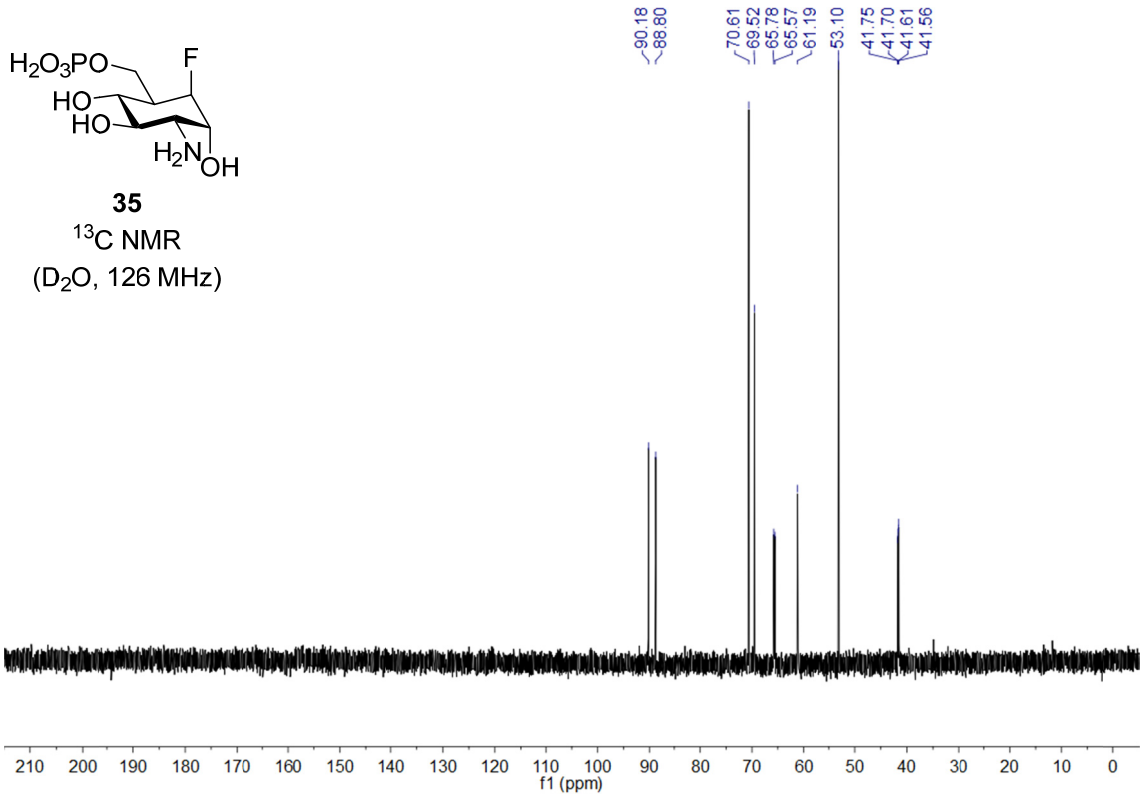

35

^{19}F NMR (^{1}H-decoupled)

(D_2O, 471 MHz)

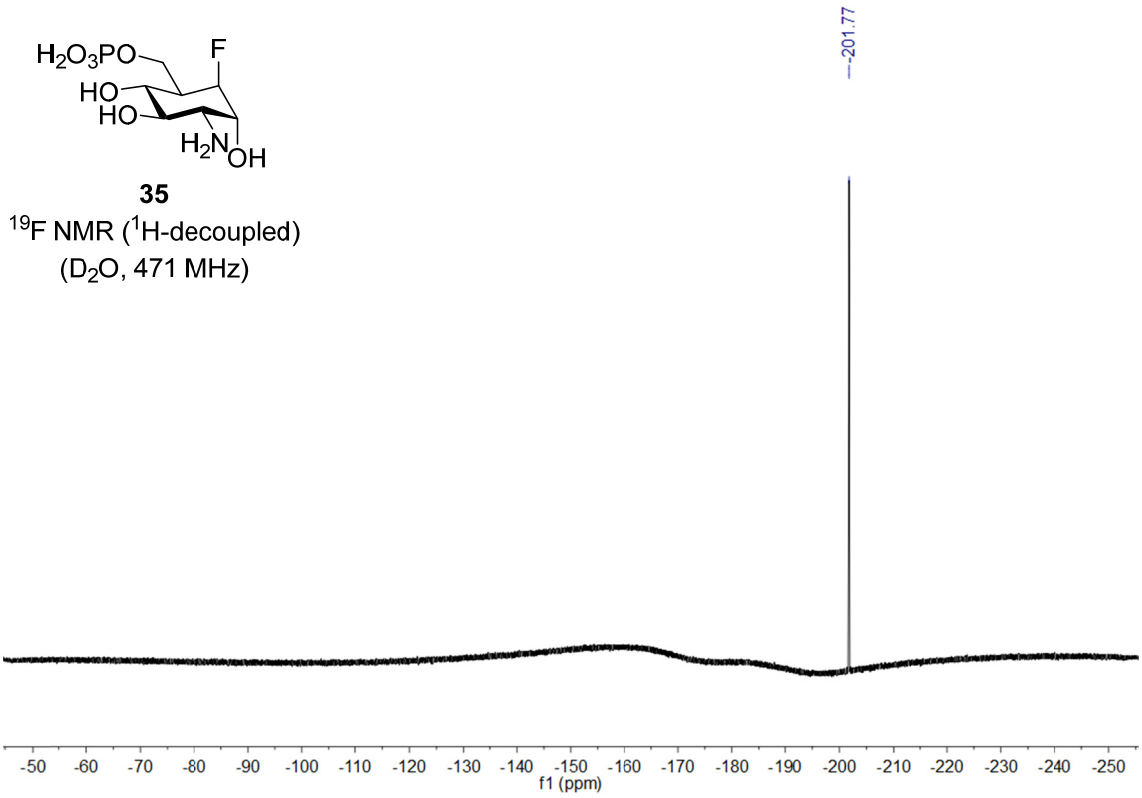

35

^{31}P NMR

(D_2O, 202 MHz)

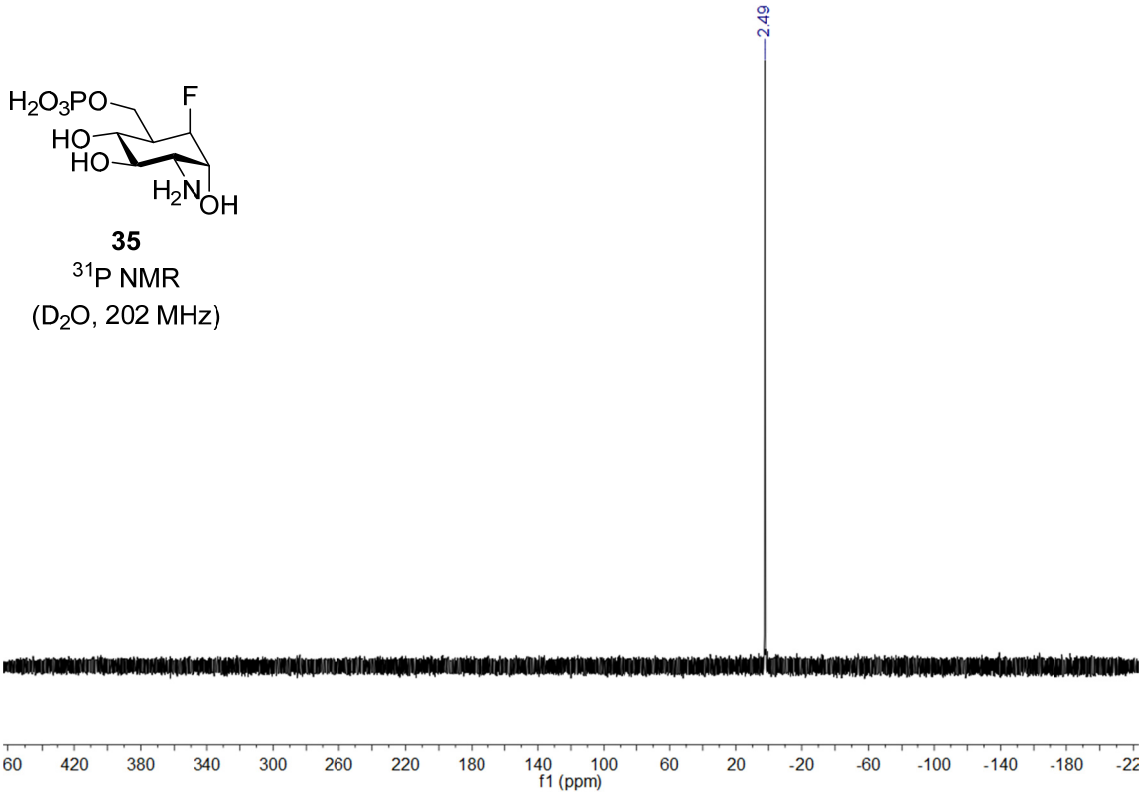

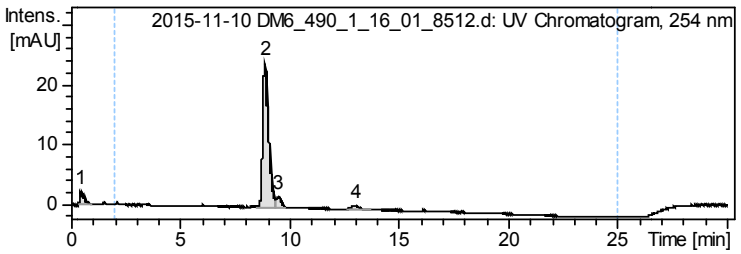

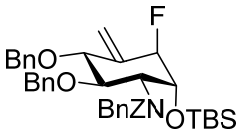

36

HPLC

ZORBAX SB-C18, 5 µm,

0.4 mL/min,

80-100% MeCN in 20 min

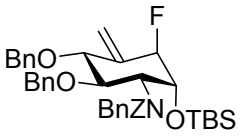

36

^{1}H NMR

($CDCl_3$, 500 MHz -40 °C)

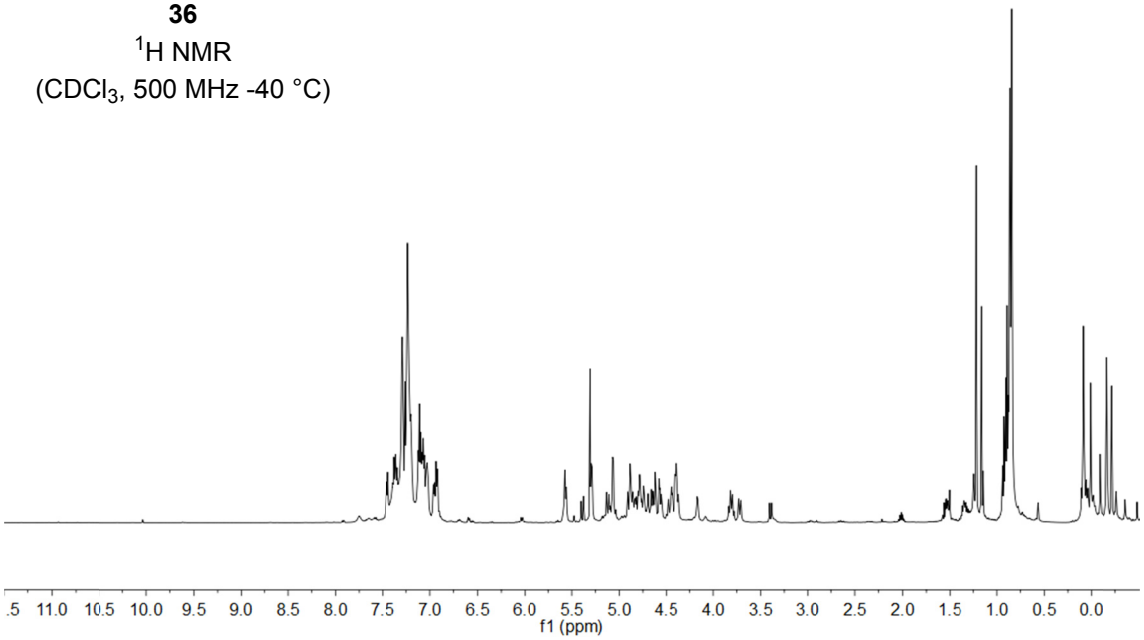

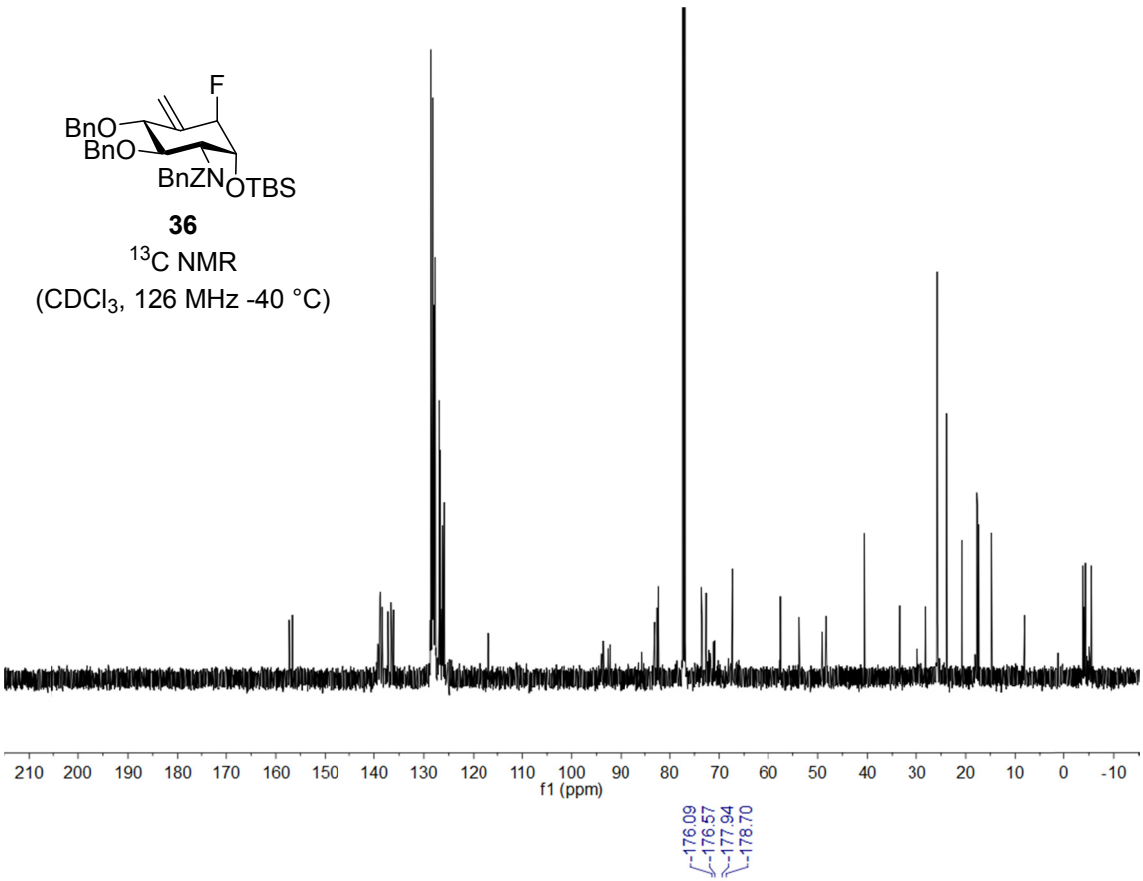

36

^{13}C NMR

($CDCl_3$, 126 MHz -40 °C)

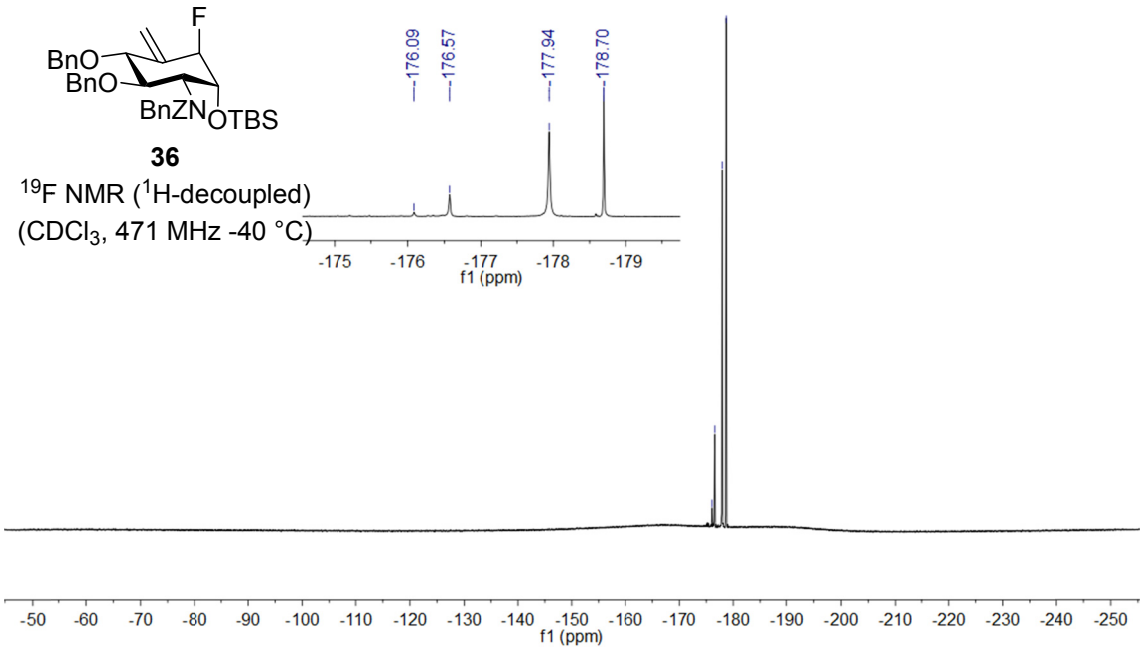

36

^{19}F NMR (^{1}H-decoupled)

($CDCl_3$, 471 MHz -40 °C)

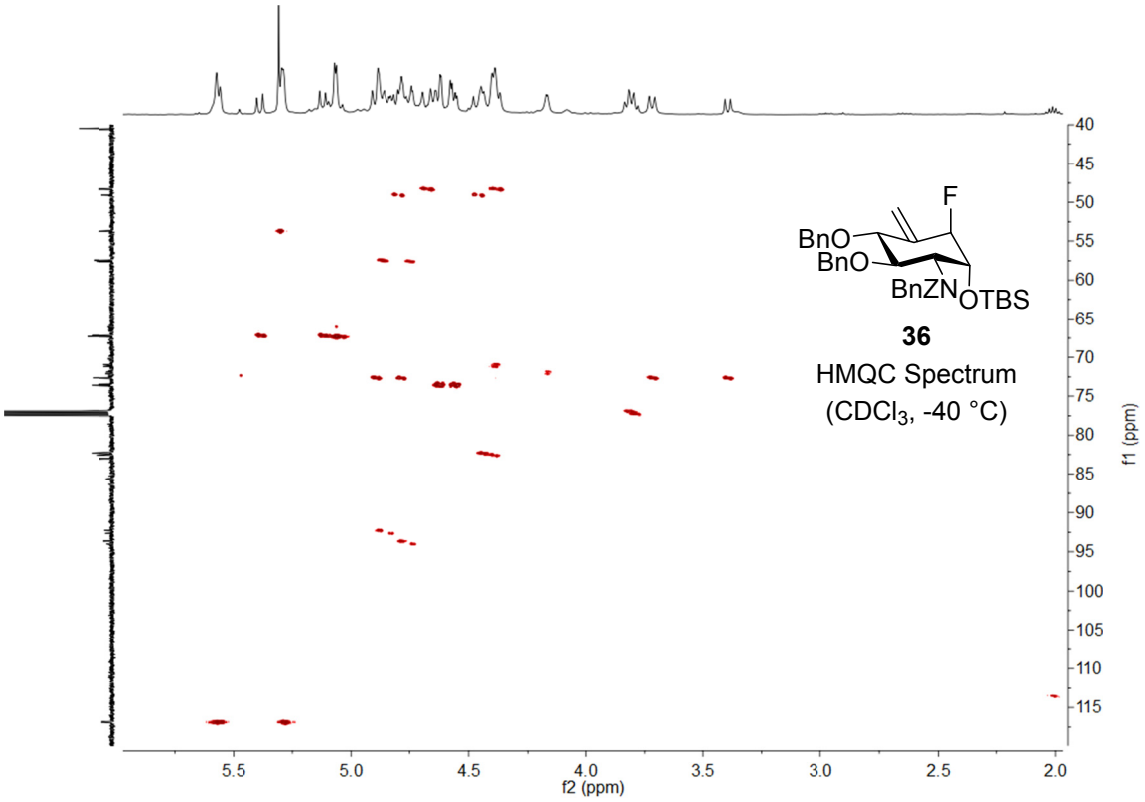
F
BnO
BnO
BnZN
OTBS
36
HMQC Spectrum
(CDCl3, -40 °C)
f2 (ppm)
f1 (ppm)

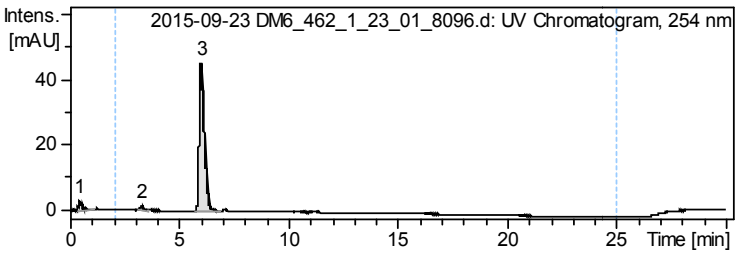

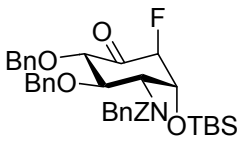

37

HPLC

ZORBAX SB-C18, 5 µm,

0.4 mL/min,

80-100% MeCN in 20 min

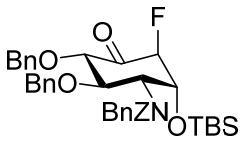

37

^{1}H NMR

($CDCl_3$, 500 MHz -40 °C)

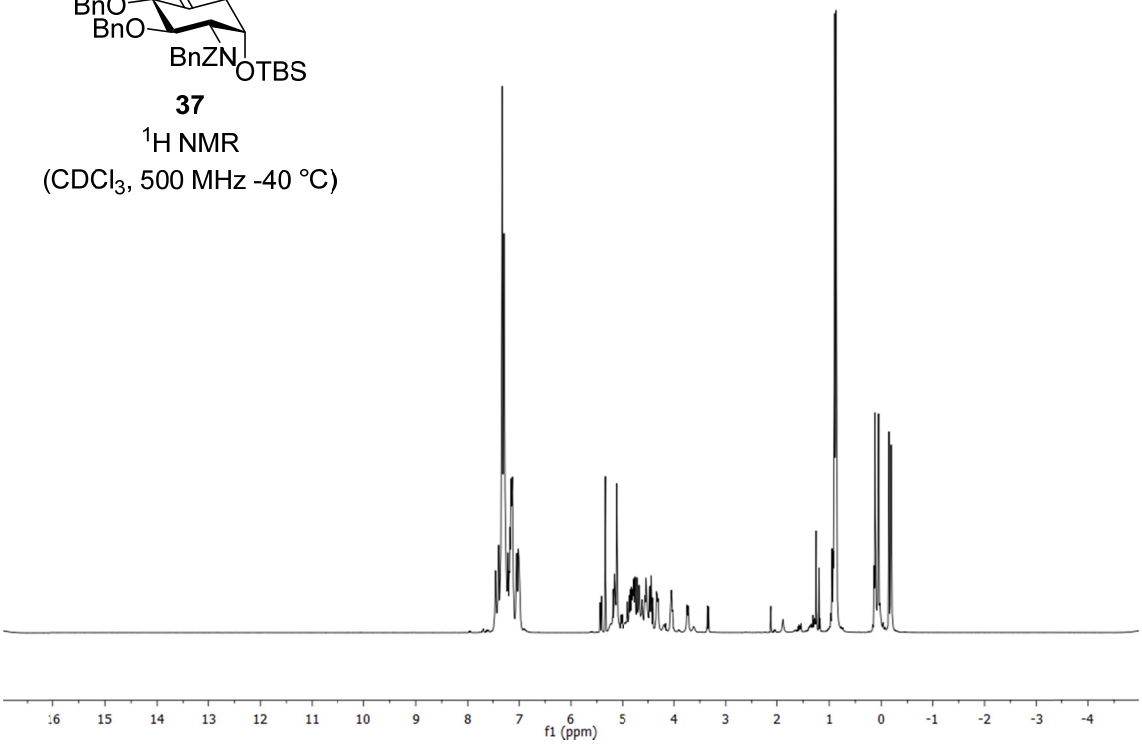

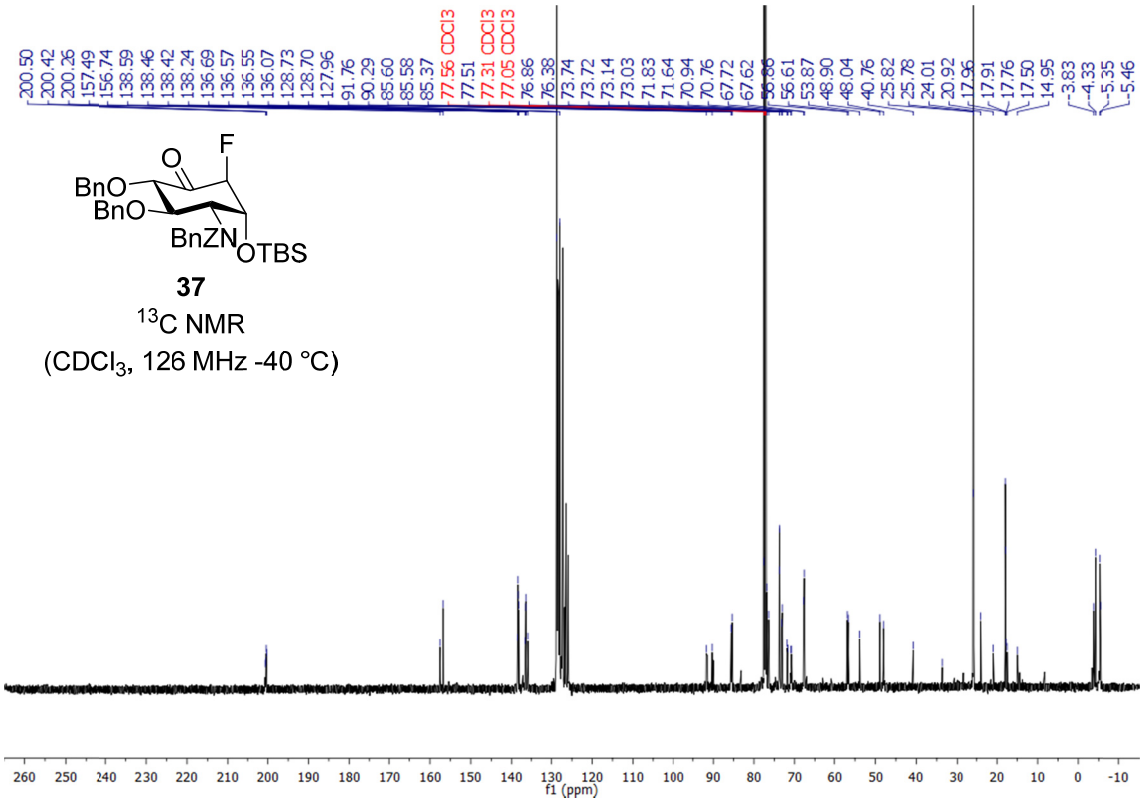

37

^{13}C NMR

($CDCl_3$, 126 MHz -40 °C)

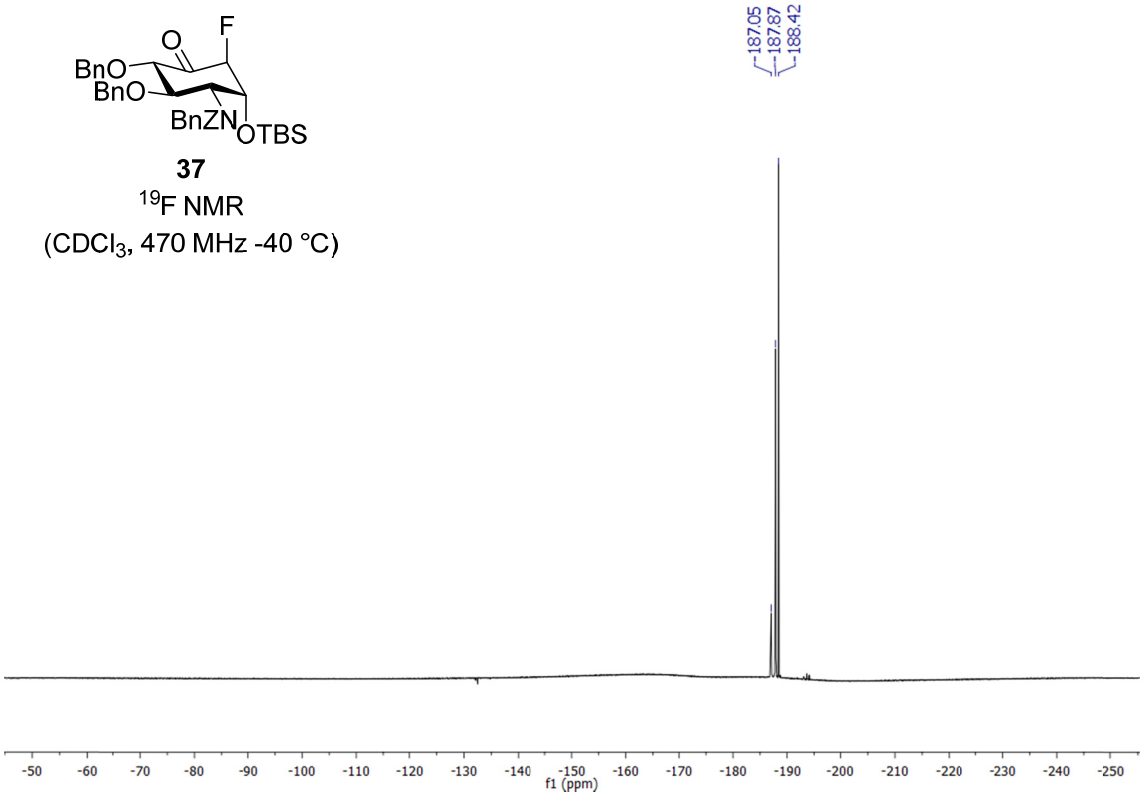

37

^{19}F NMR

($CDCl_3$, 470 MHz -40 °C)

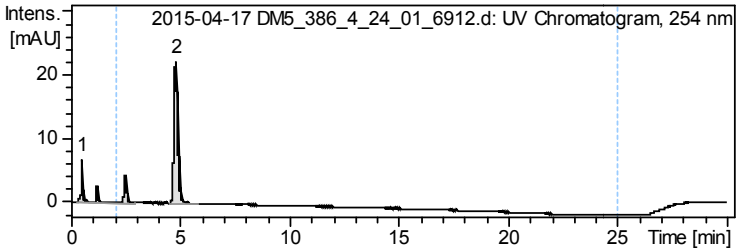

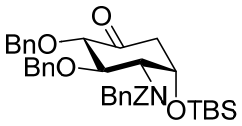

38a

HPLC

ZORBAX SB-C18, 5 µm,

0.4 mL/min,

80-100% MeCN in 20 min

38a

^{1}H NMR

($CDCl_3$, 400 MHz)

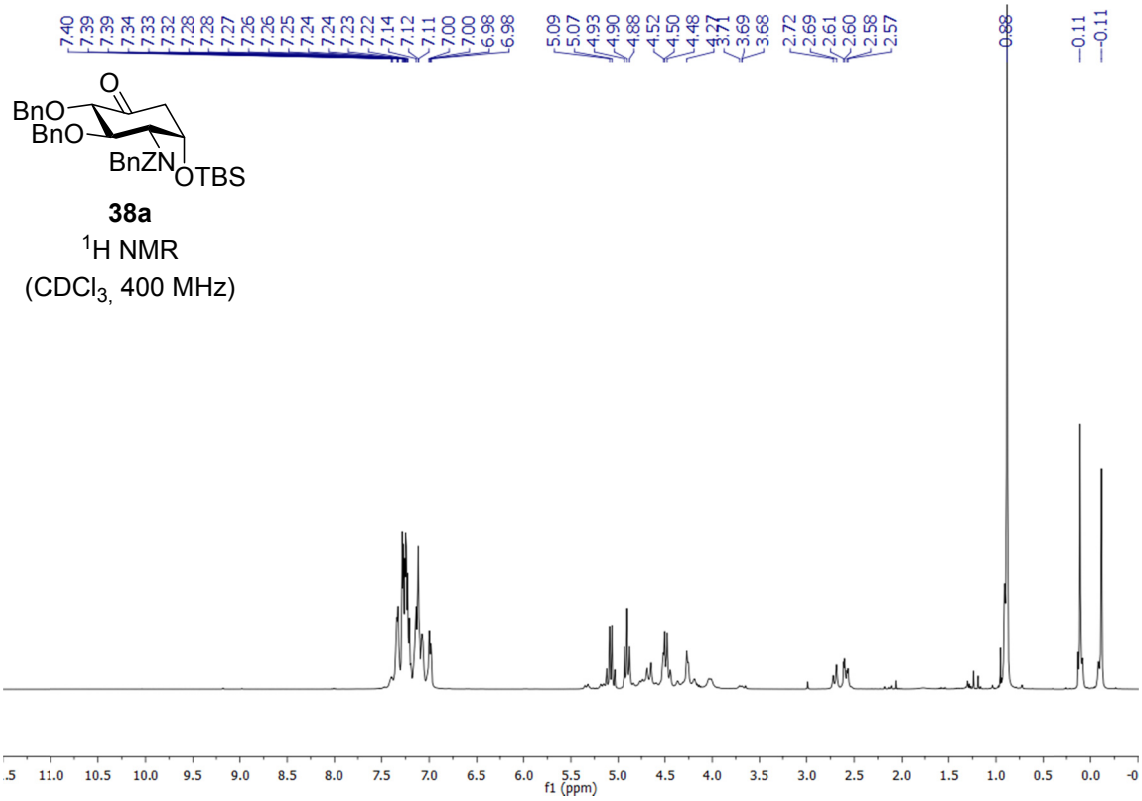

38a

^{13}C NMR

($CDCl_3$, 100 MHz)

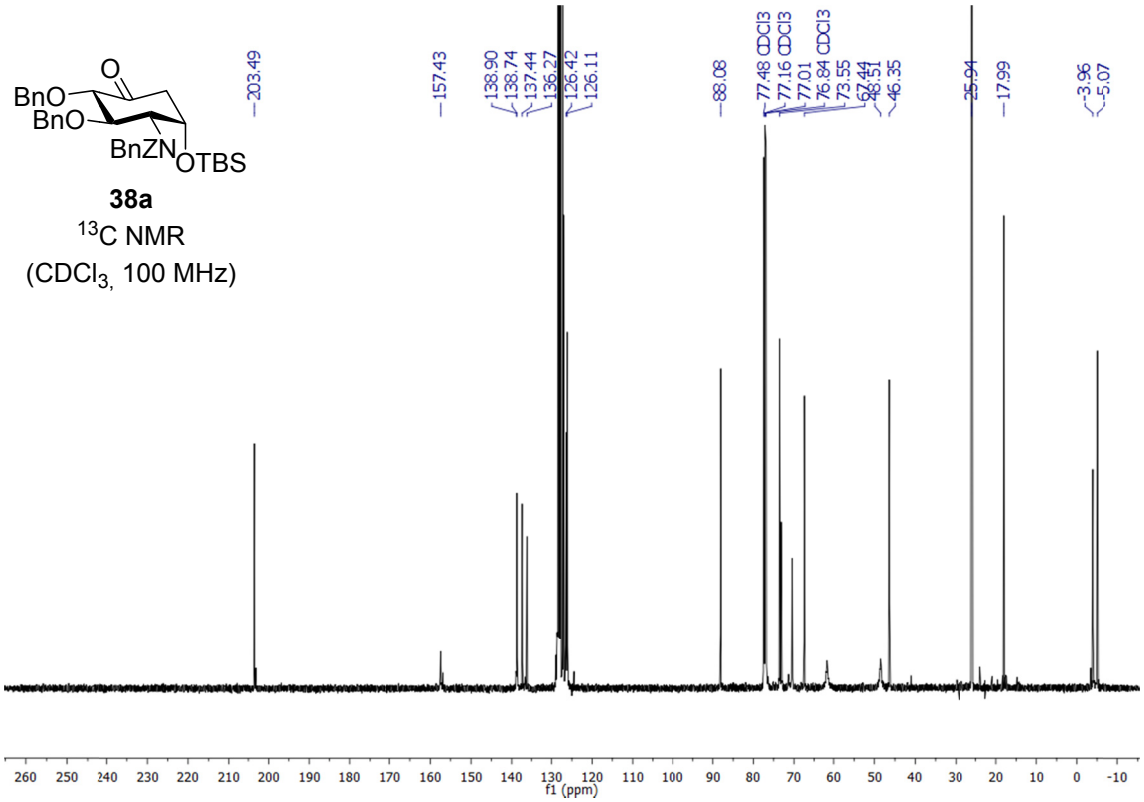

38b

^{1}H NMR

($CDCl_3$, 400 MHz)

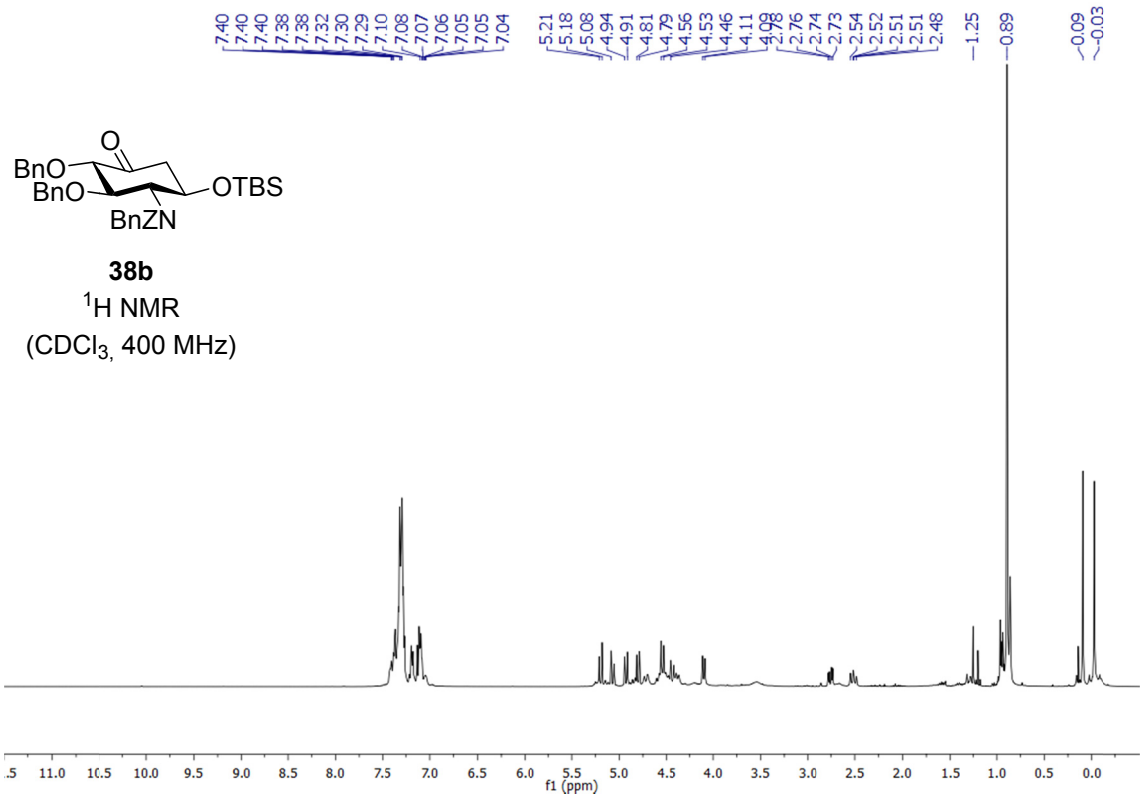

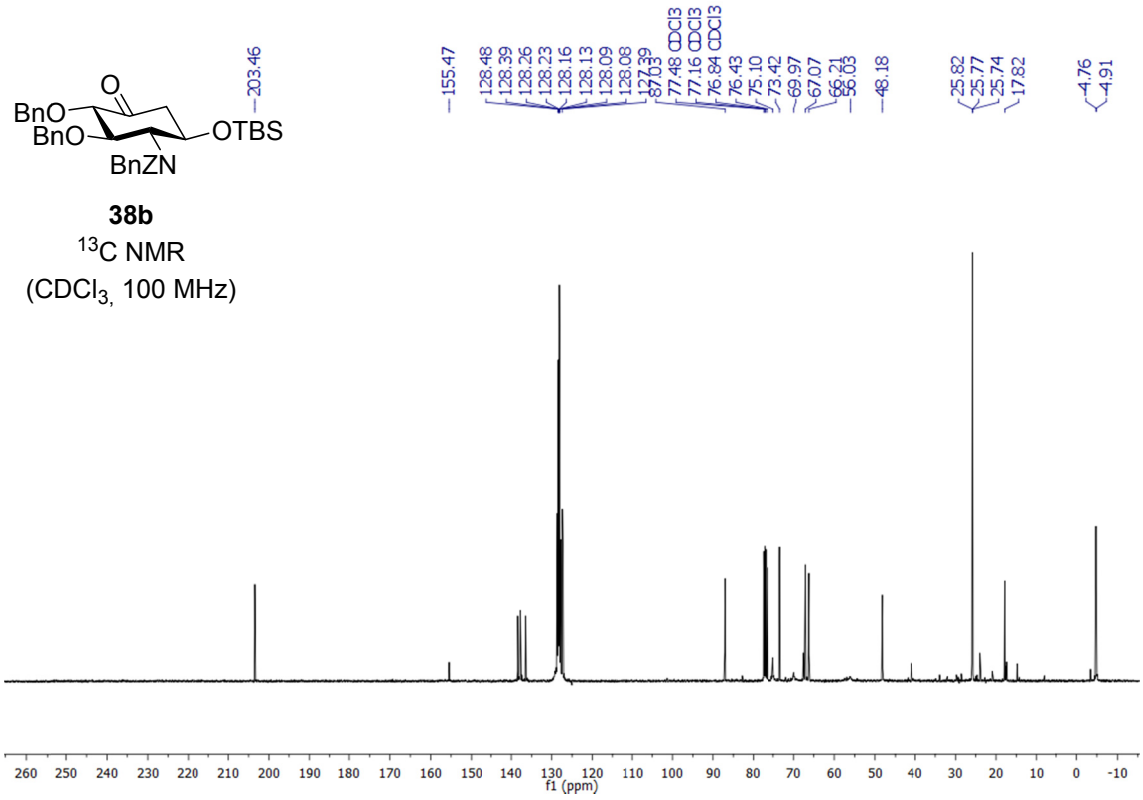

38b

^{13}C NMR

($CDCl_3$, 100 MHz)

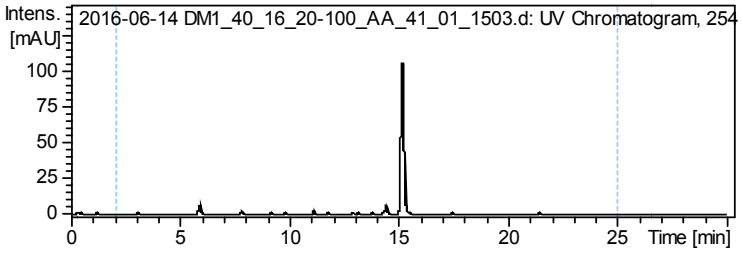

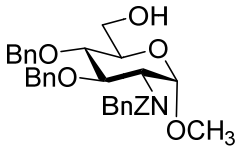

39

HPLC

ZORBAX SB-C18, 5 µm,

0.4 mL/min,

20-100% MeCN in 20 min

39

^{1}H NMR

($CDCl_3$, 400 MHz)

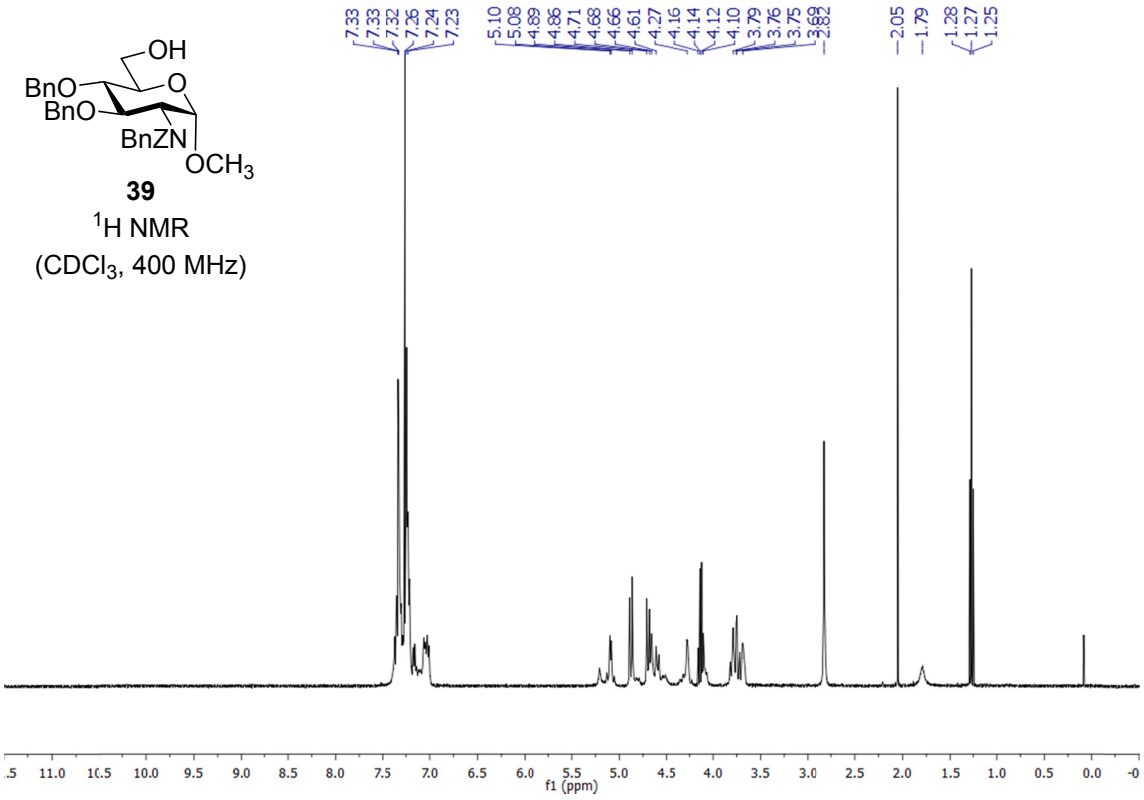

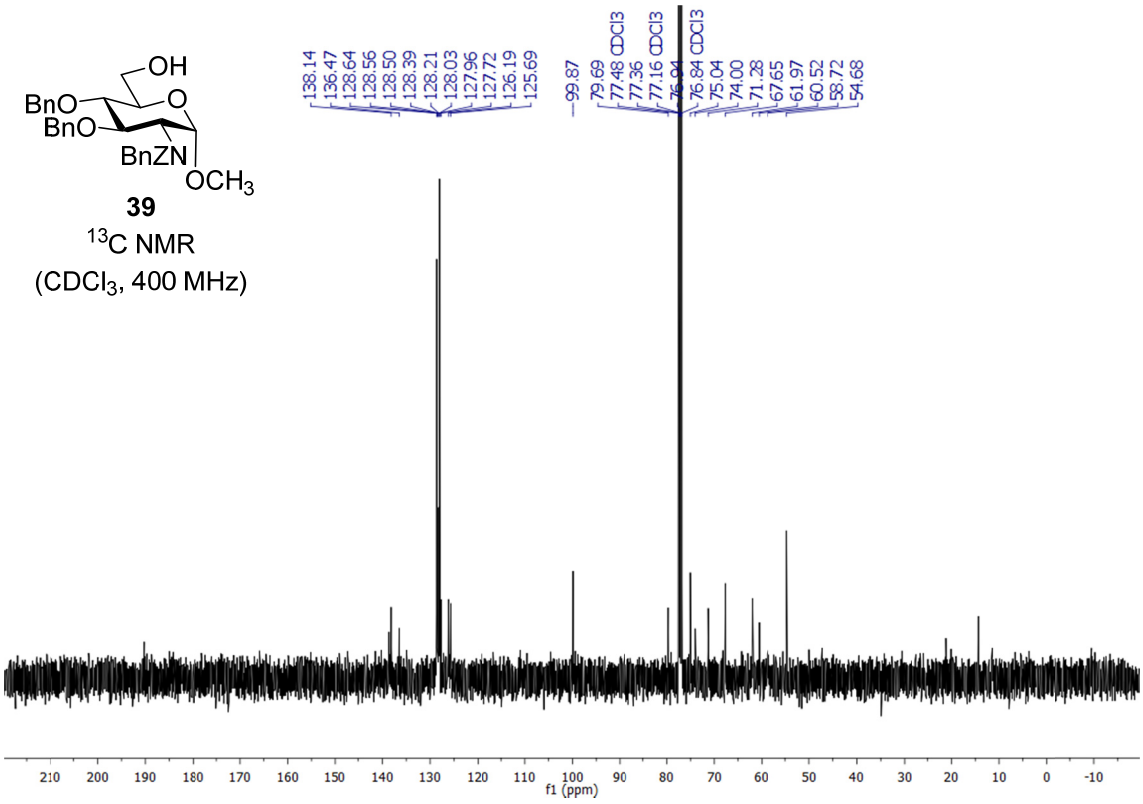
OH
BnO
O
BnO
BnZN
OCH3
39
13C NMR
(CDCl3, 400 MHz)
138.14
136.47
128.64
128.56
128.50
128.39
128.21
128.03
127.96
127.72
126.19
125.69
99.87
79.69
77.48 CDCl3
77.36
77.16 CDCl3
76.84 CDCl3
75.04
74.00
71.28
67.65
61.97
60.52
58.72
54.68
f1 (ppm)

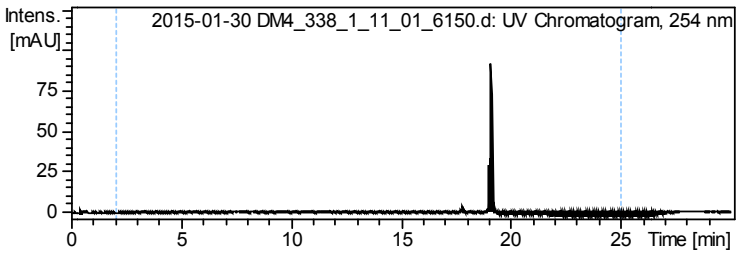

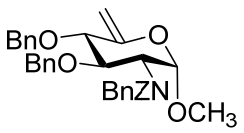

41

HPLC

ZORBAX SB-C18, 5 µm,

0.4 mL/min,

80-100% MeCN in 20 min

41

^{1}H NMR

($CDCl_3$, 400 MHz)

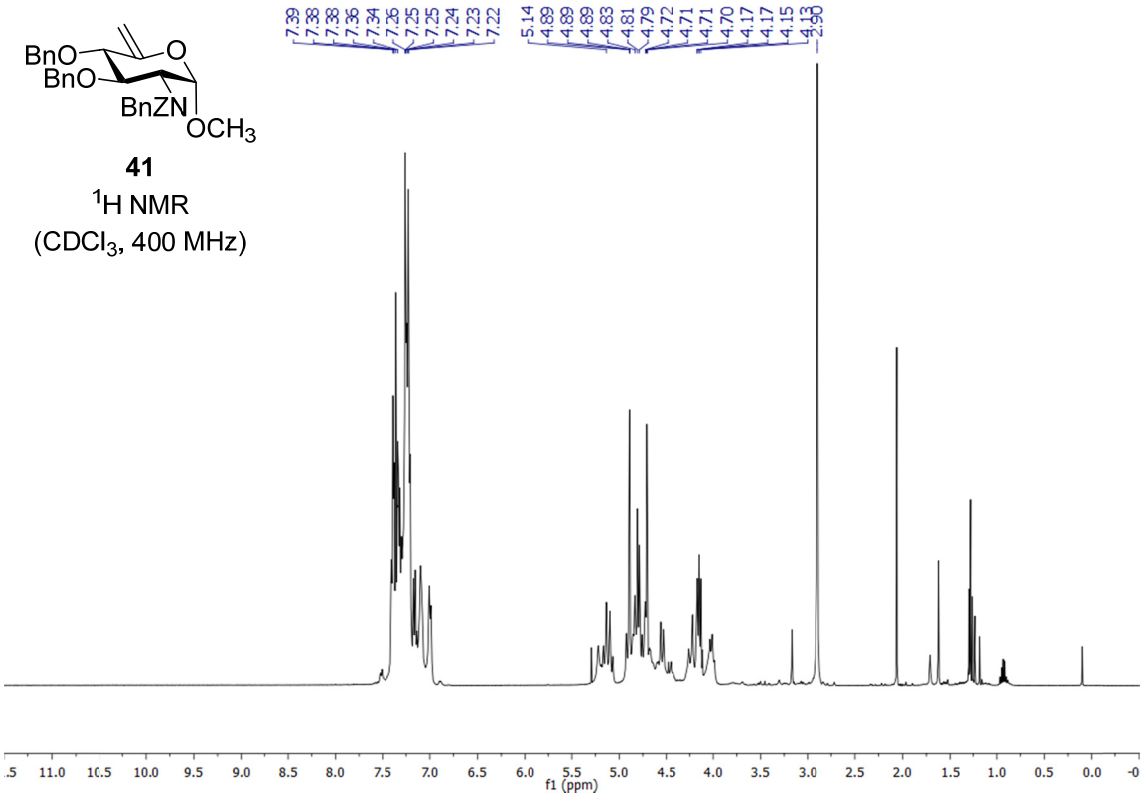

41

^{13}C NMR

($CDCl_3$, 100 MHz)

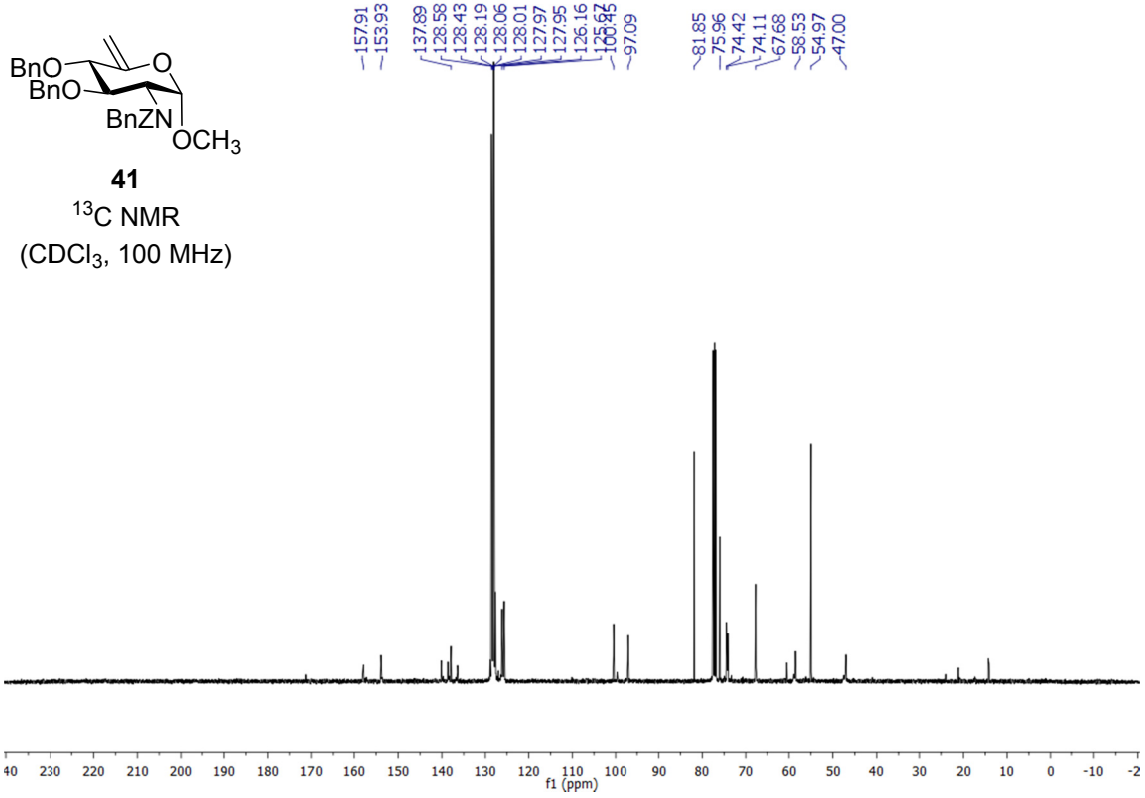

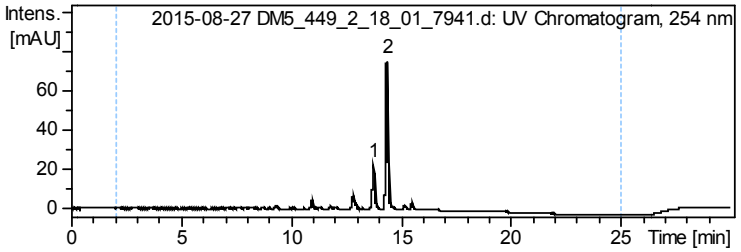

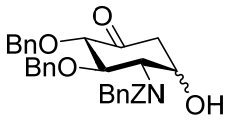

42

HPLC

ZORBAX SB-C18, 5 µm,
0.4 mL/min,
80-100% MeCN in 20 min

42

^{1}H NMR

($CDCl_3$, 500 MHz)

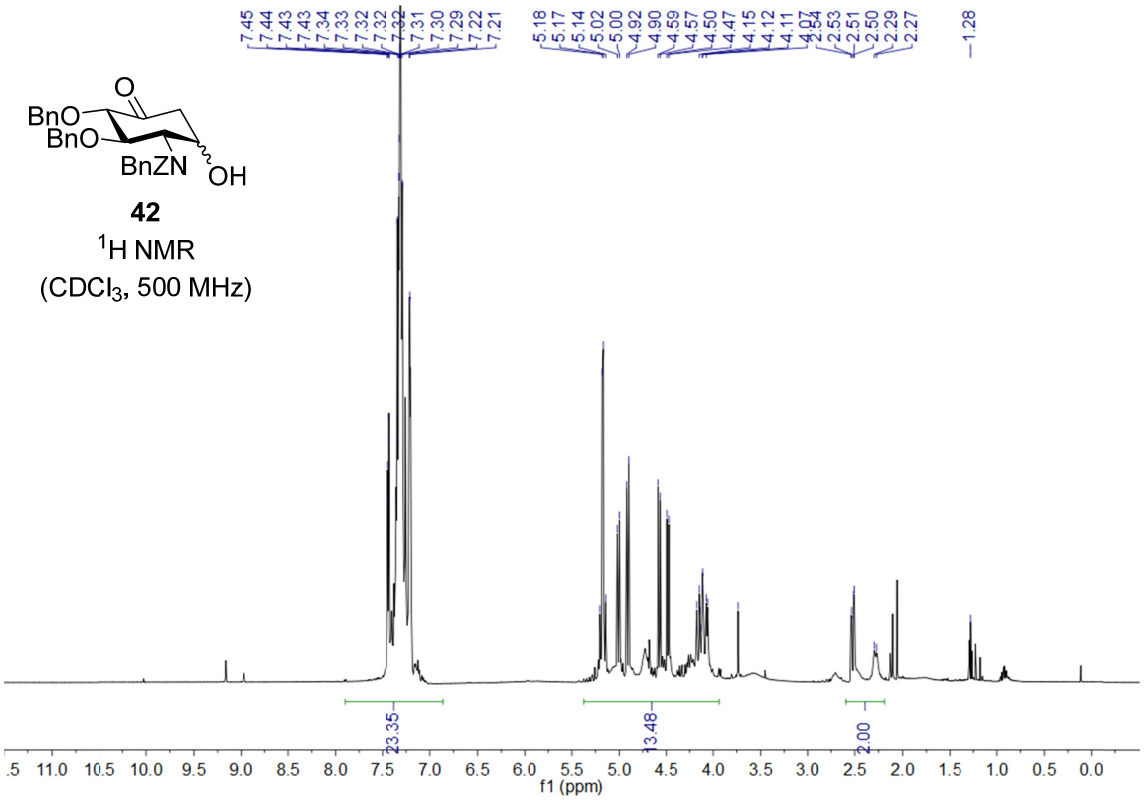

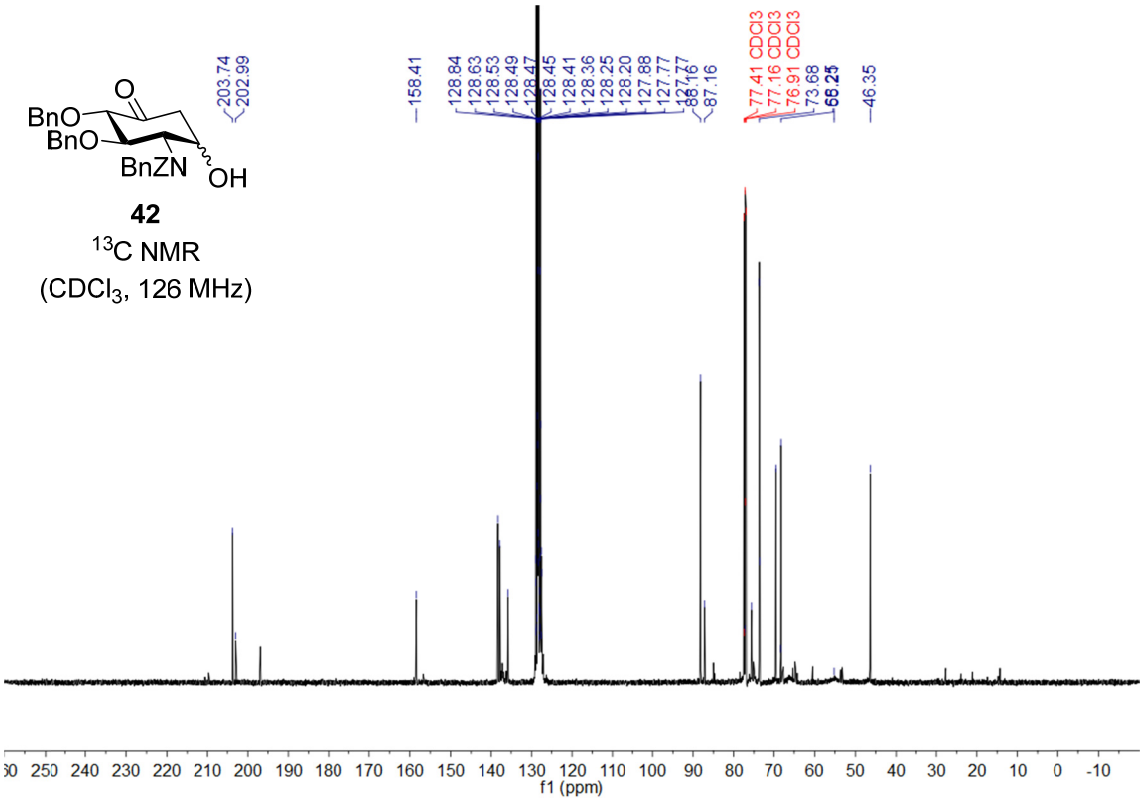
BnO
BnO
BnZN
OH
42
13C NMR
(CDCl3, 126 MHz)
203.74
202.99
158.41
128.84
128.63
128.53
128.49
128.47
128.45
128.41
128.36
128.25
128.20
127.88
127.77
127.77
88.16
87.16
77.41 CDCl3
77.16 CDCl3
76.91 CDCl3
73.68
66.25
46.35
f1 (ppm)

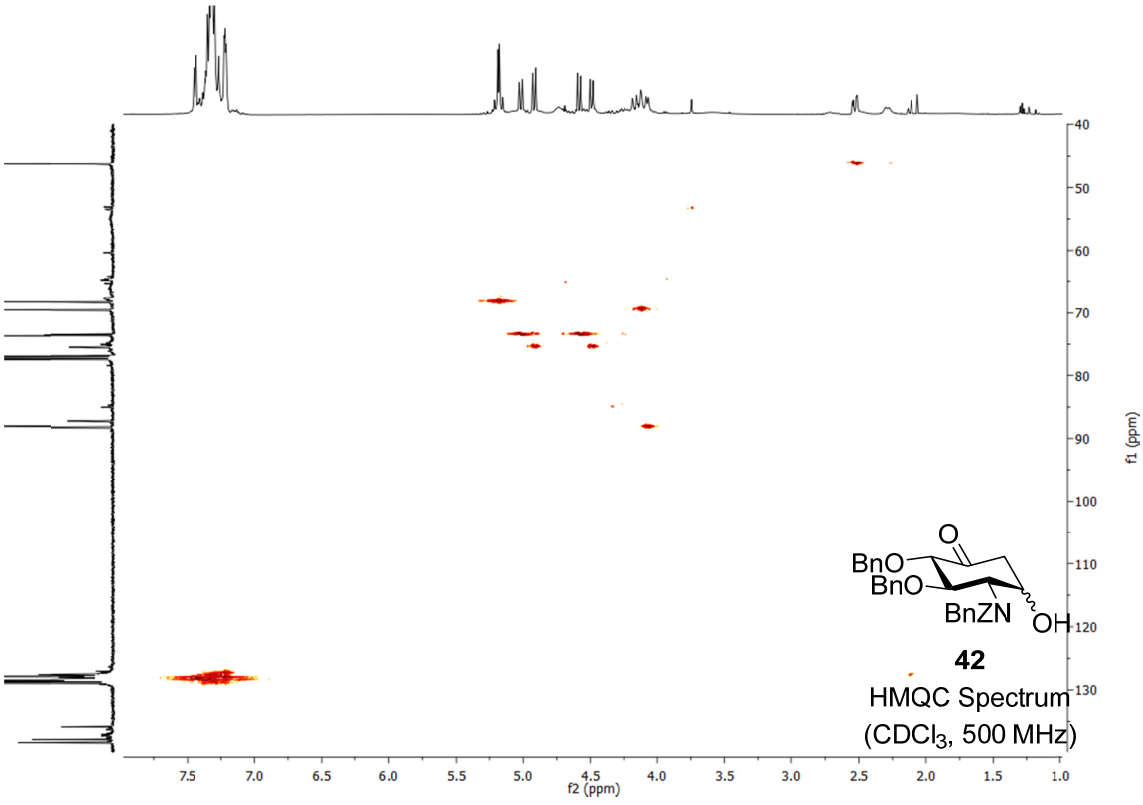
BnO
BnO
BnZN
OH
42
HMQC Spectrum
(CDCl3, 500 MHz)
f2 (ppm)
f1 (ppm)

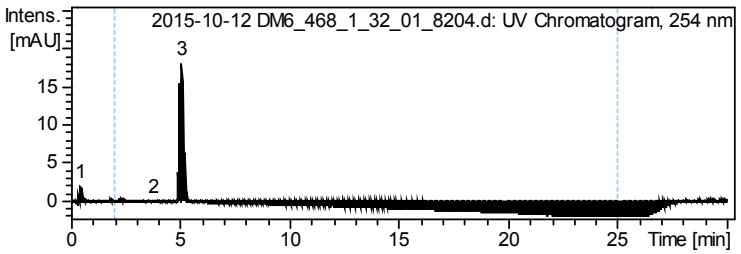

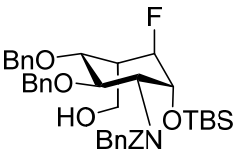

48

HPLC
ZORBAX SB-C18, 5 µm,
0.4 mL/min,
60-80 % MeCN in 20 min

48

^{1}H NMR
($CDCl_3$, 500 MHz, -40°C)

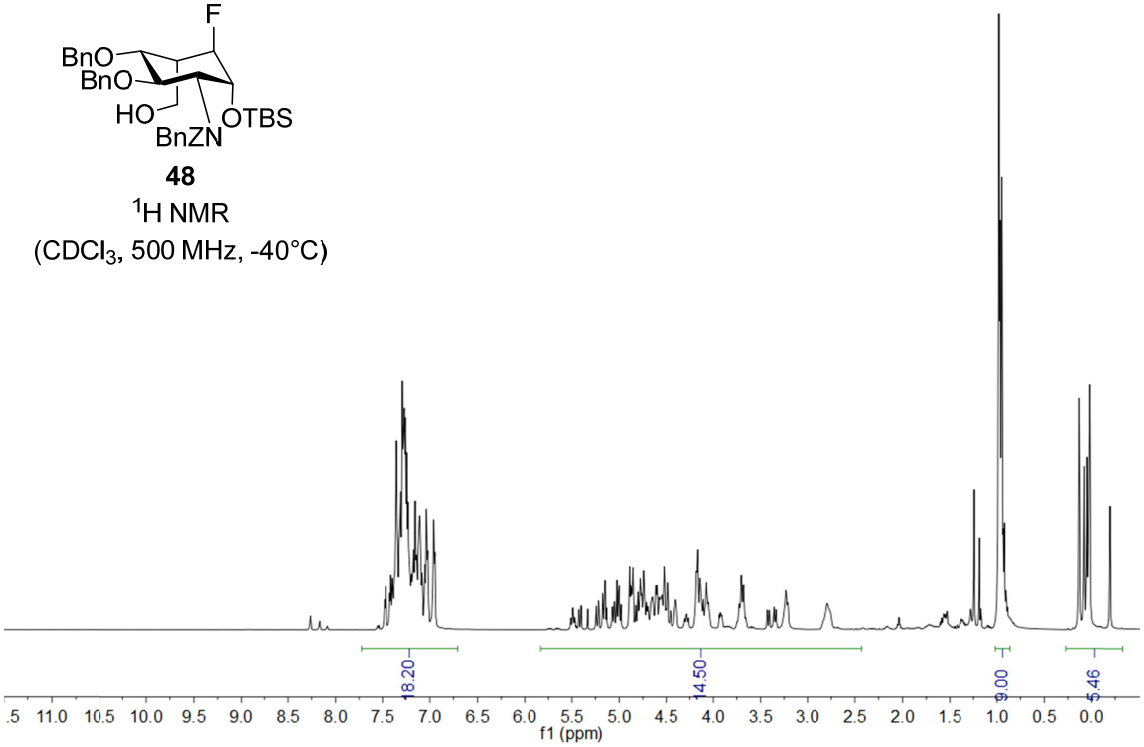

48

^{13}C NMR

($CDCl_3$, 126 MHz, -40 °C)

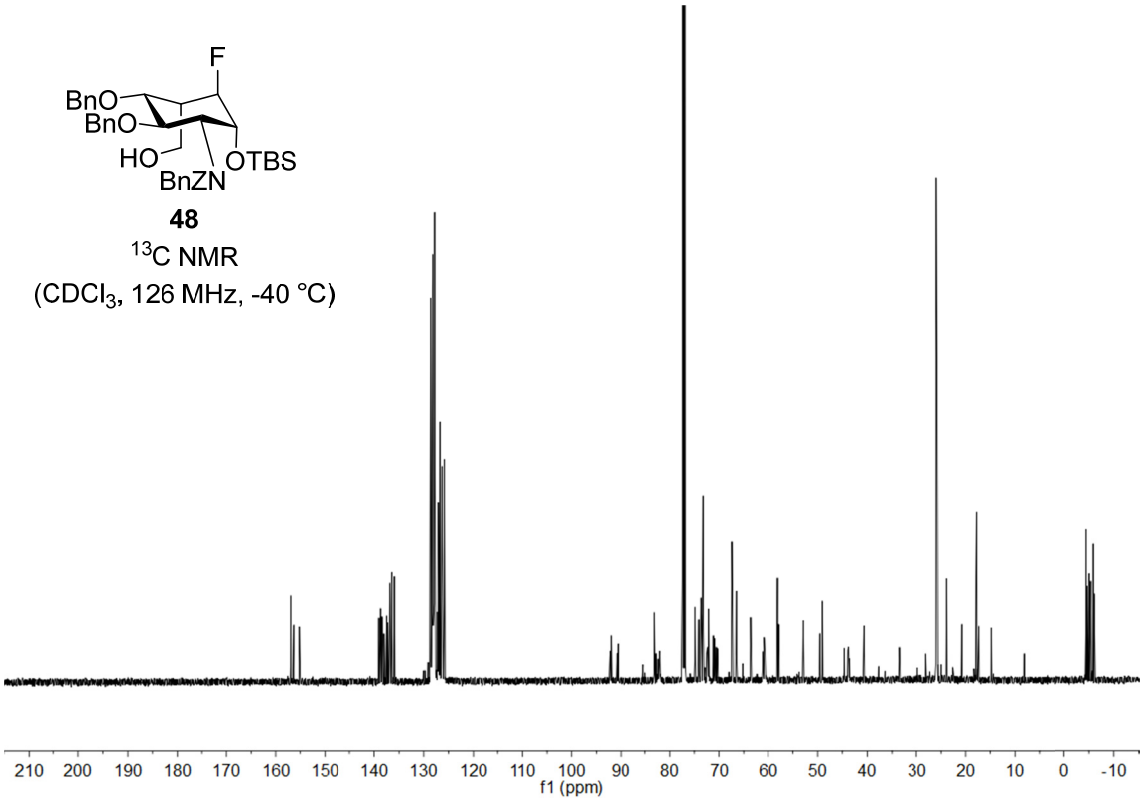

48

^{19}F NMR (^{1}H-decoupled)

($CDCl_3$, 470 MHz, -40 °C)

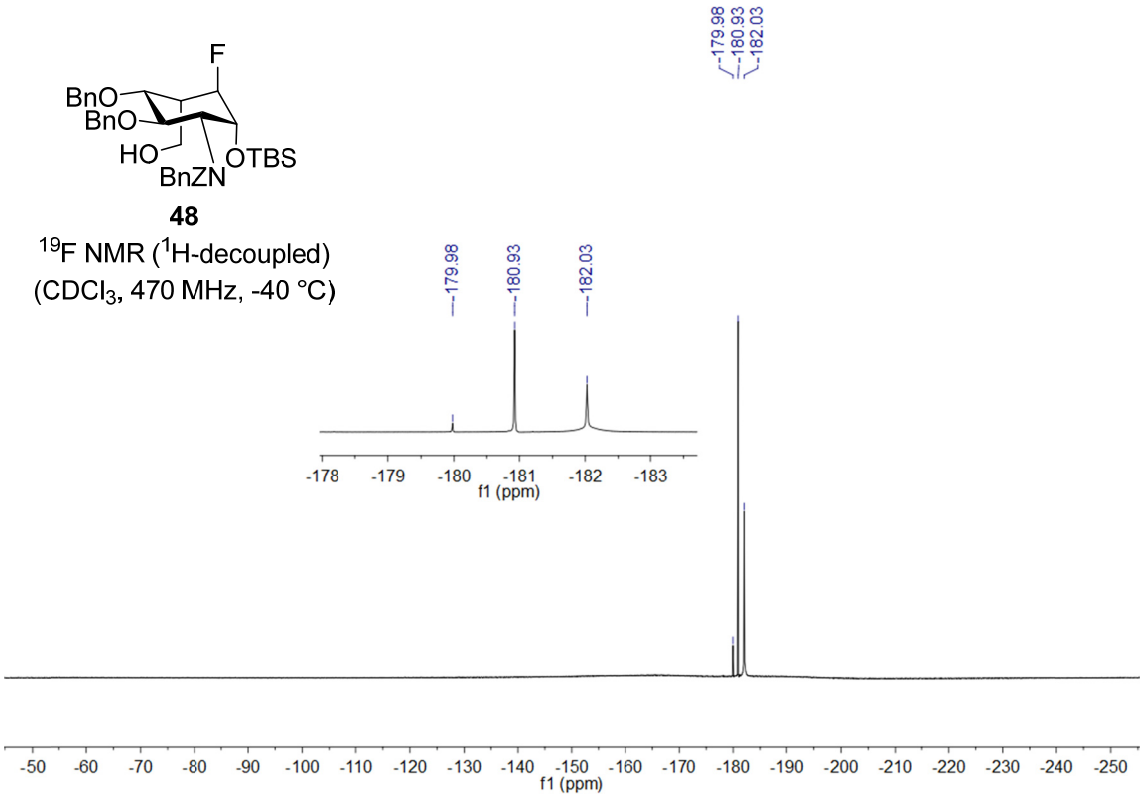

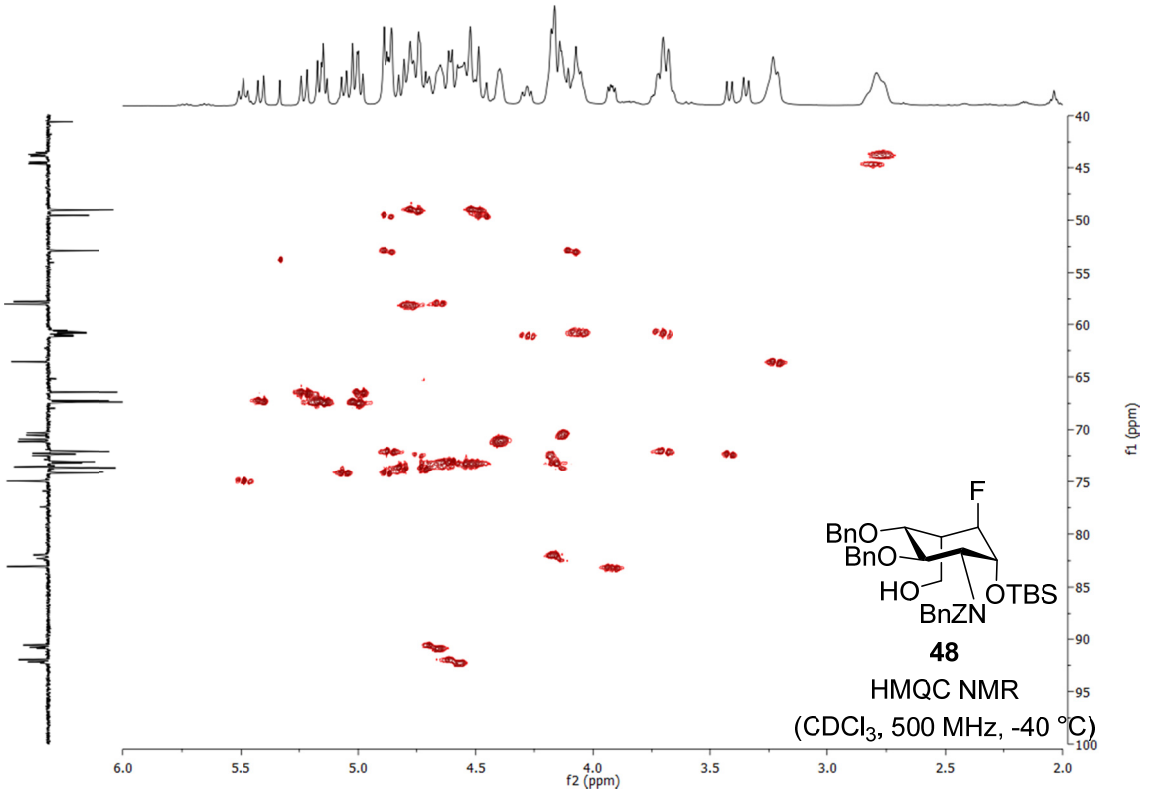
F
BnO
BnO
HO
OTBS
BnZN
48
HMQC NMR
(CDCl3, 500 MHz, -40 °C)
f2 (ppm)
f1 (ppm)

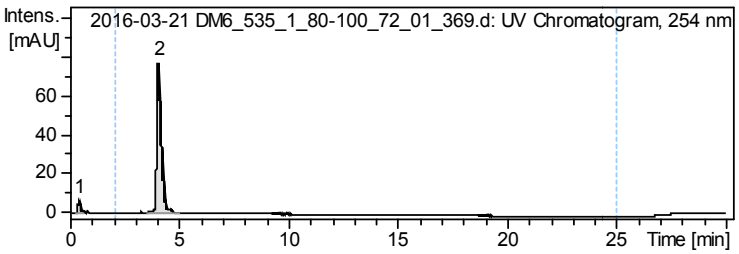

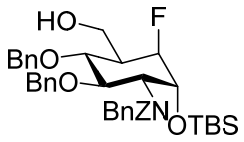

53

HPLC

ZORBAX SB-C18, 5 µm,
0.4 mL/min,
80-100 % MeCN in 20 min

53

^{1}H NMR

($CDCl_3$, 700 MHz)

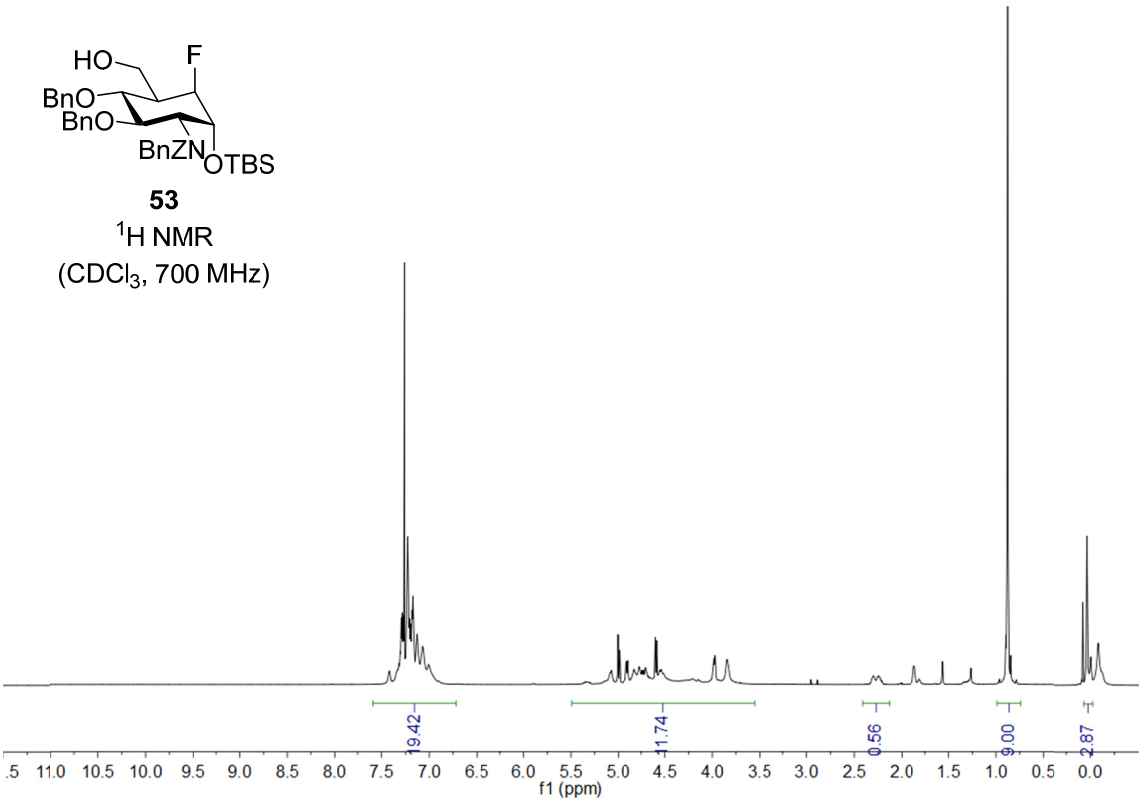

53

^{13}C NMR

($CDCl_3$, 176 MHz)

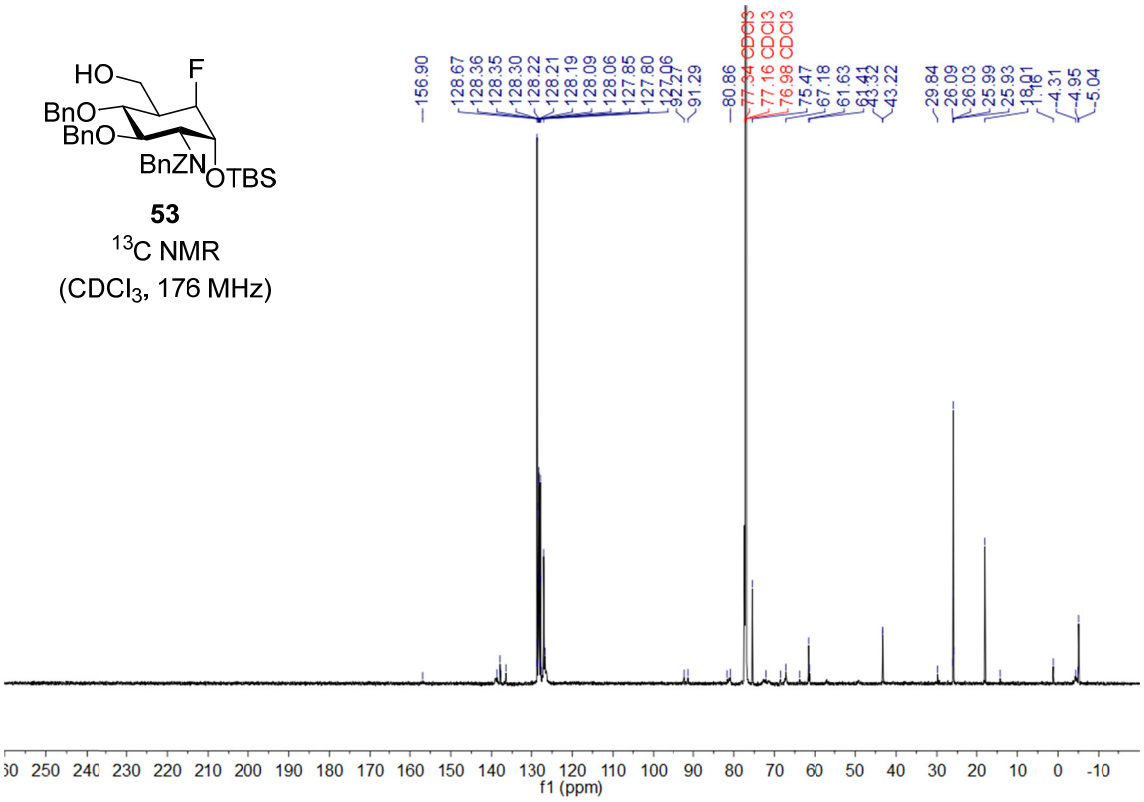

53

^{19}F NMR (^{1}H-decoupled)

($CDCl_3$, 470 MHz)

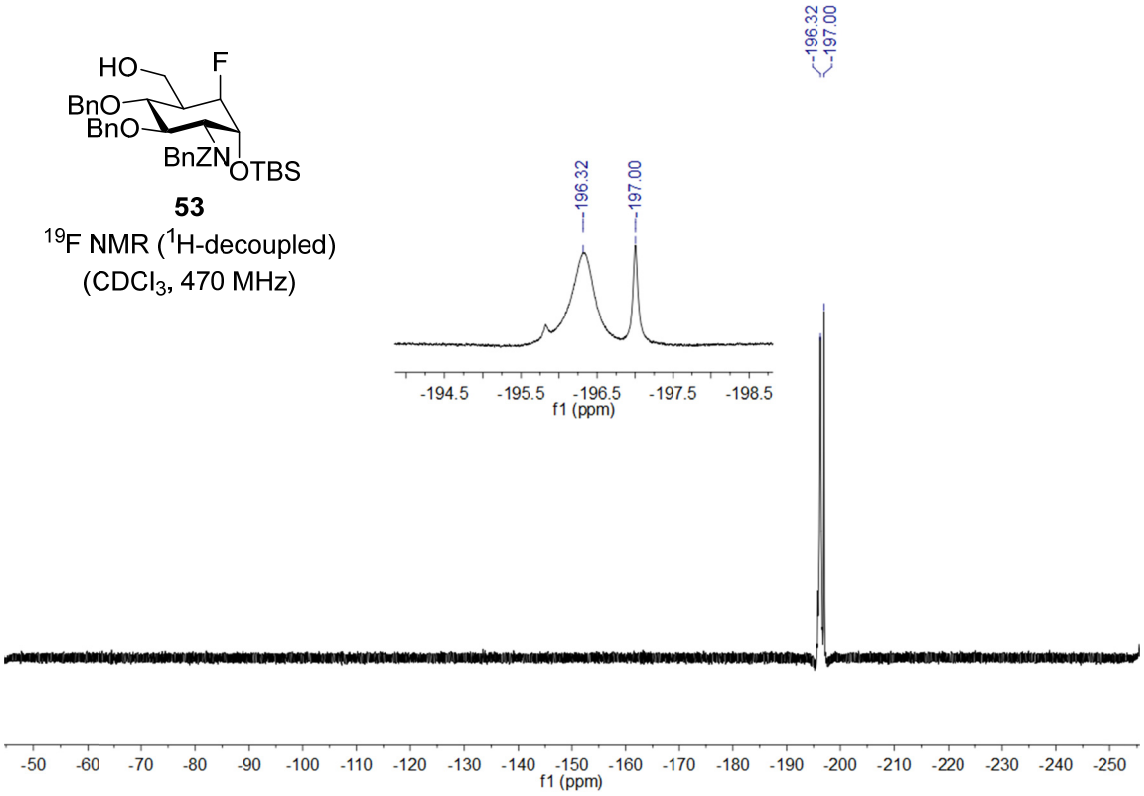

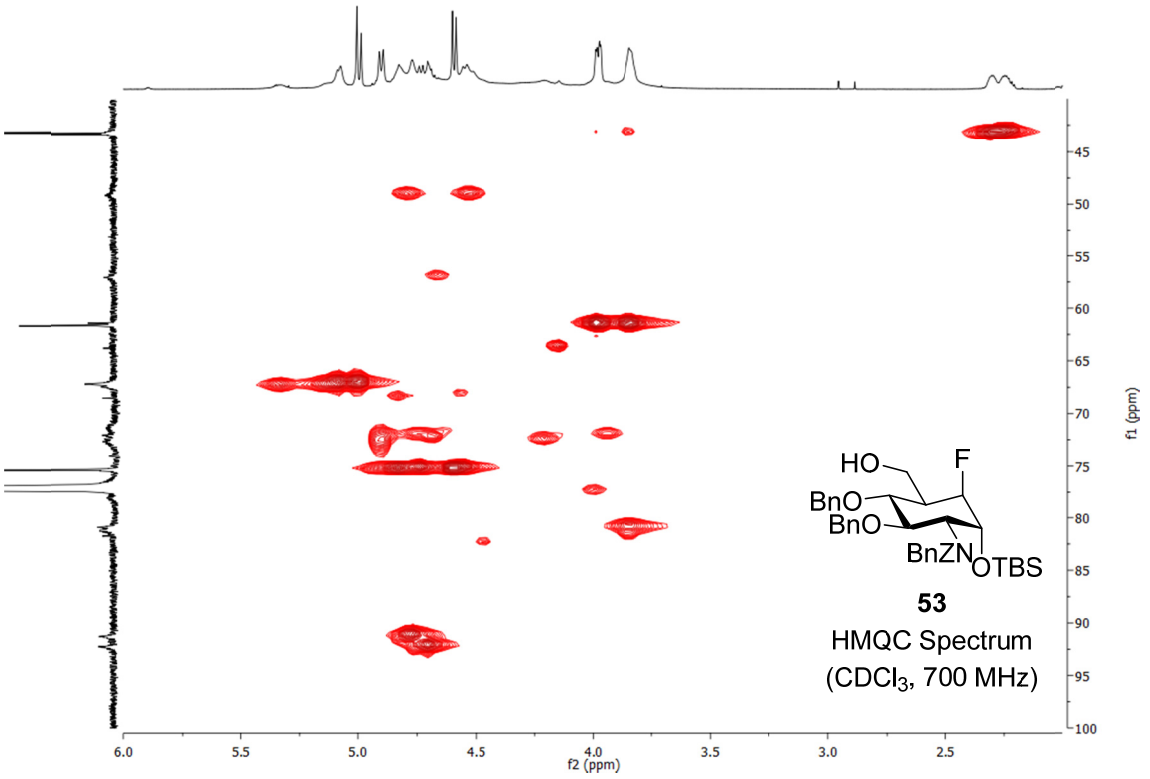
HO
F
BnO
BnO
BnZN
OTBS
53
HMQC Spectrum
(CDCl3, 700 MHz)
f2 (ppm)
f1 (ppm)

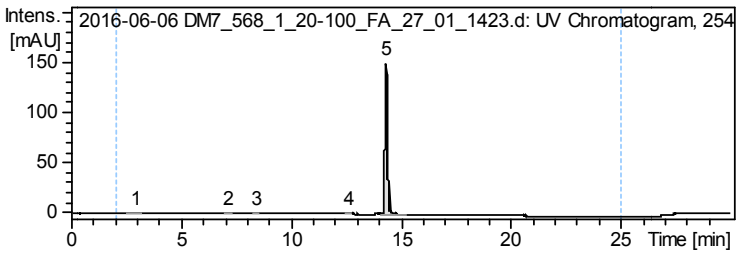

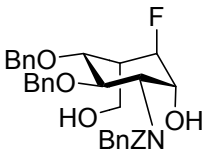

62

HPLC

ZORBAX SB-C18, 5 µm,

0.4 mL/min,

20-100% MeCN in 20 min

62

^{1}H NMR

($CDCl_3$, 500 MHz)

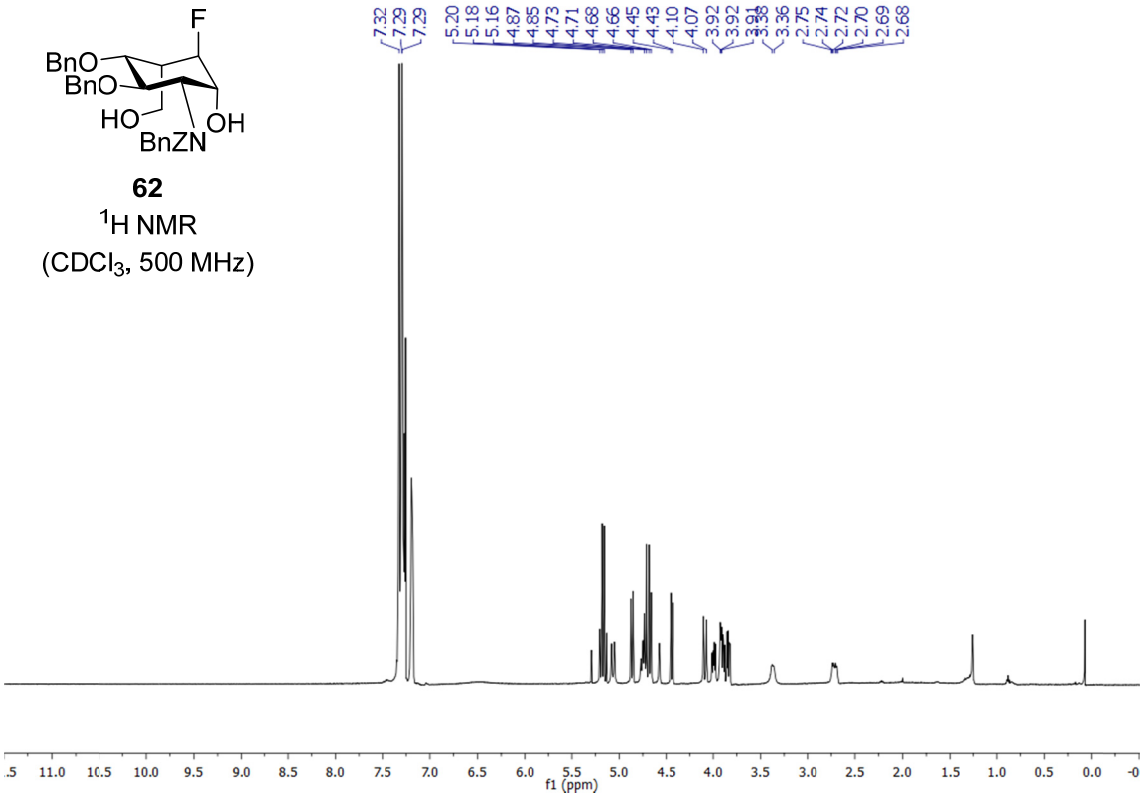

62

^{13}C NMR

($CDCl_3$, 126 MHz)

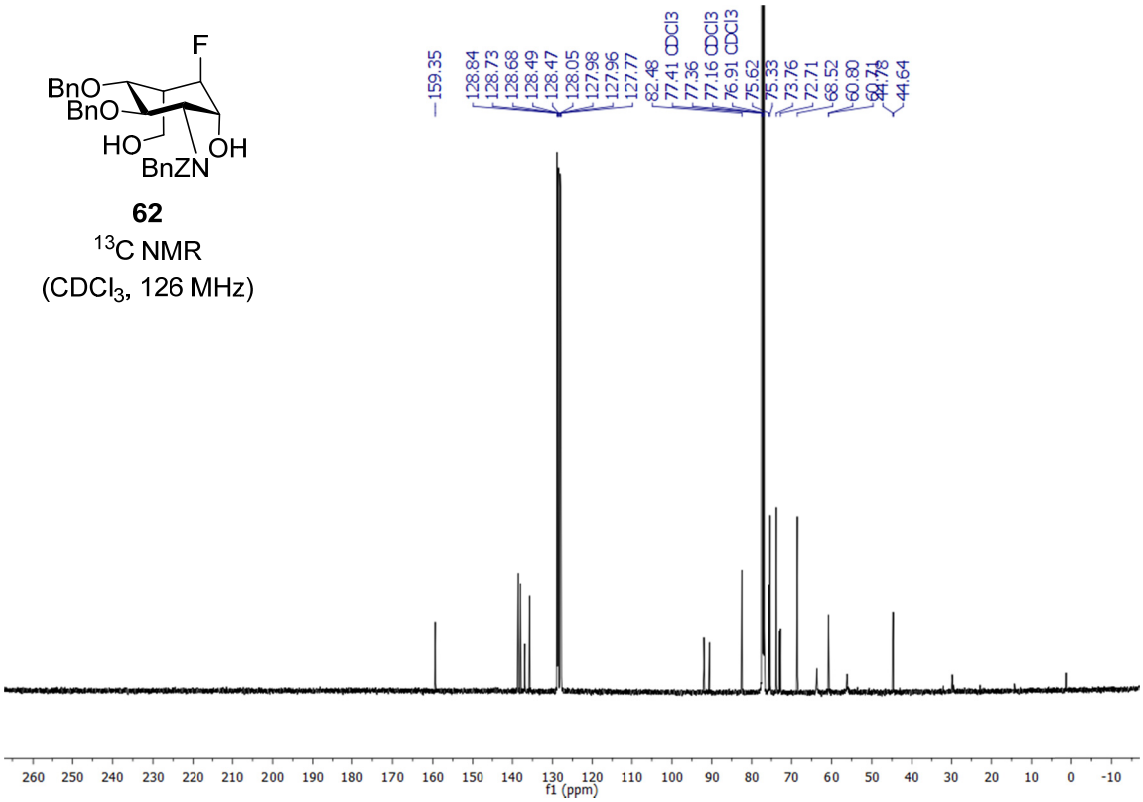

62

^{19}F NMR

($CDCl_3$, 471 MHz)

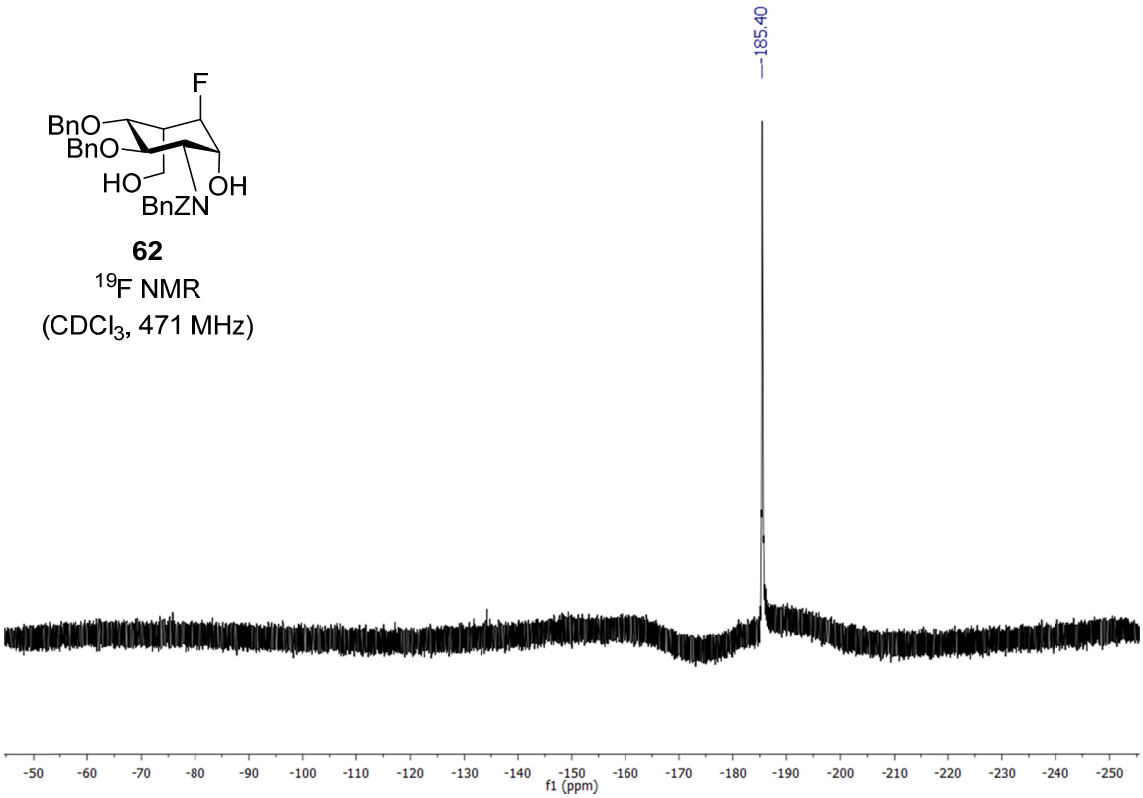

63

^{1}H NMR

(D_2O, 700 MHz)

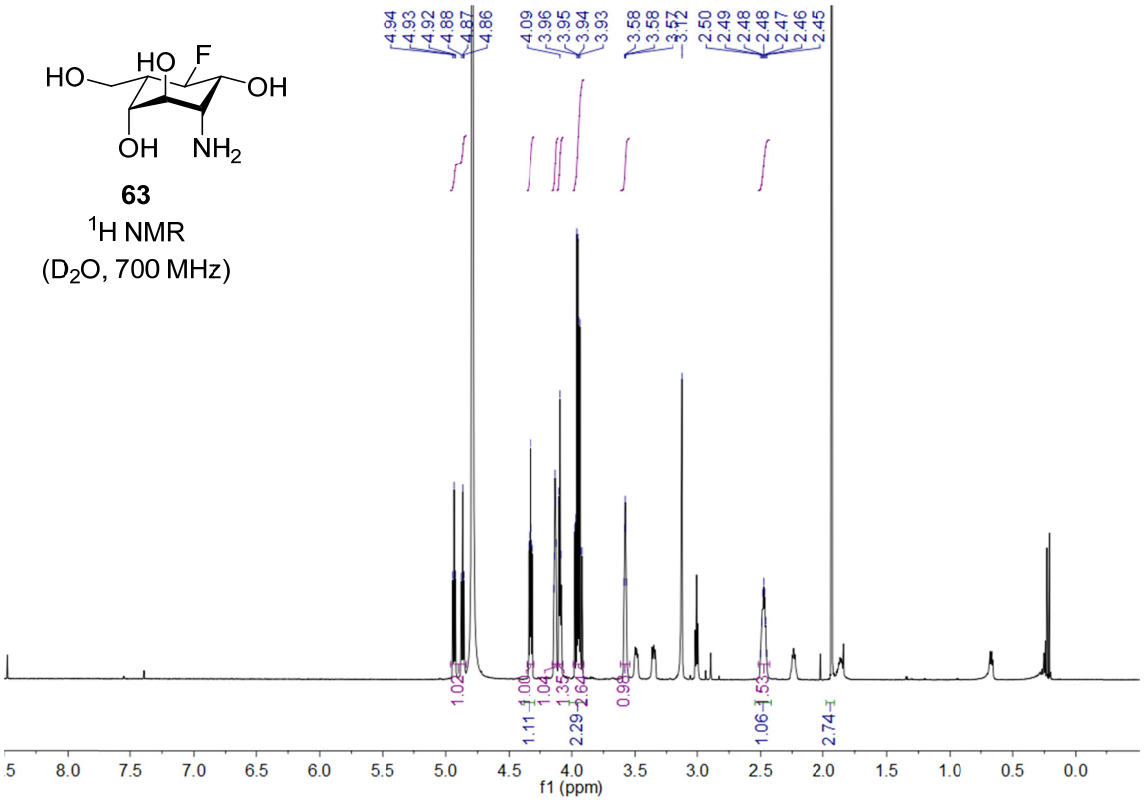

63

^{13}C NMR

(D_2O, 176 MHz)

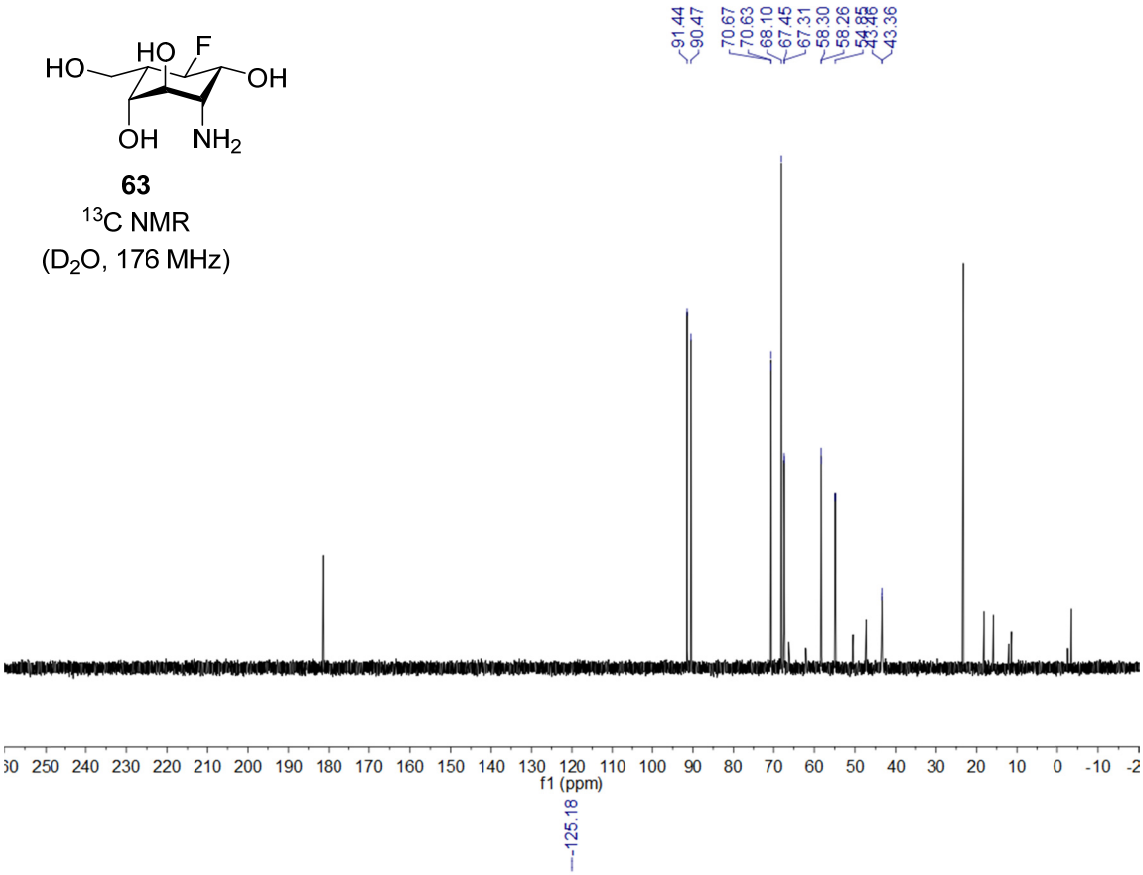

63

^{19}F NMR (^{1}H-decoupled)

(D_2O, 659 MHz)

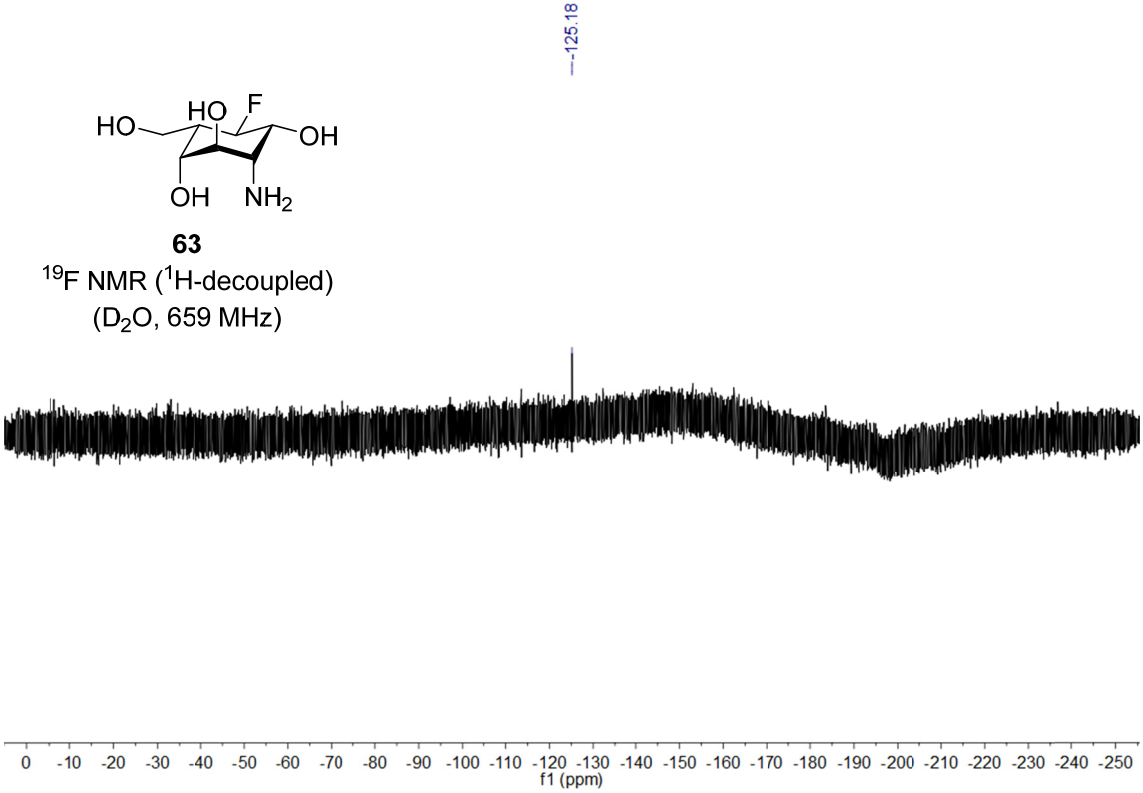

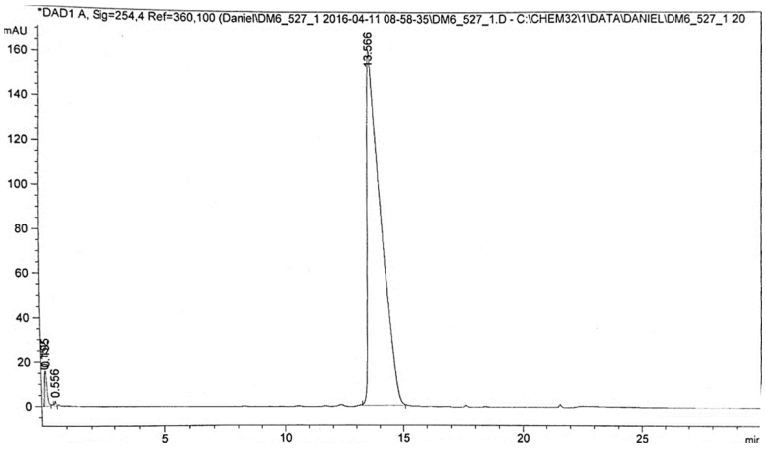

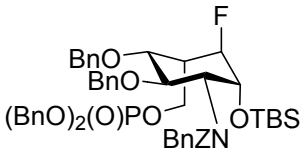

66

HPLC
Kinetex EVO C18, 2.6 µm,
0.8 mL/min,
60-80 % MeCN in 15 min

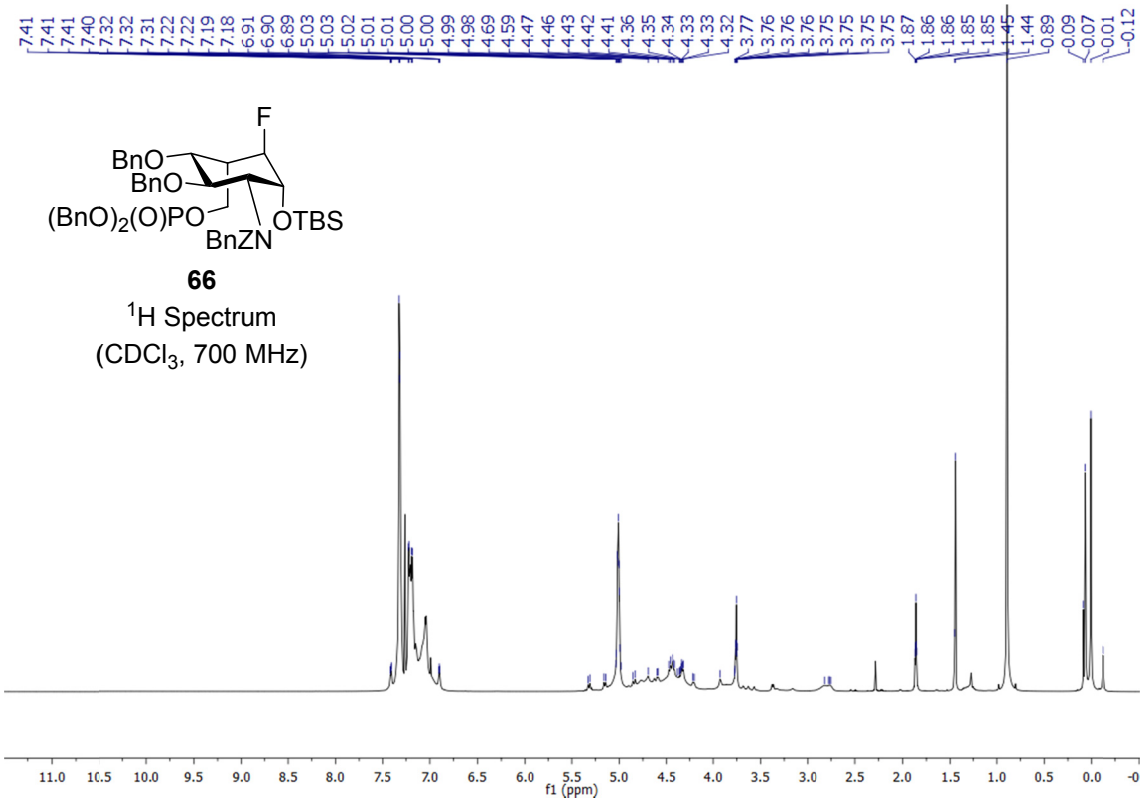

66

^{1}H Spectrum
($CDCl_3$, 700 MHz)

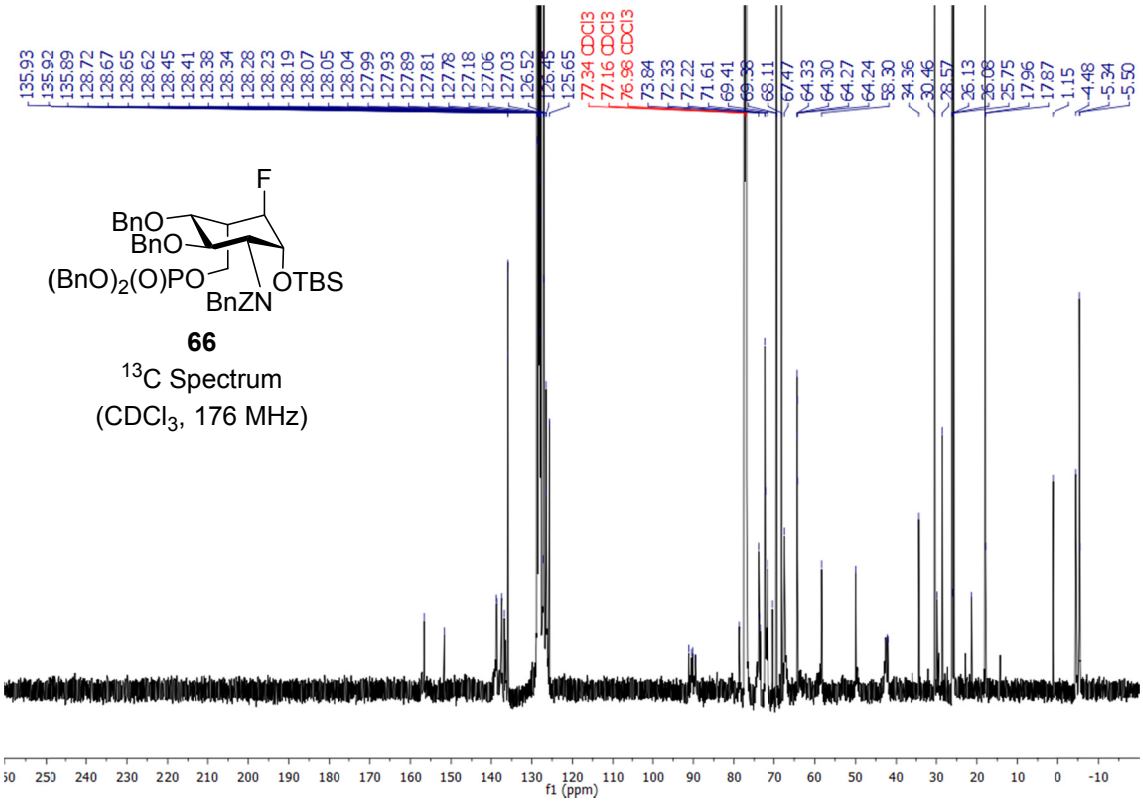

66

^{13}C Spectrum

($CDCl_3$, 176 MHz)

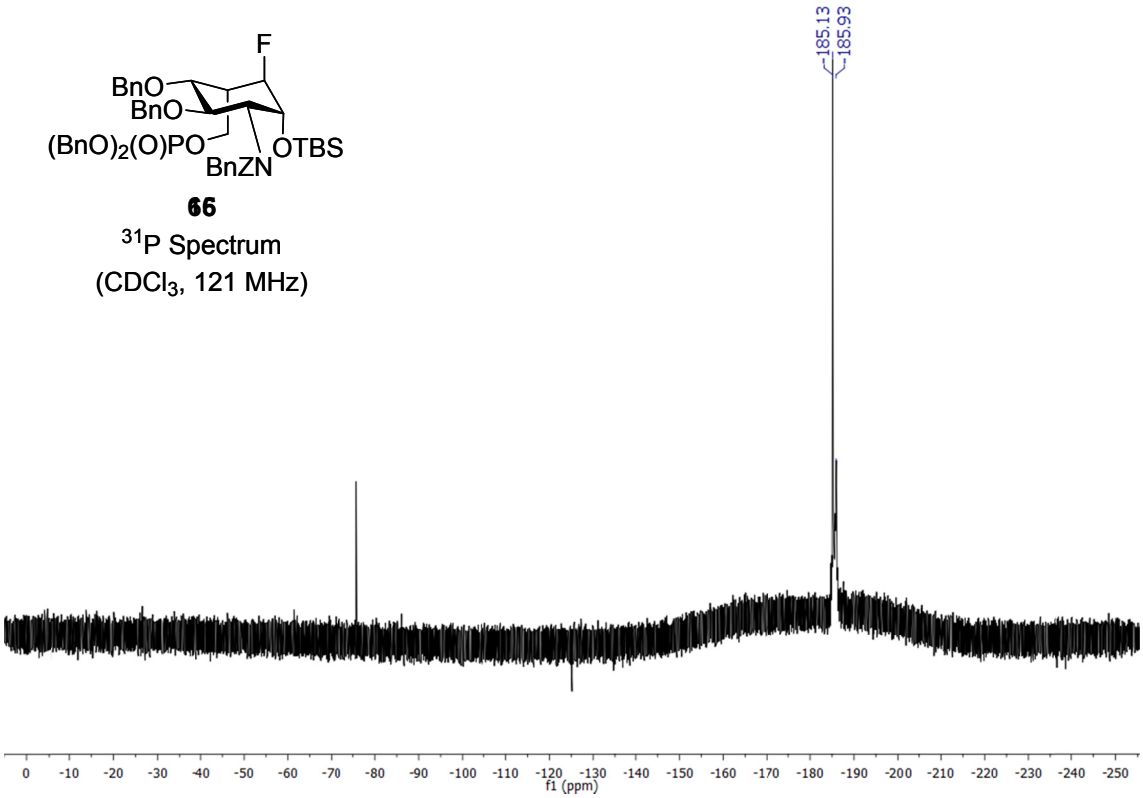

66

^{31}P Spectrum

($CDCl_3$, 121 MHz)

66

^{19}F Spectrum

($CDCl_3$, 282 MHz)

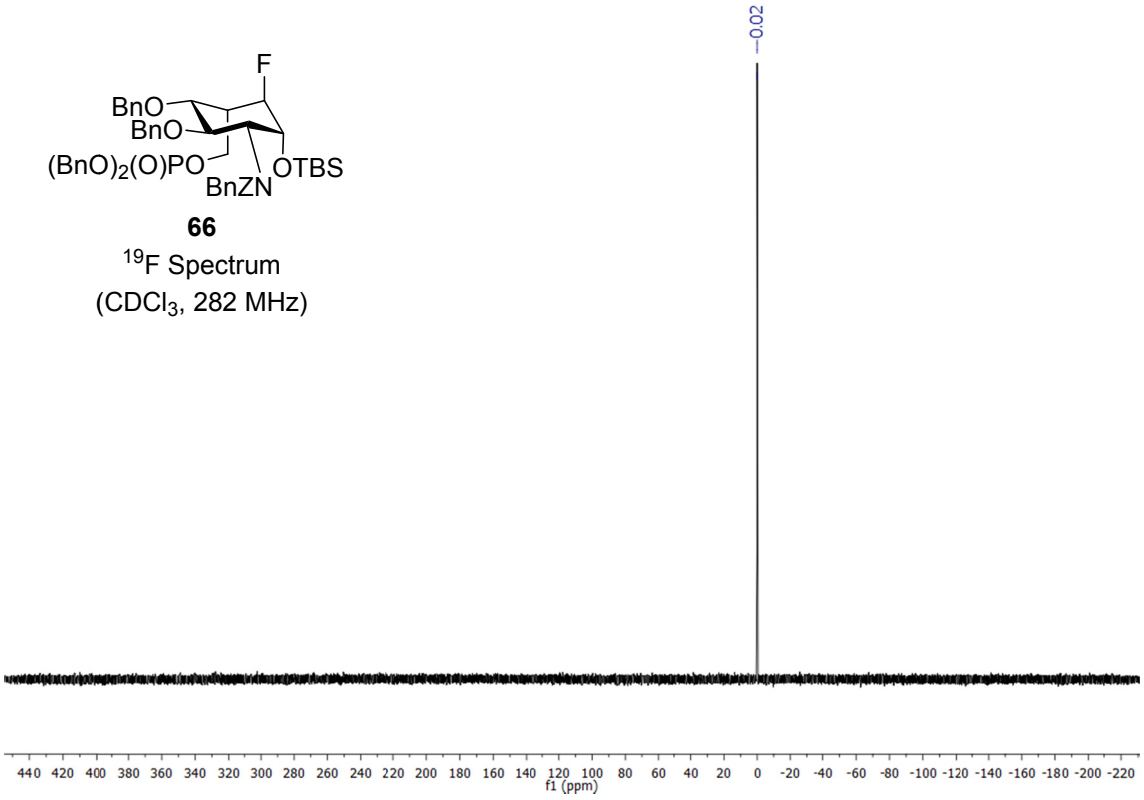

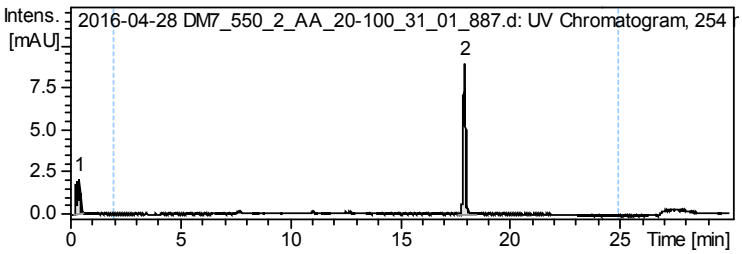

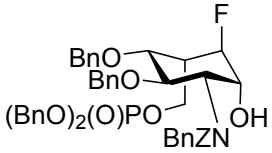

67

HPLC
ZORBAX SB-C18, 5 µm,
0.4 mL/min,
20-100% MeCN in 20 min

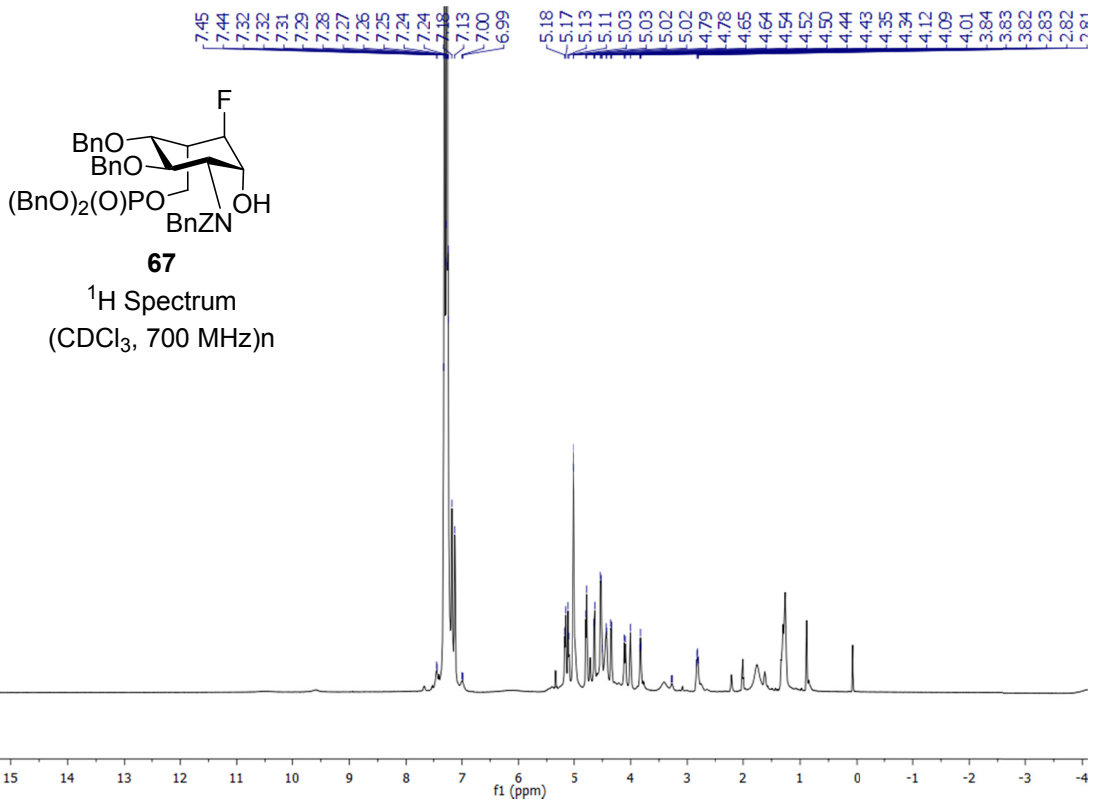

67

^{1}H Spectrum
($CDCl_3$, 700 MHz)n

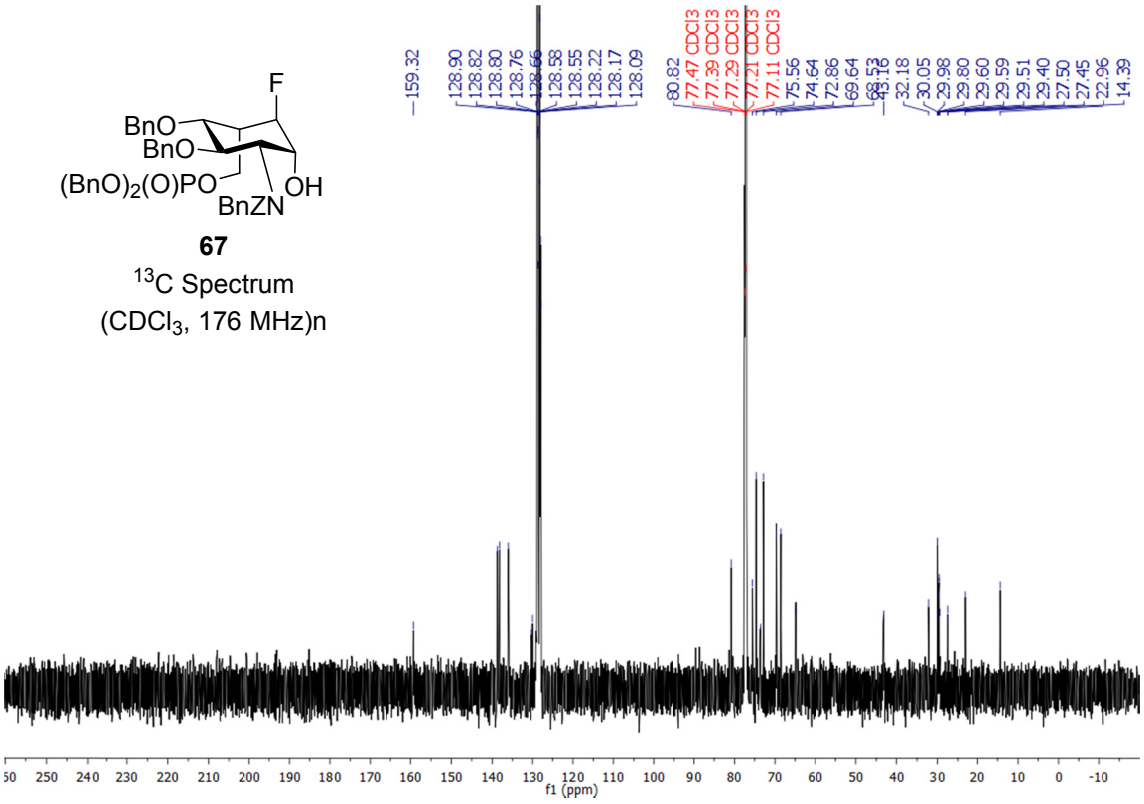

67

^{13}C Spectrum

($CDCl_3$, 176 MHz)n

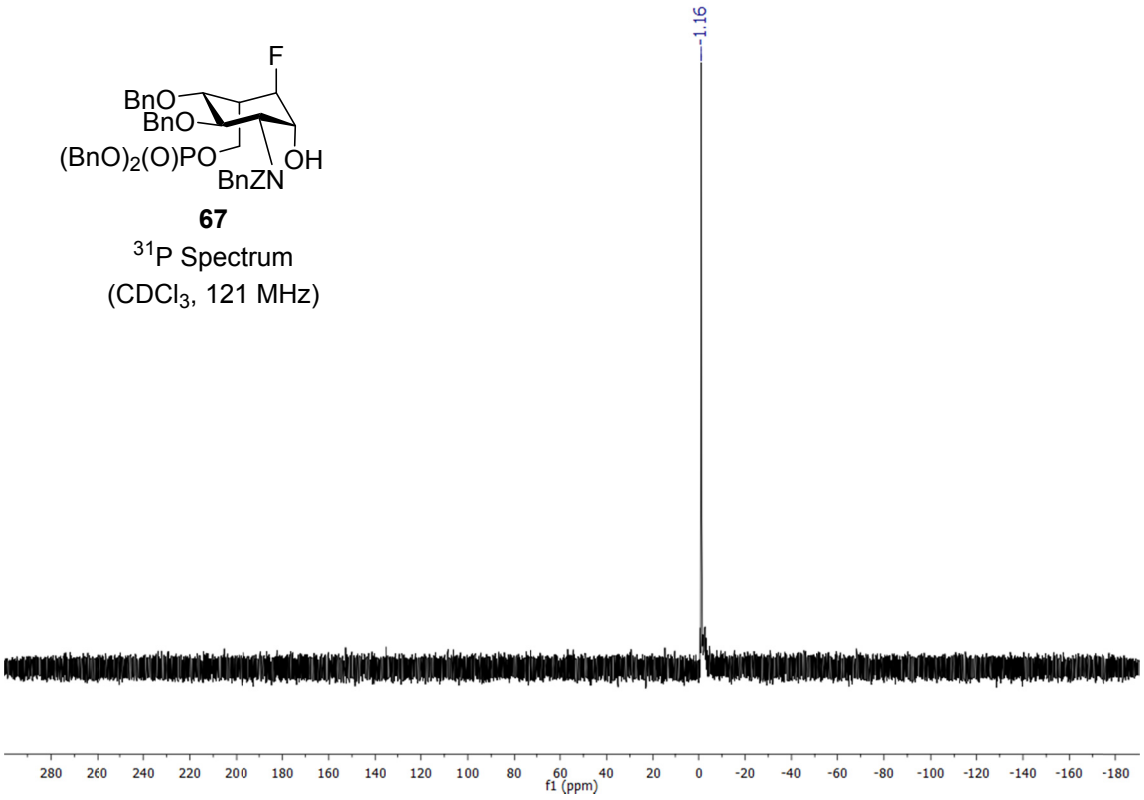

67

^{31}P Spectrum

($CDCl_3$, 121 MHz)

67

^{19}F Spectrum

($CDCl_3$, 282 MHz)

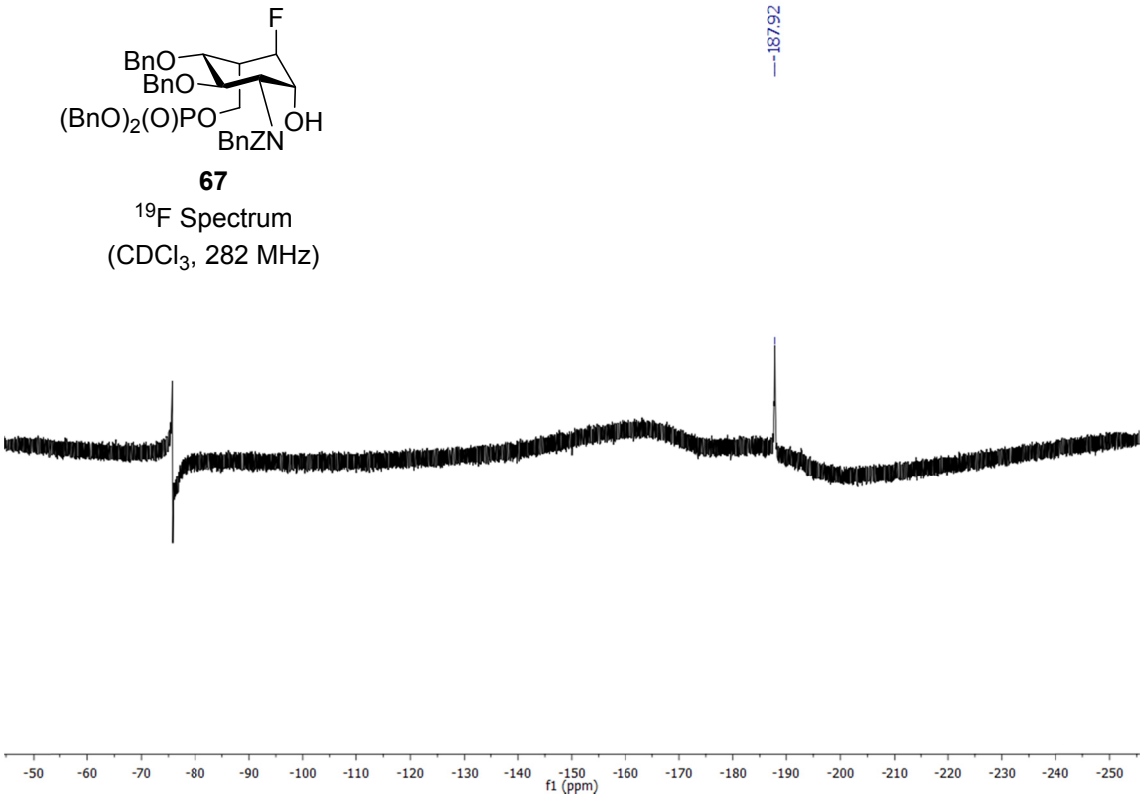

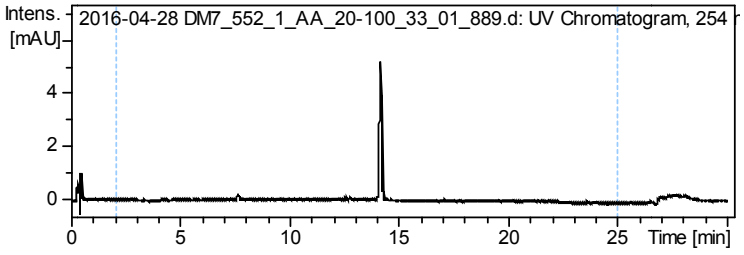

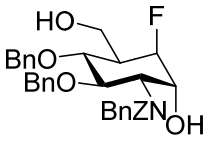

68

HPLC
ZORBAX SB-C18, 5 µm,
0.4 mL/min,
20-100 % MeCN in 20 min

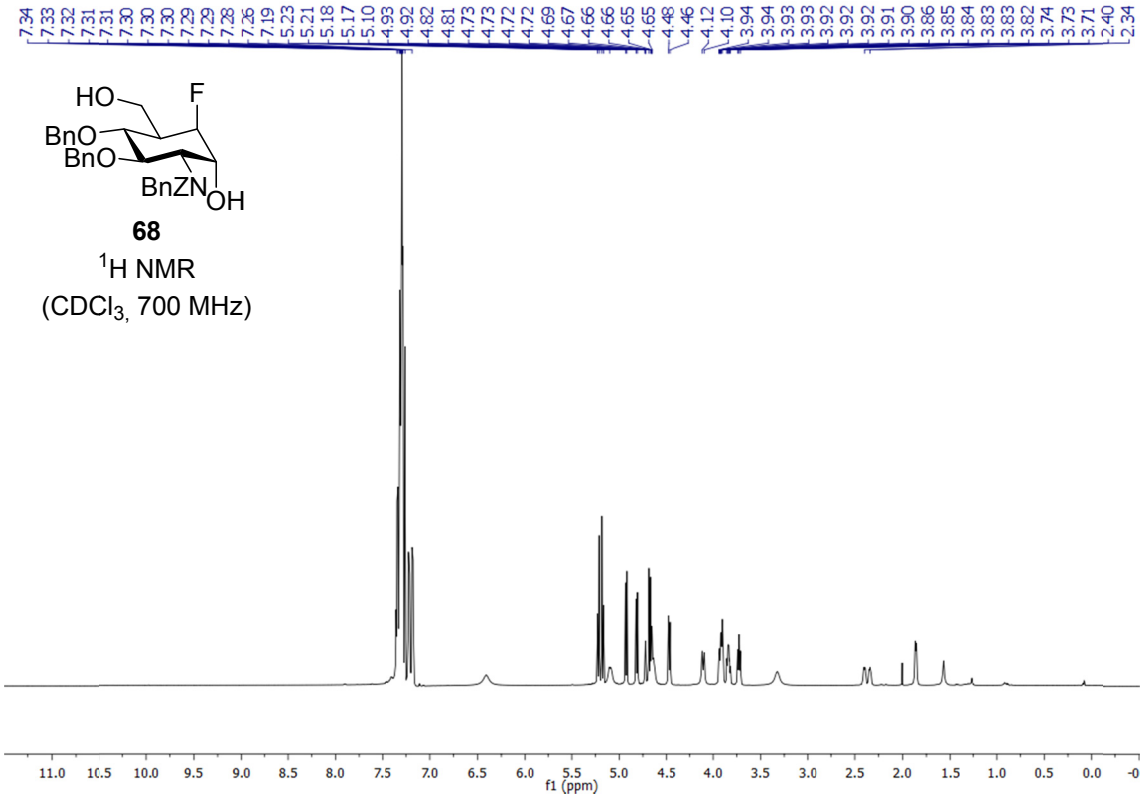

68

^{1}H NMR
($CDCl_3$, 700 MHz)

68

^{13}C NMR

($CDCl_3$, 176 MHz)

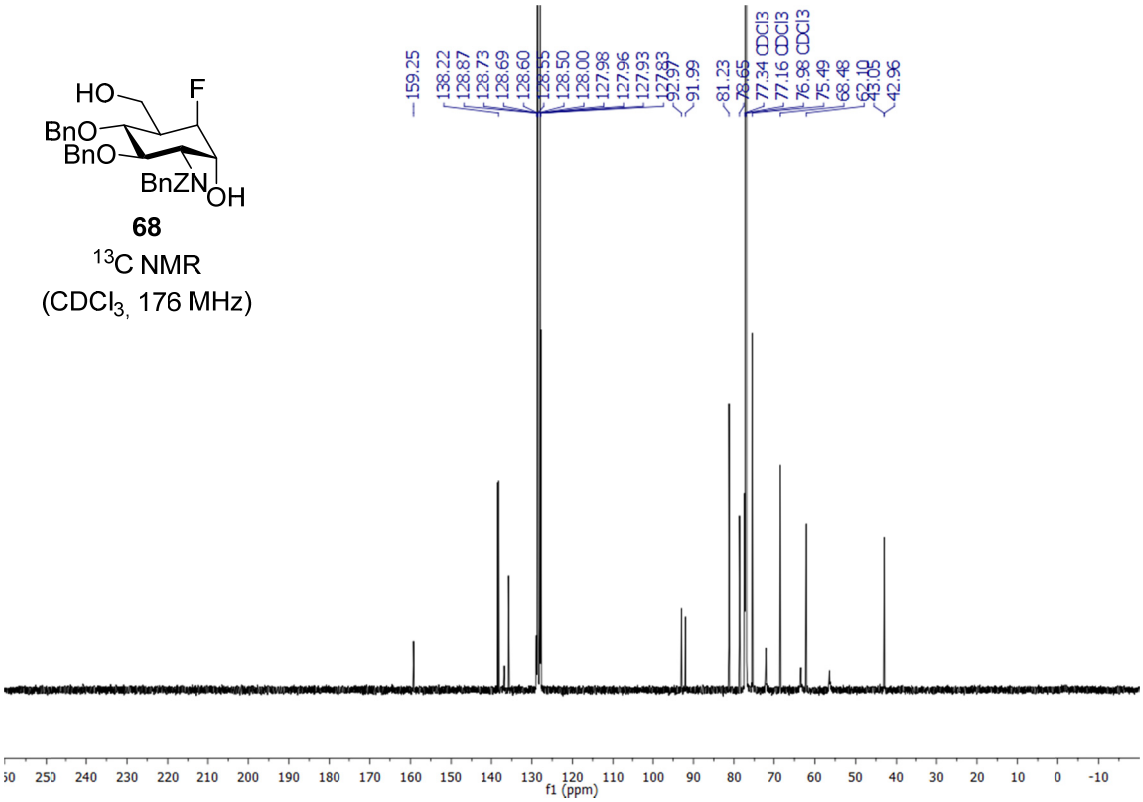

68

^{19}F NMR

($CDCl_3$, 471 MHz)

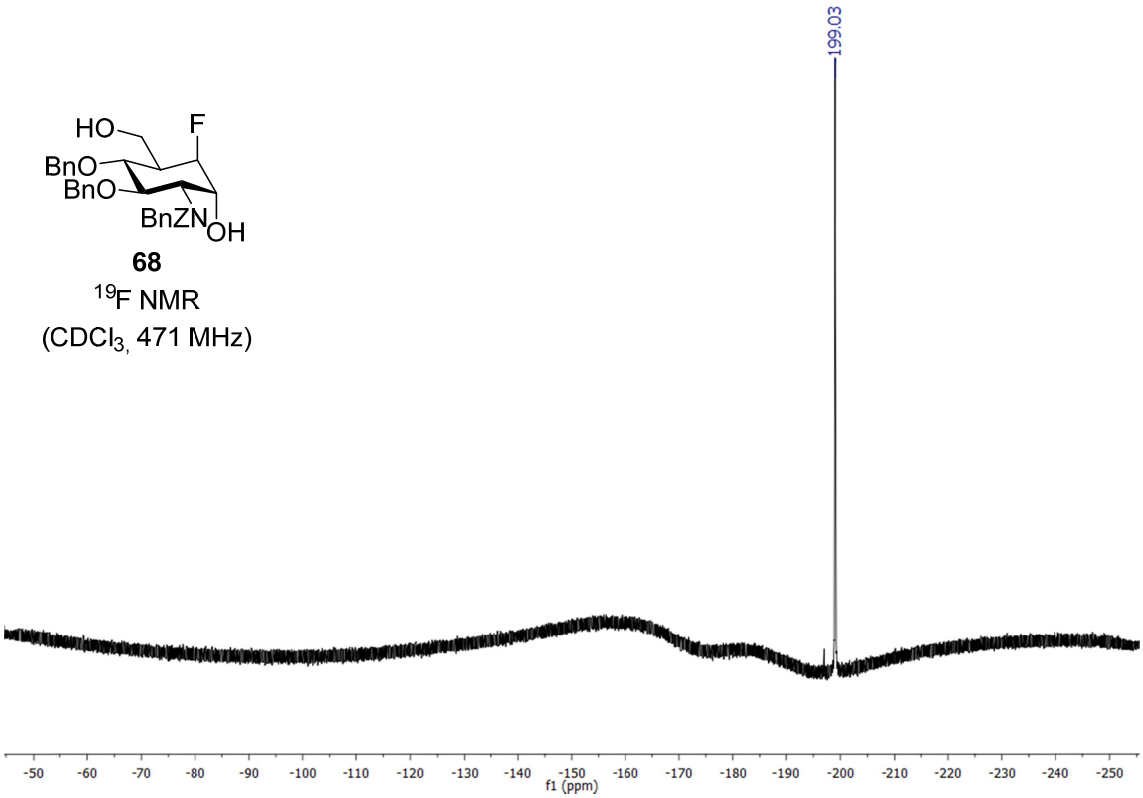

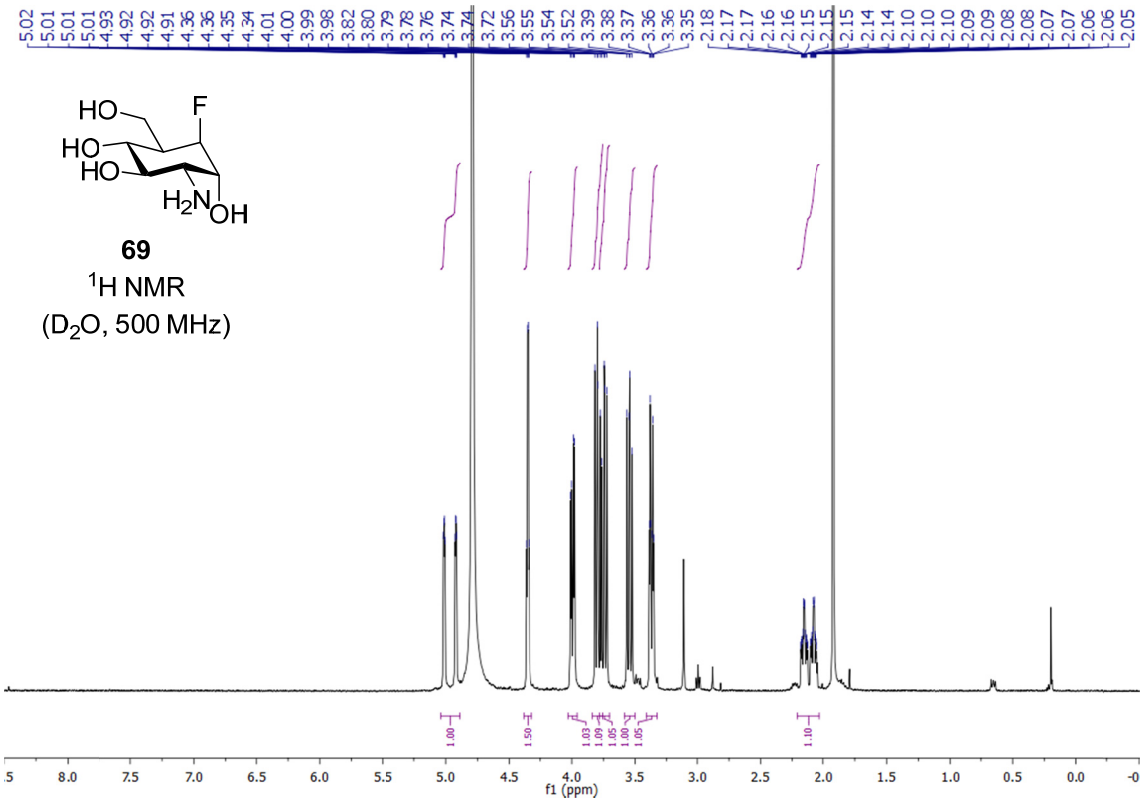
HO
F
HO
HO
H2N
OH
69
1H NMR
(D2O, 500 MHz)
f1 (ppm)

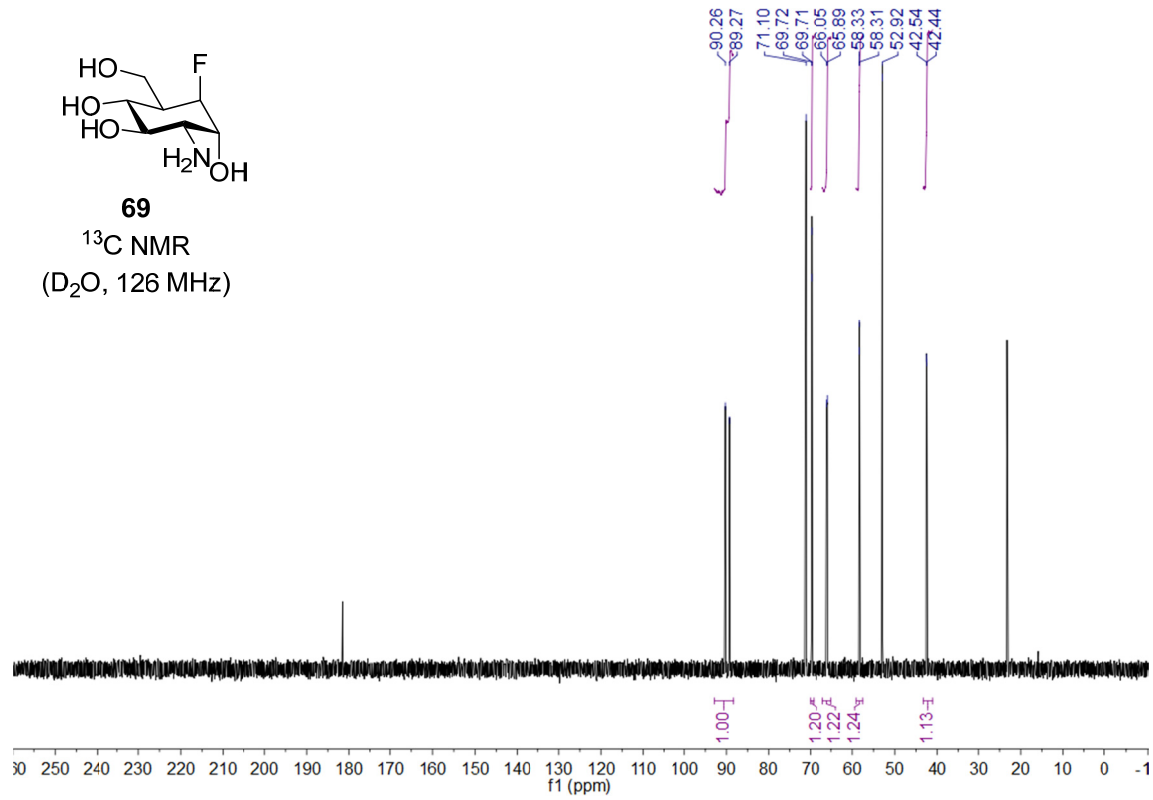
HO
F
HO
HO
H2N
OH
69
13C NMR
(D2O, 126 MHz)
f1 (ppm)

69

^{19}F NMR (^{1}H-decoupled)
(D_2O, 470 MHz)

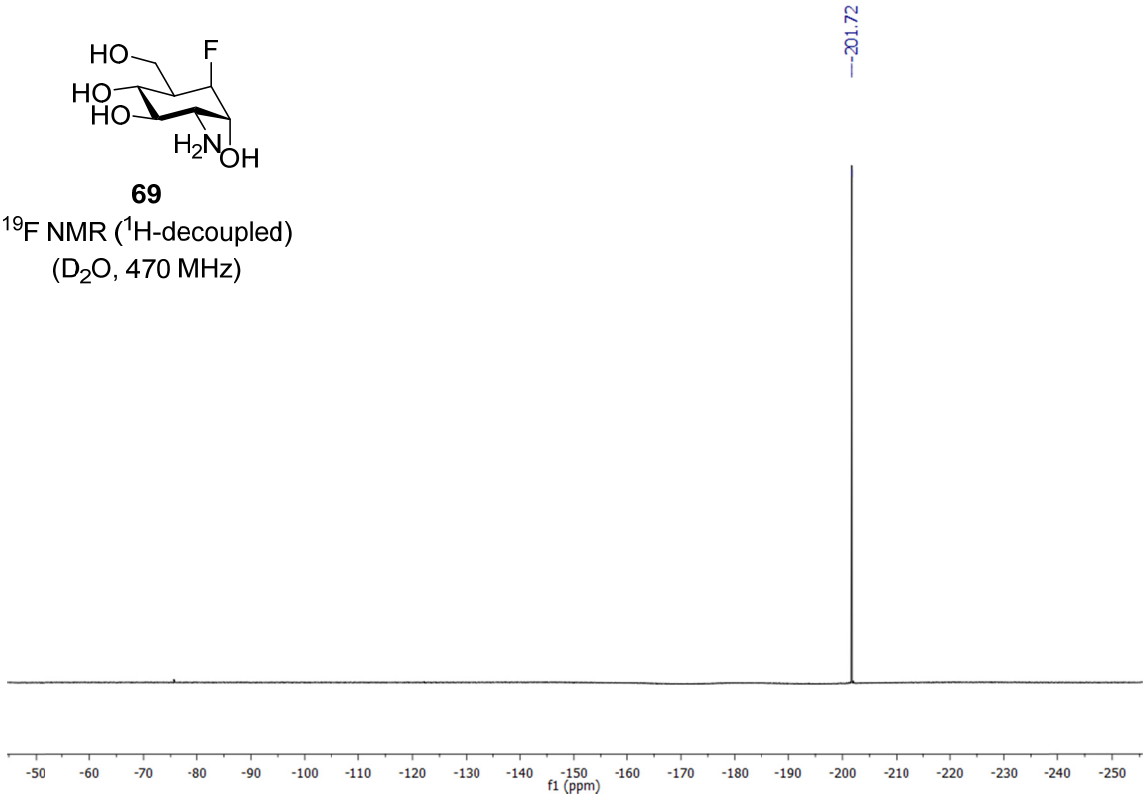

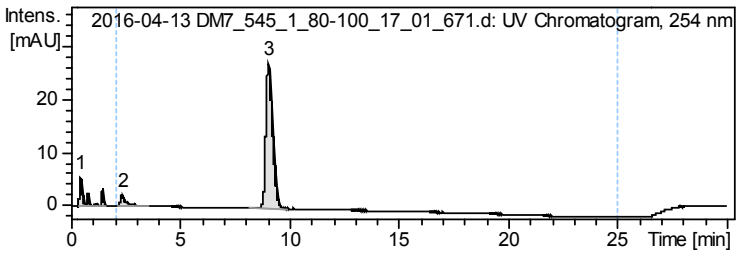

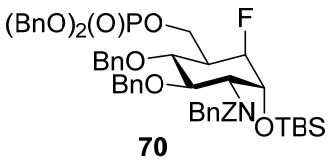

70

HPLC
ZORBAX SB-C18, 5 µm,
0.4 mL/min,
80-100 % MeCN in 20 min

70

^{1}H NMR
($CDCl_3$, 500 MHz)

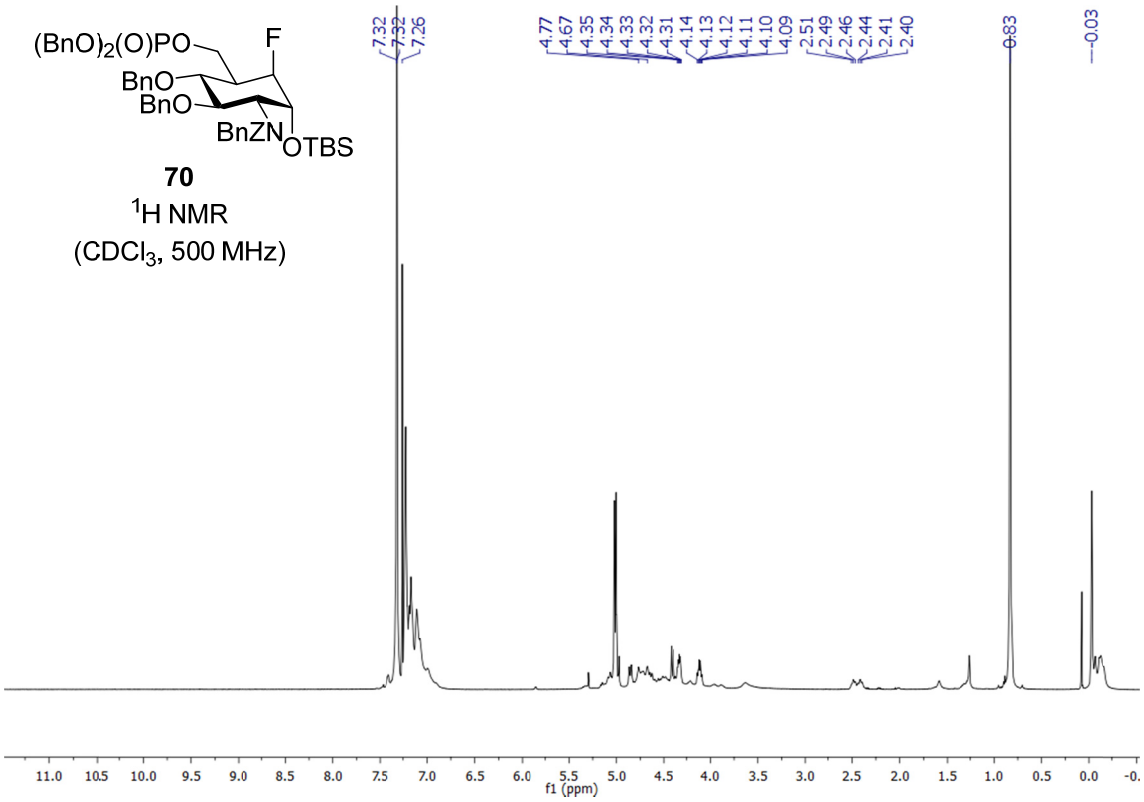

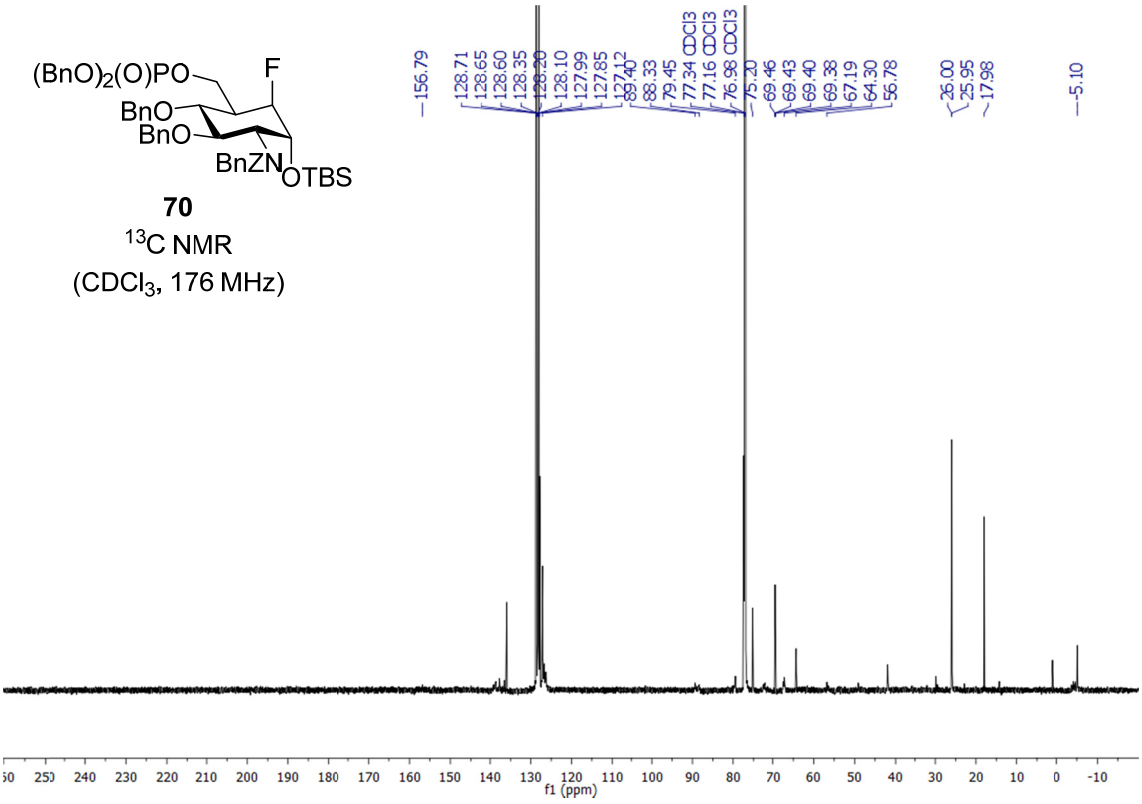

70

^{13}C NMR

($CDCl_3$, 176 MHz)

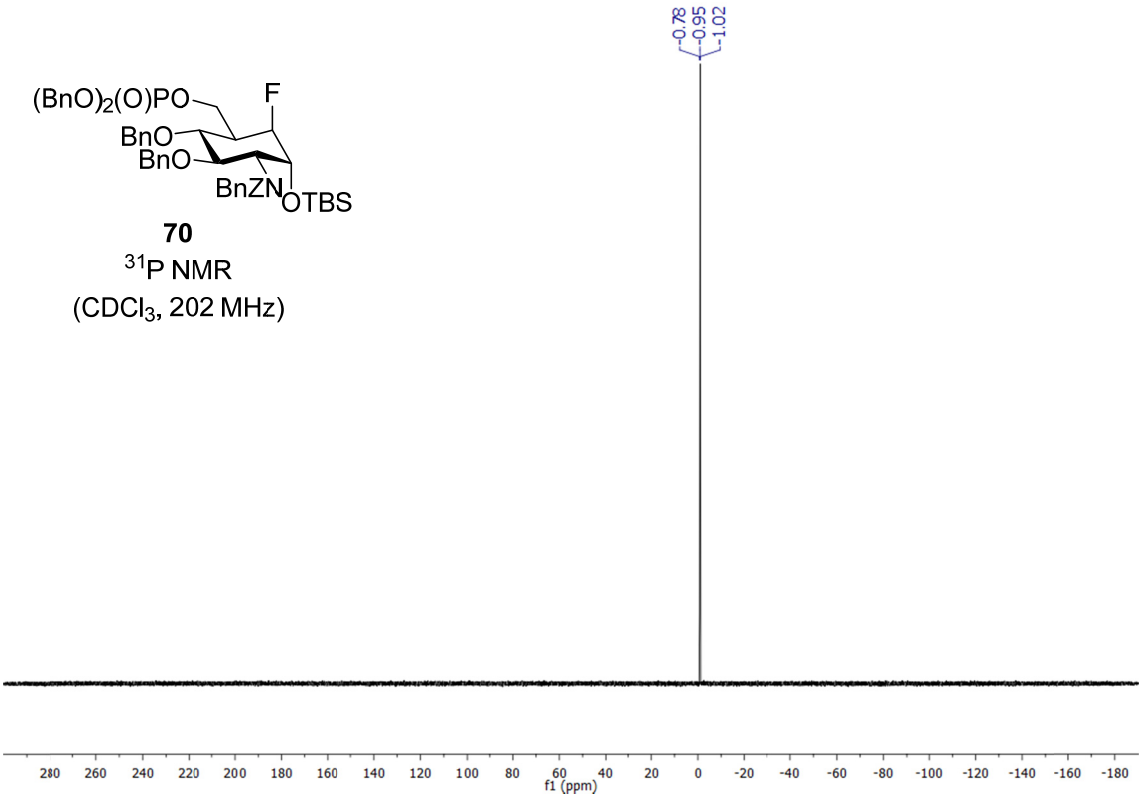

70

^{31}P NMR

($CDCl_3$, 202 MHz)

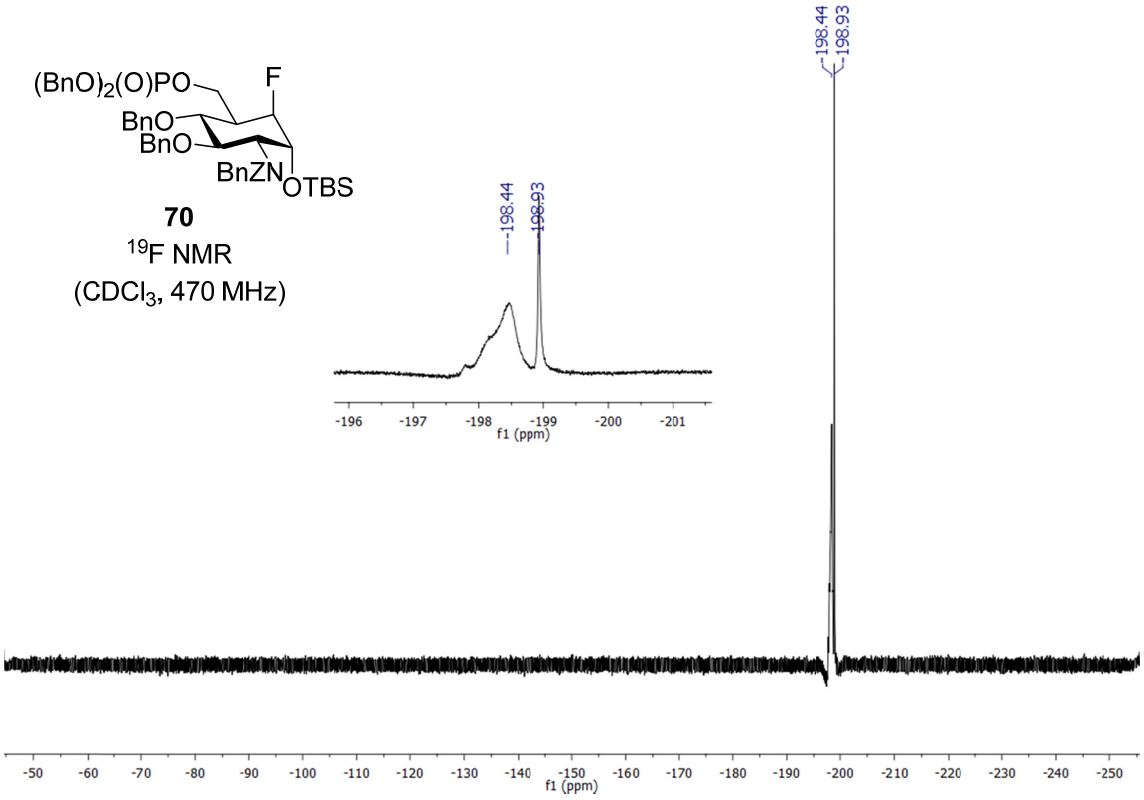
(BnO)2(O)PO
F
BnO
BnO
BnZN
OTBS
70
19F NMR
(CDCl3, 470 MHz)
198.44
198.93
-196
-197
-198
-199
-200
-201
f1 (ppm)
-50
-60
-70
-80
-90
-100
-110
-120
-130
-140
-150
-160
-170
-180
-190
-200
-210
-220
-230
-240
-250
f1 (ppm)

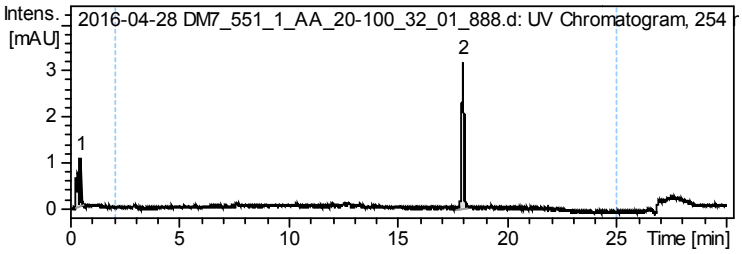

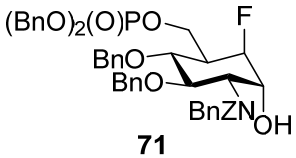

71

HPLC

ZORBAX SB-C18, 5 µm,
0.4 mL/min,
20-100 % MeCN in 20 min

71

^{1}H NMR

($CDCl_3$, 700 MHz)

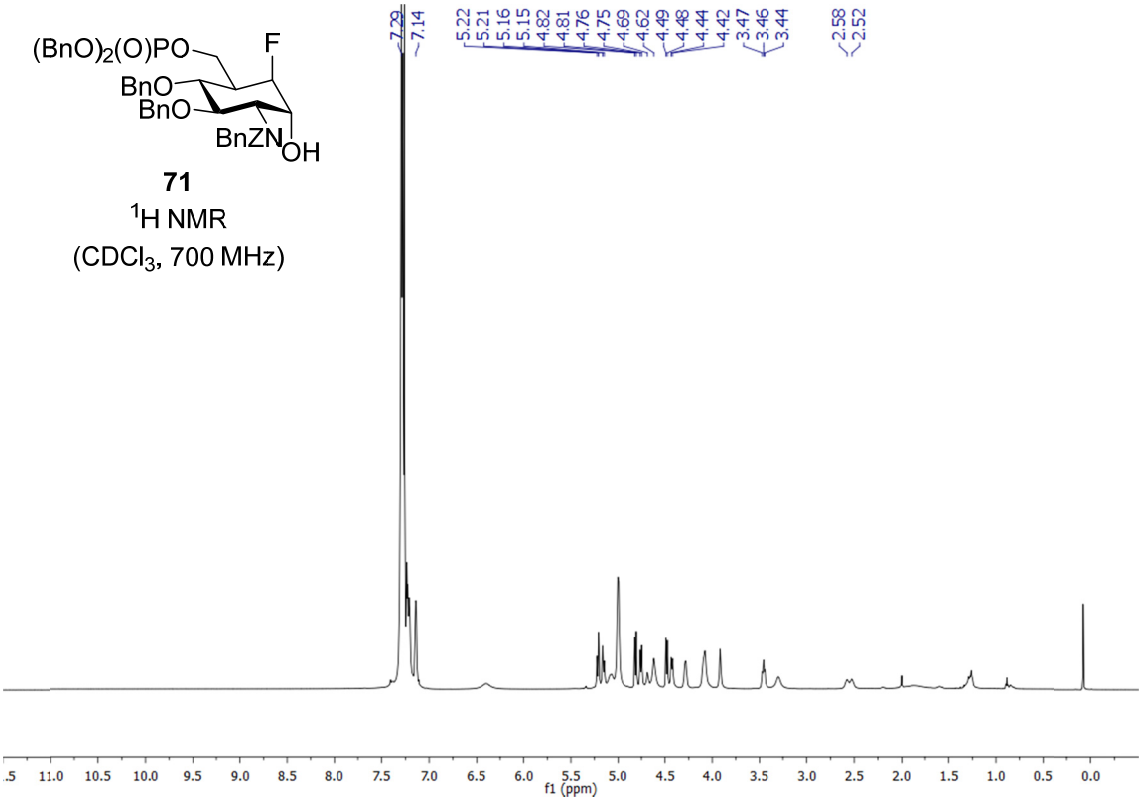

71

^{13}C NMR

($CDCl_3$, 176 MHz)

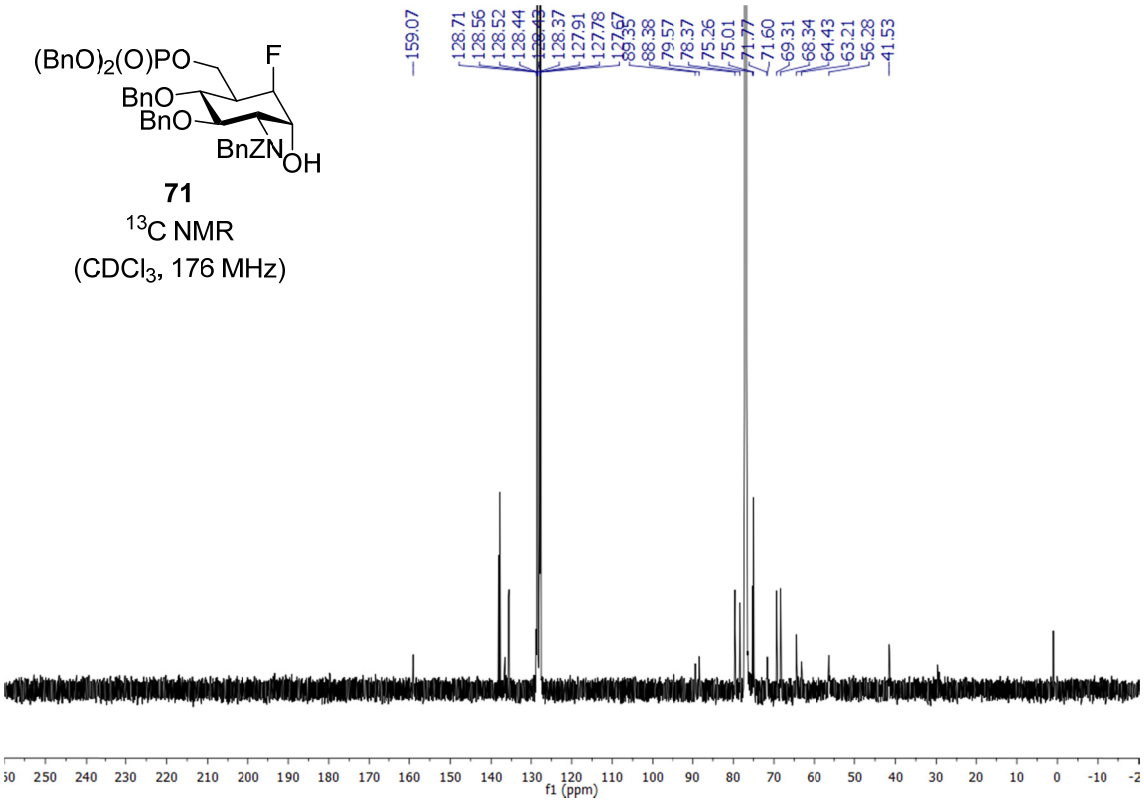

71

^{31}P NMR

($CDCl_3$, 202 MHz)

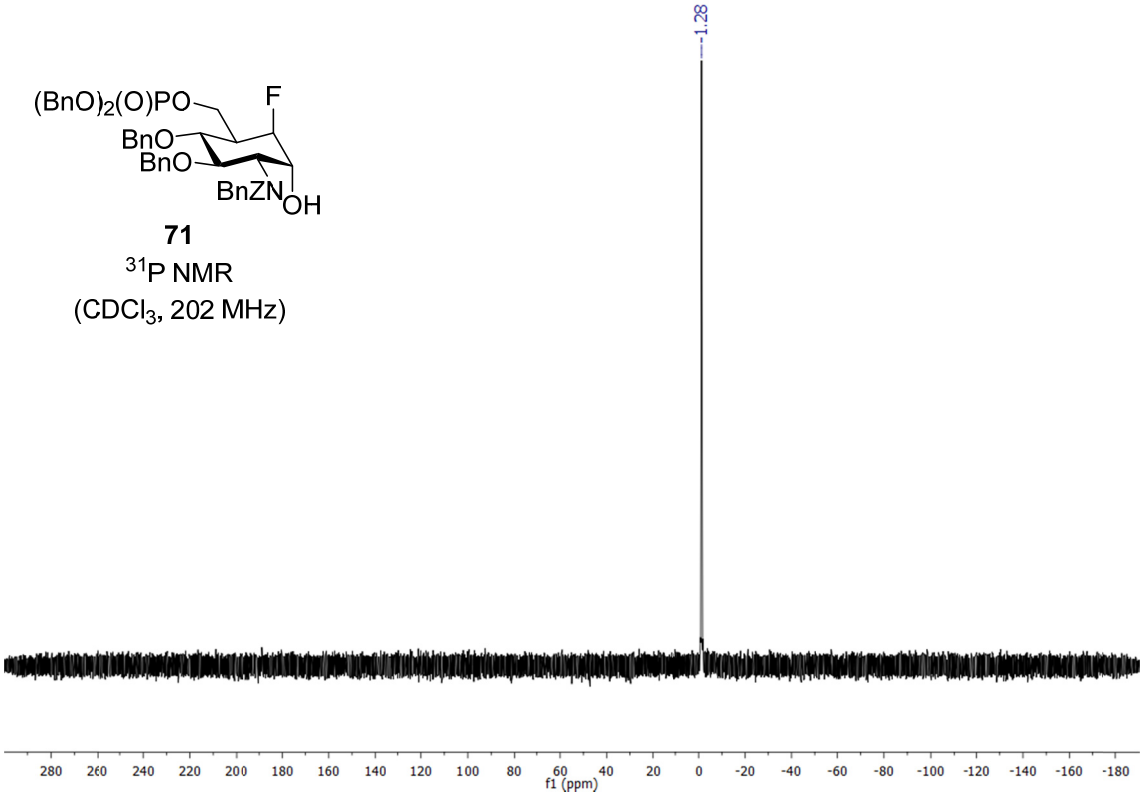

71

^{19}F NMR

($CDCl_3$, 471 MHz)

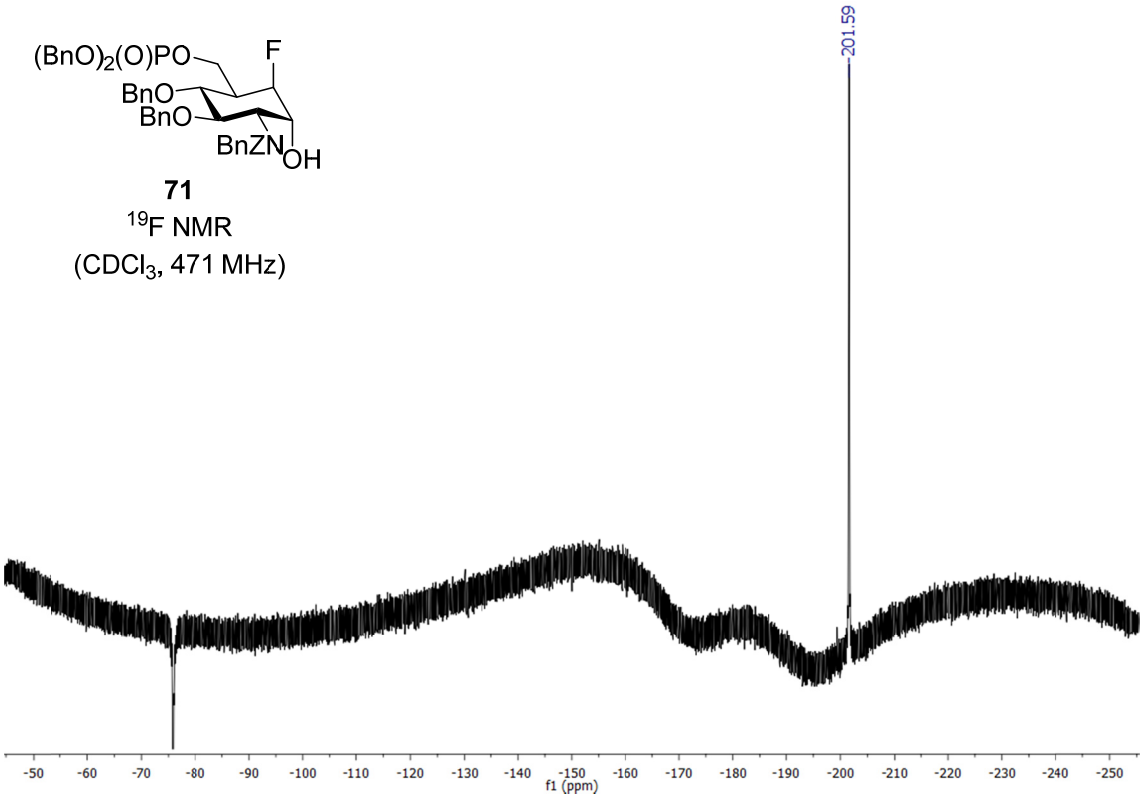

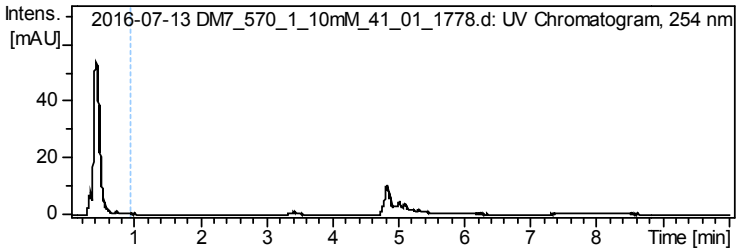

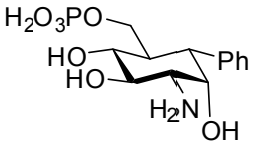

72

HPLC

ZORBAX SB-C18

50x2.3mm C18, 5 µm,

0.4 mL/min,

0-40 % MeCN in 20 min

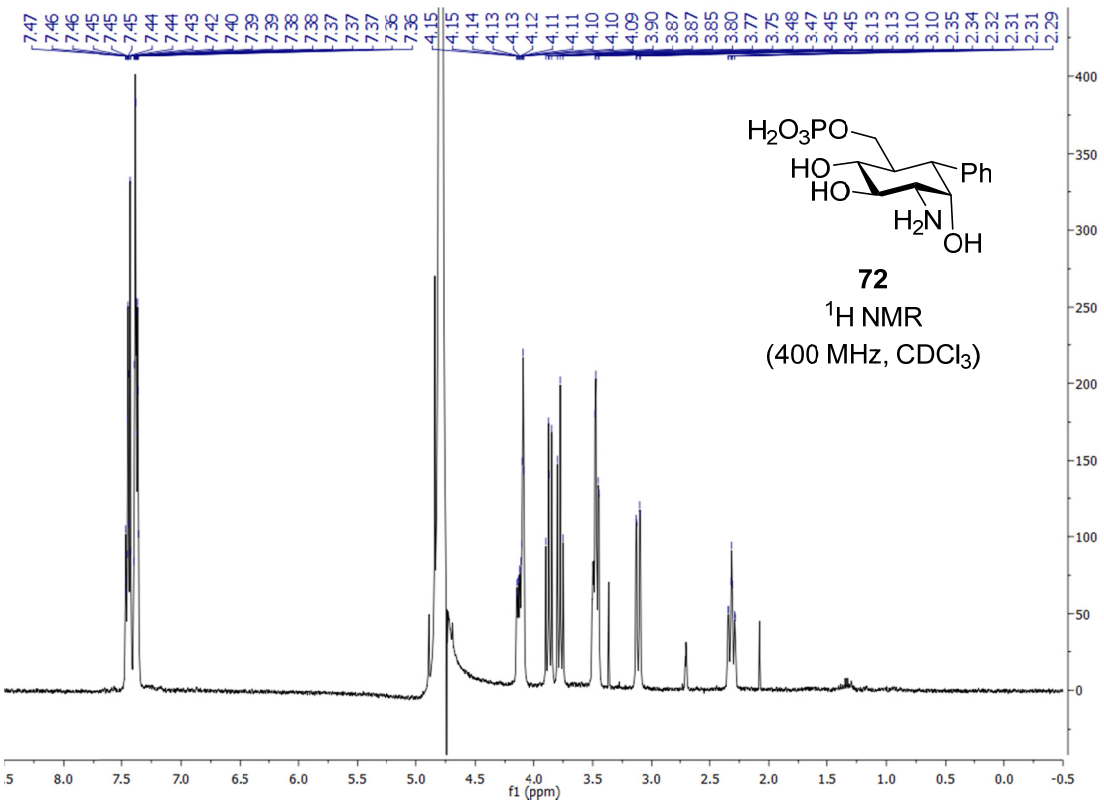

72

^{1}H NMR

(400 MHz, $CDCl_3$)

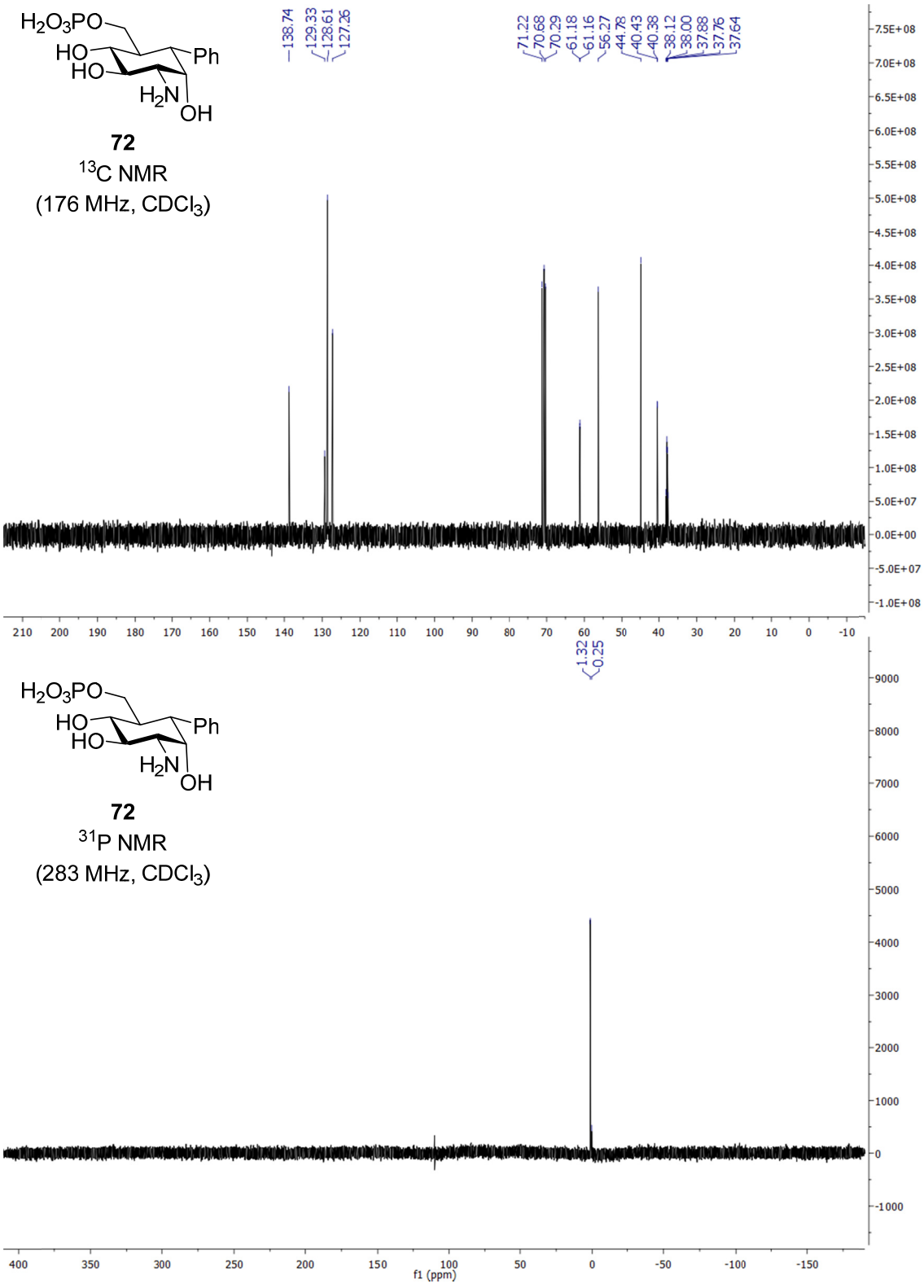
H_2O_3PO
HO
HO
Ph
H_2N
OH
72
^{13}C NMR
(176 MHz, $CDCl_3$)
138.74
129.33
128.61
127.26
71.22
70.68
70.29
61.18
61.16
56.27
44.78
40.43
40.38
38.12
38.00
37.88
37.76
37.64
H_2O_3PO
HO
HO
Ph
H_2N
OH
72
^{31}P NMR
(283 MHz, $CDCl_3$)
1.32
0.25
f1 (ppm)

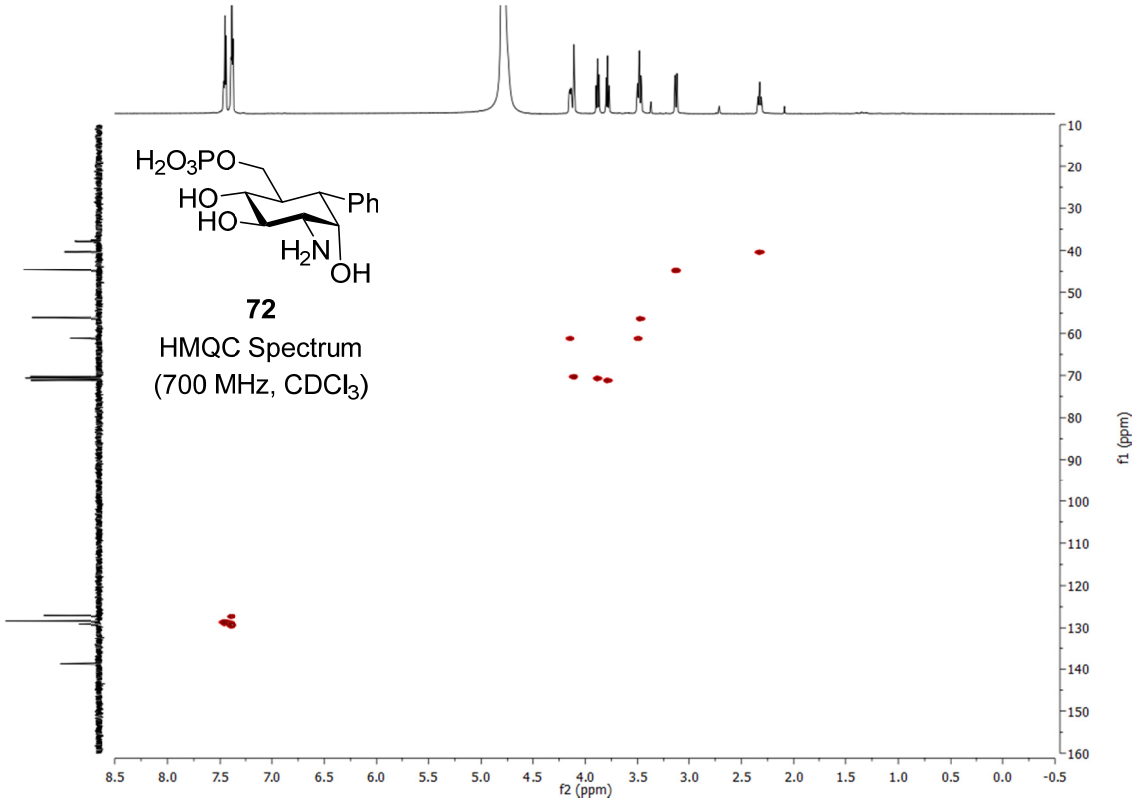
H_2O_3PO
HO
HO
Ph
H_2N
OH
72
HMQC Spectrum
(700 MHz, $CDCl_3$)
f2 (ppm)
f1 (ppm)

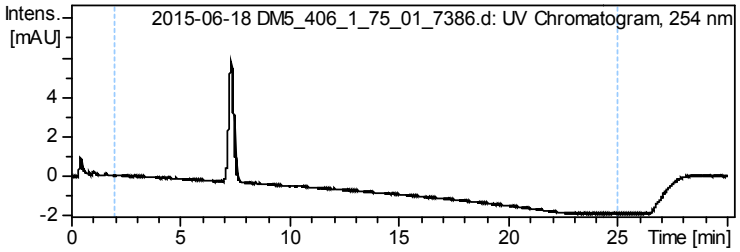

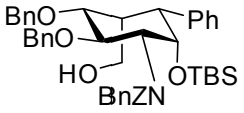

73

HPLC

ZORBAX SB-C18

50x2.3mm C18, 5 µm,

0.4 mL/min,

80-100 % MeCN in 20 min

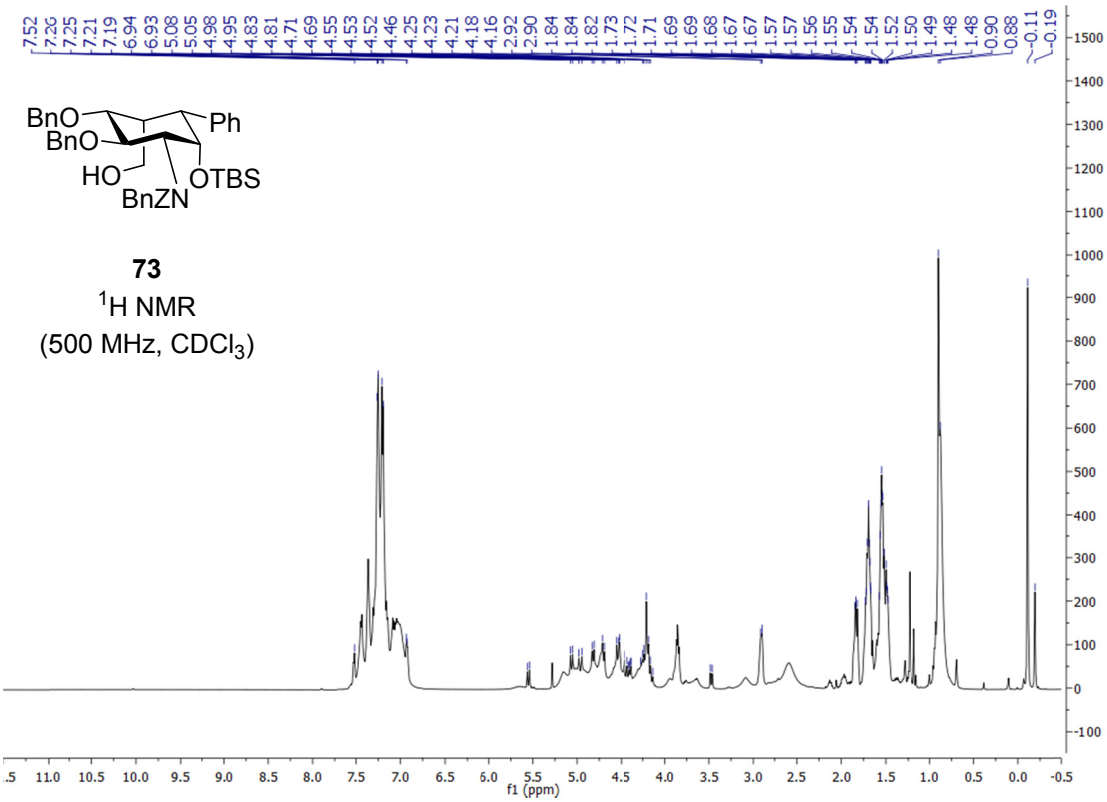

73

^{1}H NMR

(500 MHz, $CDCl_3$)

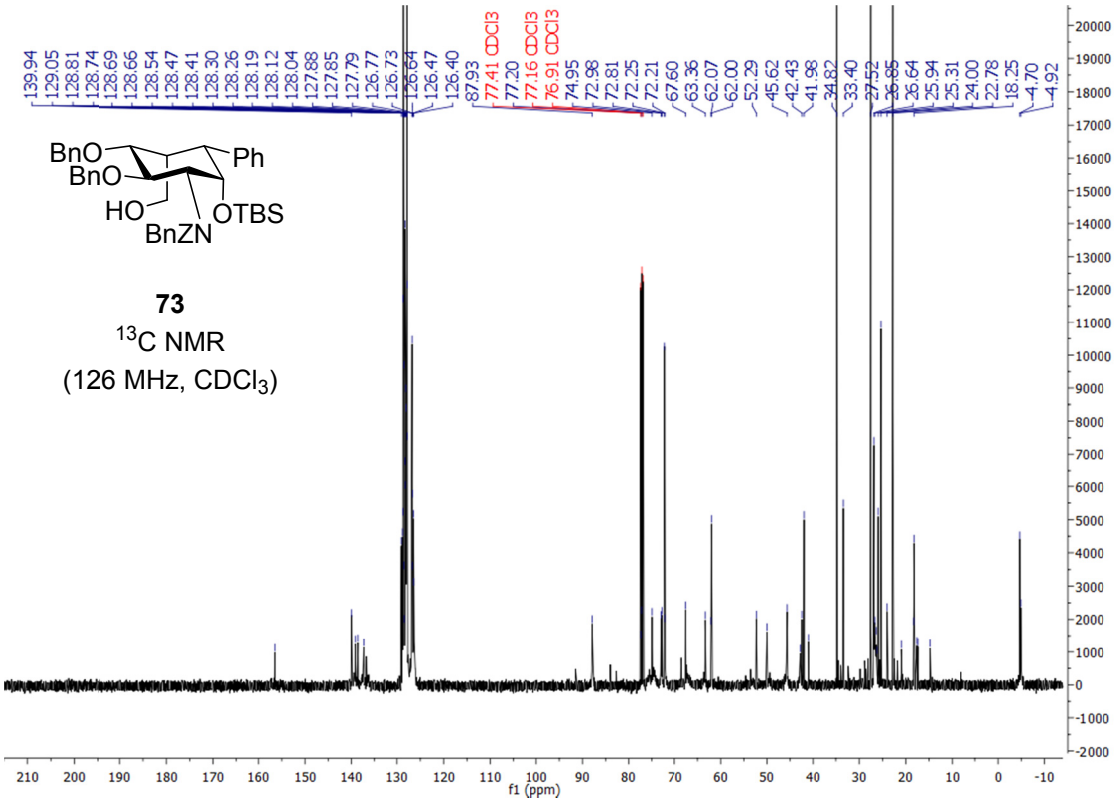
BnO
BnO
Ph
HO
OTBS
BnZN
73
13C NMR
(126 MHz, CDCl3)
f1 (ppm)

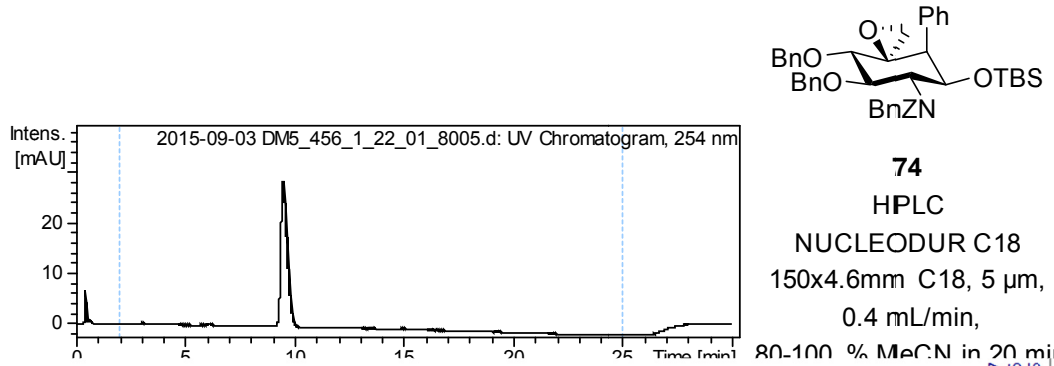

74

HPLC

NUCLEODUR C18

150x4.6mm C18, 5 µm,

0.4 mL/min,

80-100 % MeCN in 20 min

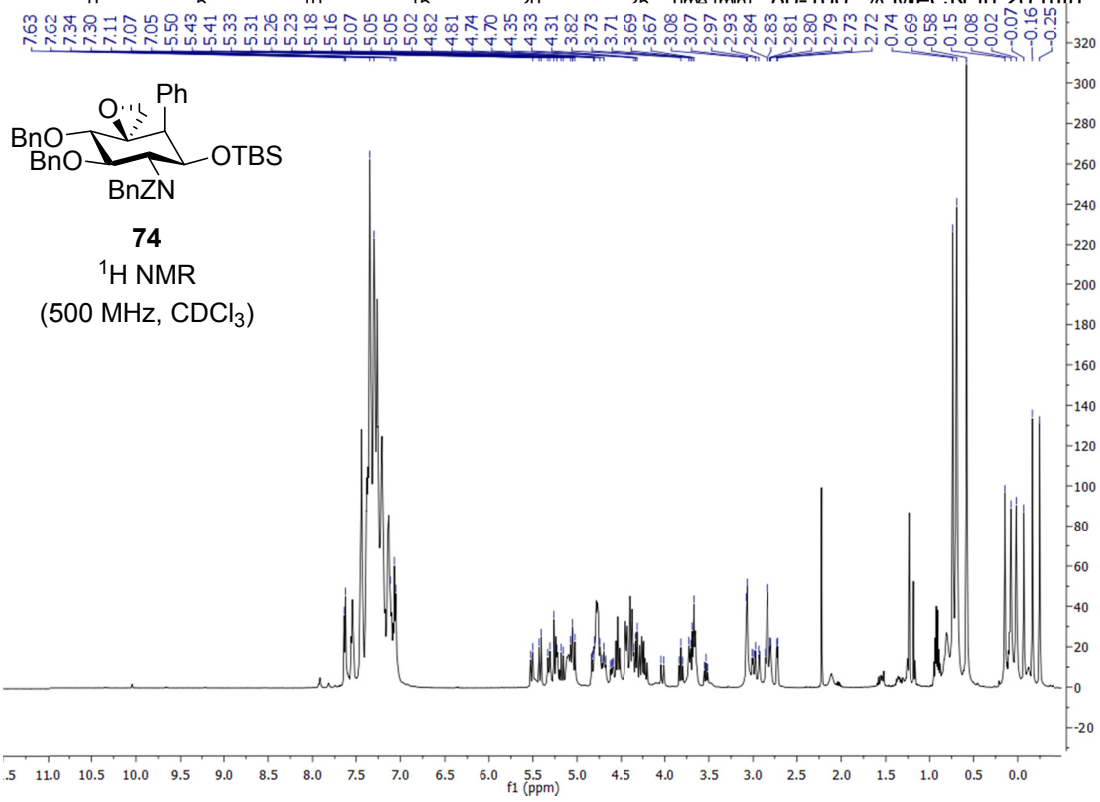

74

^{1}H NMR

(500 MHz, $CDCl_3$)

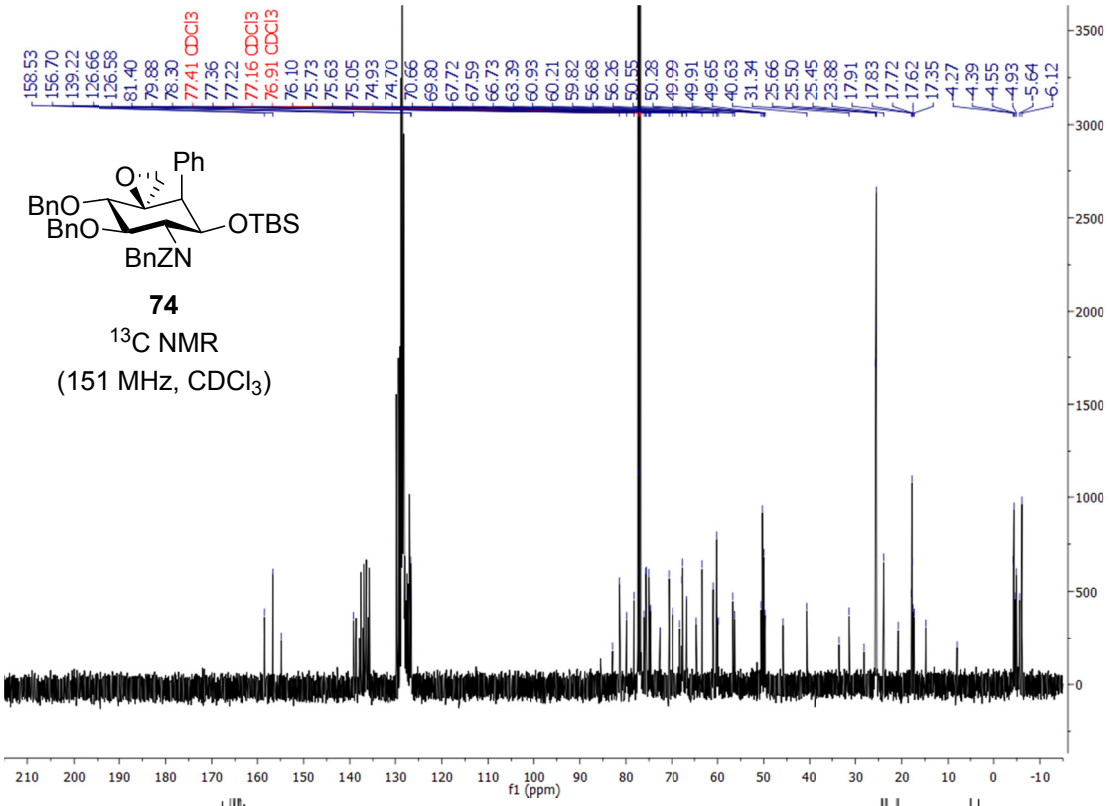
158.53
156.70
139.22
126.66
126.58
81.40
79.88
78.30
77.41 CDCl3
77.36
77.22
77.16 CDCl3
76.91 CDCl3
76.10
75.73
75.63
75.05
74.93
74.70
70.66
69.80
67.72
67.59
66.73
63.39
60.93
60.21
59.82
56.68
56.26
50.55
50.28
49.99
49.91
49.65
40.63
31.34
25.66
25.50
25.45
23.88
17.91
17.83
17.72
17.62
17.35
4.27
4.39
4.55
4.93
5.64
6.12
Ph
O
BnO
BnO
OTBS
BnZN
74
13C NMR
(151 MHz, CDCl3)
f1 (ppm)

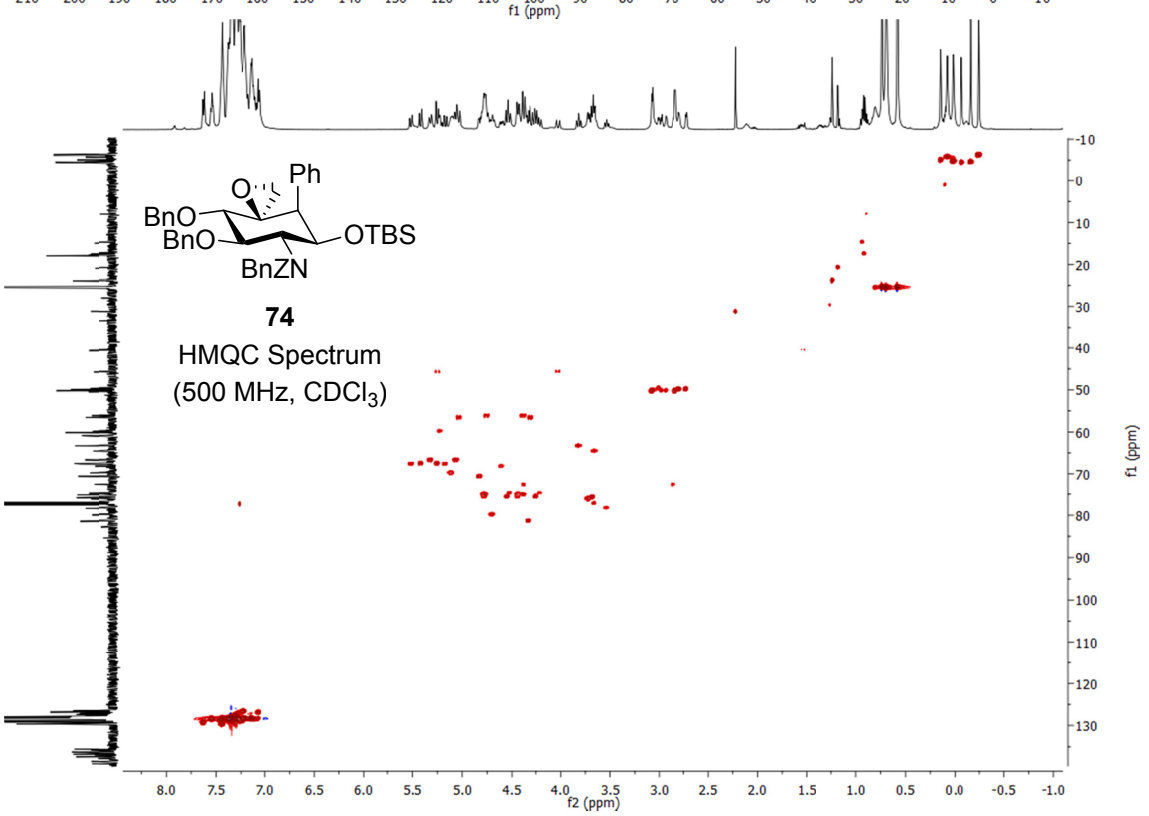
Ph
O
BnO
BnO
OTBS
BnZN
74
HMQC Spectrum
(500 MHz, CDCl3)
f2 (ppm)
f1 (ppm)

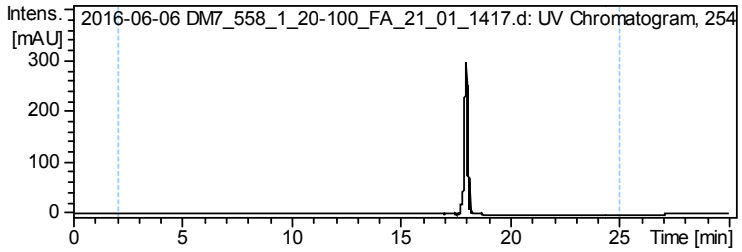

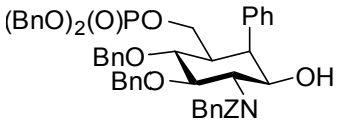

75

HPLC

ZORBAX SB-C18

50x2.3mm C18, 5 µm,

0.4 mL/min,

20-100 % MeCN in 20 min

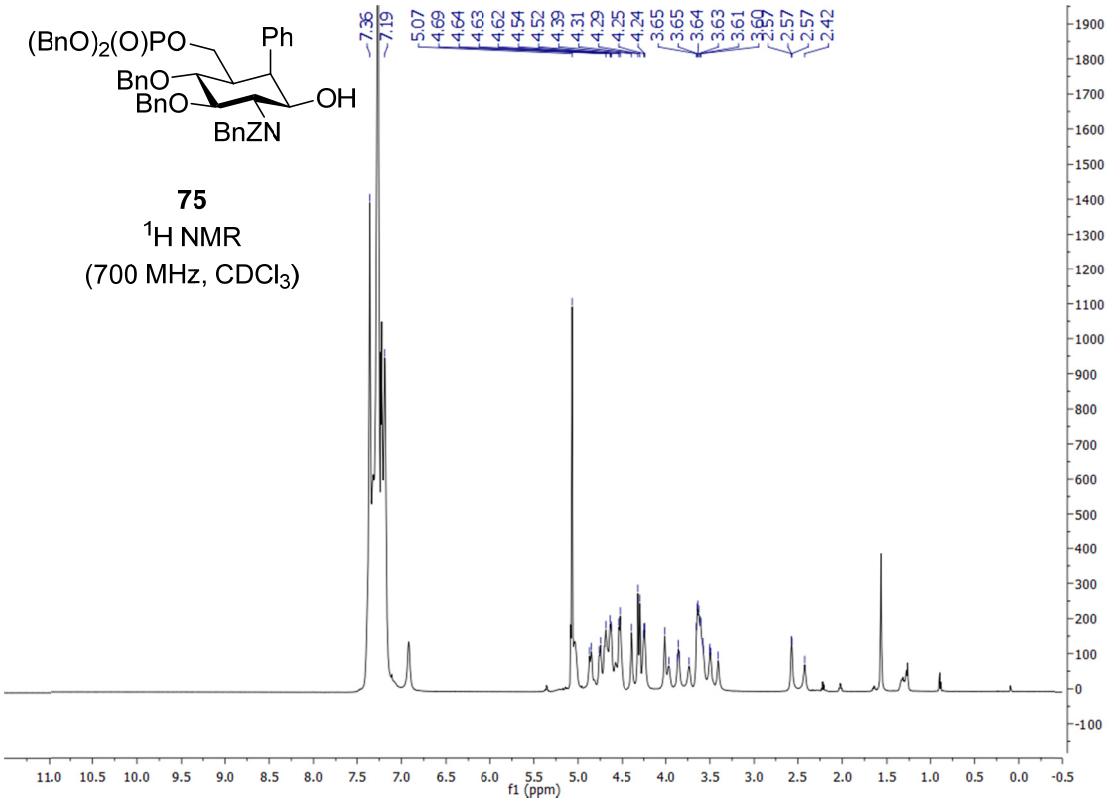

75

^{1}H NMR

(700 MHz, $CDCl_3$)

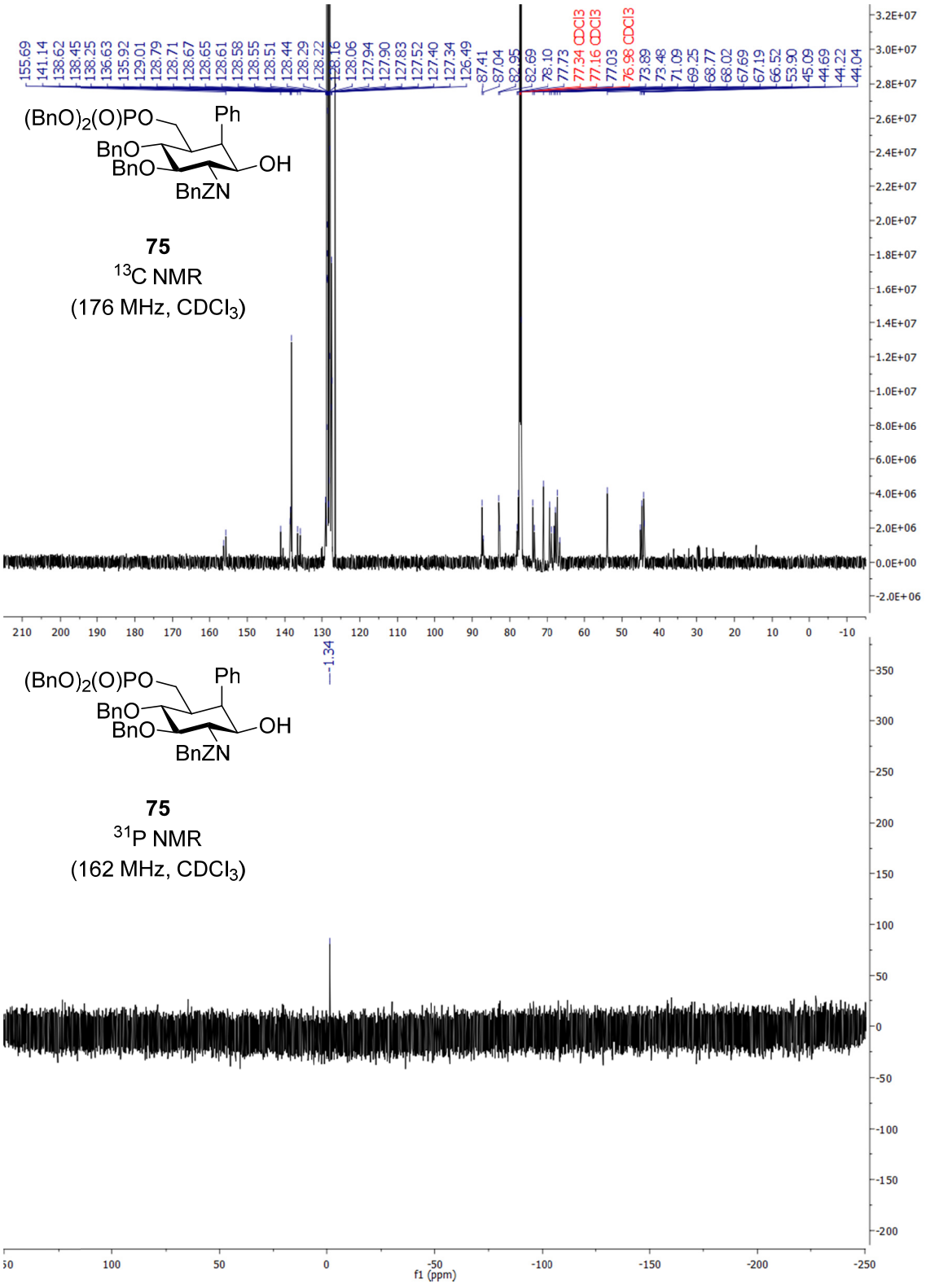
(BnO)2(O)PO
Ph
BnO
BnO
OH
BnZN
75
13C NMR
(176 MHz, CDCl3)
(BnO)2(O)PO
Ph
BnO
BnO
OH
BnZN
75
31P NMR
(162 MHz, CDCl3)
f1 (ppm)

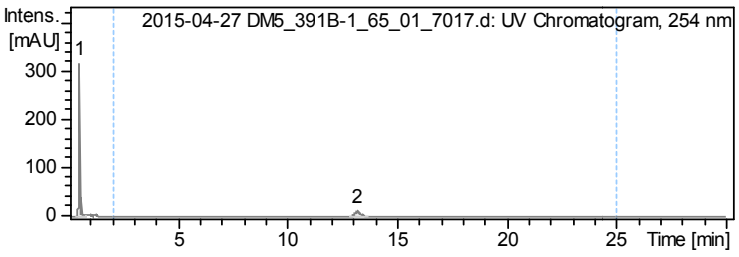

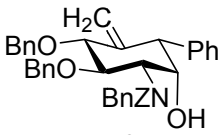

76

HPLC
NUCLEODUR C18
150x4.6mm C18, 5 µm,
0.4 mL/min,
80-100 % MeCN in 20 min

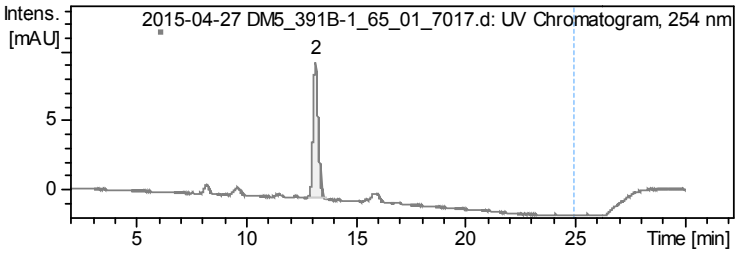

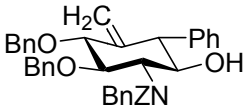

77

HPLC
NUCLEODUR C18
150x4.6mm C18, 5 µm,
0.4 mL/min,
80-100 % MeCN in 20 min

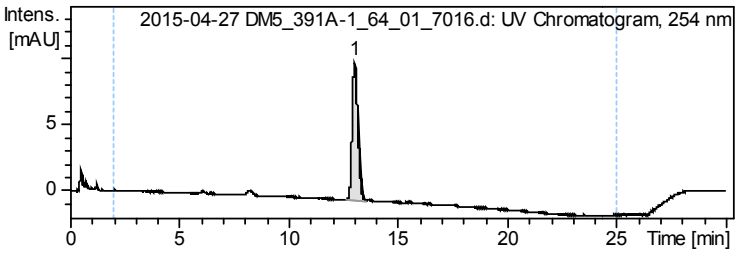

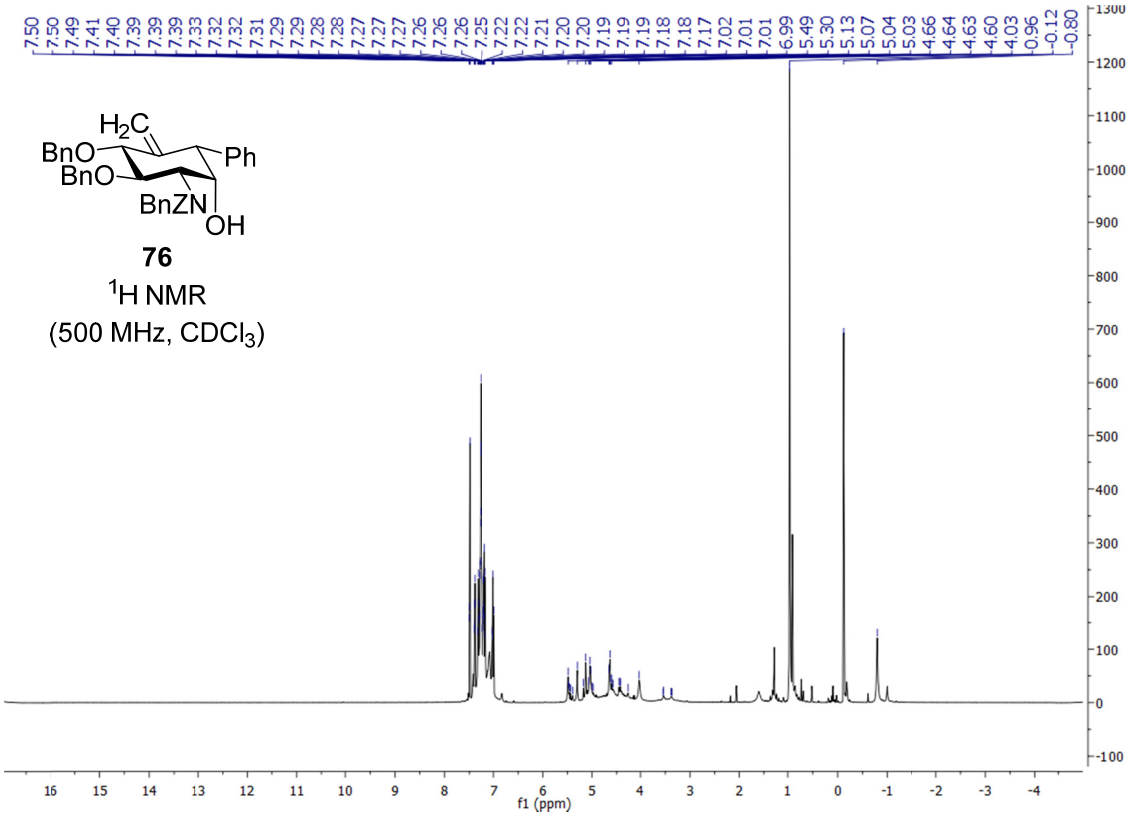

76

^{1}H NMR
(500 MHz, $CDCl_3$)

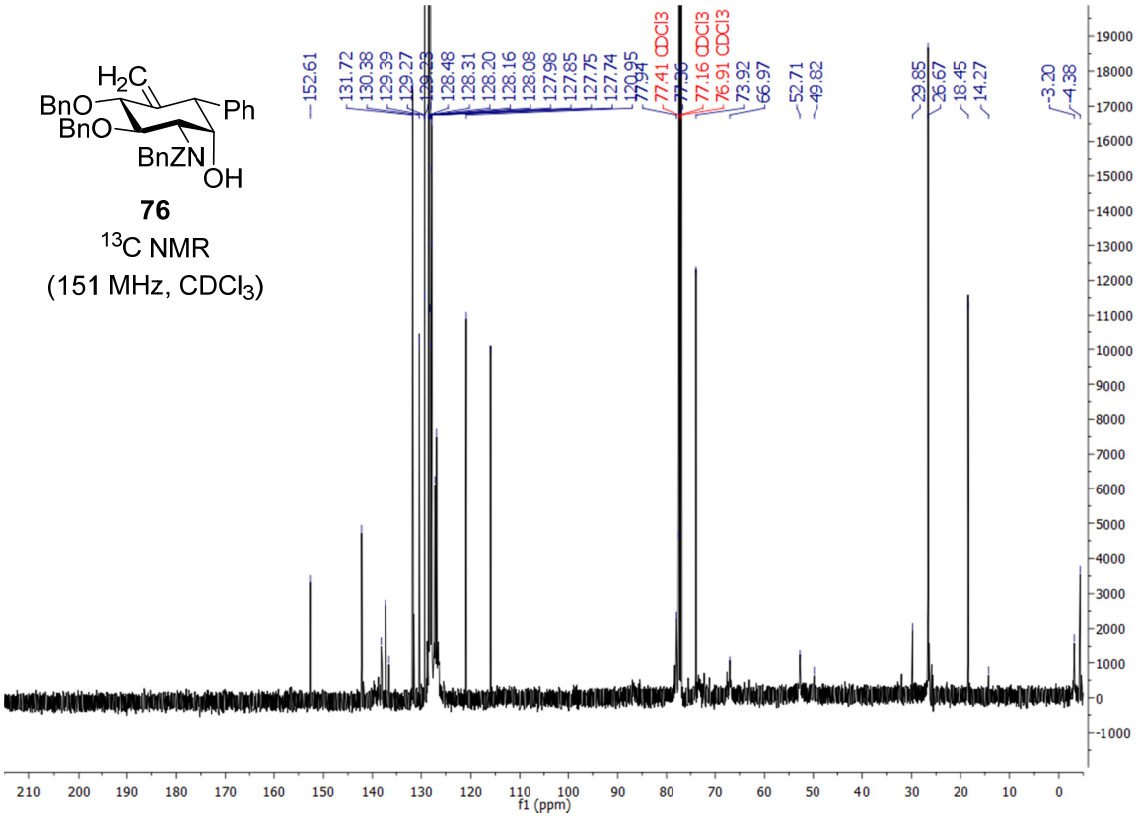
H2C
BnO
BnO
Ph
BnZN
OH
76
13C NMR
(151 MHz, CDCl3)
f1 (ppm)

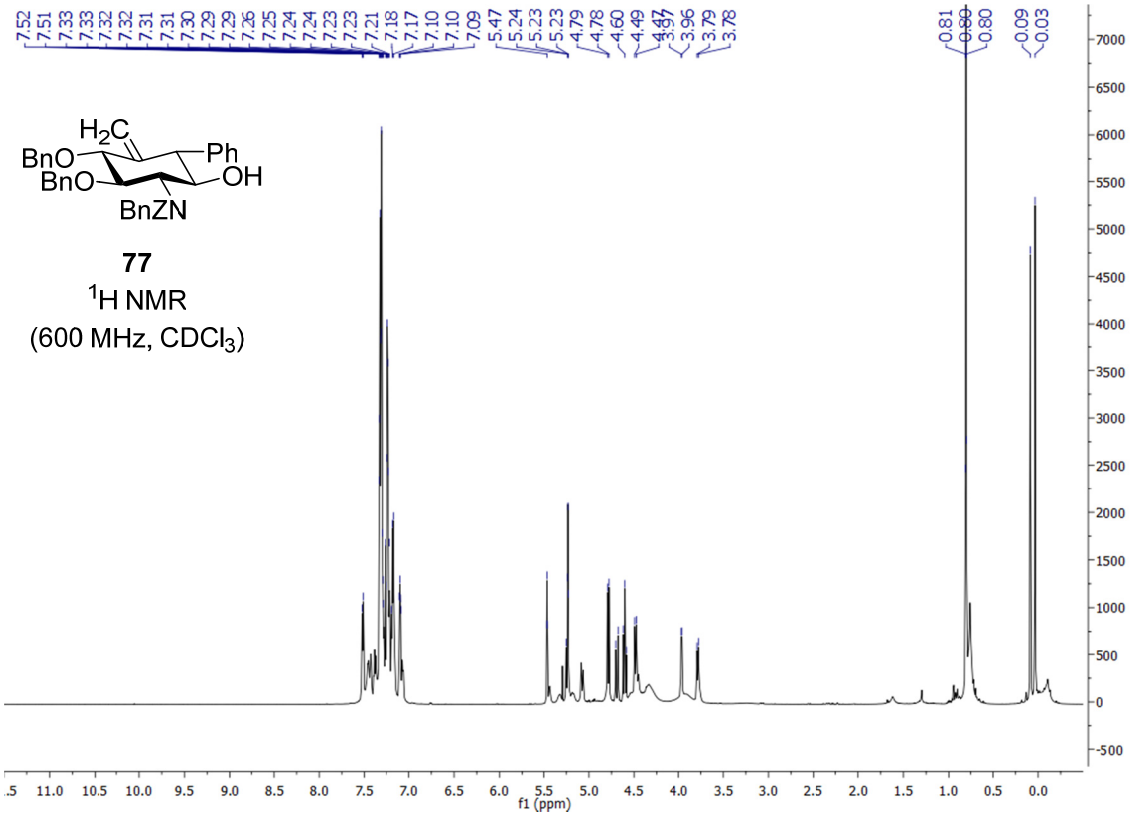
H2C
BnO
BnO
Ph
OH
BnZN
77
1H NMR
(600 MHz, CDCl3)
f1 (ppm)

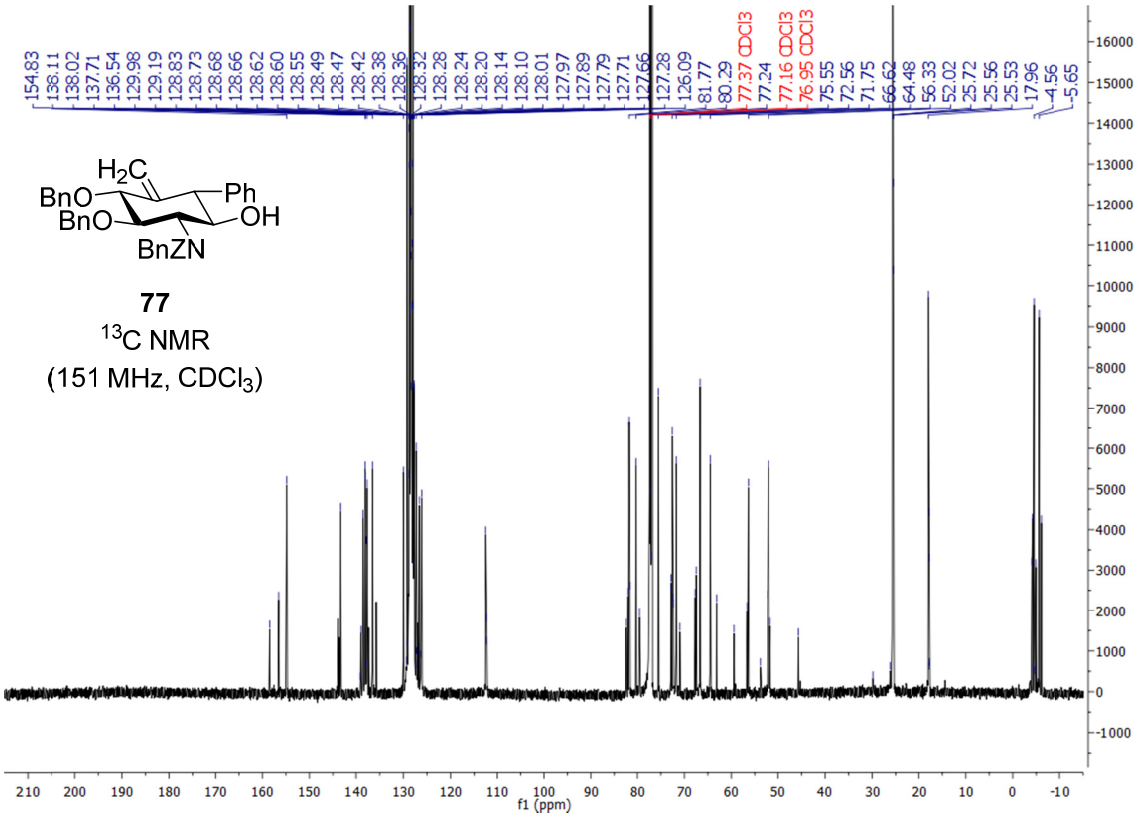

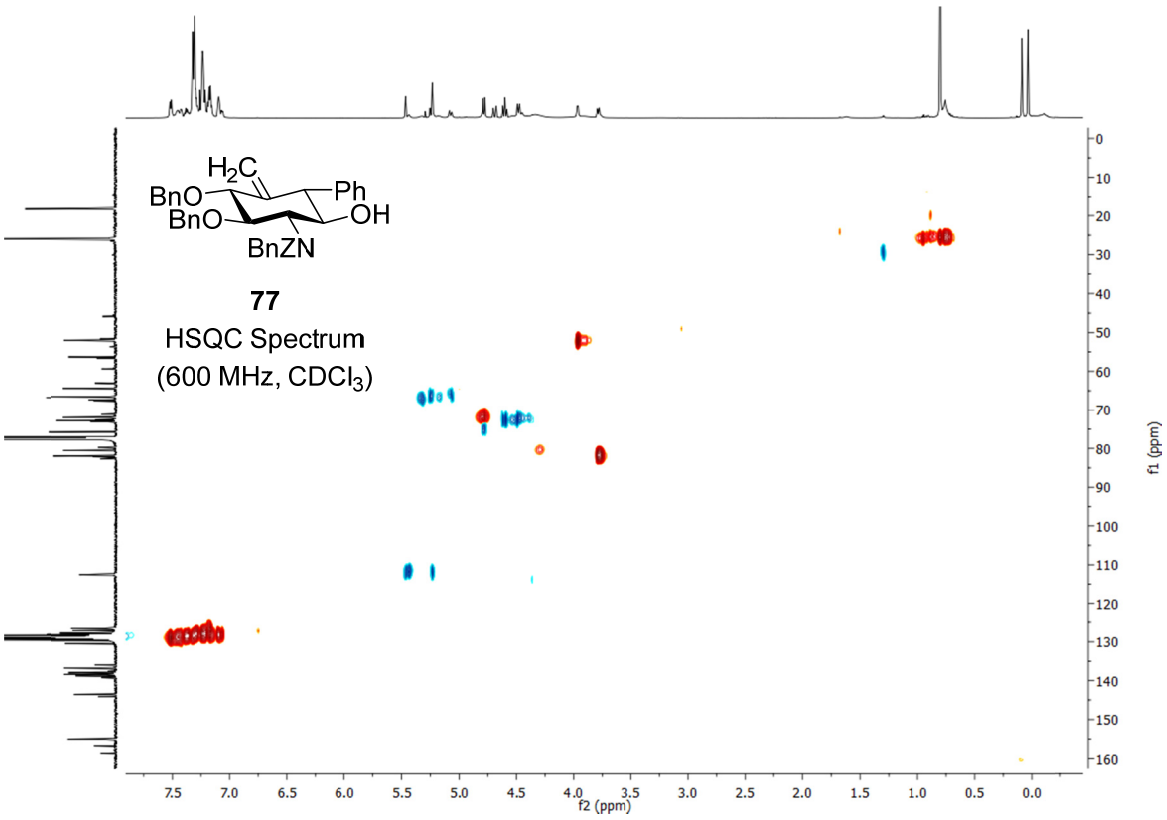

77

^{13}C NMR

(151 MHz, $CDCl_3$)

77

HSQC Spectrum

(600 MHz, $CDCl_3$)

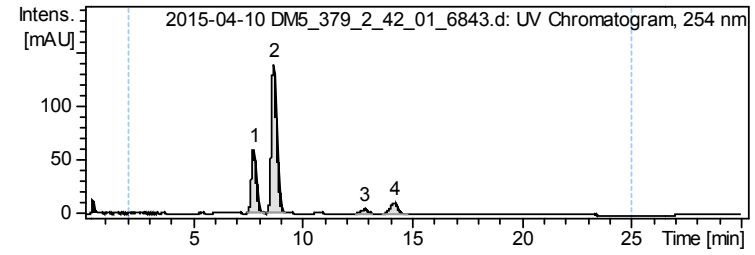

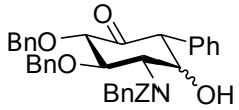

78/79
HPLC
EC 125/4 Nucleodur
Gravity C18, 5 µm,
0.4 mL/min,
80-100 % MeCN in 20 min

78
^{1}H NMR
(400 MHz, $CDCl_3$)

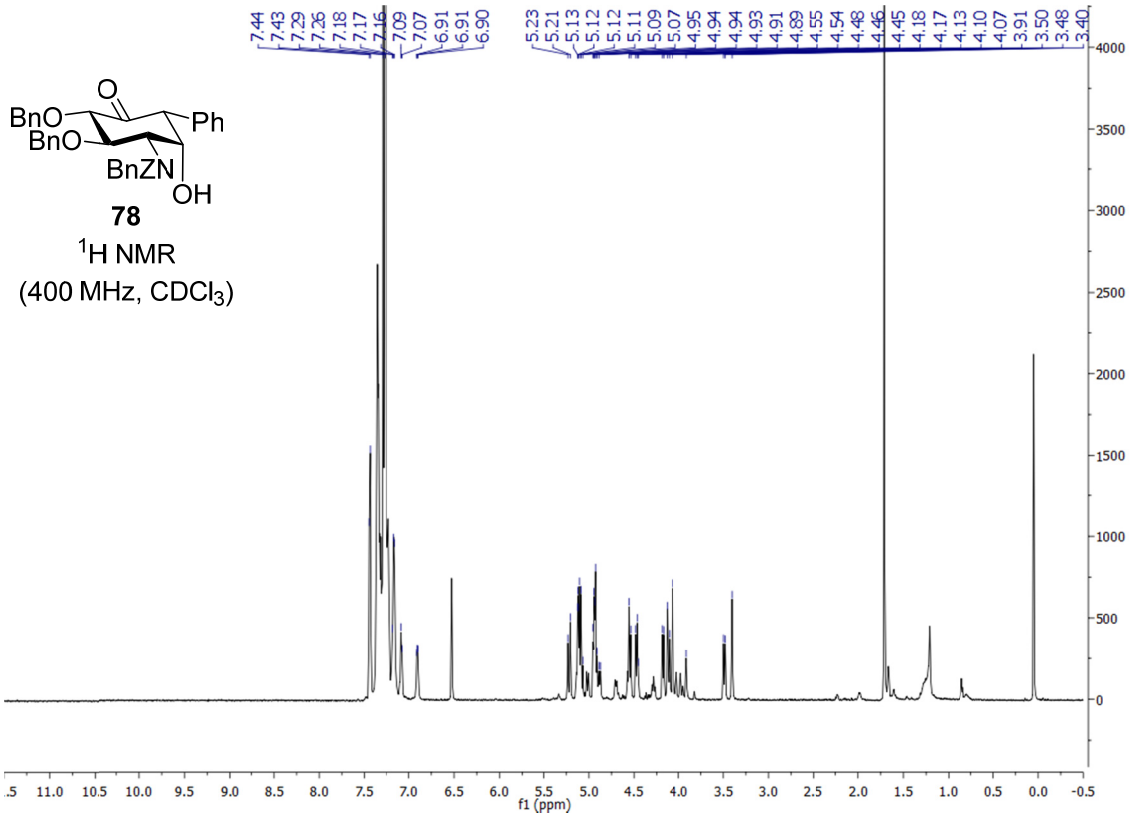

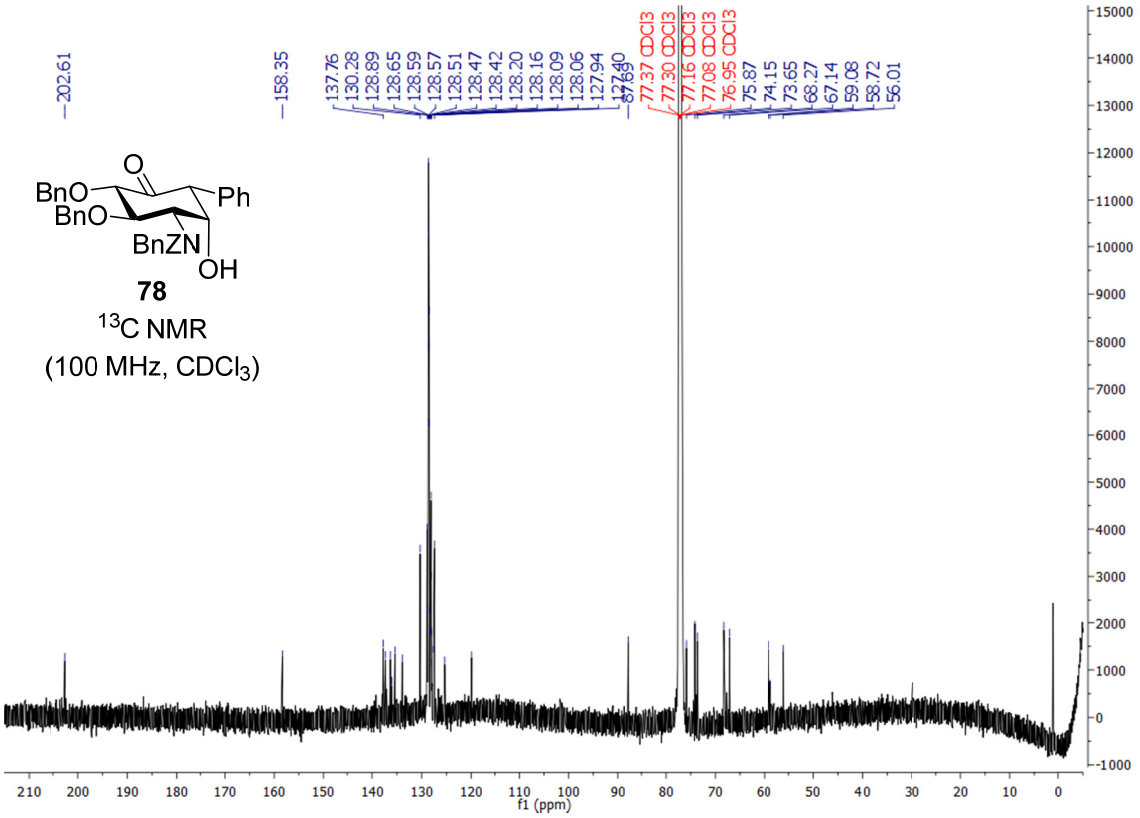
202.61
158.35
137.76
130.28
128.89
128.65
128.59
128.57
128.51
128.47
128.42
128.20
128.16
128.09
128.06
127.94
127.40
77.37 CDCl3
77.30 CDCl3
77.16 CDCl3
77.08 CDCl3
76.95 CDCl3
75.87
74.15
73.65
68.27
67.14
59.08
58.72
56.01
BnO
BnO
Ph
BnZN
OH
78
13C NMR
(100 MHz, CDCl3)
f1 (ppm)

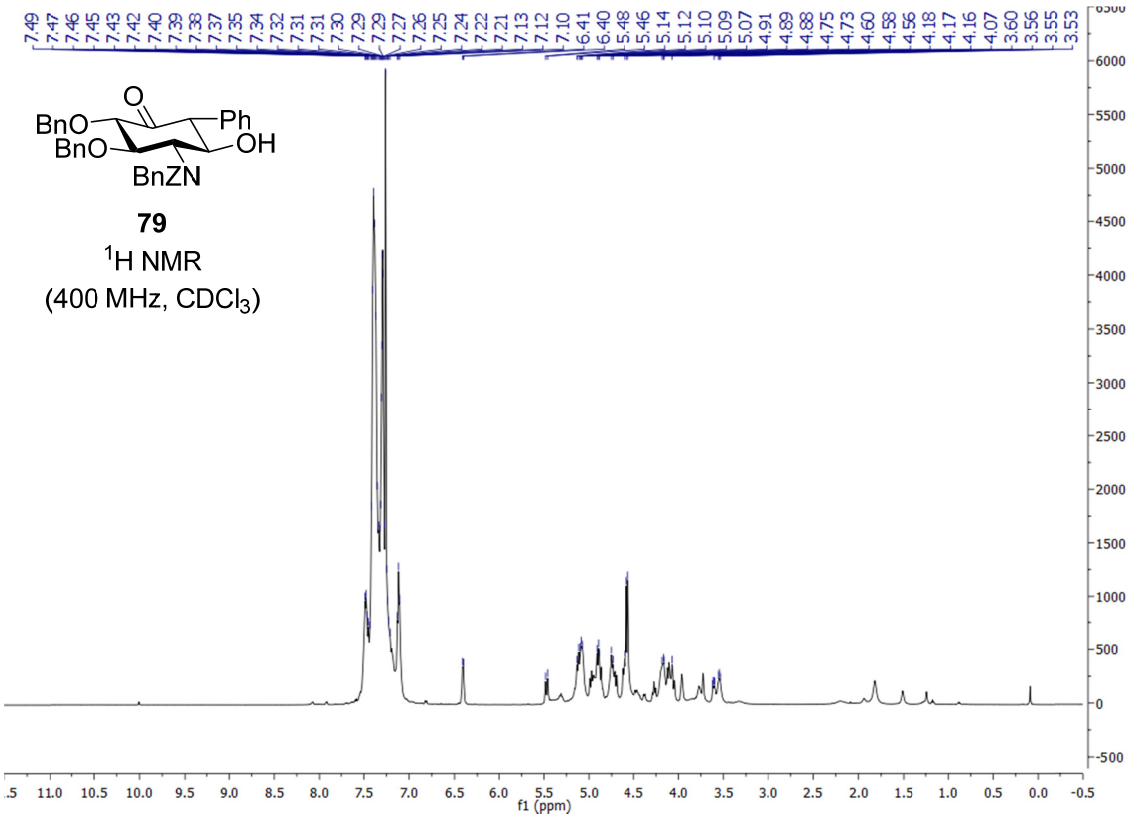
7.49
7.47
7.46
7.45
7.43
7.42
7.40
7.39
7.38
7.37
7.35
7.34
7.32
7.31
7.31
7.30
7.29
7.29
7.27
7.26
7.25
7.24
7.22
7.21
7.13
7.12
7.10
6.41
6.40
5.48
5.46
5.14
5.12
5.10
5.09
5.07
4.91
4.89
4.88
4.75
4.73
4.60
4.58
4.56
4.18
4.17
4.16
4.07
3.60
3.56
3.55
3.53
BnO
BnO
Ph
OH
BnZN
79
1H NMR
(400 MHz, CDCl3)
f1 (ppm)

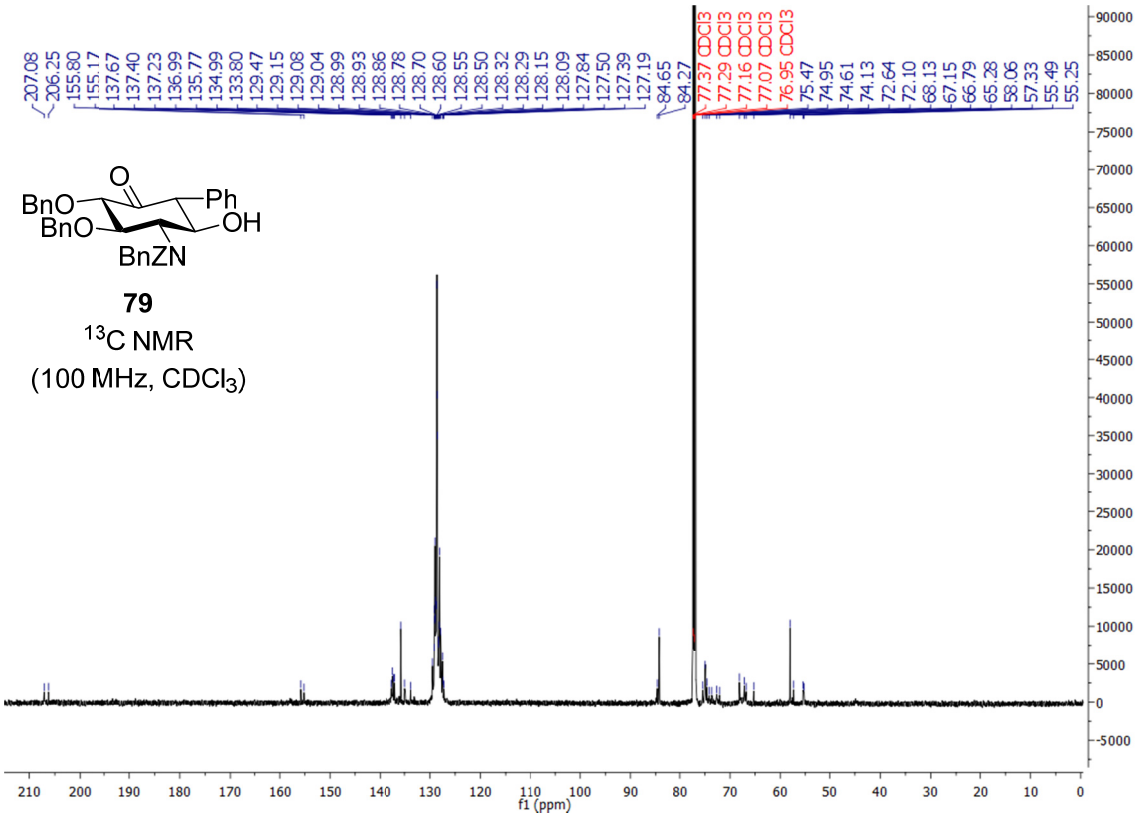
207.08
206.25
155.80
155.17
137.67
137.40
137.23
136.99
135.77
134.99
133.80
129.47
129.15
129.08
129.04
128.99
128.93
128.86
128.78
128.70
128.60
128.55
128.50
128.32
128.29
128.15
128.09
127.84
127.50
127.39
127.19
84.65
84.27
77.37 CDCl3
77.29 CDCl3
77.16 CDCl3
77.07 CDCl3
76.95 CDCl3
75.47
74.95
74.61
74.13
72.64
72.10
68.13
67.15
66.79
65.28
58.06
57.33
55.49
55.25
O
BnO
BnO
Ph
OH
BnZN
79
13C NMR
(100 MHz, CDCl3)
f1 (ppm)

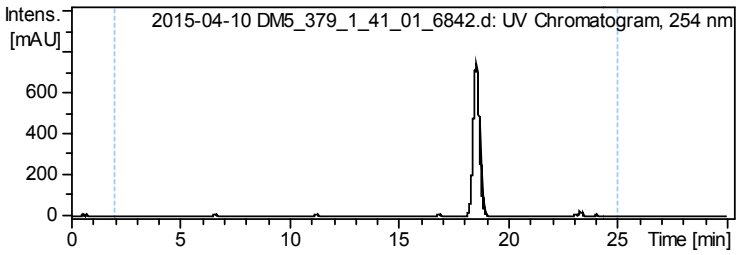

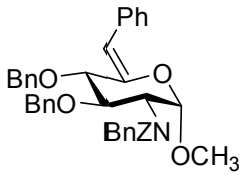

80

HPLC

ZORBAX SB-C18, 5 µm,

0.4 mL/min,

20-100 % MeCN in 20 min

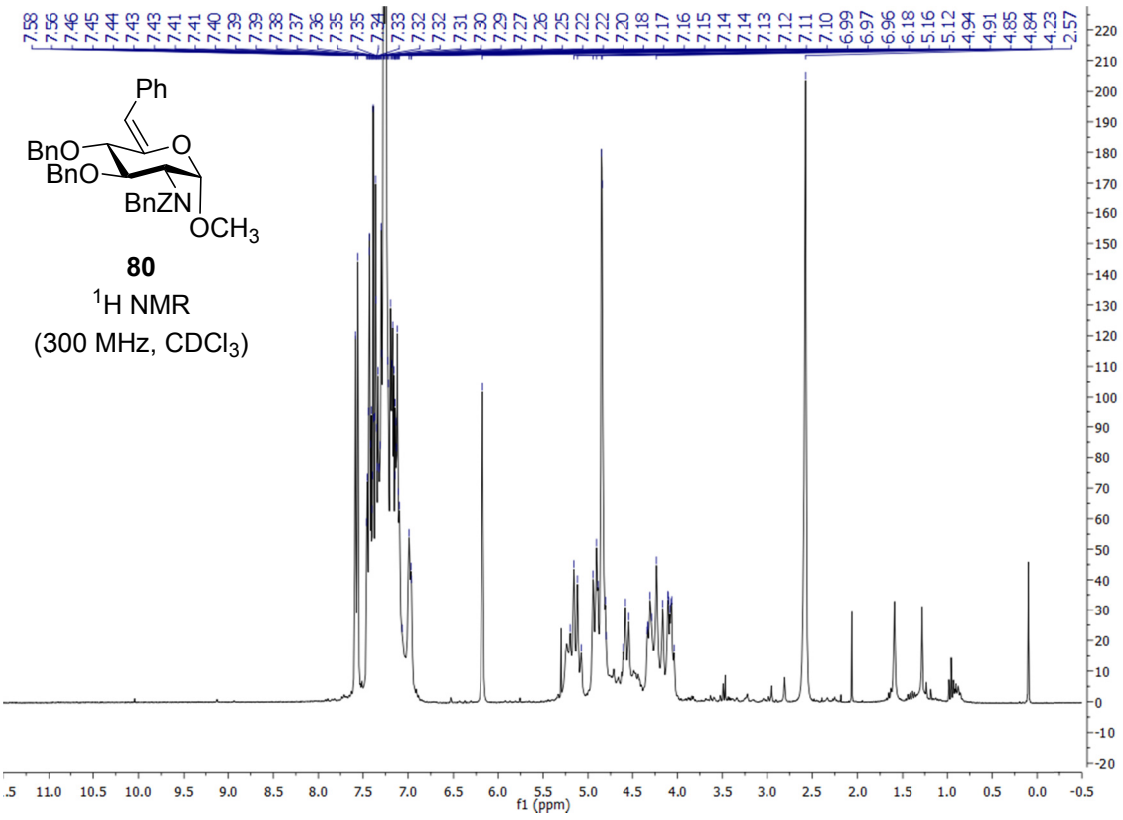

80

^{1}H NMR

(300 MHz, $CDCl_3$)

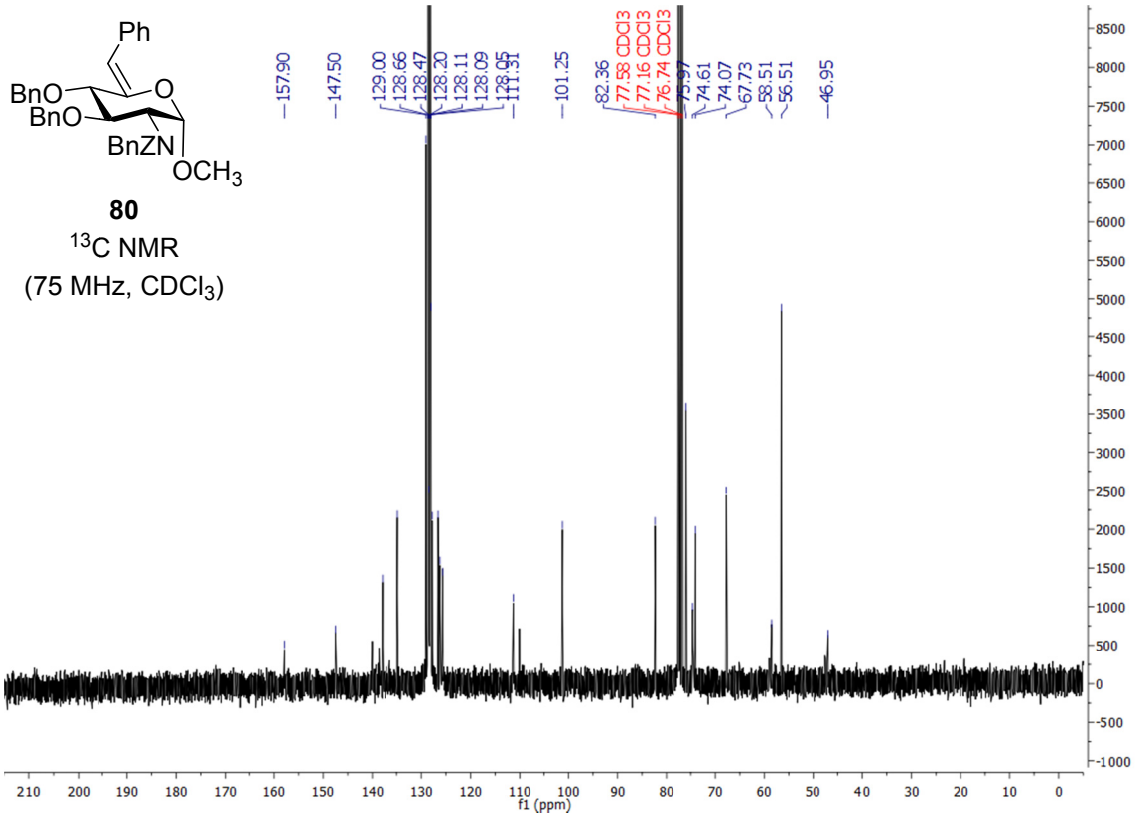

80

^{13}C NMR

(75 MHz, $CDCl_3$)

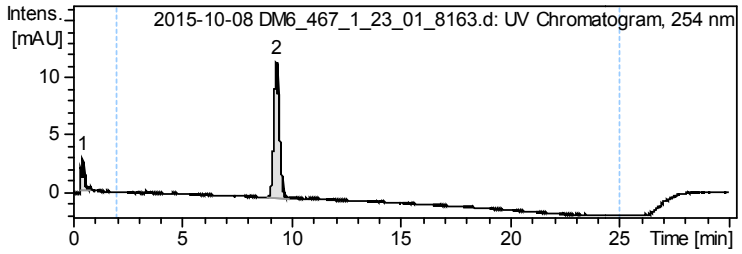

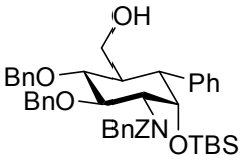

107
HPLC
ZORBAX SB-C18
50x2.3mm C18, 5 µm,
0.4 mL/min,
80-100 % MeCN in 20 min

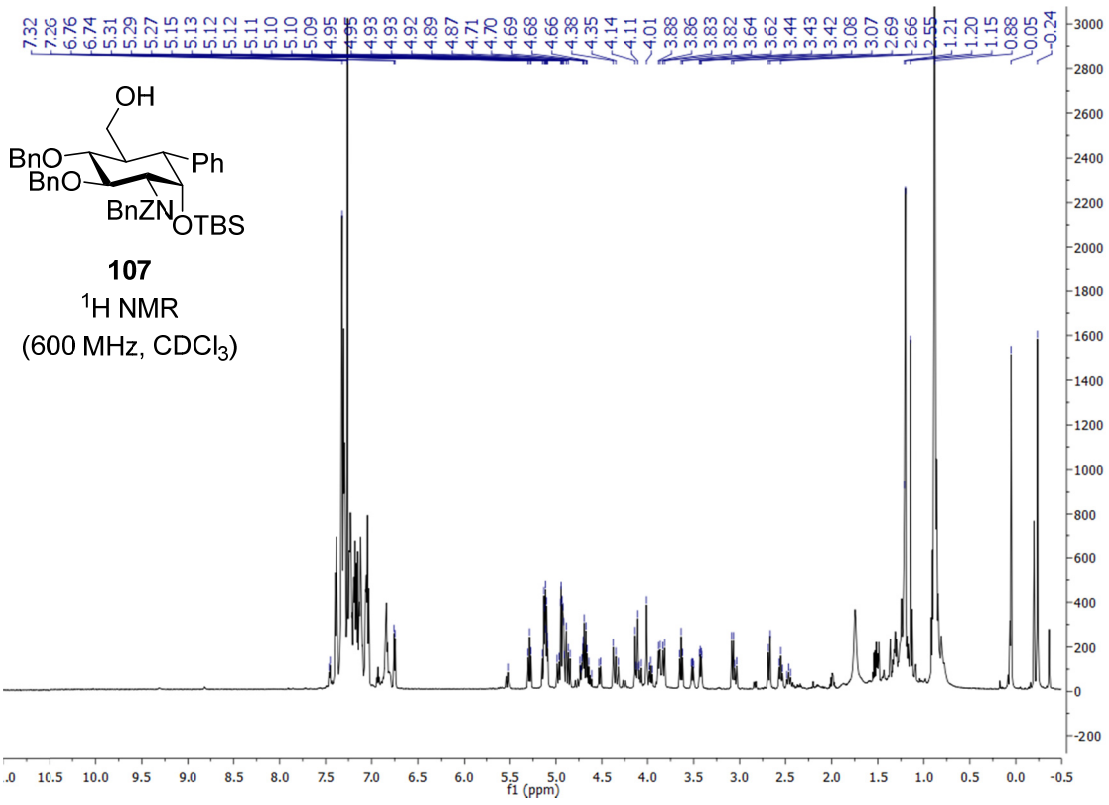

107
^{1}H NMR
(600 MHz, $CDCl_3$)

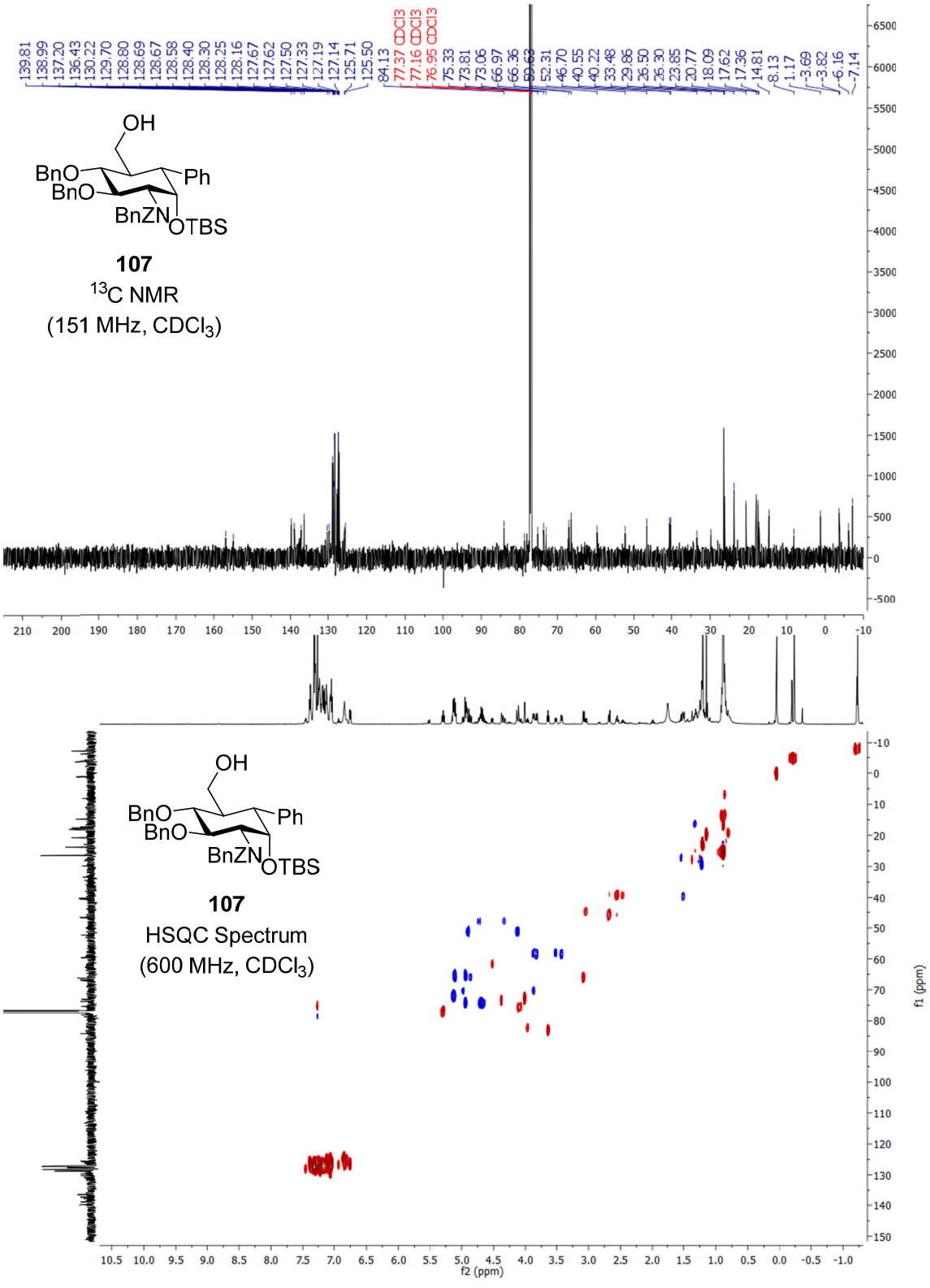
OH
BnO
BnO
Ph
BnZN
OTBS
107
13C NMR
(151 MHz, CDCl3)
OH
BnO
BnO
Ph
BnZN
OTBS
107
HSQC Spectrum
(600 MHz, CDCl3)
f2 (ppm)
f1 (ppm)

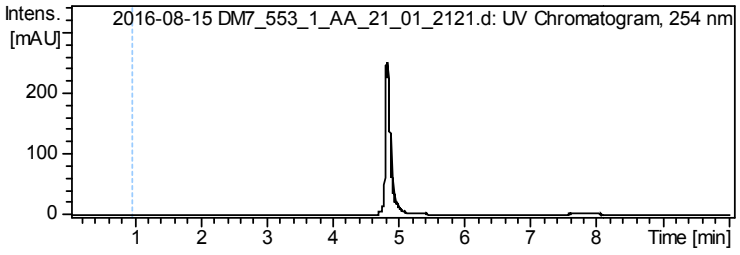

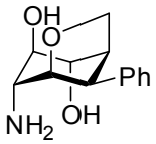

114
HPLC
ZORBAX SB-C18
50x2.3mm C18, 5 µm,
0.4 mL/min,
0-40 % MeCN in 20 min

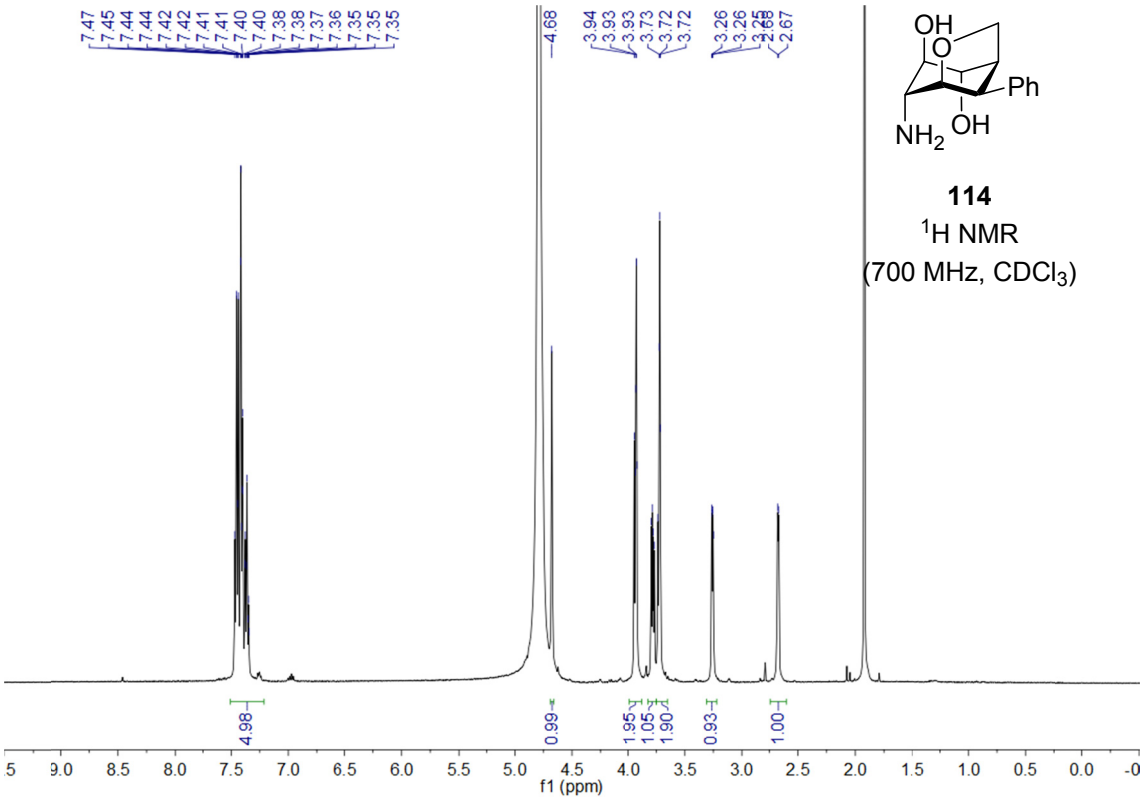

114
^{1}H NMR
(700 MHz, $CDCl_3$)

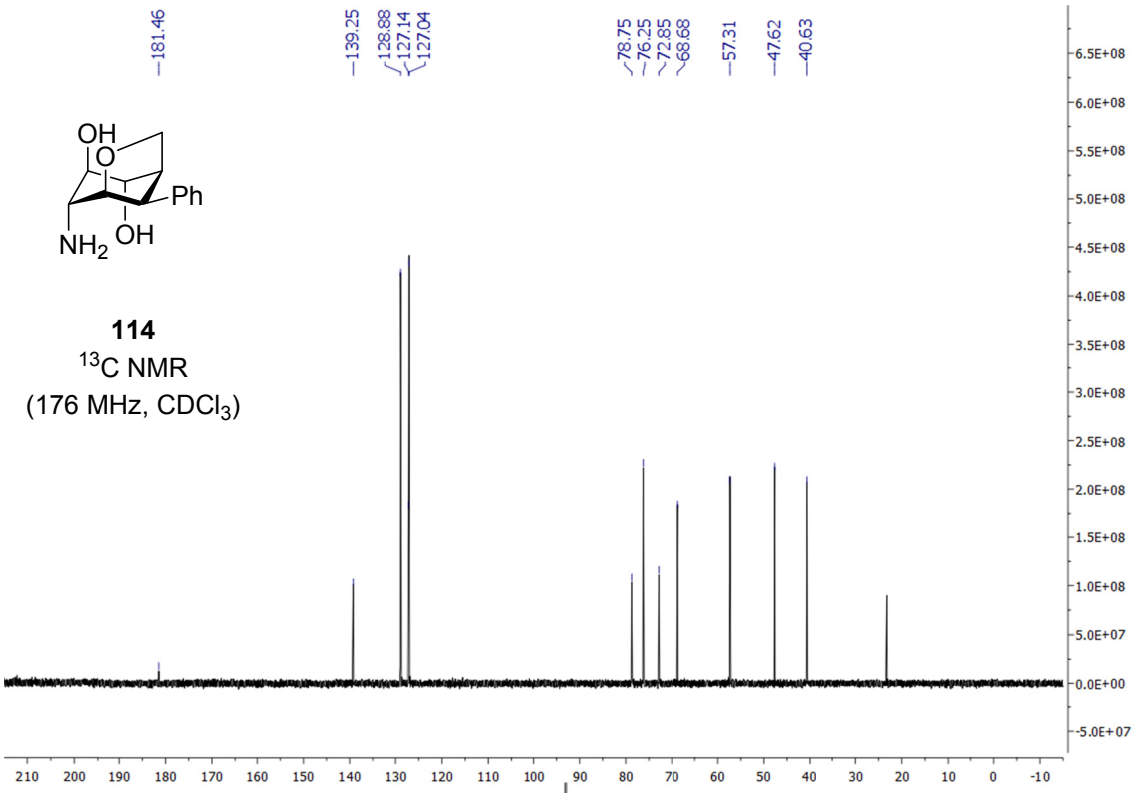

114
^{13}C NMR
(176 MHz, $CDCl_3$)

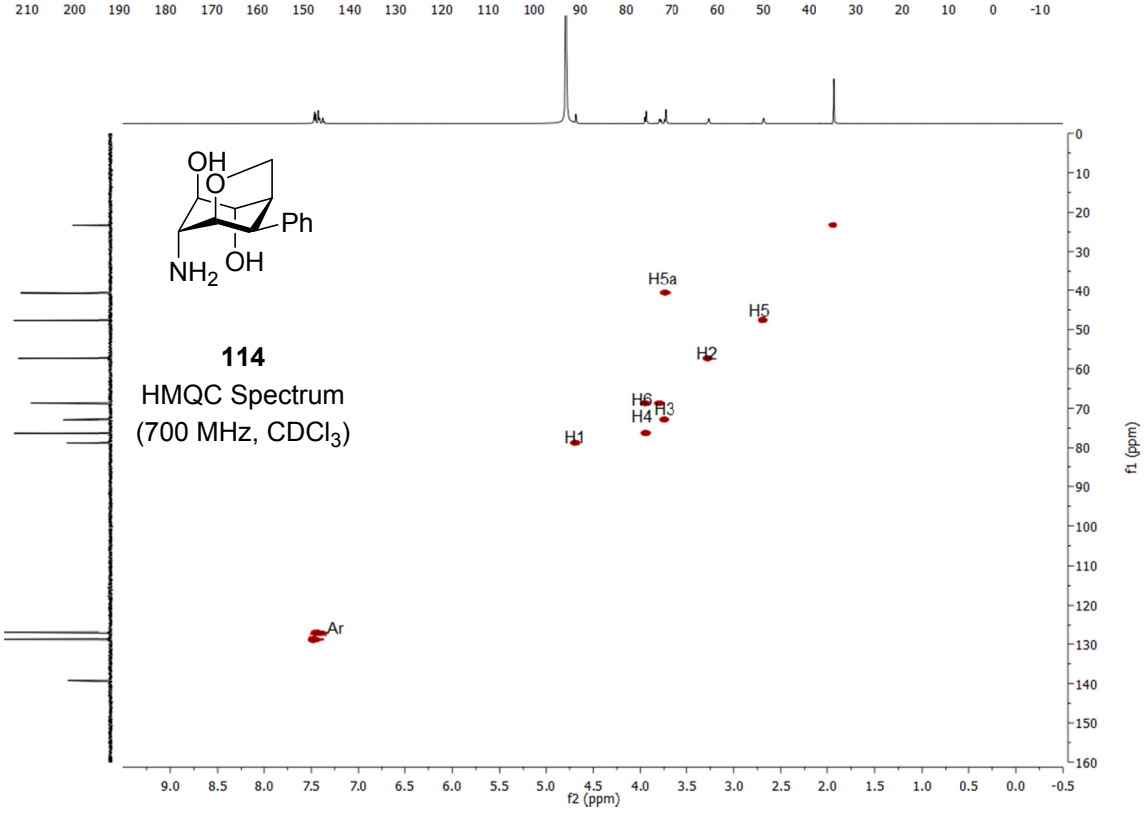

114
HMQC Spectrum
(700 MHz, $CDCl_3$)

B. List of Abbreviations

Abbreviation	Full form
ACS grade	Reagent specifications of American Chemical Society
ANOVA	Analysis of variance
B. cereus	*Bacillus cereus*
BP	Becke-Perdew exchange functional 1988
C. difficile	*Clostridium difficile*
CDC	Center for Disease Control and Prevention
CDI	*Clostridium difficile* infections
CDM	Chemically defined medium
CGlcN	Carba-α-D-glucosamine
CHD	1,4-Cyclohexadien
Coll*HCl	2,4,6-trimethylpyridine hydrochloride
COSMO	Conductor-like screening model
de	Diastereomeric excess
def2-TZVP	TZVP basis set with polarization functions (Aldrich's group 2005/2006)
DFT	Discrete Fourier transform
DMF	Dimethylformamide
DMSO	Dimethylsulfoxide
DNA	Deoxyribonucleic acid
dr	Diastereomeric ratio
E. coli	*Escherichia coli*
EC_{50}	Half maximal effective concentration
ecdc	European Centre for Disease Prevention and Control
EIIC	Component of the phosphotransferase system
FDA	Food and Drug Administration
Fru6P	Fructose-6-phosphate
gamP	Glucosamine-specific phosphotransferase system
GlcN	D-Glucosamine
GlcN1P	D-Glucosamine-1-phosphate
GlcN6P	D-Glucosamine-6-phosphate
glcP	Glucose-specific phosphotransferase system

Abbreviation	Full form
GlmS	Glutamine-fructose-6-amidotransferase
GlmU	Bifunctional protein in the biosynthetic pathway of UDP-GlcNAc
GlmY	sRNA in *E. coli*
GlmZ	sRNA in *E. coli*
HAI	Healthcare-associated infections
helD	Stress-responsive promoter (RNA)
HILIC	Hydrophilic interaction chromatography
HPLC	High-performance liquid chromatography
HPr	Histidin rich protein
HRMS	High-resolution mass spectra
HTS	High-throughput screening
IBX	2-Iodoxybenzoic acid
k_{obs}	Observed rate constant
L. monocytogenes	*Listeria monocytogenes*
LDA	Lithium diisopropylamide
lysC riboswitch	Lysine riboswitch
M. tuberculosis	*Mycobacterium tuberculosis*
*m*CPBA	*meta*-Chloroperoxybenzoic acid
MDR	Multidrug resistance
mgtA riboswitch	Rho-dependent riboswitch
MIC	Minimal inhibitory concentration
mRNA	messengerRNA
MRSA	Methicillin-resistant *Staphylococcus aureus*
MS	Mass spectrum
N. gonorrhoeae	*Neisseria gonorrhoeae*
nagE	N-Acetyl glucosamine specific PTS
NFSI	N-Fluorobenzene sulfonimide
NMR	Nuclear magnetic resonance spectroscopy
NOE	Nuclear Overhauser effect
O-GlcNAc	O-Linked N-acetylglucosamine
p.a.	Per annum
PTS	phosphoenolpyruvate: sugar phosphotransferase system
ptsH	phosphorylation subunit of PTS

Abbreviation	Full form
P*bmrC*	Stress-responsive promoter (protein synthesis)
P*helD*	Stress-responsive promoter (RNA)
P*yorB*	Promoter indicating DNA damage
P*ypuA*	Promotor indicating cell wall synthesis inhibition or cell envelope stress
QM/MM	Quantum mechanical/molecular mechanical
RapZ	RNase adaptor protein
RC	Regenerated cellulose
ribB riboswitch	Rho-dependent riboswitch
RNA	Ribonucleic acid
RNase	Ribonuclease
ROESY	Rotating frame nuclear Overhauser effect spectroscopy
RP	Reverse phase
S. aureus	*Staphylococcus aureus*
SAR	Structure-activity relationships
s.d.	Standard deviation
SD	Shine-Dalgarno sequence
SET	Single-electron-transfer
SreA riboswitch	*Trans*-acting riboswitch
SreB	*Trans*-acting riboswitch
sRNA	Small RNA
T. tengcongensis	*Thermoanaerobacter tengcongensis*
TAS-F	Tris(dimethylamino)sulfonium difluorotrimehtylsilicate
TBAF	*tetra-n*-Butylammonium fluoride
TBS	*tert*-Butyldimethylsilyl
THF	Tetrahydrofuran
TLC	thin-layer chromatography
TMS	Trimethylsilyl
TPP	Thiamin pyrophosphate
TRIS	Tris(hydroxy methylene)aminomethane
UDP-GlcNAc	Uridine diphosphate N-acetylglucosamine
UTP-GlcNAc	Uridine triphosphate N-acetylglucosamine
UTR	Untranslated region
VISA	Vancomycin intermediate resistant *Staphylococcus aureus*

Abbreviation	Full form
w/o	Without
Wt	Wild type
Z	Carboxybenzyl

C. List of Figures

D. List of Schemes

E. List of Tables

F. Bibliography

(1) Food and Agriculture Organization of the United Nations.; World Health Organization. *Carbohydrates in human nutrition : report of an expert meeting, Geneva, 17-26 September 1979*; Food and Agriculture Organization of the United Nations: Rome, 1980.

(2) Ahmed, J.; Preissner, S.; Dunkel, M.; Worth, C. L.; Eckert, A.; Preissner, R. *Nucleic Acids Res.* **2011**, *39*, D377-382.

(3) National Research Council (U.S.). Committee on Assessing the Importance and Impact of Glycomics and Glycosciences.; National Research Council (U.S.). Board on Chemical Sciences and Technology.; National Academies Press,: Washington, D.C., 2012, p 1 online resource (xvi, 191 p.).

(4) McNaught, A. D.; Wilkinson, A.; International Union of Pure and Applied Chemistry. *Compendium of chemical terminology : IUPAC recommendations*; 2nd ed.; Blackwell Science: Oxford Oxfordshire ; Malden, MA, 1997.

(5) Paulson, J. C. *Trends Biochem. Sci* **1989**, *14*, 272-276.

(6) Bertozzi, C. R.; Kiessling, L. L. *Science* **2001**, *291*, 2357-2364.

(7) Sharon, N.; Lis, H. *Sci. Am.* **1993**, *268*, 82-89.

(8) Rudd, P. M.; Elliott, T.; Cresswell, P.; Wilson, I. A.; Dwek, R. A. *Science* **2001**, *291*, 2370-2376.

(9) Lis, H.; Sharon, N. *Eur. J. Biochem.* **1993**, *218*, 1-27.

(10) Solis, D.; Bovin, N. V.; Davis, A. P.; Jimenez-Barbero, J.; Romero, A.; Roy, R.; Smetana, K., Jr.; Gabius, H. J. *Biochim. Biophys. Acta* **2015**, *1850*, 186-235.

(11) Chapleur, Y.; John Wiley & Sons.; Wiley-VCH,: Weinheim, 1998.

(12) Wong, C.-H.; John Wiley & Sons.; Wiley-VCH,: Weinheim ; New York, 2003.

(13) Bennett, L. L.; Shannon, W. M.; Allan, P. W.; Arnett, G. *Ann. N.Y. Acad. Sci.* **1975**, *255*, 342-358.

(14) Schmitt, P.; Gunther, H.; Hagele, G.; Stilke, R. *Organic Magnetic Resonance* **1984**, *22*, 446-449.

(15) Baranyovits, F. L. C. *Endeavour* **1978**, *2*, 85-92.

(16) Jackson, M.; Karwowski, J. P.; Theriault, R. J.; Hardy, D. J.; Swanson, S. J.; Barlow, G. J.; Tillis, P. M.; Mcalpine, J. B. *J. Antibiot. (Tokyo)* **1990**, *43*, 223-228.

(17) Pasetto, P.; Franck, R. W. *J. Org. Chem.* **2003**, *68*, 8042-8060.

(18) Sun, D. Y.; Hansen, M.; Clement, J. J.; Hurley, L. H. *Biochemistry* **1993**, *32*, 8068-8074.

(19) Suami, T. *Top. Curr. Chem.* **1990**, *154*, 257-283.

(20) Suami, T.; Ogawa, S. *Adv. Carbohydr. Chem. Biochem.* **1990**, *48*, 21-90.

(21) Marquez, V. E.; Lim, M. I. *Med. Res. Rev.* **1986**, *6*, 1-40.

(22) Arjona, O.; Gomez, A. M.; Lopez, J. C.; Plumet, J. *Chem. Rev.* **2007**, *107*, 1919-2036.

(23) Juaristi, E.; Cuevas, G. *The anomeric effect*; CRC Press: Boca Raton, FL, 1995.

(24) Tvaroska, I.; Bleha, T. *Anomeric and Exo-anomeric effects in carbohydrate chemistry* Macmillan Publishing Co.: New York, 1989.

(25) Kitaoka, M.; Ogawa, S.; Taniguchi, H. *Carbohydr. Res.* **1993**, *247*, 355-359.

(26) Lopez-Mendez, B.; Jia, C.; Zhang, Y.; Zhang, L. H.; Sinay, P.; Jimenez-Barbero, J.; Sollogoub, M. *Chem. - Asian J.* **2008**, *3*, 51-58.

(27) Unione, L.; Xu, B. X.; Diaz, D.; Martin-Santamaria, S.; Poveda, A.; Sardinha, J.; Rauter, A. P.; Bleriot, Y.; Zhang, Y. M.; Canada, F. J.; Sollogoub, M.; Jimenez-Barbero, J. *Chem. - Eur. J.* **2015**, *21*, 10513-10521.

(28) Xu, B.; Unione, L.; Sardinha, J.; Wu, S.; Etheve-Quelquejeu, M.; Pilar Rauter, A.; Bleriot, Y.; Zhang, Y.; Martin-Santamaria, S.; Diaz, D.; Jimenez-Barbero, J.; Sollogoub, M. *Angew. Chem.* **2014**, *53*, 9597-9602.

(29) Muller, K.; Faeh, C.; Diederich, F. *Science* **2007**, *317*, 1881-1886.

(30) Turnbull, J.; Powell, A.; Guimond, S. *Trends Cell Biol.* **2001**, *11*, 75-82.

(31) Mccasland, G. E.; Furuta, S.; Durham, L. J. *J. Org. Chem.* **1966**, *31*, 1516-&.

(32) McCasland, G. E.; Furuta, S.; Durham, L. J. *J. Org. Chem.* **1968**, *33*, 2835-2841.

(33) McCasland, G. E.; Furuta, S.; Durham, L. J. *J. Org. Chem.* **1968**, *33*, 2841-2844.

(34) Miller, T. W.; Arison, B. H.; Alberssc.G *Biotechnol. Bioeng.* **1973**, *15*, 1075-1080.

(35) Derosa, G.; Maffioli, P. *Arch. Med. Sci.* **2012**, *8*, 899-906.

(36) Schmidt, D. D.; Frommer, W.; Junge, B.; Muller, L.; Wingender, W.; Truscheit, E.; Schafer, D. *Naturwissenschaften* **1977**, *64*, 535-536.

(37) Ogawa, S.; Chida, N.; Suami, T. *Chem. Lett.* **1980**, 1559-1562.

(38) Ogawa, S.; Shibata, Y.; Nose, T.; Suami, T. *Bull. Chem. Soc. Jpn.* **1985**, *58*, 3387-3388.

(39) Krohn, K.; Börner, G.; Gringard, S. In *Carbohydrate Mimics: Concepts and Methods*; Chapleur, Y., Ed.; Wiley-VCH Verlag GmbH: Weinheim, 1998.

(40) Ferrier, R. J. *J. Chem. Soc., Perkin Trans. 1* **1979**, 1455-1458.

(41) Ferrier, R. J. *Glycoscience: Epimerisation, Isomerisation and Rearrangement Reactions of Carbohydrates*; Springer, 2001; Vol. 215.

(42) Barton, D. H. R.; Gero, S. D.; Augy, S.; Quicletsire, B. *J. Chem. Soc., Chem. Commun.* **1986**, 1399-1401.

(43) Sun, Y. S.; Nitz, M. *J. Org. Chem.* **2012**, *77*, 7401-7410.

(44) Takahashi, H.; Kittaka, H.; Ikegami, S. *J. Org. Chem.* **2001**, *66*, 2705-2716.

(45) Ferrier, R. J.; Middleton, S. *Chem. Rev.* **1993**, *93*, 2779-2831.

(46) Dubreuil, D.; Cleophax, J.; deAlmeida, M. V.; VerreSebrie, C.; Liaigre, J.; Vass, G.; Gero, S. D. *Tetrahedron* **1997**, *53*, 16747-16766.

(47) Machado, A. S.; Dubreuil, D.; Cleophax, J.; Gero, S. D.; Thomas, N. F. *Carbohydr. Res.* **1992**, *233*, C5-C8.

(48) Blattner, R.; Ferrier, R. J.; Haines, S. R. *Journal of the Chemical Society-Perkin Transactions 1* **1985**, 2413-2416.

(49) Machado, A. S.; Olesker, A.; Lukacs, G. *Carbohydr. Res.* **1985**, *135*, 231-239.

(50) Machado, A. S.; Olesker, A.; Castillon, S.; Lukacs, G. *Journal of the Chemical Society-Chemical Communications* **1985**, 330-332.

(51) Laszlo, P.; Pelyvas, I. F.; Sztaricskai, F.; Szilagyi, L.; Somogyi, A. *Carbohydr. Res.* **1988**, *175*, 227-239.

(52) Sato, K.; Sakuma, S.; Nakamura, Y.; Yoshimura, J.; Hashimoto, H. *Chem. Lett.* **1991**, 17-20.

(53) Barton, D. H. R.; Gero, S. D.; Cleophax, J.; Machado, A. S.; Quicletsire, B. *Journal of the Chemical Society-Chemical Communications* **1988**, 1184-1186.

(54) Sakairi, N.; Kuzuhara, H. *Tetrahedron Lett.* **1982**, *23*, 5327-5330.

(55) Nicotra, F.; Panza, L.; Ronchetti, F.; Russo, G. *Gazz. Chim. Ital.* **1989**, *119*, 577-579.

(56) Park, T. K.; Danishefsky, S. J. *Tetrahedron Lett.* **1994**, *35*, 2667-2670.

(57) Bender, S. L.; Budhu, R. J. *J. Am. Chem. Soc.* **1991**, *113*, 9883-9885.

(58) Park, T. K.; Danishefsky, S. J. *Tetrahedron Lett.* **1995**, *36*, 195-196.

(59) Jacob, F.; Monod, J. *J. Mol. Biol.* **1961**, *3*, 318-356.

(60) Browning, D. F.; Busby, S. J. *Nat. Rev. Microbiol.* **2004**, *2*, 57-65.

(61) Mandal, M.; Breaker, R. R. *Nature reviews. Molecular cell biology* **2004**, *5*, 451-463.

(62) Stahley, M. R.; Strobel, S. A. *Science* **2005**, *309*, 1587-1590.

(63) Torres-Larios, A.; Swinger, K. K.; Krasilnikov, A. S.; Pan, T.; Mondragon, A. *Nature* **2005**, *437*, 584-587.

(64) Levy, M.; Ellington, A. D. *Curr. Biol.* **2001**, *11*, R665-R667.

(65) Caprara, M. G.; Nilsen, T. W. *Nat. Struct. Biol.* **2000**, *7*, 831-833.

(66) Nahvi, A.; Sudarsan, N.; Ebert, M. S.; Zou, X.; Brown, K. L.; Breaker, R. R. *Chem. Biol.* **2002**, *9*, 1043.

(67) Winkler, W.; Nahvi, A.; Breaker, R. R. *Nature* **2002**, *419*, 952-956.

(68) Serganov, A.; Nudler, E. *Cell* **2013**, *152*, 17-24.

(69) Breaker, R. R. *Cold Spring Harb. Perspect. Biol.* **2012**, *4*.

(70) Matzner, D.; Mayer, G. *J. Med. Chem.* **2015**, *58*, 3275-3286.

(71) Barrick, J. E.; Breaker, R. R. *Genome Biol.* **2007**, *8*, R239.

(72) Naville, M.; Gautheret, D. *Briefings in Functional Genomics* **2010**, *9*, 178-189.

(73) Winkler, W. C.; Nahvi, A.; Roth, A.; Collins, J. A.; Breaker, R. R. *Nature* **2004**, *428*, 281-286.

(74) Collins, J. A.; Irnov, I.; Baker, S.; Winkler, W. C. *Genes Dev.* **2007**, *21*, 3356-3368.

(75) Caron, M. P.; Bastet, L.; Lussier, A.; Simoneau-Roy, M.; Masse, E.; Lafontaine, D. A. *Proc. Natl. Acad. Sci. U. S. A.* **2012**, *109*, E3444-E3453.

(76) Hollands, K.; Proshkin, S.; Sklyarova, S.; Epshtein, V.; Mironov, A.; Nudler, E.; Groisman, E. A. *Proc. Natl. Acad. Sci. U. S. A.* **2012**, *109*, 5376-5381.

(77) Loh, E.; Dussurget, O.; Gripenland, J.; Vaitkevicius, K.; Tiensuu, T.; Mandin, P.; Repoila, F.; Buchrieser, C.; Cossart, P.; Johansson, J. *Cell* **2009**, *139*, 770-779.

(78) McCown, P. J.; Corbino, K. A.; Stav, S.; Sherlock, M. E.; Breaker, R. R. *RNA* **2017**.

(79) Baker, J. L.; Sudarsan, N.; Weinberg, Z.; Roth, A.; Stockbridge, R. B.; Breaker, R. R. *Science* **2012**, *335*, 233-235.

(80) Mironov, A. S.; Gusarov, I.; Rafikov, R.; Lopez, L. E.; Shatalin, K.; Kreneva, R. A.; Perumov, D. A.; Nudler, E. *Cell* **2002**, *111*, 747-756.

(81) Cheah, M. T.; Wachter, A.; Sudarsan, N.; Breaker, R. R. *Nature* **2007**, *447*, 497-500.

(82) Sudarsan, N.; Barrick, J. E.; Breaker, R. R. *RNA* **2003**, *9*, 644-647.

(83) Bocobza, S. E.; Aharoni, A. *Plant J.* **2014**, *79*, 693-703.

(84) Croft, M. T.; Moulin, M.; Webb, M. E.; Smith, A. G. *Proc. Natl. Acad. Sci. U. S. A.* **2007**, *104*, 20770-20775.

(85) Lee, E. R.; Baker, J. L.; Weinberg, Z.; Sudarsan, N.; Breaker, R. R. *Science* **2010**, *329*, 845-848.

(86) Ferre-D'Amare, A. R. *Q. Rev. Biophys.* **2010**, *43*, 423-447.

(87) Bingaman, J. L.; Zhang, S. X.; Stevens, D. R.; Yennawar, N. H.; Hammes-Schiffer, S.; Bevilacqua, P. C. *Nat. Chem. Biol.* **2017**, *13*, 439-+.

(88) Klein, D. J.; Ferre-D'Amare, A. R. *Science* **2006**, *313*, 1752-1756.

(89) McCarthy, T. J.; Plog, M. A.; Floy, S. A.; Jansen, J. A.; Soukup, J. K.; Soukup, G. A. *Chem. Biol.* **2005**, *12*, 1221-1226.

(90) Zhang, S.; Ganguly, A.; Goyal, P.; Bingaman, J. L.; Bevilacqua, P. C.; Hammes-Schiffer, S. *J. Am. Chem. Soc.* **2015**, *137*, 784-798.

(91) Zhang, S.; Stevens, D. R.; Goyal, P.; Bingaman, J. L.; Bevilacqua, P. C.; Hammes-Schiffer, S. *J. Phys. Chem. Lett.* **2016**, *7*, 3984-3988.

(92) Klein, D. J.; Been, M. D.; Ferre-D'Amare, A. R. *J. Am. Chem. Soc.* **2007**, *129*, 14858-14859.

(93) Viladoms, J.; Fedor, M. J. *J. Am. Chem. Soc.* **2012**, *134*, 19043-19049.

(94) Lilley, D. M. *Trends Biochem. Sci* **2003**, *28*, 495-501.

(95) Klein, D. J.; Wilkinson, S. R.; Been, M. D.; Ferre-D'Amare, A. R. *J. Mol. Biol.* **2007**, *373*, 178-189.

(96) Even, S.; Pellegrini, O.; Zig, L.; Labas, V.; Vinh, J.; Brechemmier-Baey, D.; Putzer, H. *Nucleic Acids Res.* **2005**, *33*, 2141-2152.

(97) Durand, P.; Golinelli-Pimpaneau, B.; Mouilleron, S.; Badet, B.; Badet-Denisot, M. A. *Arch. Biochem. Biophys.* **2008**, *474*, 302-317.

(98) McCown, P. J.; Roth, A.; Breaker, R. R. *RNA* **2011**, *17*, 728-736.

(99) Cochrane, J. C.; Lipchock, S. V.; Strobel, S. A. *Chem. Biol.* **2007**, *14*, 97-105.

(100) Lim, J.; Grove, B. C.; Roth, A.; Breaker, R. R. *Angew. Chem. Int. Ed.* **2006**, *45*, 6689-6693.

(101) Fei, X.; Holmes, T.; Diddle, J.; Hintz, L.; Delaney, D.; Stock, A.; Renner, D.; McDevitt, M.; Berkowitz, D. B.; Soukup, J. K. *ACS Chem. Biol.* **2014**, *9*, 2875-2882.

(102) Mayer, G.; Matzner, D.; Schuller, A.; Seitz, T.; Wittmann, V. *Chemistry (Easton)* **2017**.

(103) Penchovsky, R.; Stoilova, C. C. *Expert opinion on drug discovery* **2013**, *8*, 65-82.

(104) Blount, K.; Puskarz, I.; Penchovsky, R.; Breaker, R. *RNA Biol.* **2006**, *3*, 77-81.

(105) Lunse, C. E.; Schmidt, M. S.; Wittmann, V.; Mayer, G. *ACS Chem. Biol.* **2011**, *6*, 675-678.

(106) Mayer, G.; Famulok, M. *ChemBioChem* **2006**, *7*, 602-604.

(107) Posakony, J. J.; Ferre-D'Amare, A. R. *J. Org. Chem.* **2013**, *78*, 4730-4743.

(108) Lim, J.; Winkler, W. C.; Nakamura, S.; Scott, V.; Breaker, R. R. *Angew. Chem.* **2006**, *45*, 964-968.

(109) Control, E. C. f. D. P. a. Antimicrobial resistance surveillance in Europe 2015; [Updated: Cited: Available from: http://ecdc.europa.eu/en/publications/Publications/antimicrobial-resistance-europe-2015.pdf

(110) Inoue, H.; Minghui, R. *Bull. World Health Organ.* **2017**, *95*, 242.

(111) Aminov, R. *Biochem. Pharmacol.* **2017**, *133*, 4-19.

(112) Bassetti, M.; Merelli, M.; Temperoni, C.; Astilean, A. *Ann. Clin. Microbiol. Antimicrob.* **2013**, *12*, 22.

(113) Chan, M. *Ten years in public health, 2007–2017: report by Dr Margaret Chan, Director-General, World Health Organization*, World Health Organization, 2017.

(114) Brown, E. D.; Wright, G. D. *Nature* **2016**, *529*, 336-343.

(115) Centers for Disease Control and Prevention (CDC). Antibiotic resistance threats in the United States. Published Online: 2013. http://www.cdc.gov/drugresistance/threat-report-2013/pdf/ar-threats-2013-508.pdf.

(116) European Centre for Disease Prevention and Control. ECDC/EMEA Joint technical report - The bacterial challenge: time to react. Published Online: 2009. http://www.ema.europa.eu/docs/en_GB/document_library/Report/2009/11/WC500008770.pdf.

(117) Control, E. C. f. D. P. a. Annual epidemiological report. Published Online: 2013.

(118) Paredes-Sabja, D.; Shen, A.; Sorg, J. A. *Trends Microbiol.* **2014**, *22*, 406-416.

(119) Rupnik, M.; Wilcox, M. H.; Gerding, D. N. *Nat. Rev. Microbiol.* **2009**, *7*, 526-536.

(120) Organization, W. H. Global Action Plan on Antimicrobial Resistance. Published Online: 2015.

(121) Walsh, C. *Nat. Rev. Microbiol.* **2003**, *1*, 65-70.

(122) Lewis, K. *Nat. Rev. Drug Discov.* **2013**, *12*, 371-387.

(123) Silver, L. L. *Clin. Microbiol. Rev.* **2011**, *24*, 71-109.

(124) Schatz, A.; Bugie, E.; Waksman, S. A. *Clin. Orthop. Relat. Res.* **2005**, 3-6.

(125) Lewis, K. *Nature* **2012**, *485*, 439-440.

(126) Debono, M.; Barnhart, M.; Carrell, C. B.; Hoffmann, J. A.; Occolowitz, J. L.; Abbott, B. J.; Fukuda, D. S.; Hamill, R. L.; Biemann, K.; Herlihy, W. C. *J. Antibiot. (Tokyo)* **1987**, *40*, 761-777.

(127) Andries, K.; Verhasselt, P.; Guillemont, J.; Gohlmann, H. W.; Neefs, J. M.; Winkler, H.; Van Gestel, J.; Timmerman, P.; Zhu, M.; Lee, E.; Williams, P.; de Chaffoy, D.; Huitric, E.; Hoffner, S.; Cambau, E.; Truffot-Pernot, C.; Lounis, N.; Jarlier, V. *Science* **2005**, *307*, 223-227.

(128) Cho, H.; Uehara, T.; Bernhardt, T. G. *Cell* **2014**, *159*, 1300-1311.

(129) Silver, L. L. *Nat. Rev. Drug Discov.* **2007**, *6*, 41-55.

(130) Payne, D. J.; Gwynn, M. N.; Holmes, D. J.; Pompliano, D. L. *Nat. Rev. Drug Discov.* **2007**, *6*, 29-40.

(131) Allsop, A.; Illingworth, R. *J. Appl. Microbiol.* **2002**, *92*, 7-12.

(132) Lipinski, C. A.; Lombardo, F.; Dominy, B. W.; Feeney, P. J. *Adv. Drug Del. Rev.* **2001**, *46*, 3-26.

(133) O'Shea, R.; Moser, H. E. *J. Med. Chem.* **2008**, *51*, 2871-2878.

(134) Lomovskaya, O.; Lewis, K. *Proc. Natl. Acad. Sci. U. S. A.* **1992**, *89*, 8938-8942.

(135) Tommasi, R.; Brown, D. G.; Walkup, G. K.; Manchester, J. I.; Miller, A. A. *Nat. Rev. Drug Discov.* **2015**, *14*, 529-542.

(136) Nichols, D.; Cahoon, N.; Trakhtenberg, E. M.; Pham, L.; Mehta, A.; Belanger, A.; Kanigan, T.; Lewis, K.; Epstein, S. S. *Appl. Environ. Microbiol.* **2010**, *76*, 2445-2450.

(137) Ling, L. L.; Schneider, T.; Peoples, A. J.; Spoering, A. L.; Engels, I.; Conlon, B. P.; Mueller, A.; Schaberle, T. F.; Hughes, D. E.; Epstein, S.; Jones, M.; Lazarides, L.; Steadman, V. A.; Cohen, D. R.; Felix, C. R.; Fetterman, K. A.; Millett, W. P.; Nitti, A. G.; Zullo, A. M.; Chen, C.; Lewis, K. *Nature* **2015**, *517*, 455-459.

(138) Deresinski, S. *Clin. Infect. Dis.* **2009**, *49*, 1072-1079.

(139) Firsov, A. A.; Smirnova, M. V.; Lubenko, I. Y.; Vostrov, S. N.; Portnoy, Y. A.; Zinner, S. H. *J. Antimicrob. Chemother.* **2006**, *58*, 1185-1192.

(140) Rose, W. E.; Poppens, P. T. *J. Antimicrob. Chemother.* **2009**, *63*, 485-488.

(141) Lunse, C. E.; Schuller, A.; Mayer, G. *Int. J. Med. Microbiol.* **2014**, *304*, 79-92.

(142) Blount, K. F.; Breaker, R. R. *Nat. Biotechnol.* **2006**, *24*, 1558-1564.

(143) Sudarsan, N.; Cohen-Chalamish, S.; Nakamura, S.; Emilsson, G. M.; Breaker, R. R. *Chem. Biol.* **2005**, *12*, 1325-1335.

(144) Blount, K. F.; Wang, J. X.; Lim, J.; Sudarsan, N.; Breaker, R. R. *Nat. Chem. Biol.* **2007**, *3*, 44-49.

(145) Dersch, P.; Khan, M. A.; Muhlen, S.; Gorke, B. *Front Microbiol* **2017**, *8*, 803.

(146) Winkler, W. C.; Breaker, R. R. *Annu. Rev. Microbiol.* **2005**, *59*, 487-517.

(147) Mulhbacher, J.; Brouillette, E.; Allard, M.; Fortier, L. C.; Malouin, F.; Lafontaine, D. A. *PLoS Path.* **2010**, *6*, e1000865.

(148) Howe, J. A.; Wang, H.; Fischmann, T. O.; Balibar, C. J.; Xiao, L.; Galgoci, A. M.; Malinverni, J. C.; Mayhood, T.; Villafania, A.; Nahvi, A.; Murgolo, N.; Barbieri, C. M.; Mann, P. A.; Carr, D.; Xia, E.; Zuck, P.; Riley, D.; Painter, R. E.; Walker, S. S.; Sherborne, B.; de Jesus, R.; Pan, W.; Plotkin, M. A.; Wu, J.; Rindgen, D.; Cummings, J.;

Garlisi, C. G.; Zhang, R.; Sheth, P. R.; Gill, C. J.; Tang, H.; Roemer, T. *Nature* **2015**, *526*, 672-677.

(149) Kanehisa, M.; Furumichi, M.; Tanabe, M.; Sato, Y.; Morishima, K. *Nucleic Acids Res.* **2017**, *45*, D353-D361.

(150) Kanehisa, M.; Goto, S. *Nucleic Acids Res.* **2000**, *28*, 27-30.

(151) Kanehisa, M.; Sato, Y.; Kawashima, M.; Furumichi, M.; Tanabe, M. *Nucleic Acids Res.* **2016**, *44*, D457-462.

(152) Milewski, S. *Biochim. Biophys. Acta* **2002**, *1597*, 173-192.

(153) Schuller, A.; Matzner, D.; Lunse, C. E.; Wittmann, V.; Schumacher, C.; Unsleber, S.; Brotz-Oesterhelt, H.; Mayer, C.; Bierbaum, G.; Mayer, G. *ChemBioChem* **2017**, *18*, 435-440.

(154) Barreteau, H.; Kovac, A.; Boniface, A.; Sova, M.; Gobec, S.; Blanot, D. *FEMS Microbiol. Rev.* **2008**, *32*, 168-207.

(155) Montero-Moran, G. M.; Lara-Gonzalez, S.; Alvarez-Anorve, L. I.; Plumbridge, J. A.; Calcagno, M. L. *Biochemistry* **2001**, *40*, 10187-10196.

(156) Freese, E. B.; Cole, R. M.; Klofat, W.; Freese, E. *J. Bacteriol.* **1970**, *101*, 1046-1062.

(157) Khan, M. A.; Gopel, Y.; Milewski, S.; Gorke, B. *Frontiers in Microbiology* **2016**, *7*.

(158) Persiani, S.; Rotini, R.; Trisolino, G.; Rovati, L. C.; Locatelli, M.; Paganini, D.; Antonioli, D.; Roda, A. *Osteoarthritis Cartilage* **2007**, *15*, 764-772.

(159) Deigan, K. E.; Ferre-D'Amare, A. R. *Acc. Chem. Res.* **2011**, *44*, 1329-1338.

(160) Urban, J. H.; Vogel, J. *PLoS Biol.* **2008**, *6*, e64.

(161) Reichenbach, B.; Maes, A.; Kalamorz, F.; Hajnsdorf, E.; Gorke, B. *Nucleic Acids Res.* **2008**, *36*, 2570-2580.

(162) Mengin-Lecreulx, D.; van Heijenoort, J. *J. Biol. Chem.* **1996**, *271*, 32-39.

(163) Hiramatsu, K.; Hanaki, H.; Ino, T.; Yabuta, K.; Oguri, T.; Tenover, F. C. *J. Antimicrob. Chemother.* **1997**, *40*, 135-136.

(164) Barton, D. H. R.; Augydorey, S.; Camara, J.; Dalko, P.; Delaumeny, J. M.; Gero, S. D.; Quicletsire, B.; Stutz, P. *Tetrahedron* **1990**, *46*, 215-230.

(165) Sowa, T.; Ouchi, S. *Bull. Chem. Soc. Jpn.* **1975**, *48*, 2084-2090.

(166) Wang, G. N.; Lau, P. S.; Li, Y. F.; Ye, X. S. *Tetrahedron* **2012**, *68*, 9405-9412.

(167) Drugs.com. [Internet]. U.S. Pharmaceutical Sales - 2013; [Updated: February 2014; Cited: 17.09.2017] Available from: https://www.drugs.com/stats/top100/2013/sales

(168) Purser, S.; Moore, P. R.; Swallow, S.; Gouverneur, V. *Chem. Soc. Rev.* **2008**, *37*, 320-330.

(169) Shah, P.; Westwell, A. D. *J. Enzyme Inhib. Med. Chem.* **2007**, *22*, 527-540.

(170) Gillis, E. P.; Eastman, K. J.; Hill, M. D.; Donnelly, D. J.; Meanwell, N. A. *J. Med. Chem.* **2015**, *58*, 8315-8359.

(171) Liang, T.; Neumann, C. N.; Ritter, T. *Angew. Chem. Int. Ed. Engl.* **2013**, *52*, 8214-8264.

(172) Begue, J. P.; Bonnet-Delpon, D. *J. Fluor. Chem.* **2006**, *127*, 992-1012.

(173) Wang, J.; Sanchez-Rosello, M.; Acena, J. L.; del Pozo, C.; Sorochinsky, A. E.; Fustero, S.; Soloshonok, V. A.; Liu, H. *Chem. Rev.* **2014**, *114*, 2432-2506.

(174) Neumann, C. N.; Ritter, T. *Angew. Chem.* **2015**.

(175) Hu, X. G.; Thomas, D. S.; Griffith, R.; Hunter, L. *Angewandte Chemie-International Edition* **2014**, *53*, 6176-6179.

(176) Deleuze, A.; Menozzi, C.; Sollogoub, M.; Sinay, P. *Angew. Chem. Int. Ed.* **2004**, *43*, 6680-6683.

(177) Sardinha, J.; Guieu, S.; Deleuze, A.; Fernandez-Alonso, M. C.; Rauter, A. P.; Sinay, P.; Marrot, J.; Jimenez-Barbero, J.; Sollogoub, M. *Carbohydr. Res.* **2007**, *342*, 1689-1703.

(178) Leclerc, E.; Pannecoucke, X.; Etheve-Quelquejeu, M.; Sollogoub, M. *Chem. Soc. Rev.* **2013**, *42*, 4270-4283.

(179) Sardinha, J.; Rauter, A. P.; Sollogoub, M. *Tetrahedron Lett.* **2008**, *49*, 5548-5550.

(180) Graton, J.; Wang, Z.; Brossard, A. M.; Monteiro, D. G.; Le Questel, J. Y.; Linclau, B. *Angewandte Chemie-International Edition* **2012**, *51*, 6176-6180.

(181) Sofia, M. J.; Hunter, R.; Chan, T. Y.; Vaughan, A.; Dulina, R.; Wang, H. M.; Gange, D. *J. Org. Chem.* **1998**, *63*, 2802-2803.

(182) Amano, S.; Takemura, N.; Ohtsuka, M.; Ogawa, S.; Chida, N. *Tetrahedron* **1999**, *55*, 3855-3870.

(183) Weyershausen, B.; Nieger, M.; Dotz, K. H. *J. Organomet. Chem.* **2000**, *602*, 37-44.

(184) Chida, N.; Ohtsuka, M.; Ogura, K.; Ogawa, S. *Bull. Chem. Soc. Jpn.* **1991**, *64*, 2118-2121.

(185) Boyer, F. D.; Lallemand, J. Y. *Tetrahedron* **1994**, *50*, 10443-10458.

(186) P. Henderson, A.; Riseborough, J.; Bleasdale, C.; Clegg, W.; R. J. Elsegood, M.; T. Golding, B. *J. Chem. Soc., Perkin Trans. 1* **1997**, 3407-3414.

(187) Manthey, M. K.; GonzalezBello, C.; Abell, C. *Journal of the Chemical Society-Perkin Transactions 1* **1997**, 625-628.

(188) Enders, D.; Faure, S.; Potthoff, M.; Runsink, J. *Synthesis* **2001**, 2307-2319.

(189) Garbisch, E. W. *J. Am. Chem. Soc.* **1964**, *86*, 1780-&.

(190) Anizelli, P. R.; Vilcachagua, J. D.; Neto, A. C.; Tormena, C. F. *J. Phys. Chem. A* **2008**, *112*, 8785-8789.

(191) Petasis, N. A.; Bzowej, E. I. *J. Am. Chem. Soc.* **1990**, *112*, 6392-6394.

(192) Petasis, N. A.; Lu, S. P. *Tetrahedron Lett.* **1995**, *36*, 2393-2396.

(193) Kürti, L.; Czakó, B. *Strategic applications of named reactions in organic sythesis : background and detailed mechanisms*; Elsevier: Amsterdam ; Boston, 2005.

(194) Martinez, I.; Howell, A. R. *Tetrahedron Lett.* **2000**, *41*, 5607-5611.

(195) Akita, H.; Nozawa, M.; Mitsuda, A.; Ohsawa, H. *Tetrahedron-Asymmetry* **2000**, *11*, 1375-1388.

(196) Abad, A.; Agullo, C.; Cunat, A. C.; Gonzalez-Coloma, A.; Pardo, D. *Eur. J. Org. Chem.* **2010**, 2182-2198.

(197) Carlson, R. G.; Behn, N. S. *J. Org. Chem.* **1967**, *32*, 1363-&.

(198) Johnson, C. R.; Tait, B. D.; Cieplak, A. S. *J. Am. Chem. Soc.* **1987**, *109*, 5875-5876.

(199) Cieplak, A. S. *J. Am. Chem. Soc.* **1981**, *103*, 4540-4552.

(200) ChemCraft. [Internet]. [Updated: 19.09.2017; Cited: 19.09.2017] Available from: https://www.chemcraftprog.com

(201) Rajanbabu, T. V.; Nugent, W. A.; Beattie, M. S. *J. Am. Chem. Soc.* **1990**, *112*, 6408-6409.

(202) Rajanbabu, T. V.; Nugent, W. A. *J. Am. Chem. Soc.* **1994**, *116*, 986-997.

(203) Gansauer, A.; Pierobon, M.; Bluhm, H. *Angew. Chem. Int. Ed.* **1998**, *37*, 101-103.

(204) Gansauer, A.; Kube, C.; Daasbjerg, K.; Sure, R.; Grimme, S.; Fianu, G. D.; Sadasivam, D. V.; Flowers, R. A., 2nd *J. Am. Chem. Soc.* **2014**, *136*, 1663-1671.

(205) Justicia, J.; Jimenez, T.; Morcillo, S. P.; Cuerva, J. M.; Oltra, J. E. *Tetrahedron* **2009**, *65*, 10837-10841.

(206) Luo, Y.-R.; Luo, Y.-R.; CRC Press,: Boca Raton, 2007, p 1 online resource (1,655 pages).

(207) Luo, Y.-R. *Handbook of bond dissociation energies in organic compounds*; CRC Press: Boca Raton, Fla., 2003.

(208) Kuhnel, M. F.; Lentz, D. *Angew. Chem. Int. Ed. Engl.* **2010**, *49*, 2933-2936.

(209) Kiplinger, J. L.; Richmond, T. G. *J. Am. Chem. Soc.* **1996**, *118*, 1805-1806.

(210) Daasbjert, K.; Svith, H.; Grimme, S.; Gerenkam, M.; Muck-Lichtenfeld, C.; Gansauer, A.; Barchuk, A. *Radicals in Synthesis I: Methods and Mechanisms* **2006**, *263*, 39-69.

(211) Giese, B. *Angewandte Chemie-International Edition* **1989**, *28*, 969-980.

(212) Giese, B.; Damm, W.; Witzel, T.; Zeitz, H. G. *Tetrahedron Lett.* **1993**, *34*, 7053-7056.

(213) Gansauer, A.; Bluhm, H.; Rinker, B.; Narayan, S.; Schick, M.; Lauterbach, T.; Pierobon, M. *Chem. - Eur. J.* **2003**, *9*, 531-542.

(214) Dolbier, W. R. In *Organofluorine Chemistry: Fluorinated Alkenes and Reactive Intermediates*; Chambers, R. D., Ed.; Springer Berlin Heidelberg: Berlin, Heidelberg, 1997, p 97-163.

(215) Giese, B. *Angewandte Chemie-International Edition in English* **1977**, *16*, 125-136.

(216) Neese, F. *Wiley Interdiscip. Rev.: Comput. Mol. Sci.* **2012**, *2*, 73-78.

(217) Becke, A. D. *Phys Rev A Gen Phys* **1988**, *38*, 3098-3100.

(218) Perdew, J. P. *Phys Rev B Condens Matter* **1986**, *33*, 8822-8824.

(219) Hammond, G. S. *J. Am. Chem. Soc.* **1955**, *77*, 334-338.

(220) Gold, V. *Pure Appl. Chem.* **1979**, *51*, 1725-1801.

(221) Corey, E. J.; Venkates.A *J. Am. Chem. Soc.* **1972**, *94*, 6190-&.

(222) Meyer, O.; Hoeffler, J. F.; Grosdemange-Billiard, C.; Rohmer, M. *Tetrahedron* **2004**, *60*, 12153-12162.

(223) DiLauro, A. M.; Seo, W. J.; Phillips, S. T. *J. Org. Chem.* **2011**, *76*, 7352-7358.

(224) Surfraz, M. B. U.; Akhtar, M.; Allemann, R. K. *Tetrahedron Lett.* **2004**, *45*, 1223-1226.

(225) Canales, A.; Angulo, J.; Ojeda, R.; Bruix, M.; Fayos, R.; Lozano, R.; Gimenez-Gallego, G.; Martin-Lomas, M.; Nieto, P. M.; Jimenez-Barbero, J. *J. Am. Chem. Soc.* **2005**, *127*, 5778-5779.

(226) Sinnokrot, M. O.; Sherrill, C. D. *J. Phys. Chem. A* **2006**, *110*, 10656-10668.

(227) Grimme, S. *Angewandte Chemie-International Edition* **2008**, *47*, 3430-3434.

(228) Collins, D. J.; Hibberd, A. I.; Skelton, B. W.; White, A. H. *Aust. J. Chem.* **1998**, *51*, 681-694.

(229) Wuts, P. G. M.; Greene, T. W.; Greene, T. W. *Greene's protective groups in organic synthesis*; 4th ed.; Wiley-Interscience: Hoboken, N.J., 2007.

(230) Scheidt, K. A.; Chen, H.; Follows, B. C.; Chemler, S. R.; Coffey, D. S.; Roush, W. R. *J. Org. Chem.* **1998**, *63*, 6436-6437.

(231) Yamauchi, N.; Terachi, T.; Eguchi, T.; Kakinuma, K. *Tetrahedron* **1994**, *50*, 4125-4136.

(232) Johnson, W. S.; Margrave, J. L.; Bauer, V. J.; Frisch, M. A.; Dreger, L. H.; Hubbard, W. N. *J. Am. Chem. Soc.* **1960**, *82*, 1255-1256.

(233) Anderson, C. L.; Soderquist, J. A.; Kabalka, G. W. *Tetrahedron Lett.* **1992**, *33*, 6915-6918.

(234) Sollogoub, M.; Pearce, A. J.; Herault, A.; Sinay, P. *Tetrahedron-Asymmetry* **2000**, *11*, 283-294.

(235) Tebbe, F. N.; Parshall, G. W.; Reddy, G. S. *J. Am. Chem. Soc.* **1978**, *100*, 3611-3613.

(236) Pine, S. H.; Pettit, R. J.; Geib, G. D.; Cruz, S. G.; Gallego, C. H.; Tijerina, T.; Pine, R. D. *J. Org. Chem.* **1985**, *50*, 1212-1216.

(237) Blattner, R.; Ferrier, R. J. *J. Chem. Soc., Chem. Commun.* **1987**, 1008-1009.

(238) Westheimer, F. H. *Science* **1987**, *235*, 1173-1178.

(239) Cox, J. R.; Ramsay, O. B. *Chem. Rev.* **1964**, *64*, 317-&.

(240) Lad, C.; Williams, N. H.; Wolfenden, R. *Proc. Natl. Acad. Sci. U. S. A.* **2003**, *100*, 5607-5610.

(241) Kugel, L.; Halmann, M. *J. Org. Chem.* **1967**, *32*, 642-&.

(242) Loncke, P. G.; Berti, P. J. *J. Am. Chem. Soc.* **2006**, *128*, 6132-6140.

(243) Schuller, A. *et al.* unpublished data.

(244) Schuller, A. Ph.D. thesis, University Bonn, **2017**.

(245) Lünse, C. E. Ph.D. thesis, University of Bonn, **2012**.

(246) Howard, J. A. K.; Hoy, V. J.; OHagan, D.; Smith, G. T. *Tetrahedron* **1996**, *52*, 12613-12622.

(247) Dalvit, C.; Invernizzi, C.; Vulpetti, A. *Chemistry-a European Journal* **2014**, *20*, 11058-11068.

(248) Champagne, P. A.; Desroches, J.; Paquin, J. F. *Synthesis-Stuttgart* **2015**, *47*, 306-322.

(249) Bondi, A. *J. Phys. Chem.* **1964**, *68*, 441-&.

(250) Allen, F. H.; Kennard, O.; Watson, D. G.; Brammer, L.; Orpen, A. G.; Taylor, R. *Journal of the Chemical Society-Perkin Transactions 2* **1987**, S1-S19.

(251) Sinnecker, S.; Rajendran, A.; Klamt, A.; Diedenhofen, M.; Neese, F. *J. Phys. Chem. A* **2006**, *110*, 2235-2245.

(252) Weigend, F.; Ahlrichs, R. *Phys. Chem. Chem. Phys.* **2005**, *7*, 3297-3305.

(253) Arunan, E.; Desiraju, G. R.; Klein, R. A.; Sadlej, J.; Scheiner, S.; Alkorta, I.; Clary, D. C.; Crabtree, R. H.; Dannenberg, J. J.; Hobza, P.; Kjaergaard, H. G.; Legon, A. C.; Mennucci, B.; Nesbitt, D. J. *Pure Appl. Chem.* **2011**, *83*, 1637-1641.

(254) Holleman, A. F.; Wiberg, E. *Lehrbuch der anorganischen chemie*; 57.-70., wesentlich erweiterte, umgearb. und verb. Aufl. mit einem Anhang Chemiegeschichte und einer Raumbilder-Beilage sowie 177 Figuren und 29 Struktur-Bildern in stereoskopischer Darstellung, von Egon Wiberg. ed.; De Gruyter: Berlin,, 1995.

(255) Tao, J. M.; Perdew, J. P.; Staroverov, V. N.; Scuseria, G. E. *Phys. Rev. Lett.* **2003**, *91*, 146401.

(256) Zhao, Y.; Truhlar, D. G. *J. Phys. Chem. A* **2005**, *109*, 5656-5667.

(257) Klamt, A.; Schuurmann, G. *J. Chem. Soc., Perkin Trans. 2* **1993**, 799-805.

(258) Morgenthaler, M.; Schweizer, E.; Hoffmann-Roder, A.; Benini, F.; Martin, R. E.; Jaeschke, G.; Wagner, B.; Fischer, H.; Bendels, S.; Zimmerli, D.; Schneider, J.; Diederich, F.; Kansy, M.; Muller, K. *ChemMedChem* **2007**, *2*, 1100-1115.

(259) Reizer, J.; Saier, M. H., Jr.; Deutscher, J.; Grenier, F.; Thompson, J.; Hengstenberg, W. *Crit. Rev. Microbiol.* **1988**, *15*, 297-338.

(260) Wilson, D. B. *Annu. Rev. Biochem* **1978**, *47*, 933-965.

(261) Postma, P. W.; Lengeler, J. W.; Jacobson, G. R. *Microbiol. Rev.* **1993**, *57*, 543-594.

(262) Cao, Y.; Jin, X. S.; Levin, E. J.; Huang, H.; Zong, Y. N.; Quick, M.; Weng, J.; Pan, Y. P.; Love, J.; Punta, M.; Rost, B.; Hendrickson, W. A.; Javitch, J. A.; Rajashankar, K. R.; Zhou, M. *Nature* **2011**, *473*, 50-U58.

(263) Lolkema, J. S.; ten Hoeve-Duurkens, R. H.; Dijkstra, D. S.; Robillard, G. T. *Biochemistry* **1991**, *30*, 6716-6721.

(264) Ruijter, G. J.; van Meurs, G.; Verwey, M. A.; Postma, P. W.; van Dam, K. *J. Bacteriol.* **1992**, *174*, 2843-2850.

(265) Elferink, M. G. L.; Driessen, A. J. M.; Robillard, G. T. *J. Bacteriol.* **1990**, *172*, 7119-7125.

(266) Deutscher, J.; Galinier, A.; Martin-Verstraete, I. In *Bacillus subtilis and Its Closest Relatives: from Qenes to Cells*; Sonenshein, A. L., Losick, R., Hoch, J. A., Eds.; ASM Press: Washington, D.C., 2002, p 629.

(267) Deutscher, J.; Ake, F. M. D.; Derkaoui, M.; Zebre, A. C.; Cao, T. N.; Bouraoui, H.; Kentache, T.; Mokhtari, A.; Milohanic, E.; Joyet, P. *Microbiol. Mol. Biol. Rev.* **2014**, *78*, 231-256.

(268) Deutscher, J.; Francke, C.; Postma, P. W. *Microbiol. Mol. Biol. Rev.* **2006**, *70*, 939-1031.

(269) Gaugue, I.; Oberto, J.; Putzer, H.; Plumbridge, J. *PLoS One* **2013**, *8*, e63025.

(270) Reizer, J.; Bachem, S.; Reizer, A.; Arnaud, M.; Saier, M. H., Jr.; Stulke, J. *Microbiology* **1999**, *145 (Pt 12)*, 3419-3429.

(271) Lewis, C.; Barbiers, A. R. *Antibiot Annu* **1959**, *7*, 247-254.

(272) Vavra, J. J.; Deboer, C.; Dietz, A.; Hanka, L. J.; Sokolski, W. T. *Antibiotics annual* **1959**, *7*, 230-235.

(273) Lengeler, J. *Mol. Gen. Genet.* **1980**, *179*, 49-54.

(274) Ammer, J.; Brennenstuhl, M.; Schindler, P.; Holtje, J. V.; Zahner, H. *Antimicrob. Agents Chemother.* **1979**, *16*, 801-807.

(275) Urban, A.; Eckermann, S.; Fast, B.; Metzger, S.; Gehling, M.; Ziegelbauer, K.; Rubsamen-Waigmann, H.; Freiberg, C. *Appl. Environ. Microbiol.* **2007**, *73*, 6436-6443.

(276) Mengin-Lecreulx, D.; van Heijenoort, J. *J. Bacteriol.* **1994**, *176*, 5788-5795.

(277) Seo, K. C.; Kwon, Y. G.; Kim, D. H.; Jang, I. S.; Cho, J. W.; Chung, S. K. *Chem. Commun.* **2009**, 1733-1735.

(278) Reizer, J.; Novotny, M. J.; Panos, C.; Saier, M. H. *J. Bacteriol.* **1983**, *156*, 354-361.

(279) Reizer, J.; Saier, M. H. *J. Bacteriol.* **1983**, *156*, 236-242.

(280) Lu, W.; Bennett, B. D.; Rabinowitz, J. D. *Journal of Chromatography B-Analytical Technologies in the Biomedical and Life Sciences* **2008**, *871*, 236-242.

(281) Dunn, W. B.; Ellis, D. I. *Trac-Trends in Analytical Chemistry* **2005**, *24*, 285-294.

(282) Park, B. K.; Kitteringham, N. R.; O'Neill, P. M. *Annu. Rev. Pharmacol. Toxicol.* **2001**, *41*, 443-470.

(283) Matias, V. R.; Beveridge, T. J. *Mol. Microbiol.* **2005**, *56*, 240-251.

(284) Keun, H. C.; Athersuch, T. J.; Beckonert, O.; Wang, Y.; Saric, J.; Shockcor, J. P.; Lindon, J. C.; Wilson, I. D.; Holmes, E.; Nicholson, J. K. *Anal. Chem.* **2008**, *80*, 1073-1079.

(285) O'Hagan, D.; Harper, D. B. *J. Fluor. Chem.* **1999**, *100*, 127-133.

(286) vanPee, K. H. *Annu. Rev. Microbiol.* **1996**, *50*, 375-399.

(287) Tanahashi, E.; Kiso, M.; Hasegawa, A. *Carbohydr. Res.* **1983**, *117*, 304-308.

(288) Gloster, T. M.; Zandberg, W. F.; Heinonen, J. E.; Shen, D. L.; Deng, L. H.; Vocadlo, D. J. *Nat. Chem. Biol.* **2011**, *7*, 174-181.

(289) Seitz, T. Ph.D. thesis, University Konstanz, **2017**.

(290) van de Rijn, I.; Kessler, R. E. *Infect. Immun.* **1980**, *27*, 444-448.

(291) Vriend, G. *J. Mol. Graph.* **1990**, *8*, 52-&.

(292) Trott, O.; Olson, A. J. *J. Comput. Chem.* **2010**, *31*, 455-461.

(293) Bradley, D.; Williams, G.; Lawton, M. *J. Org. Chem.* **2010**, *75*, 8351-8354.

(294) Clauss, K.; Bestian, H. *Annalen Der Chemie-Justus Liebig* **1962**, *654*, 8-19.